

BRACING REQUIREMENTS OF COLD-FORMED STEEL CEE-STUDS  
SUBJECTED TO AXIAL COMPRESSION

By

VISWANATH URALA

A THESIS PRESENTED TO THE GRADUATE SCHOOL  
OF THE UNIVERSITY OF FLORIDA IN PARTIAL FULFILLMENT  
OF THE REQUIREMENTS FOR THE DEGREE OF  
MASTER OF ENGINEERING

UNIVERSITY OF FLORIDA

2004

Copyright 2004

by

Viswanath Urala

This document is dedicated to my beloved Mother and cherished Late Father.

## ACKNOWLEDGMENTS

The author thanks his advisors, Dr. Perry S Green, and Dr. Thomas Sputo, for granting him an opportunity to work on this research and for having guided till the end. The author holds due respect to his graduate committee for their assistance and immaculate guidance. The author is grateful to the co-sponsors AISI® and SSMA® for financially supporting this research. It is the author's heartfelt gratitude to the Chairman, Department of Civil and Coastal Engineering, University of Florida, for providing the facilities and resources for completing this thesis.

The author appreciates the help offered by Mr. Darin Shearer and Ms. Kimberly Lammert, who were his colleagues and all those who directly or indirectly were part of this research. The author acknowledges the contributions of Mr. Charles Broward and Mr. Danny for their assistance in the structures laboratory. The author thanks all friends and colleagues who assisted him at various levels by boosting his morale to see this project till its completion. This research would not have been a reality without the emotional support of the author's family for which he is indebted. The author especially thanks Mr. Ratan Chand, Mr. Srinidhi Sharma, and Mr. Sudhir Gurjar, without whose support this would not have been possible.

Last but not the least the author thanks the United States of America for having accepted him as a student into their nation to fulfill his ambition to get the degree of Master of Engineering in Civil Engineering at the University of Florida.

## TABLE OF CONTENTS

|  | <u>page</u> |
|--|-------------|
| ACKNOWLEDGMENTS .....  | iv          |
| LIST OF TABLES .....   | viii        |
| LIST OF FIGURES .....  | x           |
| ABSTRACT .....   | xvi         |
| CHAPTER  |             |
| 1 INTRODUCTION .....   | 1           |
| 1.1 General.....   | 1           |
| 1.2 Objectives of Research .....   | 1           |
| 1.3 Scope of Research.....   | 3           |
| 2 LITERATURE REVIEW .....  | 6           |
| 2.1 General.....   | 6           |
| 2.2 Buckling of Columns .....  | 7           |
| 2.2.1 Elastic Buckling.....  | 7           |
| 2.2.2 Inelastic Buckling .....   | 8           |
| 2.2.3 Local Buckling and Distortional Buckling .....   | 9           |
| 2.3 Bracing Stiffness and Strength.....  | 11          |
| 2.3.1 Column with Concentric Axial Load and an Immovable Point Support<br>at Mid-height..... | 12          |
| 2.3.2 Column with Concentric Axial Load and an Elastic Lateral Support at<br>Mid-height..... | 13          |
| 2.4 Long Column Tests.....   | 19          |
| 2.4 AISC-LRFD Specification.....   | 20          |
| 2.5 AISI Specification for Cold-Formed Steel .....   | 22          |
| 3 DESCRIPTION OF EXPERIMENTAL STUDY .....  | 33          |
| 3.1 Introduction.....  | 33          |
| 3.2 Objectives of Experimental Tests .....   | 34          |
| 3.3 Material Properties of Test Specimens .....  | 34          |
| 3.4 As-Built Dimensions of the Test Specimens .....  | 35          |
| 3.5 Measured Geometric Imperfections of the Test Specimens .....                             | 36          |

|         |  |     |
|---------|--|-----|
| 3.5.1   | Global Imperfections .....   | 36  |
| 3.5.2   | Cross-Sectional Imperfections .....                                    | 37  |
| 3.6     | Test Setup and Test Procedure for Single Column Axial Load Tests ..... | 38  |
| 3.6.1   | Test Specimens of Single Column Axial Load Tests .....                 | 38  |
| 3.6.2   | Test Frame for Single Column Axial Load Tests .....                    | 38  |
| 3.6.3   | Instrumentation for Single Column Axial Load Tests .....               | 39  |
| 3.6.4   | Test Procedure of Single Column Axial Load Tests .....                 | 39  |
| 3.7     | Test Setup and Test Procedure for Bridging Tests .....                 | 40  |
| 3.7.1   | Test Specimens of Bridging Tests .....                                 | 40  |
| 3.7.2   | Test Fixture for Bridging Tests .....                                  | 42  |
| 3.7.3   | Instrumentation .....  | 43  |
| 3.7.4   | Out-of-Plane Loading Test Procedure .....                              | 43  |
| 3.7.5   | In-Plane Loading Test Procedure .....                                  | 44  |
| 4       | EXPERIMENTAL RESULTS AND EVALUATION .....                              | 60  |
| 4.1     | Single Column Axial Load Test Results .....                            | 60  |
| 4.1.1   | Bracing Strength and Stiffness .....                                   | 61  |
| 4.1.2   | Evaluation of Experimental Observations .....                          | 63  |
| 4.1.2.1 | Effect of brace stiffness on axial load capacity .....                 | 67  |
| 4.1.2.2 | Effect of brace stiffness on buckling type and mode .....              | 70  |
| 4.1.2.3 | Effect of cross-sectional dimensions of cee-studs .....                | 71  |
| 4.1.2.4 | Effect of experimental load on the brace stiffness and strength .....  | 72  |
| 4.1.2.5 | Effect of brace stiffness on lateral displacement .....                | 73  |
| 4.1.2.6 | Effect of brace stiffness on effective length of columns .....         | 73  |
| 4.1.2.7 | Effect of brace strength on axial capacity .....                       | 74  |
| 4.1.2.8 | Other effects .....  | 74  |
| 4.2     | Bridging Test Results .....  | 75  |
| 4.2.1   | Bridging Connection Strength and Stiffness .....                       | 75  |
| 4.2.2   | Observations of the Out-of-Plane Experimental Tests .....              | 77  |
| 4.2.3   | Observations of the In-Plane Experimental Tests .....                  | 79  |
| 4.2.4   | Observed Bridging Connection Failures .....                            | 80  |
| 4.2.4.1 | SS type connection .....   | 81  |
| 4.2.4.2 | WW type connection .....   | 81  |
| 4.2.4.3 | DW type connection .....   | 81  |
| 4.3     | Separation of Brace Forces in Flexural and Torsional Components .....  | 82  |
| 4.4     | Summary of Experimental Observations .....                             | 83  |
| 5       | ANALYTICAL EVALUATION .....  | 146 |
| 5.1     | Analytical Load Capacity of Unbraced and Fully Braced Studs .....      | 146 |
| 5.2     | Analytical Bridging Connection Stiffness of a Flexible Bracing .....   | 148 |
| 5.2.1   | Initial Flexural Stiffness of the Bracing Connection .....             | 148 |
| 5.2.1.1 | SS type connection .....   | 150 |
| 5.2.1.2 | WW type connection .....   | 151 |
| 5.2.1.3 | DW type connection .....   | 151 |
| 5.2.2   | Initial Torsional Stiffness of the Bracing Connection .....            | 152 |

|          |   |     |
|----------|---|-----|
| 5.3      | Total Stiffness of the Bridging Connection .....                                  | 153 |
| 5.3.1    | Initial Flexural Stiffness.....   | 153 |
| 5.3.2    | Initial Torsional Stiffness.....  | 154 |
| 6        | CONCLUSIONS AND DESIGN RECOMMENDATIONS .....                                      | 167 |
| 6.1      | General Conclusions and Recommendations.....                                      | 167 |
| 6.2      | Design Recommendations .....  | 170 |
| APPENDIX |   |     |
| A        | TEST REPORTS OF SINGLE COLUMN AXIAL LOAD TESTS .....                              | 172 |
| B        | TEST RESULTS ON BRIDGING CONNECTIONS.....   | 355 |
| C        | MATHCAD WORKSHEETS .....  | 408 |
| C.1      | Axial Load Capacity of Unbraced Cee-Studs.....                                    | 409 |
| C.1.1    | 362S125-33 with Pinned Ends.....  | 409 |
| C.1.2    | 362S125-33 with Effective Length Factors based on Experimental<br>Conditions..... | 417 |
| C.2      | Initial Flexural Stiffness of the Connection from In-Plane Load tests .....       | 419 |
| C.2.1    | SS Type Connection .....  | 419 |
| C.2.2    | WW Type Connection .....  | 426 |
|          | LIST OF REFERENCES.....   | 431 |
|          | BIOGRAPHICAL SKETCH .....   | 434 |

## LIST OF TABLES

| <u>Table</u>  | <u>page</u> |
|---|-------------|
| 3.1 As-built Material Properties from the Tension Coupon Tests .....                  | 45          |
| 3.2 As-Built Cross-Sectional Dimensions of Test Specimens .....                       | 46          |
| 3.3 Initial Geometric Imperfections .....   | 49          |
| 3.4 Average As-Built Geometric Dimensions of Each Stud Series .....                   | 50          |
| 3.5 Average As-Built Geometric Dimensions of Each Stud Series .....                   | 50          |
| 4.1 Proposed Test Matrix for the Single Column Axial Load Tests .....                 | 86          |
| 4.2 Actual Test Matrix of the Single Column Axial Load Tests.....                     | 87          |
| 4.3 Nominal Properties of the Test Specimens Using AISIWIN Program .....              | 88          |
| 4.4 Average As-built Properties of the Test Specimens Using AISIWIN Program.....      | 89          |
| 4.5 Calculated Brace Stiffness and Total Brace Stiffness of the Test Specimens.....   | 90          |
| 4.6 Summary of Experimental Test Results for Test Specimens .....                     | 92          |
| 4.7 Required Brace Stiffness Based on $P_{max}$ .....                                 | 93          |
| 4.8 Effective Length Factors Based on $P_{max}$ .....                                 | 94          |
| 4.9 Measured Values of Brace Force and Mid-height Displacement at $P_{max}$ .....     | 95          |
| 4.10 Calculated Values of Brace Force and Mid-height Displacement at $P_{max}$ .....  | 97          |
| 4.11 Proposed Test Matrix for Bridging Connection Tests .....                         | 100         |
| 4.12 Bridging Test Results for Out-of-Plane Loading .....                             | 101         |
| 4.13 Initial Torsional Stiffness of the Lower Bound Values of Out-of-Plane Tests..... | 102         |
| 4.14 Bridging Test Results for In-Plane Loading .....                                 | 104         |
| 4.15 Initial Flexural Stiffness of the In-Plane Tests.....                            | 105         |

|      |   |     |
|------|---|-----|
| 4.16 | Experimental Initial Stiffness of the In-Plane Load Tests .....                       | 107 |
| 4.17 | Experimental Initial Stiffness of the Out-of-Plane Load Tests .....                   | 108 |
| 4.18 | Maximum Flexural and Corresponding Torsional Brace Force.....                         | 109 |
| 4.19 | Maximum Torsional and Corresponding Flexural Brace Force.....                         | 110 |
| 5.1  | Axial Load Capacities of Test Specimens Using AISI (1999) MathCAD<br>Worksheets ..... | 156 |
| 5.2  | Comparison of Initial Flexural Stiffness of the In-Plane Tests.....                   | 157 |
| 5.3  | Comparison of Initial Torsional Stiffness of the In-Plane Tests.....                  | 158 |
| 5.4  | Total Flexural Stiffness of the Bridging Connections.....                             | 159 |
| 5.5  | Calculated Brace Stiffness and Total Brace Stiffness of the Test Specimens.....       | 161 |
| 5.6  | Total Torsional Stiffness of the Bridging Connections.....                            | 163 |

## LIST OF FIGURES

| <u>Figure</u>   | <u>page</u> |
|---|-------------|
| 2.1 Reduced Modulus Theory .....  | 26          |
| 2.2 Imperfect Column with Immovable Mid-height Bracing .....                                    | 26          |
| 2.3 Imperfect Column with Elastic Mid-height Bracing.....                                       | 27          |
| 2.4 Critical Loads for Elastically Supported Columns.....                                       | 27          |
| 2.5 Effect of Bracing Stiffness .....   | 28          |
| 2.6 $P_{cr}/P_e$ versus $\beta L/P_e$ for a Discrete Bracing .....                              | 29          |
| 2.7 Effect of Lateral restraint location on Brace behavior .....                                | 29          |
| 2.8 Bracing Connection Clips .....  | 30          |
| 2.9 Wall Assembly test setup .....  | 30          |
| 2.10 Types of Bracing (a) Relative Bracing and (b) Nodal Bracing.....                           | 31          |
| 2.11 Effect of Initial Out-of-Plumbness .....   | 31          |
| 2.12 Effective Length Factors for Concentrically Loaded Columns .....                           | 32          |
| 3.1 Dimensions of a Typical Tension Coupon.....   | 51          |
| 3.2 Offset Method for Determining Yield Stress .....  | 51          |
| 3.3 Autographic Diagram Method for Determining Yield Stress .....                               | 52          |
| 3.4 Typical Cross-Section of a Cee-Stud .....   | 52          |
| 3.5 Connection of Cee-Stud and Track (a) at Top, (b) at Bottom.....                             | 53          |
| 3.6 Plan View of Single Column Axial Test Setup in the Riehle Universal Testing<br>Machine..... | 53          |
| 3.7 Schematic Mid-height Bracing and Instrumentation Locations on<br>Test Specimens.....        | 54          |

|      |  |     |
|------|--|-----|
| 3.8  | Close-up View of the Location of Brace-Wires and Instrumentation at Mid-height of the Cee-Stud.....                | 54  |
| 3.9  | Types of Bridging Connections.....   | 55  |
| 3.10 | Top View of the SS Type Bridging Connection.....   | 55  |
| 3.11 | Elevation Views of Bridging Connection Test Setup.....   | 56  |
| 3.12 | Schematic Plan View of Bridging Connection Tests.....  | 57  |
| 3.13 | Overall View of the Out-of-Plane Bridging Tests.....   | 58  |
| 3.14 | Overall View of the In-Plane Bridging Tests.....   | 58  |
| 3.15 | Out-of-Plane Loading Test Instrumentation.....   | 59  |
| 3.16 | In-plane Loading Test Instrumentatio.....  | 59  |
| 4.1  | Typical Bracing for the Single Column Axial Load Tests.....  | 111 |
| 4.2  | Axial Load vs. Axial Shortening for the Stud 362S125-33 with Varying Brace Stiffness.....                          | 111 |
| 4.3  | Axial Load vs. Axial Shortening for the Stud 362S162-43 with Varying Brace Stiffness.....                          | 112 |
| 4.4  | Axial Load vs. Axial Shortening for the Stud 362S162-68 with Varying Brace Stiffness.....                          | 112 |
| 4.5  | Axial Load vs. Axial Shortening for the Stud 600S125-33 with Varying Brace Stiffness.....                          | 113 |
| 4.6  | Axial Load vs. Axial Shortening for the Stud 600S162-43 with Varying Brace Stiffness.....                          | 113 |
| 4.7  | Axial Load vs. Axial Shortening for the Stud 600S162-97 with Varying Brace Stiffness.....                          | 114 |
| 4.8  | Axial Load vs. Axial Shortening for the Stud 800S162-43 with Varying Brace Stiffness.....                          | 114 |
| 4.9  | Axial Load vs. Axial Shortening for the Stud 800S162-97 with Varying Brace Stiffness.....                          | 115 |
| 4.10 | Schematic Diagram Showing the Various Buckling Shapes and Buckling Modes Observed in the Experimental Testing..... | 115 |
| 4.11 | Comparison of Studs 362S125-33-0 and 600S125-33-0.....   | 116 |

|      |  |     |
|------|--|-----|
| 4.12 | Comparison of Studs 362S125-33-100 (1.7x) and 600S125-33-060 (1.3x) .....                            | 116 |
| 4.13 | Comparison of Studs 362S125-33-200 (6.2x) and 600S125-33-200 (7.4x) .....                            | 117 |
| 4.14 | Comparison of Studs 362S162-43-0, 600S162-43-0 and 800S162-43-0.....                                 | 117 |
| 4.15 | Comparison of Studs 362S162-43-200 (1.2x), 600S162-43-250 (1.6x) and<br>800S162-43-150 (1.3x) .....  | 118 |
| 4.16 | Comparison of Studs 362S162-43-400 (2.5x), 600S162-43-500 (3.4x) and<br>800S162-43-300 (2.3x) .....  | 118 |
| 4.17 | Comparison of Studs 600S162-97-0 and 800S162-97-0.....   | 119 |
| 4.18 | Comparison of Studs 600S162-97-1000 (1.7x) and 800S162-97-1000 (2.1x) .....                          | 119 |
| 4.19 | Comparison of Studs 600S162-97-1500 (2.7x) and 800S162-97-2100 (4.3x) .....                          | 120 |
| 4.20 | Comparison of Studs 362S125-33-0, 362S162-43-0 and 362S162-68-0.....                                 | 120 |
| 4.21 | Comparison of Studs 362S125-33-100 (1.7x), 362S162-43-200 (1.2x) and<br>362S162-68-500 (1.8x) .....  | 121 |
| 4.22 | Comparison of Studs 362S125-33-400 (6.2x), 362S162-43-800 (5.4x) and<br>362S162-68-1000 (3.3x) ..... | 121 |
| 4.23 | Comparison of Studs 600S125-33-0, 600S162-43-0 and 600S162-97-0.....                                 | 122 |
| 4.24 | Comparison of Studs 600S125-33-30 (0.2x), 600S162-43-75 (0.6x) and<br>600S162-97-160 (0.3x) .....    | 122 |
| 4.25 | Comparison of Studs 600S125-33-60 (1.3x), 600S162-43-250 (1.6x) and<br>600S162-97-1000 (1.7x) .....  | 123 |
| 4.26 | Comparison of Studs 600S125-33-200 (7.4x), 600S162-43-500 (3.4x) and<br>600S162-97-1500 (2.7x) ..... | 123 |
| 4.27 | Comparison of Studs 800S162-43-0 and 800S162-97-0.....   | 124 |
| 4.28 | Comparison of Studs 800S162-43-150(1.3x) and 800S162-97-500 (1.2x) .....                             | 124 |
| 4.29 | Comparison of Studs 800S162-43-300 (2.3x) and 800S162-97-2100 (4.3x) .....                           | 125 |
| 4.30 | Experimental Load vs. Target Brace Stiffness for 362 Series of<br>Lipped Cee Studs .....             | 125 |
| 4.31 | Experimental Load vs. Target Brace Stiffness for 600 Series of<br>Lipped Cee Studs .....             | 126 |

|      |  |     |
|------|--|-----|
| 4.32 | Experimental Load vs. Target Brace Stiffness for 800 Series of Lipped Cee Studs .....  | 126 |
| 4.33 | Total Brace Stiffness vs. Weak Axis Lateral Displacement for the 362 Series of Lipped Cee-Studs .....                            | 127 |
| 4.34 | Total Brace Stiffness vs. Weak Axis Lateral Displacement for the 600 Series of Lipped Cee Studs .....                            | 127 |
| 4.35 | Total Brace Stiffness vs. Target Brace Stiffness for the 800 Series Lipped Cee Studs .....                                       | 128 |
| 4.36 | Effective Length Factor vs. Total Brace Stiffness for 362S-125-33 Series of Lipped Cee Studs .....                               | 128 |
| 4.37 | Effective Length Factor vs. Total Brace Stiffness for 362S-162-43 Series of Lipped Cee Studs .....                               | 129 |
| 4.38 | Effective Length Factor vs. Total Brace Stiffness for 362S-162-68 Series of Lipped Cee Studs .....                               | 129 |
| 4.39 | Effective Length Factor vs. Total Brace Stiffness for 600S-125-33 Series of Lipped Cee Studs .....                               | 130 |
| 4.40 | Effective Length Factor vs. Total Brace Stiffness for 600S-162-43 Series of Lipped Cee Studs .....                               | 130 |
| 4.41 | Effective Length Factor vs. Total Brace Stiffness for 600S-162-97 Series of Lipped Cee Studs .....                               | 131 |
| 4.42 | Effective Length Factor vs. Total Brace Stiffness for 800S-162-43 Series of Lipped Cee Studs .....                               | 131 |
| 4.43 | Effective Length Factor vs. Total Brace Stiffness for 800S-162-97 Series of Lipped Cee Studs .....                               | 132 |
| 4.44 | Location of Linear Potentiometers on the Bridging Connection .....   | 132 |
| 4.45 | Plot of Applied Load vs. Calculated Rotation at the Center-line of the Web for the 362S Series of Studs.....                     | 133 |
| 4.46 | Plot of Applied Load vs. Calculated Rotation at the Center-line of the Web for the 600S Series of Studs.....                     | 133 |
| 4.47 | Plot of Applied Load vs. Calculated Rotation at the Center-line of the Web for the 800S Series of Studs with SS Connection.....  | 134 |
| 4.48 | Plot of Applied Load vs. Calculated Rotation at the Center-line of the Web for the 362S Series of Studs with WW Connection ..... | 134 |

|      |  |     |
|------|--|-----|
| 4.49 | Plot of Applied Load vs. Calculated Rotation at the Center-line of the Web for the 600S Series of Studs with WW Connection .....               | 135 |
| 4.50 | Plot of Applied Load vs. Calculated Rotation at the Center-line of the Web for the 800S Series of Studs with WW Connection .....               | 135 |
| 4.51 | Plot of Applied Load vs. Calculated Rotation at the Center-line of the Web for the 362S Series of Studs with DW Connection .....               | 136 |
| 4.52 | Plot of Applied Load vs. Calculated Rotation at the Center-line of the Web for the 600S Series of Studs with DW Connection .....               | 136 |
| 4.54 | Plot of Applied Load vs. Calculated Rotation at the Center-line of the Web for the 362S Series of Studs.....                                   | 138 |
| 4.55 | Plot of Applied Load vs. Calculated Rotation at the Center-line of the Web for the 600S Series of Studs.....                                   | 138 |
| 4.56 | Plot of Applied Load vs. Calculated Rotation at the Center-line of the Web for the 800S Series of Studs.....                                   | 139 |
| 4.57 | Plot of Applied Load vs. Calculated Rotation at the Center-line of the Web for the 362S Series of Studs.....                                   | 139 |
| 4.58 | Plot of Applied Load vs. Calculated Rotation at the Center-line of the Web for the 600S Series of Studs.....                                   | 140 |
| 4.59 | Plot of Applied Load vs. Calculated Rotation at the Center-line of the Web for the 800S Series of Studs.....                                   | 140 |
| 4.60 | Plot of Applied Load vs. Calculated Rotation at the Center-line of the Web for the 362S Series of Studs.....                                   | 141 |
| 4.61 | Plot of Applied Load vs. Calculated Rotation at the Center-line of the Web for the 600S Series of Studs.....                                   | 141 |
| 4.62 | Plot of Applied Load vs. Calculated Rotation at the Center-line of the Web for the 800S Series of Studs.....                                   | 142 |
| 4.63 | Plot of Initial Torsional Stiffness vs. Effective Flat-width to Thickness Ratio for the Out-of-Plane loading Tests on SS-type Connection ..... | 142 |
| 4.64 | Plot of Initial Torsional Stiffness vs. Effective Flat-width to Thickness Ratio for the Out-of-Plane loading Tests on WW-type Connection ..... | 143 |
| 4.65 | Plot of Initial Torsional Stiffness vs. Effective Flat-width to Thickness Ratio for the Out-of-Plane loading Tests on DW-type Connection.....  | 143 |

|      |   |     |
|------|---|-----|
| 4.66 | Plot of Initial Flexural Stiffness vs. Effective Flat-width to Thickness Ratio for the In-Plane loading Tests on SS-type Connection ..... | 144 |
| 4.67 | Plot of Initial Flexural Stiffness vs. Effective Flat-width to Thickness Ratio for the In-Plane loading Tests on WW-type Connection ..... | 144 |
| 4.68 | Plot of Initial Flexural Stiffness vs. Effective Flat-width to Thickness Ratio for the In-Plane loading Tests on DW-type Connection ..... | 145 |
| 4.69 | Brace Forces as a Resultant of Flexural and Torsional Components.....   | 145 |
| 5.1  | Flexural Stiffness of the SS Type Connection .....  | 165 |
| 5.2  | Flexural Stiffness of the WW Type Connection .....  | 165 |
| 5.3  | Flexural Stiffness of the DW Type Connection .....  | 166 |
| 5.4  | Torsional Stiffness of the SS Type Connection .....   | 166 |

Abstract of Thesis Presented to the Graduate School  
of the University of Florida in Partial Fulfillment of the  
Requirements for the Degree of Master of Engineering

BRACING REQUIREMENTS OF COLD-FORMED STEEL CEE-STUDS  
SUBJECTED TO AXIAL COMPRESSION

By

Viswanath Urala

August 2004

Chair: Perry S Green

Major Department: Civil and Coastal Engineering

An experimental testing program was carried out on single axially loaded cold-formed lipped cee-studs to determine the required flexural and torsional bracing strength and stiffness requirements of the stud. Conventional bridging or nodal bracing has been simulated in the experiments using monofilament steel wires attached to the stud flanges at mid-height. A range of brace stiffness was simulated in the testing frame by using various diameters and lengths of monofilament wire. The brace stiffness that was achieved ranged from less than 30 lbs/in. to greater than 4000 lbs/in. Brace strength was determined from the cross-sectional area of the steel wire and its experimentally determined yield strength. The axial load, individual brace forces, axial shortening, and in-plane (weak-axis) and out-of-plane (strong-axis) lateral displacements were measured in each test. The required bracing stiffness was experimentally determined by varying the brace stiffness for a given stud size and was based on the ability of the stud to develop its nominal axial compressive capacity as predicted by the 1996 AISI Cold-Formed Steel

Specification including Supplement No. 1. The experimental results were compared to existing nodal bracing models, analytical prediction models, and the current column bracing provisions that are part of the 1999 AISC-LRFD Specification for Structural Steel Buildings.

Experimental testing has also been carried out on typical industry bridging configuration to measure bridging assembly strength and stiffness relationships for bridging subjected to in-plane and out-of-plane loadings. Load versus displacement measurements have been compiled for these assemblies for various stud web depths, flange widths, and thicknesses with the goal of categorizing strength and stiffness for these various bridging assemblies.

## CHAPTER 1 INTRODUCTION

The drive to create more cost effective cold-formed steel structural systems, and the current move to designing axially loaded wall stud systems using an “all-steel” approach, has required an alternative to sheathing braced design. This has resulted in wall stud systems that are more sensitive to global stability limit states than previous designs. Ensuring global stability of axially loaded steel studs requires that the bracing system possess adequate stiffness and strength to develop the predicted axial strength.

### **1.1 General**

Cold-formed steel has been widely used in structural and non-structural wall construction for more than 60 years, and may be found in many residential, commercial and industrial facilities being built today. The lightweight property of cold-formed steel makes it easier and economical to transport and install than other construction materials such as masonry or hot-rolled steel. Other advantages include – resistance to pest attack, rapid construction, long service life and efficiently recyclable. Cold-formed steel sections can be used in most parts of a building, including roofs, trusses, frames etc.

### **1.2 Objectives of Research**

Current North American structural steel design practice using the 3rd Edition of the American Institute of Steel Construction- Load and Resistance Factor Design Specification (AISC 1999) prescribes nodal bracing strength and stiffness requirements, based on a model developed by Winter (1960) and modified by Yura (1995). However, the most recent cold-formed steel design specification, the North American Specification

by the American Iron and Steel Institute (AISI 2001a) does not contain provisions for determining nodal brace strength and stiffness requirements for axially loaded compression members. This research program was conducted to experimentally determine rational requirements for nodal bracing strength and stiffness demand of lipped cee-studs by conducting single column axial compression tests, and bridging strength and stiffness tests. The experimental results were used to formulate a rational methodology to be incorporated into the AISI Specification provisions for design purposes.

The objectives of this research included to determine:

1. the minimum bracing strength and stiffness required for cold-formed steel members subjected to axial loading;
2. the stiffness and strength of typical industry bridging systems;
3. the effective length factors based on unbraced length;
4. the effect of slenderness ratio on the buckling behavior of the cold-formed steel members;
5. the limit state or the governing buckling mode of cold-formed steel members;
6. the effect of support fixity on global buckling of cold-formed steel members.

The strength and stiffness required for bracing hot-rolled steel sections has been investigated by numerous researchers (Winter 1960, Yura 1995) based on experimental testing, analytical studies and feasible design considerations. Research has been conducted on the buckling phenomena of cold-formed steel subjected to axial compression by many researchers including Winter (1959), Miller (1990), Kwon and Hancock (1991), Miller and Pekoz (1994), Young and Rasmussen (1999), Schafer (2000), Beshara and LaBoube (2001). The current research has been directed towards establishing the strength and stiffness requirements of the bracing and bridging requirements for cold-formed steel lipped cee-studs.

### 1.3 Scope of Research

The scope of this research is limited to determining the strength and stiffness requirements for cold-formed steel lipped cee-studs subjected to axial compression. The lipped cee-studs were tested to determine their axial load capacity in a manner consistent with a typical field installation. With this as a basis, the scope of the single column axial tests was:

1. Standard lipped cee-studs that are widely used in structural and non-structural wall assemblies were tested. The section nominal web depths were 3.625, 6.00, and 8.00 inches, the nominal thickness were 33, 43, 68 and 97 mil. The flange width of the 33 mil studs was 1.25 inches and the flange width of the other studs was 1.625 inches (1 mil = 1/1000 inches).
2. The lipped cee-studs were mounted in industry standard shallow track and attached with #10 self-drilling screws. The lengths of the cee-studs were 8'-0" for all the single column tests.
3. The number of nodal brace points was limited to one, at the mid-height of the lipped cee-stud.
4. The support fixity was limited to a shallow track 1.25 inch deep and 12 inches long, attached to the stud with one self-drilling screws on each flange. The track was loosely fixed to the loading plates with two bolts.
5. The simulated bridging used in the single column axial load tests was comprised of high strength steel wires attached to the each flange on both sides of the web. Four wires were used to brace the cee-stud so that for any global buckling at least two brace wires would be effective.

The steel stud industry has employed the use of several typical bridging details for a number of years. The strength of typical bridging has been studied and previously reported (Beshara and LaBoube 2001). However, there is little published information available regarding as-constructed bracing demand. Based on previous testing, and because of the relatively low bracing force required to brace steel studs, bridging strength does not appear to be a significant concern. The most apparent criteria for the bridging

are the strength and stiffness of the connection of the bridging to the stud and the stiffness of the total bridging system. The scope of this experimental program involved:

- The bridging tests were limited to three types of typical industry bridging connections, namely screwed-screwed, welded-welded and direct-welded. In the first two types, a standard clip angle was used to secure the channel bridging to the web of the cee-stud. In the third type, the channel bridging was directly welded to the web punchout.
- The bridging was tested for its in-plane strength and out-of-plane torsional stiffness for all the stud sizes used in the single column axial tests. The load was applied with an actuator attached to the bridging at a distance away from the bridging to stud connection to avoid localized effects of load application.

While the stiffness required to develop the strength of the member will vary depending on whether the member is under axial compression or flexural loading, the actual physical stiffness of the bridging system is independent of the type of loading. Therefore, the stiffness of the bridging system (flexural or torsional stiffness) may be considered independently of the loading.

A general test procedure was developed such that the results of this research may be extended to other types of stud cross-sections, to determine the requirements of any type of bridging. Conventional bridging or nodal bracing was simulated in the single column axial load tests using steel wires attached to the stud flanges at mid-height. A range of brace stiffness, from less than 30 lbs/in. to greater than 4000 lbs/in., was simulated in the testing frame by using various diameters and lengths of high strength steel wire. Brace strength was determined from the cross-sectional area of the steel wire and the experimentally determined yield strength. The axial load, individual brace forces, axial shortening, and in-plane (weak axis) and out-of-plane (strong axis) lateral displacements at mid-height of the cee-stud were measured in each test.

The required bracing stiffness was experimentally determined by varying the brace stiffness for a given stud size and was based on the ability of the stud to develop the nominal axial compressive capacity as predicted by the provisions of AISI Cold-Formed Steel Specification (AISI 1996) including Supplement No. 1 (AISI 1999). The experimental results were compared to existing nodal bracing models, analytical prediction models, and the current column bracing provisions that are part of the 1999 AISC-LRFD Specification for Structural Steel Buildings (AISC 1999).

## CHAPTER 2 LITERATURE REVIEW

### 2.1 General

The use of cold-formed steel in building construction dates back to the 1850s, but cold-formed steel was not widely used until the 1940's (Yu 1991). It is used in constructing walls, slab-decks, beams, columns, storage-racks, and is typically found in small to medium rise structures. This wide application of cold-formed steel in building construction has required a comprehensive understanding of its behavior. The increased use of cold-formed steel as an alternative building material necessitated, in 1946, the first "Specification for the Design of Light Gage Steel Structural Members". Since then, there have been several revisions to the specification as well as design manuals with aids issued by American Iron and Steel Institute (AISI). In 1991, Load and Resistance Factor Design (LRFD) was introduced into the cold-formed steel specification. Today, the current specification edition is the North American Specification for Design of Cold-Formed Steel Structural Members (AISI 2001a).

While considerable research effort has been directed at the problem of bracing hot-rolled structural steel columns, little published information exists specifically addressing the bracing requirements for cold-formed steel columns. This chapter includes a comprehensive review of relevant work done in the field relating cold-formed steel members on – lateral beam bracing, sheathed bracing of wall studs, local and distortional buckling on channel sections, and eccentric loading on wall stud assemblies. Several

analytical models formulated by past researchers to determine the bracing strength and stiffness requirements for axially loaded compression members are also reviewed.

## 2.2 Buckling of Columns

The global buckling of columns has been studied since the 18th century. Even today, in spite of numerous investigations in past decades, research in this specialized field has by no means produced a complete understanding. Based on length and slenderness ratios, columns can be classified as long, intermediate and short. The slenderness ratio is a function of the ratio of effective length of the column and the radius of gyration of the column cross-section.

### 2.2.1 Elastic Buckling

The history of column theory dates back to 1744 when the Swiss mathematician Leonard Euler published the equation for the critical load or the buckling load of an axially loaded prismatic column, assuming that the material is linear and elastic. It is given by

$$P_e = \frac{\pi^2 EI}{L^2} \quad (2.1)$$

where E = Elastic modulus

I = Moment of inertia about the axis orthogonal to buckling plane

L = Unbraced length of the column

This equation is valid for loads acting through the centroidal axis on a perfectly straight column whose ends are perfectly pinned. In practice, it is impossible to realize such conditions, hence the equation serves as an upper bound solution to the buckling problem.

The above equation may be modified to calculate the buckling load for other end conditions by introducing an effective length factor (K). The modified equation is

$$P_e = \frac{\pi^2 EI}{(KL)^2} \quad (2.2)$$

where  $KL$  = effective length of the column

(length between points of zero curvature of the buckled shape)

Eq. 2.2 can be modified to calculate the critical buckling stress by dividing both sides by the cross-sectional area 'A' of the column and replacing the moment of inertia (I) by the second moment of area ( $A r^2$ ), where 'r' is the radius of gyration corresponding to the axis about which the moment of inertia is being computed. The elastic critical buckling stress is thus given by the equation

$$\sigma_e = \frac{\pi^2 E}{\left(\frac{KL}{r}\right)^2} \quad (2.3)$$

where  $\sigma_e$  = critical elastic buckling stress

This equation is applicable when the value of "E" does not change before buckling occurs, meaning the material is completely elastic at the instant of buckling.

### 2.2.2 Inelastic Buckling

In cases of intermediate and short columns, the elastic limit of the material is exceeded before buckling occurs. The modulus of elasticity 'E' hence becomes a function of the critical buckling stress, and to solve this Engesser put forth the Tangent Modulus theory, in 1889. Instead of the elastic modulus 'E', the tangent modulus ' $E_T$ ' was substituted into Eq. 2.3 to calculate the critical buckling stress. This was called the Euler-Engesser Equation and is given by

$$\sigma_e = \frac{\pi^2 E_T}{\left(\frac{K L}{r}\right)^2} \quad (2.4)$$

However, Considère recognized that an axially loaded column stressed beyond the proportional limit starts to bend, and the stresses on the concave side increase according to the compressive stress-strain curve of the material, whereas the stresses on the convex side decrease proportionally to the strain. In 1895, Engesser formulated the Double Modulus theory of buckling, with use of a reduced modulus 'E<sub>R</sub>' in place of the tangent modulus in the Euler-Engesser Equation (see Figure 2.). The reduced modulus is given by

$$E_R = \frac{E I_1 + E_T I_2}{I} \quad (2.5)$$

where  $I_1, I_2$ , represent the moment of inertia of the cross-sectional areas separated by the neutral axis as shown in Figure 2.1.

### 2.2.3 Local Buckling and Distortional Buckling

In calculating the strengths of elastic and inelastic columns, the stability criteria are based on the column as a whole. Other than prismatic sections, columns are made up of plate elements, which are subjected to compressive stresses when the column is loaded. The effect of these compressive stresses on slender plate elements may cause them to buckle locally, which leads to a part of the cross-section to reach its critical buckling stress and become ineffective in carrying the applied load. In local buckling, the instability arises due to a change of cross-sectional shape in a localized region and does not directly alter the overall configuration of the member as a whole (Shanley 1957).

Local buckling of individual compression elements can be calculated by two different approaches to facilitate design – one based on an effective width criterion, the other based on an average or reduced stress criterion. For each approach, the degree of the edge restraint influences the behavior. The cross-section elements are classified as edge-stiffened or unstiffened. An unstiffened compression element is one that is stiffened at only one edge parallel to the direction of applied stress. A stiffened compression element is stiffened at both edges parallel to the direction of applied stress (Galambos 1998). The effective width of locally buckled elements is given by

$$b_e = \frac{b(1 - 0.22/\lambda)}{\lambda} \quad (2.6)$$

where  $b_e$  = Effective width  
 $b$  = Flat width of plate element  
 $\lambda$  =  $(\sigma_e/\sigma_{cr})^{1/2}$   
 $\sigma_e$  = Maximum elastic stress  
 $\sigma_{cr}$  = Plate buckling stress defined by

$$\sigma_{cr} = \frac{\pi^2 Ek}{12(1 - \nu^2)} \left(\frac{t}{b}\right)^2 \quad (2.7)$$

$E$  = Elastic modulus of material  
 $k$  = Plate-buckling coefficient  
 ( $k = 4$  for stiffened elements,  $k = 0.425$  for unstiffened elements)  
 $t$  = Plate thickness  
 $\nu$  = Poisson's ratio

Distortional buckling, also called as “stiffener buckling” by Desmond, Pekoz and Winter in 1981, or “local-torsional buckling” by Sridharan in 1982, is a mode

characterized by rotation of the flanges at the flange/web junction in members with edge stiffened elements. Formulae for computing the elastic distortional buckling stress were provided by Lau and Hancock (1987). Strength tests of cold-formed channel sections, undergoing distortional buckling, were investigated by Kwon and Hancock (1991). The distortional mode of buckling occurs at longer half-wavelengths than local buckling and involves element displacements of the edge or intermediate stiffeners forming the section or of complete flanges (Galambos 1998). A historical review of distortional buckling was compiled by Schafer and Hancock (Schafer 2000). Distortional buckling of cold-formed steel columns was investigated by Schafer (2000) for a project sponsored by AISI. The investigation compares the design methods using the effective width approach and the direct strength approach and states design recommendations for AISI Specification. Teng (2002) extended the axially loaded column investigations by Lau and Hancock (1987) and examined distortional buckling of beam-columns.

### **2.3 Bracing Stiffness and Strength**

Zuk (1956) analytically derived the magnitudes of brace forces by solving the basic second order differential equation of equilibrium assuming elastic behavior of the compression member. It was determined by Zuk that the lateral force is a direct function of the initial crookedness and the critical buckling load. Eight different cases were considered with discrete or continuous lateral bracing on laterally loaded flexural members, axially loaded compression members and eccentrically loaded compression members, all with either fixed or pinned support conditions. Out of these eight cases, the first two are relevant to the present investigation and are summarized below

### 2.3.1 Column with Concentric Axial Load and an Immovable Point Support at Mid-height

In Figure 2.2 (Zuk 1956), the centroidal axis of the column is shown as a straight line passing through the top and bottom pin ends. The initial crookedness is defined by the following

$$y_0 = a \sin \left( \frac{x}{L} \right) \quad (2.8)$$

where  $a$  = Maximum amplitude at the center and is represented by a dashed line in the figure.

Due to the brace at mid-height, the column assumes a buckled shape as shown by the continuous line, and is defined as a function of ' $y_1$ ' and ' $y_2$ ' in the upper and lower halves of the column respectively. The curves ' $y_1$ ' and ' $y_2$ ' represent the additional displacements due to the applied load ' $P$ '. When the applied compressive load on the column, with a fully effective brace, reaches the critical elastic buckling load, given by

$$P_{cr} = \frac{4\pi^2 B_1}{L^2} \quad (2.9a)$$

the maximum brace force, ' $F_{max}$ ', is calculated from the second order differential equation of equilibrium, which reduces to

$$F_{max} = \frac{64\pi^2 B_1 a}{3L^3} \quad (2.9b)$$

where  $B_1$  = Flexural rigidity =  $E I$

$L$  = Length of column from the top pin end to the bottom pin end

$a$  = Amplitude of initial crookedness

It can be seen here that an initial crookedness of  $L/1000$ , shows that  $F_{\max}$  is 0.53% of the critical buckling load ' $P_{cr}$ '. As mentioned earlier, the equation for the brace force is a direct function of the initial crookedness of the column.

### **2.3.2 Column with Concentric Axial Load and an Elastic Lateral Support at Mid-height**

This case is the same as that derived by Winter (1947) and was included by Zuk for purpose of comparison. Winter analytically determined that for a concentrically loaded pin-ended column with mid-height elastic bracing, the brace force is about 2% of the critical load, ' $P_{cr}$ '.

Winter (1960) published the results of a simple analytical model to calculate the required bracing stiffness and strength for both beams and columns. It was found that both bracing strength and stiffness contribute to the critical buckling load of a compression member. Both forms of bracing, discrete and continuous, were considered in Winter's investigation. For an axially loaded column (see Figure 2.3 (Winter 1960)), a nodal brace at mid-height can increase its axial load capacity only if the brace is stiff enough to restrain the column from flexural buckling or flexural-torsional buckling. For a column with mid-height bracing, Winter considered that the unsupported length of the column to be half the overall length of the column. There is a minimum stiffness requirement to effectively brace a member laterally and this is defined as the ideal stiffness, and such bracing is called "full bracing". If an axially loaded column has an initial crookedness ' $d_0$ ', the required strength of the lateral brace increases with the magnitude of the imperfection, but the stiffness demand does not likewise increase. For the column with mid-height bracing shown in Figure 2.3 (Winter 1960), Winter obtained the required bracing stiffness as given by the equation

$$k_{\text{req}} = \frac{2 P_e}{L} \left( \frac{d_o}{d} + 1 \right) \quad (2.10a)$$

where  $L$  = Unbraced length of the column  
 $P_e$  = Euler's critical buckling load for a column of length,  $L$   
 $d_o$  = Amplitude of initial crookedness  
 $d$  = Additional displacement due to buckling

For an ideal column,  $d_o = 0$ , the above equation reduces to

$$k_{\text{ideal}} = \frac{2 P_e}{L} \quad (2.10b)$$

and the strength of the bracing is given by

$$S_{\text{req}} = \frac{2 P_e}{L} (d_o + d) \quad (2.11)$$

Winter also developed the required stiffness and strength for two, three and four symmetric brace points along the length of a column. It was recommended to take the value of  $d_o = 1/500$  or  $1/1000$  and that of  $d = L/250$  or  $L/500$ , depending on the type of cross-section (e.g. wide flange). This is because 'd' is the displacement at incipient failure and under design loads it would be less than half of the above values. Figure 2.4 (Winter 1960) shows the critical loads for elastically supported columns.

Plaut (1993) mathematically derived relations for elastic translational springs at arbitrary points along the length of a column with a pin support at the base and with either a pin support or a brace at the top of the column. Both perfect and imperfect columns were considered and the effect of span length, bracing stiffness and initial imperfection were determined. Plaut stated that for imperfect columns the deflections and the bracing forces tend to increase with the applied load.

If  $P = P_\infty$  then,

$$k = k_{id} \left( 1 + \eta \frac{d_o}{d} \right) \quad (2.12)$$

where for this case  $k_{id} = 16\pi^2 \frac{EI}{L^2}$

For  $P < P_\infty$ , and for a range of  $d_o/d$

$$k = \frac{4P}{L} \left( 1 + \eta \frac{d_o}{d} \right) \quad (2.13)$$

- where
- L = Length of column
  - P = Non-dimensional axial load as a fraction of  $P_\infty$
  - $P_\infty$  = Dimensional axial load for an infinitely stiff brace
  - $d_o$  = Initial deflection at location of the brace
  - d = Additional deflection at location of the brace due to buckling
  - $\eta$  = Dimensionless parameter

When  $\eta = 1.41$ , it gives the upper bound to the required stiffness. Figure 2.5(a), (b), (c) (Plaut 1993) shows the effect of bracing stiffness on the deflection ratio ( $d_o/d$ ), load ratio ( $P/P_\infty$ ), and bracing force to axial load ratio ( $F_1/P$ ), respectively.

Yura (1995) focused on simplicity and easy formulations for the bracing strength and stiffness required for bracing compression members. Relative, discrete, continuous, and lean-on bracing systems were considered in this work. Yura concluded that simply satisfying the strength requirement of 2% of applied compressive load might be detrimental if the bracing is too flexible to restrain displacement. Stiffness of the bridging also affects the behavior of the compression member. It was observed from column tests that the larger the stiffness of the bracing, the smaller was the measured

brace force. Yura proposed the ideal nodal brace stiffness,  $\beta_{ideal}$ , for an axially loaded column to be

$$\beta_{ideal} = \frac{[4 - 2/n]P_n}{L_b} \quad (2.14)$$

and the required brace strength, assuming an initial out-of-straightness of  $L/500$  to be

$$P_{brace} = 0.02 P_n \quad (2.15)$$

where  $L_b$  = Unbraced length  
 $P_{brace}$  = Minimum required brace strength  
 $P_n$  = Nominal axial capacity when the assumed brace stiffness is greater than or equal to  $\beta_{ideal}$   
 $n$  = Number of equally spaced intermediate brace locations  
 $\beta_{ideal}$  = Minimum required brace stiffness

Yura made the following recommendations for design

The brace stiffness should be equal to twice the ideal requirement to limit displacement; and

The brace strength should be 1% of the nominal capacity of the compression member at the ideal bracing

Figure 2.6 (Yura 1995) shows a plot of  $P_{cr}/P_e$  versus  $\beta L/P_e$  for several discrete bracing systems. The recommendations made by Yura were later incorporated into the American Institute of Steel Construction- Load and Resistance Factor Design Specification (AISC 1999).

Helwig and Yura (1999) conducted a finite element investigation of torsional buckling behavior of columns with lateral bracing located at different points on the cross-section. Their paper describes that many column-bracing details employed in steel construction do not prevent twist, and subsequently torsional buckling may control the

column capacity. Equations were developed for strength and stiffness requirements of bracing to control torsional buckling of doubly-symmetric sections. Connection details for torsional bracing were described and presented. For a doubly-symmetric section, the torsional buckling capacity of a compression member can be computed using Eq. 2.16 (Timoshenko and Gere 1961).

$$P_T = \frac{P_{ey}(d^2/4) + GJ}{r_x^2 + r_y^2} \quad (2.16)$$

When the locations of intermediate lateral restraint are offset from the centroid of the cross-section, the torsional buckling capacity is given by Eq. 2.17 when the offset lies in the plane of the web, and Eq. 2.18 when the offset lies along the strong axis.

$$P_T = \frac{P_{ey}[(d^2/4) + a^2] + GJ}{a^2 + r_x^2 + r_y^2} \quad (2.17)$$

$$P_T = \frac{P_{ey}[(d^2/4) + (I_x/I_y)b^2] + GJ}{b^2 + r_x^2 + r_y^2} \quad (2.18)$$

- where  $G$  = Shear modulus
- $I_x$  = Strong axis moment of inertia
- $I_y$  = Weak axis moment of inertia
- $J$  = Torsional constant
- $P_{ey}$  = Elastic flexural buckling load, based on a column length between points of zero twist (Eq. 2.19)
- $a, b$  = Distances to an axis away from centroidal axis
- $d$  = Distance between flange centroids
- $r_x, r_y$  = Strong-axis and weak-axis radii of gyration

$$P_{ey} = \frac{\pi^2 E I_y}{L_T^2} \quad (2.19)$$

E = elastic modulus

$L_T$  = unbraced length for torsion

Helwig used eight-node shell elements to model a W16x26 wide flange section. Shell elements were also used to model the braces, which consisted of angle sections. Torsional stiffness of the brace was determined by separate analysis (of the brace) by determining the rotation caused by a concentrated moment. Eigenvalue buckling analyses were conducted on straight columns to determine the stiffness requirements of the bracing. Imperfect columns were also considered in the analyses and were analyzed by accounting for the large displacements. Figure 2.7 (Helwig 1999) shows the effect of lateral restraint location on the brace behavior. It was determined that when the lateral bracing is at the centroid of the section and is adequate to control flexural buckling, the torsional bracing behavior is not sensitive to the lateral brace stiffness. Therefore, the recommended lateral brace stiffness is twice the ideal value when the lateral bracing is at the centroid and four times the ideal value when the lateral bracing is at the flange. The equations, formulated to determine the capacity of a compression member, may be found elsewhere (Helwig 1999).

Beshara and LaBoube (2001) conducted an experimental pilot study on lateral bracing of C-sections in flexure. In this investigation, typical industry bridging connections, along with two proprietary systems, were tested for the bracing requirements. It was found that the screw attached typical industry clip and the SPAZZER 5400™ spacer bar provided adequate bracing to achieve the computed moment capacity for all the 3-5/8" and 6" deep sections, but failed to provide adequate

bracing for the 8" deep sections. The STEEL Network BridgeClip™ provided adequate bracing to achieve the computed moment capacity for all the 3-5/8" and 6"-18 gauge sections, but failed to provide adequate bracing for the 6"-16 gauge and 8" sections. Overall, it was found that the typical industry clip provided the highest resistance against rotation followed by the SPAZZER 5400™ and the STEEL Network BridgeClip™. Figure 2.8 (Beshara and LaBoube 2001) shows the three connections tested in the investigation. The observed failure was classified broadly as torsional-flexural buckling and individual tests indicate the actual mechanism of failure.

#### **2.4 Long Column Tests**

Miller (1990) conducted a series of tests on cold-formed steel cee studs at Cornell University. Individual column tests with a length of 8'-0" were performed on studs with depths of 3-5/8" and 6". Load was applied to the studs both concentrically and eccentrically with either pin end or fixed end conditions. Several of the studs were tested with one or more perforations in the web. Geometric imperfections were measured and considered when the experimental results were compared to the analytical results. No bridging or bracing was installed as part of the test set-up.

Additionally, Miller conducted wall assembly axial tests on 8'-0" members, spaced (typically) at 24" on-center and having depths of 3-5/8" and 6" (see Figure 2.9 (Miller 1990)). Bracing was applied to the wall members in one of three forms: continuous flat straps screwed to both flanges, continuous channel bridging installed through web perforations, and gypsum sheathing screwed to one of the flanges of the members. As in the individual long column tests, end conditions of the studs were either pin-ended or fixed. Miller noted that the use of flat strap bracing and channel bridging resulted in similar ultimate axial loads, while the presence of mid-height bridging increased the load

carrying capacity by at least 25% for 6” members and by at least 60% for 3-5/8” members, over those tested without any bridging or bracing.

Miller (1993) presented the results of effectiveness of the bracing for imperforated two stud wall assembly tests. The investigation found that for 6 inch, 20 gage studs, the predicted capacities were about 20% higher than the experimental results, where the predicted capacity was based on the AISI Specification’s Cold-Formed Steel Design, (AISI 1986). This was because the AISI Specification considered the load to act through the centroid, while Miller calculated the effect of eccentric load acting through the gross centroids and found that the predicted loads were conservative in most cases. Individual long column and flat-ended stud tests were also conducted. The flat-ended studs were fitted with short tracks on both the ends, prior to testing.

The effective length factors for the wall studs with and without mid-height bracing were determined for flexure and torsion, and the recommended values by Miller (1993) are

- Unbraced:  $K_x = K_y = K_t = 0.65$
- Braced at mid-height:  $K_x = 0.65, \quad K_y = K_t = 0.4$

#### **2.4 AISI-LRFD Specification**

The AISI-LRFD Specification, 3<sup>rd</sup> Edition (AISC 1999) contains provisions for the stability bracing of structural steel members and frames, in Chapter C3. There are two general types of bracing – relative bracing and nodal bracing. The relative brace system shown in Figure 2.10(a) (Figure C-C3.1, AISC 1999) consists of a diagonal and a strut that control the movement at one end of the unbraced length, A, with respect to the other end of the unbraced length, B. A nodal brace controls the movement only at the

particular brace point, as shown in Figure 2.10(b) (Figure C-C3.1, AISC 1999), without interaction with adjacent brace points.

The minimum bracing requirements as given in the AISC-LRFD Specification (AISC 1999), Chapter C3-3, for nodal bracing, are as follows

Required brace strength

$$P_{br} = 0.01P_u \quad (2.20)$$

Brace stiffness:

$$\beta_{br} = \frac{8P_u}{\phi L_b} \quad (2.21)$$

where  $P_u$  = Required compressive strength of the column

$L_b$  = Distance between braces

$\phi$  = 0.75

Recall that Winter (1958) recommended that the brace stiffness for frames, columns, beams be equal to twice the critical stiffness and this same recommendation has been adopted by the AISC-LRFD Specification (1999). The  $\phi = 0.75$  specified for all brace stiffness requirements is consistent with the implied resistance factor for the Euler column buckling. i.e.  $0.877 \times \phi_c = 0.75$ . The initial displacement also known as initial out-of-plumbness,  $\Delta_o$ , for the relative or nodal bracing is defined with respect to the distance between adjacent braces, as shown in Figure 2.11 (Figure C-C3.3, AISC 1999). The brace strength recommendations for frames, columns, and beam lateral bracing are based on an assumed  $\Delta_o = 0.002L$ , where  $L$  is the distance between adjacent brace points. The flexibility or ability of a brace connection to slip should be considered in the evaluation of the actual bracing system stiffness,  $\beta_{act}$ , as follows

$$\frac{1}{\beta_{act}} = \frac{1}{\beta_{conn}} + \frac{1}{\beta_{brace}} \quad (2.22)$$

where  $\beta_{conn}$  = Stiffness of the Connection

$\beta_{brace}$  = Stiffness of the brace

## 2.5 AISI Specification for Cold-Formed Steel

In case of concentrically loaded compression members, there are three limit states namely, (1) yielding, (2) overall column buckling (flexural, torsional, flexural-torsional buckling), and (3) local buckling of individual elements.

Flexural buckling occurs in a slender, axially loaded column about the either of the principal axes. The critical elastic buckling stress for a column is given by Eq. 2.3, which is discussed earlier. The Commentary on North American Specification for Design of Cold-Formed Steel (AISI 2001b) gives the equation for critical inelastic buckling stress as

$$F_{cr} = F_y \left( 1 - \frac{F_y}{4(F_{cr})_e} \right) \quad (2.23)$$

where  $E$  = Elastic modulus of steel

$F_y$  = Yield stress of the material

$(F_{cr})_e$  = Critical elastic buckling stress, given by Eq. 2.24

$$(F_{cr})_e = \left( \frac{\pi^2 E}{(KL/r)^2} \right) \quad (2.24)$$

$KL$  = Effective length of column

$r$  = Minimum radius of gyration

In the above equation, the critical buckling stress is directly proportional to the yield strength of the steel. For cold-formed steel compression members with large width-

to-thickness ratios, local buckling of individual component plates may occur before the applied load reaches the nominal axial strength determined by Eq. 4.4 (Section C4, AISI 2001) for locally stable columns

$$P_n = A_g F_{cr} \quad (2.25)$$

where  $A_g$  = Full cross-sectional area of the compression member

$F_{cr}$  = Critical buckling stress, either elastic or inelastic

The interaction effect of the local and overall column buckling may result in a reduction of the overall column strength. In order to reflect the effect of local buckling on the reduction of column strength, the nominal axial strength is determined by the critical buckling stress and the effective area,  $A_e$ , instead of the full sectional area. The nominal axial strength of cold-formed steel compression members can be determined by the following equation

$$P_n = A_e F_{cr} \quad (2.26)$$

where  $A_e$  = Effective area at  $F_{cr}$

$F_{cr}$  = Critical buckling stress, either elastic or inelastic

However, Eq. 2.26 is limited to its applicability in case of singly symmetric or point symmetric sections. The design equations for calculating the inelastic and elastic flexural buckling stresses have been changed to those used in AISC-LRFD Specification (AISC 1999). The AISI Specification (2001a) gives the equations for critical buckling stress as

$$\text{For } \lambda_c \leq 1.5 \quad F_n = \left( 0.658^{\lambda_c^2} \right) F_y \quad (2.27)$$

$$\text{For } \lambda_c > 1.5 \quad F_n = \left[ \frac{0.877}{\lambda_c^2} \right] F_y \quad (2.28)$$

where  $F_n$  = Nominal flexural buckling stress

$$\lambda_c = \sqrt{F_y / F_e}$$

$F_e$  = Elastic flexural buckling stress calculated using Eq. 2.24

Consequently, the nominal axial compressive strength is given by

$$P_n = A_e F_n \quad (2.29)$$

The effective length factor,  $K$ , accounts for influence of restraint against rotation and translation at the ends of a column on its load carrying capacity. For concentrically loaded compression members, the recommended values of effective length factors are given in Figure 2.12 (AISI 1996).

For inelastic buckling, the critical torsional buckling stress is calculated according to Eqs. 2.27 and 2.28 by using  $\sigma_t$  instead of  $F_e$  in calculation of  $\lambda_c$ . In certain cold-formed steel cross-sections, the design strength is limited by the torsional buckling of columns. For relatively short members the elastic torsional buckling stress is given by,  $\sigma_t$ , calculated as follows

$$\sigma_t = \frac{1}{A r_o} \left[ G J + \frac{\pi^2 E C_w}{(K_t L_t)^2} \right] \quad (2.30)$$

where  $A$  = Full cross-sectional area

$C_w$  = Torsional warping constant

$G$  = Shear modulus

$J$  = Saint Venant's torsion constant of the cross-section

$K_t L_t$  = Effective length of twisting

$r_o$  = Polar radius of gyration of the cross-section about the shear center

In case of flexural-torsional buckling of a column, the column undergoes flexural buckling about one of the principal axes, with simultaneous torsional buckling about the shear center. This limit state is to be checked only when there is a chance of flexural-torsional buckling to occur. The governing elastic flexural-torsional buckling stress of a column is given by

$$F_e = \frac{1}{2\beta} \left[ (\sigma_{ex} + \sigma_t) - \sqrt{(\sigma_{ex} + \sigma_t)^2 - 4\beta \sigma_{ex} \sigma_t} \right] \quad (2.31)$$

where  $\sigma_{ex} = \pi^2 E / (K_x L_x / r_x)^2$  is the flexural buckling stress about the x-axis

$\sigma_t =$  torsional buckling stress

$\beta = 1 - (x_o/r_o)^2$

The flexural-torsional buckling stress is always lower than the Euler stress  $\sigma_{ex}$  for flexural buckling about the axis of axis of symmetry. For inelastic buckling, the torsional buckling stress is given by Eq. 2.27.

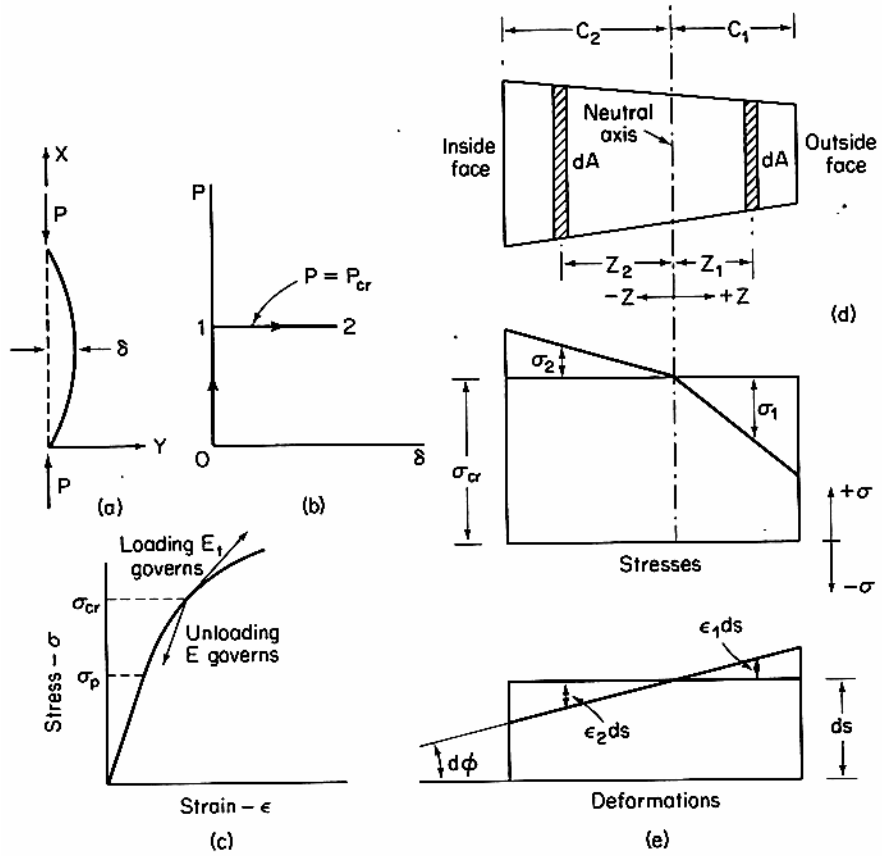


Figure 2.1 Reduced Modulus Theory

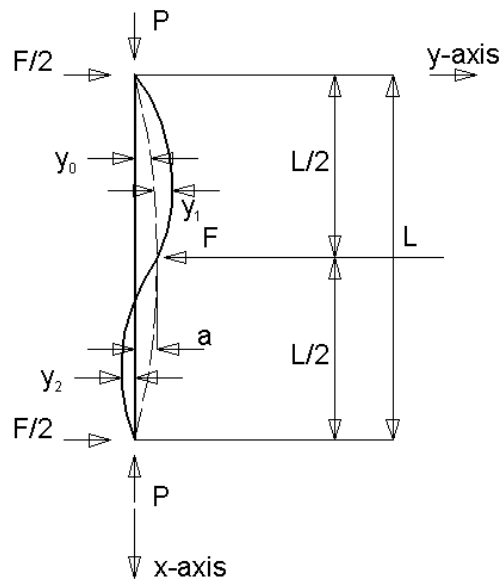


Figure 2.2 Imperfect Column with Immovable Mid-height Bracing

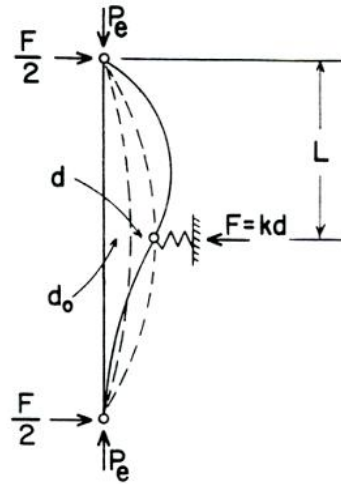


Figure 2.3 Imperfect Column with Elastic Mid-height Bracing

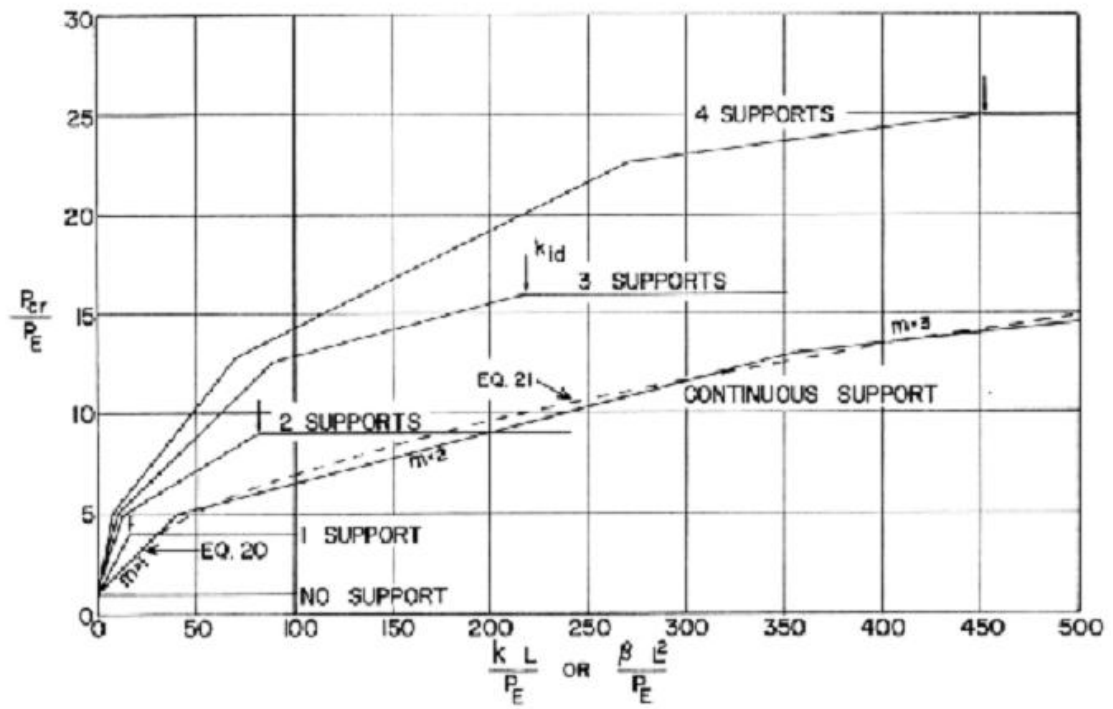
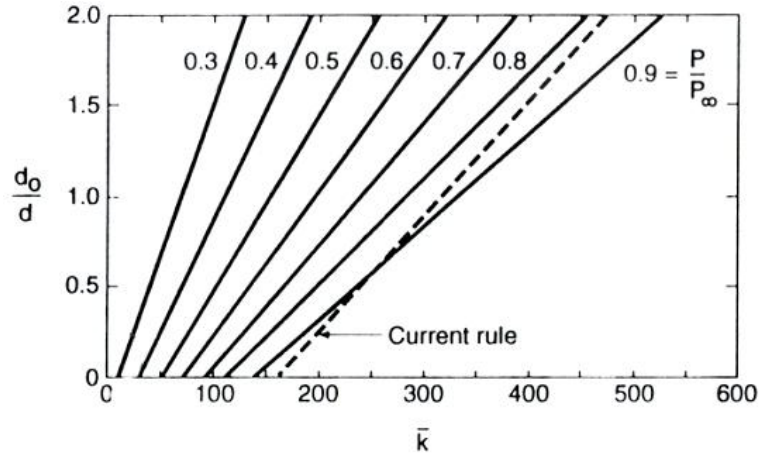
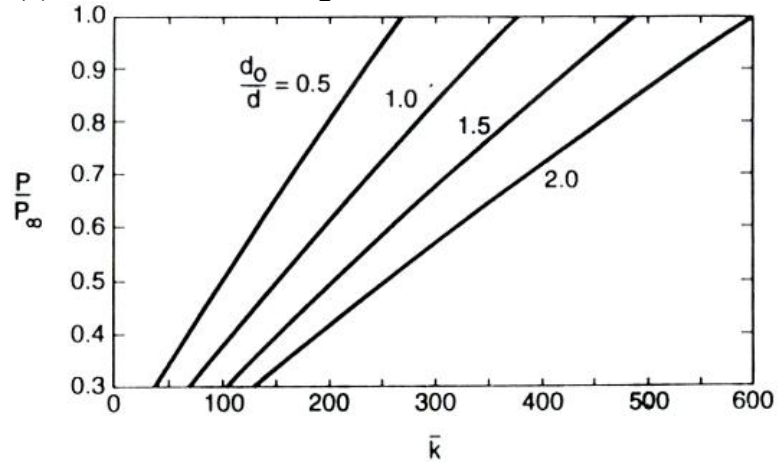


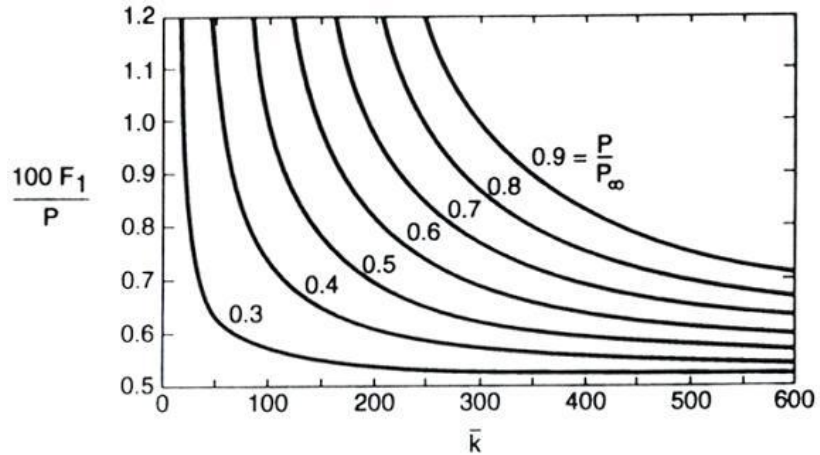
Figure 2.4 Critical Loads for Elastically Supported Columns



(a) Effect of Bracing Stiffness on Deflection Ratio  $d_0/d$



(b) Effect of Bracing Stiffness on Load Ratio  $P/P_\infty$



(c) Effect of Bracing Stiffness on Bracing Force as Percentage of Axial Load for given Load Ratio  $P/P_\infty$

Figure 2.5 Effect of Bracing Stiffness

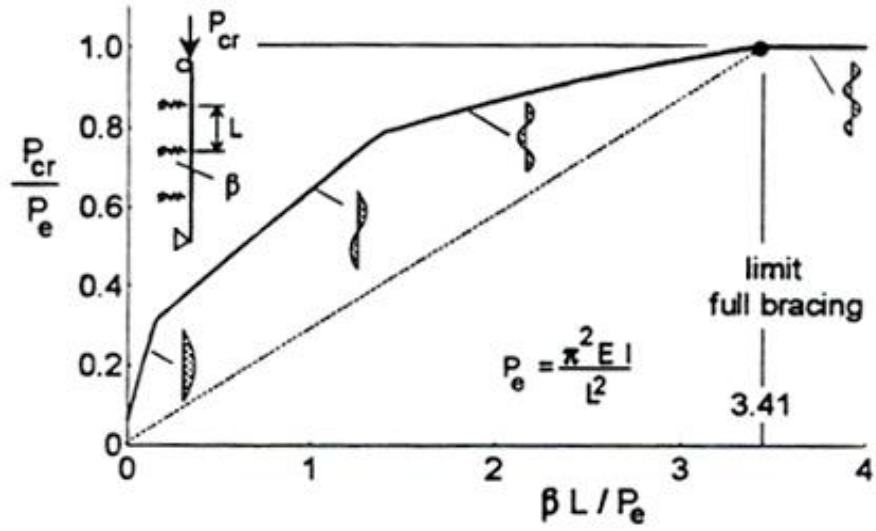


Figure 2.6  $P_{cr}/P_e$  versus  $\beta L/P_e$  for a Discrete Bracing

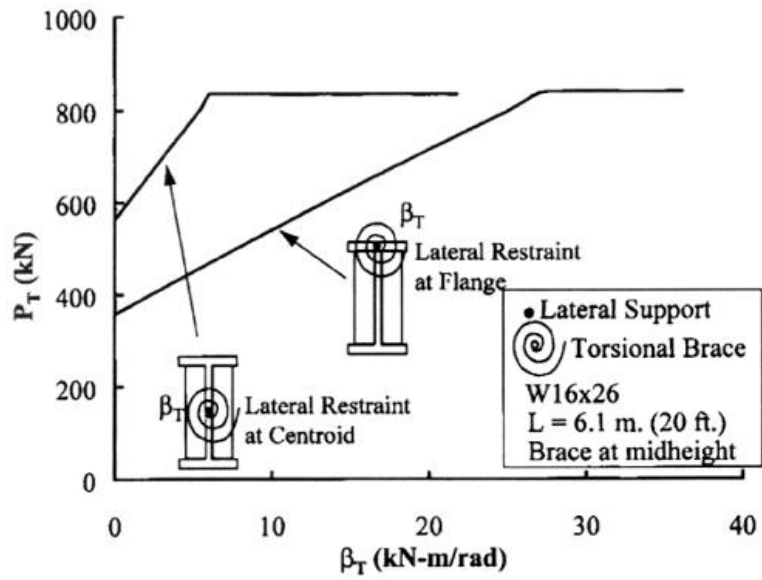


Figure 2.7 Effect of Lateral restraint location on Brace behavior

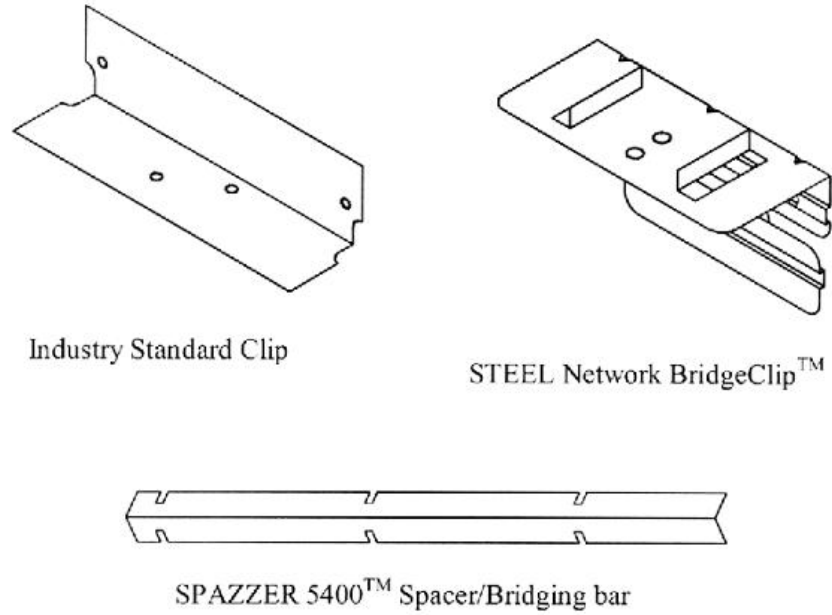


Figure 2.8 Bracing Connection Clips

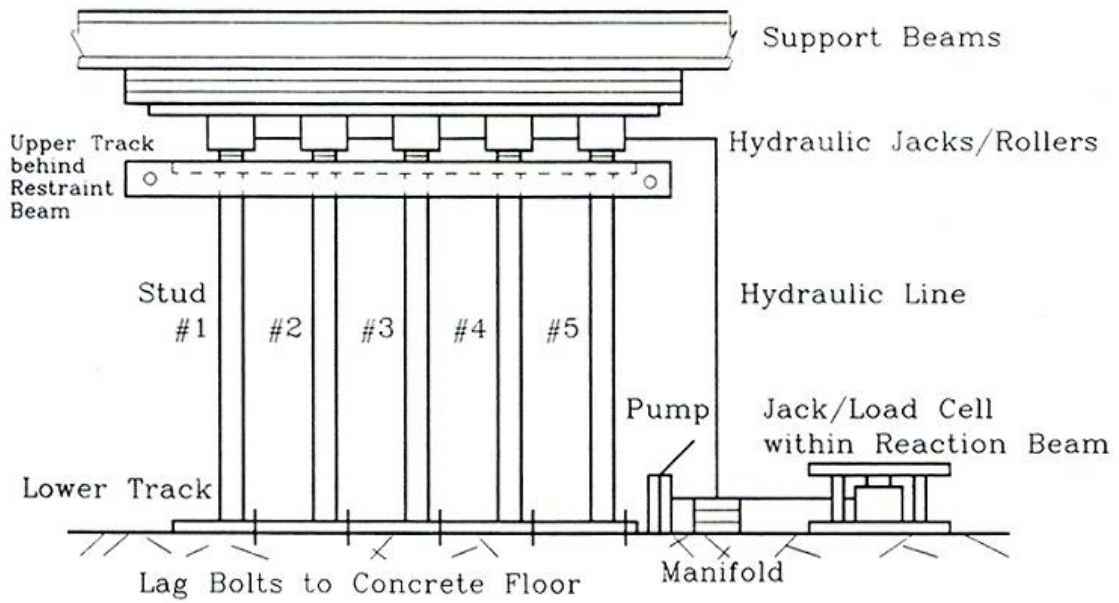


Figure 2.9 Wall Assembly test setup

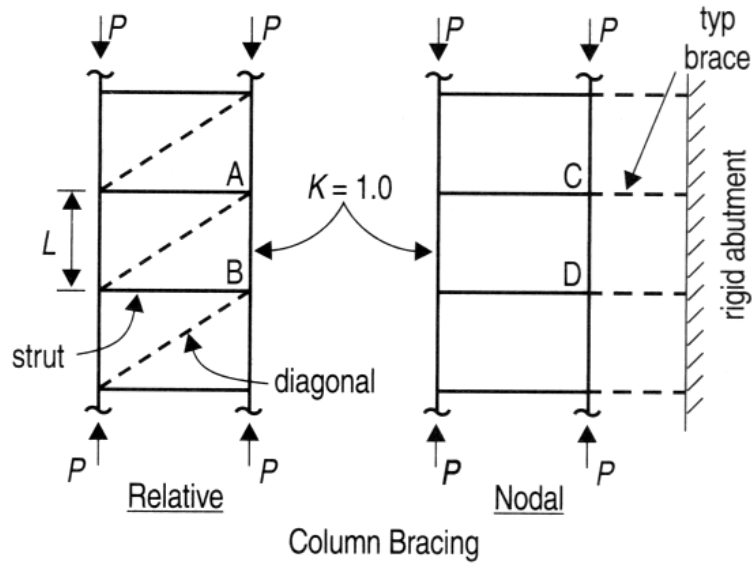


Figure 2.10 Types of Bracing (a) Relative Bracing and (b) Nodal Bracing

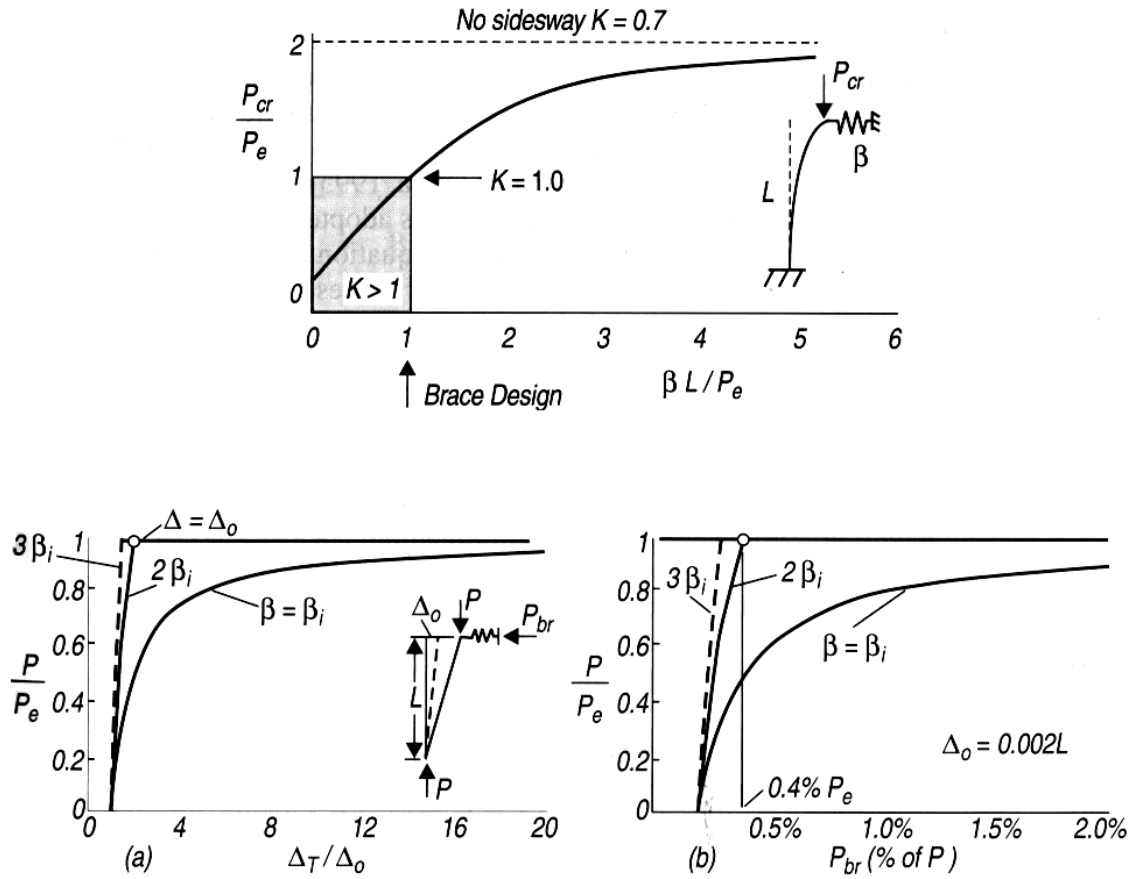


Figure 2.11 Effect of Initial Out-of-Plumbness

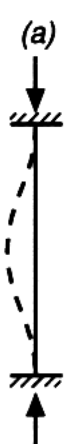
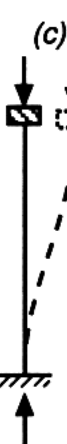
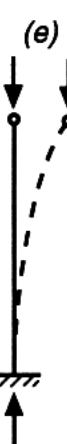
|   |   |   |  |   |   |   |
|---|---|---|--|---|---|---|
| <p>Buckled shape of column is shown by dashed line</p>            |    |    |  |  |  |  |
| <p>Theoretical K value</p>  | <p>0.5</p>  | <p>0.7</p>  | <p>1.0</p>   | <p>1.0</p>  | <p>2.0</p>  | <p>2.0</p>  |
| <p>Recommended K value when ideal conditions are approximated</p> | <p>0.65</p>   | <p>0.80</p>   | <p>1.2</p>   | <p>1.0</p>  | <p>2.10</p>   | <p>2.0</p>  |
| <p>End condition code</p>   | <br><br><br> | <p>Rotation fixed, Translation fixed</p> <p>Rotation free, Translation fixed</p> <p>Rotation fixed, Translation free</p> <p>Rotation free, Translation free</p> |  |   |   |   |

Figure 2.12 Effective Length Factors for Concentrically Loaded Columns

## CHAPTER 3 DESCRIPTION OF EXPERIMENTAL STUDY

The purpose of this chapter is to give a brief description of the objectives of the experimental program, the material properties and measured as-built geometry of the test specimens, the test setups, and the test procedures employed in the project. The experimental program consisted of two phases of testing:

- Phase-I: Axial Compression Tests
- Phase-II: Bridging Tests

### **3.1 Introduction**

Phase-I of the experimental program consisted of examining the behavior of single axially loaded cee-studs, with and without mid-height bracing (or bridging). In Phase-II, typical industry bridging was examined for its strength and stiffness by in-plane and out-of-plane loading. Description of the test setups and the test procedures are given in Sections 3.6 and 3.7. Three types of typical industry bridging were tested:

- Type-1: Screwed-Screwed (SS), where the bridging channel and clip angle are screwed to each other and to the web of the cee-stud.
- Type-2: Welded-Welded (WW), where the bridging channel and clip angle is fillet welded to each other and to the web of the cee-stud.
- Type-3: Direct-Welded (DW), where the bridging channel is directly welded to the web of the cee-stud.

The stud specimens tested had nominal web depths of 3.625, 6.00, and 8.00 inches with specified thicknesses ranging from 33 mils to 97 mils. The 33 mil, 43 mil, and 68 mil studs were manufactured by Steel Construction Systems, Orlando, FL and the 97 mil

studs were manufactured at the Wildwood, FL plant of Dietrich Metal Framing Inc., Pittsburgh, PA. The mechanical properties of the stud material used to fabricate the test specimens were determined by tension coupon tests. The as-built dimensions and geometric imperfections of the fabricated test specimens were recorded and this data was utilized in the calculation of the resistance properties of each specimen.

### 3.2 Objectives of Experimental Tests

The main objectives of the experimental study are summarized as follows:

- To investigate the behavior of cold-formed steel cee-studs with and without mid-height lateral bracing by testing a range of studs, subjected to axial compression while providing different bracing stiffnesses and strengths
- To investigate the strength and stiffness of the lateral bridging over the same range of studs subjected to in-plane and out-of-plane loading
- To provide the experimental data for determining the minimum bracing requirements of cold-formed steel cee-studs subjected to axial compression

### 3.3 Material Properties of Test Specimens

A series of standard 2" gage length ASTM tension tests were performed on coupons cut from the web material of the cee-studs. The dimensions of a typical tension coupon are shown in Figure 3.1. The nomenclature used to identify the group of cee-stud to which the coupon belonged was represented as:

TC DDDS FFF-TT

where TC = Tension coupon

DDD = Overall stud depth (362 = 3.625", 600 = 6.000", and 800= 8.000")

S = Lipped stud section

FFF = Flange width (125 = 1.25", 162 = 1.625")

TT = Nominal sheet thickness (mils, 1 mil = 0.001 inch)

The tension tests were performed in accordance with ASTM E8-01e2 (ASTM 2001) on a 60 Kip capacity Tinius-Olsen testing machine. The applied load was measured through a load cell and the gage elongation of each coupon was measured using two extensometers, one fixed on the front and the other on the back of the tension coupon. The applied load and the corresponding elongation data was used to plot the stress-strain relationship. From the stress-strain plot, the yield and ultimate stresses were determined as per ASTM E8-01e2 (ASTM 2001). The elastic modulus of the material was not determined by testing and was assumed to be equal to 29500 ksi (AISI 1996). For each cee-stud section, a minimum of three tests were performed. The average values of yield and ultimate stresses were calculated based on either the 0.2% offset method for a continuously yielding material or the autographic diagram method for materials exhibiting discontinuous yielding. Figure 3.2 shows the 0.2% offset method for determination of the yield stress, and Figure 3.3 shows the autographic diagram method for determination of the yield stress. The tension coupon test results are summarized in Table 3.1.

### 3.4 As-Built Dimensions of the Test Specimens

For the single axial load tests, 8'-0" long cee-studs were cut from the as-delivered 20'-6" long members. For the bridging tests, short 3'-6" stubs were cut from the 20'-6" long members. For the purposes of this study, each tested stud was identified using a modified Steel Stud Manufacturers Association (SSMA) nomenclature:

DDD S FFF-TT-KKKK

where DDD = Overall stud depth (362 = 3.62"; 600 = 6.00"; 800 = 8.00")

S = Lipped stud section

FFF = Flange width (125 = 1.25"; 162 = 1.62")

TT = Nominal steel thickness (mils; 1 mil = 0.001")

KKK = Axial stiffness of one brace wire in pounds per inch

For each specimen, the cross-section dimensions were measured at three locations along the length of each 8'-0" stud with a digital micrometer and tabulated in Table 3.2. The tables provide the stud designation and corresponding brace stiffness used in the testing along with the measured dimensions A through F and thicknesses 't<sub>a</sub>' through 't<sub>e</sub>' (see Figure 3.4) for each test specimen. The (+) and (-) symbols denote the direction of camber and sweep of the stud. The camber and sweep were measured as described in Section 3.5.1.

### 3.5 Measured Geometric Imperfections of the Test Specimens

The geometric imperfections of a stud can be categorized as a global imperfection and/or a local imperfection as described in Sections 3.5.1 and 3.5.2.

#### 3.5.1 Global Imperfections

The bow/sweep and camber of the studs were measured with a digital micrometer to a least count of 0.005". A nylon monofilament line was stretched from one end to the other end of a stud and then was clamped tight. The out-of-straightness of each flat surface of a stud was measured at mid-height. The distance from the string to the surface of the stud was the initial global imperfection for the stud and tabulated in Table 3.3. The measured out-of-straightness of each stud was found to be within the permissible values as stated, which is 1/32 inches per foot for both bow and camber. The permissible values are found in the Standard Specifications for Load Bearing Steel Studs ASTM C955-01 (ASTM 2001) and for nonstructural steel framing members ASTM C645-00 (ASTM 2000). The measured cambers were negligible in all the tested specimens except for the 600S162-43 series where it ranged from 0.0 to a maximum of 0.065 inches, or L/1500.

The sweep measurements were more significant as these might directly influence the axial behavior of the cee-studs during testing. The measured sweep ranged from 0.0 to 0.04 inches, or  $L/2400$  for the 362S162-43 and 600S162-43 series; from 0.0 to 0.075 inches, or  $L/1300$  for the 600S162-97 series; and from 0.0 to 0.14 inches, or  $L/700$  for the 362S162-68 series. No geometric imperfection measurements were made of the 800S162-97 series studs. In a few studs there was an initial twist over its length but it would disappear when the bottom end was plumbed with the top end while setting up for a compression test. A note was made of the initial twist, but the degree of twist was not measured.

### **3.5.2 Cross-Sectional Imperfections**

The as-built out-to-out measurements of the cross-section of a stud showed that it was neither symmetric nor of uniform thickness. Also, the intersecting corners of the flange-lip and the web-flange junctions were typically right angular. However, the cross-section was considered to be mono-symmetric and of uniform thickness for calculation purposes. It was observed that in some of the studs the punchout were offset from the web centerline by as much as  $1/8''$ , and this was documented along with the test data. The average cross-sectional measurements of each of the test specimen series are given in Tables 3.4 and 3.5. In order to calculate the gross cross-section area, the radius of the bend was taken as the maximum of  $3/32''$  or two times the base-metal thickness, based on the SSMA Manual (SSMA 2001). The studs were fabricated from galvanized steel. The base metal thickness was calculated by subtracting a thickness of two mils from the average of the measured values of thickness.

### **3.6 Test Setup and Test Procedure for Single Column Axial Load Tests**

A total of 37 studs were tested in this phase of the experimental study. Each stud was tested in a 400 Kip, screw driven Riehle Universal Testing Machine. The test setup and test procedure for the single column axial load tests is described below.

#### **3.6.1 Test Specimens of Single Column Axial Load Tests**

To simulate actual field installation conditions, each stud was mounted in standard track of type “T DDD 125-43” (where T = track, DDD = depth of stud, 1-1/4” flange, 43 mil thickness). Figure 3.5 shows a stud attached to the track with a single #10 self-drilling screw on each flange. The track was then mounted to end bearing plates with two 0.150" diameter bolts to simulate attachment to a concrete support or other structural member using 0.144" diameter drive pins. Figure 3.5(a) shows the top of the stud attached to the end bearing plate being held in position against the movable crosshead of the Riehle Universal Testing Machine. Figure 3.5(b) shows the bottom of the stud attached to the other end bearing plate that sits just above another plate holding a 150 Kip axial load cell in place and resting on the fixed platen of the testing machine.

#### **3.6.2 Test Frame for Single Column Axial Load Tests**

An adjustable frame attached to the Riehle testing machine was used to hold the flexural-torsional bracing system in place. Figure 3.6 is an overall view of the test frame and its accompanying instrumentation. The mid-height lateral bracing was simulated using steel wires of varying diameters and lengths. As indicated in the figure, the wires were attached to the corners of the flanges of the test specimens using #10 screws. The brace wires terminated at the S-Beam load cells, which were used to measure the tension force in the brace wires during the testing.

### 3.6.3 Instrumentation for Single Column Axial Load Tests

Five load cells and six linear potentiometers were used to measure the loads and displacements for each single axial compression test for the braced stud specimens. Figure 3.7 shows the locations of the instruments mounted on the test frame. Four S-Beam load cells (Load Cells 1, 2, 3, 4) were used to measure the brace forces in the brace wires. A 150 kip capacity load cell (Load Cell 5) was used to measure the axial load at the base of the stud. The minor axis lateral displacement of a stud was measured by a complementary set of four linear potentiometers (LINEAR POTS 1, 2, 3, 4) positioned directly adjacent to the individual brace wires that made up the lateral bracing system. The major axis lateral displacement was measured at mid-height, by a single linear potentiometer (LINEAR POT 5) located along the minor axis attached to the south flange of a stud. Axial shortening of a stud was measured along the north flange of the test specimen parallel to the longitudinal axis of a stud (LINEAR POT 6). Figure 3.8 shows a close-up view of the stud cross-section at mid-height that shows the attachment points of the bracing wires to their corresponding load cells: A-NE BRACE (BF-1), B-SE BRACE (BF-2), C-NW BRACE (BF-3), and D-SW BRACE (BF-4).

### 3.6.4 Test Procedure of Single Column Axial Load Tests

Each cee-stud was fixed in the Riehle Universal Testing Machine with the tracks bolted to the top crosshead and bottom base plate and was plumbed along both the strong and weak axis prior to testing. The measuring instruments, described in Section 3.6.2 were connected to an electronic data acquisition system to collect and display the run-time data. The tests were conducted under displacement control since the Riehle is a mechanically screw-driven testing machine, which allowed the studs to be loaded at a rate of approximately 5 to 20 lbs/sec to ensure a static response to the applied load.

Initially, each stud was loaded up to an axial load of 200 lbs to 500 lbs then unloaded. At this time all the instrumentation was checked and balanced. This preliminary loading and unloading cycle also ensured proper seating of the specimen in the Riehle UTM. During the continued loading, the buckling behavior of the stud was observed and photographs were taken at notable points and at certain load levels. Failure was considered to have occurred when the stud could no longer carry additional load or significant axial or cross-sectional deformation of the stud was observed and recorded. The stud was then unloaded and the test was then terminated.

### **3.7 Test Setup and Test Procedure for Bridging Tests**

A total of 54 specimens were tested in this phase of the experimental study to evaluate the strength and stiffness of typical industry bridging. The tests were conducted on 3'-6" long cee-stud sections. As previously stated, three types of typical industry bridging were tested. The specimens were divided into two groups based on the direction of loading namely, in-plane loading and out-of-plane loading. Twenty-eight specimens were tested in the out-of-plane loading group while twenty-six specimens were tested in the in-plane loading group.

#### **3.7.1 Test Specimens of Bridging Tests**

The 3'-6" long cee-stud sections were cut from the 20'-6" long studs such that the elevation to the center of the web punchout was maintained at 23 inches. The test specimens were identified using a modified SSMA nomenclature:

DDD S FFF-TT-N CC

where DDD = Overall stud depth (362 = 3.62"; 600 = 6.00"; 800 = 8.00")

S = Lipped stud section

FFF = Flange width (125 = 1.25"; 162 = 1.62")

|    |   |  |
|----|---|--|
| TT | = | Nominal steel thickness (mils; 1 mil = 0.001")     |
| N  | = | Number of the test specimen in each series of stud |
| CC | = | Bridging connection type ( SS, WW, DW)             |

Figure 3.9(a) through (c) show the types of bridging connections tested and they are described below:

**3.7.1.1 Screwed-Screwed (SS) Connection:** The clip angle was first screwed to the bridging channel with two #10 self-drilling screws, as shown in Figure 3.9(a) and Figure 3.10. Position of the screws on the clip angle was marked and then it was centered on the centerline of the web at a height of 23 inches from the bottom. The clip angle was then screwed to the web of the stud. This connection type was called Screwed-Screwed (SS).

**3.7.1.2 Welded-Welded (WW) Connection:** The bridging channel was welded at its flange-web junction to the clip, as shown in Figure 3.9(b). The clip angle was then positioned along the centerline of the web and fillet welded on the edges of the in-line leg. The bridging channel was slid through the punch out and then fillet welded to the outstanding leg of the clip angle. The welding specifications used were – Metal alloy: ER7056, Heat: 1026° F, Gas shielding: Argon-CO2 (75%-25%). This connection type was called Welded-Welded (WW).

**3.7.1.3 Direct-Welded (DW) Connection:** The bridging channel was slid through the web punchout and then the flanges were welded to the web of the stud, as shown in Figure 3.9(c). The weld specification used was same as in Type-2 connection. This connection type was called Direct Welded (DW).

### 3.7.2 Test Fixture for Bridging Tests

The test fixture used to secure the specimens for the bridging tests is shown in Figure 3.11(a). Figure 3.12(a) and (b) are schematic plan views of the test fixture positioned for the out-of-plane and in-plane bridging tests, respectively, while Figure 3.13 and Figure 3.14 show an overall view of each experimental test setup. The fixture consists of a Specimen Mounting Frame (see Figure 3.11(a)) and an Actuator Armature (see Figure 3.11(b)). The load was applied to the bridging channel by a manually operated screw-driven actuator, fixed to the Actuator Armature (see Figure 3.11 through Figure 3.14). The Specimen Mounting Frame was used to secure the cee-stud in place and to isolate the web portion of the specimen (see Figure 3.11(a)). One end of the actuator was connected to an S-beam load cell, and the other end was connected to the vertical channel of the Actuator Armature by a 3/4" diameter SAE Grade 5 bolt. The Actuator Armature was bolted to the web of C8x11.5. The channel section was welded to top flange of a W8x24 whose bottom flange was bolted to the test fixture base plate. A plate-coupler was introduced between the bridging and the S-beam load cell at Point A (see Figure 3.11 and Figure 3.12), that allowed the load to be transmitted to the bridging channel through the plate-coupler by a 3/8" diameter SAE Grade 8 bolt. The joint between the actuator and the vertical channel of the Actuator Armature was free to rotate horizontally, while the joint between the plate-coupler and the bridging channel was free to rotate vertically. All members and connections were checked prior to the commencement of any testing to verify that the limit state of the loading system would be at the bridging connection and not at any of the components of the test fixture. A shear test was performed on the 3/8"  $\emptyset$  bolt, the design strength of the plate coupler was calculated based on its as-built measurements, and the weld strength used to fabricate the plate-coupler was checked.

For the out-of-plane load tests, a 500 lb load cell was used and for the in-plane load tests, a 10 Kip load cell was used. This change was necessary since the strength predictions for the in-plane tests were found to be beyond the safe working range of the 500 lb load cell.

### **3.7.3 Instrumentation**

The instruments used for the out-of-plane loading tests are shown in Figure 3.15 and for the in-plane loading tests in Figure 3.16. For both the loading conditions, three linear string type potentiometers were used to capture the spatial movement of Point A on the bridging where it is connected to the load actuator, each measuring the X, Y and Z displacements, respectively. Five linear potentiometers were used to measure the displacement of the bridging connection and the stud web, two on the front side (LP-1, LP-2), two on the back side (LP-3, LP-4), and an additional one on the back side (LP-5) located approximately one foot above the location of the bridging connection to the stud web. For the SS type connection, LP-1 and LP-2 were attached to the screw heads to measure the pullout of the screws, while LP-3 and LP-4 were attached on the back to measure the movement of the web plate just below the screws. The measurements being recorded by LP-5 is to show that the web is completely isolated and is unaffected by the loading. For the WW type connection, LP-1 and LP-2 were attached at relatively the same location as in SS type connection, but to measure the horizontal movement of the vertical leg of the clip angle. For the DW type connection, LP-1 and LP-2 were attached at relatively the same location as in SS type connection, but to measure the horizontal movement of the stud web.

### **3.7.4 Out-of-Plane Loading Test Procedure**

The specimen mounting-frame and the Actuator Armature were aligned and anchored to the floor (see Figure 3.11). In this setup, the Actuator Armature was placed

perpendicular to the centerline of the bridging channel, with the armature centerline passing through Point A. The test specimen was placed in the specimen mounting-frame and aligned horizontally and vertically. Figure 3.13 shows an overall view of the specimen in the test fixture, and Figure 3.15(a) shows a view of the connection between the bridging channel and the actuator. The specimen was secured on the front and on the back by four rigid hot-rolled steel members, to isolate the web for testing. To maintain the same spatial position of Point A for all the tests, it was triangulated and the locations of the linear string type potentiometers were adjusted to achieve an orthogonal coordinate system to a reasonable accuracy of 0.10 inch.

### **3.7.5 In-Plane Loading Test Procedure**

The specimen mounting-frame and the Actuator Armature were placed in line with the bridging channel of the stud specimen and anchored to the floor (see Figure 3.12). The test specimen was placed in the specimen mounting-frame and aligned horizontally and vertically. The specimen was then secured on the front and on the back by four rigid hot-rolled steel members, to isolate the web for testing. Figure 3.13 shows the overall view of a specimen in the test fixture, and a shows a view of the connection between the bridging channel and the load actuator. The cranking arm of the actuator was turned at approximately one-half a revolution per second until the bridging failed.

Table 3.1 As-built Material Properties from the Tension Coupon Tests

| Specimen ID |     |   |     |    |    | Yield Stress<br>(0.2% offset) | Upper<br>Yield<br>Stress | Lower<br>Yield<br>Stress | Ultimate<br>Stress |
|-------------|-----|---|-----|----|----|-------------------------------|--------------------------|--------------------------|--------------------|
| TC          | D   | S | B   | t  | ID | ksi                           | ksi                      | ksi                      | ksi                |
| TC          | 362 | S | 125 | 33 | 1  | -                             | 47.26                    | 46.40                    | 54.68              |
| TC          | 362 | S | 125 | 33 | 2  | 48.51                         | 49.17                    | 48.59                    | 55.88              |
| TC          | 362 | S | 125 | 33 | 3  | 48.55                         | 49.17                    | 49.40                    | 55.89              |
| Average     |     |   |     |    |    | 48.53                         | 48.53                    | 48.13                    | 55.48              |
| TC          | 362 | S | 162 | 43 | 2  | 46.65                         | 46.90                    | 46.43                    | 57.62              |
| TC          | 362 | S | 162 | 43 | 3  | 46.73                         | 46.84                    | 46.13                    | 57.64              |
| TC          | 362 | S | 162 | 43 | 4  | 47.98                         | 48.31                    | 47.22                    | 58.60              |
| TC          | 362 | S | 162 | 43 | 5  | 46.80                         | 47.83                    | 47.25                    | 58.94              |
| Average     |     |   |     |    |    | 47.04                         | 47.47                    | 46.76                    | 58.20              |
| TC          | 362 | S | 162 | 68 | 2  | 50.12                         | 51.91                    | 51.72                    | 66.62              |
| TC          | 362 | S | 162 | 68 | 3  | 51.75                         | 51.78                    | 51.24                    | 67.34              |
| TC          | 362 | S | 162 | 68 | 4  | 54.15                         | 54.35                    | 53.96                    | 69.43              |
| Average     |     |   |     |    |    | 52.01                         | 52.68                    | 52.30                    | 67.80              |
| TC          | 600 | S | 125 | 33 | 1  | 23.82                         | -                        | -                        | 45.22              |
| TC          | 600 | S | 125 | 33 | 3  | 26.97                         | -                        | -                        | 45.56              |
| TC          | 600 | S | 125 | 33 | 5  | 26.73                         | -                        | -                        | 44.93              |
| TC          | 600 | S | 125 | 33 | 7  | 18.61                         | -                        | -                        | 35.70              |
| TC          | 600 | S | 125 | 33 | 8  | -                             | -                        | -                        | 36.88              |
| Average     |     |   |     |    |    | 24.03                         | -                        | -                        | 45.24              |
| TC          | 600 | S | 162 | 43 | 2  | 45.12                         | 45.48                    | 44.06                    | 53.03              |
| TC          | 600 | S | 162 | 43 | 3  | 46.65                         | 47.49                    | 48.37                    | 55.65              |
| TC          | 600 | S | 162 | 43 | 4  | 46.75                         | 47.28                    | 45.86                    | 55.65              |
| TC          | 600 | S | 162 | 43 | 5  | 46.43                         | 47.79                    | 47.16                    | 55.18              |
| Average     |     |   |     |    |    | 46.24                         | 47.01                    | 46.36                    | 54.88              |
| TC          | 600 | S | 162 | 43 | 3a | 50.27                         | 50.81                    | 50.63                    | 59.21              |
| TC          | 600 | S | 162 | 43 | 4a | 50.34                         | 51.58                    | 51.24                    | 59.56              |
| Average     |     |   |     |    |    | 50.30                         | 51.19                    | 50.94                    | 59.38              |
| TC          | 600 | S | 162 | 97 | 3a | 60.40                         | 60.70                    | 59.23                    | 70.38              |
| TC          | 600 | S | 162 | 97 | 3b | 61.10                         | 62.05                    | 59.31                    | 70.28              |
| TC          | 600 | S | 162 | 97 | 4  | 59.10                         | 59.87                    | 58.30                    | 69.96              |
| Average     |     |   |     |    |    | 60.20                         | 60.87                    | 58.94                    | 70.21              |
| TC          | 800 | S | 162 | 43 | 1  | -                             | 40.65                    | 40.20                    | 55.03              |
| TC          | 800 | S | 162 | 43 | 3  | -                             | 40.50                    | 40.20                    | 54.47              |
| TC          | 800 | S | 162 | 43 | 4  | -                             | 40.88                    | 40.30                    | 55.20              |
| Average     |     |   |     |    |    | -                             | 40.68                    | 40.23                    | 54.90              |
| TC          | 800 | S | 162 | 97 | 1  | 42.12                         | 45.62                    | 44.39                    | 66.79              |
| TC          | 800 | S | 162 | 97 | 3  | 43.32                         | 44.55                    | 44.51                    | 68.00              |
| TC          | 800 | S | 162 | 97 | 4  | 42.06                         | 47.01                    | 46.56                    | 67.69              |
| Average     |     |   |     |    |    | 42.50                         | 45.73                    | 45.15                    | 67.49              |

Table 3.2 As-Built Cross-Sectional Dimensions of Test Specimens

| Stud Designation |   |     |    |    | Target<br>Brace<br>Stiffness | Average As-Built Measurements |        |       |        |       |       |        |        |       |        |       |
|------------------|---|-----|----|----|------------------------------|-------------------------------|--------|-------|--------|-------|-------|--------|--------|-------|--------|-------|
|                  |   |     |    |    |                              | Lip                           | Flange | Web   | Flange | Lip   | Web   | Lip    | Flange | Web   | Flange | Lip   |
| D                | S | B   | t  | ID | lbs/in.                      | A                             | B      | C     | D      | E     | F     | ta     | tb     | tc    | td     | te    |
|                  |   |     |    |    |                              | in.                           | in.    | in.   | in.    | in.   | in.   | in.    | in.    | in.   | in.    | in.   |
| 362              | S | 125 | 33 | 1  | 200                          | 0.252                         | 1.317  | 3.613 | 1.259  | 0.209 | 3.589 | 0.033  | 0.039  | 0.034 | 0.034  | 0.032 |
| 362              | S | 125 | 33 | 2  | 400                          | 0.252                         | 1.316  | 3.613 | 1.258  | 0.205 | 3.584 | 0.036  | 0.035  | 0.033 | 0.035  | 0.032 |
| 362              | S | 125 | 33 | 3  | 100                          | 0.251                         | 1.321  | 3.616 | 1.258  | 0.206 | 3.603 | 0.036  | 0.036  | 0.034 | 0.036  | 0.034 |
| 362              | S | 125 | 33 | 4  | 100                          | 0.253                         | 1.318  | 3.616 | 1.259  | 0.208 | 3.593 | 0.034  | 0.035  | 0.033 | 0.035  | 0.032 |
| 362              | S | 125 | 33 | 5  | 0                            | 0.251                         | 1.319  | 3.612 | 1.256  | 0.203 | 3.589 | 0.031  | 0.036  | 0.034 | 0.035  | 0.032 |
| 362              | S | 125 | 33 | 6  | 100                          | 0.250                         | 1.318  | 3.612 | 1.256  | 0.204 | 3.597 | 0.032  | 0.035  | 0.034 | 0.035  | 0.031 |
| 362              | S | 125 | 33 |    |                              | 0.252                         | 1.318  | 3.613 | 1.258  | 0.206 | 3.590 | 0.033  | 0.036  | 0.034 | 0.035  | 0.032 |
|                  |   |     |    |    |                              |                               |        |       |        |       |       |        |        |       |        |       |
| 362              | S | 162 | 43 | 1  | 0                            | 0.541                         | 1.637  | 3.562 | 1.603  | 0.531 | 3.547 | 0.044  | 0.042  | 0.042 | 0.042  | 0.044 |
| 362              | S | 162 | 43 | 2  | 200                          | 0.530                         | 1.606  | 3.563 | 1.642  | 0.538 | 3.541 | 0.045  | 0.043  | 0.043 | 0.043  | 0.043 |
| 362              | S | 162 | 43 | 3  | 800                          | 0.536                         | 1.640  | 3.563 | 1.607  | 0.534 | 3.540 | 0.044  | 0.042  | 0.042 | 0.043  | 0.044 |
| 362              | S | 162 | 43 | 4  | 400                          | 0.528                         | 1.602  | 3.569 | 1.639  | 0.538 | 3.541 | 0.042  | 0.042  | 0.042 | 0.042  | 0.042 |
| 362              | S | 162 | 43 |    |                              | 0.534                         | 1.621  | 3.564 | 1.623  | 0.535 | 3.542 | 0.044  | 0.042  | 0.042 | 0.043  | 0.043 |
|                  |   |     |    |    |                              |                               |        |       |        |       |       |        |        |       |        |       |
| 362              | S | 162 | 68 | 2  | 1000                         | 0.526                         | 1.628  | 3.642 | 1.706  | 0.539 | 3.631 | 0.0717 | 0.070  | 0.070 | 0.070  | 0.072 |
| 362              | S | 162 | 68 | 3  | 500                          | 0.546                         | 1.701  | 3.638 | 1.629  | 0.524 | 3.633 | 0.074  | 0.070  | 0.070 | 0.070  | 0.072 |
| 362              | S | 162 | 68 | 4  | 750                          | 0.542                         | 1.705  | 3.635 | 1.630  | 0.536 | 3.635 | ---    | 0.069  | 0.069 | 0.069  | 0.069 |
| 362              | S | 162 | 68 | 5  | 0                            | 0.543                         | 1.703  | 3.636 | 1.629  | 0.523 | 3.634 | 0.076  | 0.068  | 0.068 | 0.068  | 0.073 |
| 362              | S | 162 | 68 |    |                              | 0.540                         | 1.684  | 3.638 | 1.649  | 0.530 | 3.633 | 0.074  | 0.069  | 0.069 | 0.069  | 0.071 |

Table 3.2 (Continued) As-Built Cross-Sectional Dimensions of Test Specimens

| Stud Designation |   |     |    |    | Target<br>Brace<br>Stiffness | Average As-Built Measurements |        |       |        |       |       |       |        |       |        |       |
|------------------|---|-----|----|----|------------------------------|-------------------------------|--------|-------|--------|-------|-------|-------|--------|-------|--------|-------|
|                  |   |     |    |    |                              | Lip                           | Flange | Web   | Flange | Lip   | Web   | Lip   | Flange | Web   | Flange | Lip   |
| D                | S | B   | t  | ID | lbs/in.                      | A                             | B      | C     | D      | E     | F     | ta    | tb     | tc    | td     | te    |
|                  |   |     |    |    |                              | in.                           | in.    | in.   | in.    | in.   | in.   | in.   | in.    | in.   | in.    | in.   |
| 600              | S | 125 | 33 | 1  | 200                          | 0.206                         | 1.243  | 6.022 | 1.307  | 0.243 | 5.999 | 0.032 | 0.032  | 0.030 | 0.032  | 0.032 |
| 600              | S | 125 | 33 | 2  | 0                            | 0.205                         | 1.247  | 6.019 | 1.309  | 0.245 | 6.004 | 0.031 | 0.030  | 0.031 | 0.030  | 0.031 |
| 600              | S | 125 | 33 | 3  | 60                           | 0.208                         | 1.247  | 6.019 | 1.305  | 0.246 | 6.008 | 0.031 | 0.030  | 0.030 | 0.031  | 0.031 |
| 600              | S | 125 | 33 | 4  | 30                           | 0.210                         | 1.248  | 6.019 | 1.308  | 0.242 | 6.008 | 0.032 | ---    | 0.031 | ---    | 0.033 |
| 600              | S | 125 | 33 |    |                              | 0.207                         | 1.246  | 6.020 | 1.307  | 0.244 | 6.005 | 0.032 | 0.031  | 0.031 | 0.031  | 0.032 |
|                  |   |     |    |    |                              |                               |        |       |        |       |       |       |        |       |        |       |
| 600              | S | 162 | 43 | 1  | 250                          | 0.531                         | 1.603  | 5.994 | 1.592  | 0.536 | 5.993 | 0.041 | 0.044  | 0.044 | 0.044  | 0.042 |
| 600              | S | 162 | 43 | 2  | 75                           | 0.526                         | 1.612  | 6.017 | 1.596  | 0.534 | 6.041 | 0.042 | 0.044  | 0.044 | 0.044  | 0.042 |
| 600              | S | 162 | 43 | 4  | 500                          | 0.533                         | 1.595  | 6.036 | 1.616  | 0.530 | 6.068 | 0.044 | 0.045  | 0.044 | 0.044  | 0.042 |
| 600              | S | 162 | 43 | 5  | 30                           | 0.531                         | 1.596  | 6.026 | 1.612  | 0.529 | 6.052 | 0.044 | 0.044  | 0.044 | 0.044  | 0.042 |
| 600              | S | 162 | 43 | 6  | 0                            | 0.528                         | 1.616  | 6.034 | 1.598  | 0.535 | 6.066 | 0.043 | 0.044  | 0.044 | 0.044  | 0.043 |
| 600              | S | 162 | 43 | 6a | 0                            | 0.536                         | 1.707  | 5.984 | 1.609  | 0.535 | 6.092 | 0.044 | 0.046  | 0.046 | 0.046  | 0.045 |
| 600              | S | 162 | 43 |    |                              | 0.530                         | 1.604  | 6.021 | 1.603  | 0.533 | 6.044 | 0.043 | 0.044  | 0.044 | 0.044  | 0.042 |
|                  |   |     |    |    |                              |                               |        |       |        |       |       |       |        |       |        |       |
| 600              | S | 162 | 97 | 1  | 1000                         | 0.544                         | 1.652  | 6.069 | 1.675  | 0.610 | ---   | 0.100 | 0.104  | 0.099 | 0.110  | 0.102 |
| 600              | S | 162 | 97 | 2  | 1500                         | 0.533                         | 1.665  | 6.065 | 1.671  | 0.562 | ---   | 0.103 | 0.102  | 0.100 | 0.107  | 0.106 |
| 600              | S | 162 | 97 | 3  | 500                          | 0.557                         | 1.656  | 6.106 | 1.658  | 0.580 | ---   | 0.099 | 0.102  | 0.101 | 0.103  | 0.099 |
| 600              | S | 162 | 97 | 4  | 160                          | 0.527                         | 1.649  | 6.077 | 1.673  | 0.576 | 6.063 | 0.100 | 0.104  | 0.100 | 0.105  | 0.105 |
| 600              | S | 162 | 97 | 5  | 0                            | 0.542                         | 1.648  | 6.091 | 1.683  | 0.584 | 6.106 | 0.100 | 0.101  | 0.101 | 0.101  | 0.102 |
| 600              | S | 162 | 97 |    |                              | 0.541                         | 1.654  | 6.082 | 1.672  | 0.582 | 6.084 | 0.100 | 0.103  | 0.100 | 0.105  | 0.103 |

Table 3.2 (Continued) As-Built Cross-Sectional Dimensions of Test Specimens

| Stud Designation |   |     |    |    | Target<br>Brace<br>Stiffness | Average As-Built Measurements |        |       |        |       |     |                |                |                |                |                |
|------------------|---|-----|----|----|------------------------------|-------------------------------|--------|-------|--------|-------|-----|----------------|----------------|----------------|----------------|----------------|
|                  |   |     |    |    |                              | Lip                           | Flange | Web   | Flange | Lip   | Web | Lip            | Flange         | Web            | Flange         | Lip            |
| D                | S | B   | t  | ID | lbs/in.                      | A                             | B      | C     | D      | E     | F   | t <sub>a</sub> | t <sub>b</sub> | t <sub>c</sub> | t <sub>d</sub> | t <sub>e</sub> |
|                  |   |     |    |    |                              | in.                           | in.    | in.   | in.    | in.   | in. | in.            | in.            | in.            | in.            | in.            |
| 800              | S | 162 | 43 | 2  | 75                           | 0.537                         | 1.597  | 7.912 | 1.604  | 0.530 | --- | 0.042          | 0.043          | 0.043          | 0.043          | 0.042          |
| 800              | S | 162 | 43 | 3  | 150                          | 0.535                         | 1.598  | 7.925 | 1.605  | 0.533 | --- | 0.042          | 0.043          | 0.043          | 0.043          | 0.043          |
| 800              | S | 162 | 43 | 4  | 0                            | 0.533                         | 1.597  | 7.929 | 1.608  | 0.532 |     | 0.043          | 0.043          | 0.043          | 0.043          | 0.043          |
| 800              | S | 162 | 43 | 5  | 300                          | 0.528                         | 1.606  | 7.920 | 1.597  | 0.532 | --- | 0.042          | 0.043          | 0.044          | 0.044          | 0.041          |
| 800              | S | 162 | 43 |    |                              | 0.533                         | 1.599  | 7.921 | 1.603  | 0.532 | --- | 0.042          | 0.043          | 0.043          | 0.043          | 0.042          |
|                  |   |     |    |    |                              |                               |        |       |        |       |     |                |                |                |                |                |
| 800              | S | 162 | 97 | 1  | 1000                         | 0.562                         | 1.631  | 8.053 | 1.670  | 0.659 | --- | 0.101          | 0.102          | 0.102          | 0.103          | 0.103          |
| 800              | S | 162 | 97 | 2  | 500                          | 0.651                         | 1.649  | 8.048 | 1.647  | 0.561 | --- | 0.102          | 0.103          | 0.103          | 0.103          | 0.102          |
| 800              | S | 162 | 97 | 3  | 0                            | 0.553                         | 1.629  | 8.041 | 1.650  | 0.661 | --- | 0.101          | 0.103          | 0.104          | 0.103          | 0.103          |
| 800              | S | 162 | 97 | 4  | 2100                         | 0.656                         | 1.647  | 8.033 | 1.632  | 0.556 | --- | 0.100          | 0.105          | 0.103          | 0.104          | 0.101          |
| 800              | S | 162 | 97 |    |                              | 0.605                         | 1.639  | 8.044 | 1.650  | 0.609 | --- | 0.101          | 0.103          | 0.103          | 0.103          | 0.102          |

Table 3.3 Initial Geometric Imperfections

| Stud Designation |   |     |    |    | Target<br>Brace<br>Stiffness | Initial Imperfection |       |        |
|------------------|---|-----|----|----|------------------------------|----------------------|-------|--------|
|                  |   |     |    |    |                              | Camber               |       | Sweep  |
|                  |   |     |    |    |                              | B                    | D     | C      |
| D                | S | B   | t  | ID | lbs/in.                      | in.                  | in.   | in.    |
| 362              | S | 125 | 33 | 1  | 200                          | 0                    | 0     | 0      |
| 362              | S | 125 | 33 | 2  | 400                          | 0                    | 0     | 0      |
| 362              | S | 125 | 33 | 3  | 100                          | 0                    | 0     | 0      |
| 362              | S | 125 | 33 | 4  | 100                          | 0                    | 0     | 0      |
| 362              | S | 125 | 33 | 5  | 0                            | 0                    | 0     | 0      |
| 362              | S | 125 | 33 | 6  | 100                          | 0                    | 0     | 0      |
| 362              | S | 162 | 43 | 1  | 0                            | 0                    | 0     | 0      |
| 362              | S | 162 | 43 | 2  | 200                          | 0                    | 0     | 0      |
| 362              | S | 162 | 43 | 3  | 800                          | 0                    | 0     | 0.01   |
| 362              | S | 162 | 43 | 4  | 400                          | 0.01                 | 0.02  | 0      |
| 362              | S | 162 | 68 | 2  | 1000                         | 0                    | 0     | -0.187 |
| 362              | S | 162 | 68 | 3  | 500                          | 0                    | 0     | -0.155 |
| 362              | S | 162 | 68 | 4  | 750                          | 0                    | 0     | 0.14   |
| 362              | S | 162 | 68 | 5  | 0                            | 0                    | 0     | 0.1    |
| 600              | S | 125 | 33 | 1  | 200                          | 0                    | 0     | 0.1    |
| 600              | S | 125 | 33 | 2  | 0                            | 0                    | 0.07  | 0.13   |
| 600              | S | 125 | 33 | 3  | 60                           | 0                    | 0     | 0.12   |
| 600              | S | 125 | 33 | 4  | 30                           | 0                    | 0     | 0.075  |
| 600              | S | 162 | 43 | 1  | 250                          | 0                    | 0     | 0.04   |
| 600              | S | 162 | 43 | 2  | 75                           | 0                    | 0     | 0.03   |
| 600              | S | 162 | 43 | 4  | 500                          | 0.055                | 0.045 | 0      |
| 600              | S | 162 | 43 | 5  | 30                           | 0.055                | 0.053 | 0      |
| 600              | S | 162 | 43 | 6  | 0                            | 0.065                | 0.065 | 0      |
| 600              | S | 162 | 43 | 6a | 0                            | 0                    | 0     | -0.036 |
| 600              | S | 162 | 97 | 1  | 1000                         | ---                  | ---   | ---    |
| 600              | S | 162 | 97 | 2  | 1500                         | ---                  | ---   | ---    |
| 600              | S | 162 | 97 | 3  | 500                          | ---                  | ---   | ---    |
| 600              | S | 162 | 97 | 4  | 160                          | 0                    | 0     | 0.075  |
| 600              | S | 162 | 97 | 5  | 0                            | 0                    | 0     | 0.015  |
| 800              | S | 162 | 43 | 2  | 75                           | 0                    | 0     | 0.09   |
| 800              | S | 162 | 43 | 3  | 150                          | 0                    | 0     | 0.11   |
| 800              | S | 162 | 43 | 4  | 0                            | 0                    | 0     | 0.11   |
| 800              | S | 162 | 43 | 5  | 300                          | 0                    | 0.12  | 0      |
| 800              | S | 162 | 97 | 1  | 1000                         | ---                  | ---   | ---    |
| 800              | S | 162 | 97 | 2  | 500                          | ---                  | ---   | ---    |
| 800              | S | 162 | 97 | 3  | 0                            | ---                  | ---   | ---    |
| 800              | S | 162 | 97 | 4  | 2100                         | 0                    | 0     | 0.12   |

Table 3.4 Average As-Built Geometric Dimensions of Each Stud Series

| Stud Designation |   |     |     | Clear O/O Dimensions |        |        |        |        |        | Average Width |        |
|------------------|---|-----|-----|----------------------|--------|--------|--------|--------|--------|---------------|--------|
|                  |   |     |     | Lip                  | Flange | Web    | Flange | Lip    | Web    | Lip           | Flange |
|                  |   |     |     | A                    | B      | C      | D      | E      | F      |               |        |
| D                | S | B   | t   | in.                  | in.    | in.    | in.    | in.    | in.    | in.           | in.    |
| 362              | S | 125 | 33  | 0.2515               | 1.3175 | 3.6131 | 1.2577 | 0.2058 | 3.5904 | 0.2287        | 1.2876 |
| 362              | S | 162 | 43  | 0.5335               | 1.6212 | 3.5643 | 1.6229 | 0.5352 | 3.5423 | 0.5344        | 1.6220 |
| 362              | S | 162 | 68  | 0.5396               | 1.6842 | 3.6377 | 1.6485 | 0.5304 | 3.6329 | 0.5350        | 1.6664 |
| 600              | S | 125 | 33  | 0.2071               | 1.2462 | 6.0197 | 1.3073 | 0.2439 | 6.0045 | 0.2255        | 1.2768 |
| 600              | S | 162 | 43  | 0.5298               | 1.6042 | 6.0213 | 1.6028 | 0.5328 | 6.0439 | 0.5313        | 1.6035 |
| 600              | S | 162 | 43a | 0.5363               | 1.7070 | 5.9842 | 1.6092 | 0.5352 | 6.0920 | 0.5358        | 1.6581 |
| 600              | S | 162 | 97  | 0.5405               | 1.6539 | 6.0816 | 1.6717 | 0.5824 | 6.0843 | 0.5615        | 1.6628 |
| 800              | S | 162 | 43  | 0.5330               | 1.5994 | 7.9213 | 1.6033 | 0.5316 | ---    | 0.5323        | 1.6014 |
| 800              | S | 162 | 97  | 0.6053               | 1.6388 | 8.0436 | 1.6498 | 0.6091 | ---    | 0.6072        | 1.6443 |

Table 3.5 Average As-Built Geometric Dimensions of Each Stud Series

| Stud Designation |   |     |     | Thickness |        |        |        |        |           | Radius of Bend | Base Metal Thickness | Internal Radius |
|------------------|---|-----|-----|-----------|--------|--------|--------|--------|-----------|----------------|----------------------|-----------------|
|                  |   |     |     | Lip       | Flange | Web    | Flange | Lip    | $t_{avg}$ |                |                      |                 |
|                  |   |     |     | $t_a$     | $t_b$  | $t_c$  | $t_d$  | $t_e$  |           | R              | $t_{net}$            | $R_{int}$       |
| D                | S | B   | t   | in.       | in.    | in.    | in.    | in.    | in.       | in.            | in.                  |                 |
| 362              | S | 125 | 33  | 0.0333    | 0.0360 | 0.0336 | 0.0348 | 0.0318 | 0.0339    | 0.0938         | 0.0319               | 0.07781         |
| 362              | S | 162 | 43  | 0.0437    | 0.0424 | 0.0425 | 0.0425 | 0.0432 | 0.0429    | 0.0938         | 0.0409               | 0.07332         |
| 362              | S | 162 | 68  | 0.0735    | 0.0691 | 0.0691 | 0.0693 | 0.0714 | 0.0705    | 0.1409         | 0.0685               | 0.10669         |
| 600              | S | 125 | 33  | 0.0316    | 0.0307 | 0.0307 | 0.0308 | 0.0315 | 0.0310    | 0.0938         | 0.0290               | 0.07923         |
| 600              | S | 162 | 43  | 0.0427    | 0.0441 | 0.0442 | 0.0443 | 0.0423 | 0.0435    | 0.0938         | 0.0415               | 0.07299         |
| 600              | S | 162 | 43a | 0.0442    | 0.0458 | 0.0460 | 0.0460 | 0.0447 | 0.0453    | 0.0938         | 0.0433               | 0.07209         |
| 600              | S | 162 | 97  | 0.1002    | 0.1027 | 0.1004 | 0.1053 | 0.1028 | 0.1023    | 0.2045         | 0.1003               | 0.15440         |
| 800              | S | 162 | 43  | 0.0421    | 0.0431 | 0.0431 | 0.0430 | 0.0422 | 0.0427    | 0.0938         | 0.0407               | 0.07340         |
| 800              | S | 162 | 97  | 0.1008    | 0.1031 | 0.1029 | 0.1031 | 0.1021 | 0.1024    | 0.2048         | 0.1004               | 0.15458         |

Note: Radius of Bend = max [(2  $t_{avg}$ ), 3/32"], Clark's tables. Internal Radii = (Radius of Bend -  $t_{net}$  / 2)

Base Metal Thickness = [ $t_{avg}$  - 2 mils for galvanizing]

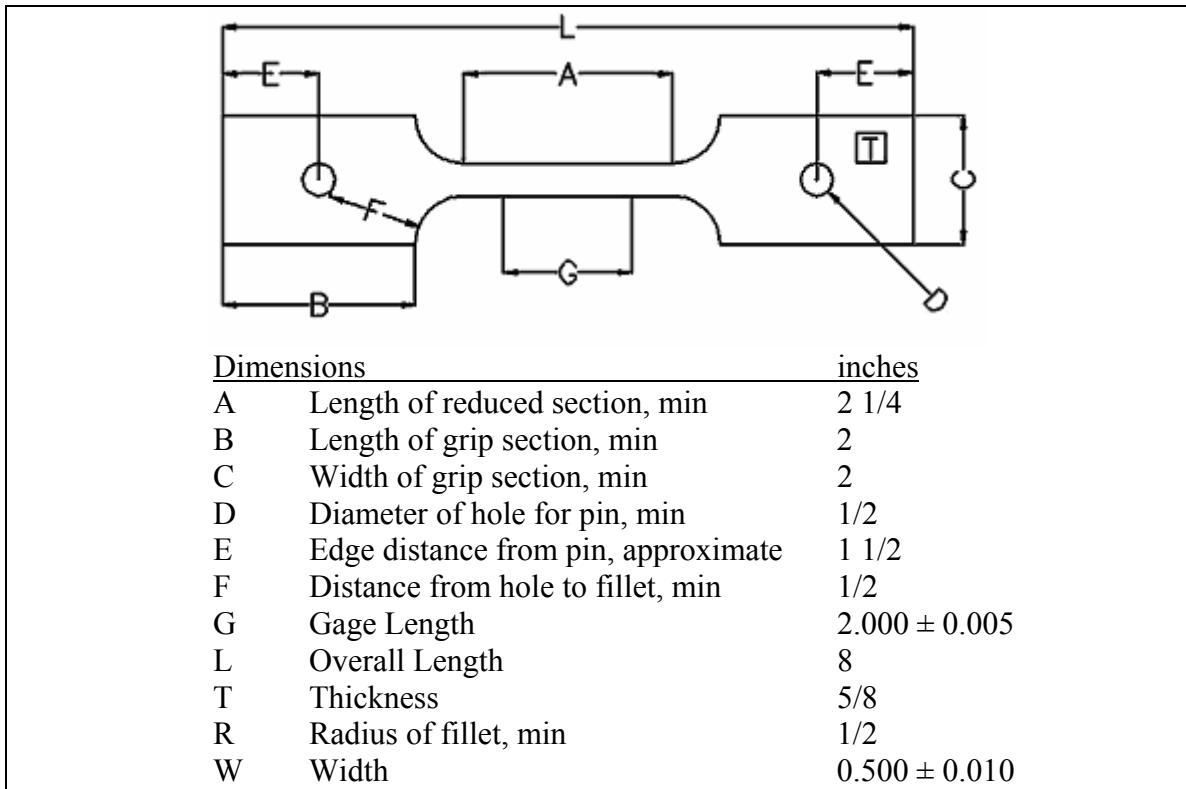


Figure 3.1 Dimensions of a Typical Tension Coupon

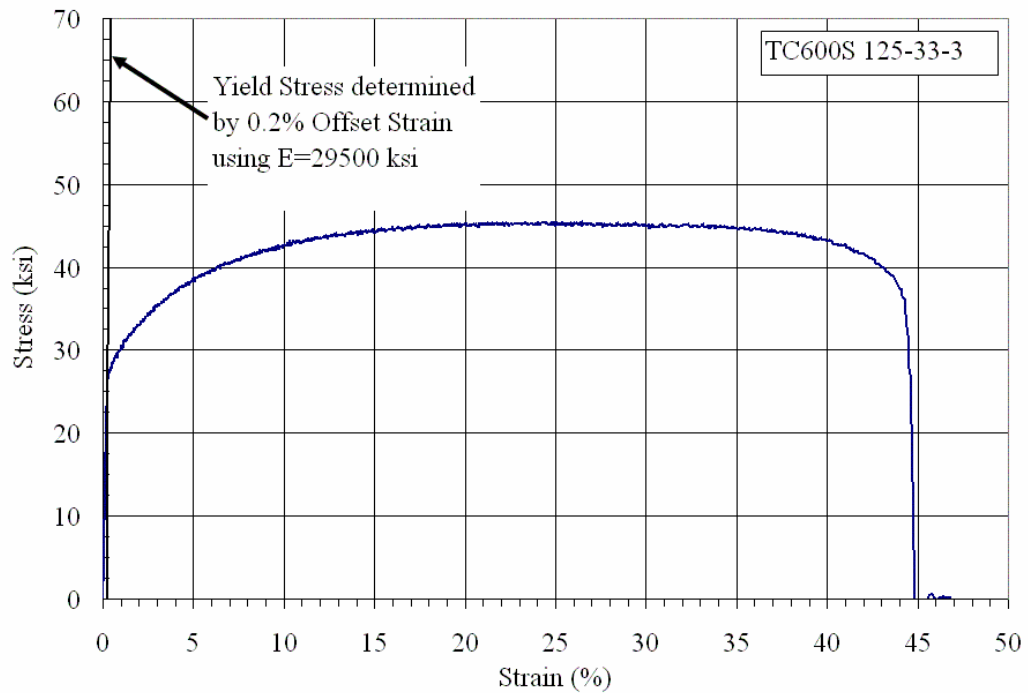


Figure 3.2 Offset Method for Determining Yield Stress

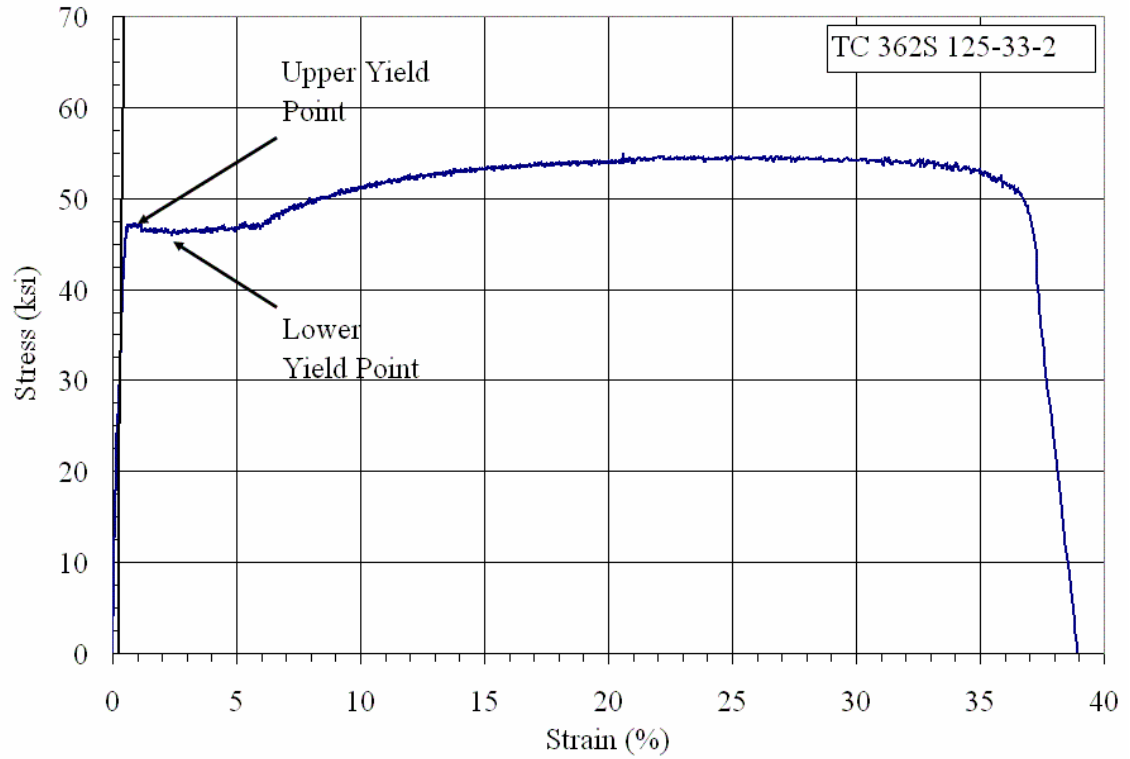


Figure 3.3 Autographic Diagram Method for Determining Yield Stress

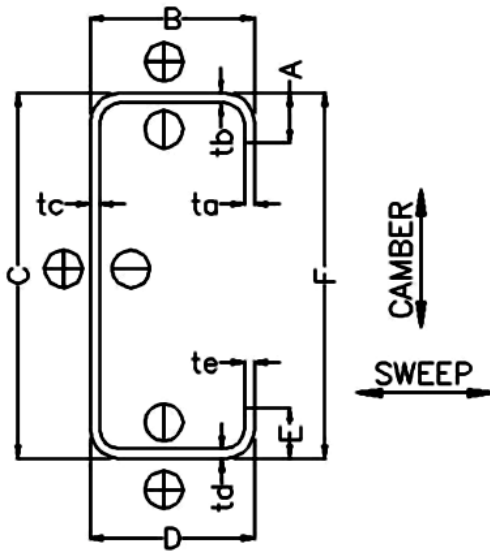


Figure 3.4 Typical Cross-Section of a Cee-Stud



Figure 3.5 Connection of Cee-Stud and Track (a) at Top, (b) at Bottom

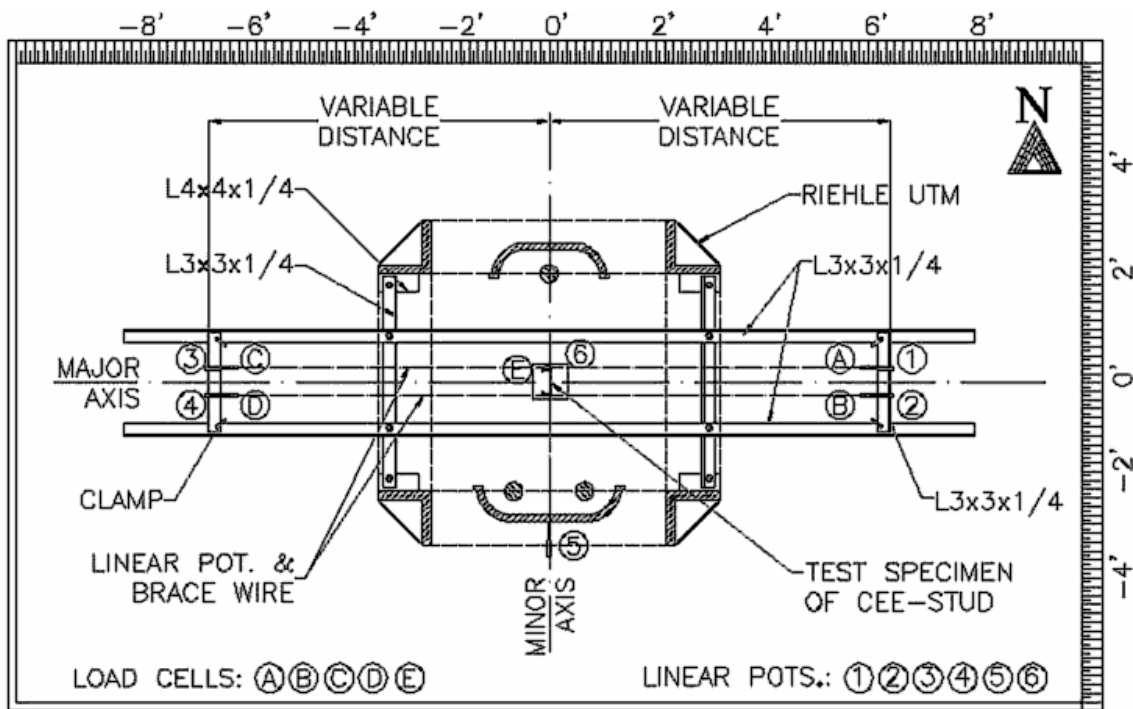


Figure 3.6 Plan View of Single Column Axial Test Setup in the Riehle Universal Testing Machine

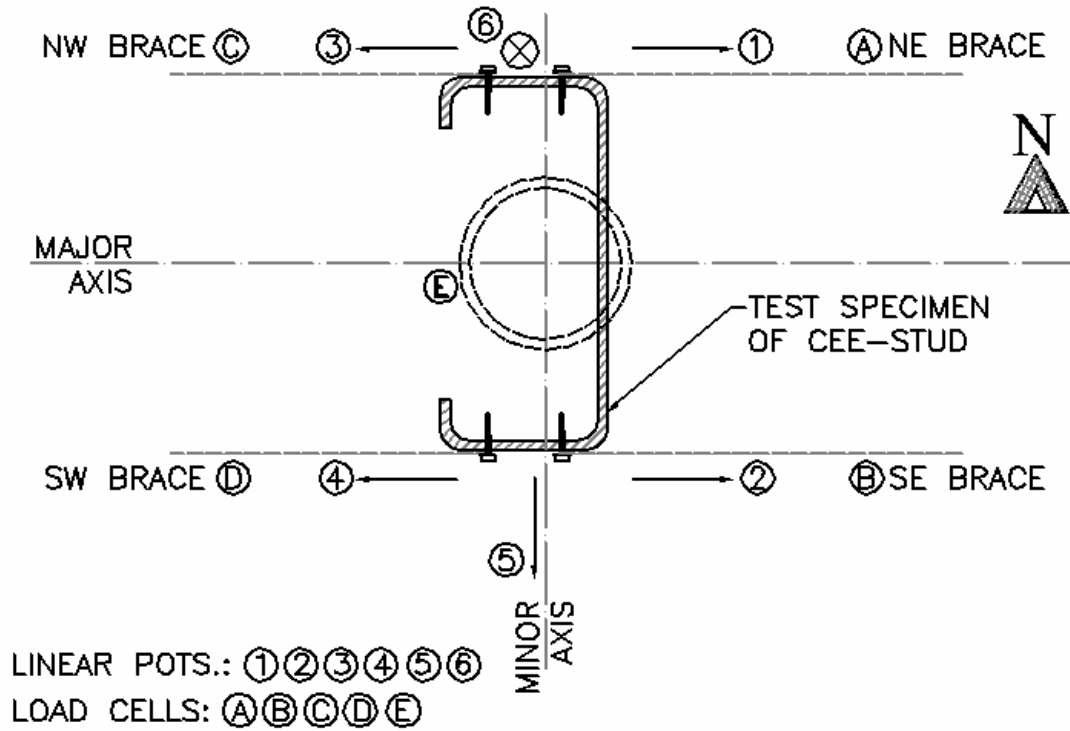


Figure 3.7 Schematic Mid-height Bracing and Instrumentation Locations on Test Specimens

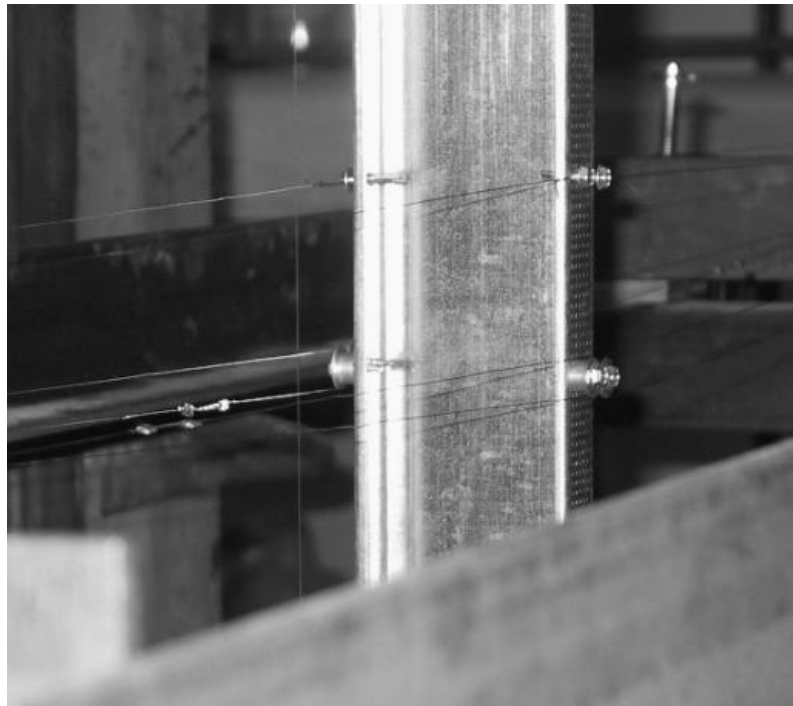


Figure 3.8 Close-up View of the Location of Brace-Wires and Instrumentation at Mid-height of the Cee-Stud. (Screws at the bottom are location of looped brace-wires, and Screws at the top are location of the Linear Potentiometers)

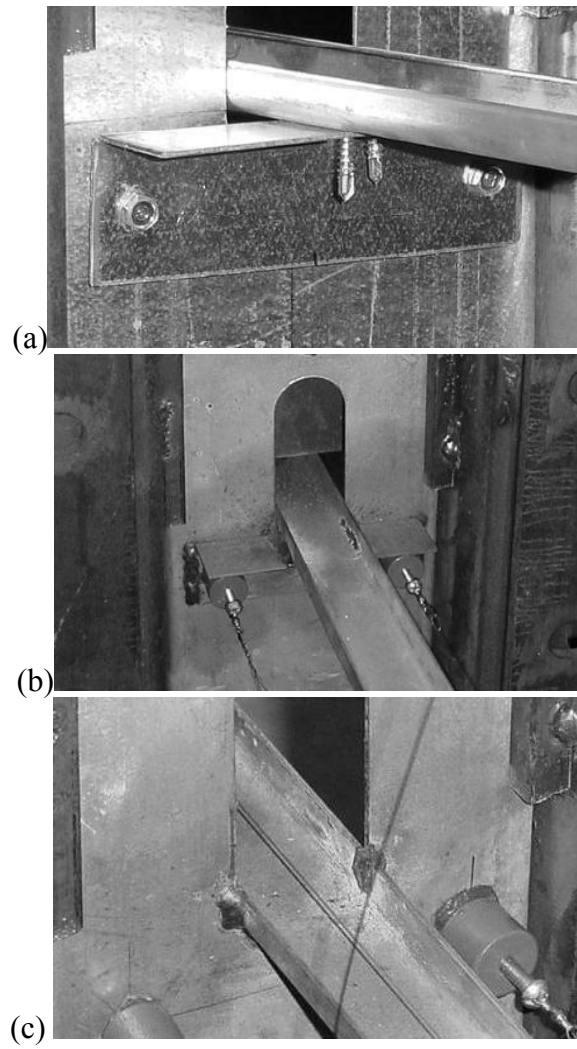


Figure 3.9 Types of Bridging Connections (a) SS (b) WW and (c) DW

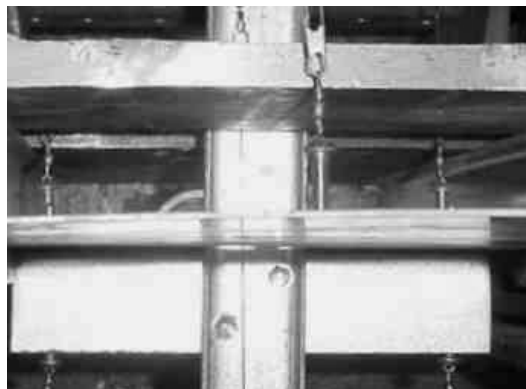
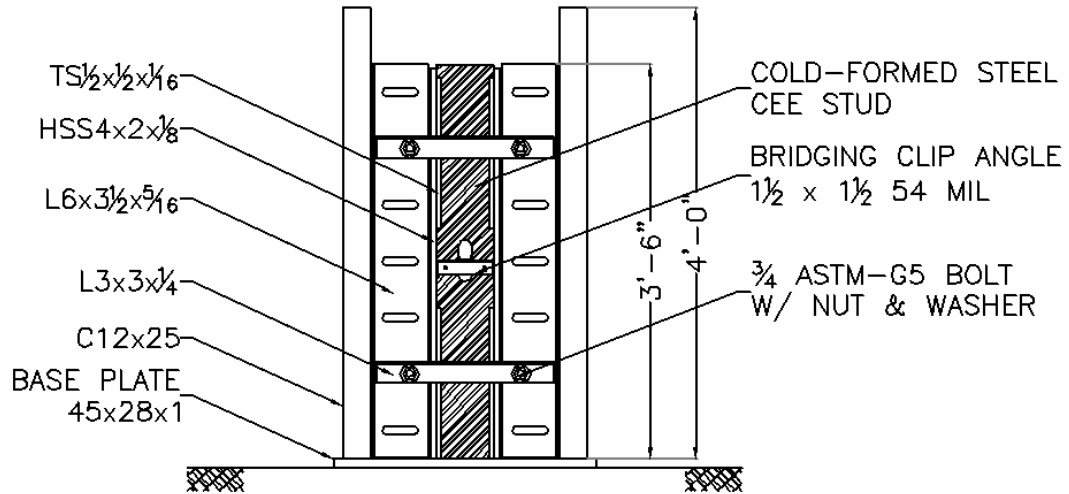
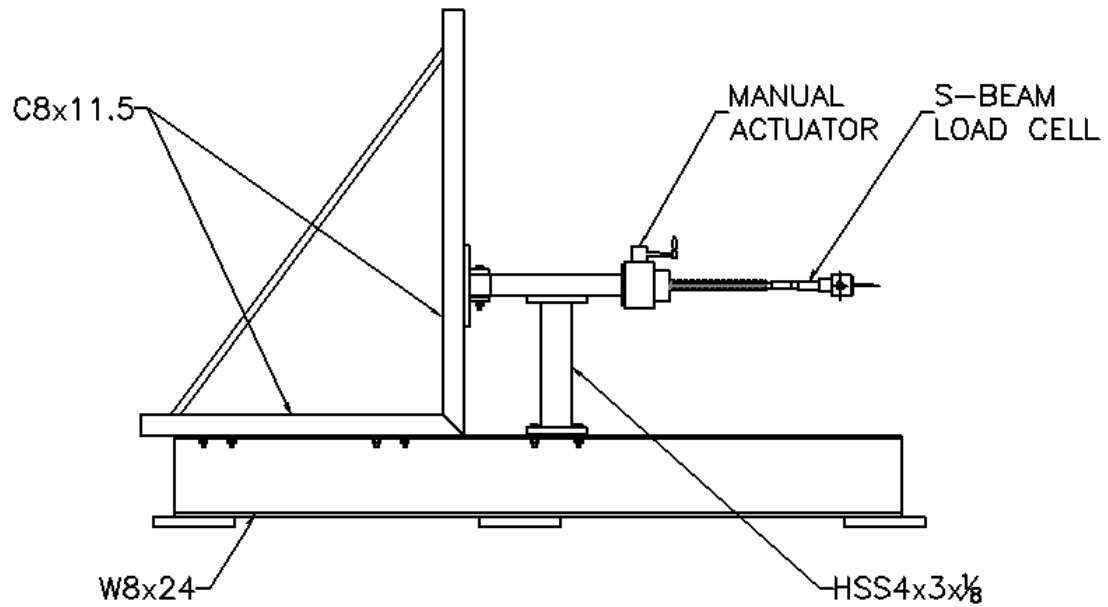


Figure 3.10 Top View of the SS Type Bridging Connection



(a) Elevation View of the Specimen Mounting Frame



(b) Loading Actuator Armature

Figure 3.11 Elevation Views of Bridging Connection Test Setup

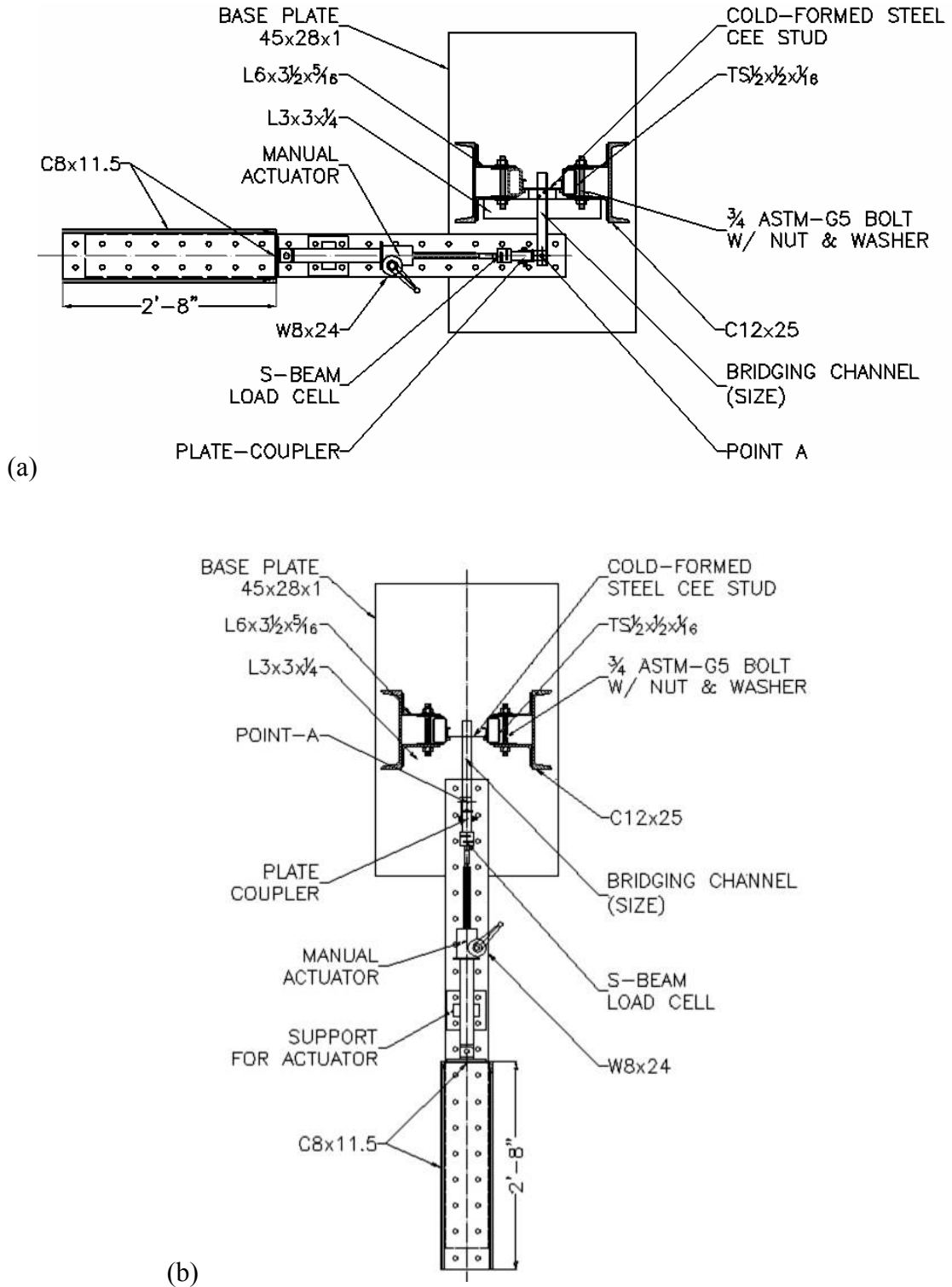


Figure 3.12 Schematic Plan View of the (a) Out-of-Plane Bridging Test (b) In-Plane Bridging Test

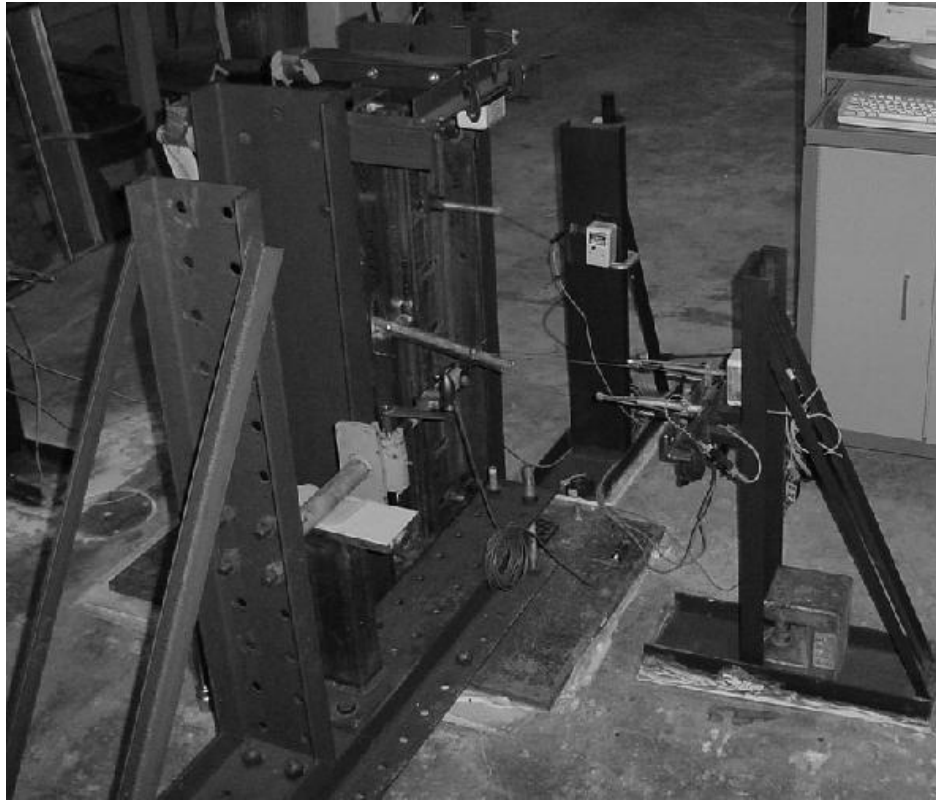


Figure 3.13 Overall View of the Out-of-Plane Bridging Tests

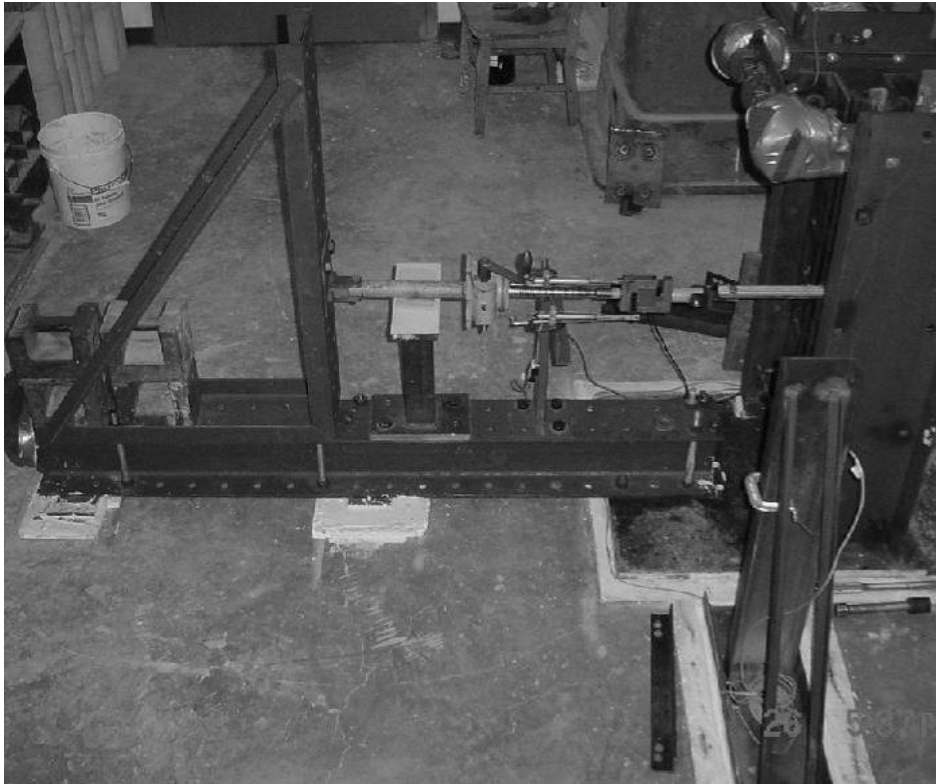


Figure 3.14 Overall View of the In-Plane Bridging Tests



Figure 3.15 Out-of-Plane Loading Test Instrumentation on the (a) Front (b) Back

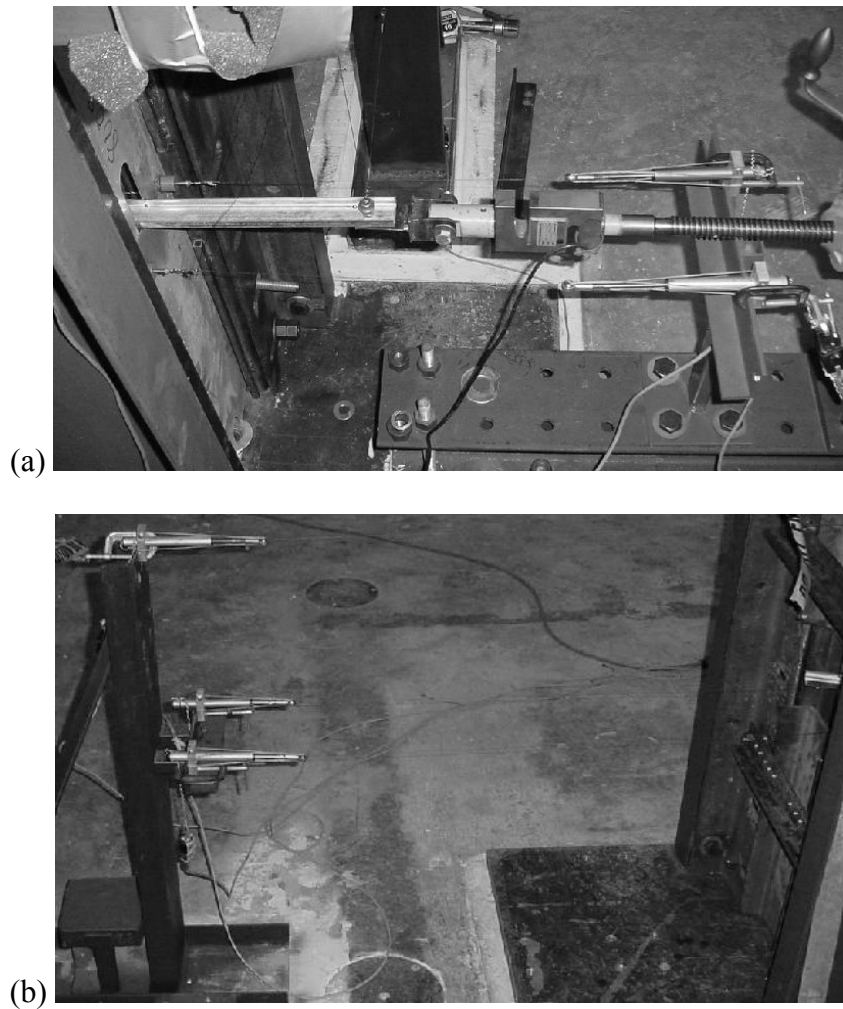


Figure 3.16 In-plane Loading Test Instrumentation on the (a) Front (b) Back

## CHAPTER 4 EXPERIMENTAL RESULTS AND EVALUATION

Experimental tests on single column specimens and bridging specimens were performed as per the test protocols described in Chapter 3. The individual test reports for the single column tests are discussed in Appendix A and the results of the bridging tests are available in Appendix B. This chapter is divided into four sections, the first section deals with the results of the single column axial tests and discusses the effect of brace stiffness and strength on the load carrying capacity, mid-height lateral displacement and effective length of the braced columns. The second section deals with the axial pullout strength and torsional stiffness of the three bridging connections for eight series of cee-studs. The third section deals with the relationship between the flexible bracing and the bridging strength and stiffness. The fourth section summarizes the experimental evaluation.

### 4.1 Single Column Axial Load Test Results

In the single column axial load tests a total of 37 studs were tested based on the following parameters:

- Cross-sections
  - 362S125-33, 362S162-43, 362S162-68
  - 600S 125-33, 600S 162-43, 600S 162-97
  - 800S 162-43, 800S 162-97
- Unbraced Test Specimens versus Braced Test Specimens
- Bracing Stiffness
  - Under-Braced – less than ideal bracing
  - Ideally-Braced – equal to ideal bracing
  - Over-Braced – greater than ideal bracing

Table 4.1 provides the proposed test matrix for the 8'-0" long single column axially loaded cee-stud specimens. Due to certain experimental limitations, the actual test matrix is as given in Table 4.2, where the numbers in the table represent the number of tests conducted at that brace stiffness. The specific reasons for the changes from the proposed test matrix compared to the actual test matrix are described in the course of this chapter.

#### **4.1.1 Bracing Strength and Stiffness**

Eight groups of cee-studs were tested with a total of 37 test specimens. The AISIWIN software program (AISIWIN 2000) was used to determine the nominal properties of the eight groups of test specimens, with appropriate nominal values of material yield and ultimate stress. Table 4.3 gives the ultimate and unfactored capacities of each of the stud groups. The target brace stiffness, for single nodal bracing ( $n=1$ ), was calculated using Eq. 2.14, as recommended by Yura (1995), where the unbraced length of the column was taken as the distance between the support and the point of bracing ( $L_b = 48.0$  inches). The target bracing stiffness is also tabulated and provided in Table 4.3.

The measured geometric dimensions and the results of the material tension coupon tests for each group of cee-studs were then used to recalculate the ideal brace stiffness using AISIWIN (2002). Table 4.4 gives the values of the required ideal bracing stiffness for each of the studs. The single column axial load tests were conducted on cee-stud specimens with varying brace stiffnesses, which were lesser than, equal to, or greater than the ideal brace stiffness. As discussed earlier, at least one cee-stud per series was tested without any lateral (or torsional) bracing.

The cee-studs were braced with four steel wires attached at mid-height of the member to the flanges, as shown in Figure 4.1. By varying the length and diameter of the brace wires the brace stiffness was varied from one test specimen to the other. The brace strength was

calculated as the product of the cross-sectional area of the wire and its nominal tensile strength. The actual brace stiffness ( $k_{br}$ ) was calculated as the average value of the brace stiffnesses of all four wires. The brace stiffness of each wire was calculated using Eq.4.1a.

$$k_{br} = \frac{AE}{L_{br}} \quad (4.1a)$$

where: A = Cross-sectional area of the wire  
 E = Young's Modulus = 29,000,000 psi.  
 $L_{br}$  = Length of brace wire

At any time during the test only two brace wires, out of the four, were effective in bracing the stud. If the stud buckled in a flexural mode, the two brace wires on the same side of the web were effective, whereas if the stud buckled in a torsional mode, the two diagonally opposite brace wires were effective in bracing the stud. Therefore, the total brace stiffness was taken as twice the average stiffness of the four brace wires, and is given in Table 4.5. The ratio of the total brace stiffness provided to the required ideal brace stiffness, ( $\beta_{provided}/\beta_{required}$ ) is defined as the *brace-factor*. The brace-factor for each of the 37 test specimens is listed in Table 4.5, which was used to categorize the cee-studs as: *under-braced*, *ideally-braced* or *over-braced* (i.e. brace-factor <1.0, =1.0, or >1.0).

The column effective length factors were taken from Table C-C4-1 of the Commentary to the North American Specification for Cold-Formed Steel (AISI 2000). For flexural buckling about the weak axis the effective length factor was taken as  $K_y=1.0$  for the unbraced studs and  $K_y=0.5$  for the braced studs. This effective length factor was assumed to be the same for all three categories of braced studs. For flexural buckling about the strong axis, it was considered that the track offered near full base fixity, and hence the effective length

factor was taken as  $K_x=0.5$ . Since the top and bottom supports prevented the stud from twisting, and the effective length factor was taken as  $K_x=0.5$ .

#### 4.1.2 Evaluation of Experimental Observations

The evaluation of the experiments provided below will be based on a review of the test parameters such as the effect of cee-stud dimensions, the brace stiffness and the brace strength. The experimental results are compared to analytically calculated values of axial load capacity and the expected brace forces based on the measured lateral displacements. The effect of brace stiffness on the axial load capacity has been studied and the graphically illustrated in Figure 4.2 to 4.9 and has been discussed in this section. Figure 4.10 gives the buckling modes and shapes of the experimental observations, which is explained later in this chapter.

While keeping the brace-factor constant between two or more studs, the following parametric studies were performed based on the cross-section dimensions:

- Web depth, keeping the brace-factor relatively the same.
  - a. Comparing 362S125-33 and 600S125-33 (Figures 4.11 to 4.13)
  - b. Comparing 362S162-43, 600S162-43 and 800S162-43 (Figures 4.14 to 4.16)
  - c. Comparing 600S162-97 and 800S162-97 (Figures 4.17 to 4.19)
- Thickness, keeping the brace-factor relatively the same:
  - a. Comparing 362S125-33, 362S162-43 and 362S125-68 (Figures 4.20 to 4.22)
  - b. Comparing 600S125-33, 600S162-43 and 600S162-97 (Figures 4.23 to 4.26)
  - c. Comparing 800S162-43 and 800S162-97 (Figures 4.27 to 4.29)

Figures 4.11 through 4.29 have been normalized with respect to the analytical values of axial load and the corresponding axial shortening obtained from AISIWIN (2002) using the average as-built properties of each stud group. The effect of different material properties has

been considered in the above normalization by including it in the AISIWIN program. With increasing web depth and flange width, the slenderness ratio of the web and flange plate elements increases. This leads to a loss of elastic stiffness in the web and hence the load carrying capacity of the studs decreases and is evident in the comparisons described above. Figures 4.11 to 4.13 indicate that the 600S125-33 studs have undergone nearly twice the axial deformation compared to the 362S125-33 studs, for nearly the same brace factor. Both, the unbraced 362S and 600S studs have attained almost a normalized load of 1.35 times than the analytical prediction, but their normalized axial deformations at the maximum load being 1.6 and 4.6, respectively. In Figure 4.12, the 362S and 600S studs with a brace factor of 1.7x and 1.3x, have attained nearly 1.0 and 1.4 times the analytical prediction for a mid-height braced stud, respectively. Comparing the 362S and 600S studs in Figure 4.13, with brace factors 6.2x and 7.4x, respectively, shows that the normalized axial shortening being 1.25 and 3.3 at normalized axial loads of 1.25 and 1.15, respectively.

Figures 4.14, 4.15 and 4.16 show the comparison of the 362S, 600S and 800S studs for the same plate thickness of 43 mils. The 362S, 600S and the 800S unbraced studs recorded a normalized axial load of 2.6, 1.4 and 2.0 at corresponding normalized axial shortening of 2.6, 3.0 and 3.8, respectively. Comparing the 362S (1.2x), 600S (1.6x) and 800S (1.3x) studs in Figure 4.15 shows that normalized axial loads are 1.4, 1.05 and 0.85 for corresponding normalized axial shortening of 1.75, 2.2 and 2.1 respectively. In the 800S162-43-150 stud the buckling mode was distortional hence the experimental maximum load was less than the analytical value. When the brace factor was greater than 2.0, as in the case of 362S (2.5x), 600S (3.4x) and 800S (2.3x) studs, the normalized axial loads were 1.35, 1.0 and 1.0 with corresponding normalized axial shortening being 1.8, 2.0 and 1.0, respectively. It can be

observed from all the three figures that the 362S studs not only have the highest elastic stiffness but also have the highest load enhancement. In Figure 4.16, due to strong axis buckling of the 800S162-43-300 stud, the axial shortening was neutralized by the elongation in the north flange. However, the slope of latter part of the plot shows that this stud had an elastic stiffness that was less than the stiffness of the other two studs that are in the comparison.

The comparison of the 600S and 800S studs with a plate thickness of 97 mils with varying brace stiffness is shown in Figures 4.17 to 4.19. It can be observed that the 800S (0x, 2.1x, and 4.3x) studs have lesser elastic stiffness and the maximum normalized axial loads attained are 2.5, 1.1, and 1.1 at corresponding normalized axial shortening of 2.5, 2.7, and 2.15, respectively. On the other hand, the 600S (0x, 1.7x, and 2.7x) studs have higher elastic stiffness and the normalized axial loads attained are 2.8, 1.2 and 1.25 at corresponding normalized axial shortenings of 1.4, 1.65, and 1.05. The 800S studs have a higher web-depth to thickness ratio than that of the 600S studs resulting in lesser elastic stiffness.

Figures 4.20 to 4.22 (362S), Figures 4.23 to 4.26 (600S), and Figures 4.27 to 4.29 (800S) show the comparison of studs with constant web-depth while varying the thicknesses. The brace-factors are maintained approximately the same in these comparisons.

Figure 4.20 compares the 362S unbraced studs with 33, 43 and 68 mil thicknesses. The failure modes were first mode flexural-torsional for all the three studs, where as the maximum normalized axial loads were 1.25, 2.6 and 1.5 at corresponding normalized axial shortenings of 1.3, 2.6 and 6.6, respectively. For the 362S braced studs (see Figure 4.21) of thicknesses 33 mils, 43 mils and 68 mil, with respective brace factors of 1.7x, 1.2x, and 1.8x, the maximum normalized axial load were 1.0, 1.4 and 1.35 at corresponding normalized axial

shortenings of 0.7, 1.75, and 1.7, respectively. In Figure 4.22, the studs had respective brace factors of 6.2x, 5.4x, and 3.3x with maximum normalized axial loads of 1.25, 1.25, and 1.5, at corresponding normalized axial shortenings of 1.2, 1.6, and 2.3, respectively.

Figure 4.23 compares the 600S studs with thicknesses of 33, 43 and 97 mils. For the unbraced studs the maximum normalized axial loads were 1.3, 1.45, and 2.85, at corresponding normalized axial shortenings of 4.1, 3.0, and 1.5, respectively. For the braced studs (see Figure 4.24) with respective brace factors of 0.2x, 0.6x, and 0.3x, the maximum normalized axial loads were 1.05, 0.85, and 1.2, at corresponding normalized axial shortenings of 3.4, 2.0, and 1.05, respectively. In Figure 4.25, the 600S studs with brace factors 1.3x, 1.6x, and 1.7x were compared, and the maximum normalized axial loads were 1.25, 1.05, and 1.25, at corresponding normalized axial shortenings of 3.1, 2.2, and 1.6, respectively. In Figure 4.26, the 600S studs with brace factors 7.4x, 3.4x, and 2.7x were compared, and the maximum normalized axial loads were 1.2, 1.05, and 1.25, at corresponding normalized axial shortenings of 3.3, 2.1, and 1.35, respectively.

For the 800S studs with 43 and 97 mil thicknesses shown in Figure 4.27, with no bracing, the normalized axial load reached maximum values of 2.0 and 2.5 at corresponding normalized axial shortenings of 3.6 and 2.5, respectively. For the braced studs with 1.3x and 1.2x, respective brace factors, the maximum normalized axial load was 0.85 and 1.05 at corresponding normalized axial shortenings of 2.1 and 1.4, respectively. Both, the 800S162-43-150 and 800S162-97-500 studs failed in distortional buckling mode. The distortional buckling prevented the stud to reach the analytically calculated fully braced capacity, in spite of the brace factor being greater than ideal bracing. When the 800S studs with respective brace factors of 2.3x and 4.3x were compared (see Figure 4.29), the maximum normalized

axial loads were 1.0 and 1.1 at corresponding normalized axial shortenings of 0.95 and 2.15, respectively.

#### 4.1.2.1 Effect of brace stiffness on axial load capacity

It can be observed from the combined plots of each series of the studs that there is a considerable enhancement in the load carrying capacity of a braced stud in comparison to an unbraced stud. Figures 4.2 to 4.9 indicate that for brace stiffnesses higher than the ideal bracing requirement, the experimental maximum loads attained remain unchanged. Table 4.6 gives both, the experimental maximum load and the percentage in crease in the axial load, which clearly indicates the load enhancement.

Figure 4.2 to 4.9 also show that the initial elastic stiffness (k) line, which was calculated using:

$$k = \frac{A_g E}{L} \quad (4.1b)$$

where  $A_g$  = Gross cross-sectional area of the cee-stud

$E$  = Young's Modulus = 29,500,000 psi

$L$  = Length of an unbraced stud = 8'-0"

The 362S125-33 studs failed by flexural-torsional buckling with flexural buckling occurring about the weak and strong axes and torsional buckling occurring about the shear center. Due to the strong axis flexural buckling, the north flange was elongating and the south flange was shortening, this in combination with the torsional buckling influenced the axial shortening and the studs hence exhibited unanticipated behavior. Beyond the ultimate capacity, these studs seem to lose load gradually. Figure 4.2 shows the plot of axial load versus axial shortening of the 362S125-33 series studs.

It can be observed from Figure 4.3 that the load-deformation behavior of 362S162-43 studs have the same slope as that of the initial elastic stiffness line up to an axial load of approximately 5200 lbs at which the unbraced stud failed. Beyond this load, the plot indicates that the braced studs begin to lose stiffness, and on reaching the ultimate load the failure is instantaneous.

In the case of 362S162-68 series studs, the load-deformation behavior, shown in Figure 4.4, seem to have an initial stiffness that is almost comparable to the initial elastic stiffness up to their ultimate capacities. There is a substantial increase in the ultimate load capacity of the braced studs over the unbraced stud and the studs failed instantaneously on reaching the ultimate load.

The 600S125-33 and 600S162-43 series studs had lower stiffness than the calculated initial elastic stiffness, which can be observed in Figures 4.5 and 4.6. In the 600S125-33 series, the under-braced stud failed by first mode flexural buckling and all the others failed by distortional buckling. In the 600S162-43 series, the unbraced stud failed in first mode flexure, and the remaining studs failed by distortional buckling. In both the series, distortional buckling seems to affect the elastic stiffness in comparison to the 362S series of studs that failed by global buckling. The load-deformation behavior of the 600S162-97 series of studs, shown in Figure 4.7, seems to have the same slope as the initial elastic stiffness line, and braced studs seem to have almost the same ultimate loads.

The 800S162-43 series of studs did not exhibit a very high load enhancement in spite of them being either ideally-braced or over-braced. Due to certain limitations in the experimental setup, two of the studs exhibited strong axis buckling that caused stretching of their north flange, which affected the measured axial shortening. When the axial load

reached a value that was critical to weak axis buckling, the stud exhibited weak axis buckling and the slope of the load-deformation plot changed sharply, which is shown in Figure 4.8. The slope of the remaining plot indicates that the studs had lesser stiffness than the initial elastic stiffness. The ultimate capacities of these studs were comparable to the calculated axial capacities. This indicates that the top and bottom supports do not have any partial restraint and the supports act like a pinned connection. This clearly indicates the requirement of an independent study on the affect of support conditions on the buckling of the cee-studs.

In the case of 800S162-97 stud group, the ultimate capacities of the braced studs are slightly greater than that of the unbraced stud. Figure 4.9 shows that the cee-studs have a lower elastic stiffness than the initial elastic stiffness.

The results of the experimental tests are tabulated in Table 4.6 which gives the maximum experimental load measured, observed failure modes and percentage increase in the axial capacity of the braced stud over the unbraced stud. It was generally observed that the maximum experimental loads are higher than the predicted capacities from AISIWIN (2002). For all the unbraced studs the predicted axial load capacity with nominal cross-section properties and nominal yield strength, in the AISIWIN (2002) program, was less than the measured maximum experimental loads. This is because the AISIWIN (2002) program considers a perfect pin-ended support condition for both flexural and torsional buckling. In the experimental investigation, the cee-studs were seated in standard track at both ends that provided end-conditions of partial fixity for weak axis flexural buckling and near full fixity for both strong axis flexural buckling and torsional buckling. These end restraints led to higher axial load capacities for the studs that failed by global buckling, i.e. flexural, flexural-torsional or torsional buckling. The 600S125-33, 600S162-43 series of studs failed by a

distortional buckling limit state at axial loads lower than those predicted by AISIWIN (2002) for a perfectly pin-ended column. This necessitates the consideration of distortional buckling as a possible controlling and critical limit state for certain stud geometries. AISIWIN does not consider the distortional buckling limit state while predicting the axial capacity of cold-formed lipped cee studs.

The enhancement in the load carrying capacity of a stud is directly related to the type of buckling failure that occurred. The percentage enhancement in the experimental load for the braced studs compared to an unbraced stud, within the same series, is given in Table 4.6. The braced studs of the 362S125-33 series attained nearly 140% more load capacity than the unbraced stud, and the buckling was mainly global second mode flexural-torsional buckling. The braced studs of the 362S162-43, 362S162-68 series showed a load increase of about 35% and 115%, respectively. Though the 600S125-33 and 600S162-43 series studs failed by distortional buckling, they exhibited an average load increase of 87%, and 34%, respectively and the 600S162-97 showed an average load increase of about 38%. The 800S series studs, both 43 and 97 mils, showed only a slight load enhancement as their experimental maximum capacities were in the range of the predicted axial capacities from AISIWIN. As discussed earlier, this indicates that the partial support fixity has reduced with increasing column depth.

#### **4.1.2.2 Effect of brace stiffness on buckling type and mode**

Figure 4.10 is a schematic diagram of the observed buckling shapes and modes of the test specimens. The abbreviations in Table 4.6 and Figure 4.10 represent: F = Flexural Buckling, T = Torsional Buckling and the digit in brackets represents the number of half-sine waves or the order of buckling mode. This figure does not include the distortional buckling mode, which may or may not be associated with the global buckling modes.

It was observed that with an increase in the brace stiffness the test specimens failed after attaining a higher order buckling mode. In some cases, under-braced studs failed at loads higher than the over-braced studs. However, in the former, the failure has been sudden and in the latter, the failure has been gradual. With increasing brace stiffness, the 362S studs exhibited flexural-torsional buckling changing from first mode to second mode. The 600S125-33 and the 600S162-43 studs failed by distortional buckling irrespective of the bracing stiffness, whereas the 600S162-97 studs failed by flexural and/or flexural-torsional buckling. The 800S studs failed by flexural, flexural-torsional and distortional buckling. Among the 33, 43 and 68 mil studs, irrespective of the total depth of the stud, local elastic buckling waves were observed in the web and distortional buckling waves were observed in the flanges. The local elastic buckling is related to the flat-widths to thickness ratio of the web and the flanges. The reader is advised to refer to Appendix A for photographs of the buckling modes for various studs.

#### **4.1.2.3 Effect of cross-sectional dimensions of cee-studs**

The 33, 43 and 68 mils studs underwent elastic local and distortional buckling at loads in the range of 10 to 25% of their ultimate capacities. On the other hand, the 97 mil studs did not show the same elastic local buckling. However local buckling was observed near the punchout, at axial deformations beyond those corresponding to the ultimate capacities and was inelastic permanent deformations. The two types of inelastic local buckling generally observed in the 600S162-97 and the 800S162-97 series were local yielding of the lip-flange junction and local distortion around the web-punchouts. The sensitivity of the member to local buckling depends upon its width-to-thickness ratio (Gotluru 2000). It has been experimentally shown by Young and Rasmussen (1999) that local buckling does not induce overall bending of fixed-fixed singly symmetric columns, as it does for pin-ended singly

symmetric columns. In the current research, the cee-studs were supported by the track at the top and bottom, and the degree of fixity offered by the track has to be ascertained. In a later section in this chapter, the effective length factor for each of the cee-studs is determined based on the analytical value of the load capacity that corresponds to the maximum experimental load achieved for each of the test specimens.

#### **4.1.2.4 Effect of experimental load on the brace stiffness and strength**

As discussed earlier, most of the unbraced studs failed at loads higher than the AISIWIN predicted capacities. The higher capacities for the studs necessitated recalculating the ideal brace stiffness as per Eq. 2.14. Table 4.7 gives the required ideal brace stiffness based on these higher load capacities of the unbraced studs. The higher load capacity would require a higher demand on the lateral bracing as given in Table 4.7. This higher demand on the bracing stiffness renders some of the braced cee-studs to fall into the category of under-braced cee-studs since the provided brace stiffness is now less than the new ideal bracing requirement. The bracing strength however remained satisfactory since the brace wires were capable of carrying the increased brace force.

It was observed in the plots of experimental load versus target brace stiffness in Figures 4.3 to 4.9 that by increasing the brace stiffness there is a gradual increase in the axial capacity of the stud. Figures 4.30 to 4.32 show an increase in capacity of the columns with a corresponding increase in target brace stiffness. The axial load carrying capacity for the 362S125-33 studs increased by 162%, for the 362S162-43 studs increased by 25.0% and for the 362S162-68 studs it increased by 129.0% while varying the brace stiffness from an unbraced stud to an over braced stud. It can also be observed in the figure that there is not much of an increase in the load carrying capacity from an ideally braced stud to an over braced stud. There was a similar increase in the 600S series of studs, for the 33, 43 and 97

mil thicknesses, with respective increases of 32%, 37%, and 40.0%. It must be made note of here that all the 33 and 43 mil studs failed by distortional buckling and that a few of them had lesser experimental maximum loads (see Table 4.6) compared to the analytical prediction of a mid-height braced stud. In the case of the 800S studs with 43 and 97 mils, there is a respective increase of 19.0% and 35% in the axial load carrying capacity.

#### **4.1.2.5 Effect of brace stiffness on lateral displacement**

For any group of cee-studs, the mid-height lateral displacement of the weak axis decreased with increasing brace stiffness, as reported by Yura (1995), which was adopted by the latest edition of the AISC-LRFD Specification (AISC 1999). The plots of axial load versus mid-height strong axis lateral displacement and weak axis lateral displacement for all the cee-studs are given in the individual test reports provided in Appendix A. Figs 4.33 to 4.35 plot the actual total bracing stiffness versus the mid-height weak axis lateral displacement for the 362s, 600s, and 800s series of studs. These plots show that with increasing brace stiffness, the mid-height lateral displacement of the weak axis decreases. In all the series of studs, there was a decrease in the mid-height lateral displacement by more than 75% from an unbraced stud to an over braced stud.

#### **4.1.2.6 Effect of brace stiffness on effective length of columns**

Table 4.8 gives the effect of total brace stiffness and the effective length factors for the cee-studs. The effective length factors were determined using a MathCAD worksheet developed by Chen (1996) for the AISI Committee on Specifications for the Design of Cold-Formed Steel Structural Members. The effective length factors  $K_x$ ,  $K_y$  and  $K_t$  were varied to arrive at a predicted load close to the experimental load capacity of each of the 37 cee-studs. It can be observed in Figures 4.36 to 4.43 that by increasing the total bracing stiffness, the effective length factor of the columns decrease. The effective length cannot be less than

0.25, hence the plots have been truncated below the limiting value of 0.25. For a column with fully fixed ends, the effective length factor is 0.5, and for such a column with fully effective mid-height bracing, the effective length factor reduces to 0.25. For most of the over-braced studs, the effective length factor was 0.25 in strong axis flexural buckling and torsional buckling. For weak axis buckling, the effective length factor is 0.5, assuming there is no partial rigidity at the supports.

#### **4.1.2.7 Effect of brace strength on axial capacity**

The brace strength, which is dependent upon the cross-sectional area of the wire and its yield stress, does not affect the buckling of the single axial column specimens because the brace forces that were generated during the testing were often less than the capacities of the brace wires. However, the yield strength of the brace wires does affect the behavior of the stud only when the brace forces reach the yield load of the brace wires. In some preliminary tests, outside the scope of the test matrix, it was observed that mild steel brace wires did not provide enough brace strength. When the brace force in the mild steel wire reached its yield capacity, the brace wire stretched at a constant brace force until failure, causing a non-linear lateral displacement. It was then decided to conduct the tests with high-strength steel wires. The steel wire had a tendency to coil and to keep it straight, a threshold brace force of approximately 2 lbs was applied to each of the four braces prior to testing.

#### **4.1.2.8 Other effects**

Among other effects are effects due to geometric imperfections, mechanical properties of the stud material, track resistance and bearing ends of the stud. The measured geometric imperfections of the test specimens are listed in Table 3.3. As per Winter (1960), the effect of initial imperfection is to increase the brace force, thus necessitating higher brace stiffness. It is stated that the stiffness required to attain “full bracing” in an imperfect column (see Eq.

2.3) exceeds that required for the ideal column (see Eq. 2.4), the more so the larger the imperfection 'd<sub>o</sub>'. Hence, the required brace stiffness is given by:

$$\beta_{\text{req}} = \beta_{\text{ideal}} \times (d_o / d + 1) \quad (4.2)$$

where  $\beta_{\text{ideal}}$  = ideal brace stiffness for perfect column

$d_o$  = measured imperfection in the stud

$d$  = deformation of the brace at the maximum brace force

The total measured brace forces at the maximum axial load for all the studs are tabulated in Table 4.9. The measured weak axis lateral displacement at the maximum axial load for all the studs is tabulated in Table 4.10. It is observed that the calculated brace forces based on the measured displacements, given in Table 4.10, are higher than the corresponding values of the measured brace forces, given in Table 4.9. This is because of the initial seating, slipping of brace wires at the loops. However compared to the global effects and at full capacities, these initial limitations are negligible. Yura (1995) had proposed that the required brace strength to be 2.0% of the nominal axial capacity of the column, as discussed earlier in Chapter 2. Table 4.9 gives the measured brace forces as a percentage of the ultimate load. It is observed that the percentage of measured brace forces ranges from as low as 0.08% to as high as 1.34% of the ultimate capacity of the cee-studs.

## 4.2 Bridging Test Results

### 4.2.1 Bridging Connection Strength and Stiffness

In the bridging connection strength and stiffness tests, three types of typical industry bridging connection specimens were fabricated and tested. The connection types and specimen details are described under Section 3.7.1 of this report. A total number of 54 specimens were tested, with 28 specimens subjected to out-of-plane loading and 26

specimens subjected to in-plane loading. In the out-of-plane loading, the load was applied parallel to the web at a distance of 11 inches away on the bridging channel (see Figure 3.13). In the in-plane loading tests, the load was applied perpendicular to the web at a distance of 11 inches away on the bridging channel (see Figure 3.14). Both the test protocols are described in Section 3.7.5 of this report. The proposed test matrix is given in Table 4.11. The results of all the experimental tests are presented in Appendix B, which is divided into two sections, with the results of the out-of-plane loading tests in one section and the results of the in-plane loading tests in another section. The data collected from the out-of-plane loading tests was used to plot (see Figures 3.11b, 3.12a, 3.15, and 4.44, for visualization):

- the applied load versus the X-direction displacement of Point A;
- the applied load versus the left screw displacement bearing on the adjacent web plate, and
- the applied load versus the right screw pull out displacement from the adjacent web plate.

The data collected from the in-plane load tests were used to generate three plots (see Figures 3.11b, 3.12b, 3.16 and 4.44 for visualization):

- the plot of the applied load versus the Y-direction displacement of Point A,
- the plot of the applied load versus the left screw bearing displacement on the adjacent web plate, and
- the plot of the applied load versus the right screw pull out displacement from the adjacent web plate.

Under both the series of tests, the ultimate load capacity of the connection was taken as the load at which there was a complete failure or at which there was sufficient deformation in the test specimen. Sufficient deformation was considered to have occurred when the measured deformation in the bridging tests, when compared to the single column axially loaded studs tests, would result in influencing the global limit states of the single column

axially loaded studs. The torsional stiffness of the connection was calculated as a secant ratio defines as ratio of ultimate load to the rotation of the connection and the flexural stiffness was calculated as the ratio of the ultimate load to the measured in-plane displacement. The rotation angle for the torsional stiffness was the angle between the initial center-line and the final center-line of the bridging channel. The X-direction displacement was used to calculate the change in angle as the inverse tangent of ratio of the measured displacement and the distance to Point A from the web of stud.

For the out-of-plane load tests, the right side displacement measured by LP-2 was used in calculating the torsional stiffness of the bridging. For the in-plane load tests, the average of the displacements measured by LP-1 and LP-2 (see Figure 4.44) was used to calculate the flexural stiffness of the bridging. The observed failure modes of the bridging systems are described later in this chapter.

As described in Chapter 3, the displacements of the clip angle and/or the web were measured using two linear potentiometers, LP-1 and LP-2, attached to the web as shown in Figure 4.44 and the displacements of the back of the web were measured using two linear potentiometers, LP-3 and LP-4. These measurements were common to both out-of-plane and in-plane loading directions and are given in Tables 4.12 and 4.14. Spatial displacement of Point A was measured, the purpose of which is described in Chapter 3. The experimental observations for each connection type and the failure mode are described in the following two sections.

#### **4.2.2 Observations of the Out-of-Plane Experimental Tests**

The observations of the out-of-plane loading tests for the three types of connections are as follows:

- SS type connection (Figure 3.9a): With the application of the out-of-plane load on the bridging channel, the eccentricity of the load created a moment on the connection. The center of rotation of the moment was at the center-line of the stud causing the right screw to pull out and the left-half of the clip-angle to bear against the web plate of the stud. The load capacity of the SS type connection increased with increasing thickness of the web as and is shown in the plots of applied load versus rotation about the center-line of the web in Figures 4.45 to 4.47. The clip-angles failed by forming multiple yield-lines. The increase in plate thickness resulted in proportional increase in the contact area of the screw and the stud causing the increase in pull out capacity.
- WW type connection (Figure 3.9b): On application of the out-of-plane load, the right half of the clip angle started to pull on the stud web, developing tension in the weld, with the left half bearing on the web. In all the tests with WW type connections, failure occurred at the connection of the clip angle to the stud web. The observed failure types are described in a subsequent section in this chapter. The plot of the applied load versus the rotation about the center-line of the web is shown in Figures 4.48 through 4.50.
- DW type connection (Figure 3.9c): In this connection type, the flange of the bridging channel was welded to the stud web at the punchout. This connection failed mainly by tearing of the weld. The plot of the applied load versus the rotation about the center-line of the web is shown in Figures 4.51 through 4.53. It can be seen from these plots, that the initial connection stiffness is not dependent upon the depth of the stud. The effect of the varying web thickness on the connection stiffness cannot be determined, since only one thickness per depth of stud was tested with the DW type connection.

The maximum loads attained and corresponding displacements measured by LP-1 are given in Table 4.12. The values of displacement given in the table were measured on the front and on the back, to the right half of the centerline of the web. The final torsional stiffness of the connection was calculated as a ratio of the maximum load to the corresponding X-direction displacement at Point A. The initial torsional stiffness was calculated as the initial slope of the load versus rotation plots shown in Figures 4.45 through 4.53. Table 4.13 gives the initial torsional stiffness of the out-of-plane loading tests, at 10% of the maximum load, calculated as the ratio of the load to the corresponding rotation. It was observed that within this load range, the initial slope of the plot was linear. For the three connection types, the plots of torsional stiffness versus the flat-width to thickness ratio are given in Figures 4.63 through 4.65. It can be observed in Figure 4.63 that for all the three

groups of studs, the slope of the trend line is nearly equal and with the increase in the flat-width to thickness ratio the stiffness of the connection drops. However, in Figure 4.64 for the WW-type connection, the stiffness increases with increase in the depth of stud, whereas the same trend is not true for the DW connection (see Figure 4.65). The DW connection has the least torsional stiffness, followed by SS type and the maximum torsional stiffness is observed in the WW type connection.

### 4.2.3 Observations of the In-Plane Experimental Tests

The observations of the in-plane loading tests for three types of connections were as follows:

- SS type connection (see Figure 3.9a): With the application of the in-plane load, the screws began to pull out. It was observed that when the clip angle deformed by forming the yield-lines between the two screws attached to the web, there was tilting of the screws. This tilting of the screw caused an increase in the pull out capacity and hence an increase in both, the connection strength and stiffness. However, at this load the connection had undergone sufficient deformation and hence failure was considered to have occurred at the load at which this stiffening effect was observed in the plot of the applied load versus the X-axis displacement. The plots of the applied load versus Y-direction displacement for the three groups of stud are shown in Figures 4.54 to 4.56.
- WW type connection (see Figure 3.9b): On application of the in-plane load, the load was transferred from the bridging channel to the clip angle and finally to the stud web through the connecting welds. In all the tests with WW type connection, the failure occurred at the connection of the clip angle to the stud web, either at the weld or the base metal. The plot of applied load versus Y-Direction displacement is given in Figures 4.57 to 4.59.
- DW type connection (see Figure 3.9c): In this connection type, the flanges of the bridging channel were welded to the web at the punchout. In this case too, the load path was from the bridging channel to the stud web across these small lengths of weld between the channel flanges. This type of connection was very strong due to the high stiffness of the stud webs and the capacity of the welds. The plot of applied load versus Y-Direction displacement is given in Figures 4.60 to 4.62.

The maximum load and the corresponding displacement of the connection measured on the front of the web by LP-1 and LP-2 are given in Table 4.14. The displacement values in

the table were measured on the left and right sides on the front of the web. The final flexural stiffness of the connection was calculated as a ratio of the maximum load to the corresponding average displacements measured by LP-1 and LP-2. The initial flexural stiffness was calculated as the initial slope of the load versus displacement plots in Figures 4.54 through 4.62. Table 4.15 gives the initial flexural stiffness at 10% of the maximum load, calculated as the ratio of the load to the corresponding Y-displacement. The 10% of the maximum load was taken since it was found that the plot of the load versus displacement was initially linear within this load range.

The plots of flexural stiffness versus the flat-width to thickness ratio are given in Figures 4.66 through 4.68 for each connection type. It can be observed that the slopes of the linear fit trend lines in Figure 4.66 are not the same for the three groups of studs and with the increasing flat-width to thickness ratio, the flexural stiffness decreases. In Figures 4.67 and 4.68 it can be observed that flexural stiffness decreases with an increase in the depth of the stud for both WW type and DW type connections. With increasing web thickness and for a constant web depth, the flexural stiffness of the SS type connection increases for a selected series of cee-stud. For a given thickness the flexural stiffness decreases with the increase in web depth. On comparing the three connection types, the SS type has the least flexural stiffness, followed by the WW type with highest being for the DW type connection.

#### **4.2.4 Observed Bridging Connection Failures**

The observed failure types in the out-of-plane loading tests and the in-plane loading tests for each of the three types of bridging connection are described below. The figures showing the failure types are given in Appendix B, and the failure types for each test specimen are given in Tables 4.12 and 4.14.

#### 4.2.4.1 SS type connection

- Single screw pull out without distortion of the clip angle: This occurred when the clip angle separated from the web plate without any bending deformation or cross-sectional distortion.
- Single screw pull out with either deformation or distortion of the clip angle: When the clip angle separated from the web plate by either bending deformation or by distorting. The bending deformation of the clip occurred in the out-of-plane tests, where the clip angle behaved as a cantilever beam subjected to a point load at the right screw, with the fixity at the left screw. For the in-plane tests, the cross-section distortion occurred when the clip angle formed a yield line in the angle leg connected to the stud web, at the level of the screws.
- Tensile failure of the screw connecting the clip angle to the stud web: The axial tension in the screws attached to the web exceeded the axial tension capacity of the screw, resulting in a sudden failure. These screws failed in the neck region.
- Shear failure of screw connecting the bridging channel to the clip angle: The failure of the connection occurred when the screw capacity in single shear of the screws attaching the clip angle to the bridging channel was exceeded.

#### 4.2.4.2 WW type connection

- Weld failure without angle distortion: In this case, tearing of the weld material between the angle and the cee-stud was observed. Connection failure occurred when the weld strength was exceeded. This was the anticipated mode of failure.
- Angle tear along the leg welded to the cee-stud: In this case, the tearing strength of the clip angle was exceeded, whereas the weld remained intact. In a few specimens, the weld thickness was greater than the design weld, and in few other specimens there was a weld return at the root of the clip angle.
- Weld separation between the clip angle and the cee-stud: The weld remained intact and stripped off with the clip angle, which indicates poor weld penetration. This is due to the galvanization of the stud, when the weld material cannot melt into the stud material.

#### 4.2.4.3 DW type connection

- Tearing of weld between the bridging channel and the cee-stud: This occurred when the load on the weld exceeded the weld strength and there was a good weld between the connected elements.
- Tearing of cee-stud web around the weld material: This occurred when there was complete weld penetration and there was block tear out of the web plate.

- Weld separation between the bridging channel and the cee-stud: The weld remained intact and stripped off with the bridging channel, which indicates poor weld penetration. This is due to the galvanization of the stud.

The summary of results for the out-of-plane load tests and in-plane load tests, giving the initial torsional stiffness and initial flexural stiffness are given in Table 4.16 and 4.17, respectively. The initial stiffnesses have been arranged based on the web depth and on the thickness of the cross-section. This table represents the same data discussed previously and is provided for convenience purposes.

### **4.3 Separation of Brace Forces in Flexural and Torsional Components**

The brace forces BF-1, BF-2, BF-3 and BF-4 were measured using load cells A, B, C, D (as shown in Figure 3.6) and are plotted against the axial load for all 36 stud tests, which are presented in Appendix A. The axially loaded braced cee-studs buckled either in flexural, torsional or flexural-torsional buckling. Due to the aforementioned configuration of the brace wires, the center of torsional buckling shifted from the shear center to the centroid of the brace forces. Flexural buckling of the stud resulted in brace forces in two brace wires on the same side of the minor axis of the stud cross-section. Torsional buckling resulted in brace forces in the brace wires that were on the diagonally opposite corners of the stud cross-section. In the case of flexural-torsional buckling there were both flexural and torsional brace forces.

The total brace force was a resultant of the flexural and the torsional components, which can be resolved as shown in Figure 4.69. The measured brace forces in the brace wires were the resultant brace force due to global buckling. At any axial load level, the measured brace force was separated into two components, namely flexural and torsional brace force components. The flexural brace force component is the brace force in the two brace wires as shown in Figure 4.69(b), which have the same magnitude and direction. The

torsional brace force component is the brace force in the two brace wires as shown in Figure 4.69(c), which have the same magnitude but opposite directions. The maximum magnitude of the flexural brace force component, the corresponding torsional brace force component and the corresponding axial load are given in Table 4.18. Similarly, the maximum magnitude of the torsional brace force component, the corresponding flexural component and the corresponding axial load are given in Table 4.19. In most specimens, the above maximum values did not occur at the same axial load, and depended upon the buckling shape and mode at the maximum axial load. The sum of maximum flexural brace force component and the corresponding torsional brace force component was compared to the sum of maximum torsional brace force component and the corresponding flexural brace force component. The greater of the two values was considered as the total maximum brace force.

The brace forces as a percentage of the axial load was computed and is given in Tables 4.18 and 4.19, and the magnitude of the brace factors are given in Table 4.5 for comparison. It is observed that from an under-braced stud to an over-braced stud in the 362S125-33, 362S162-43, 600S162-97 and 800S162-43 series, the total maximum brace force increased with the increase in the brace factor. In the case of 600S125-33 and 600S162-43 series of studs, the observed failure was mainly due to distortional buckling, resulting in brace forces that did not bear any relation to the brace factor. In the case of the 362S162-68 and 800S162-97 series, the provided brace factors were greater than the ideal requirement and hence the total maximum brace forces are almost the same.

#### **4.4 Summary of Experimental Observations**

The axial capacities of the cee-studs were determined by the AISIWIN (2002) program by considering the nominal cross-section dimensions and nominal yield stress of 33 ksi. and of 50 ksi. These values were used to calculate the ideal brace stiffness. The test matrix given

in Table 4.1 was proposed for target bracing stiffnesses less than, equal to and more than the ideal bracing stiffness, and the studs being categorized as being – under-braced, ideally-braced or over-braced. The nominal values from AISIWIN and the average as-built values of test specimen geometry and the material yield and ultimate strength are given in Tables 4.3 and 4.2B, respectively. The target brace stiffness, the total brace stiffness and the brace-factor was determined for each stud, which is given in Table 4.5. The single column axial load tests on the unbraced cee-studs showed that the predicted axial capacities were lower than the experimental maximum loads. Since the bracing stiffness and strength are functions of the axial capacity, they increase with an increase in the axial capacity. This required recalculation of the brace stiffness and modification of the test matrix as given in Table 4.2. The required brace stiffnesses and the brace-factors were determined as given in Table 4.7.

The observed failure types were broadly classified as global or local. Figure 4.10 shows the global buckling types (flexural, torsional and flexural-torsional) and modes (first and second). The local buckling types were elastic plate buckling and distortional buckling. Table 4.6 gives the buckling type and mode for each stud at failure. The bracing was not designed to prevent flexural buckling about the strong axis. The elastic waves in the web owing to local elastic plate buckling were observed in the 33, 43, 68 mils cee-studs at loads as low as 10% of the ultimate capacity. The elastic waves had a half wavelength equal to width of the web. In addition to the elastic waves, the 600S series (33, 43 mils) and the 800S series (43 mils) exhibited distortional buckling in the flanges with a half wavelength of about 18 inches. The 600S series studs with a plate thickness of 33 and 43 mils, failed by distortional buckling of the flanges. The strength prediction using AISIWIN (2002) does not consider the effect of distortional buckling, and in the case of the stud 600S125-43 with total

brace stiffness of 148 lbs/in, the analytical value was greater than the experimental maximum load. The 600S and 800S series of studs with a plate thickness of 97 mils exhibited local inelastic plate buckling at loads beyond the ultimate capacity. These studs failed by global buckling in first mode, which indicates that the brace stiffness was inadequate to force the stud to buckle in a higher mode. This may be attributed to the decrease in the resistance offered by the support because of the lower flange-width to web-depth ratio than the 362S series of studs.

Enhancement in the load carrying capacity of the cee-studs with increase in the bracing stiffness is observed in Figures 4.2 to 4.9 and in Figures 4.30 to 4.32. The mid-height lateral displacement of the weak axis decreases with increasing brace stiffness, and is shown in Figures 4.33 to 4.35, and the average of the measured value (north & south flange) as a factor of  $L/250$ , is given in Table 4.9. The column effective length factors also decrease with increasing brace stiffness and is shown in Figures 4.36 to 4.43. Table 4.9 gives the total measured brace force as a percentage of the ultimate load, which ranged from 0.08% to 1.34%.

In the bridging connection tests, for both out-of-plane loading and in-plane loading tests, the maximum load attained, corresponding displacements are given in Table 4.12 and 4.14, respectively. The initial flexural stiffness and the initial torsional stiffness were computed at 10% of the applied load and the corresponding displacement. These are given in Tables 4.13 and 4.15, respectively. Figures 4.63 through 4.68 give the initial torsional stiffness of each of the tested specimen. The summary of calculated initial stiffnesses from the bridging connection tests are given in Tables 4.16 and 4.17 for the in-plane and out-of-plane load tests.

Table 4.1 Proposed Test Matrix for the Single Column Axial Load Tests

| Series | Stud Designation |   |     |    | Unbraced Studs | Total Bracing Stiffness of Braced Studs |                         |                   |
|--------|------------------|---|-----|----|----------------|---|-------------------------|-------------------|
|        | D                | S | B   | t  |                | $< \beta_{ideal}$                       | $\approx \beta_{ideal}$ | $> \beta_{ideal}$ |
| 1      | 362              | S | 125 | 33 | X              | X                                       | X                       | X                 |
| 2      | 362              | S | 162 | 43 | X              | X                                       | X                       | X                 |
| 3      | 362              | S | 162 | 68 | X              | X                                       | X                       | X                 |
| 4      | 600              | S | 125 | 33 | X              | X                                       | X                       | X                 |
| 5      | 600              | S | 162 | 43 | X              | X                                       | X                       | X                 |
| 6      | 600              | S | 162 | 97 | X              | X                                       | X                       | X                 |
| 7      | 800              | S | 162 | 43 | X              | X                                       | X                       | X                 |
| 8      | 800              | S | 162 | 97 | X              | X                                       | X                       | X                 |

Table 4.2 Actual Test Matrix of the Single Column Axial Load Tests

| Series | Stud Designation |   |     |    | Unbraced Studs | Total Bracing Stiffness of Braced Studs |                         |                           |                     |
|--------|------------------|---|-----|----|----------------|---|-------------------------|---------------------------|---------------------|
|        | D                | S | B   | t  |                | $< \beta_{ideal}$                       | $\approx \beta_{ideal}$ | $\approx 2 \beta_{ideal}$ | $> 2 \beta_{ideal}$ |
| 1      | 362              | S | 125 | 33 | 1              | 0                                       | 1                       | 2                         | 2                   |
| 2      | 362              | S | 162 | 43 | 1              | 0                                       | 1                       | 1                         | 1                   |
| 3      | 362              | S | 162 | 68 | 1              | 0                                       | 0                       | 1                         | 2                   |
| 4      | 600              | S | 125 | 33 | 1              | 1                                       | 1                       | 0                         | 1                   |
| 5      | 600              | S | 162 | 43 | 2              | 2                                       | 0                       | 1                         | 1                   |
| 6      | 600              | S | 162 | 97 | 1              | 2                                       | 0                       | 1                         | 1                   |
| 7      | 800              | S | 162 | 43 | 1              | 1                                       | 1                       | 1                         | 0                   |
| 8      | 800              | S | 162 | 97 | 1              | 0                                       | 1                       | 1                         | 1                   |



Table 4.4 Average As-built Properties of the Test Specimens Using AISIWIN Program

| Stud Designation |   |     |     | Tension Coupon Test Results |                 | AISIWIN               |                                      |                 |  |                 | Required Ideal Brace Stiffness |
|------------------|---|-----|-----|-----------------------------|-----------------|-----------------------|--------------------------------------|-----------------|--|-----------------|--------------------------------|
|                  |   |     |     | Yield Stress                | Ultimate Stress | As-Built Section Area | As-Built Ultimate Capacity ( $P_u$ ) |                 | As-Built Unfactored Capacity ( $P_n$ ) |                 | $\beta_{ideal}$                |
|                  |   |     |     | $F_y$                       | $F_u$           |                       | Unbraced                             | Mid-Point Brace | No Brace                               | Mid-Point Brace |                                |
| D                | S | B   | t   | ksi                         | ksi             | in <sup>2</sup>       | lbs                                  | lbs             | lbs                                    | lbs             | lb/in.                         |
| 362              | S | 125 | 33  | 48.53                       | 55.48           | 0.2028                | 704                                  | 1978            | 828                                    | 2327            | 97                             |
| 362              | S | 162 | 43  | 47.04                       | 58.20           | 0.3089                | 1688                                 | 4411            | 1986                                   | 5189            | 216                            |
| 362              | S | 162 | 68  | 52.01                       | 67.80           | 0.5154                | 3515                                 | 8448            | 4135                                   | 9939            | 414                            |
| 600              | S | 125 | 33  | 24.03                       | 45.24           | 0.2537                | 592                                  | 1548            | 696                                    | 1821            | 76                             |
| 600              | S | 162 | 43  | 46.24                       | 54.88           | 0.4135                | 2156                                 | 5832            | 2536                                   | 6861            | 286                            |
| 600              | S | 162 | 43a | 50.30                       | 59.38           | 0.4346                | 2465                                 | 6721            | 2900                                   | 7907            | 329                            |
| 600              | S | 162 | 97  | 60.20                       | 70.21           | 0.9807                | 6277                                 | 19888           | 7385                                   | 23398           | 975                            |
| 800              | S | 162 | 43  | 40.23                       | 54.90           | 0.4829                | 1967                                 | 5180            | 2314                                   | 6094            | 254                            |
| 800              | S | 162 | 97  | 42.50                       | 67.49           | 1.1843                | 6686                                 | 17989           | 7866                                   | 21164           | 882                            |

AISIWIN program was used to calculate the As-Built values of the test specimens  
Ideal Brace Stiffness was obtained using Yura's Bracing Equation 2.14 (Yura 1995)  
Design factor used in calculating the Unfactored Capacity is 0.85

Table 4.5 Calculated Brace Stiffness and Total Brace Stiffness of the Test Specimens

| Stud Designation |   |     |    |    | Target<br>Brace<br>Stiffness | Wire  |                 |       |      | Actual<br>Stiffness<br>per Wire | AISIWIN<br>Unfactored<br>Load $P_n$ | Total<br>Brace<br>Stiffness | Ideal<br>Brace<br>Stiffness | Brace<br>Factor    |
|------------------|---|-----|----|----|------------------------------|-------|-----------------|-------|------|---------------------------------|-------------------------------------|-----------------------------|-----------------------------|--------------------|
|                  |   |     |    |    |                              | Dia.  | Area            | L     | Nos. |                                 |                                     |                             |                             | $\beta_{provided}$ |
| D                | S | B   | t  | ID | lbs/in.                      | in.   | in <sup>2</sup> | in.   |      | lb/in                           | lbs                                 | lb/in                       | lbs/in                      | $\beta_{ideal}$    |
| 362              | S | 125 | 33 | 1  | 200                          | 0.016 | 0.000201        | 56.50 | 2    | 206                             | 2327                                | 413                         | 97                          | 4.3                |
| 362              | S | 125 | 33 | 2  | 400                          | 0.016 | 0.000201        | 30.50 | 2    | 382                             | 2327                                | 765                         | 97                          | 7.9                |
| 362              | S | 125 | 33 | 3  | 100                          | 0.016 | 0.000201        | 60.75 | 1    | 96                              | 2327                                | 192                         | 97                          | 2.0                |
| 362              | S | 125 | 33 | 4  | 100                          | 0.016 | 0.000201        | 60.75 | 1    | 96                              | 2327                                | 192                         | 97                          | 2.0                |
| 362              | S | 125 | 33 | 5  | 0                            | 0     | 0.000000        | 0     | 0    | 0                               | 828                                 | Not Braced                  |                             |                    |
| 362              | S | 125 | 33 | 6  | 100                          | 0.016 | 0.000201        | 58.00 | 1    | 101                             | 2327                                | 201                         | 99                          | 1.9                |
| 362              | S | 162 | 43 | 1  | 0                            |       |                 |       |      |                                 | 1986                                | Not Braced                  |                             |                    |
| 362              | S | 162 | 43 | 2  | 200                          | 0.024 | 0.000452        | 70.75 | 1    | 185                             | 5189                                | 371                         | 216                         | 1.7                |
| 362              | S | 162 | 43 | 3  | 800                          | 0.024 | 0.000452        | 35.50 | 2    | 739                             | 5189                                | 1478                        | 216                         | 6.8                |
| 362              | S | 162 | 43 | 4  | 400                          | 0.024 | 0.000452        | 35.75 | 1    | 367                             | 5189                                | 734                         | 216                         | 3.4                |
| 362              | S | 162 | 68 | 2  | 1000                         | 0.033 | 0.000855        | 24.25 | 1    | 1023                            | 9939                                | 2046                        | 414                         | 4.9                |
| 362              | S | 162 | 68 | 3  | 500                          | 0.033 | 0.000855        | 48.50 | 1    | 511                             | 9939                                | 1023                        | 414                         | 2.5                |
| 362              | S | 162 | 68 | 4  | 750                          | 0.033 | 0.000855        | 32.25 | 1    | 769                             | 9939                                | 1538                        | 414                         | 3.7                |
| 362              | S | 162 | 68 | 5  | 0                            |       |                 |       |      | 0                               | 4135                                | Not Braced                  |                             |                    |

Table 4.5 (Continued) Calculated Brace Stiffness and Total Brace Stiffness of the Test Specimens

| Stud Designation |   |     |    |    | Target<br>Brace<br>Stiffness | Wire   |                 |       |      | Actual<br>Stiffness<br>per Wire | AISIWIN<br>Unfactored<br>Load $P_n$ | Total<br>Brace<br>Stiffness | Ideal<br>Brace<br>Stiffness | Brace<br>Factor    |
|------------------|---|-----|----|----|------------------------------|--------|-----------------|-------|------|---------------------------------|-------------------------------------|-----------------------------|-----------------------------|--------------------|
|                  |   |     |    |    |                              | Dia.   | Area            | L     | Nos. |                                 |                                     |                             |                             | $\beta_{provided}$ |
| D                | S | B   | t  | ID | lbs/in.                      | in.    | in <sup>2</sup> | in.   |      | lb/in                           | lbs                                 | lb/in                       | lbs/in                      | $\beta_{ideal}$    |
| 600              | S | 125 | 33 | 1  | 200                          | 0.016  | 0.000201        | 29.00 | 1    | 201                             | 1821                                | 402                         | 76                          | 5.3                |
| 600              | S | 125 | 33 | 2  | 0                            |        |                 |       |      | 0                               | 696                                 | Not Braced                  |                             |                    |
| 600              | S | 125 | 33 | 3  | 60                           | 0.01   | 0.000079        | 37.00 | 1    | 62                              | 1821                                | 123                         | 76                          | 1.6                |
| 600              | S | 125 | 33 | 4  | 30                           | 0.01   | 0.000079        | 75.00 | 1    | 30                              | 1821                                | 61                          | 76                          | 0.8                |
| 600              | S | 162 | 43 | 1  | 250                          | 0.024  | 0.000452        | 52.75 | 1    | 249                             | 6861                                | 497                         | 286                         | 1.7                |
| 600              | S | 162 | 43 | 2  | 75                           | 0.016  | 0.000201        | 79.00 | 1    | 74                              | 6861                                | 148                         | 286                         | 0.5                |
| 600              | S | 162 | 43 | 4  | 500                          | 0.024  | 0.000452        | 26.50 | 1    | 495                             | 6861                                | 990                         | 286                         | 3.5                |
| 600              | S | 162 | 43 | 5  | 30                           | 0.01   | 0.000079        | 75.25 | 1    | 30                              | 6861                                | 61                          | 286                         | 0.2                |
| 600              | S | 162 | 43 | 6  | 0                            |        |                 |       |      | 0                               | 2536                                | Not Braced                  |                             |                    |
| 600              | S | 162 | 43 | 6a | 0                            |        |                 |       |      | 0                               | 2900                                | Not Braced                  |                             |                    |
| 600              | S | 162 | 97 | 1  | 1000                         | 0.0625 | 0.003068        | 86.00 | 1    | 1035                            | 23398                               | 2069                        | 975                         | 2.1                |
| 600              | S | 162 | 97 | 2  | 1500                         | 0.0625 | 0.003068        | 53.00 | 1    | 1679                            | 23398                               | 3357                        | 975                         | 3.4                |
| 600              | S | 162 | 97 | 3  | 500                          | 0.0348 | 0.000951        | 53.00 | 1    | 520                             | 23398                               | 1041                        | 975                         | 1.1                |
| 600              | S | 162 | 97 | 4  | 160                          | 0.024  | 0.000452        | 81.00 | 1    | 162                             | 23398                               | 324                         | 975                         | 0.3                |
| 600              | S | 162 | 97 | 5  | 0                            |        |                 |       |      | 0                               | 7385                                | Not Braced                  |                             |                    |
| 800              | S | 162 | 43 | 2  | 75                           | 0.016  | 0.000201        | 78.25 | 1    | 75                              | 6094                                | 149                         | 254                         | 0.6                |
| 800              | S | 162 | 43 | 3  | 150                          | 0.016  | 0.000201        | 39.00 | 1    | 150                             | 6094                                | 299                         | 254                         | 1.2                |
| 800              | S | 162 | 43 | 4  | 0                            |        |                 |       |      | 0                               | 2314                                | Not Braced                  |                             |                    |
| 800              | S | 162 | 43 | 5  | 300                          | 0.016  | 0.000201        | 38.75 | 2    | 301                             | 6094                                | 602                         | 254                         | 2.4                |
| 800              | S | 162 | 97 | 1  | 1000                         | 0.0625 | 0.003068        | 85.00 | 1    | 1047                            | 21164                               | 2093                        | 882                         | 2.4                |
| 800              | S | 162 | 97 | 2  | 500                          | 0.0348 | 0.000951        | 53.00 | 1    | 520                             | 21164                               | 1041                        | 882                         | 1.2                |
| 800              | S | 162 | 97 | 3  | 0                            |        |                 |       |      | 0                               | 7866                                | Not Braced                  |                             |                    |
| 800              | S | 162 | 97 | 4  | 2100                         | 0.0475 | 0.001772        | 24.50 | 1    | 2098                            | 21164                               | 4195                        | 882                         | 4.8                |

Table 4.6 Summary of Experimental Test Results for Test Specimens

| Stud Designation |   |     |    |    | Target<br>Brace<br>Stiffness | Axial Capacity |                 |                      | Observed<br>Failure<br>Mode | Increase in<br>$P_{max}$ of<br>Braced<br>over<br>Unbraced<br>Studs |
|------------------|---|-----|----|----|------------------------------|----------------|-----------------|----------------------|-----------------------------|--|
|                  |   |     |    |    |                              | Analytical     |                 | Experimental<br>Load |                             |  |
|                  |   |     |    |    |                              | No<br>Brace    | Mid-Pt<br>Brace |                      |                             |  |
| D                |   | B   | t  | ID | lbs/in.                      | $P_n$ (lbs)    | $P_n$ (lbs)     | $P_{max}$ (lbs)      |                             | %  |
| 362              | S | 125 | 33 | 5  | 0                            | 828            | -               | 1127                 | F[1] - T[1]                 | 0.00   |
| 362              | S | 125 | 33 | 3  | 100                          | -              | 2327            | 2749                 | F[2] - T[2]                 | 143.80   |
| 362              | S | 125 | 33 | 4  | 100                          | -              | 2327            | 2306                 | F[2] - T[2]                 | 104.51   |
| 362              | S | 125 | 33 | 6  | 100                          | -              | 2327            | 2399                 | Distortional                | 112.79   |
| 362              | S | 125 | 33 | 1  | 200                          | -              | 2327            | 3012                 | F[2]                        | 167.17   |
| 362              | S | 125 | 33 | 2  | 400                          | -              | 2327            | 2959                 | F[2] - T[2]                 | 162.47   |
| 362              | S | 162 | 43 | 1  | 0                            | 1986           | -               | 5223                 | T[1] - F[1]                 | 0.00   |
| 362              | S | 162 | 43 | 2  | 200                          | -              | 5189            | 7268                 | F[1] - T[2]                 | 39.15  |
| 362              | S | 162 | 43 | 4  | 400                          | -              | 5189            | 7029                 | F[1] - T[2]                 | 34.58  |
| 362              | S | 162 | 43 | 3  | 800                          | -              | 5189            | 6557                 | T[2]                        | 25.54  |
| 362              | S | 162 | 68 | 5  | 0                            | 4135           | -               | 6451                 | F[1] - T[1]                 | 0.00   |
| 362              | S | 162 | 68 | 3  | 500                          | -              | 9939            | 13384                | T[1] - F[1]                 | 107.47   |
| 362              | S | 162 | 68 | 4  | 750                          | -              | 9939            | 14029                | T[2]                        | 117.47   |
| 362              | S | 162 | 68 | 2  | 1000                         | -              | 9939            | 14792                | T[2]                        | 129.30   |
| 600              | S | 125 | 33 | 2  | 0                            | 696            | -               | 984                  | Distortional                | 0.00   |
| 600              | S | 125 | 33 | 4  | 30                           | -              | 1821            | 1951                 | F[1]                        | 98.27  |
| 600              | S | 125 | 33 | 3  | 60                           | -              | 1821            | 2271                 | Distortional                | 130.79   |
| 600              | S | 125 | 33 | 1  | 200                          | -              | 1821            | 1302                 | Distortional                | 32.32  |
| 600              | S | 162 | 43 | 6  | 0                            | 2536           | -               | 5144                 | Distortional                | 0.00   |
| 600              | S | 162 | 43 | 6a | 0                            | 2900           | -               | 4258                 | F[1]                        | 0.00   |
| 600              | S | 162 | 43 | 5  | 30                           | -              | 6861            | 7163                 | Distortional                | 39.25  |
| 600              | S | 162 | 43 | 2  | 75                           | -              | 6861            | 6052                 | Distortional                | 17.65  |
| 600              | S | 162 | 43 | 1  | 250                          | -              | 6861            | 7308                 | Distortional                | 42.07  |
| 600              | S | 162 | 43 | 4  | 500                          | -              | 6861            | 7075                 | Distortional                | 37.54  |
| 600              | S | 162 | 97 | 5  | 0                            | 7385           | -               | 21029                | F[1]                        | 0.00   |
| 600              | S | 162 | 97 | 4  | 160                          | -              | 23398           | 28306                | F[1] - T[1]                 | 34.60  |
| 600              | S | 162 | 97 | 3  | 500                          | -              | 23398           | 30085                | F[1] - T[1]                 | 43.06  |
| 600              | S | 162 | 97 | 1  | 1000                         | -              | 23398           | 28553                | T[1]                        | 35.78  |
| 600              | S | 162 | 97 | 2  | 1500                         | -              | 23398           | 29472                | T[1]                        | 40.15  |
| 800              | S | 162 | 43 | 4  | 0                            | 2314           | -               | 4591                 | F[1]                        | 0.00   |
| 800              | S | 162 | 43 | 2  | 75                           | -              | 6094            | 4306                 | F[1]                        | -6.21  |
| 800              | S | 162 | 43 | 3  | 150                          | -              | 6094            | 5333                 | Distortional                | 16.16  |
| 800              | S | 162 | 43 | 5  | 300                          | -              | 6094            | 6213                 | F[2]                        | 35.33  |
| 800              | S | 162 | 97 | 3  | 0                            | 7866           | -               | 19703                | F[1]                        | 0.00   |
| 800              | S | 162 | 97 | 2  | 500                          | -              | 21164           | 21626                | Distortional                | 9.76   |
| 800              | S | 162 | 97 | 1  | 1000                         | -              | 21164           | 23811                | Distortional                | 20.85  |
| 800              | S | 162 | 97 | 4  | 2100                         | -              | 21164           | 23537                | T[1]                        | 19.46  |

Table 4.7 Required Brace Stiffness Based on  $P_{max}$ 

| Stud Designation |   |     |    |    | Total Brace Stiffness | Brace Factor       | AISIWIN Unfactored Load | Experimental Load | Required Total Stiffness | Brace Factor       |
|------------------|---|-----|----|----|-----------------------|--------------------|-------------------------|-------------------|--------------------------|--------------------|
|                  |   |     |    |    | $\beta_{provided}$    | $\beta_{provided}$ | $P_n$                   | $P_{max}$         | $\beta_{required}$       | $\beta_{provided}$ |
| D                | S | B   | t  | ID | lbs/in.               | $\beta_{ideal}$    | lbs                     | lbs               | lbs/in.                  | $\beta_{required}$ |
| 362              | S | 125 | 33 | 5  | 0                     | -                  | 828                     | 1127              | -                        | -                  |
| 362              | S | 162 | 43 | 1  | 0                     | -                  | 1986                    | 5223              | -                        | -                  |
| 362              | S | 162 | 68 | 5  | 0                     | -                  | 4135                    | 6451              | -                        | -                  |
| 600              | S | 125 | 33 | 2  | 0                     | -                  | 696                     | 984               | -                        | -                  |
| 600              | S | 162 | 43 | 6  | 0                     | -                  | 2536                    | 5144              | -                        | -                  |
| 600              | S | 162 | 43 | 6a | 0                     | -                  | 2900                    | 4258              | -                        | -                  |
| 600              | S | 162 | 97 | 5  | 0                     | -                  | 7385                    | 21029             | -                        | -                  |
| 800              | S | 162 | 43 | 4  | 0                     | -                  | 2314                    | 4591              | -                        | -                  |
| 800              | S | 162 | 97 | 3  | 0                     | -                  | 7866                    | 19703             | -                        | -                  |
| 600              | S | 125 | 33 | 4  | 61                    | 0.8                | 1821                    | 1951              | 81                       | 0.7                |
| 600              | S | 162 | 43 | 5  | 61                    | 0.2                | 6861                    | 7163              | 298                      | 0.2                |
| 600              | S | 162 | 43 | 2  | 148                   | 0.5                | 6861                    | 6052              | 252                      | 0.6                |
| 600              | S | 162 | 97 | 4  | 324                   | 0.3                | 23398                   | 28306             | 1179                     | 0.3                |
| 800              | S | 162 | 43 | 2  | 149                   | 0.6                | 6094                    | 4306              | 179                      | 0.8                |
| 600              | S | 125 | 33 | 3  | 123                   | 1.6                | 1821                    | 2271              | 95                       | 1.3                |
| 600              | S | 162 | 97 | 3  | 1041                  | 1.1                | 23398                   | 30085             | 1254                     | 0.8                |
| 800              | S | 162 | 43 | 3  | 299                   | 1.2                | 6094                    | 5333              | 222                      | 1.3                |
| 800              | S | 162 | 97 | 2  | 1041                  | 1.2                | 21164                   | 21626             | 901                      | 1.2                |
| 362              | S | 125 | 33 | 3  | 192                   | 2.0                | 2327                    | 2749              | 115                      | 1.7                |
| 362              | S | 125 | 33 | 4  | 192                   | 2.0                | 2327                    | 2306              | 96                       | 2.0                |
| 362              | S | 125 | 33 | 6  | 201                   | 1.9                | 2327                    | 2399              | 100                      | 2.0                |
| 362              | S | 162 | 43 | 2  | 371                   | 1.7                | 5189                    | 7268              | 303                      | 1.2                |
| 362              | S | 162 | 68 | 3  | 1023                  | 2.5                | 9939                    | 13384             | 558                      | 1.8                |
| 600              | S | 162 | 43 | 1  | 497                   | 1.7                | 6861                    | 7308              | 305                      | 1.6                |
| 600              | S | 162 | 97 | 1  | 2069                  | 2.1                | 23398                   | 28553             | 1190                     | 1.7                |
| 800              | S | 162 | 43 | 5  | 602                   | 2.4                | 6094                    | 6213              | 259                      | 2.3                |
| 800              | S | 162 | 97 | 1  | 2093                  | 2.4                | 21164                   | 23811             | 992                      | 2.1                |
| 362              | S | 125 | 33 | 1  | 413                   | 4.3                | 2327                    | 3012              | 126                      | 3.3                |
| 362              | S | 125 | 33 | 2  | 765                   | 7.9                | 2327                    | 2959              | 123                      | 6.2                |
| 362              | S | 162 | 43 | 4  | 734                   | 3.4                | 5189                    | 7029              | 293                      | 2.5                |
| 362              | S | 162 | 43 | 3  | 1478                  | 6.8                | 5189                    | 6557              | 273                      | 5.4                |
| 362              | S | 162 | 68 | 4  | 1538                  | 3.7                | 9939                    | 14029             | 585                      | 2.6                |
| 362              | S | 162 | 68 | 2  | 2046                  | 4.9                | 9939                    | 14792             | 616                      | 3.3                |
| 600              | S | 125 | 33 | 1  | 402                   | 5.3                | 1821                    | 1302              | 54                       | 7.4                |
| 600              | S | 162 | 43 | 4  | 990                   | 3.5                | 6861                    | 7075              | 295                      | 3.4                |
| 600              | S | 162 | 97 | 2  | 3357                  | 3.4                | 23398                   | 29472             | 1228                     | 2.7                |
| 800              | S | 162 | 97 | 4  | 4195                  | 4.8                | 21164                   | 23537             | 981                      | 4.3                |

Table 4.8 Effective Length Factors Based on  $P_{max}$ 

| Stud Designation |   |     |    |    | Total<br>Brace<br>Stiffness | Observed<br>Failure<br>Mode | Effective Length Factors based<br>on $P_{max}$ |       |       |       |
|------------------|---|-----|----|----|-----------------------------|-----------------------------|--|-------|-------|-------|
|                  |   |     |    |    |                             |                             | $\beta_{provided}$                             | $K_x$ | $K_y$ | $K_t$ |
| D                | S | B   | t  | ID | lbs/in.                     |                             |  |       |       | lbs   |
| 362              | S | 125 | 33 | 5  | 0                           | F[1] - T[1]                 | 0.50   | 0.67  | 0.64  | 1127  |
| 362              | S | 125 | 33 | 3  | 192                         | F[2] - T[2]                 | 0.50   | 0.25  | 0.25  | 2749  |
| 362              | S | 125 | 33 | 4  | 192                         | F[2] - T[2]                 | 0.50   | 0.36  | 0.34  | 2306  |
| 362              | S | 125 | 33 | 6  | 201                         | Distortional                | 0.50   | 0.33  | 0.31  | 2399  |
| 362              | S | 125 | 33 | 1  | 413                         | F[2]                        | 0.50   | 0.25  | 0.25  | 3012  |
| 362              | S | 125 | 33 | 2  | 765                         | F[2] - T[2]                 | 0.50   | 0.25  | 0.25  | 2959  |
| 362              | S | 162 | 43 | 1  | 0                           | T[1] - F[1]                 | 0.50   | 0.52  | 0.43  | 5223  |
| 362              | S | 162 | 43 | 2  | 371                         | F[1] - T[2]                 | 0.50   | 0.25  | 0.25  | 7268  |
| 362              | S | 162 | 43 | 4  | 734                         | F[1] - T[2]                 | 0.50   | 0.25  | 0.25  | 7029  |
| 362              | S | 162 | 43 | 3  | 1478                        | T[2]                        | 0.50   | 0.25  | 0.25  | 6557  |
| 362              | S | 162 | 68 | 5  | 0                           | F[1] - T[1]                 | 0.50   | 0.69  | 0.62  | 6451  |
| 362              | S | 162 | 68 | 3  | 1023                        | T[1] - F[1]                 | 0.50   | 0.25  | 0.25  | 13384 |
| 362              | S | 162 | 68 | 4  | 1538                        | T[2]                        | 0.50   | 0.25  | 0.25  | 14029 |
| 362              | S | 162 | 68 | 2  | 2046                        | T[2]                        | 0.50   | 0.25  | 0.25  | 14792 |
| 600              | S | 125 | 33 | 2  | 0                           | Distortional                | 0.50   | 0.80  | 0.96  | 984   |
| 600              | S | 125 | 33 | 4  | 61                          | F[1]                        | 0.50   | 0.45  | 0.52  | 1951  |
| 600              | S | 125 | 33 | 3  | 123                         | Distortional                | 0.50   | 0.32  | 0.37  | 2271  |
| 600              | S | 125 | 33 | 1  | 402                         | Distortional                | 0.50   | 0.68  | 0.80  | 1302  |
| 600              | S | 162 | 43 | 6  | 0                           | Distortional                | 0.50   | 0.65  | 0.70  | 5144  |
| 600              | S | 162 | 43 | 6a | 0                           | F[1]                        | 0.50   | 0.80  | 0.85  | 4258  |
| 600              | S | 162 | 43 | 5  | 61                          | Distortional                | 0.50   | 0.47  | 0.49  | 7163  |
| 600              | S | 162 | 43 | 2  | 148                         | Distortional                | 0.50   | 0.57  | 0.60  | 6052  |
| 600              | S | 162 | 43 | 1  | 497                         | Distortional                | 0.50   | 0.46  | 0.47  | 7308  |
| 600              | S | 162 | 43 | 4  | 990                         | Distortional                | 0.50   | 0.48  | 0.50  | 7075  |
| 600              | S | 162 | 97 | 5  | 0                           | F[1]                        | 0.50   | 0.54  | 0.65  | 21029 |
| 600              | S | 162 | 97 | 4  | 324                         | F[1] - T[1]                 | 0.50   | 0.39  | 0.45  | 28306 |
| 600              | S | 162 | 97 | 3  | 1041                        | F[1] - T[1]                 | 0.50   | 0.35  | 0.40  | 30085 |
| 600              | S | 162 | 97 | 1  | 2069                        | T[1]                        | 0.50   | 0.39  | 0.44  | 28553 |
| 600              | S | 162 | 97 | 2  | 3357                        | T[1]                        | 0.50   | 0.37  | 0.41  | 29472 |
| 800              | S | 162 | 43 | 4  | 0                           | F[1]                        | 0.50   | 0.66  | 0.77  | 4591  |
| 800              | S | 162 | 43 | 2  | 149                         | F[1]                        | 0.50   | 0.69  | 0.80  | 4306  |
| 800              | S | 162 | 43 | 3  | 299                         | Distortional                | 0.50   | 0.58  | 0.67  | 5333  |
| 800              | S | 162 | 43 | 5  | 602                         | F[2]                        | 0.50   | 0.48  | 0.56  | 6213  |
| 800              | S | 162 | 97 | 3  | 0                           | F[1]                        | 0.50   | 0.52  | 0.66  | 19703 |
| 800              | S | 162 | 97 | 2  | 1041                        | Distortional                | 0.50   | 0.46  | 0.58  | 21626 |
| 800              | S | 162 | 97 | 1  | 2093                        | Distortional                | 0.50   | 0.39  | 0.48  | 23811 |
| 800              | S | 162 | 97 | 4  | 4195                        | T[1]                        | 0.50   | 0.40  | 0.49  | 23537 |

Table 4.9 Measured Values of Brace Force and Mid-height Displacement at  $P_{max}$

| Stud Designation |   |     |    |    | Target<br>Brace<br>Stiffness | Experimental<br>Load | Measured<br>Initial<br>Bow | Measured Values at $P_{max}$ |                |                                    |         | $P_{br}$ as<br>% of<br>$P_{max}$ | Average<br>$\Delta_w$ in<br>terms of<br>L/250 |
|------------------|---|-----|----|----|------------------------------|----------------------|----------------------------|------------------------------|----------------|------------------------------------|---------|----------------------------------|---|
|                  |   |     |    |    |                              |                      |                            | $P_{max}$                    | Brace<br>Force | Weak Axis Displacement, $\Delta_w$ |         |                                  |   |
|                  |   |     |    |    |                              | $P_{br}$             |                            |                              | N-Flange       | S-<br>Flange                       | Average |                                  |   |
| D                | S | B   | t  | ID | lbs/in.                      | lbs                  | in.                        | lbs                          | in.            | in.                                | in.     | %                                |   |
| 362              | S | 125 | 33 | 5  | 0                            | 1127                 | 0.000                      | -                            | 0.4065         | 0.8289                             | 0.618   | -                                | 1.61  |
| 362              | S | 125 | 33 | 3  | 100                          | 2749                 | 0.000                      | 9.55                         | 0.0835         | 0.0661                             | 0.075   | 0.35                             | 0.19  |
| 362              | S | 125 | 33 | 4  | 100                          | 2306                 | 0.000                      | 22.41                        | 0.1577         | 0.0006                             | 0.079   | 0.97                             | 0.21  |
| 362              | S | 125 | 33 | 6  | 100                          | 2399                 | 0.000                      | 14.47                        | 0.0099         | 0.1561                             | 0.083   | 0.60                             | 0.22  |
| 362              | S | 125 | 33 | 1  | 200                          | 3012                 | 0.000                      | 10.55                        | 0.0173         | 0.0451                             | 0.031   | 0.35                             | 0.08  |
| 362              | S | 125 | 33 | 2  | 400                          | 2959                 | 0.000                      | 32.43                        | 0.0906         | 0.1925                             | 0.142   | 1.10                             | 0.37  |
| 362              | S | 162 | 43 | 1  | 0                            | 5223                 | 0.000                      | -                            | 0.8281         | 0.0845                             | 0.456   | -                                | 1.19  |
| 362              | S | 162 | 43 | 2  | 200                          | 7268                 | 0.000                      | 19.37                        | 0.1007         | 0.0411                             | 0.071   | 0.27                             | 0.18  |
| 362              | S | 162 | 43 | 4  | 400                          | 7029                 | 0.000                      | 39.07                        | 0.0815         | 0.0324                             | 0.057   | 0.56                             | 0.15  |
| 362              | S | 162 | 43 | 3  | 800                          | 6557                 | 0.010                      | 34.67                        | 0.0852         | -0.0246                            | 0.055   | 0.53                             | 0.08  |
| 362              | S | 162 | 68 | 5  | 0                            | 6451                 | 0.100                      | -                            | 2.8548         | -0.2529                            | 1.554   | -                                | 3.39  |
| 362              | S | 162 | 68 | 3  | 500                          | 13384                | -0.155                     | 159.31                       | 0.4032         | -0.0366                            | 0.220   | 1.19                             | 0.48  |
| 362              | S | 162 | 68 | 4  | 750                          | 14029                | 0.140                      | 131.92                       | 0.1315         | 0.0118                             | 0.072   | 0.94                             | 0.19  |
| 362              | S | 162 | 68 | 2  | 1000                         | 14792                | -0.187                     | 144.26                       | 0.0644         | 0.1814                             | 0.123   | 0.98                             | 0.32  |
| 600              | S | 125 | 33 | 2  | 0                            | 984                  | 0.130                      | -                            | 0.7034         | 0.2548                             | 0.479   | -                                | 1.25  |
| 600              | S | 125 | 33 | 4  | 30                           | 1951                 | 0.075                      | 25.05                        | 0.6312         | 0.2406                             | 0.436   | 1.28                             | 1.14  |
| 600              | S | 125 | 33 | 3  | 60                           | 2271                 | 0.120                      | 11.86                        | -0.1936        | -0.0529                            | 0.123   | 0.52                             | -0.32   |
| 600              | S | 125 | 33 | 1  | 200                          | 1302                 | 0.100                      | 1.10                         | -0.0146        | -0.0208                            | 0.018   | 0.08                             | -0.05   |

Table 4.9 (Continued) Measured Values of Brace Force and Mid-height Displacement at  $P_{max}$

| Stud Designation |   |     |    |    | Target<br>Brace<br>Stiffness | Experimental<br>Load | Measured<br>Initial<br>Bow | Measured Values at $P_{max}$ |                        |         |       | $P_{br}$ as<br>Percentage<br>of $P_{max}$ | Average<br>$\Delta_w$ in<br>terms of<br>L/250 |
|------------------|---|-----|----|----|------------------------------|----------------------|----------------------------|------------------------------|------------------------|---------|-------|---|---|
|                  |   |     |    |    |                              |                      |                            | Brace<br>Force               | Weak Axis Displacement |         |       |   |   |
|                  |   |     |    |    |                              | $P_{br}$             |                            | N-Flange                     | S-Flange               | Average | %     |   |   |
| D                | S | B   | t  | ID | lbs/in.                      | lbs                  | in.                        | lbs                          | in.                    | in.     | in.   | %   |   |
| 600              | S | 162 | 43 | 6  | 0                            | 5144                 | 0.015                      | -                            | 0.3305                 | 0.2255  | 0.278 | -   | 0.72  |
| 600              | S | 162 | 43 | 6a | 0                            | 4258                 | 0.090                      | -                            | -1.0398                | -0.9219 | 0.981 | -   | -2.55   |
| 600              | S | 162 | 43 | 5  | 30                           | 7163                 | 0.075                      | 15.51                        | 0.0298                 | -0.4001 | 0.215 | 0.22                                      | -0.48   |
| 600              | S | 162 | 43 | 2  | 75                           | 6052                 | -                          | 57.49                        | 1.0127                 | 0.0393  | 0.526 | 0.95                                      | 1.37  |
| 600              | S | 162 | 43 | 1  | 250                          | 7308                 | -                          | 7.43                         | -0.0378                | -0.0064 | 0.022 | 0.10                                      | -0.06   |
| 600              | S | 162 | 43 | 4  | 500                          | 7075                 | -                          | 14.85                        | 0.0238                 | 0.0102  | 0.017 | 0.21                                      | 0.04  |
| 600              | S | 162 | 97 | 5  | 0                            | 21029                | -                          | -                            | -0.1614                | -0.9538 | 0.558 | -   | -1.45   |
| 600              | S | 162 | 97 | 4  | 160                          | 28306                | -                          | 45.23                        | 0.0961                 | -0.1869 | 0.142 | 0.16                                      | -0.12   |
| 600              | S | 162 | 97 | 3  | 500                          | 30085                | 0.000                      | 137.53                       | -0.3179                | 0.0125  | 0.165 | 0.46                                      | -0.40   |
| 600              | S | 162 | 97 | 1  | 1000                         | 28553                | 0.110                      | 171.51                       | -0.3955                | -0.0472 | 0.221 | 0.60                                      | -0.58   |
| 600              | S | 162 | 97 | 2  | 1500                         | 29472                | 0.110                      | 154.42                       | -0.0220                | -0.2422 | 0.132 | 0.52                                      | -0.34   |
| 800              | S | 162 | 43 | 4  | 0                            | 4591                 | 0.000                      | -                            | -0.4082                | -0.8840 | 0.646 | -   | -1.68   |
| 800              | S | 162 | 43 | 2  | 75                           | 4306                 | -                          | 24.69                        | -0.0027                | 0.4608  | 0.232 | 0.57                                      | 0.60  |
| 800              | S | 162 | 43 | 3  | 150                          | 5333                 | 0.120                      | 71.52                        | 0.3110                 | -0.2260 | 0.269 | 1.34                                      | 0.11  |
| 800              | S | 162 | 43 | 5  | 300                          | 6213                 | 0.000                      | 16.81                        | -0.0482                | -0.0811 | 0.065 | 0.27                                      | -0.17   |
| 800              | S | 162 | 97 | 3  | 0                            | 19703                | 0.000                      | -                            | 0.4080                 | 0.3385  | 0.373 | -   | 0.97  |
| 800              | S | 162 | 97 | 2  | 500                          | 21626                | 0.000                      | 85.60                        | 0.1250                 | 0.2550  | 0.190 | 0.40                                      | 0.49  |
| 800              | S | 162 | 97 | 1  | 1000                         | 23811                | 0.000                      | 115.45                       | 0.2014                 | 0.1889  | 0.195 | 0.48                                      | 0.51  |
| 800              | S | 162 | 97 | 4  | 2100                         | 23537                | 0.000                      | 69.64                        | 0.2314                 | 0.0723  | 0.152 | 0.30                                      | 0.40  |

Table 4.10 Calculated Values of Brace Force and Mid-height Displacement at  $P_{max}$

| Stud Designation |   |     |    |    | Target<br>Brace<br>Stiffness | Experimental<br>Load | Measured<br>Initial<br>Bow | Measured Weak Axis<br>Displacement at $P_{max}$ |          | Calculated Brace Force for<br>Measured Weak Axis<br>Displacement |          |       | $P_{br}$ as<br>% of<br>$P_{max}$ |
|------------------|---|-----|----|----|------------------------------|----------------------|----------------------------|---|----------|--|----------|-------|----------------------------------|
|                  |   |     |    |    |                              | $P_{max}$            |                            | N-Flange  | S-Flange | N-Flange   | S-Flange | Total |                                  |
| D                | S | B   | t  | ID | lbs/in.                      | lbs                  | in.                        | in.   | in.      | lbs  | lbs      | lbs   | %                                |
| 362              | S | 125 | 33 | 5  | 0                            | 1127                 | 0.000                      | 0.4065  | 0.8289   | -  | -        |       |                                  |
| 362              | S | 125 | 33 | 3  | 100                          | 2749                 | 0.000                      | 0.0835  | 0.0661   | 9.6  | 7.6      | 17.1  | 0.62                             |
| 362              | S | 125 | 33 | 4  | 100                          | 2306                 | 0.000                      | 0.1577  | 0.0006   | 15.2   | 0.1      | 15.2  | 0.66                             |
| 362              | S | 125 | 33 | 6  | 100                          | 2399                 | 0.000                      | 0.0099  | 0.1561   | 1.0  | 15.6     | 16.6  | 0.69                             |
| 362              | S | 125 | 33 | 1  | 200                          | 3012                 | 0.000                      | 0.0173  | 0.0451   | 2.2  | 5.7      | 7.8   | 0.26                             |
| 362              | S | 125 | 33 | 2  | 400                          | 2959                 | 0.000                      | 0.0906  | 0.1925   | 11.2   | 23.7     | 34.9  | 1.18                             |
| 362              | S | 162 | 43 | 1  | 0                            | 5223                 | 0.000                      | 0.8281  | 0.0845   | -  | -        |       |                                  |
| 362              | S | 162 | 43 | 2  | 200                          | 7268                 | 0.000                      | 0.1007  | 0.0411   | 30.5   | 12.5     | 43.0  | 0.59                             |
| 362              | S | 162 | 43 | 4  | 400                          | 7029                 | 0.000                      | 0.0815  | 0.0324   | 23.9   | 9.5      | 33.4  | 0.47                             |
| 362              | S | 162 | 43 | 3  | 800                          | 6557                 | 0.010                      | 0.0852  | -0.0246  | 26.0   | 4.0      | 30.0  | 0.46                             |
| 362              | S | 162 | 68 | 5  | 0                            | 6451                 | 0.100                      | 2.8548  | -0.2529  | -  | -        |       |                                  |
| 362              | S | 162 | 68 | 3  | 500                          | 13384                | -0.155                     | 0.4032  | -0.0366  | 138.4  | 106.9    | 245.3 | 1.83                             |
| 362              | S | 162 | 68 | 4  | 750                          | 14029                | 0.140                      | 0.1315  | 0.0118   | 158.7  | 88.8     | 247.5 | 1.76                             |
| 362              | S | 162 | 68 | 2  | 1000                         | 14792                | -0.187                     | 0.0644  | 0.1814   | 75.6   | 3.5      | 79.0  | 0.53                             |
| 600              | S | 125 | 33 | 2  | 0                            | 984                  | 0.130                      | 0.7034  | 0.2548   | -  | -        |       |                                  |
| 600              | S | 125 | 33 | 4  | 30                           | 1951                 | 0.075                      | 0.6312  | 0.2406   | 57.4   | 25.7     | 83.1  | 4.26                             |
| 600              | S | 125 | 33 | 3  | 60                           | 2271                 | 0.120                      | -0.1936   | -0.0529  | 7.0  | 6.3      | 13.3  | 0.59                             |
| 600              | S | 125 | 33 | 1  | 200                          | 1302                 | 0.100                      | -0.0146   | -0.0208  | 4.6  | 4.3      | 8.9   | 0.69                             |

Table 4.10 (Continued) Calculated Values of Brace Force and Mid-height Displacement at  $P_{max}$

| Stud Designation |   |     |    |    | Target<br>Brace<br>Stiffness | Experimental<br>Load | Measured<br>Initial<br>Bow | Measured Weak<br>Axis Displacement<br>at $P_{max}$ |              | Calculated Brace Force for<br>Measured Weak Axis<br>Displacement |              |       | $P_{br}$ as %<br>of $P_{max}$ |
|------------------|---|-----|----|----|------------------------------|----------------------|----------------------------|--|--------------|--|--------------|-------|-------------------------------|
|                  |   |     |    |    |                              | $P_{max}$            |                            | N-<br>Flange                                       | S-<br>Flange | N-<br>Flange   | S-<br>Flange | Total |                               |
| D                | S | B   | t  | ID | lbs/in.                      | lbs                  | in.                        | in.  | in.          | lbs  | lbs          | lbs   | %                             |
| 600              | S | 125 | 33 | 2  | 0                            | 984                  | 0.130                      | 0.7034   | 0.2548       | -  | -            |       |                               |
| 600              | S | 125 | 33 | 4  | 30                           | 1951                 | 0.075                      | 0.6312   | 0.2406       | 57.4   | 25.7         | 83.1  | 4.26                          |
| 600              | S | 125 | 33 | 3  | 60                           | 2271                 | 0.120                      | -0.1936  | -0.0529      | 7.0  | 6.3          | 13.3  | 0.59                          |
| 600              | S | 125 | 33 | 1  | 200                          | 1302                 | 0.100                      | -0.0146  | -0.0208      | 4.6  | 4.3          | 8.9   | 0.69                          |
| 600              | S | 162 | 43 | 6  | 0                            | 5144                 | 0.000                      | 0.3305   | 0.2255       | -  | -            |       |                               |
| 600              | S | 162 | 43 | 6a | 0                            | 4258                 | -0.036                     | -1.0398  | -0.9219      | -  | -            |       |                               |
| 600              | S | 162 | 43 | 5  | 30                           | 7163                 | 0.000                      | 0.0298   | -0.4001      | 8.9  | 119.4        | 128.3 | 1.79                          |
| 600              | S | 162 | 43 | 2  | 75                           | 6052                 | 0.030                      | 1.0127   | 0.0393       | 262.9  | 17.5         | 280.4 | 4.63                          |
| 600              | S | 162 | 43 | 1  | 250                          | 7308                 | 0.040                      | -0.0378  | -0.0064      | 0.7  | 10.2         | 10.9  | 0.15                          |
| 600              | S | 162 | 43 | 4  | 500                          | 7075                 | 0.000                      | 0.0238   | 0.0102       | 7.0  | 3.0          | 10.0  | 0.14                          |
| 600              | S | 162 | 97 | 5  | 0                            | 21029                | 0.015                      | -0.1614  | -0.9538      | -  | -            |       |                               |
| 600              | S | 162 | 97 | 4  | 160                          | 28306                | 0.075                      | 0.0961   | -0.1869      | 201.8  | 220.4        | 422.2 | 1.49                          |
| 600              | S | 162 | 97 | 3  | 500                          | 30085                | -                          | -0.3179  | 0.0125       | 398.6  | 15.7         | 414.3 | 1.38                          |
| 600              | S | 162 | 97 | 1  | 1000                         | 28553                | -                          | -0.3955  | -0.0472      | 470.5  | 56.1         | 526.6 | 1.84                          |
| 600              | S | 162 | 97 | 2  | 1500                         | 29472                | -                          | -0.0220  | -0.2422      | 27.0   | 297.4        | 324.4 | 1.10                          |

Table 4.10 (Continued) Calculated Values of Brace Force and Mid-height Displacement at  $P_{max}$

| Stud Designation |   |     |    |    | Target<br>Brace<br>Stiffness | Experimental<br>Load | Measured<br>Initial<br>Bow | Measured Weak<br>Axis Displacement<br>at $P_{max}$ |              | Calculated Brace Force for<br>Measured Weak Axis<br>Displacement |              |       | $P_{br}$ as %<br>of $P_{max}$ |
|------------------|---|-----|----|----|------------------------------|----------------------|----------------------------|--|--------------|--|--------------|-------|-------------------------------|
|                  |   |     |    |    |                              | $P_{max}$            |                            | N-<br>Flange                                       | S-<br>Flange | N-<br>Flange   | S-<br>Flange | Total |                               |
| D                | S | B   | t  | ID | lbs/in.                      | lbs                  | in.                        | in.  | in.          | lbs  | lbs          | lbs   | %                             |
| 800              | S | 162 | 43 | 4  | 0                            | 4591                 | 0.110                      | -0.4082  | -0.8840      | -  | -            |       |                               |
| 800              | S | 162 | 43 | 2  | 75                           | 4306                 | 0.090                      | -0.0027  | 0.4608       | 15.7   | 82.7         | 98.3  | 2.28                          |
| 800              | S | 162 | 43 | 3  | 150                          | 5333                 | 0.110                      | 0.3110   | -0.2260      | 93.5   | 25.8         | 119.3 | 2.24                          |
| 800              | S | 162 | 43 | 5  | 300                          | 6213                 | 0.000                      | -0.0482  | -0.0811      | 12.5   | 21.0         | 33.5  | 0.54                          |
| 800              | S | 162 | 97 | 3  | 0                            | 19703                | -                          | 0.4080   | 0.3385       | -  | -            |       |                               |
| 800              | S | 162 | 97 | 2  | 500                          | 21626                | -                          | 0.1250   | 0.2550       | 112.6  | 229.8        | 342.4 | 1.58                          |
| 800              | S | 162 | 97 | 1  | 1000                         | 23811                | -                          | 0.2014   | 0.1889       | 199.8  | 187.4        | 387.2 | 1.63                          |
| 800              | S | 162 | 97 | 4  | 2100                         | 23537                | 0.120                      | 0.2314   | 0.0723       | 344.6  | 188.5        | 533.2 | 2.27                          |

Table 4.11 Proposed Test Matrix for Bridging Connection Tests

| Specimen Type | Stud Designation |   |     |    |   |    | Number of Tests |          |
|---------------|------------------|---|-----|----|---|----|-----------------|----------|
|               | D                | S | B   | t  | N | C  | Out-of-Plane    | In-Plane |
| 1             | 362              | S | 125 | 33 | 1 | SS | 2               | 2        |
| 2             | 362              | S | 162 | 43 | 1 | SS | 2               | 2        |
| 3             | 362              | S | 162 | 68 | 1 | SS | 2               | 2        |
| 4             | 362              | S | 162 | 68 | 1 | WW | 2               | 2        |
| 5             | 362              | S | 162 | 68 | 1 | DW | 2               | 2        |
| 6             | 600              | S | 125 | 33 | 1 | SS | 2               | 2        |
| 7             | 600              | S | 162 | 43 | 1 | SS | 2               | 2        |
| 8             | 600              | S | 162 | 97 | 3 | SS | 2               | 2        |
| 9             | 600              | S | 162 | 97 | 1 | WW | 2               | 2        |
| 10            | 600              | S | 162 | 97 | 1 | DW | 2               | 2        |
| 11            | 800              | S | 162 | 43 | 1 | SS | 2               | 2        |
| 12            | 800              | S | 162 | 97 | 1 | SS | 2               | 2        |
| 13            | 800              | S | 162 | 97 | 1 | WW | 2               | 2        |
| 14            | 800              | S | 162 | 97 | 1 | DW | 2               | 2        |

Table 4.12 Bridging Test Results for Out-of-Plane Loading

| Stud Designation |   |     |    |   |    | Applied Load     | Displacement       |                   | Final Torsional Stiffness | Failure Types                   |
|------------------|---|-----|----|---|----|------------------|--------------------|-------------------|---------------------------|---------------------------------|
|                  |   |     |    |   |    |                  | R <sub>FRONT</sub> | R <sub>BACK</sub> |                           |                                 |
|                  |   |     |    |   |    | T <sub>max</sub> | Δ <sub>RB</sub>    | Δ <sub>RF</sub>   | K <sub>T</sub>            |                                 |
| D                | S | B   | t  | N | C  | lbs.             | in.                | in.               | lbs./in.                  |                                 |
| 362              | S | 125 | 33 | 1 | SS | 57.37            | 0.184              | -0.008            | 311                       | Screw Pullout                   |
| 362              | S | 125 | 33 | 2 | SS | 71.10            | 0.208              | -0.005            | 342                       | Screw Pullout                   |
| 362              | S | 162 | 43 | 1 | SS | 69.19            | 0.073              | 0.014             | 945                       | Screw Pullout, Angle Distortion |
| 362              | S | 162 | 43 | 2 | SS | 63.05            | 0.098              | 0.002             | 640                       | Screw Pullout, Angle Distortion |
| 362              | S | 162 | 68 | 1 | SS | 128.91           | 0.067              | 0.003             | 1925                      | Screw Pullout, Angle Distortion |
| 362              | S | 162 | 68 | 2 | SS | 102.39           | 0.059              | -0.002            | 1731                      | Screw Pullout, Angle Distortion |
| 362              | S | 162 | 68 | 1 | WW | 138.81           | 0.028              | 0.009             | 4908                      | Angle Tear                      |
| 362              | S | 162 | 68 | 2 | WW | 150.23           | 0.031              | 0.008             | 4917                      | Angle Tear                      |
| 362              | S | 162 | 68 | 1 | DW | 166.15           | 0.04               | 0.027             | 4491                      | Weld Failure                    |
| 362              | S | 162 | 68 | 2 | DW | 149.83           | 0.036              | 0.031             | 4149                      | Weld Failure                    |
| 600              | S | 125 | 33 | 1 | SS | 113.91           | 0.31               | 0.024             | 370                       | Screw Pullout                   |
| 600              | S | 125 | 33 | 2 | SS | 83.59            | 0.200              | 0.019             | 418                       | Screw Pullout                   |
| 600              | S | 162 | 43 | 1 | SS | 66.09            | 0.109              | -0.008            | 605                       | Screw Pullout, Angle Distortion |
| 600              | S | 162 | 43 | 2 | SS | 137.95           | 0.202              | -0.009            | 682                       | Screw Pullout                   |
| 600              | S | 162 | 97 | 3 | SS | 280.33           | 0.061              | 0.001             | 4564                      | Screw Pullout                   |
| 600              | S | 162 | 97 | 4 | SS | 272.34           | 0.067              | 0.002             | 4094                      | Screw Pullout                   |
| 600              | S | 162 | 97 | 1 | WW | 380.67           | 0.044              | 0.014             | 8747                      | Angle Tear                      |
| 600              | S | 162 | 97 | 2 | WW | 421.57           | 0.067              | 0.021             | 6276                      | Angle Tear                      |
| 600              | S | 162 | 97 | 1 | DW | 199.59           | 0.047              | 0.041             | 4267                      | Weld Failure                    |
| 600              | S | 162 | 97 | 2 | DW | 156.88           | 0.042              | 0.019             | 3753                      | Weld Failure                    |
| 800              | S | 162 | 43 | 1 | SS | 161.23           | 0.150              | 0.002             | 1075                      | Screw Pullout, Angle Distortion |
| 800              | S | 162 | 43 | 2 | SS | 145.14           | 0.129              | 0.000             | 1128                      | Screw Pullout, Angle Distortion |
| 800              | S | 162 | 97 | 1 | SS | 255.75           | 0.029              | 0.004             | 8735                      | Screw Shear Failure             |
| 800              | S | 162 | 97 | 2 | SS | 273.51           | 0.039              | 0.003             | 7049                      | Screw Shear Failure             |
| 800              | S | 162 | 97 | 1 | WW | 291.13           | 0.015              | 0.002             | 20036                     | Weld Failure, Angle Distortion  |
| 800              | S | 162 | 97 | 2 | WW | 388.28           | 0.026              | 0.014             | 14797                     | Weld Failure, Angle Distortion  |
| 800              | S | 162 | 97 | 1 | DW | 207.52           | 0.038              | 0.030             | 5503                      | Weld Separation                 |
| 800              | S | 162 | 97 | 2 | DW | 162.02           | 0.031              | 0.020             | 5272                      | -                               |

Table 4.13 Initial Torsional Stiffness of the Lower Bound Values of Out-of-Plane Tests

| Stud Designation |   |     |    |   |    | Initial Load at 10% of $T_{max}$ ( $T_{10}$ ) | Experimental X-Displacement ( $\Delta$ ) | Rotation ( $\Phi=\Delta/I_a$ ) | Initial Slope ( $T_{10}^*I_a/\Phi$ ) | Flat-width at Hole ( $w-d_h$ ) | Flat-width to Thickness Ratio | Slenderness Factor ( $\lambda$ ) |
|------------------|---|-----|----|---|----|---|--|--------------------------------|--------------------------------------|--------------------------------|-------------------------------|----------------------------------|
| D                | S | B   | t  | N | C  | lbs.  | in.                                      | rad.                           | kip-in/rad.                          | in.                            | ( $w-d_h$ )/t                 | ( $w-d_h/t$ )/ $\sqrt{(f_y/E)}$  |
| 362              | S | 125 | 33 | 2 | SS | 7.18  | 0.294                                    | 0.027                          | 2.95                                 | 1.90                           | 57.71                         | 2.34                             |
| 362              | S | 125 | 33 | 1 | SS | 5.45  | 0.165                                    | 0.015                          | 4.00                                 | 1.90                           | 57.71                         | 2.34                             |
| 362              | S | 162 | 43 | 1 | SS | 7.31  | 0.166                                    | 0.015                          | 5.33                                 | 1.89                           | 44.06                         | 1.76                             |
| 362              | S | 162 | 43 | 2 | SS | 7.35  | 0.126                                    | 0.011                          | 7.04                                 | 1.89                           | 44.06                         | 1.76                             |
| 362              | S | 162 | 68 | 1 | SS | 12.79   | 0.112                                    | 0.010                          | 13.88                                | 1.79                           | 26.25                         | 1.10                             |
| 362              | S | 162 | 68 | 2 | SS | 10.42   | 0.080                                    | 0.007                          | 15.72                                | 1.79                           | 26.25                         | 1.10                             |
| 600              | S | 125 | 33 | 2 | SS | 8.86  | 0.153                                    | 0.014                          | 7.02                                 | 4.28                           | 129.83                        | 3.71                             |
| 600              | S | 125 | 33 | 1 | SS | 11.01   | 0.185                                    | 0.017                          | 7.20                                 | 4.28                           | 129.83                        | 3.71                             |
| 600              | S | 162 | 43 | 1 | SS | 6.81  | 0.039                                    | 0.004                          | 21.04                                | 4.27                           | 99.41                         | 3.94                             |
| 600              | S | 162 | 43 | 2 | SS | 15.60   | 0.078                                    | 0.007                          | 24.08                                | 4.27                           | 99.41                         | 3.94                             |
| 600              | S | 162 | 97 | 3 | SS | 32.91   | 0.127                                    | 0.012                          | 31.38                                | 4.02                           | 41.44                         | 1.87                             |
| 600              | S | 162 | 97 | 4 | SS | 31.24   | 0.087                                    | 0.008                          | 43.60                                | 4.02                           | 41.44                         | 1.87                             |

Table 4.13 (Continued) Initial Torsional Stiffness of the Lower Bound Values from the Out-of-Plane Tests

| Stud Designation |   |     |    |   |    | Initial Load at 10% of $T_{max}$ ( $T_{10}$ ) | Experimental X-Displacement ( $\Delta$ ) | Rotation ( $\Phi=\Delta/l_a$ ) | Initial Slope ( $T_{10}^*l_a/\Phi$ ) | Flat-width at Hole ( $w-d_h$ ) | Flat-width to Thickness Ratio | Slenderness Factor ( $\lambda$ )  |
|------------------|---|-----|----|---|----|---|--|--------------------------------|--------------------------------------|--------------------------------|-------------------------------|-----------------------------------|
| D                | S | B   | t  | N | C  | lbs.  | in.                                      | rad.                           | kip-in/rad.                          | in.                            | ( $w-d_h$ )/t                 | ( $w-d_h/t$ )<br>$\sqrt{(f_v/E)}$ |
| 800              | S | 162 | 43 | 2 | SS | 13.22   | 0.031                                    | 0.003                          | 51.41                                | 6.27                           | 145.92                        | 5.39                              |
| 800              | S | 162 | 43 | 1 | SS | 31.77   | 0.064                                    | 0.006                          | 60.32                                | 6.27                           | 145.92                        | 5.39                              |
| 800              | S | 162 | 97 | 2 | SS | 28.30   | 0.049                                    | 0.004                          | 70.32                                | 6.02                           | 62.06                         | 2.36                              |
| 800              | S | 162 | 97 | 1 | SS | 29.99   | 0.046                                    | 0.004                          | 78.95                                | 6.02                           | 62.06                         | 2.36                              |
| 362              | S | 162 | 68 | 1 | WW | 11.03   | 0.018                                    | 0.002                          | 75.79                                | 1.79                           | 26.25                         | 1.06                              |
| 362              | S | 162 | 68 | 2 | WW | 13.51   | 0.016                                    | 0.001                          | 99.27                                | 1.79                           | 26.25                         | 1.06                              |
| 600              | S | 162 | 97 | 2 | WW | 49.88   | 0.031                                    | 0.003                          | 197.38                               | 4.02                           | 41.44                         | 1.68                              |
| 600              | S | 162 | 97 | 1 | WW | 41.71   | 0.024                                    | 0.002                          | 211.10                               | 4.02                           | 41.44                         | 1.68                              |
| 800              | S | 162 | 97 | 2 | WW | 132.07  | 0.068                                    | 0.006                          | 236.61                               | 6.02                           | 62.06                         | 2.52                              |
| 800              | S | 162 | 97 | 1 | WW | 144.52  | 0.056                                    | 0.005                          | 314.45                               | 6.02                           | 62.06                         | 2.52                              |
| 362              | S | 162 | 68 | 2 | DW | 21.84   | 0.091                                    | 0.008                          | 28.89                                | 2.06                           | 30.25                         | 1.23                              |
| 362              | S | 162 | 68 | 1 | DW | 21.40   | 0.080                                    | 0.007                          | 32.40                                | 2.06                           | 30.25                         | 1.23                              |
| 600              | S | 162 | 97 | 2 | DW | 21.67   | 0.100                                    | 0.009                          | 26.31                                | 4.41                           | 45.44                         | 1.84                              |
| 600              | S | 162 | 97 | 1 | DW | 22.02   | 0.100                                    | 0.009                          | 26.72                                | 4.41                           | 45.44                         | 1.84                              |
| 800              | S | 162 | 97 | 2 | DW | 14.12   | 0.095                                    | 0.009                          | 18.04                                | 6.41                           | 66.06                         | 2.68                              |
| 800              | S | 162 | 97 | 1 | DW | 21.26   | 0.093                                    | 0.008                          | 27.58                                | 6.41                           | 66.06                         | 2.68                              |

Note: Elastic Modulus = 29500.0 ksi.  
 Lever Arm for Moment = 11.0 in.  
 Width of punchout = 1.5 in.

Table 4.14 Bridging Test Results for In-Plane Loading

| Stud Designation |   |     |    |   |    | Applied Load     | Displacement of    |                    | Flexural Stiffness | Failure Type                    |
|------------------|---|-----|----|---|----|------------------|--------------------|--------------------|--------------------|---------------------------------|
|                  |   |     |    |   |    |                  | L <sub>FRONT</sub> | R <sub>FRONT</sub> |                    |                                 |
| D                | S | B   | t  | N | C  | F <sub>max</sub> | Δ <sub>LF</sub>    | Δ <sub>RF</sub>    | K <sub>F</sub>     |                                 |
|                  |   |     |    |   |    | lbs.             | in.                | in.                | lbs./in.           |                                 |
| 362              | S | 125 | 33 | 3 | SS | 391.94           | 0.219              | 0.229              | 1752               | Screw Pullout                   |
| 362              | S | 125 | 33 | 4 | SS | 431.48           | 0.321              | 0.174              | 1743               | Screw Pullout                   |
| 362              | S | 162 | 43 | 3 | SS | 545.56           | 0.130              | 0.088              | 5005               | Screw Pullout, Angle Distortion |
| 362              | S | 162 | 43 | 4 | SS | 448.67           | 0.100              | 0.089              | 4755               | Screw Pullout, Angle Distortion |
| 362              | S | 162 | 68 | 3 | SS | 937.28           | 0.087              | 0.092              | 10496              | Angle Distortion                |
| 362              | S | 162 | 68 | 4 | SS | 889.78           | 0.092              | 0.054              | 12225              | Angle Distortion, Screw Tension |
| 362              | S | 162 | 68 | 3 | WW | 1503.76          | 0.118              | 0.127              | 12263              | Weld Failure                    |
| 362              | S | 162 | 68 | 4 | WW | 1462.17          | 0.121              | 0.127              | 11817              | Angle Tear                      |
| 362              | S | 162 | 68 | 3 | DW | 3064.03          | 0.31               | 0.307              | 9883               | Block Shear Rupture of Web      |
| 362              | S | 162 | 68 | 4 | DW | 2642.63          | 0.349              | 0.401              | 7054               | Block Shear Rupture of Web      |
| 600              | S | 125 | 33 | 3 | SS | 425.80           | 0.29               | 0.223              | 1658               | Screw Pullout                   |
| 600              | S | 125 | 33 | 4 | SS | 302.94           | 0.174              | 0.186              | 1684               | Screw Pullout                   |
| 600              | S | 162 | 43 | 4 | SS | 640.80           | 0.131              | 0.125              | 5001               | Screw Pullout                   |
| 600              | S | 162 | 43 | 5 | SS | 587.06           | 0.214              | 0.381              | 5001               | Screw Pullout                   |
| 600              | S | 162 | 97 | 1 | SS | 1514.38          | 0.131              | 0.147              | 10902              | Angle Distortion, Screw Tension |
| 600              | S | 162 | 97 | 2 | SS | 1172.38          | 0.105              | 0.130              | 9996               | Angle Distortion, Screw Tension |
| 600              | S | 162 | 97 | 3 | WW | 1169.53          | 0.163              | 0.200              | 6444               | Weld Failure                    |
| 600              | S | 162 | 97 | 4 | WW | 1653.71          | 0.212              | 0.230              | 7477               | Angle Tear                      |
| 600              | S | 162 | 97 | 3 | DW | -                | -                  | -                  | -                  | -                               |
| 600              | S | 162 | 97 | 4 | DW | 3159.07          | 0.469              | 0.464              | 6772               | -                               |
| 800              | S | 162 | 43 | 3 | SS | 275.60           | 0.073              | 0.093              | 3307               | Screw Pullout                   |
| 800              | S | 162 | 43 | 4 | SS | 522.66           | 0.137              | 0.151              | 3632               | Screw Tension                   |
| 800              | S | 162 | 97 | 3 | SS | 1402.04          | 0.064              | 0.030              | 29965              | Screw Tension                   |
| 800              | S | 162 | 97 | 4 | SS | 1719.25          | 0.221              | 0.427              | 5303               | Screw Tension                   |
| 800              | S | 162 | 97 | 3 | WW | 1238.18          | 0.143              | 0.148              | 8493               | Angle Tear                      |
| 800              | S | 162 | 97 | 4 | WW | 1101.97          | 0.151              | 0.111              | 8417               | Angle Tear                      |
| 800              | S | 162 | 97 | 3 | DW | 2908.04          | 0.526              | 0.553              | 5390               | Weld Failure                    |
| 800              | S | 162 | 97 | 4 | DW | -                | -                  | -                  | -                  | -                               |

Table 4.15 Initial Flexural Stiffness of the In-Plane Tests

| Stud Designation |   |     |    |   |    | Initial Load at<br>10% of $F_{max}$<br>( $F_{10}$ ) | Experimental<br>Y-Displacement<br>( $D$ ) | Initial Flexural<br>Stiffness ( $F_{10}/\Delta$ ) | Flat-width to<br>Thickness<br>Ratio | Slenderness<br>Factor ( $\lambda$ ) |
|------------------|---|-----|----|---|----|---|---|---|-------------------------------------|-------------------------------------|
| D                | S | B   | t  | N | C  | lbs.  | in.                                       | kip/in.   | $(w-d_h)/t$                         | $(w-d_h/t) \sqrt{f_y/E}$            |
| 362              | S | 125 | 33 | 4 | SS | 45.25   | 0.027                                     | 1.68  | 57.71                               | 2.34                                |
| 362              | S | 125 | 33 | 3 | SS | 46.65   | 0.023                                     | 2.07  | 57.71                               | 2.34                                |
| 362              | S | 162 | 43 | 3 | SS | 52.00   | 0.015                                     | 3.57  | 44.06                               | 1.76                                |
| 362              | S | 162 | 43 | 4 | SS | 44.26   | 0.011                                     | 4.20  | 44.06                               | 1.76                                |
| 362              | S | 162 | 68 | 3 | SS | 104.77  | 0.017                                     | 6.10  | 26.25                               | 1.10                                |
| 362              | S | 162 | 68 | 4 | SS | 104.83  | 0.013                                     | 7.94  | 26.25                               | 1.10                                |
| 600              | S | 125 | 33 | 4 | SS | 30.21   | 0.030                                     | 1.00  | 129.83                              | 3.71                                |
| 600              | S | 125 | 33 | 3 | SS | 44.59   | 0.039                                     | 1.14  | 129.83                              | 3.71                                |
| 600              | S | 162 | 43 | 4 | SS | 69.11   | 0.018                                     | 3.78  | 99.41                               | 3.94                                |
| 600              | S | 162 | 43 | 3 | SS | 58.36   | 0.015                                     | 3.82  | 99.41                               | 3.94                                |
| 600              | S | 162 | 97 | 1 | SS | 149.64  | 0.027                                     | 5.57  | 41.44                               | 1.87                                |
| 600              | S | 162 | 97 | 2 | SS | 370.12  | 0.054                                     | 6.86  | 41.44                               | 1.87                                |
| 800              | S | 162 | 43 | 4 | SS | 99.58   | 0.048                                     | 2.07  | 145.92                              | 5.39                                |
| 800              | S | 162 | 43 | 3 | SS | 156.23  | 0.063                                     | 2.46  | 145.92                              | 5.39                                |
| 800              | S | 162 | 97 | 3 | SS | 124.78  | 0.018                                     | 7.08  | 62.06                               | 2.36                                |

Table 4.15 (Continued) Initial Flexural Stiffness of the In-Plane Tests

| Stud Designation |   |     |    |   |    | Initial Load<br>at 10% of<br>$F_{max}$ ( $F_{10}$ ) | Experimental<br>Y-Displacement<br>( $D$ ) | Initial Flexural<br>Stiffness ( $F_{10}/\Delta$ ) | Flat-width to<br>Thickness<br>Ratio | Slenderness<br>Factor ( $\lambda$ ) |
|------------------|---|-----|----|---|----|---|---|---|-------------------------------------|-------------------------------------|
| D                | S | B   | t  | N | C  | lbs.  | in.                                       | kip/in.   | ( $w-d_h$ )/ $t$                    | ( $w-d_h/t$ ) $\sqrt{(f_y/E)}$      |
| 800              | S | 162 | 97 | 4 | SS | 172.05  | 0.058                                     | 2.95  | 62.06                               | 2.36                                |
| 362              | S | 162 | 68 | 4 | WW | 137.82  | 0.005                                     | 30.42   | 26.25                               | 1.06                                |
| 362              | S | 162 | 68 | 3 | WW | 183.14  | 0.004                                     | 40.79   | 26.25                               | 1.06                                |
| 600              | S | 162 | 97 | 3 | WW | 109.88  | 0.007                                     | 16.52   | 41.44                               | 1.68                                |
| 600              | S | 162 | 97 | 4 | WW | 95.25   | 0.006                                     | 15.24   | 41.44                               | 1.68                                |
| 800              | S | 162 | 97 | 4 | WW | 114.06  | 0.011                                     | 10.51   | 62.06                               | 2.52                                |
| 800              | S | 162 | 97 | 3 | WW | 178.58  | 0.009                                     | 19.67   | 62.06                               | 2.52                                |
| 362              | S | 162 | 68 | 3 | DW | 378.77  | 0.008                                     | 45.36   | 30.25                               | 1.23                                |
| 362              | S | 162 | 68 | 4 | DW | 206.19  | 0.004                                     | 50.41   | 30.25                               | 1.23                                |
| 600              | S | 162 | 97 | 3 | DW | 363.78  | 0.044                                     | 8.26  | 45.44                               | 1.84                                |
| 600              | S | 162 | 97 | 4 | DW | -   | -   | -   | -                                   | -                                   |
| 800              | S | 162 | 97 | 3 | DW | 364.75  | 0.152                                     | 2.40  | 66.06                               | 2.68                                |
| 800              | S | 162 | 97 | 4 | DW | -   | -   | -   | -                                   | -                                   |

Note: Elastic Modulus = 29500.0 ksi.  
 Lever Arm for Moment = 11.0 in.  
 Width of punchout = 1.5 in.

Table 4.16 Experimental Initial Stiffness of the In-Plane Load Tests

| <b>SS Type Connection</b>           |           |           |           |           |
|-------------------------------------|-----------|-----------|-----------|-----------|
| <b>Initial Stiffness in kip/in.</b> |           |           |           |           |
| <b>D vs. T</b>                      | <b>33</b> | <b>43</b> | <b>68</b> | <b>97</b> |
| 362                                 | 1.68      | 3.57      | 6.10      |           |
|                                     | 2.07      | 4.20      | 7.94      |           |
| 600                                 | 1.00      | 3.78      |           | 5.57      |
|                                     | 1.14      | 3.82      |           | 6.86      |
| 800                                 |           | 2.07      |           | 7.08      |
|                                     |           | 2.46      |           | 2.95      |
| <b>WW Type Connection</b>           |           |           |           |           |
| <b>Initial Stiffness in kip/in.</b> |           |           |           |           |
| <b>D vs. T</b>                      | <b>33</b> | <b>43</b> | <b>68</b> | <b>97</b> |
| 362                                 |           |           | 30.42     |           |
|                                     |           |           | 40.79     |           |
| 600                                 |           |           |           | 16.52     |
|                                     |           |           |           | 15.24     |
| 800                                 |           |           |           | 10.51     |
|                                     |           |           |           | 19.67     |
| <b>DW Type Connection</b>           |           |           |           |           |
| <b>Initial Stiffness in kip/in.</b> |           |           |           |           |
| <b>D vs. T</b>                      | <b>33</b> | <b>43</b> | <b>68</b> | <b>97</b> |
| 362                                 |           |           | 45.36     |           |
|                                     |           |           | 50.41     |           |
| 600                                 |           |           |           | 8.26      |
|                                     |           |           |           |           |
| 800                                 |           |           |           | 2.40      |
|                                     |           |           |           |           |

Table 4.17 Experimental Initial Stiffness of the Out-of-Plane Load Tests

| <b>SS Type Connection</b>                |           |           |           |           |
|--|-----------|-----------|-----------|-----------|
| <b>Initial Stiffness in kip-in./rad.</b> |           |           |           |           |
| <b>D vs. T</b>                           | <b>33</b> | <b>43</b> | <b>68</b> | <b>97</b> |
| 362                                      | 2.95      | 5.33      | 13.88     |           |
|  | 4.00      | 7.04      | 15.72     |           |
| 600                                      | 7.02      | 21.04     |           | 31.38     |
|  | 7.20      | 24.08     |           | 43.60     |
| 800                                      |           | 51.41     |           | 70.32     |
|  |           | 60.32     |           | 78.95     |
| <b>WW Type Connection</b>                |           |           |           |           |
| <b>Initial Stiffness in kip-in./rad.</b> |           |           |           |           |
| <b>D vs. T</b>                           | <b>33</b> | <b>43</b> | <b>68</b> | <b>97</b> |
| 362                                      |           |           | 75.79     |           |
|  |           |           | 99.27     |           |
| 600                                      |           |           |           | 197.38    |
|  |           |           |           | 211.10    |
| 800                                      |           |           |           | 236.61    |
|  |           |           |           | 314.45    |
| <b>DW Type Connection</b>                |           |           |           |           |
| <b>Initial Stiffness in kip-in./rad.</b> |           |           |           |           |
| <b>D vs. T</b>                           | <b>33</b> | <b>43</b> | <b>68</b> | <b>97</b> |
| 362                                      |           |           | 28.89     |           |
|  |           |           | 32.40     |           |
| 600                                      |           |           |           | 26.31     |
|  |           |           |           | 26.72     |
| 800                                      |           |           |           | 18.04     |
|  |           |           |           | 27.58     |

Table 4.18 Maximum Flexural and Corresponding Torsional Brace Force

| Stud Designation |   |     |    |    | Target<br>Brace<br>Stiffness | Brace Force         |                    | Corr.<br>Axial<br>Load | Flexural<br>BF as<br>% of P |
|------------------|---|-----|----|----|------------------------------|---------------------|--------------------|------------------------|-----------------------------|
|                  |   |     |    |    |                              | Maximum<br>Flexural | Corr.<br>Torsional |                        |                             |
| D                | S | B   | t  | ID | lbs/in.                      | lbs                 | lbs                | lbs                    | %                           |
|                  |   |     |    |    |                              |                     |                    |                        |                             |
| 362              | S | 125 | 33 | 3  | 100                          | 5.92                | 0.44               | 1866.86                | 0.32                        |
| 362              | S | 125 | 33 | 4  | 100                          | 11.28               | 2.42               | 2299.90                | 0.49                        |
| 362              | S | 125 | 33 | 6  | 100                          | 7.23                | 7.22               | 2398.96                | 0.30                        |
| 362              | S | 125 | 33 | 1  | 200                          | 5.28                | 1.78               | 3012.17                | 0.18                        |
| 362              | S | 125 | 33 | 2  | 400                          | 16.22               | 2.15               | 2959.05                | 0.55                        |
|                  |   |     |    |    |                              |                     |                    |                        |                             |
| 362              | S | 162 | 43 | 2  | 200                          | 13.31               | 3.09               | 6190.00                | 0.22                        |
| 362              | S | 162 | 43 | 4  | 400                          | 25.53               | 4.59               | 5197.30                | 0.49                        |
| 362              | S | 162 | 43 | 3  | 800                          | 18.97               | 7.23               | 4466.38                | 0.42                        |
|                  |   |     |    |    |                              |                     |                    |                        |                             |
| 362              | S | 162 | 68 | 3  | 500                          | 79.65               | 76.57              | 13384.46               | 0.60                        |
| 362              | S | 162 | 68 | 4  | 750                          | 67.63               | 49.63              | 13787.71               | 0.49                        |
| 362              | S | 162 | 68 | 2  | 1000                         | 73.35               | 50.17              | 14596.98               | 0.50                        |
|                  |   |     |    |    |                              |                     |                    |                        |                             |
| 600              | S | 125 | 33 | 4  | 30                           | 12.53               | 6.50               | 1951.03                | 0.64                        |
| 600              | S | 125 | 33 | 3  | 60                           | 6.86                | 4.77               | 2241.37                | 0.31                        |
| 600              | S | 125 | 33 | 1  | 200                          | 1.47                | 0.65               | 823.73                 | 0.18                        |
|                  |   |     |    |    |                              |                     |                    |                        |                             |
| 600              | S | 162 | 43 | 5  | 30                           | 7.75                | 6.77               | 7163.83                | 0.11                        |
| 600              | S | 162 | 43 | 2  | 75                           | 28.74               | 27.45              | 6052.34                | 0.47                        |
| 600              | S | 162 | 43 | 1  | 250                          | 5.05                | 0.61               | 1310.44                | 0.39                        |
| 600              | S | 162 | 43 | 4  | 500                          | 10.78               | 3.74               | 4231.99                | 0.25                        |
|                  |   |     |    |    |                              |                     |                    |                        |                             |
| 600              | S | 162 | 97 | 4  | 160                          | 22.61               | 12.37              | 28306.23               | 0.08                        |
| 600              | S | 162 | 97 | 3  | 500                          | 68.77               | 62.12              | 30085.90               | 0.23                        |
| 600              | S | 162 | 97 | 1  | 1000                         | 85.76               | 45.83              | 28553.51               | 0.30                        |
| 600              | S | 162 | 97 | 2  | 1500                         | 77.21               | 48.38              | 29472.16               | 0.26                        |
|                  |   |     |    |    |                              |                     |                    |                        |                             |
| 800              | S | 162 | 43 | 2  | 75                           | 12.35               | 10.36              | 4306.04                | 0.29                        |
| 800              | S | 162 | 43 | 3  | 150                          | 35.76               | 9.92               | 5333.03                | 0.67                        |
| 800              | S | 162 | 43 | 5  | 300                          | 21.42               | 12.67              | 3917.25                | 0.55                        |
|                  |   |     |    |    |                              |                     |                    |                        |                             |
| 800              | S | 162 | 97 | 2  | 500                          | 37.05               | 16.85              | 21626.00               | 0.17                        |
| 800              | S | 162 | 97 | 1  | 1000                         | 53.18               | 2.34               | 23811.17               | 0.22                        |
| 800              | S | 162 | 97 | 4  | 2100                         | 34.82               | 25.29              | 23537.15               | 0.15                        |

Table 4.19 Maximum Torsional and Corresponding Flexural Brace Force

| Stud Designation |   |     |    |    | Target<br>Brace<br>Stiffness | Brace Force       |                      | Corr.<br>Axial<br>Load | Torsional<br>BF as %<br>of P |
|------------------|---|-----|----|----|------------------------------|-------------------|----------------------|------------------------|------------------------------|
|                  |   |     |    |    |                              | Corr.<br>Flexural | Maximum<br>Torsional |                        |                              |
| D                | S | B   | t  | ID | lbs/in.                      | lbs               | lbs                  | lbs                    | %                            |
|                  |   |     |    |    |                              |                   |                      |                        |                              |
| 362              | S | 125 | 33 | 3  | 100                          | 4.78              | 2.67                 | 2748.51                | 0.10                         |
| 362              | S | 125 | 33 | 4  | 100                          | 7.48              | 5.53                 | 2066.30                | 0.27                         |
| 362              | S | 125 | 33 | 6  | 100                          | 7.23              | 7.22                 | 2398.96                | 0.30                         |
| 362              | S | 125 | 33 | 1  | 200                          | 5.28              | 1.78                 | 3012.17                | 0.06                         |
| 362              | S | 125 | 33 | 2  | 400                          | 12.86             | 2.37                 | 2940.58                | 0.08                         |
|                  |   |     |    |    |                              |                   |                      |                        |                              |
| 362              | S | 162 | 43 | 2  | 200                          | 9.69              | 5.77                 | 7268.46                | 0.08                         |
| 362              | S | 162 | 43 | 4  | 400                          | 19.53             | 16.96                | 7029.71                | 0.24                         |
| 362              | S | 162 | 43 | 3  | 800                          | 13.50             | 14.53                | 6338.90                | 0.23                         |
|                  |   |     |    |    |                              |                   |                      |                        |                              |
| 362              | S | 162 | 68 | 3  | 500                          | 79.65             | 76.57                | 13384.46               | 0.57                         |
| 362              | S | 162 | 68 | 4  | 750                          | 65.96             | 59.11                | 14029.50               | 0.42                         |
| 362              | S | 162 | 68 | 2  | 1000                         | 72.13             | 54.23                | 14792.16               | 0.37                         |
|                  |   |     |    |    |                              |                   |                      |                        |                              |
| 600              | S | 125 | 33 | 4  | 30                           | 12.53             | 6.50                 | 1951.03                | 0.33                         |
| 600              | S | 125 | 33 | 3  | 60                           | 6.85              | 4.77                 | 2249.36                | 0.21                         |
| 600              | S | 125 | 33 | 1  | 200                          | 1.11              | 1.15                 | 1566.29                | 0.07                         |
|                  |   |     |    |    |                              |                   |                      |                        |                              |
| 600              | S | 162 | 43 | 5  | 30                           | 7.75              | 6.77                 | 7163.83                | 0.09                         |
| 600              | S | 162 | 43 | 2  | 75                           | 28.74             | 27.45                | 6052.34                | 0.45                         |
| 600              | S | 162 | 43 | 1  | 250                          | 3.37              | 3.96                 | 7079.07                | 0.06                         |
| 600              | S | 162 | 43 | 4  | 500                          | 9.86              | 3.86                 | 3954.20                | 0.10                         |
|                  |   |     |    |    |                              |                   |                      |                        |                              |
| 600              | S | 162 | 97 | 4  | 160                          | 22.61             | 12.37                | 28306.23               | 0.04                         |
| 600              | S | 162 | 97 | 3  | 500                          | 68.77             | 62.12                | 30085.90               | 0.21                         |
| 600              | S | 162 | 97 | 1  | 1000                         | 84.46             | 45.87                | 28549.18               | 0.16                         |
| 600              | S | 162 | 97 | 2  | 1500                         | 77.21             | 48.38                | 29472.16               | 0.16                         |
|                  |   |     |    |    |                              |                   |                      |                        |                              |
| 800              | S | 162 | 43 | 2  | 75                           | 12.35             | 10.36                | 4306.04                | 0.24                         |
| 800              | S | 162 | 43 | 3  | 150                          | 35.76             | 9.92                 | 5333.03                | 0.19                         |
| 800              | S | 162 | 43 | 5  | 300                          | 21.10             | 12.84                | 4001.41                | 0.32                         |
|                  |   |     |    |    |                              |                   |                      |                        |                              |
| 800              | S | 162 | 97 | 2  | 500                          | 28.81             | 19.10                | 20549.82               | 0.09                         |
| 800              | S | 162 | 97 | 1  | 1000                         | 20.66             | 14.66                | 19679.07               | 0.07                         |
| 800              | S | 162 | 97 | 4  | 2100                         | 34.82             | 25.29                | 23537.15               | 0.11                         |

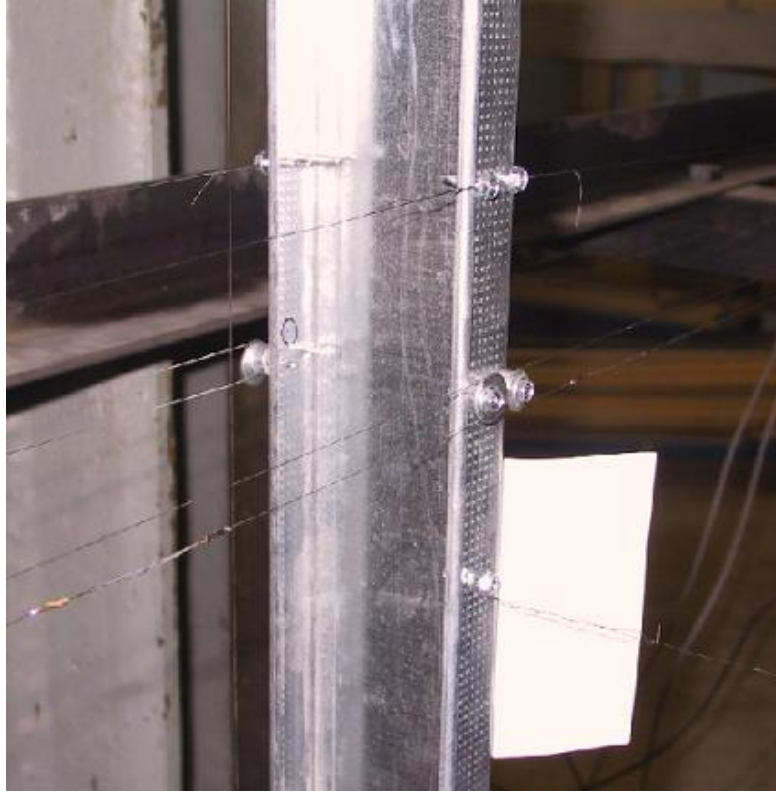


Figure 4.1 Typical Bracing for the Single Column Axial Load Tests

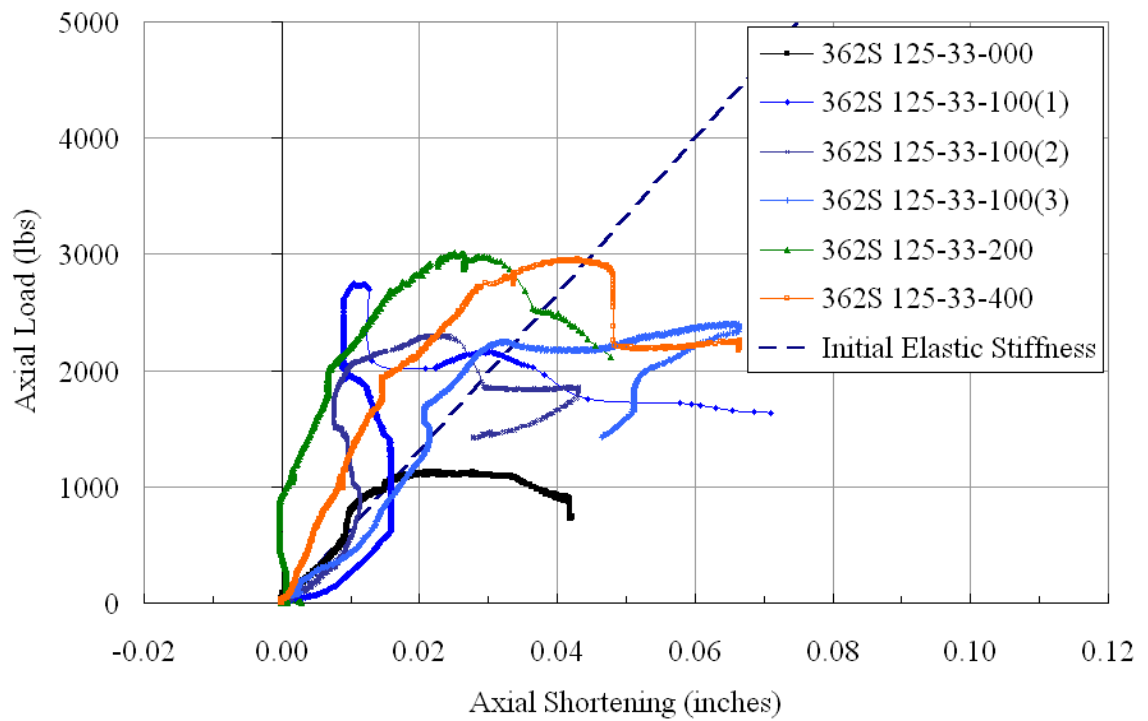


Figure 4.2 Axial Load vs. Axial Shortening for the Stud 362S125-33 with Varying Brace Stiffness

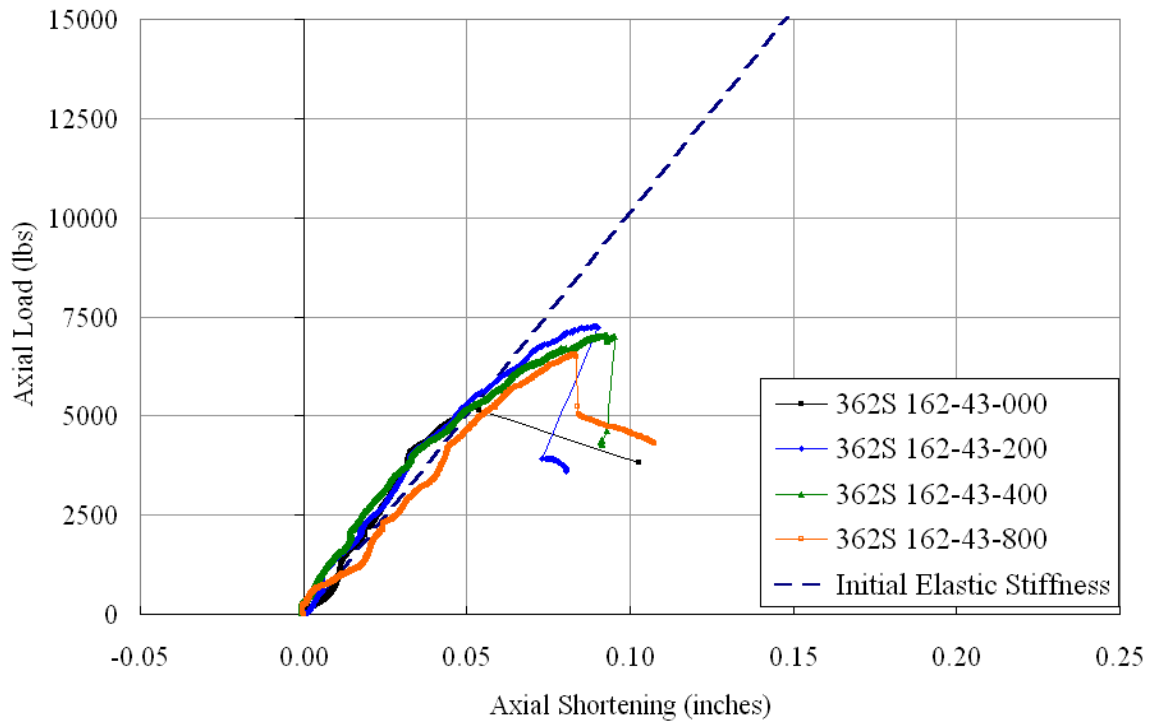


Figure 4.3 Axial Load vs. Axial Shortening for the Stud 362S162-43 with Varying Brace Stiffness

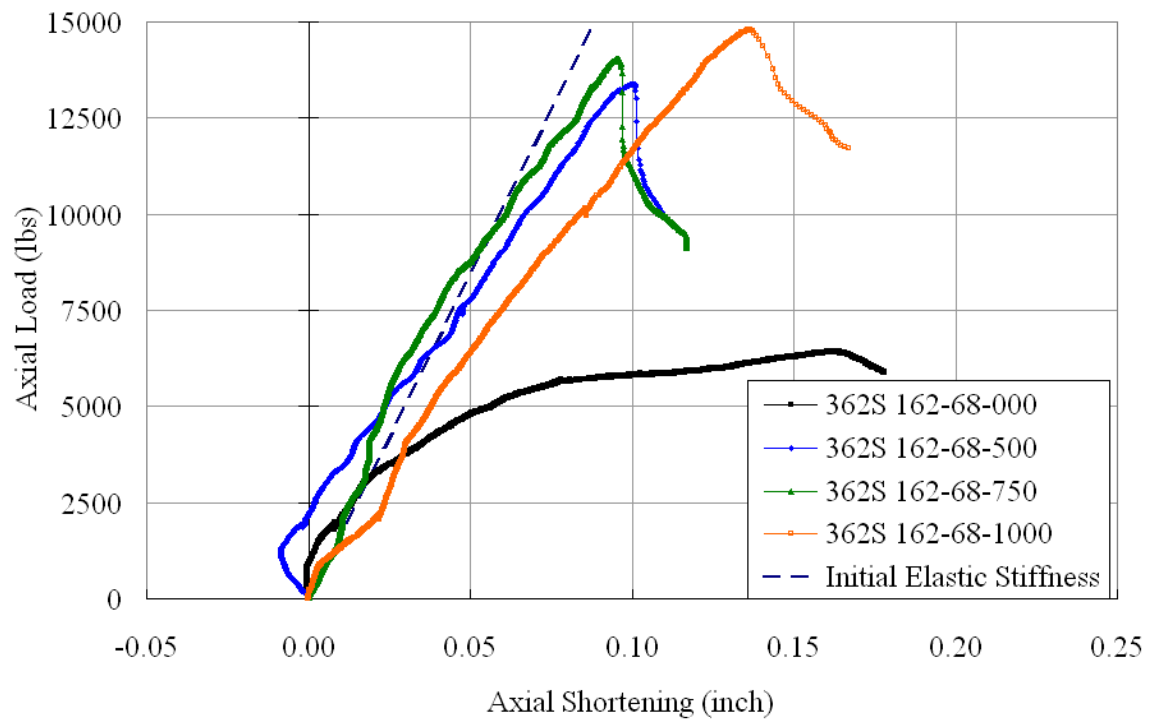


Figure 4.4 Axial Load vs. Axial Shortening for the Stud 362S162-68 with Varying Brace Stiffness

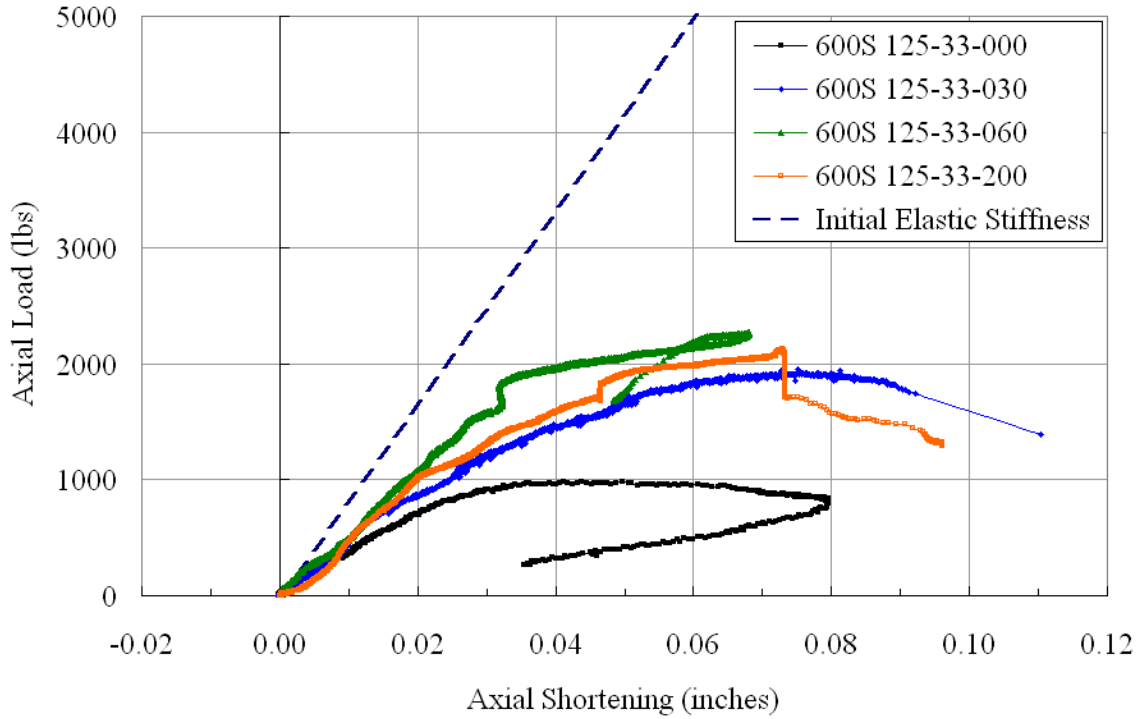


Figure 4.5 Axial Load vs. Axial Shortening for the Stud 600S125-33 with Varying Brace Stiffness

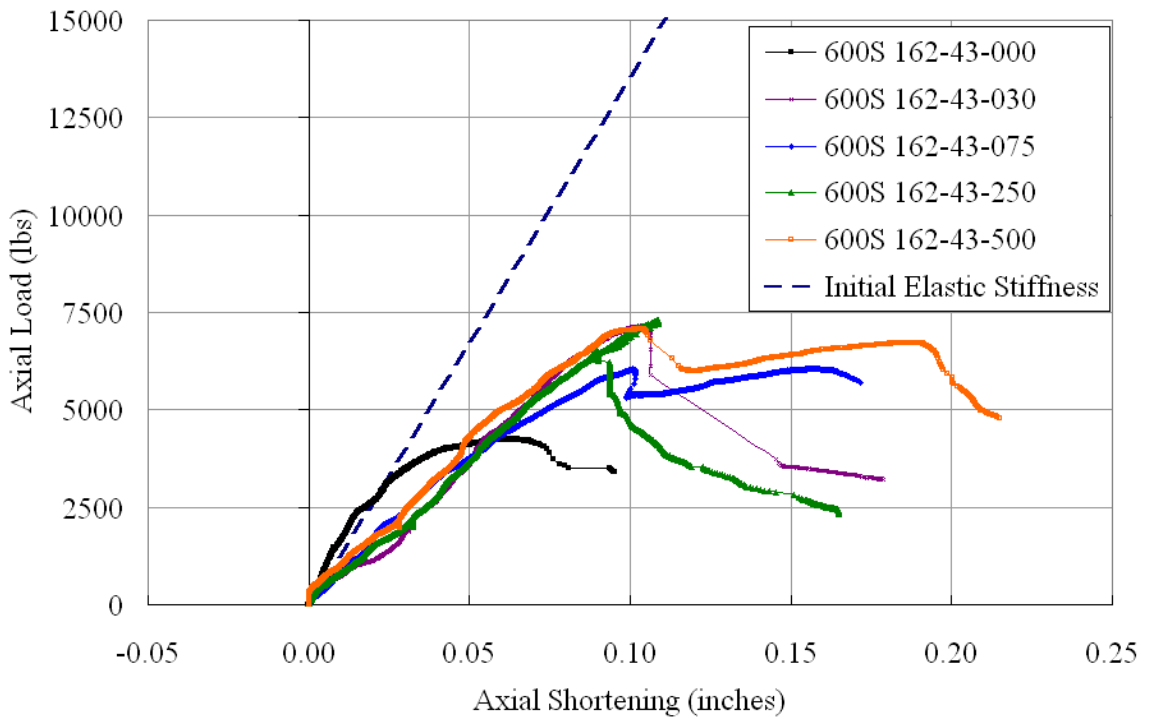


Figure 4.6 Axial Load vs. Axial Shortening for the Stud 600S162-43 with Varying Brace Stiffness

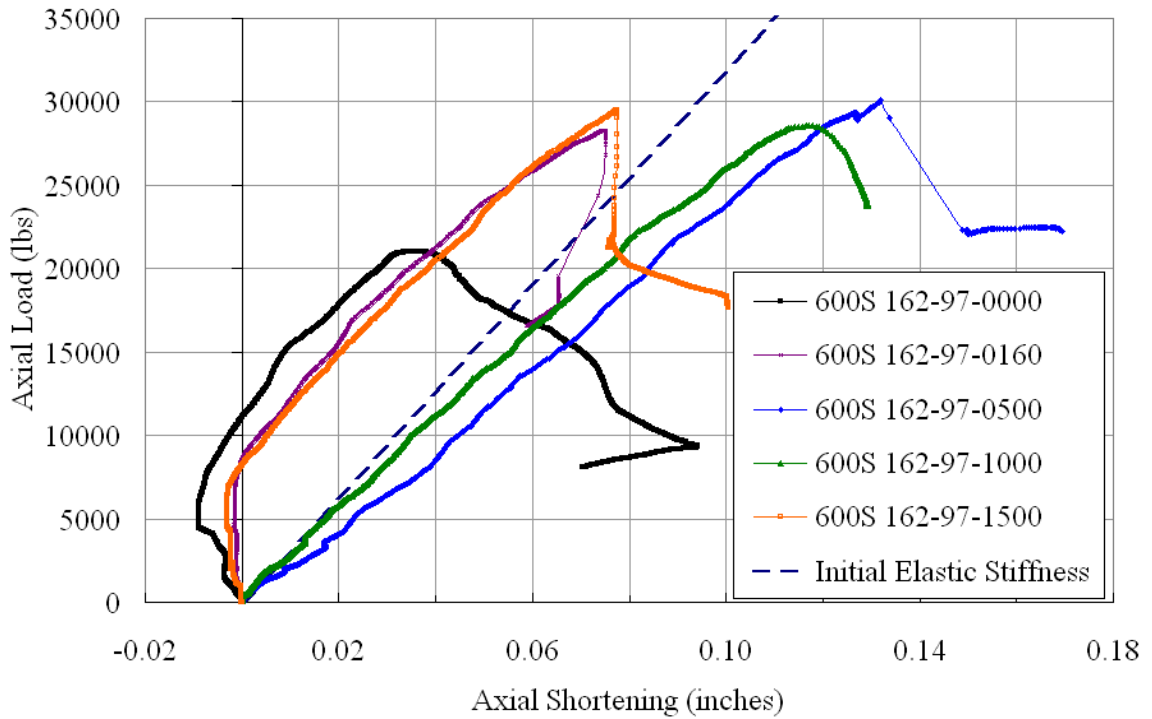


Figure 4.7 Axial Load vs. Axial Shortening for the Stud 600S162-97 with Varying Brace Stiffness

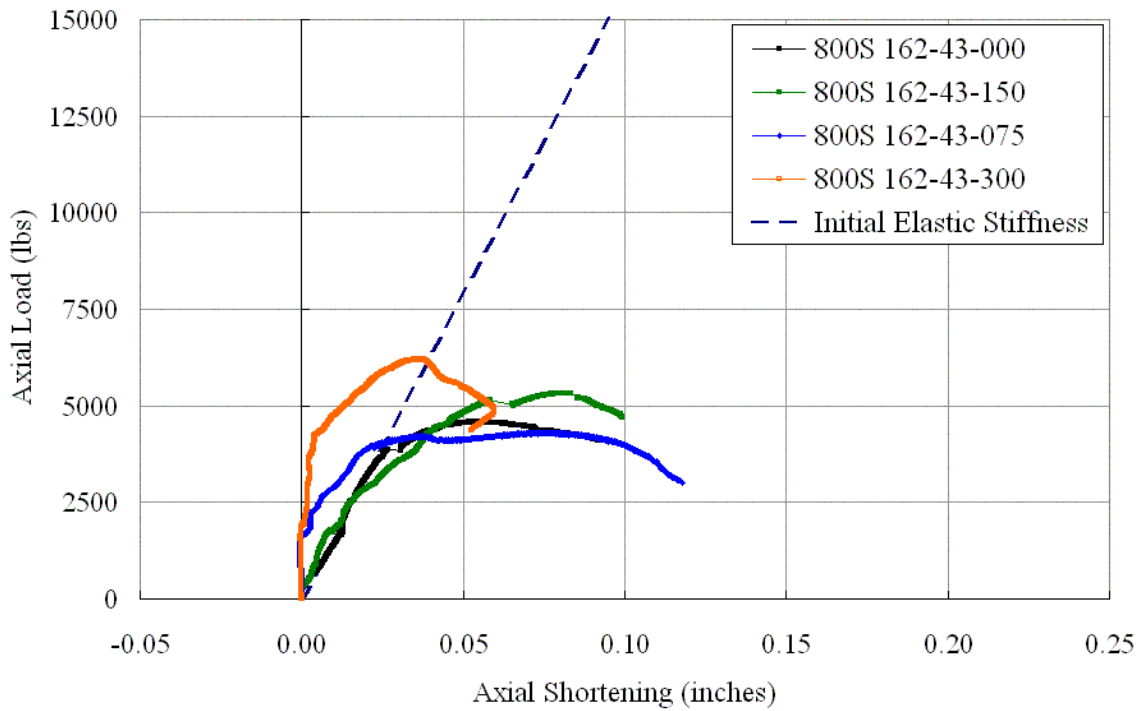


Figure 4.8 Axial Load vs. Axial Shortening for the Stud 800S162-43 with Varying Brace Stiffness

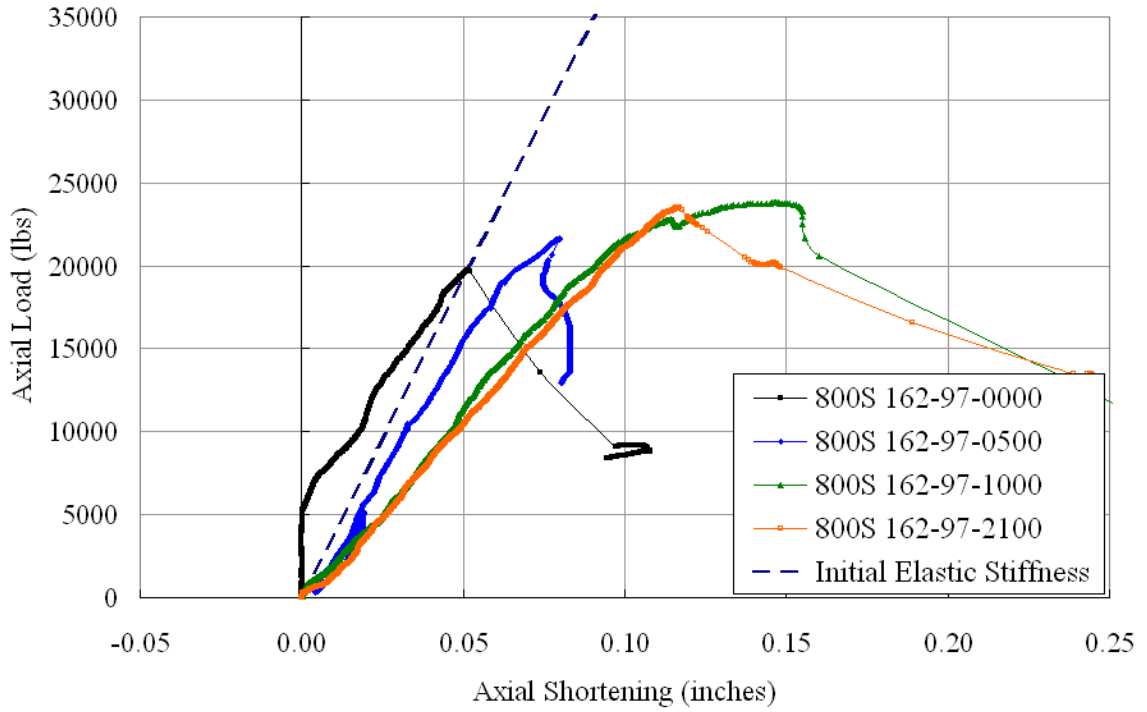


Figure 4.9 Axial Load vs. Axial Shortening for the Stud 800S162-97 with Varying Brace Stiffness

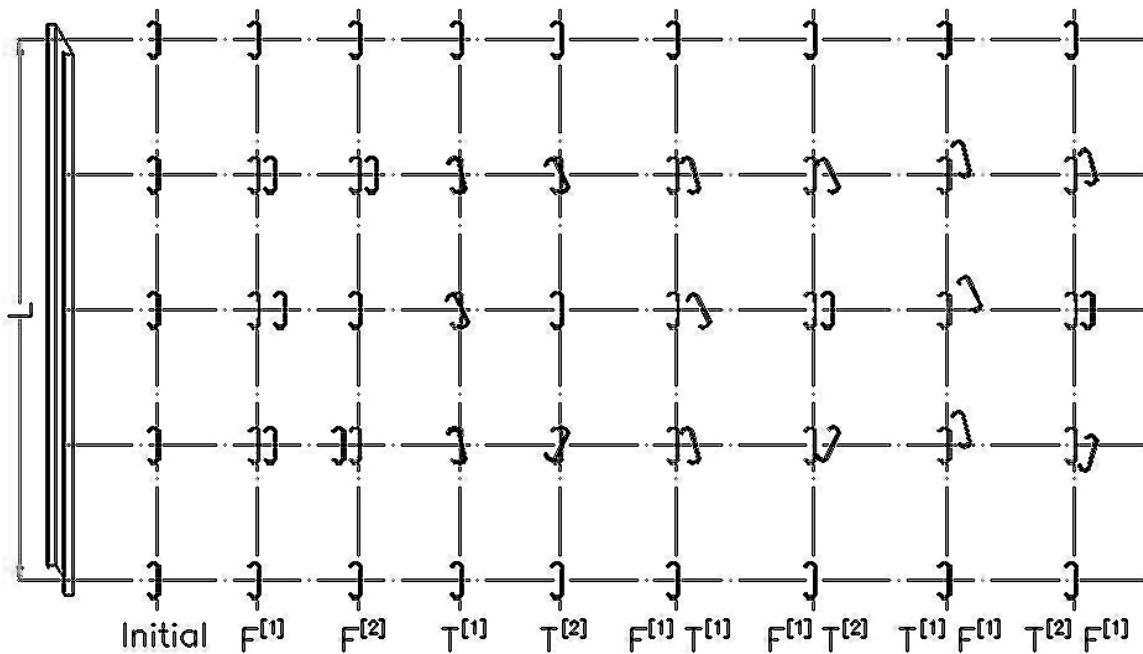


Figure 4.10 Schematic Diagram Showing the Various Buckling Shapes and Buckling Modes Observed in the Experimental Testing

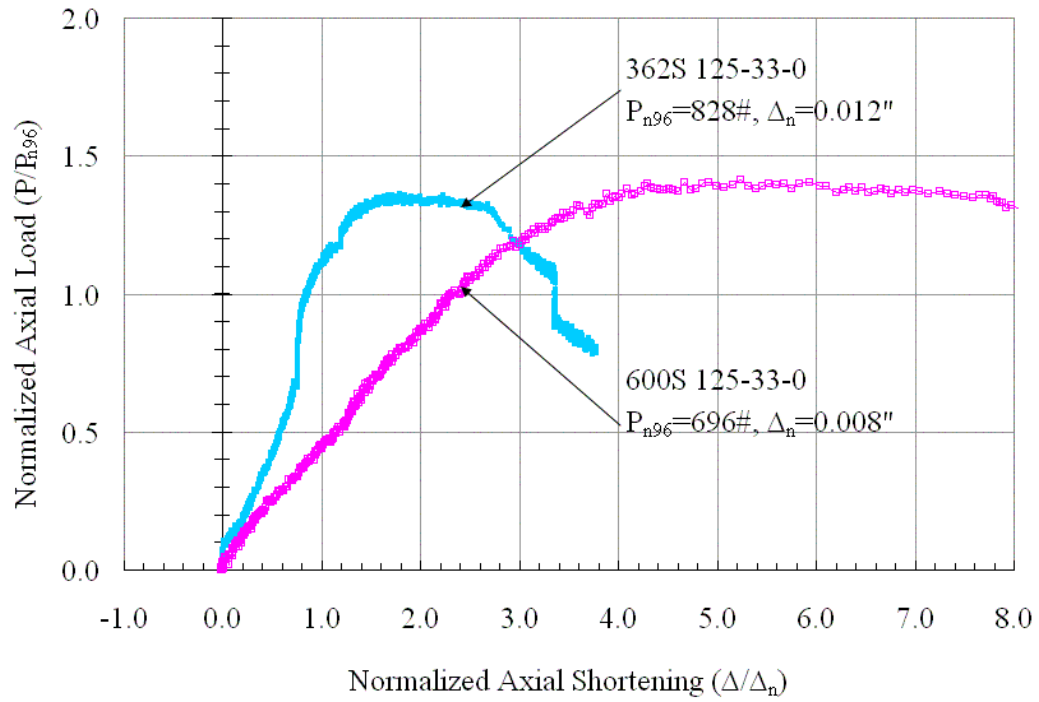


Figure 4.11 Comparison of Studs 362S125-33-0 and 600S125-33-0

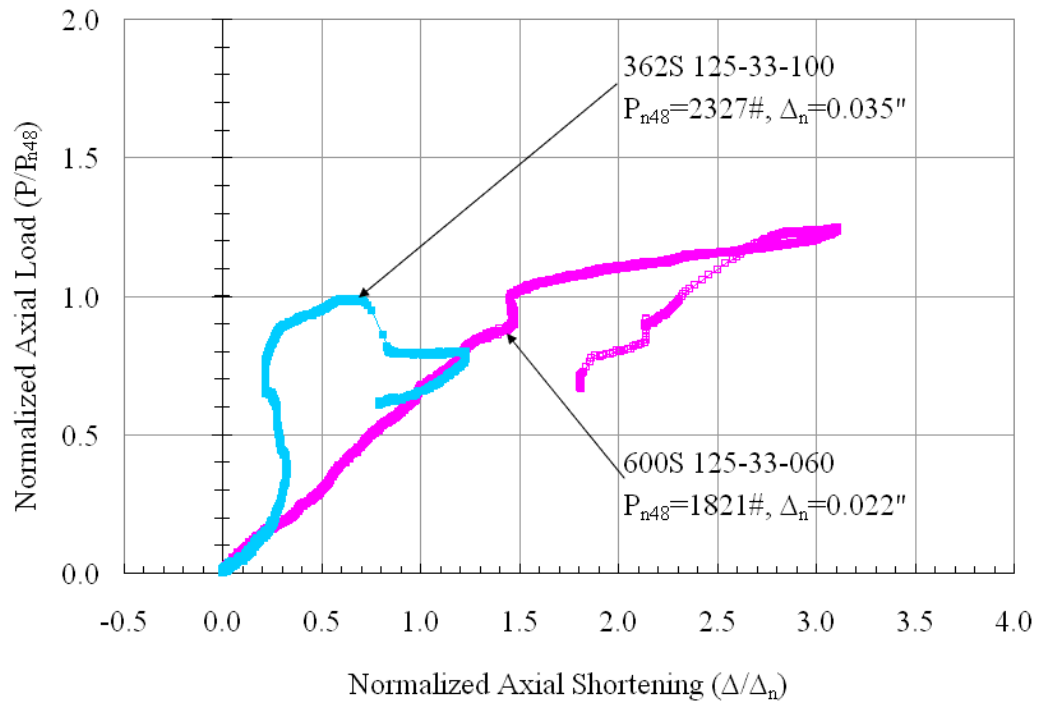


Figure 4.12 Comparison of Studs 362S125-33-100 (1.7x) and 600S125-33-060 (1.3x)

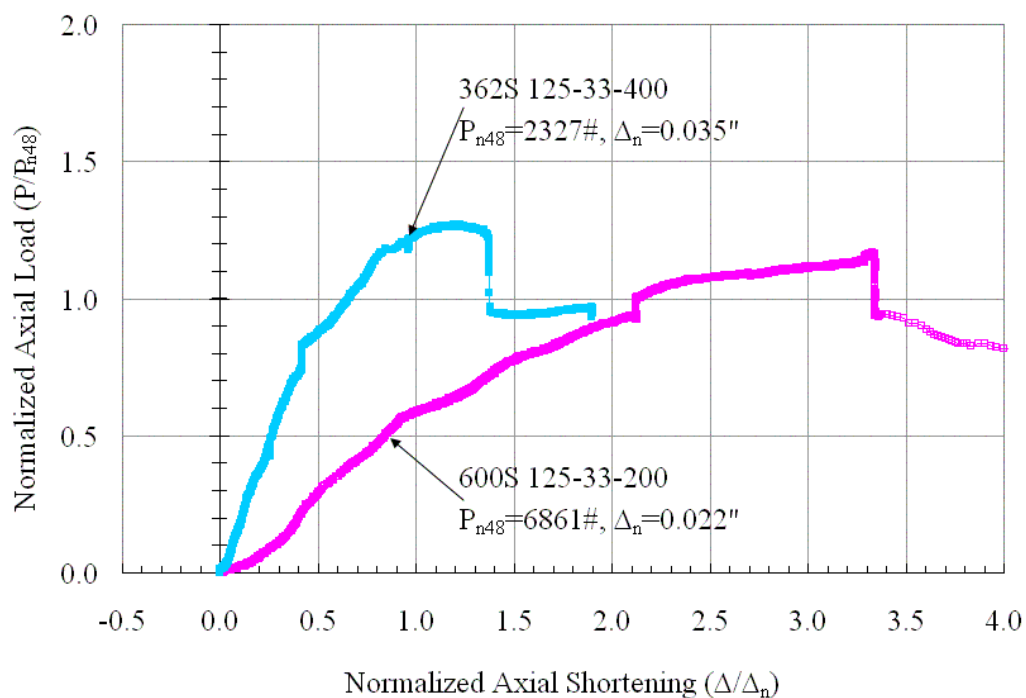


Figure 4.13 Comparison of Studs 362S125-33-200 (6.2x) and 600S125-33-200 (7.4x)

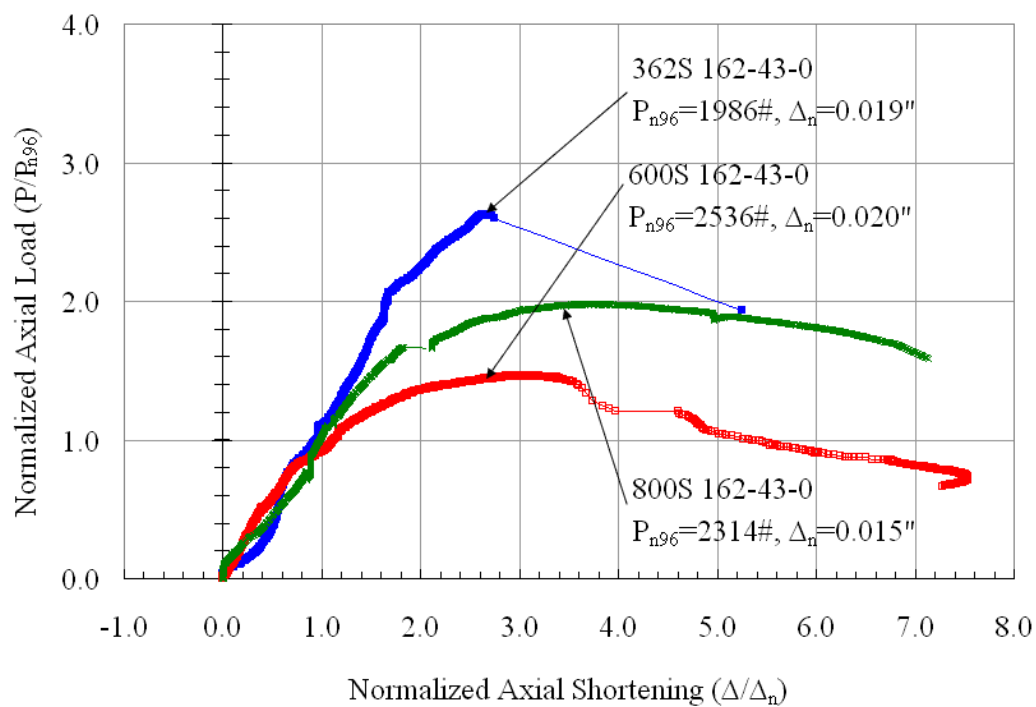


Figure 4.14 Comparison of Studs 362S162-43-0, 600S162-43-0 and 800S162-43-0

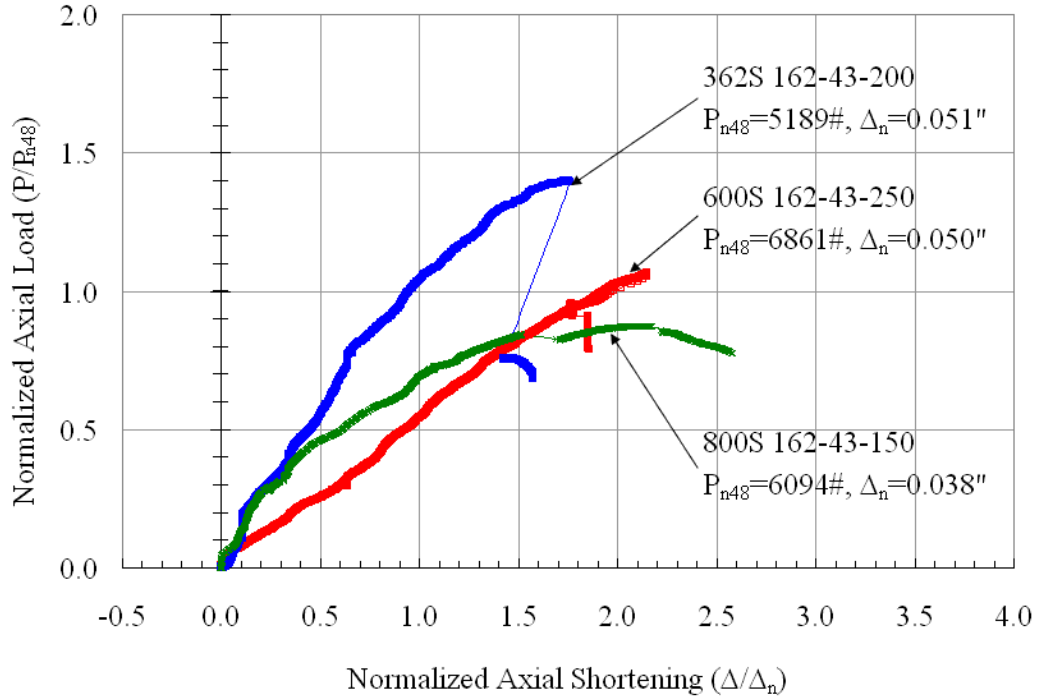


Figure 4.15 Comparison of Studs 362S162-43-200 (1.2x), 600S162-43-250 (1.6x) and 800S162-43-150 (1.3x)

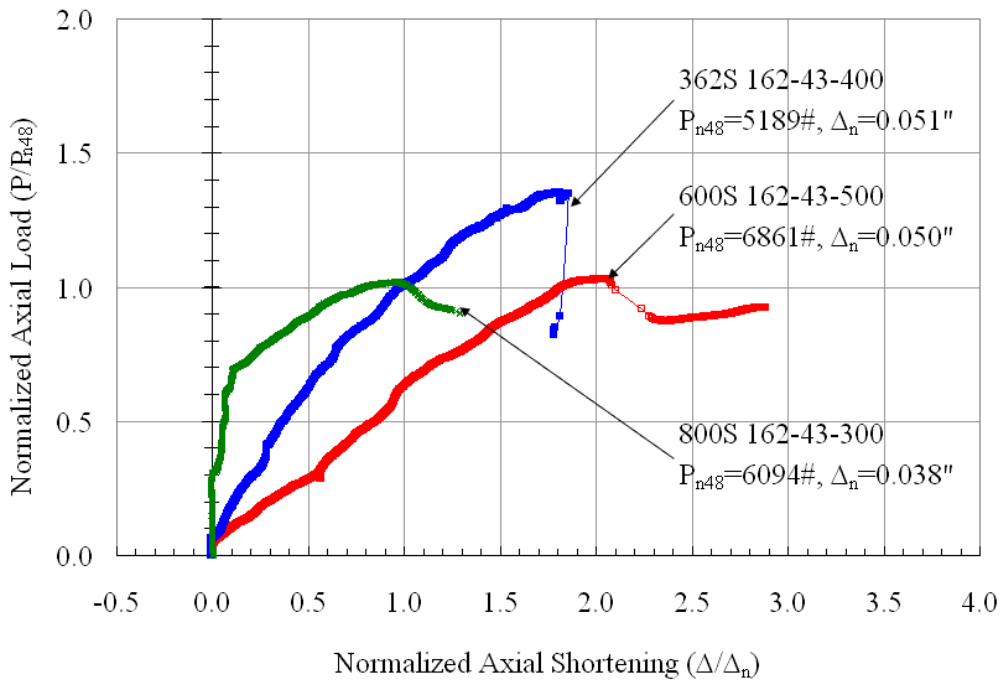


Figure 4.16 Comparison of Studs 362S162-43-400 (2.5x), 600S162-43-500 (3.4x) and 800S162-43-300 (2.3x)

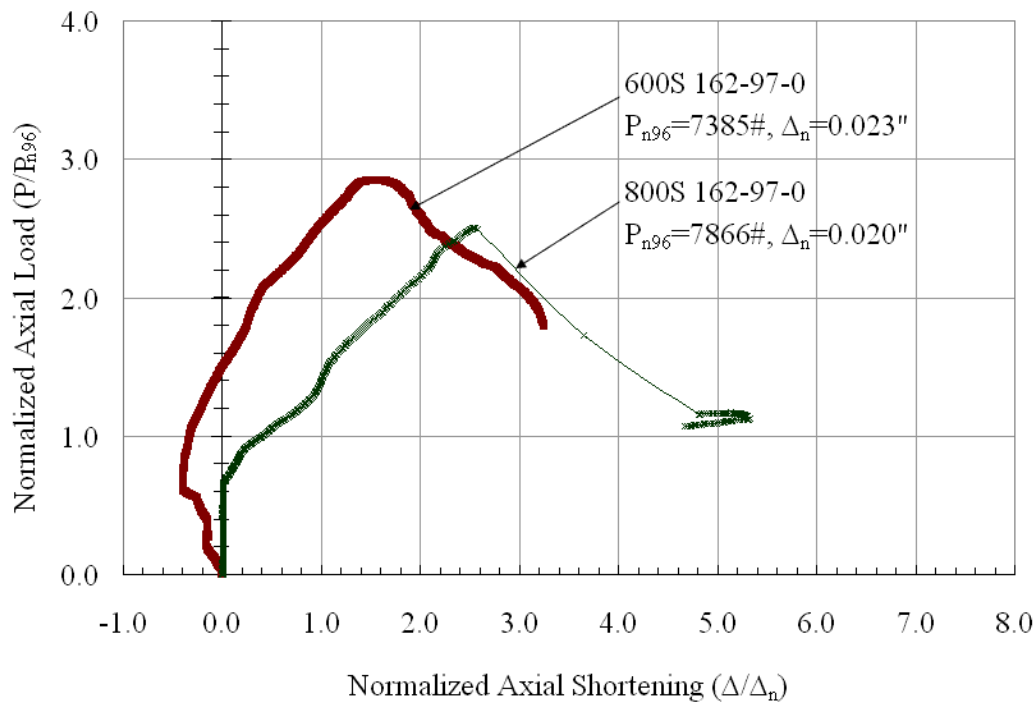


Figure 4.17 Comparison of Studs 600S162-97-0 and 800S162-97-0

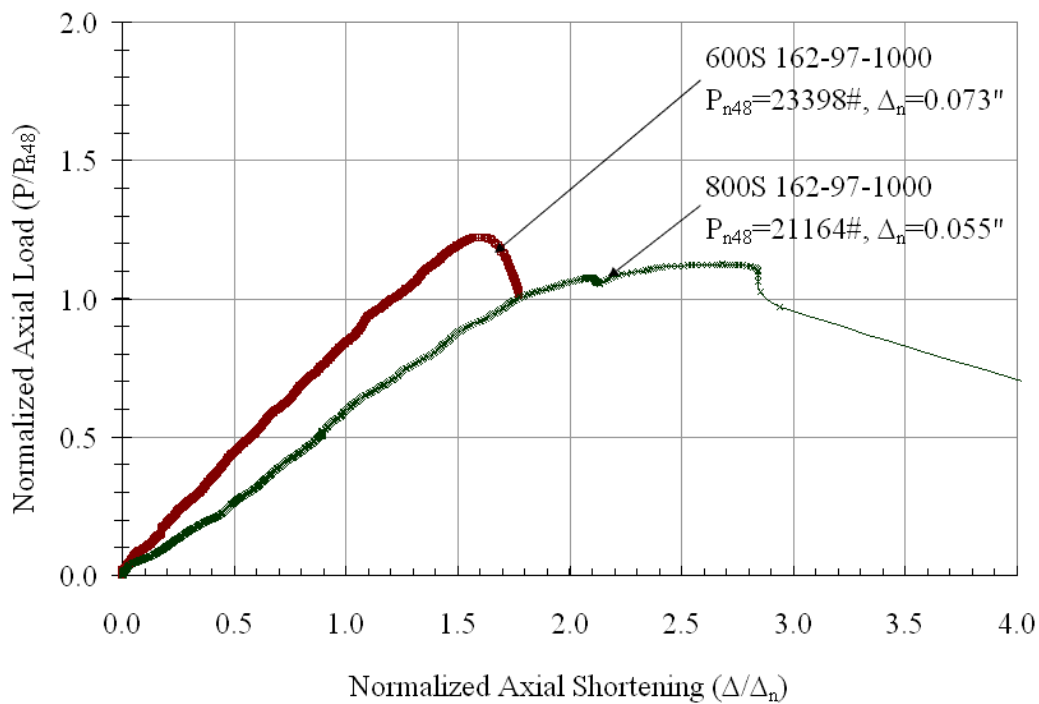


Figure 4.18 Comparison of Studs 600S162-97-1000 (1.7x) and 800S162-97-1000 (2.1x)

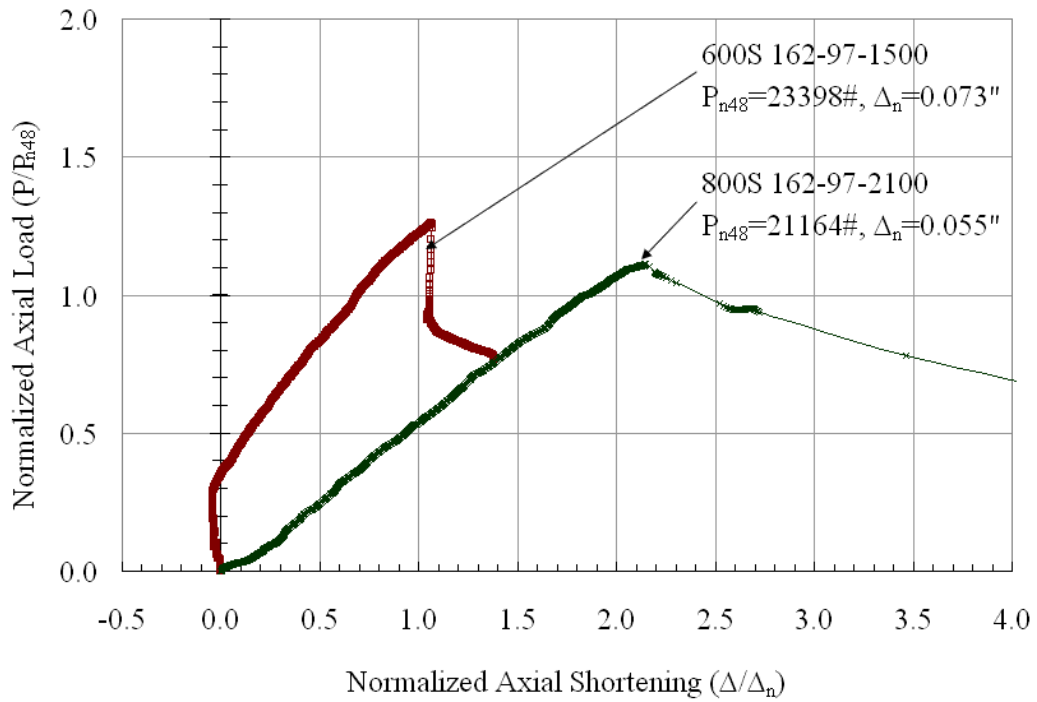


Figure 4.19 Comparison of Studs 600S162-97-1500 (2.7x) and 800S162-97-2100 (4.3x)

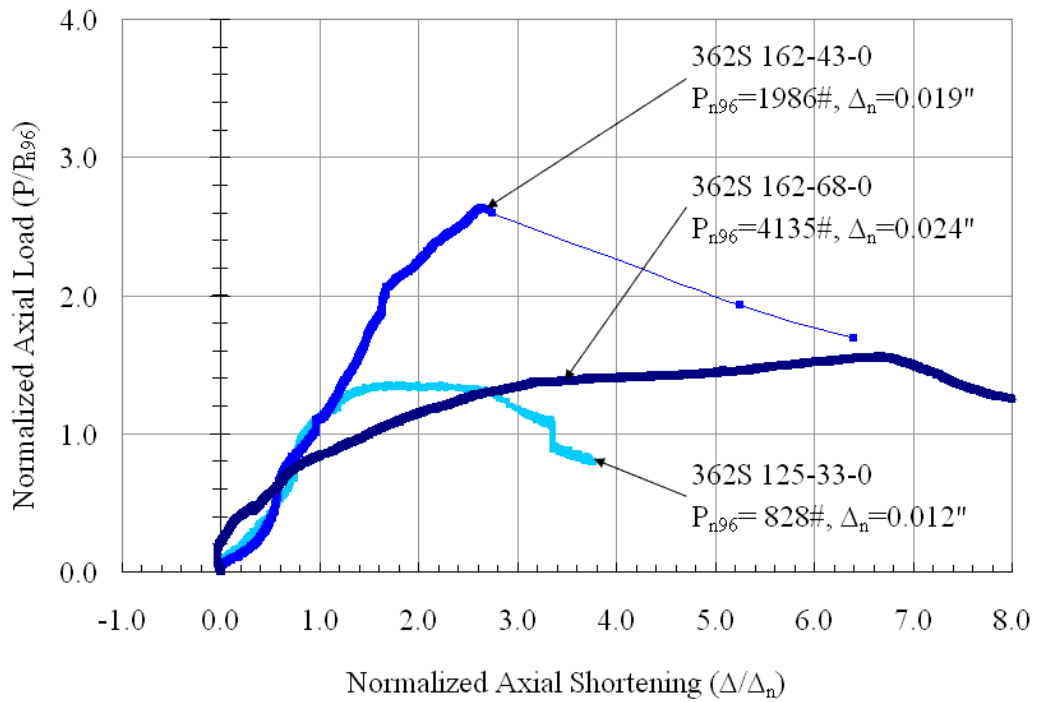


Figure 4.20 Comparison of Studs 362S125-33-0, 362S162-43-0 and 362S162-68-0

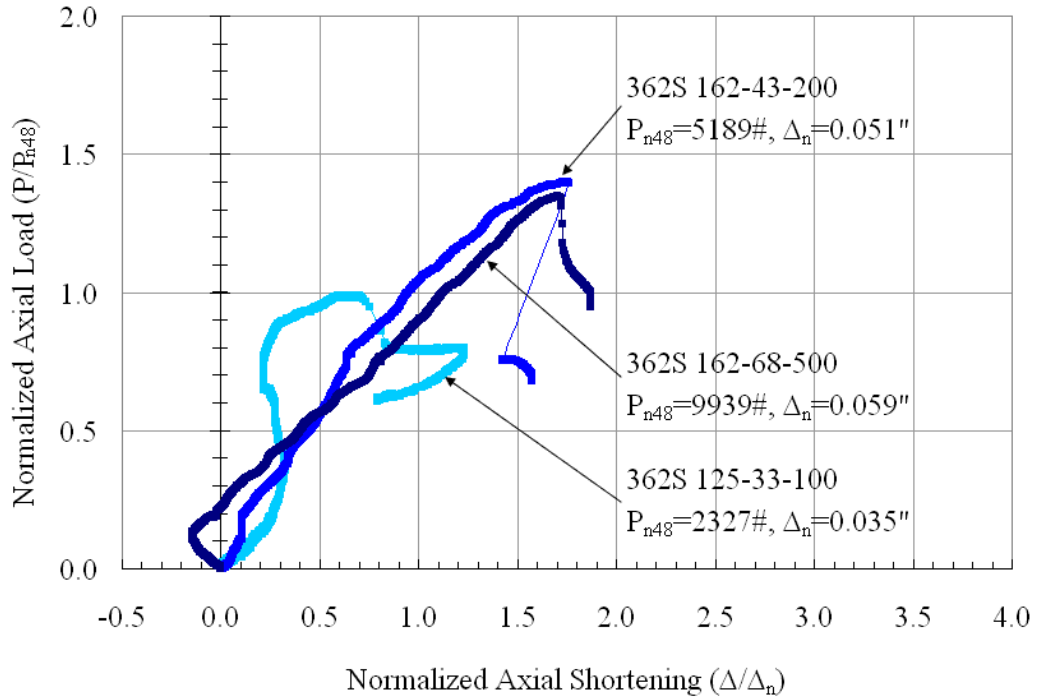


Figure 4.21 Comparison of Studs 362S125-33-100 (1.7x), 362S162-43-200 (1.2x) and 362S162-68-500 (1.8x)

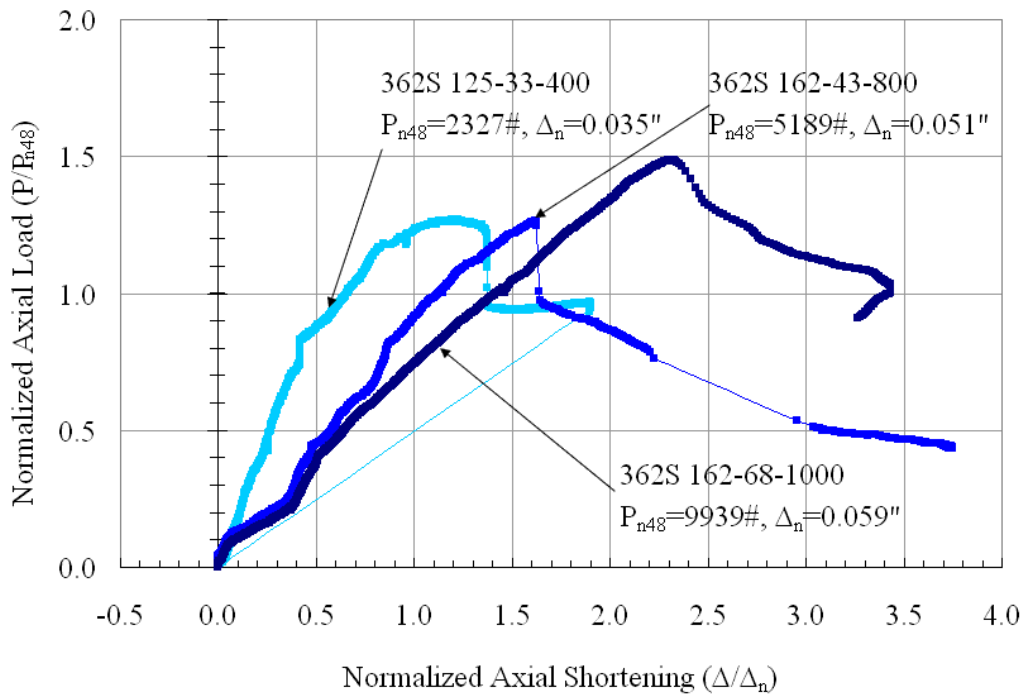


Figure 4.22 Comparison of Studs 362S125-33-400 (6.2x), 362S162-43-800 (5.4x) and 362S162-68-1000 (3.3x)

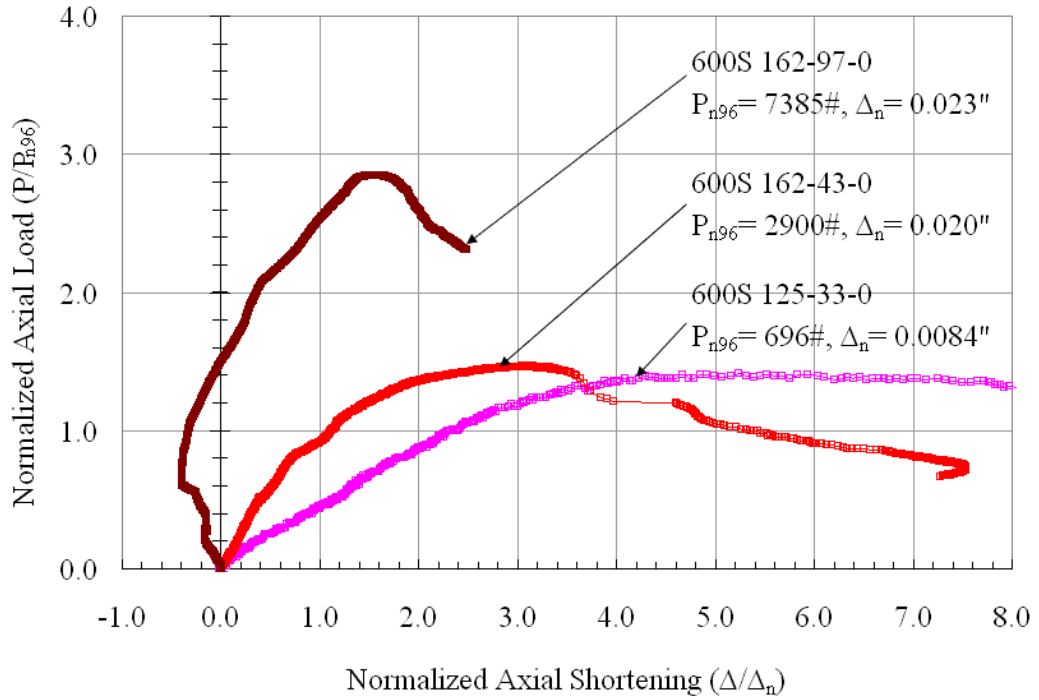


Figure 4.23 Comparison of Studs 600S125-33-0, 600S162-43-0 and 600S162-97-0

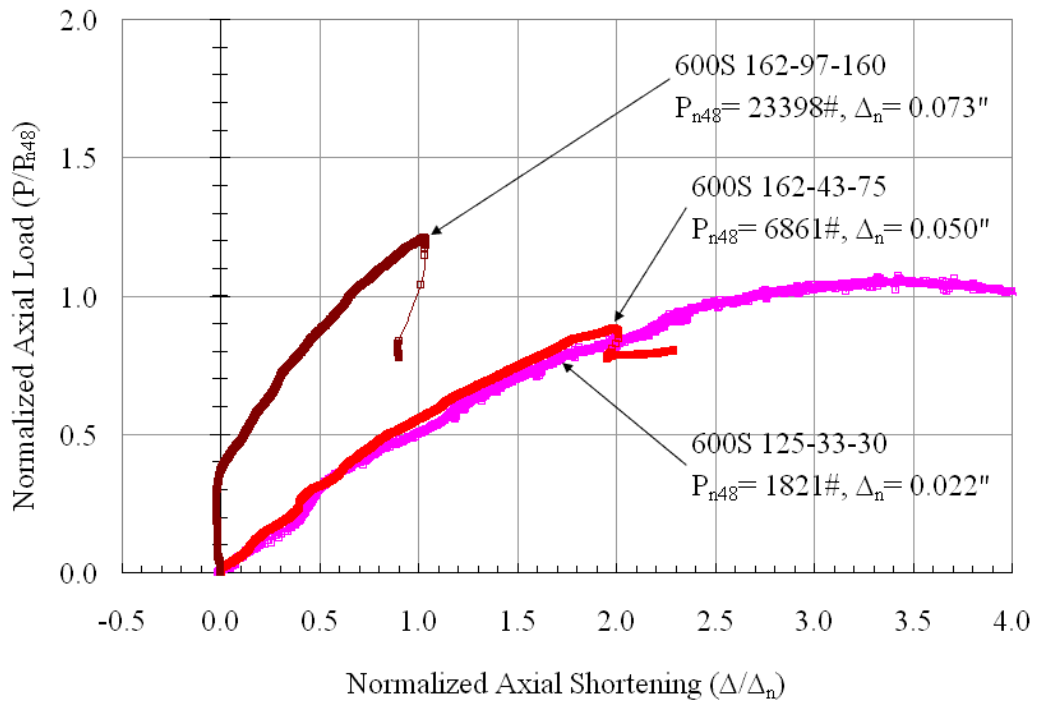


Figure 4.24 Comparison of Studs 600S125-33-30 (0.2x), 600S162-43-75 (0.6x) and 600S162-97-160 (0.3x)

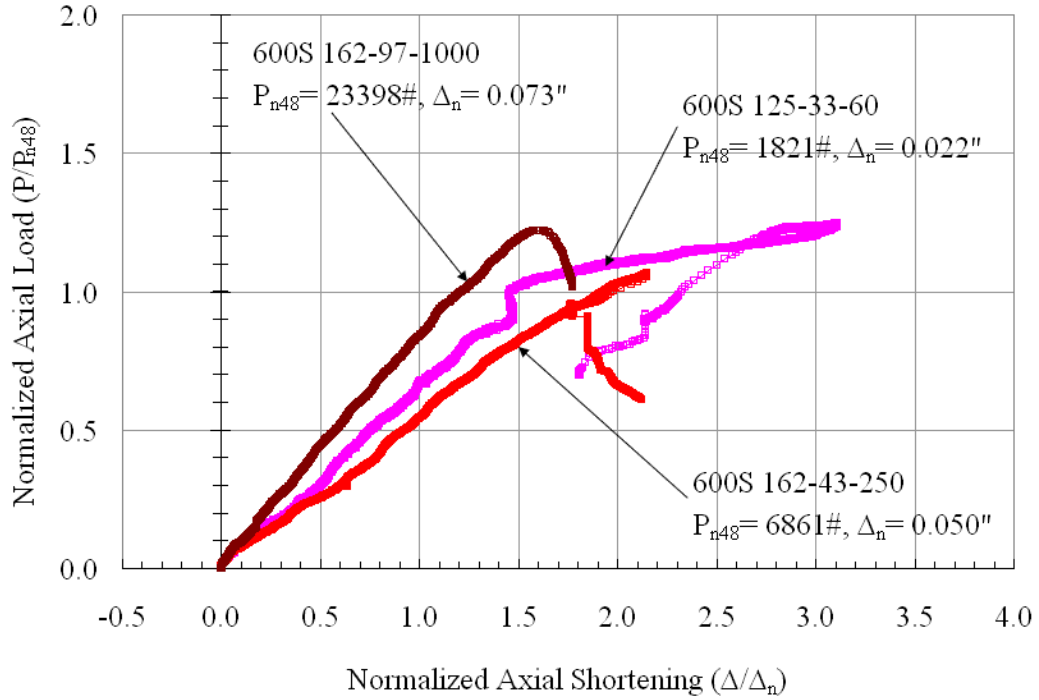


Figure 4.25 Comparison of Studs 600S125-33-60 (1.3x), 600S162-43-250 (1.6x) and 600S162-97-1000 (1.7x)

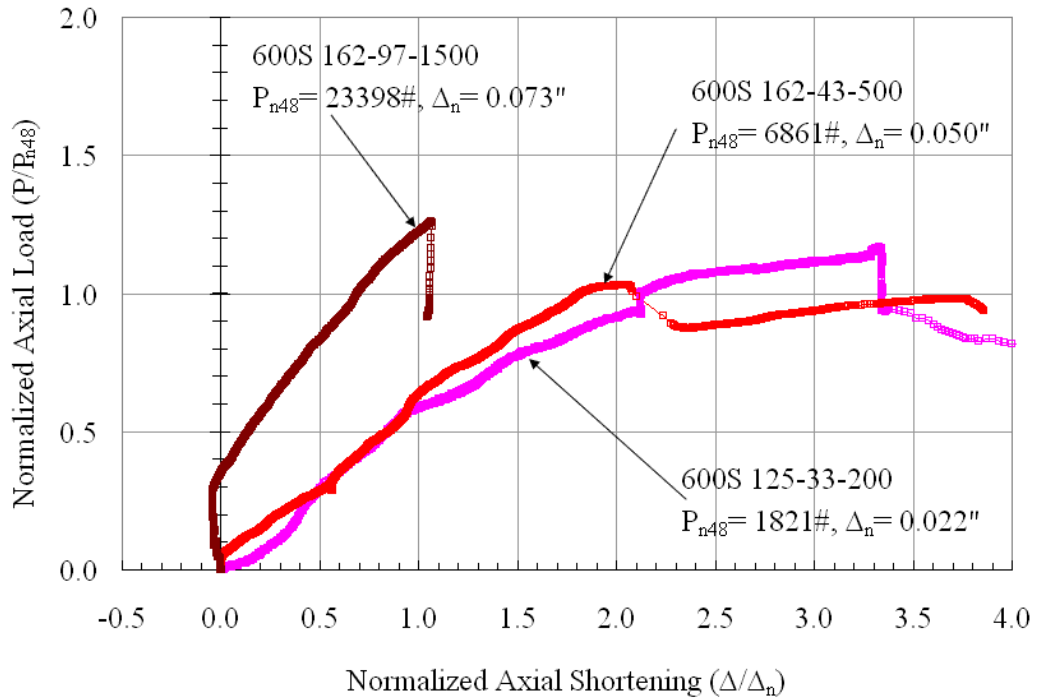


Figure 4.26 Comparison of Studs 600S125-33-200 (7.4x), 600S162-43-500 (3.4x) and 600S162-97-1500 (2.7x)

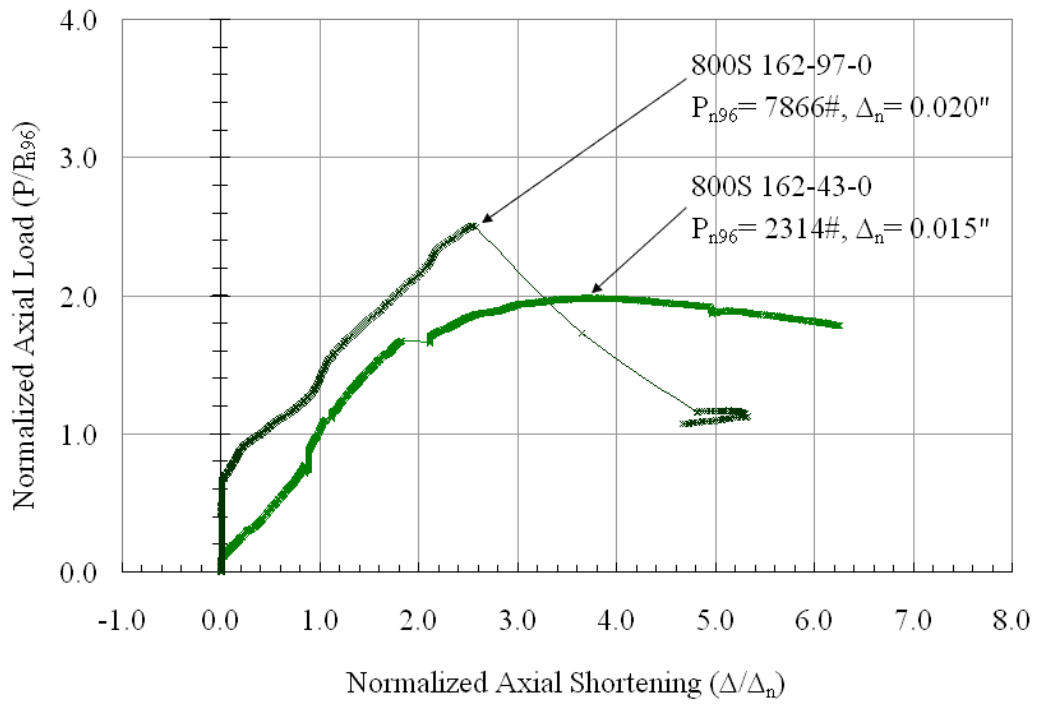


Figure 4.27 Comparison of Studs 800S162-43-0 and 800S162-97-0

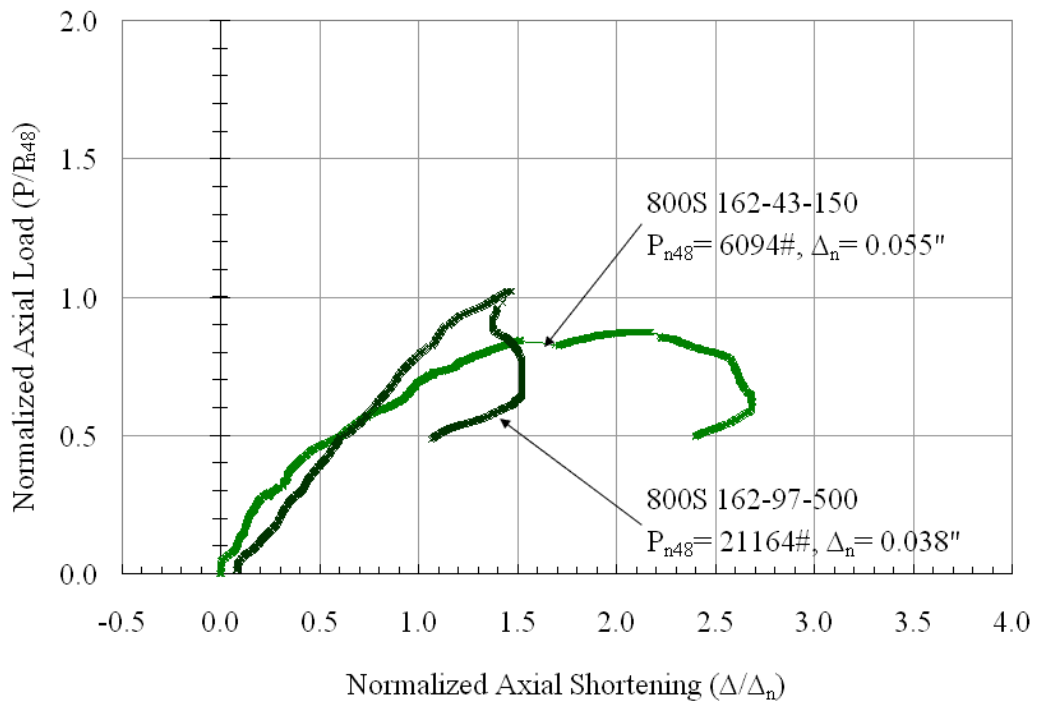


Figure 4.28 Comparison of Studs 800S162-43-150(1.3x) and 800S162-97-500 (1.2x)

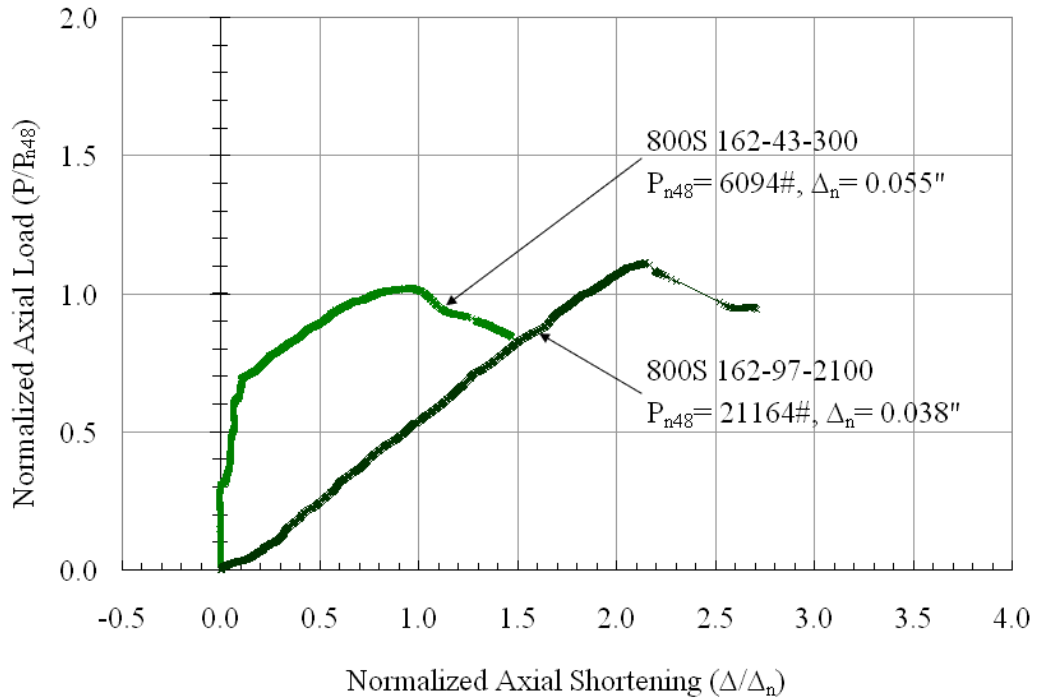


Figure 4.29 Comparison of Studs 800S162-43-300 (2.3x) and 800S162-97-2100 (4.3x)

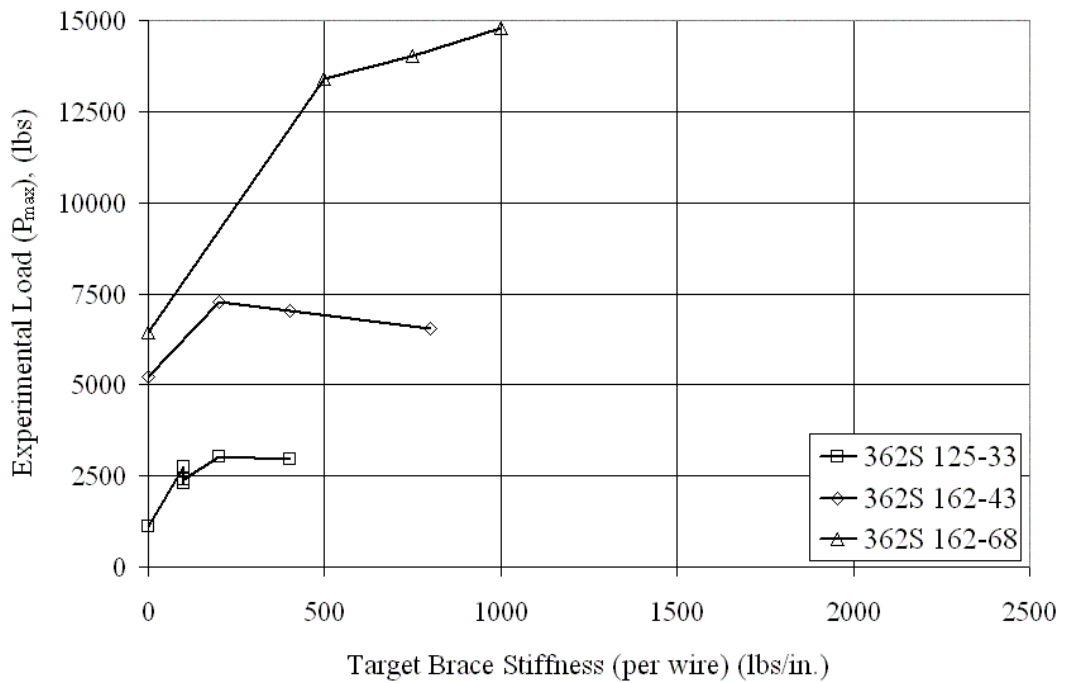


Figure 4.30 Experimental Load vs. Target Brace Stiffness for 362 Series of Lipped Cee Studs

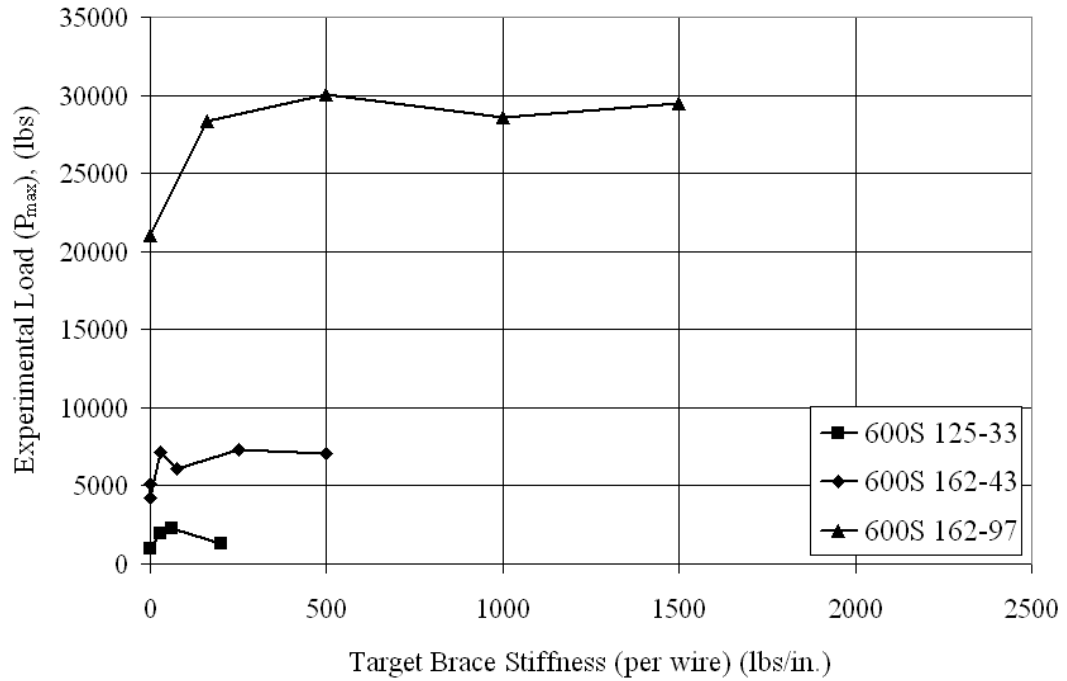


Figure 4.31 Experimental Load vs. Target Brace Stiffness for 600 Series of Lipped Cee Studs

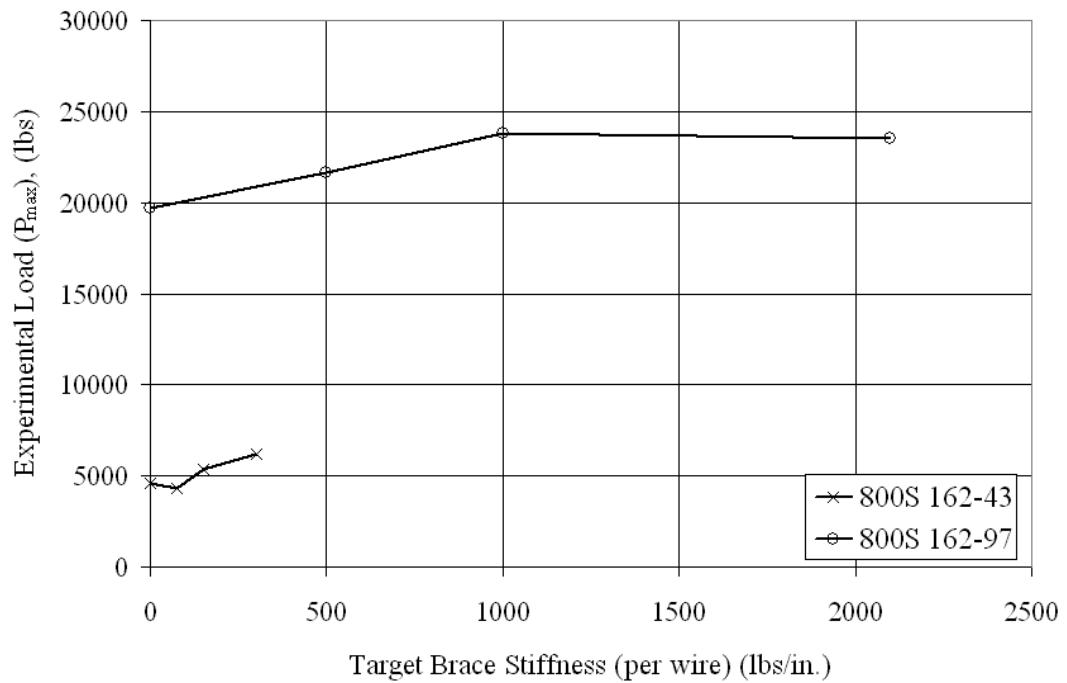


Figure 4.32 Experimental Load vs. Target Brace Stiffness for 800 Series of Lipped Cee Studs

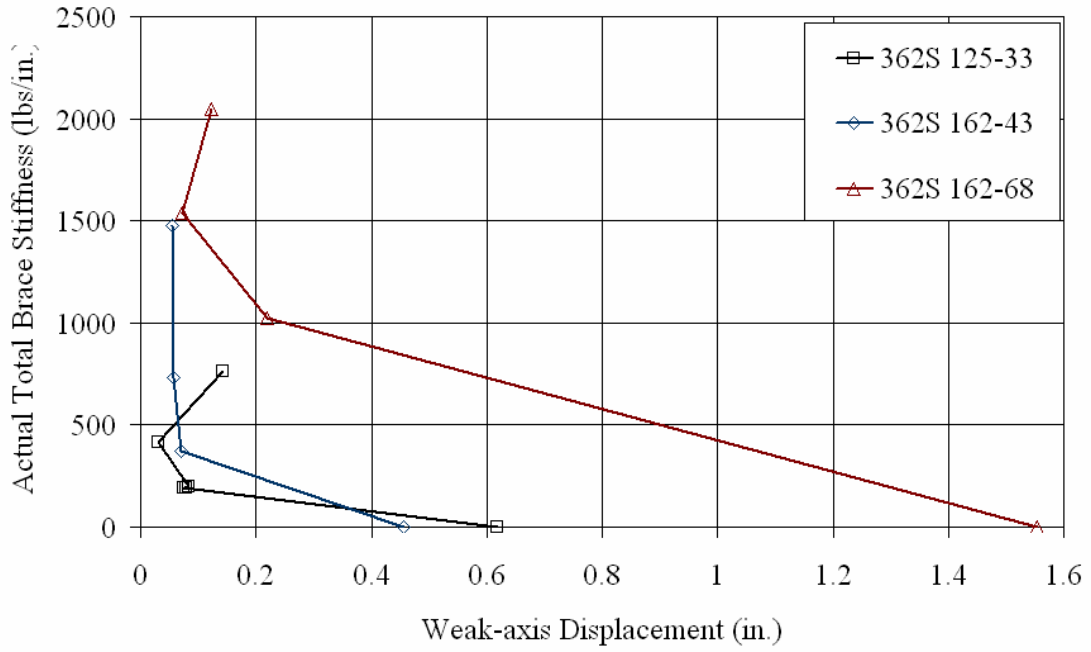


Figure 4.33 Total Brace Stiffness vs. Weak Axis Lateral Displacement for the 362 Series of Lipped Cee-Studs

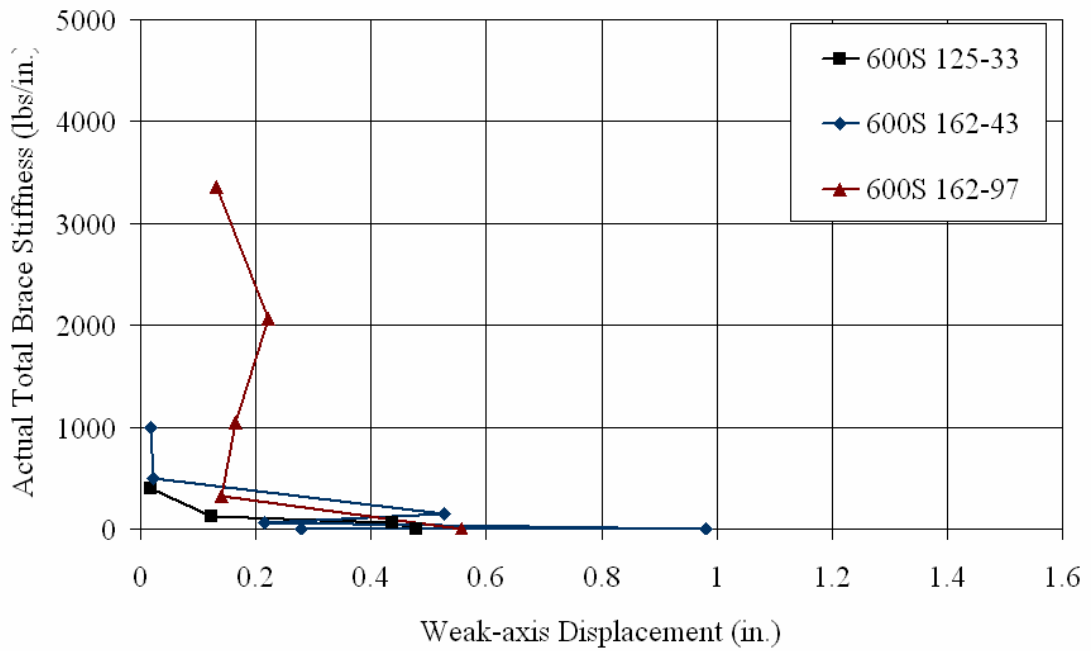


Figure 4.34 Total Brace Stiffness vs. Weak Axis Lateral Displacement for the 600 Series of Lipped Cee-Studs

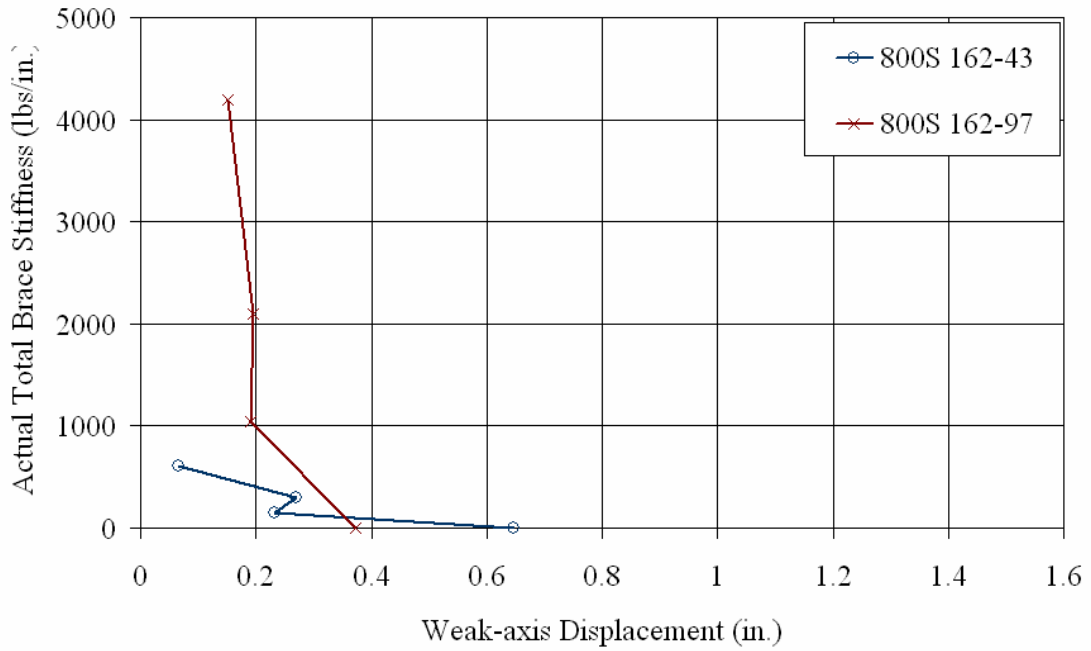


Figure 4.35 Total Brace Stiffness vs. Target Brace Stiffness for the 800 Series Lipped Cee Studs



Figure 4.36 Effective Length Factor vs. Total Brace Stiffness for 362S-125-33 Series of Lipped Cee Studs

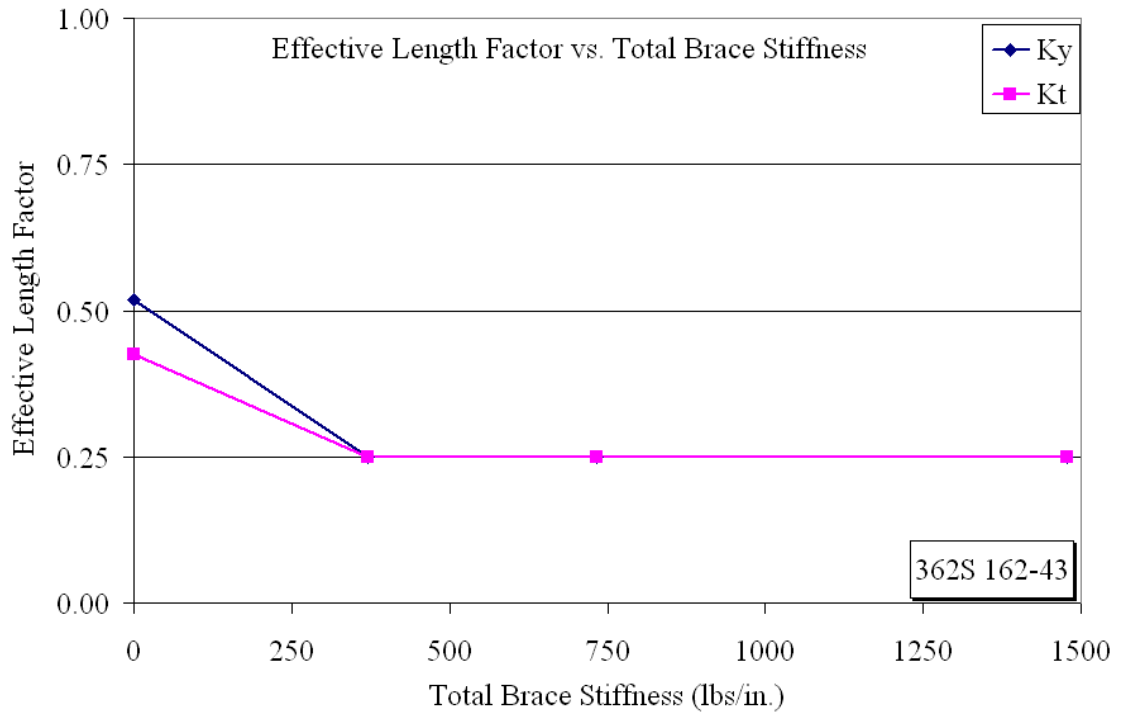


Figure 4.37 Effective Length Factor vs. Total Brace Stiffness for 362S-162-43 Series of Lipped Cee Studs

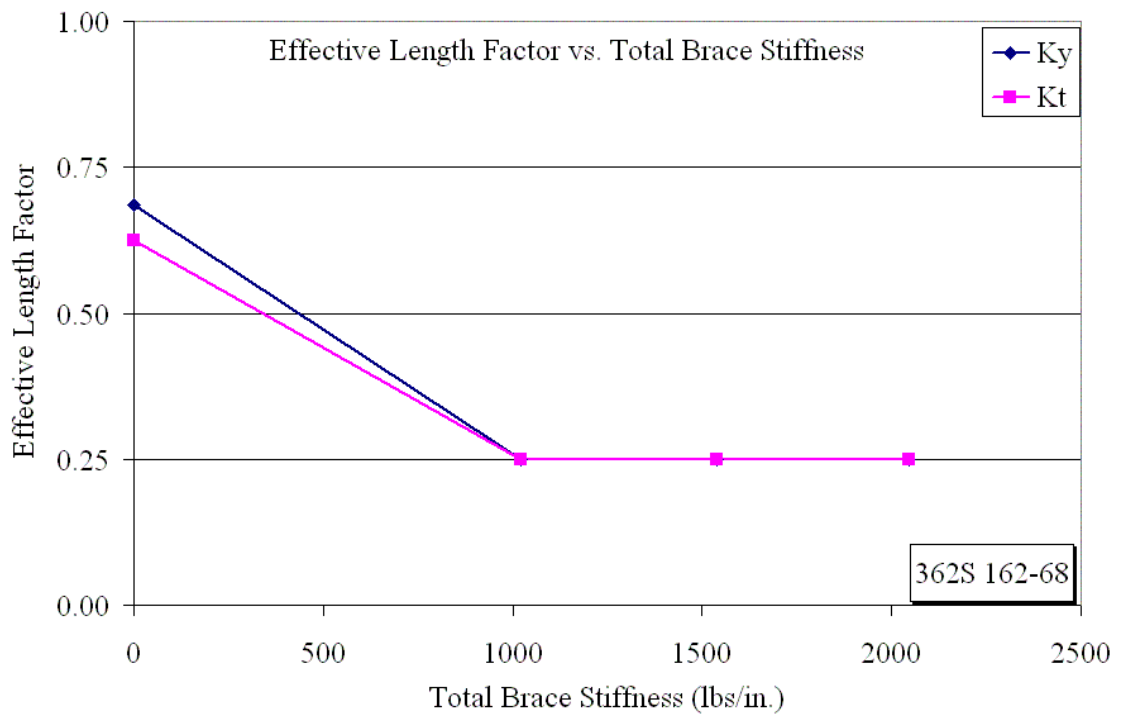


Figure 4.38 Effective Length Factor vs. Total Brace Stiffness for 362S-162-68 Series of Lipped Cee Studs

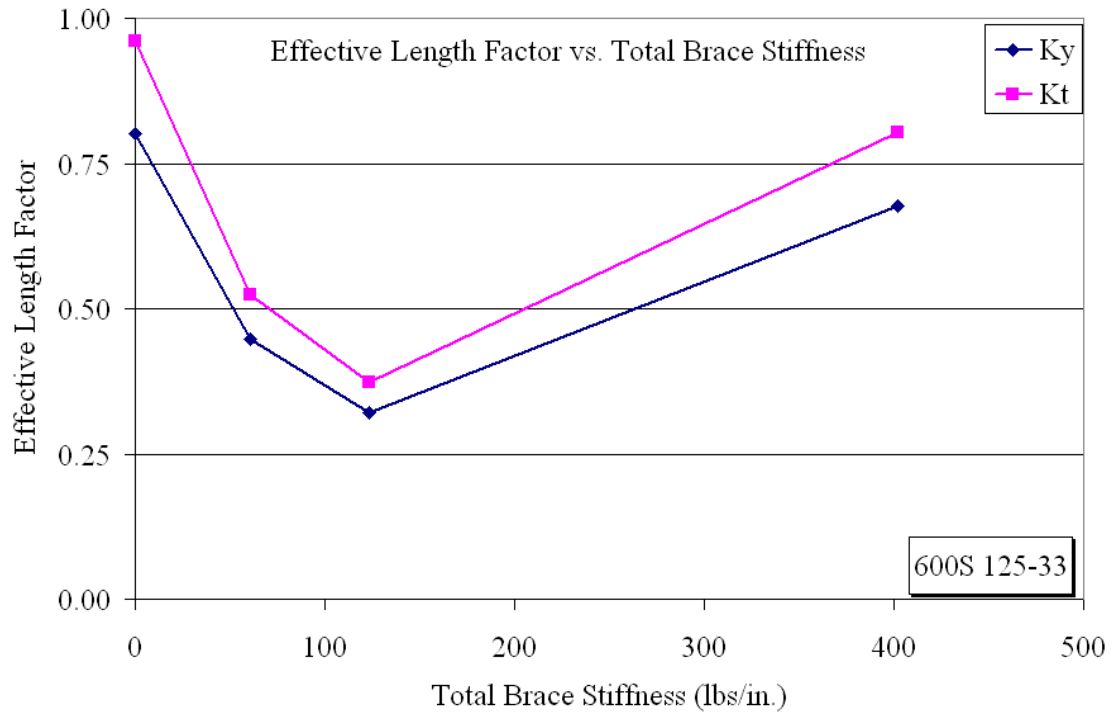


Figure 4.39 Effective Length Factor vs. Total Brace Stiffness for 600S-125-33 Series of Lipped Cee Studs

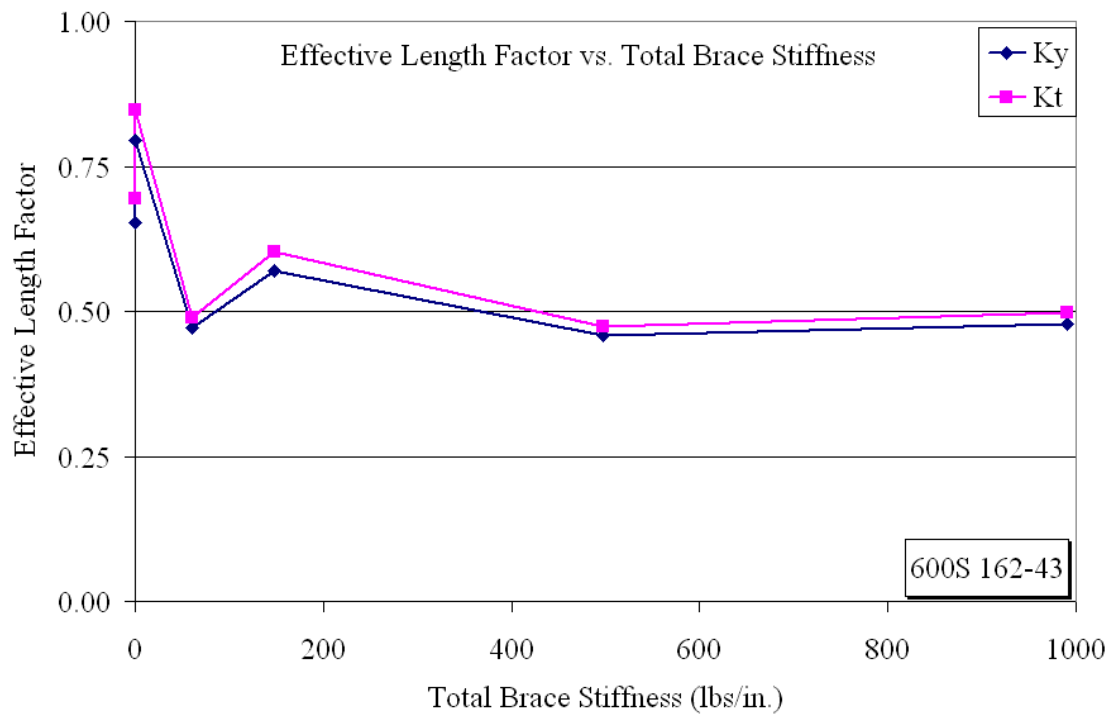


Figure 4.40 Effective Length Factor vs. Total Brace Stiffness for 600S-162-43 Series of Lipped Cee Studs

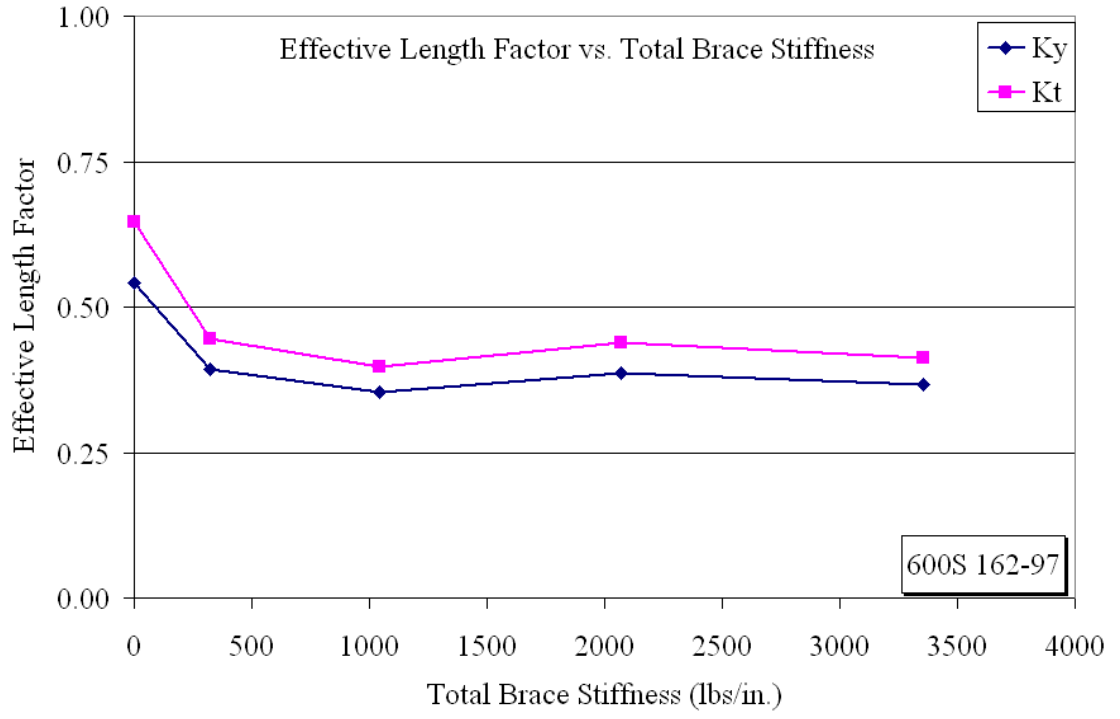


Figure 4.41 Effective Length Factor vs. Total Brace Stiffness for 600S-162-97 Series of Lipped Cee Studs

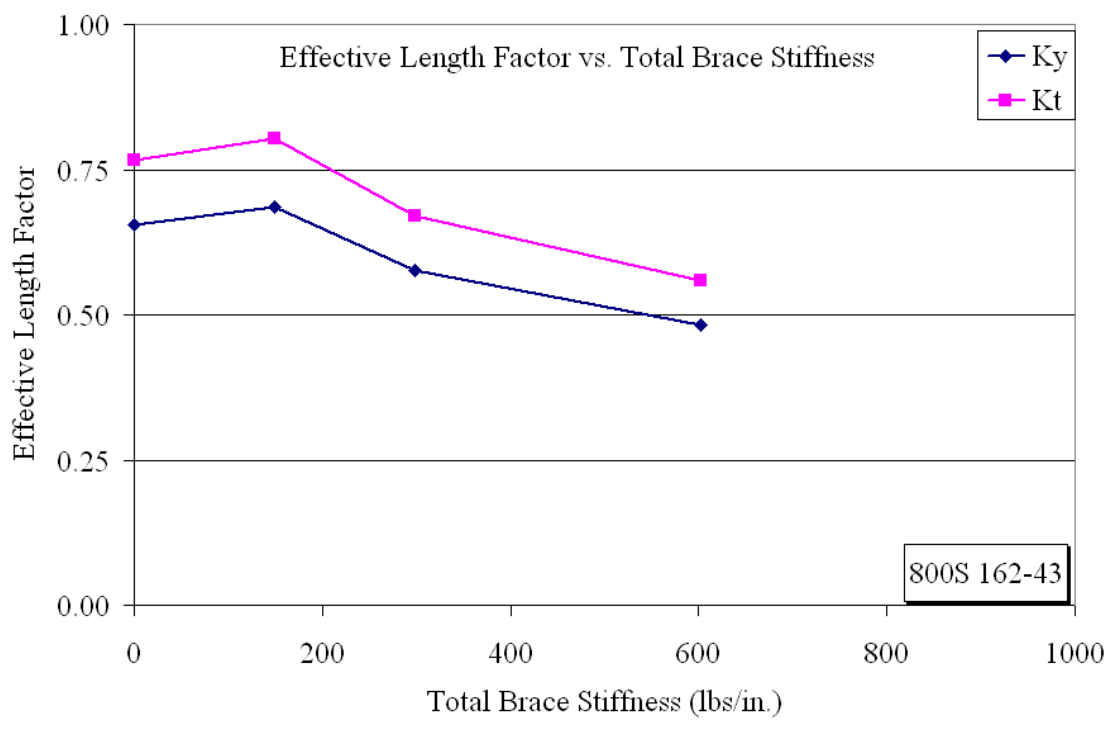


Figure 4.42 Effective Length Factor vs. Total Brace Stiffness for 800S-162-43 Series of Lipped Cee Studs

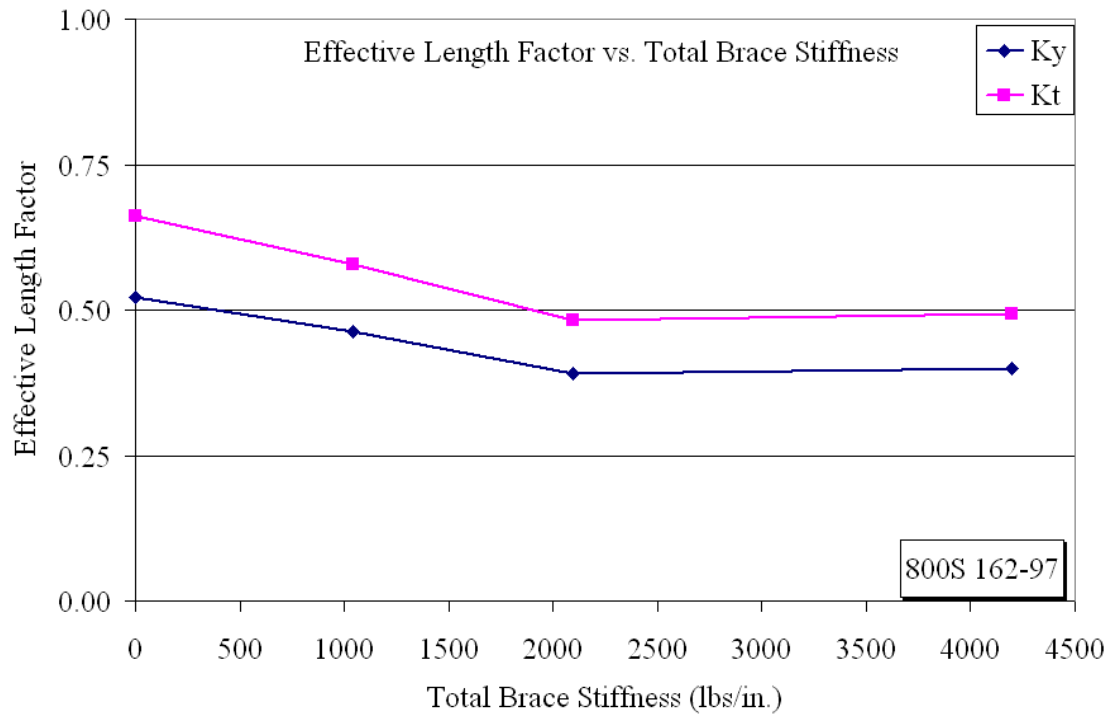


Figure 4.43 Effective Length Factor vs. Total Brace Stiffness for 800S-162-97 Series of Lipped Cee Studs

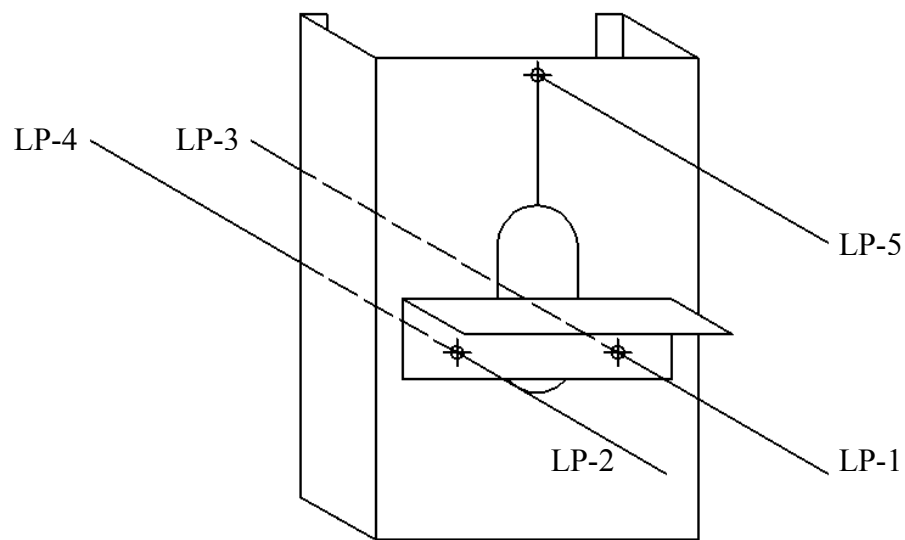


Figure 4.44 Location of Linear Potentiometers on the Bridging Connection

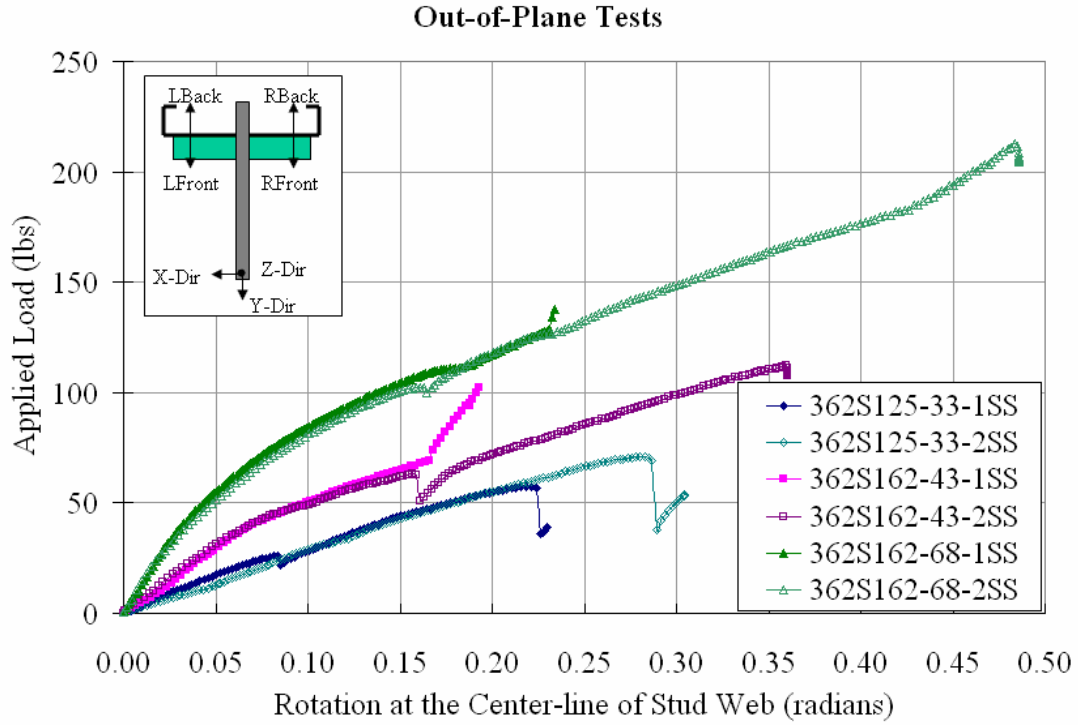


Figure 4.45 Plot of Applied Load vs. Calculated Rotation at the Center-line of the Web for the 362S Series of Studs

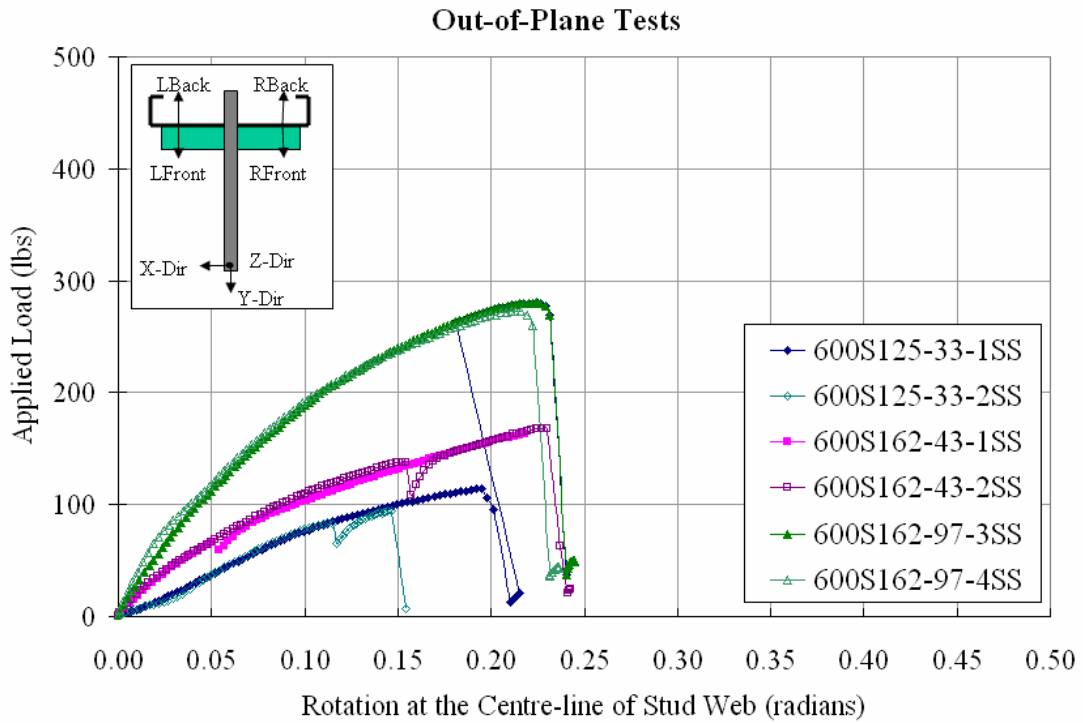


Figure 4.46 Plot of Applied Load vs. Calculated Rotation at the Center-line of the Web for the 600S Series of Studs.

Out-of-Plane Tests

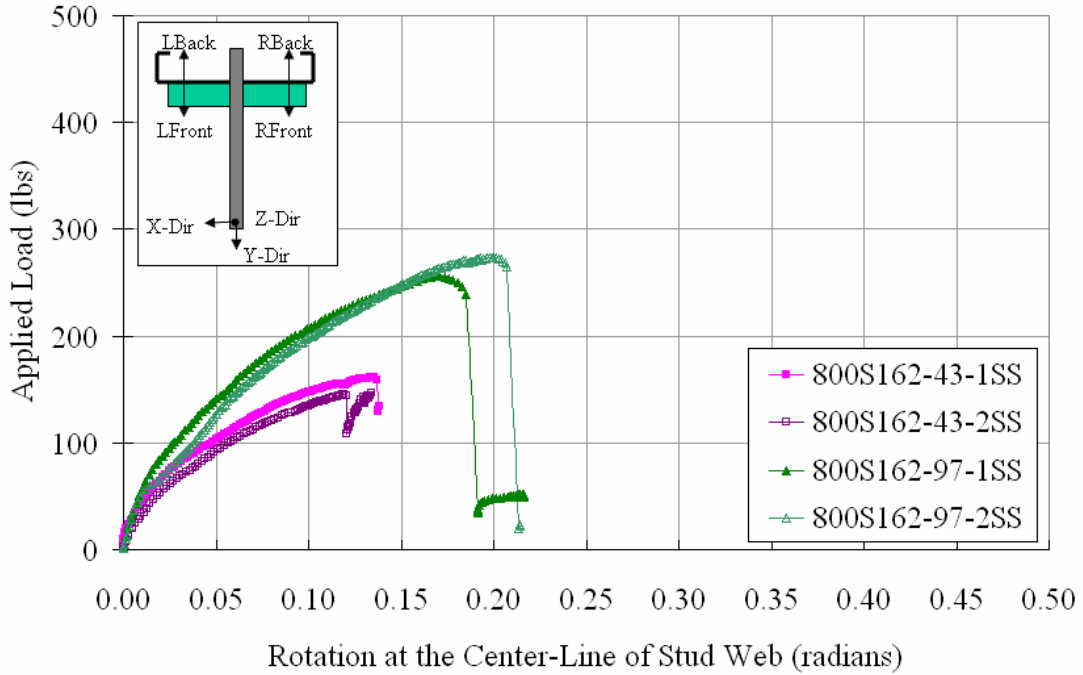


Figure 4.47 Plot of Applied Load vs. Calculated Rotation at the Center-line of the Web for the 800S Series of Studs with SS Connection.

Out-of-Plane Tests

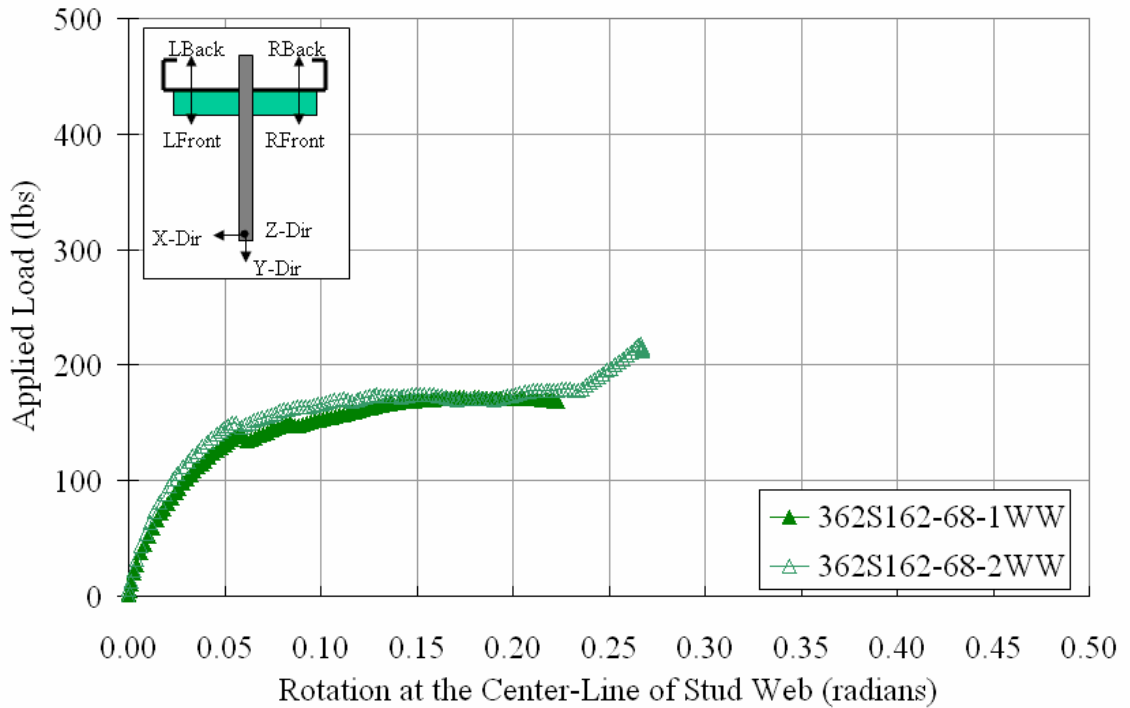


Figure 4.48 Plot of Applied Load vs. Calculated Rotation at the Center-line of the Web for the 362S Series of Studs with WW Connection

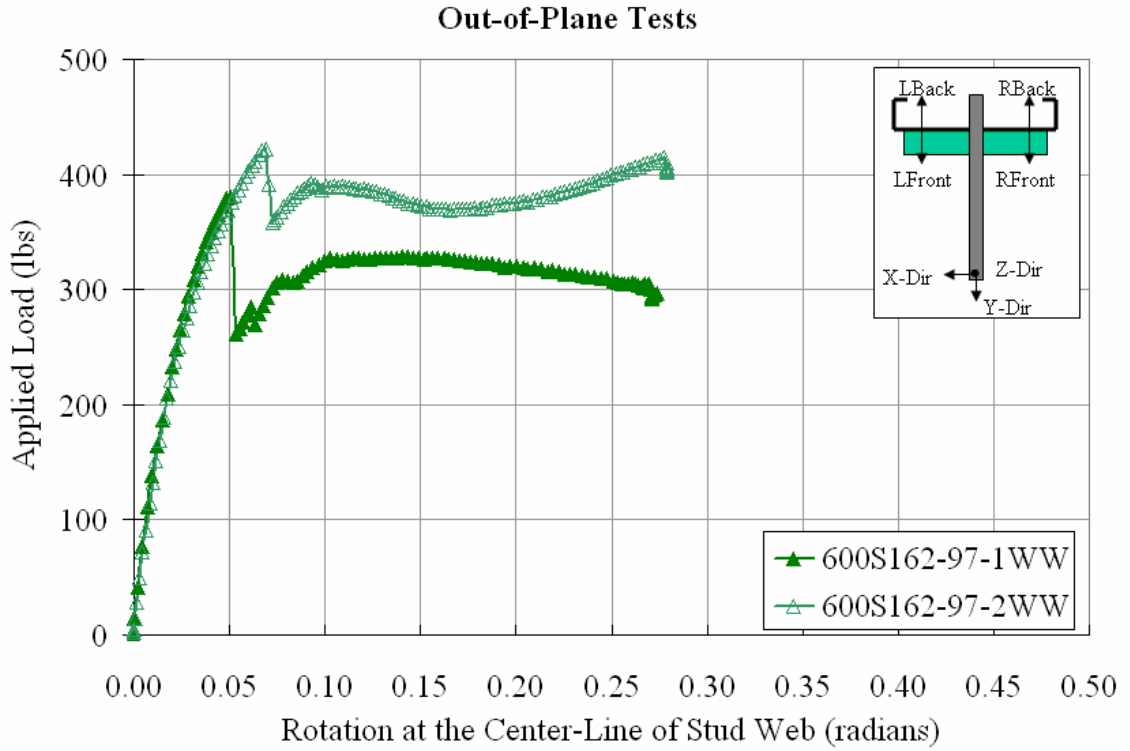


Figure 4.49 Plot of Applied Load vs. Calculated Rotation at the Center-line of the Web for the 600S Series of Studs with WW Connection

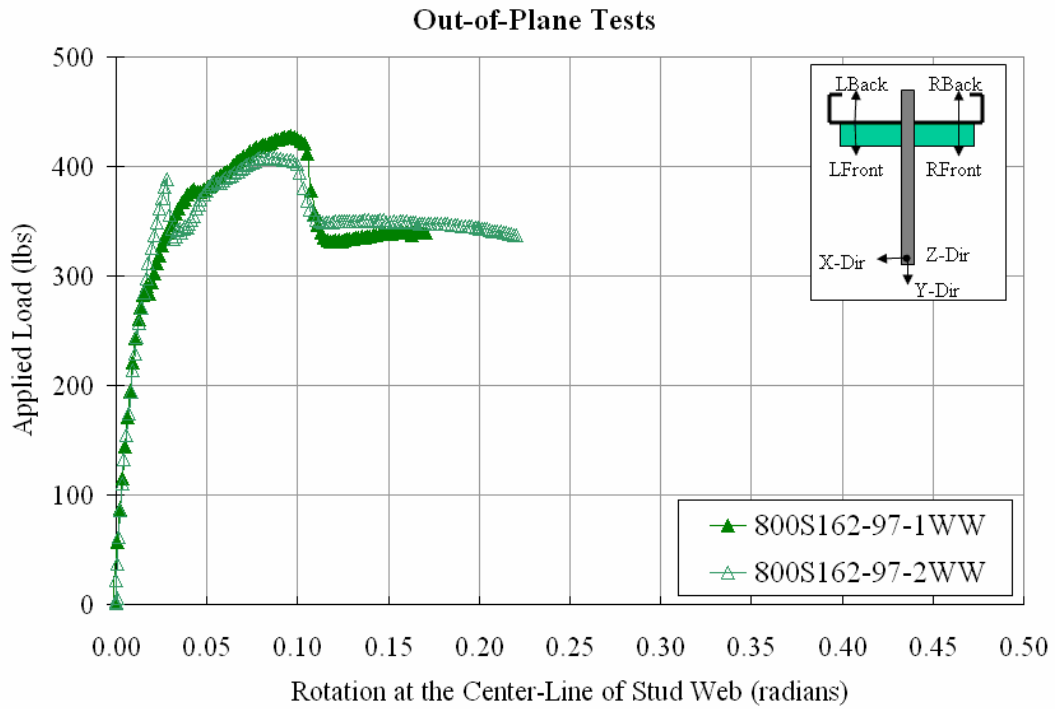


Figure 4.50 Plot of Applied Load vs. Calculated Rotation at the Center-line of the Web for the 800S Series of Studs with WW Connection

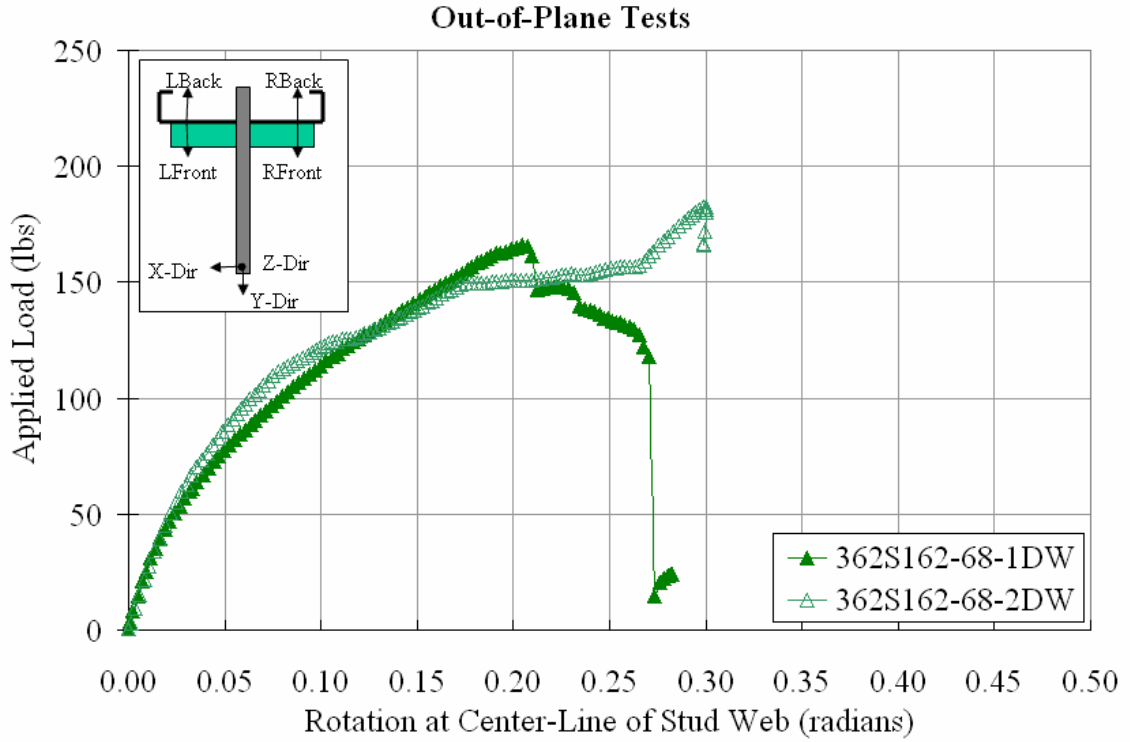


Figure 4.51 Plot of Applied Load vs. Calculated Rotation at the Center-line of the Web for the 362S Series of Studs with DW Connection

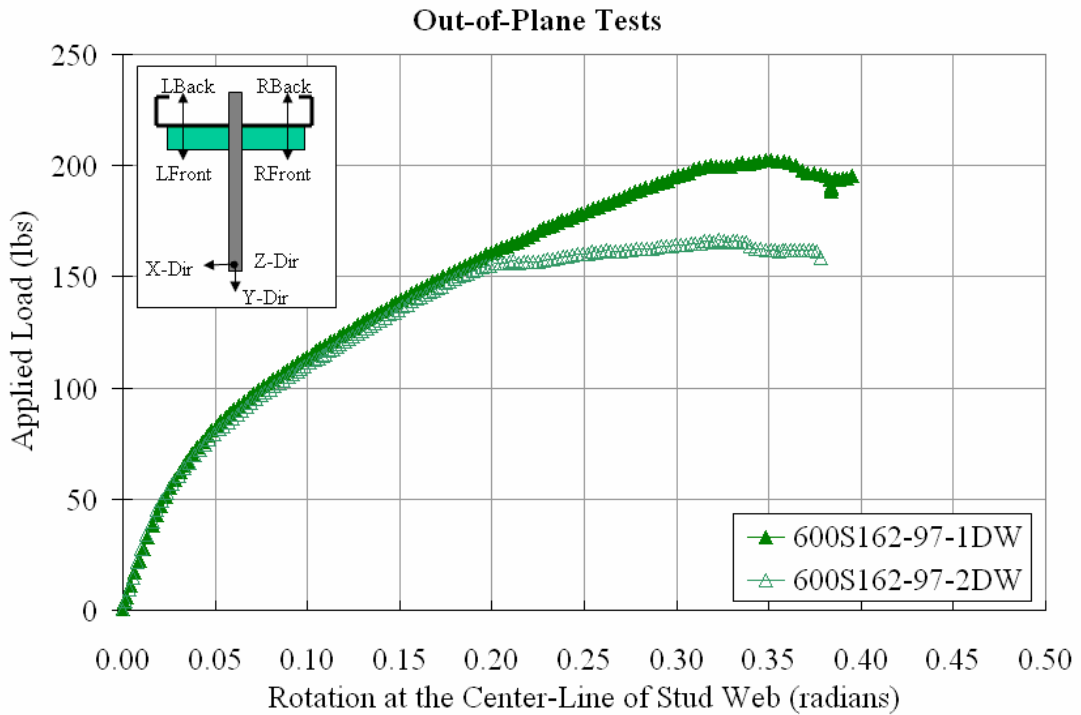


Figure 4.52 Plot of Applied Load vs. Calculated Rotation at the Center-line of the Web for the 600S Series of Studs with DW Connection

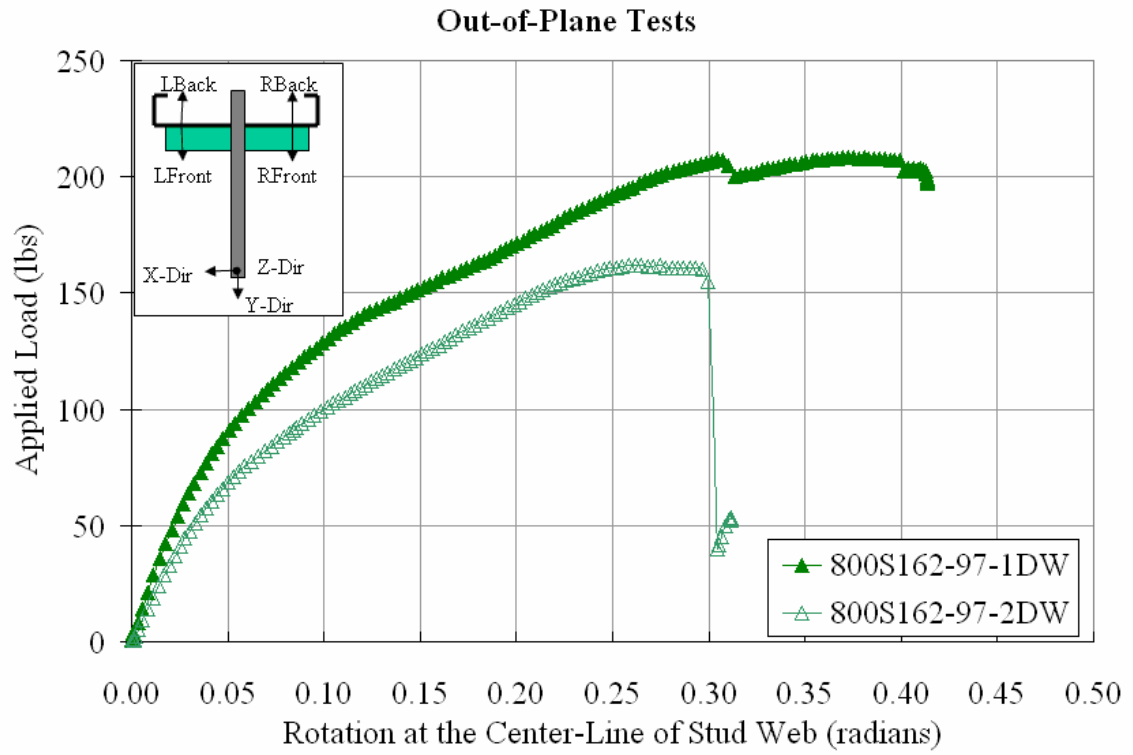


Figure 4.53. Plot of Applied Load vs. Calculated Rotation at the Center-line of the Web for the 800S Series of Studs with DW Connection

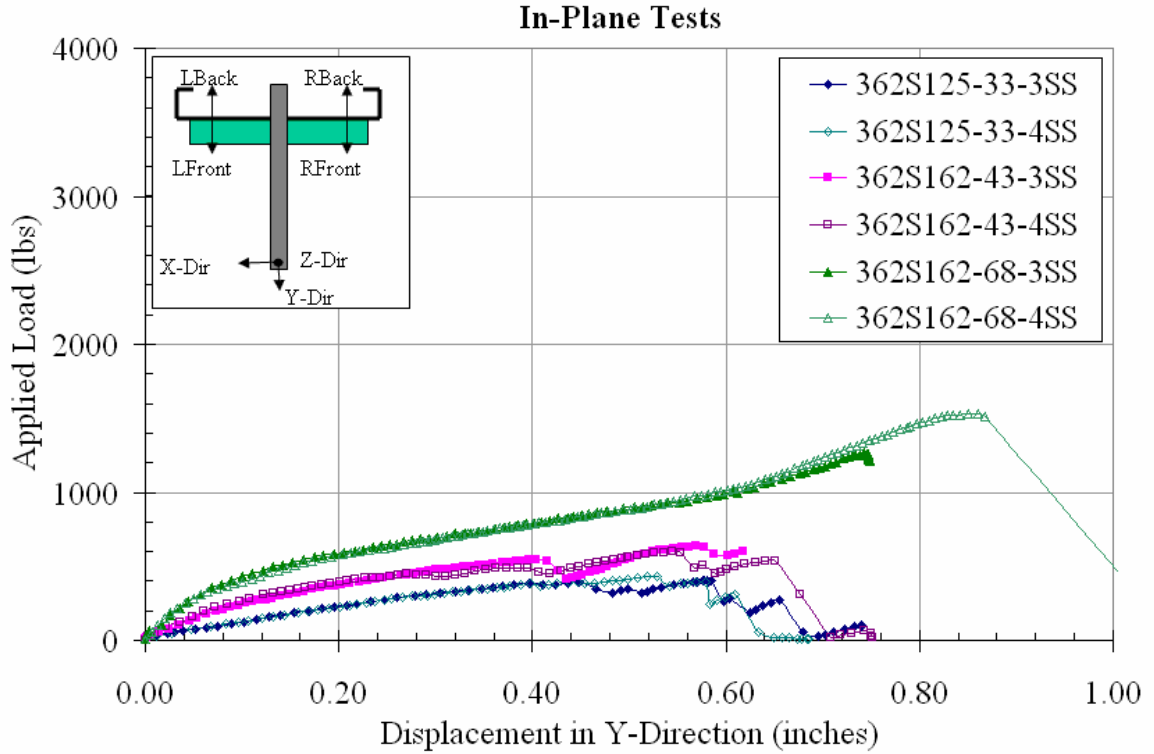


Figure 4.54 Plot of Applied Load vs. Calculated Rotation at the Center-line of the Web for the 362S Series of Studs

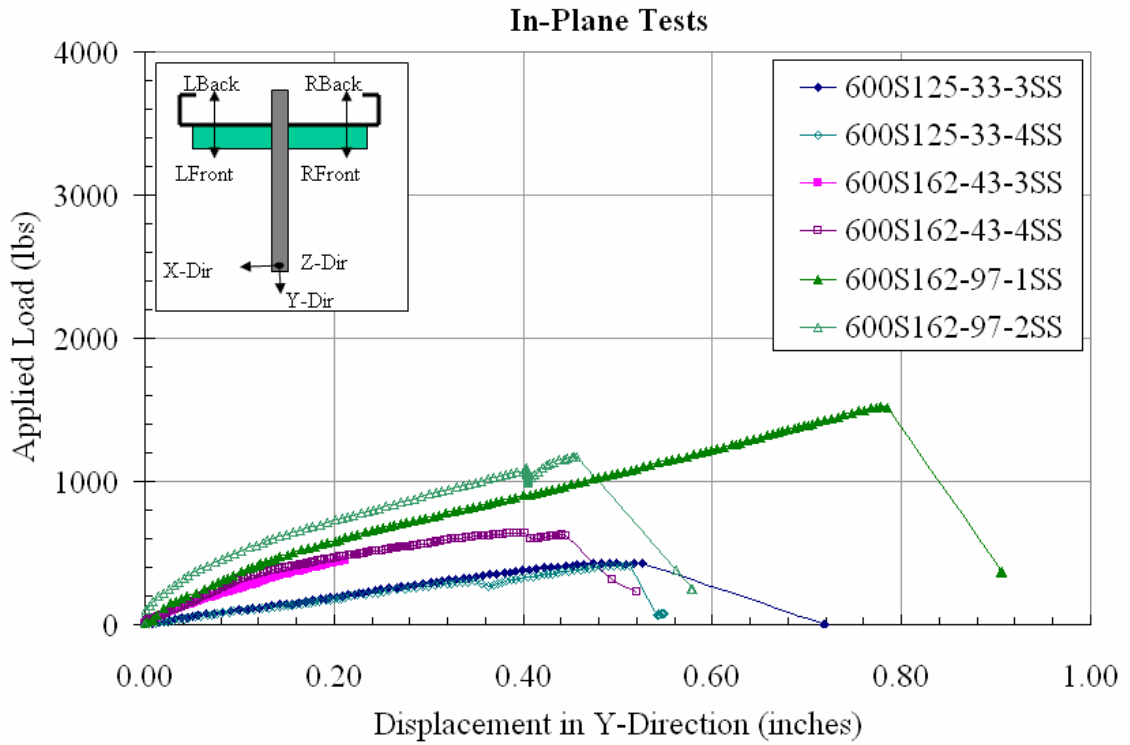


Figure 4.55 Plot of Applied Load vs. Calculated Rotation at the Center-line of the Web for the 600S Series of Studs

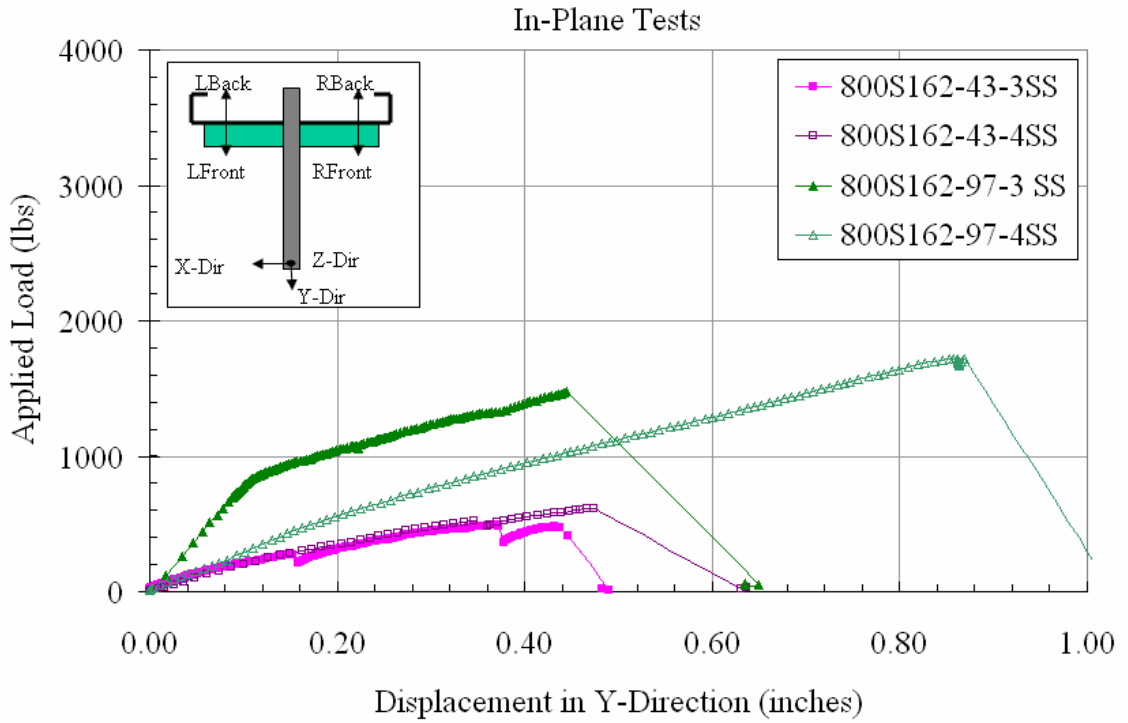


Figure 4.56 Plot of Applied Load vs. Calculated Rotation at the Center-line of the Web for the 800S Series of Studs

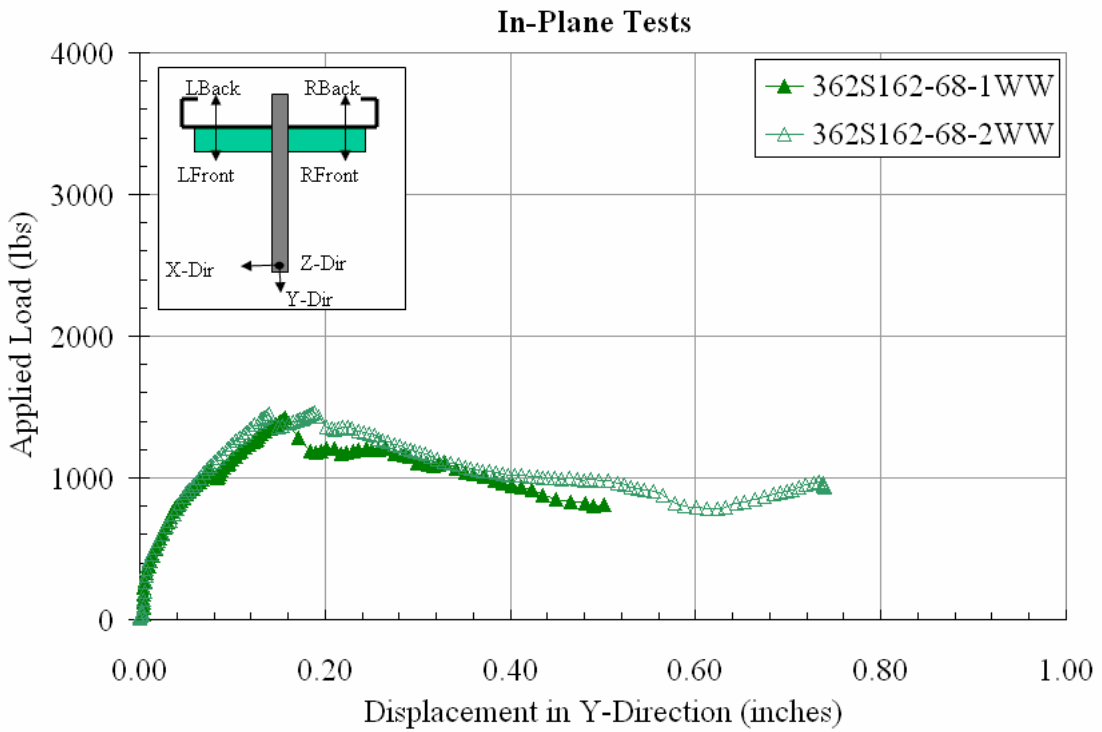


Figure 4.57 Plot of Applied Load vs. Calculated Rotation at the Center-line of the Web for the 362S Series of Studs

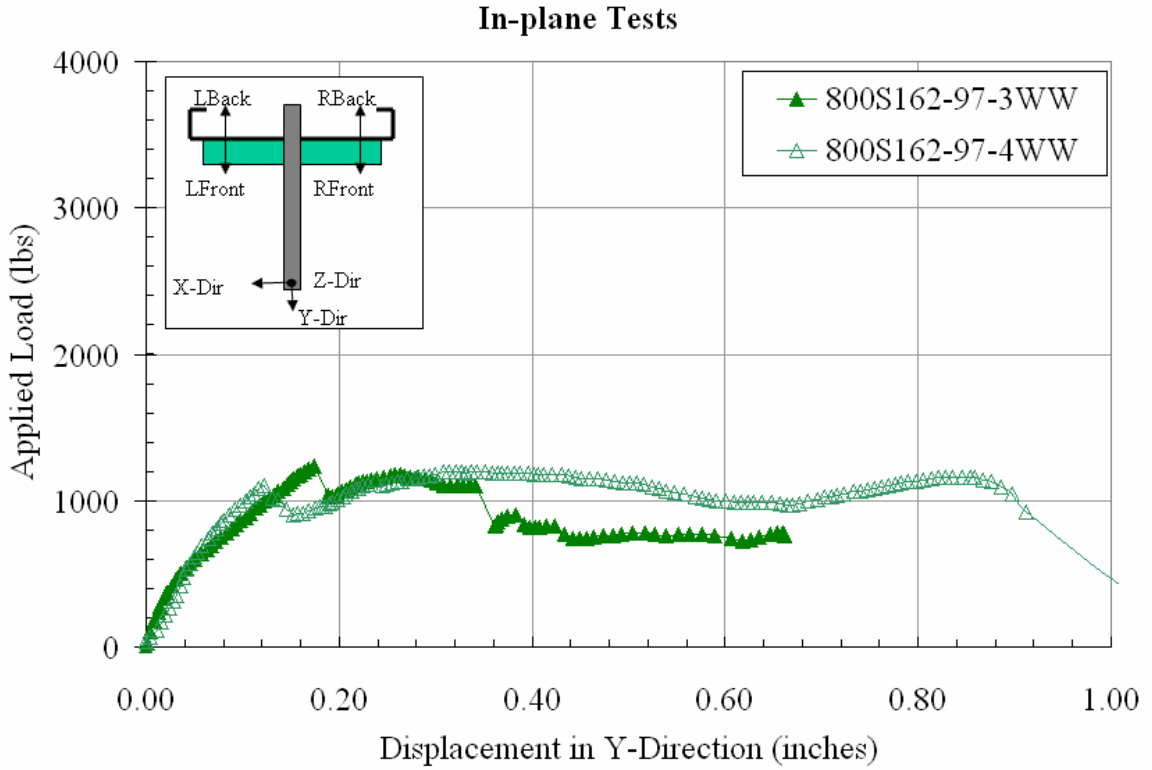


Figure 4.58 Plot of Applied Load vs. Calculated Rotation at the Center-line of the Web for the 600S Series of Studs

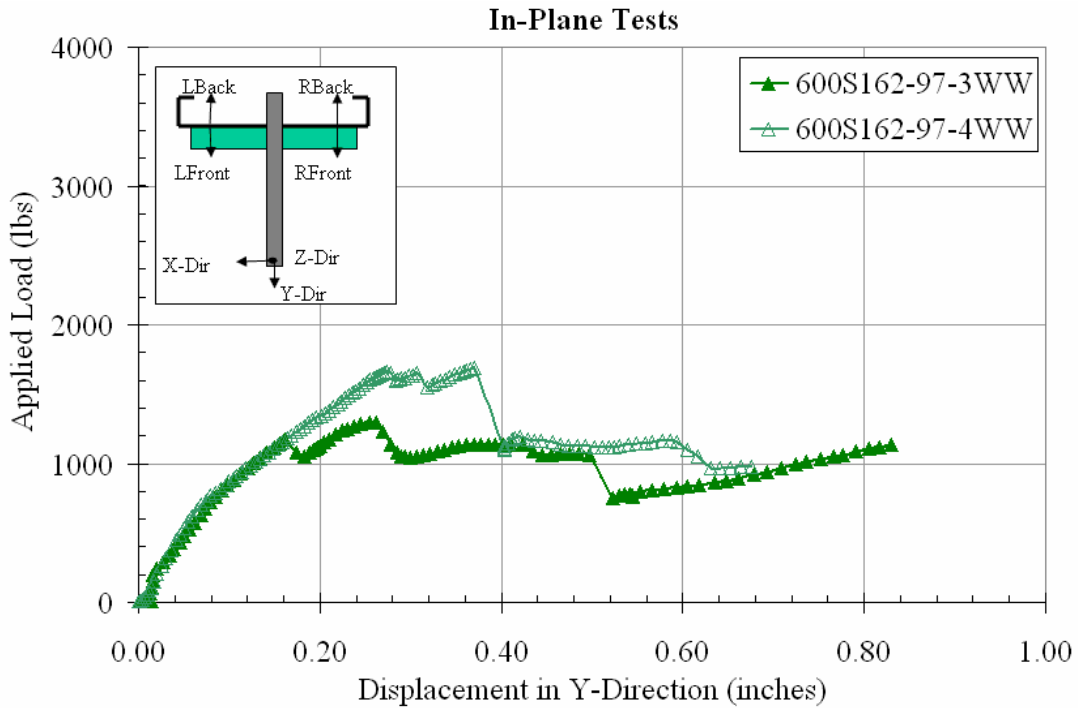


Figure 4.59 Plot of Applied Load vs. Calculated Rotation at the Center-line of the Web for the 800S Series of Studs

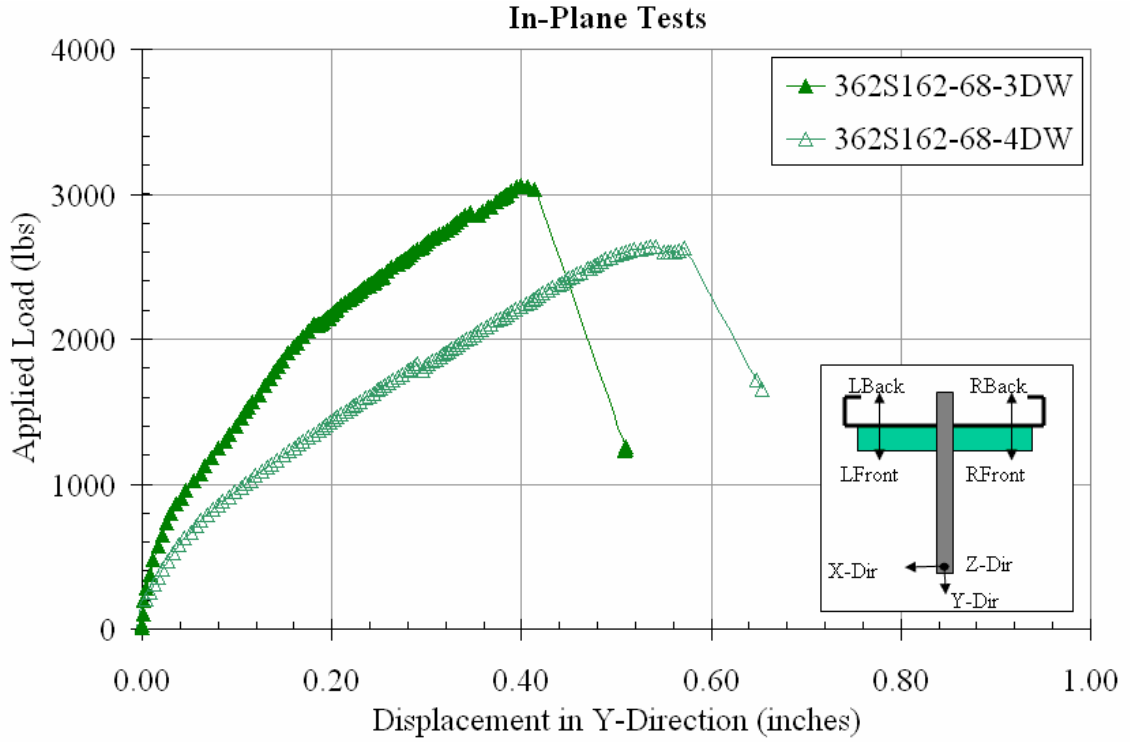


Figure 4.60 Plot of Applied Load vs. Calculated Rotation at the Center-line of the Web for the 362S Series of Studs

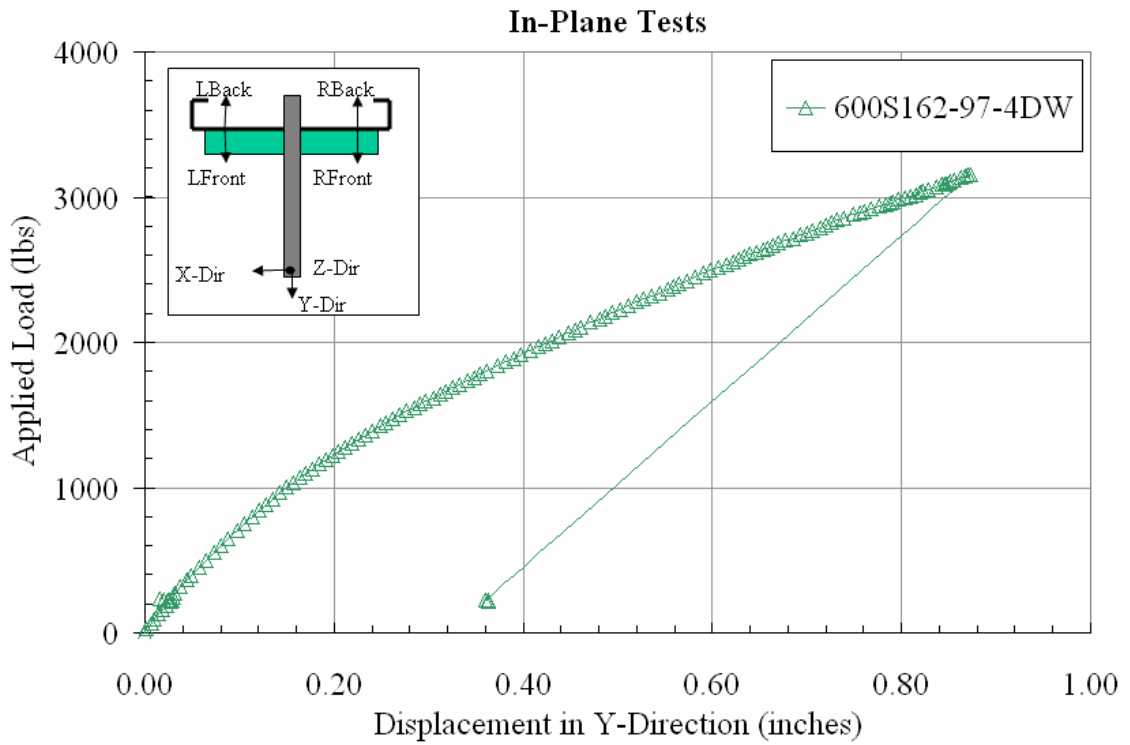


Figure 4.61 Plot of Applied Load vs. Calculated Rotation at the Center-line of the Web for the 600S Series of Studs

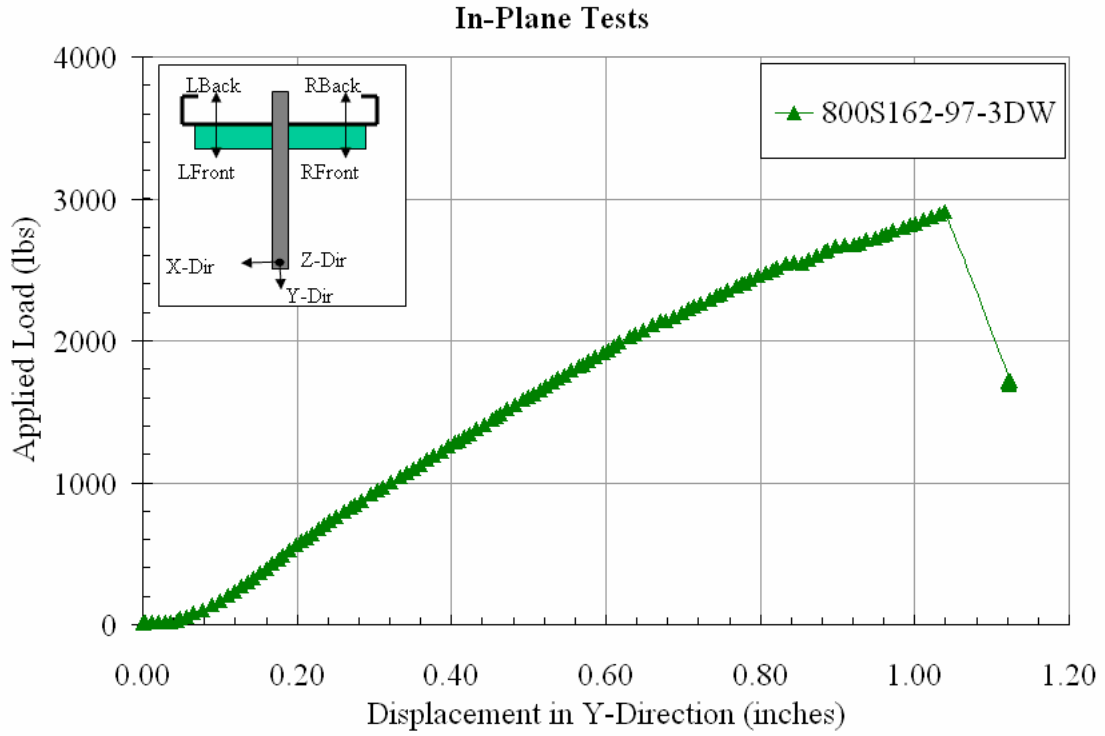


Figure 4.62 Plot of Applied Load vs. Calculated Rotation at the Center-line of the Web for the 800S Series of Studs

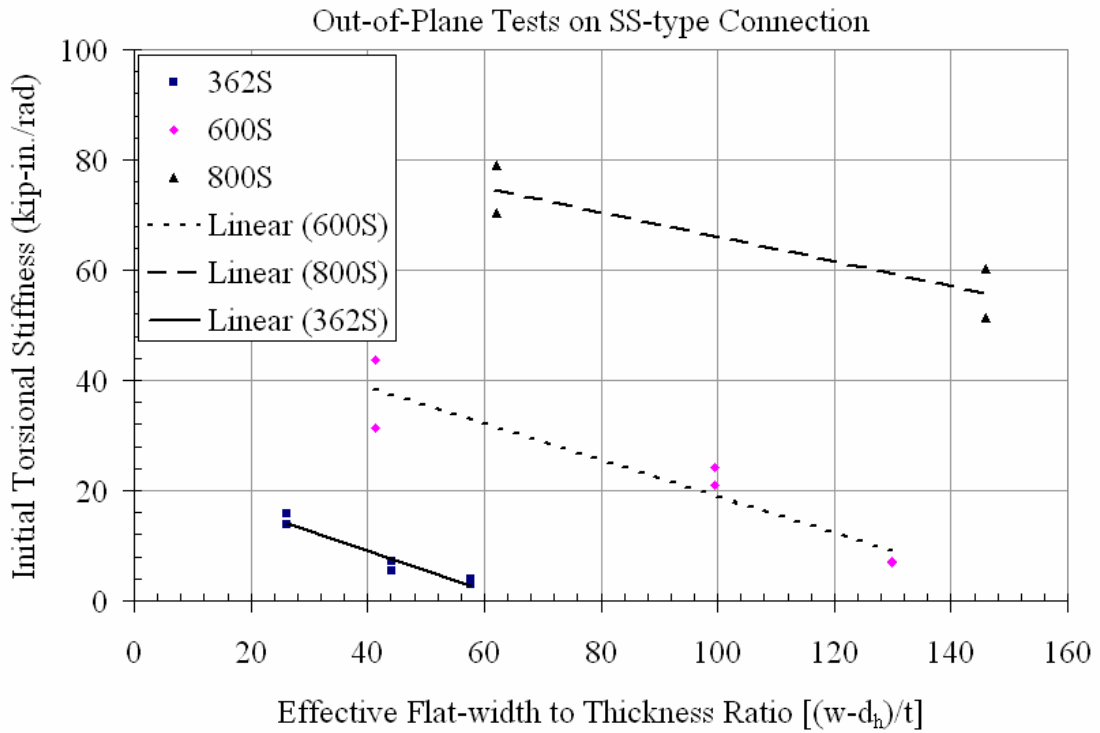


Figure 4.63 Plot of Initial Torsional Stiffness vs. Effective Flat-width to Thickness Ratio for the Out-of-Plane loading Tests on SS-type Connection

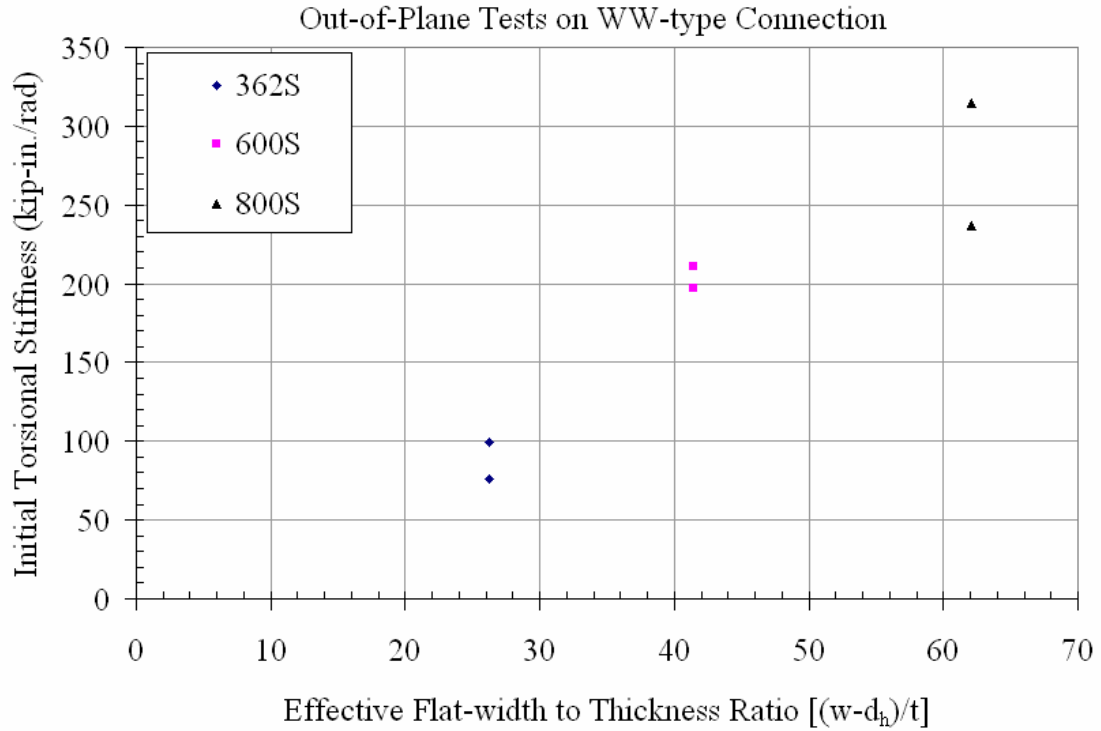


Figure 4.64 Plot of Initial Torsional Stiffness vs. Effective Flat-width to Thickness Ratio for the Out-of-Plane loading Tests on WW-type Connection

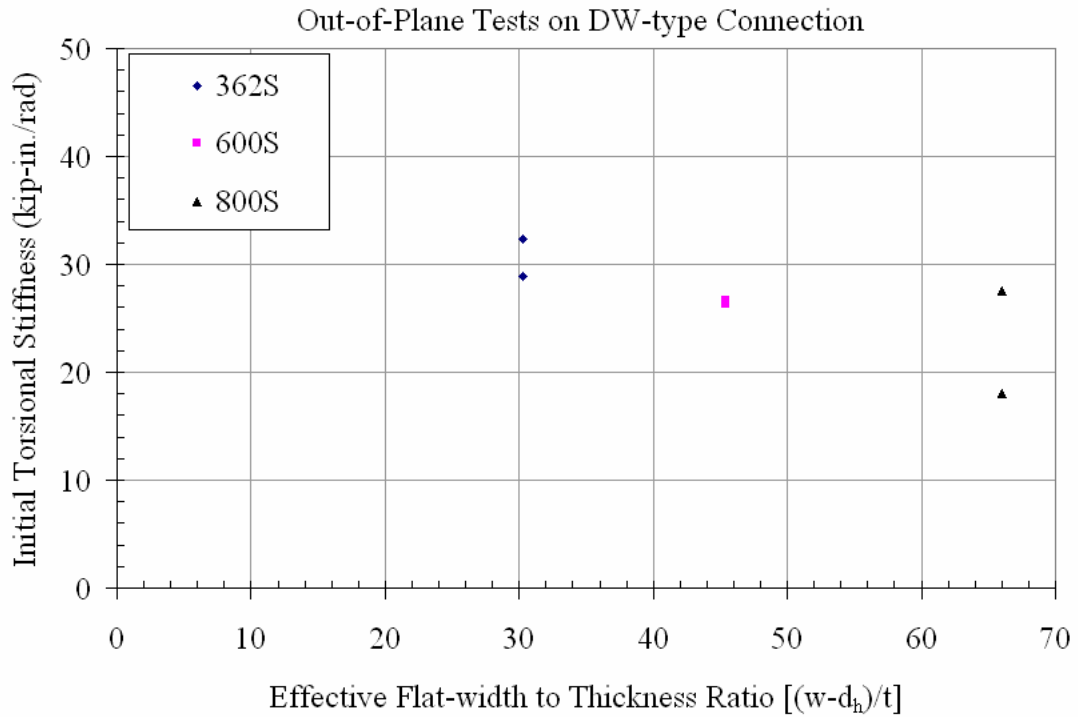


Figure 4.65 Plot of Initial Torsional Stiffness vs. Effective Flat-width to Thickness Ratio for the Out-of-Plane loading Tests on DW-type Connection

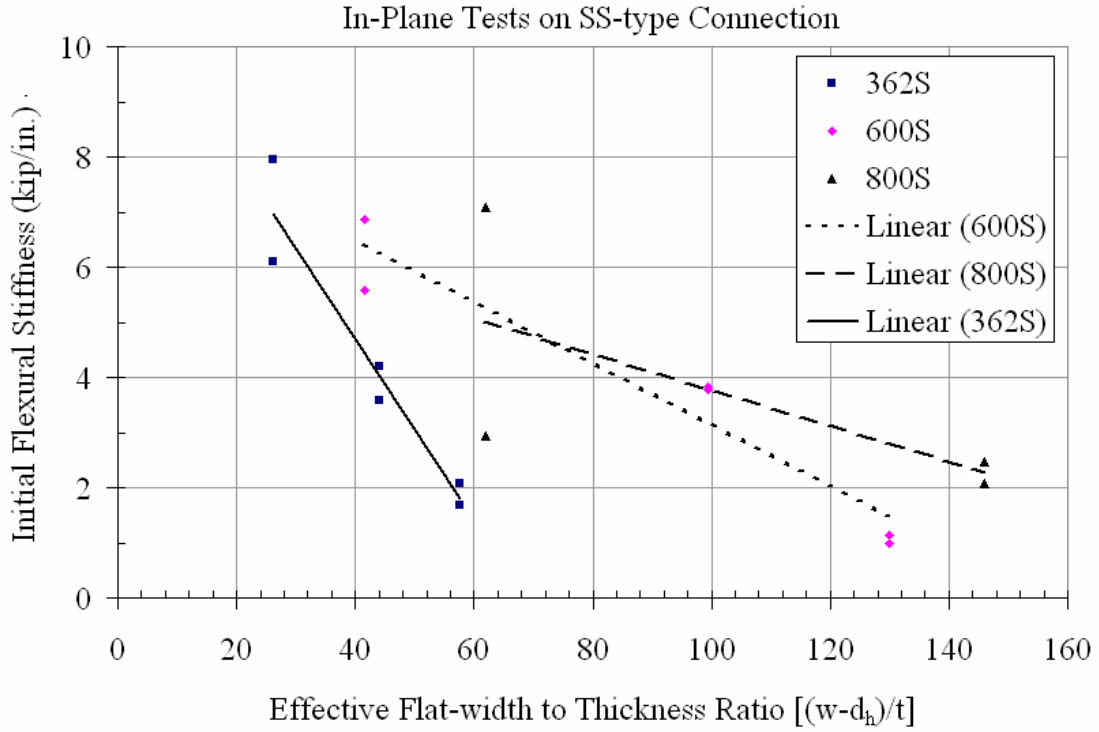


Figure 4.66 Plot of Initial Flexural Stiffness vs. Effective Flat-width to Thickness Ratio for the In-Plane loading Tests on SS-type Connection

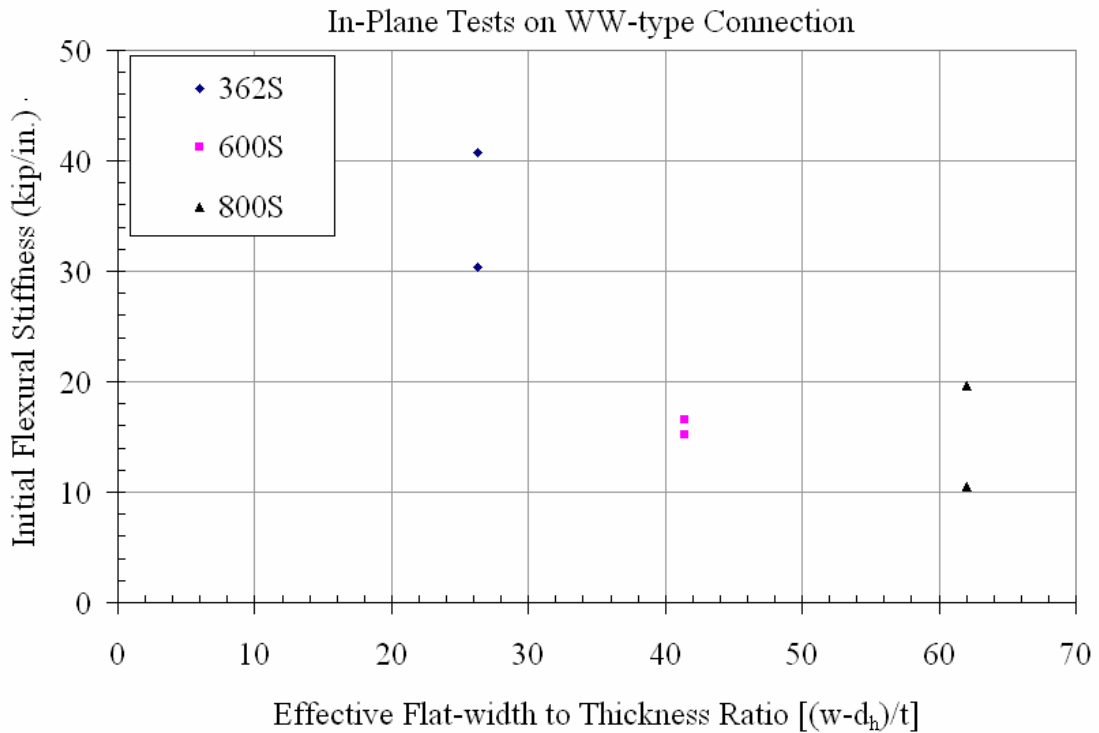


Figure 4.67 Plot of Initial Flexural Stiffness vs. Effective Flat-width to Thickness Ratio for the In-Plane loading Tests on WW-type Connection

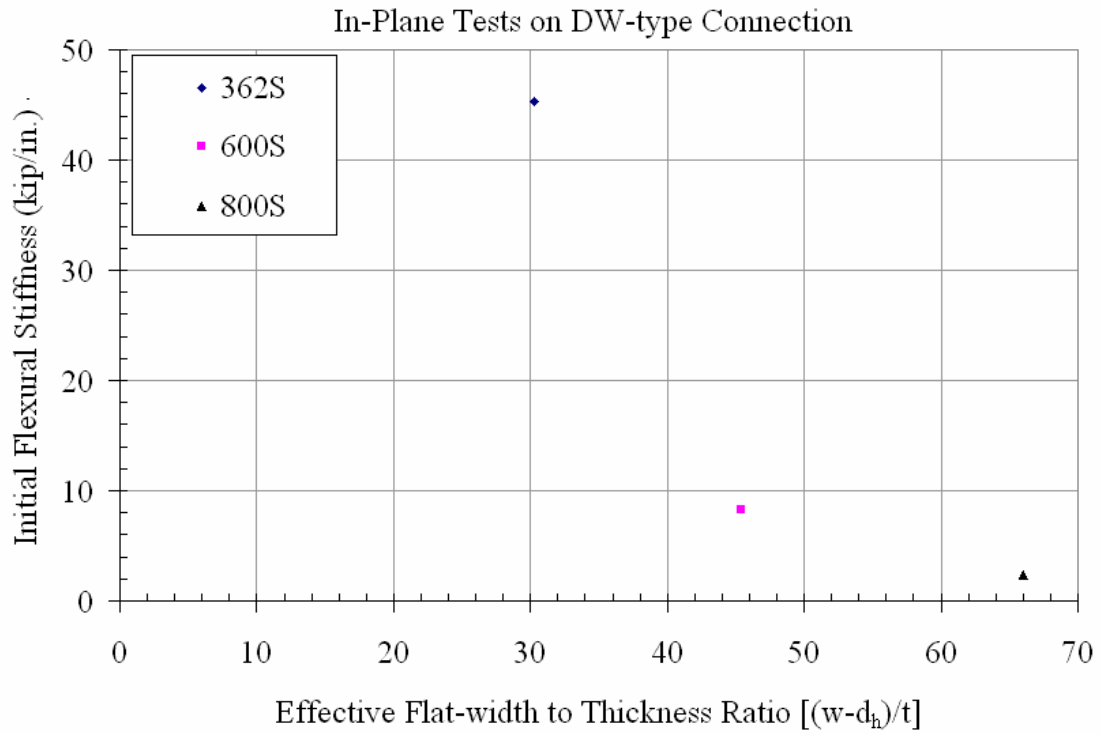


Figure 4.68 Plot of Initial Flexural Stiffness vs. Effective Flat-width to Thickness Ratio for the In-Plane loading Tests on DW-type Connection

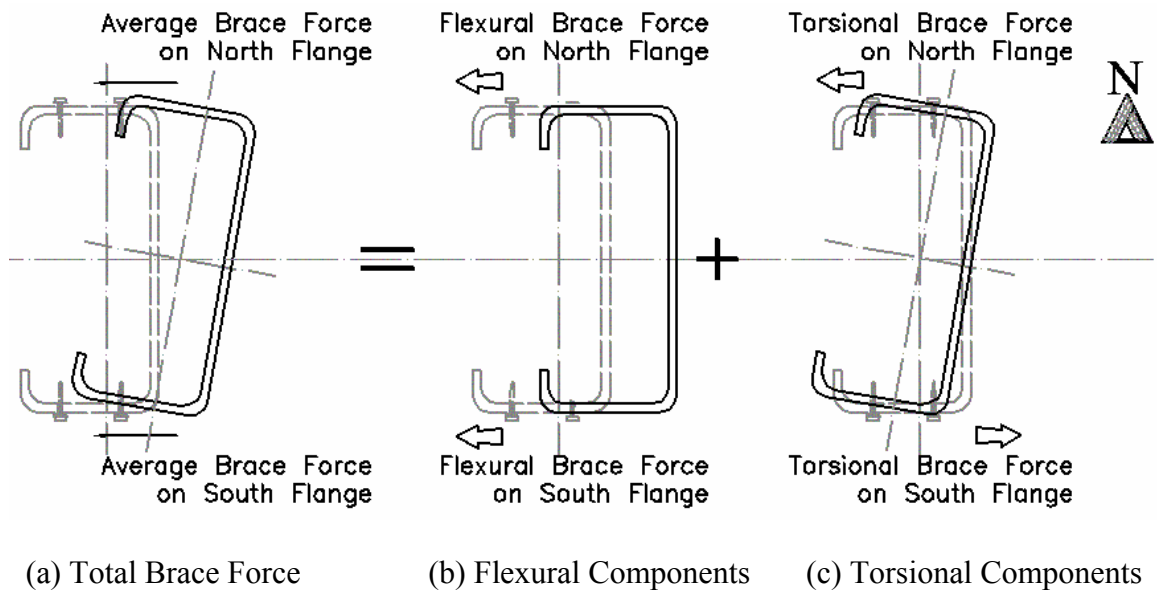


Figure 4.69 Brace Forces as a Resultant of Flexural and Torsional Components

## CHAPTER 5 ANALYTICAL EVALUATION

This chapter discusses the analytical methods used to determine the axial load capacity of the cee-stud, initial flexural stiffness and initial torsional stiffness of the bracing connections. The calculations of the total connection stiffness from the experimental results are also presented. The axial capacity was calculated for each stud cross-section using the experimentally determined mechanical properties of the eight groups of cee-studs. The flexural and torsional stiffness of the bracing connections were determined using basic structural mechanics and applying the elastic spring analogy to the connection components.

### **5.1 Analytical Load Capacity of Unbraced and Fully Braced Studs**

The axial load capacity of braced and unbraced studs was determined using MathCAD worksheets developed by Chen for AISI (1999). Table 5.1 gives the calculated axial load capacities based on two different effective length factors. The end conditions of the stud were considered pinned for weak axis flexural buckling, fixed for strong axis flexural buckling and fixed for torsional buckling about the shear center. The reasons for choosing these support conditions and the effects on stud behavior have been discussed in Chapter 4. The effective length factor for the case of an unbraced stud, for strong axis flexural buckling,  $K_x = 0.5$ , for weak axis flexural buckling,  $K_y = 1.0$  and for torsional buckling,  $K_t = 0.5$ . The effective length factor for the case of a braced stud, for strong axis flexural buckling,  $K_x = 0.5$ , for weak axis flexural buckling,  $K_y = 0.5$  and for torsional buckling,  $K_t = 0.25$ . The MathCAD worksheets accounts for the size of the

punchouts and their locations. The axial load capacity is affected by the size of the punchout, the effect of which is in reduction of the axial load capacity. The effective cross-sectional area is determined based on the effective width of the web across the punchout as per Section B2.2, AISI (1999). The critical buckling stress is computed as the minimum of the strong axis buckling stress, the weak axis buckling stress or the torsional buckling stress. The axial loads predicted by the AISIWIN (2000) program whose results are given in Tables 4.3 and 4.4 did not include the effect of punchouts and hence are greater than the values given in Table 5.1 for the same cross-section of the cee-stud. It may be observed that in both the analytical determinations of axial load capacities fall below the actual experimental maximum load. This is because of the support restraint that is present in the test specimens.

These MathCAD worksheets were used to compare the results obtained from AISIWIN (2000). It can be observed that AISIWIN gives a higher prediction of the axial load capacity than the MathCAD worksheets results. It must be noted here that, using both these analytical methods, the axial capacity was far conservative due to which the brace stiffness and demand happens to be less than the experimentally required value. This leads to a bracing requirement that is unconservative for all practical purposes. The reason being that the support conditions in the standard industry practice, using standard tracks, offers far more rigidity than the ideal cases of pinned ends. The two analytical methods used to determine the axial load capacities of the cee-studs though have the option of specifying the effective lengths, it is a judgment call by the practicing engineer to safely choose the effective lengths.

## 5.2 Analytical Bridging Connection Stiffness of a Flexible Bracing

The experimental values of initial connection stiffness have been determined in Chapter 4. Referring back to Table 4.13, the initial torsional stiffness at 10% of the maximum load is calculated as the ratio of the applied load to the corresponding rotation of the web. It was observed that within this load range, the initial slopes of the plots were nearly linear. Similarly, Table 4.15 gives the initial flexural stiffness at 10% of the maximum load, calculated as the ratio of the applied load to the corresponding Y-displacement of Point A, the point of application of the load on the channel bridging, measured by a string potentiometer.

The total actual stiffness of the bridging system is calculated using Eq. 2.22, as described in Chapter 2. The total actual stiffness is the reciprocal of the sum of reciprocals of the connection stiffness and the brace stiffness, because the bridging connection is in series with the bracing system. The bridging connection is comprised of several connecting elements that are in series with one another and their equivalent connection stiffness determination is given in Appendix C. The total connection stiffness was determined from both the experimental results of the bridging tests and the analytical models developed for each connection type. The comparisons of the calculated experimental stiffness with calculated analytical stiffness are presented in Tables 5.2 and 5.3 for the initial flexural stiffness and the initial torsional stiffness, respectively.

### 5.2.1 Initial Flexural Stiffness of the Bracing Connection

The following assumptions were made in finding the analytical value of initial flexural stiffness:

- The bridging channel was considered to be under tension due to the applied load and the deformation was computed using the following equation:

$$\frac{\Delta}{P} = \frac{L}{A E} \quad (5.1)$$

- The clip angle acts as a beam supported at two points, subjected to two point loads. The moment of inertia of the angle was taken about its horizontal leg. For the SS type connection, the angle was considered to be simply-supported between the screws, and for the WW type connection, the angle was considered to be fixed at the welds. The MathCAD worksheet for this calculation is given in Appendix C and provides the calculations for this analytical determination.
- The web was considered as a rectangular plate with either simple or fixed edges at the boundaries. The plate was considered to be subjected to concentrated loads at the location of the screws or the welds. The plate buckling equation (Roark 1985) for a rectangular plate subjected to a concentrated load is given as:

$$\frac{\Delta}{P} = C(1 - \mu^2) \frac{a b}{E t^3} \quad (5.2)$$

|       |          |   |   |
|-------|----------|---|---|
| where | C        | = | Support fixity coefficient of the steel plate |
|       | E        | = | Elastic modulus of cold-formed steel          |
|       | P        | = | Applied load                                  |
|       | a, b     | = | Dimensions of the rectangular plate           |
|       | t        | = | Thickness of the rectangular plate            |
|       | $\Delta$ | = | Displacement due to applied load, P           |
|       | $\mu$    | = | Poisson's ratio of steel, 0.3                 |

The effective width of the web plate was calculated as per Section B2.2, AISI (1999) which is as follows:

$$b = \frac{w}{\lambda} \left[ 1 - \frac{0.22}{\lambda} - \frac{0.8 d_h}{w} \right] \quad (5.3a)$$

when  $\lambda > 0.673$  or

$$b = w - d_h \quad (5.3b)$$

where  $d_h$  = Diameter of the elongated circular punchout

The slenderness factor is calculated using the relation

$$\lambda = \frac{1.052}{\sqrt{k}} \frac{w}{t} \sqrt{\frac{f_y}{E}} \quad (5.4)$$

where  $k$  = Plate buckling coefficient  
 = 24.0 for simply-supported edges  
 = 40.8 for fixed-fixed edges

The effect of the length of the punchout was considered to be negligible since the web is assumed to be infinite in that direction while the predominant flexural displacement was along the shorter span direction between the flanges of the cee-stud cross-section. In all the cases, the stiffness and deformation of the screws or the welds was calculated and found that these components had little effect on the overall connection stiffness, and hence they were later neglected for simplicity.

The flexural stiffness values are plotted in Figures 5.1, 5.2 and 5.3 against the slenderness factor of the stud web, determined using Eq. 5.4 for the three connection types (SS, WW and DW), respectively. The plots contain four different data sets representing the following cases of initial flexural stiffness for the in-plane loading tests:

- Experimental lower bound values (LBV)
- Experimental upper bound values (UBV)
- Analytical value for a rectangular plate with four simply-supported edges
- Analytical value for a rectangular plate with four fixed edges

#### **5.2.1.1 SS type connection**

It can be observed that in Figure 5.1 for the SS Type connection the analytical calculation of the initial flexural stiffness increases exponentially with decrease in the web slenderness factor ( $\lambda$ ). It can also be observed that the analytical flexural stiffness

values for the rectangular plate with either fixed edges or simply-supported edges form the upper and lower bounds to the experimental values of the initial flexural stiffness for the SS Type connection. For the eight groups of studs in the experimental program, the slenderness factor varied from 0.43 to 1.43 and the experimental initial flexural stiffness varied from 7.92 to 2.46 kip/in., respectively. The analytical flexural stiffness for the lower slenderness factors show a greater difference for the type of support condition than the higher slenderness factors that show almost equal values for the different types of support conditions.

#### **5.2.1.2 WW type connection**

The analytical initial flexural stiffness values, shown in Figure 5.2 for the WW Type connection, decrease linearly with increasing web slenderness factor ( $\lambda$ ). It was clearly observed that the analytical flexural stiffness values for a rectangular plate with either fixed edges or simply-supported edges form the upper and lower bounds to the experimental values of the initial flexural stiffness for the WW Type connection. For the three groups of studs in the experimental program, the slenderness varied from 0.43 to 0.63 and the corresponding experimental initial flexural stiffness varied from 40.8 to 19.7 kip/in, respectively.

#### **5.2.1.3 DW type connection**

The analytical initial flexural stiffness values shown in Figure 5.3 for the DW Type connection, decrease linearly with increasing web slenderness factor. ( $\lambda$ ). Except for one value of experimental stiffness, the analytical values form the upper and lower bound values to the experimental initial flexural stiffness values. For the three groups of studs in the experimental program, the slenderness varied from 0.43 to 0.63 and the

corresponding experimental initial flexural stiffness varied from 50.4 to 2.4 kip/in, respectively.

From the above three figures, it can be generalized that the analytical determination of initial flexural stiffness values is close enough to the values determined from the experimental results.

### **5.2.2 Initial Torsional Stiffness of the Bracing Connection**

The following assumptions were made in determining the initial torsional stiffness of the bracing connection:

- The bridging channel was considered to be rigid enough to deform under the influence of the applied out-of-plane load. This assumption was verified and found to be true since all the torsional deformation was occurring at the stud web.
- The clip angles in case of the SS and WW Type connections were considered to be initially rigid compared to the stiffness of the web.
- The web was considered as a rectangular plate with fixed edges. The plate was considered to be subjected to two point loads. The first point load was a direct pull at the location of the screw or the weld. The second point load was the resultant of the bearing pressure of the clip angle on the web. For simplicity, the two point loads were considered to be of equal magnitude and equidistant from the vertical centerline of the web.

The initial torsional stiffness values determined using Eq. 5.4 are plotted in Figure 5.4 against the web slenderness factor for the SS Type connection. The plot contains four different data sets representing the following cases of initial torsional stiffness for the out-of-plane loading tests:

- Experimental lower bound values (LBV)
- Experimental upper bound values (UBV)
- Analytical value for a rectangular plate with four fixed edges

With calculations based on above assumptions the results obtained for the analytical initial torsional stiffness of the SS Type connection is not accurate or even in

the same range as that of the values determined from the experimental tests and can be observed in Figure 5.4 and Table 5.3. This requires a further study and more exact model of the connection has to be developed. There are several factors contributing to the torsional stiffness and the flexural stiffness of the clip angle and the bracing channel has to be converted to an equivalent torsional stiffness. The bearing of the clip angle is causes uniformly varying load on the web which has a resultant that is not at the same distance as the location of the connection point load. This causes an unsymmetrical load distribution about the vertical centerline of the web. This uniformly varying load is also affected by the presence of the web punchout causing a trapezoidal load on the loaded portion of the web. Based on some of the experimental observations during the test, the clip angle has been the controlling critically stiff element and hence its stiffness is important in calculating the initial torsional stiffness of the connection. Further analysis is required to assess the initial torsional stiffness analytically.

### 5.3 Total Stiffness of the Bridging Connection

The determination of the total stiffness of the bridging system has been discussed in detail in Chapter 4. The initial stiffness of the bridging connection is determined experimentally at an applied load of 10% of the maximum load attained during the bracing tests and is explained in Section 4.2 of this report.

#### 5.3.1 Initial Flexural Stiffness

The determination of the total flexural stiffness of the bridging connection has been discussed in Chapter 2 and is given by Eq. 2.2, which is given as:

$$\frac{1}{\beta_{\text{act}}} = \frac{1}{\beta_{\text{conn}}} + \frac{1}{\beta_{\text{brace}}} \quad (2.22)$$

For each cee-stud any of the three connection types can be used to secure the mid-height bracing. The stiffness of each connection type is given in Table 4.16 which is based on two test results per stud and connection type. Table 5.4 gives the total equivalent flexural stiffness of the bridging connection for each of the 37 axially loaded studs. It is assumed that the bridging connection remains elastic when the axially loaded cee-stud has reached its full capacity. This is evident by the fact that the connection stiffness is greater than the brace stiffness. However the total actual stiffness is slightly lower than the total brace stiffness. This is because the connection itself undergoes deformations under the applied load. The connection stiffness given in Table 5.4 is obtained as the average value from the two tests for each stud and connection type.

### 5.3.2 Initial Torsional Stiffness

The determination of the total torsional stiffness of the bridging connection has been discussed in Chapter 2 and is given by Eq. 2.2, as given above. For each cee-stud any of the three connection types can be used to secure the mid-height bracing. The torsional stiffness of the brace wire is determined assuming that the torsional buckling occurs about the centroid of the gross-section rather than the shear center. This is because the brace wires restrain the stud from strong axis displacement. If the force in the brace wire is  $P$ , the deformation of the brace is  $\Delta$ , then the stiffness of the brace wire is given by:

$$\frac{P}{\Delta} = \frac{A E}{L} \quad (5.5)$$

If the cross-section rotates by an angle  $\theta$ , then for small angular deformations,

$$\theta = \frac{\Delta}{D/2} \quad (5.6)$$

Substituting Eq. 5.5 in 5.6, we get the torsional stiffness of the bracing as:

$$\frac{PL}{\theta} = \frac{AED}{2} \quad (5.7)$$

- where A = Area of cross-section of brace wire  
 E = Elastic modulus of steel wire = 29,000 ksi.  
 D = Distance between the brace wires = depth of the cee-stud  
 L = Length of brace wire  
 P = Force in the brace wire

Table 5.5 gives the calculated values of torsional stiffness of the brace wire. Table 5.6 gives the total equivalent torsional stiffness of the bridging connection for each of the 36 axially loaded studs. The values of the experimental initial torsional stiffness for two test specimens per stud cross section and connection type has been previously given in Table 4.17 and the average value of those two is given in Table 5.6

Table 5.1 Axial Load Capacities of Test Specimens Using AISI (1999) MathCAD Worksheets

| Stud Designation |   |     |     | Tension Coupon Test Results |                  | AISI (1999) MathCAD worksheets |  |                 |  |                 | Required Ideal Brace Stiffness |
|------------------|---|-----|-----|-----------------------------|------------------|--------------------------------|--|-----------------|--|-----------------|--------------------------------|
|                  |   |     |     | Yield Stress                | Ultimate. Stress | As-Built Section Area          | As-Built Ultimate Capacity (P <sub>u</sub> ) |                 | As-Built Unfactored Capacity (P <sub>n</sub> ) |                 | β <sub>ideal</sub>             |
|                  |   |     |     | F <sub>y</sub>              | F <sub>u</sub>   |                                | Unbraced                                     | Mid-Point Brace | No Brace                                       | Mid-Point Brace |                                |
| D                | S | B   | t   | ksi                         | Ksi              | in. <sup>2</sup>               | lbs  | lbs             | lbs  | lbs             | lbs/in.                        |
| 362              | S | 125 | 33  | 48.53                       | 55.48            | 0.2028                         | 429.13                                       | 1586.53         | 505  | 1867            | 78                             |
| 362              | S | 162 | 43  | 47.04                       | 58.20            | 0.3089                         | 2221.17                                      | 6967.64         | 2613   | 8197            | 342                            |
| 362              | S | 162 | 68  | 52.01                       | 67.80            | 0.5154                         | 3713.37                                      | 11548.77        | 4369   | 13587           | 566                            |
| 600              | S | 125 | 33  | 24.03                       | 45.24            | 0.2537                         | 586.66                                       | 1541.69         | 690  | 1814            | 76                             |
| 600              | S | 162 | 43  | 46.24                       | 54.88            | 0.4135                         | 2156.02                                      | 5832.46         | 2536   | 6862            | 286                            |
| 600              | S | 162 | 43a | 50.30                       | 59.38            | 0.4346                         | 2460.57                                      | 6715.21         | 2895   | 7900            | 329                            |
| 600              | S | 162 | 97  | 60.20                       | 70.21            | 0.9807                         | 6286.86                                      | 19904.25        | 7396   | 23417           | 976                            |
| 800              | S | 162 | 43  | 40.23                       | 54.90            | 0.4829                         | 1967.02                                      | 5155.93         | 2314   | 6066            | 253                            |
| 800              | S | 162 | 97  | 42.50                       | 67.49            | 1.1841                         | 6694.4                                       | 17467.54        | 7876   | 20550           | 856                            |

As-Built sectional properties were based on the experimentally measured dimensions  
 Ideal Brace Stiffness was obtained using Yura's Bracing Equation 2.14 (Yura 1995)  
 Design factor used in calculating the Unfactored Capacity was 0.85

Table 5.2 Comparison of Initial Flexural Stiffness of the In-Plane Tests

| Stud Designation |   |     |    |    | Slenderness Factor | Initial Stiffness |         | Analytical Stiffness |         |
|------------------|---|-----|----|----|--------------------|-------------------|---------|----------------------|---------|
| D                | S | B   | t  | C  | $\lambda$          | Lower             | Upper   | Simple               | Fixed   |
|                  |   |     |    |    |                    | kip./in           | kip./in | kip./in              | kip./in |
| 362              | S | 125 | 33 | SS | 0.8984             | 1.683             | 2.068   | 0.65                 | 1.34    |
| 362              | S | 162 | 43 | SS | 0.6768             | 3.574             | 4.200   | 1.45                 | 2.97    |
| 362              | S | 162 | 68 | SS | 0.4343             | 6.102             | 7.942   | 6.25                 | 12.64   |
| 600              | S | 125 | 33 | SS | 1.0733             | 1.000             | 1.143   | 0.17                 | 0.35    |
| 600              | S | 162 | 43 | SS | 1.1406             | 3.785             | 3.822   | 0.38                 | 0.78    |
| 600              | S | 162 | 97 | SS | 0.5493             | 5.571             | 6.860   | 4.78                 | 9.62    |
| 800              | S | 162 | 43 | SS | 1.4328             | 2.066             | 2.463   | 0.19                 | 0.39    |
| 800              | S | 162 | 97 | SS | 0.6296             | 2.947             | 7.082   | 2.34                 | 4.71    |
| 362              | S | 162 | 68 | WW | 0.4343             | 30.423            | 40.788  | 25.82                | 49.78   |
| 600              | S | 162 | 97 | WW | 0.5493             | 15.241            | 16.524  | 14.13                | 27.63   |
| 800              | S | 162 | 97 | WW | 0.6296             | 10.512            | 19.668  | 7.29                 | 14.40   |
| 362              | S | 162 | 68 | DW | 0.4343             | 45.361            | 50.412  | 15.70                | 31.09   |
| 600              | S | 162 | 97 | DW | 0.5493             | 8.260             | 8.260   | 7.55                 | 15.25   |
| 800              | S | 162 | 97 | DW | 0.6296             | 2.401             | 2.401   | 3.23                 | 6.60    |

Table 5.3 Comparison of Initial Torsional Stiffness of the In-Plane Tests

| Stud Designation |   |     |    |    | Slenderness Factor | Initial Stiffness |             | Analytical Stiffness |             |
|------------------|---|-----|----|----|--------------------|-------------------|-------------|----------------------|-------------|
| D                | S | B   | t  | C  | $\lambda$          | Lower             | Upper       | Simple               | Fixed       |
|                  |   |     |    |    |                    | kip-in/rad.       | kip-in/rad. | kip-in/rad.          | kip-in/rad. |
| 362              | S | 125 | 33 | SS | 0.8984             | 2.955             | 3.998       | -                    | 0.51        |
| 362              | S | 162 | 43 | SS | 0.6768             | 5.334             | 7.043       | -                    | 1.12        |
| 362              | S | 162 | 68 | SS | 0.4343             | 13.876            | 15.718      | -                    | 4.13        |
| 600              | S | 125 | 33 | SS | 1.0733             | 7.019             | 7.200       | -                    | 0.62        |
| 600              | S | 162 | 43 | SS | 1.1406             | 21.040            | 24.077      | -                    | 1.37        |
| 600              | S | 162 | 97 | SS | 0.5493             | 31.376            | 43.597      | -                    | 14.25       |
| 800              | S | 162 | 43 | SS | 1.4328             | 51.413            | 60.318      | -                    | 1.73        |
| 800              | S | 162 | 97 | SS | 0.6296             | 70.320            | 78.946      | -                    | 18.44       |
| 362              | S | 162 | 68 | WW | 0.4343             | 75.788            | 99.267      | -                    | -           |
| 600              | S | 162 | 97 | WW | 0.5493             | 197.375           | 211.103     | -                    | -           |
| 800              | S | 162 | 97 | WW | 0.6296             | 236.610           | 314.449     | -                    | -           |
| 362              | S | 162 | 68 | DW | 0.4343             | 28.888            | 32.404      | -                    | -           |
| 600              | S | 162 | 97 | DW | 0.5493             | 26.307            | 26.725      | -                    | -           |
| 800              | S | 162 | 97 | DW | 0.6296             | 18.044            | 27.576      | -                    | -           |

Table 5.4 Total Flexural Stiffness of the Bridging Connections

| Stud Designation |   |     |    |    | Total<br>Brace<br>Stiffness | Experimental Initial Flexural Stiffness<br>of the Bridging Connection |         |         | Total Flexural Stiffness of the<br>Bridging Connection |         |         |
|------------------|---|-----|----|----|-----------------------------|---|---------|---------|--|---------|---------|
|                  |   |     |    |    |                             | $\beta_{provided}$  | SS Type | WW Type | DW Type  | SS Type | WW Type |
| D                | S | B   | t  | ID | lbs/in.                     | lbs/in.   | lbs/in. | lbs/in. | lbs/in.  | lbs/in. | lbs/in. |
| 362              | S | 125 | 33 | 5  | 0                           | 0   |         |         |  |         |         |
| 362              | S | 125 | 33 | 3  | 192                         | 1875  |         |         | 174  |         |         |
| 362              | S | 125 | 33 | 4  | 192                         | 1875  |         |         | 174  |         |         |
| 362              | S | 125 | 33 | 6  | 201                         | 1875  |         |         | 182  |         |         |
| 362              | S | 125 | 33 | 1  | 413                         | 1875  |         |         | 338  |         |         |
| 362              | S | 125 | 33 | 2  | 765                         | 1875  |         |         | 543  |         |         |
| 362              | S | 162 | 43 | 1  | 0                           | 0   |         |         |  |         |         |
| 362              | S | 162 | 43 | 2  | 371                         | 3885  |         |         | 339  |         |         |
| 362              | S | 162 | 43 | 4  | 734                         | 3885  |         |         | 617  |         |         |
| 362              | S | 162 | 43 | 3  | 1478                        | 3885  |         |         | 1071   |         |         |
| 362              | S | 162 | 68 | 5  | 0                           | 0   |         |         |  |         |         |
| 362              | S | 162 | 68 | 3  | 1023                        | 7020  | 35605   | 47885   | 893  | 994     | 1001    |
| 362              | S | 162 | 68 | 4  | 1538                        | 7020  | 35605   | 47885   | 1262   | 1475    | 1490    |
| 362              | S | 162 | 68 | 2  | 2046                        | 7020  | 35605   | 47885   | 1584   | 1935    | 1962    |
| 600              | S | 125 | 33 | 2  | 0                           |   |         |         |  |         |         |
| 600              | S | 125 | 33 | 4  | 61                          | 1070  |         |         | 57   |         |         |
| 600              | S | 125 | 33 | 3  | 123                         | 1070  |         |         | 110  |         |         |
| 600              | S | 125 | 33 | 1  | 402                         | 1070  |         |         | 292  |         |         |

Table 5.4 (Continued) Total Flexural Stiffness of the Bridging Connections

| Stud Designation |   |     |    |    | Total<br>Brace<br>Stiffness | Experimental Initial Flexural Stiffness<br>of the Bridging Connection |         |         | Total Flexural Stiffness of the<br>Bridging Connection |         |         |
|------------------|---|-----|----|----|-----------------------------|---|---------|---------|--|---------|---------|
|                  |   |     |    |    |                             | $\beta_{provided}$  | SS Type | WW Type | DW Type  | SS Type | WW Type |
| D                | S | B   | t  | ID | lbs/in.                     | lbs/in.   | lbs/in. | lbs/in. | lbs/in.  | lbs/in. | lbs/in. |
| 600              | S | 162 | 43 | 6  | 0                           |   |         |         |  |         |         |
| 600              | S | 162 | 43 | 6a | 0                           |   |         |         |  |         |         |
| 600              | S | 162 | 43 | 5  | 61                          | 3800  |         |         | 60   |         |         |
| 600              | S | 162 | 43 | 2  | 148                         | 3800  |         |         | 142  |         |         |
| 600              | S | 162 | 43 | 1  | 497                         | 3800  |         |         | 440  |         |         |
| 600              | S | 162 | 43 | 4  | 990                         | 3800  |         |         | 785  |         |         |
| 600              | S | 162 | 97 | 5  | 0                           |   |         |         |  |         |         |
| 600              | S | 162 | 97 | 4  | 324                         | 6215  | 15880   | 8260    | 308  | 317     | 312     |
| 600              | S | 162 | 97 | 3  | 1041                        | 6215  | 15880   | 8260    | 892  | 977     | 924     |
| 600              | S | 162 | 97 | 1  | 2069                        | 6215  | 15880   | 8260    | 1552   | 1831    | 1655    |
| 600              | S | 162 | 97 | 2  | 3357                        | 6215  | 15880   | 8260    | 2180   | 2771    | 2387    |
| 800              | S | 162 | 43 | 4  | 0                           |   |         |         |  |         |         |
| 800              | S | 162 | 43 | 2  | 149                         | 2265  |         |         | 140  |         |         |
| 800              | S | 162 | 43 | 3  | 299                         | 2265  |         |         | 264  |         |         |
| 800              | S | 162 | 43 | 5  | 602                         | 2265  |         |         | 476  |         |         |
| 800              | S | 162 | 97 | 3  | 0                           |   |         |         |  |         |         |
| 800              | S | 162 | 97 | 2  | 1041                        | 5015  | 15090   | 2400    | 862  | 974     | 726     |
| 800              | S | 162 | 97 | 1  | 2093                        | 5015  | 15090   | 2400    | 1477   | 1838    | 1118    |
| 800              | S | 162 | 97 | 4  | 4195                        | 5015  | 15090   | 2400    | 2284   | 3283    | 1527    |

Table 5.5 Calculated Brace Stiffness and Total Brace Stiffness of the Test Specimens

| Stud Designation |   |     |    |    | Target<br>Brace<br>Stiffness | As-Built<br>Depth of<br>Stud | Wire  |                 |       |      | Torsional Stiffness of<br>Wire |
|------------------|---|-----|----|----|------------------------------|------------------------------|-------|-----------------|-------|------|--------------------------------|
|                  |   |     |    |    |                              |                              | Dia.  | Area            | L     | Nos. |                                |
| D                | S | B   | t  | ID | lbs/in.                      | in.                          | in.   | in <sup>2</sup> | in.   |      | lbs-in/rad.                    |
| 362              | S | 125 | 33 | 5  | 0                            | 3.613                        | -     | -               | -     | -    | 0                              |
| 362              | S | 125 | 33 | 3  | 100                          | 3.613                        | 0.016 | 0.000201        | 60.75 | 1    | 11                             |
| 362              | S | 125 | 33 | 4  | 100                          | 3.613                        | 0.016 | 0.000201        | 60.75 | 1    | 11                             |
| 362              | S | 125 | 33 | 6  | 100                          | 3.613                        | 0.016 | 0.000201        | 58    | 1    | 11                             |
| 362              | S | 125 | 33 | 1  | 200                          | 3.613                        | 0.016 | 0.000201        | 56.5  | 2    | 21                             |
| 362              | S | 125 | 33 | 2  | 400                          | 3.613                        | 0.016 | 0.000201        | 30.5  | 2    | 21                             |
| 362              | S | 162 | 43 | 1  | 0                            | 3.564                        | -     | -               | -     | -    | 0                              |
| 362              | S | 162 | 43 | 2  | 200                          | 3.564                        | 0.024 | 0.000452        | 70.75 | 1    | 23                             |
| 362              | S | 162 | 43 | 4  | 400                          | 3.564                        | 0.024 | 0.000452        | 35.75 | 1    | 23                             |
| 362              | S | 162 | 43 | 3  | 800                          | 3.564                        | 0.024 | 0.000452        | 35.5  | 2    | 47                             |
| 362              | S | 162 | 68 | 5  | 0                            | 3.638                        | -     | -               | -     | -    | 0                              |
| 362              | S | 162 | 68 | 3  | 500                          | 3.638                        | 0.033 | 0.000855        | 48.5  | 1    | 45                             |
| 362              | S | 162 | 68 | 4  | 750                          | 3.638                        | 0.033 | 0.000855        | 32.25 | 1    | 45                             |
| 362              | S | 162 | 68 | 2  | 1000                         | 3.638                        | 0.033 | 0.000855        | 24.25 | 1    | 45                             |
| 600              | S | 125 | 33 | 2  | 0                            | 6.020                        | -     | -               | -     | -    | 0                              |
| 600              | S | 125 | 33 | 4  | 30                           | 6.020                        | 0.01  | 0.000079        | 75    | 1    | 7                              |
| 600              | S | 125 | 33 | 3  | 60                           | 6.020                        | 0.01  | 0.000079        | 37    | 1    | 7                              |
| 600              | S | 125 | 33 | 1  | 200                          | 6.020                        | 0.016 | 0.000201        | 29    | 1    | 18                             |

Table 5.5 (Continued) Calculated Brace Stiffness and Total Brace Stiffness of the Test Specimens

| Stud Designation |   |     |    |    | Target Brace Stiffness | As-Built Depth of Stud | Wire   |                 |       |      | Torsional Stiffness of Wire |
|------------------|---|-----|----|----|------------------------|------------------------|--------|-----------------|-------|------|-----------------------------|
|                  |   |     |    |    |                        |                        | Dia.   | Area            | L     | Nos. |                             |
| D                | S | B   | t  | ID | lbs/in.                | in.                    | in.    | in <sup>2</sup> | in.   |      | lbs-in/rad.                 |
| 600              | S | 162 | 43 | 6  | 0                      | 6.021                  | -      |                 |       |      | 0                           |
| 600              | S | 162 | 43 | 6a | 0                      | 5.984                  | -      |                 |       |      | 0                           |
| 600              | S | 162 | 43 | 5  | 30                     | 6.021                  | 0.01   | 0.000079        | 75.25 | 1    | 7                           |
| 600              | S | 162 | 43 | 2  | 75                     | 6.021                  | 0.016  | 0.000201        | 79    | 1    | 18                          |
| 600              | S | 162 | 43 | 1  | 250                    | 6.021                  | 0.024  | 0.000452        | 52.75 | 1    | 39                          |
| 600              | S | 162 | 43 | 4  | 500                    | 6.021                  | 0.024  | 0.000452        | 26.5  | 1    | 39                          |
| 600              | S | 162 | 97 | 5  | 0                      | 6.082                  | -      |                 |       |      | 0                           |
| 600              | S | 162 | 97 | 4  | 160                    | 6.082                  | 0.024  | 0.000452        | 81    | 1    | 40                          |
| 600              | S | 162 | 97 | 3  | 500                    | 6.082                  | 0.0348 | 0.000951        | 53    | 1    | 84                          |
| 600              | S | 162 | 97 | 1  | 1000                   | 6.082                  | 0.0625 | 0.003068        | 86    | 1    | 271                         |
| 600              | S | 162 | 97 | 2  | 1500                   | 6.082                  | 0.0625 | 0.003068        | 53    | 1    | 271                         |
| 800              | S | 162 | 43 | 4  | 0                      | 7.921                  | -      |                 |       |      | 0                           |
| 800              | S | 162 | 43 | 2  | 75                     | 7.921                  | 0.016  | 0.000201        | 78.25 | 1    | 23                          |
| 800              | S | 162 | 43 | 3  | 150                    | 7.921                  | 0.016  | 0.000201        | 39    | 1    | 23                          |
| 800              | S | 162 | 43 | 5  | 300                    | 7.921                  | 0.016  | 0.000201        | 38.75 | 2    | 46                          |
| 800              | S | 162 | 97 | 3  | 0                      | 8.044                  | -      |                 |       |      | 0                           |
| 800              | S | 162 | 97 | 2  | 500                    | 8.044                  | 0.0348 | 0.000951        | 53    | 1    | 111                         |
| 800              | S | 162 | 97 | 1  | 1000                   | 8.044                  | 0.0625 | 0.003068        | 85    | 1    | 358                         |
| 800              | S | 162 | 97 | 4  | 2100                   | 8.044                  | 0.0475 | 0.001772        | 24.5  | 1    | 207                         |

Table 5.6 Total Torsional Stiffness of the Bridging Connections

| Stud Designation |   |     |    |    | Torsional Stiffness of the Brace | Experimental Initial Flexural Stiffness of the Bridging Connection |              |              | Total Flexural Stiffness of the Bridging Connection |              |              |
|------------------|---|-----|----|----|----------------------------------|--|--------------|--------------|---|--------------|--------------|
|                  |   |     |    |    |                                  | SS Type  | WW Type      | DW Type      | SS Type   | WW Type      | DW Type      |
| D                | S | B   | t  | ID | lbs-in./rad.                     | lbs-in./rad.   | lbs-in./rad. | lbs-in./rad. | lbs-in./rad.  | lbs-in./rad. | lbs-in./rad. |
| 362              | S | 125 | 33 | 5  | 0                                | 0  |              |              |   |              |              |
| 362              | S | 125 | 33 | 3  | 11                               | 3475   |              |              | 11  |              |              |
| 362              | S | 125 | 33 | 4  | 11                               | 3475   |              |              | 11  |              |              |
| 362              | S | 125 | 33 | 6  | 11                               | 3475   |              |              | 11  |              |              |
| 362              | S | 125 | 33 | 1  | 21                               | 3475   |              |              | 21  |              |              |
| 362              | S | 125 | 33 | 2  | 21                               | 3475   |              |              | 21  |              |              |
| 362              | S | 162 | 43 | 1  | 0                                | 0  |              |              |   |              |              |
| 362              | S | 162 | 43 | 2  | 23                               | 6185   |              |              | 23  |              |              |
| 362              | S | 162 | 43 | 4  | 23                               | 6185   |              |              | 23  |              |              |
| 362              | S | 162 | 43 | 3  | 47                               | 6185   |              |              | 46  |              |              |
| 362              | S | 162 | 68 | 5  | 0                                | 0  |              |              |   |              |              |
| 362              | S | 162 | 68 | 3  | 45                               | 14800  | 87530        | 30645        | 45  | 45           | 45           |
| 362              | S | 162 | 68 | 4  | 45                               | 14800  | 87530        | 30645        | 45  | 45           | 45           |
| 362              | S | 162 | 68 | 2  | 45                               | 14800  | 87530        | 30645        | 45  | 45           | 45           |
| 600              | S | 125 | 33 | 2  | 0                                | 0  |              |              |   |              |              |
| 600              | S | 125 | 33 | 4  | 7                                | 7110   |              |              | 7   |              |              |
| 600              | S | 125 | 33 | 3  | 7                                | 7110   |              |              | 7   |              |              |
| 600              | S | 125 | 33 | 1  | 18                               | 7110   |              |              | 18  |              |              |

Table 5.6 (Continued) Total Torsional Stiffness of the Bridging Connections

| Stud Designation |   |     |    |    | Torsional Stiffness of the Brace | Experimental Initial Flexural Stiffness of the Bridging Connection |              |              | Total Flexural Stiffness of the Bridging Connection |              |              |
|------------------|---|-----|----|----|----------------------------------|--|--------------|--------------|---|--------------|--------------|
|                  |   |     |    |    |                                  | SS Type  | WW Type      | DW Type      | SS Type   | WW Type      | DW Type      |
| D                | S | B   | t  | ID | lbs-in./rad.                     | lbs-in./rad.   | lbs-in./rad. | lbs-in./rad. | lbs-in./rad.  | lbs-in./rad. | lbs-in./rad. |
| 600              | S | 162 | 43 | 6  | 0                                | 0  |              |              |   |              |              |
| 600              | S | 162 | 43 | 6a | 0                                | 0  |              |              |   |              |              |
| 600              | S | 162 | 43 | 5  | 7                                | 22560  |              |              | 7   |              |              |
| 600              | S | 162 | 43 | 2  | 18                               | 22560  |              |              | 18  |              |              |
| 600              | S | 162 | 43 | 1  | 39                               | 22560  |              |              | 39  |              |              |
| 600              | S | 162 | 43 | 4  | 39                               | 22560  |              |              | 39  |              |              |
| 600              | S | 162 | 97 | 5  | 0                                | 0  |              |              |   |              |              |
| 600              | S | 162 | 97 | 4  | 40                               | 37490  | 204240       | 26515        | 40  | 40           | 40           |
| 600              | S | 162 | 97 | 3  | 84                               | 37490  | 204240       | 26515        | 84  | 84           | 84           |
| 600              | S | 162 | 97 | 1  | 271                              | 37490  | 204240       | 26515        | 269   | 270          | 268          |
| 600              | S | 162 | 97 | 2  | 271                              | 37490  | 204240       | 26515        | 269   | 270          | 268          |
| 800              | S | 162 | 43 | 4  | 0                                | 0  |              |              |   |              |              |
| 800              | S | 162 | 43 | 2  | 23                               | 55865  |              |              | 23  |              |              |
| 800              | S | 162 | 43 | 3  | 23                               | 55865  |              |              | 23  |              |              |
| 800              | S | 162 | 43 | 5  | 46                               | 55865  |              |              | 46  |              |              |
| 800              | S | 162 | 97 | 3  | 0                                | 0  |              |              |   |              |              |
| 800              | S | 162 | 97 | 2  | 111                              | 74635  | 275530       | 22810        | 111   | 111          | 110          |
| 800              | S | 162 | 97 | 1  | 358                              | 74635  | 275530       | 22810        | 356   | 357          | 352          |
| 800              | S | 162 | 97 | 4  | 207                              | 74635  | 275530       | 22810        | 206   | 207          | 205          |

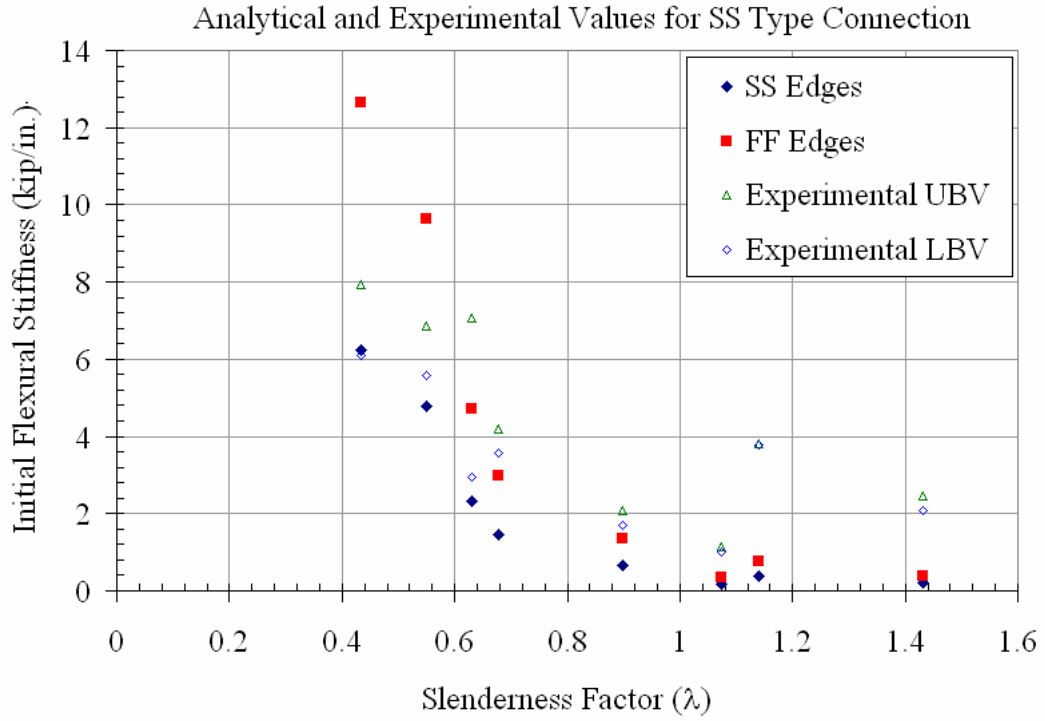


Figure 5.1 Flexural Stiffness of the SS Type Connection

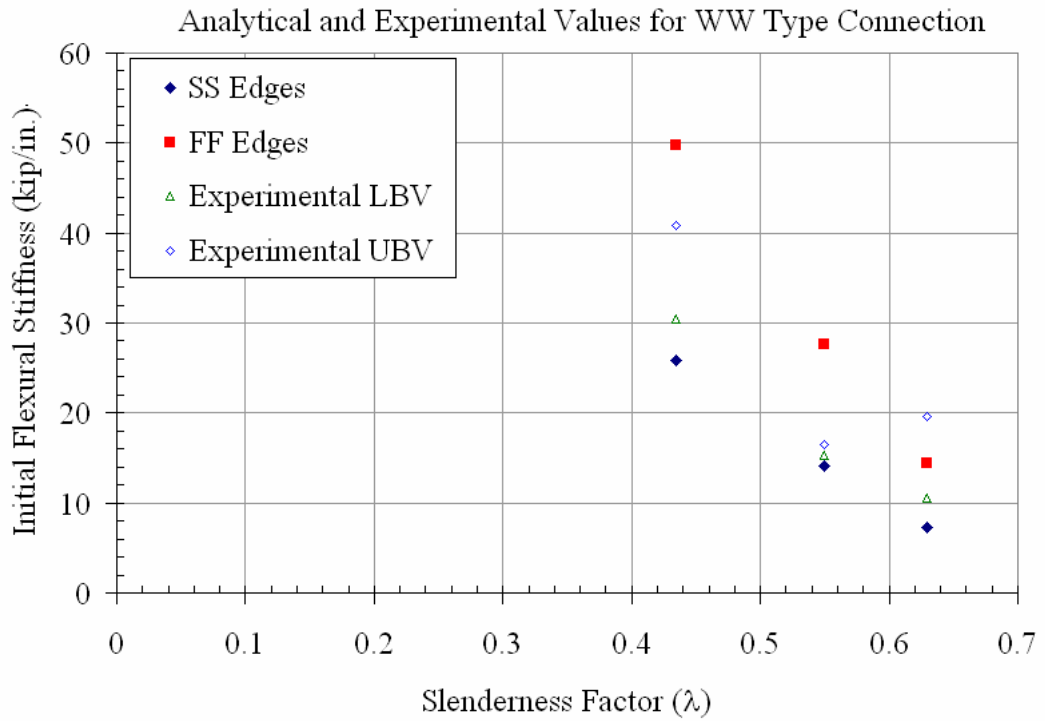


Figure 5.2 Flexural Stiffness of the WW Type Connection

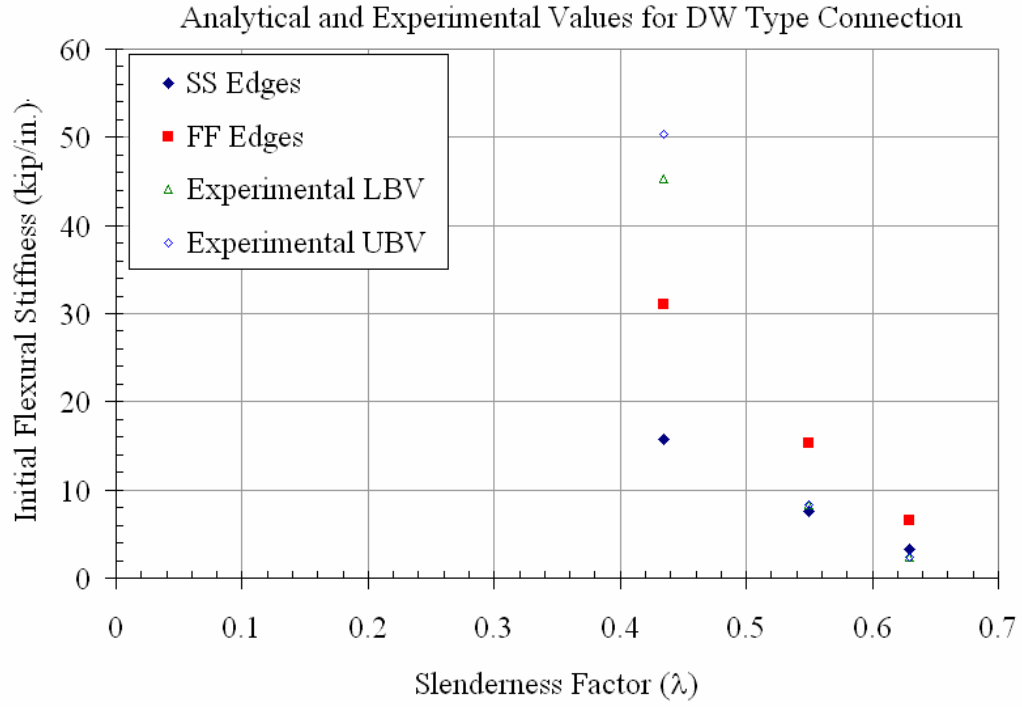


Figure 5.3 Flexural Stiffness of the DW Type Connection

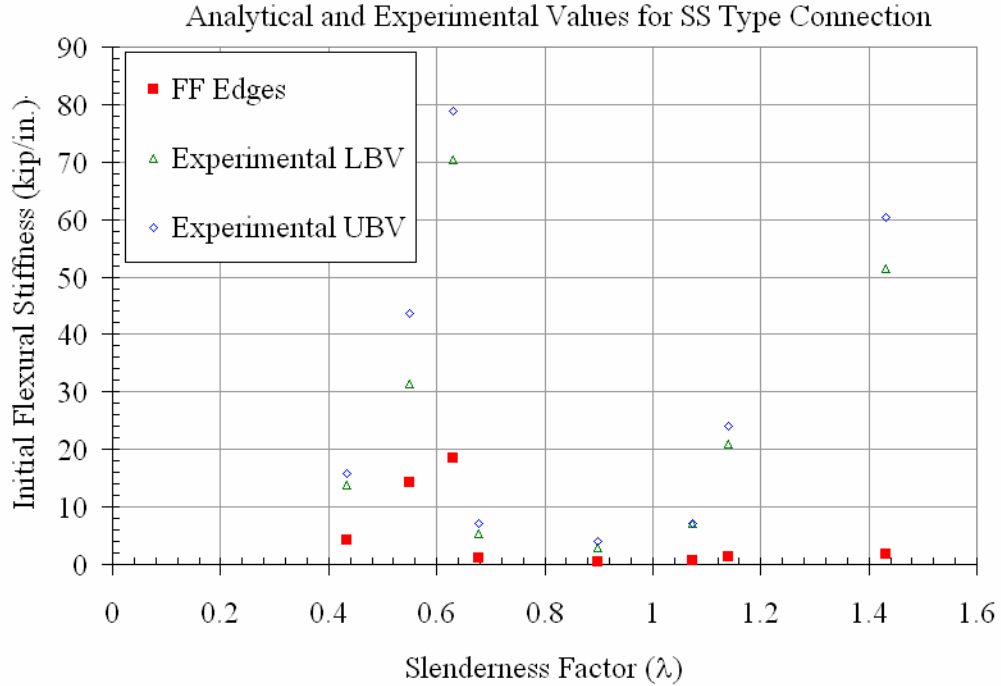


Figure 5.4 Torsional Stiffness of the SS Type Connection

## CHAPTER 6 CONCLUSIONS AND DESIGN RECOMMENDATIONS

The current provisions of the North American Cold-Formed Steel Specification do not specify the minimum requirements of the bracing strength and stiffness for structural wall stud assembly systems. These load bearing steel studs can also be used as stand-alone columns. The current provisions of the AISC-LRFD Specification (AISC 1999) have been discussed in Section 2.5 for hot-rolled steel members, but there are no equivalent provisions in the current North American Cold-Formed Steel Specification (2001). An experimental investigation was conducted at the Structures Laboratory, Department of Civil and Coastal Engineering, University of Florida, Gainesville, to ascertain the bracing strength and stiffness requirements for single column axially loaded cee-studs with mid-height lateral bracing about the weak axis. The experimental results and analytical evaluations of this investigation have been provided in Chapters 3, 4 and 5. This chapter describes the proposed minimum bracing requirements based on the experimental results and analytical calculation that were performed. In addition, a standard test procedure for determining the bracing connection strength and stiffness has been developed.

### **6.1 General Conclusions and Recommendations**

The following observations can be made based on the results of this research through its experimental investigation and analytical evaluation:

1. The compressive axial load capacity of a cold-formed cee-stud predicted by the current provisions of the AISI Specification (1999), under-predicts the axial capacity owing to ideal support conditions that are non-existent in general practice.

The bracing strength and stiffness is directly proportional to the axial load capacity leading to under-prediction of the actual ideal bracing requirement.

2. The mounting of the cee-stud in industry standard track offers partial base fixity and causes a reduction in the effective length of the compression member, leading to higher axial load capacity of the cee-stud. This, in turn, leads to higher demand on the mid-height lateral bracing for flexural and torsional buckling. The fixity factor varies for each stud cross-section and a separate study is recommended to ascertain these values.
3. The depth of the track and its connection type surely affects the axial load capacity of the stud and hence a separate study is recommended to determine the effect of different track geometry on the support fixity.
4. The support fixities are different for different buckling modes that the mono-symmetric cee-stud section is subjected to and hence the same effective length factors cannot be used for all the different buckling modes. An analytical tool must be developed for the practicing engineer to determine the effective length factor based on the stud cross-section and its length.
5. Based on the type of mid-height bracing, the stud is either forced into flexural buckling or flexural-torsional buckling even if the unbraced stud predominantly would fail by torsional buckling. This seriously affects the performance of the stud in a wall-stud panel system. The critical buckling stresses for each of the buckling modes has to be evaluated and the axial capacity needs to be determined based on the application of the stud.
6. The critical buckling stress, using the provisions in the AISI Specification (1999), is a minimum of weak axis flexural buckling stress, strong axis buckling stress and torsional buckling stress. The bracing required to ideally brace the cee-stud must be meet the demands not only in flexural buckling but also in torsional buckling due to the any of the limiting critical buckling stress states.
7. The initial flexural stiffness of the three industry standard bracing connections has been predicted from basic structural mechanics. Based on the fixity of a rectangular web plate, two cases were developed that form the upper and lower bounds to the experimental results. A similar procedure to determine the initial torsional stiffness was also undertaken.
8. The stiffness and strength of the mid-height lateral bracing was drastically affected by the higher axial capacities in the experiments. The tests showed more than a 50% increase in the axial capacity of the unbraced cee-stud due to non-ideal support conditions. This led to unconservative prediction of the ideal bracing requirement for the eight groups of cee-studs that were evaluated in the investigation. Thus, bracing strength and stiffness of a few studs, which were classified as over braced, were actually under braced in the experiments.

9. The braced studs reached axial capacities greater than the unbraced studs and exhibited higher stiffness. The brace factor hence must be increased by a certain multiplier to account for this increased demand.
10. With increasing the brace stiffness for a particular cee-stud cross-section, the mid-height lateral displacement decreased, however, the axial capacities remained nearly the same. For global stability in wall stud systems it is important that the mid-height lateral displacement be a minimum, hence a stiffer brace is required.
11. The braced studs that failed by distortional buckling did not attain their predicted axial capacity since the critical buckling stress due to distortional buckling mode is less than that for the global buckling modes. It is necessary to consider distortional buckling as one of the limiting critical buckling modes for certain ranges of effective web depth-to-thickness ratios.
12. The effect of the size, shape and location of the web punchouts is critical for an analytical axial load capacity prediction. In the experiments, it was observed that maximum deformation occurred in the vicinity of the punchouts at close to ultimate loads. This surely indicates that even a better prediction of the axial load considering the support fixity will be affected by the punchouts, and hence a separate study is required to determine these effects.
13. Three standard industry bracing connections were tested for their strength and initial stiffness. The SS Type and the WW Type performed equally well in both the out-of-plane load tests and in-plane load tests. The WW Type had definitely higher stiffness when compared to the SS Type connection. The DW Type connection performed extremely well in the in-plane tests but was not good enough in the out-of-plane tests. Based on the stud cross-section and its usage, a suitable connection type should be chosen for the purpose of mid-height lateral bracing of the cee-stud.
14. It was observed that in the WW Type and DW Type tests, the connections failed due to poor performance of the weld due to the effect of galvanization of the stud. It must be made sure that, before the welding, the base metal is exposed. However, this may not be a very critical requirement due to the reasons mentioned below.
15. In all the bracing connection tests the analytical evaluation of the connection stiffness showed that the bracing stiffness is controlled by the stiffness of the stud web and the effects of other components are negligible.
16. Comparison of the experimental brace stiffness to the experimental connection stiffness shows that the former values are less compared to the latter and hence the effect of the latter on the total system stiffness is negligible. The total actual stiffness is slightly less than the brace stiffness. A suitable stiffness reduction factor can be used based on the connection type to simplify the calculations.
17. Initial imperfections in the studs affect their axial load capacity and hence the maximum allowable imperfections must be as per the ASTM C645-00 (2000) for non-structural steel studs and ASTM C955-01 (2001) for structural steel studs.

## 6.2 Design Recommendations

This section gives the minimum requirements of the mid-height lateral bracing for the cold-formed lipped cee-studs subjected to compressive axial loading. The equations given below are as per Yura's (1995) recommendations. It must be made note of here that the out-of-straightness of the stud was taken at  $\Delta_o = L / 384$ .

The ideal brace stiffness is given by:

$$\beta_{\text{brace, ideal}} = \frac{[4 - 2/n]P_n}{L_b}$$

The required brace stiffness is at least:

$$\beta_{\text{brace, required}} = 2\beta_{\text{brace, ideal}}$$

The ideal brace strength is given by:

$$P_{\text{brace, ideal}} = 0.004 P_n$$

The minimum required brace strength is at least:

$$P_{\text{brace, required}} = 0.01 P_n$$

|       |                                  |   |  |
|-------|----------------------------------|---|--|
| where | $L_b$                            | = | Unbraced length, or distance between the braces, inches.   |
|       | $P_{\text{brace, ideal}}$        | = | Ideal bracing of the cee-stud, kips.   |
|       | $P_{\text{brace, required}}$     | = | Minimum required brace strength, kips.   |
|       | $P_n$                            | = | Nominal axial capacity when the assumed brace stiffness is greater than or equal to $\beta_{\text{ideal}}$ , kips. |
|       | $n$                              | = | Number of equally spaced intermediate brace locations  |
|       | $\beta_{\text{brace, ideal}}$    | = | Ideal brace stiffness  |
|       | $\beta_{\text{brace, required}}$ | = | Minimum required brace stiffness   |

The flexibility or ability of a brace connection to slip should be considered in the evaluation of the actual bracing system stiffness,  $\beta_{act}$ , as follows:

$$\frac{1}{\beta_{act}} = \frac{1}{\beta_{conn}} + \frac{1}{\beta_{brace}} \quad (2.22)$$

where  $\beta_{conn}$  = Stiffness of the connection

$\beta_{brace}$  = Stiffness of the brace

The flexural stiffness and torsional stiffness have to be determined separately and then the connection system employed in bracing the cee-stud must be checked for the above minimum requirements. The unit for the initial flexural stiffness is (kip/in.) and that of the initial torsional stiffness is (kip-in/rad).

APPENDIX A  
TEST REPORTS OF SINGLE COLUMN AXIAL LOAD TESTS

This appendix contains the individual test reports of the 37 experimental tests conducted on single columns subjected to axial compression. The reports describe the observations during each experiment the buckling modes developed at various stages of loading and proves the displacements and brace forces at corresponding load levels. During each experiment, photographs were taken at the initial, intermediate and final stages of loading and some of the photographs are given in these test reports.

The plots of applied load versus the 1) Axial Shortening, 2) Brace Forces, 3) Weak-axis Displacement, and 4) Strong-Axis Displacement are shown for each experiment.

The test reports are arranged in the following order:

| <b>Serial No</b> | <b>Specimen Number</b> |
|------------------|------------------------|
| 1                | 362S125-33-000         |
| 2                | 362S125-33-100(1)      |
| 3                | 362S125-33-100(2)      |
| 4                | 362S125-33-100(3)      |
| 5                | 362S125-33-200         |
| 6                | 362S125-33-400         |
| 7                | 362S162-43-000         |
| 8                | 362S162-43-200         |
| 9                | 362S162-43-400         |
| 10               | 362S162-43-800         |
| 11               | 362S162-68-0000        |
| 12               | 362S162-68-0500        |
| 13               | 362S162-68-0750        |
| 14               | 362S162-68-1000        |
| 15               | 600S125-33-000         |

|    |                   |
|----|-------------------|
| 16 | 600S125-33-030    |
| 17 | 600S125-33-060    |
| 18 | 600S125-33-200    |
| 19 | 600S162-43-000(1) |
| 20 | 600S162-43-000(2) |
| 21 | 600S162-43-075    |
| 22 | 600S162-43-250    |
| 23 | 600S162-43-300    |
| 24 | 600S162-43-500    |
| 25 | 600S162-97-0000   |
| 26 | 600S162-97-0160   |
| 27 | 600S162-97-0500   |
| 28 | 600S162-97-1000   |
| 29 | 600S162-97-1500   |
| 30 | 800S162-43-000    |
| 31 | 800S162-43-075    |
| 32 | 800S162-43-150    |
| 33 | 800S162-43-300    |
| 34 | 800S162-97-0000   |
| 35 | 800S162-97-0500   |
| 36 | 800S162-97-1000   |
| 37 | 800S162-97-2100   |

**362S125-33-000**

The test specimen, 362S125-33-000, was tested without mid-height lateral bracing. Figure A1.1 shows the cee stud specimen in the Riehle Universal Testing Machine prior to testing. To ensure static response of the stud to the applied load, it was loaded at 5 lbs/sec during the entire test. The weak axis lateral displacement was measured with linear potentiometers LP-1 & LP-3, attached to the north flange, and LP-2 & LP-4, attached to the south flange. The strong axis displacement was measured using LP-5, attached to the south flange.

From an axial load of zero to 275 lbs, the north and south flanges laterally displaced to the east by 0.070 and 0.053 inches, respectively, (see Figure A1.7). From zero up to 600 lbs, the axial compression of the stud is comparable and parallel to the initial elastic stiffness line, as shown in Figure A1.5. At this load level, there was no strong axis movement, as shown in Figure A1.7, and the north and south flanges had moved by 0.074 inches and 0.13 inches, respectively. The mid-height differential lateral displacement of the two flanges indicates the flexural-torsional buckling of the stud, as shown in Figure A1.2. From 600 lbs to 1000 lbs of axial load, strong axis buckling of the stud was observed and the lateral displacement of the mid-height section increased from 0.014 inches to 0.061 inches (see Figure A1.7). The axial shortening due to the compressive load was equaled by the elongation of the north flange due to strong-axis flexural buckling of the stud. This resulted in no change in axial shortening as measured by LP-6, attached to the north flange. At 1000 lbs of axial load, the north and the south flanges had moved east by 0.25 inches and 0.50 inches respectively, and the strong axis had moved north by 0.055 inches (see Figure A1.3).

On further loading, the stud reached its maximum capacity at an axial load of approximately 1127 lbs. With the load being constant at this critical load, the axial shortening increased from 0.017 inches to 0.034 inches, causing the stud to buckle in first mode flexural-torsion. The axial load started to drop gradually with the formation of a local buckle on the south flange-lip junction, at about 3 feet from the bottom end of the stud. Figures A1.4a and A1.4b show the partial and overall views of the stud at failure. In these figures, the local buckle in the flange can be seen in the lower half of the stud.



Figure A1.1 Overall View of Stud 362S125-33-000 in the Riehle UTM (Looking East)



Figure A1.2 Elastic Flexural-Torsional Buckling of Stud 362S125-33-000 at an Axial Load of 500 lbs



Figure A1.3 Elastic Flexural-Torsional Buckling of Stud 362S125-33-000 at an Axial Load of 1000 lbs (Looking North)



(a) Local Buckle at 1'-6" from Mid-Height  
 (b) Overall View (Looking East)  
 Figure A1.4 Final Buckled Shape of Stud 362S125-33-000



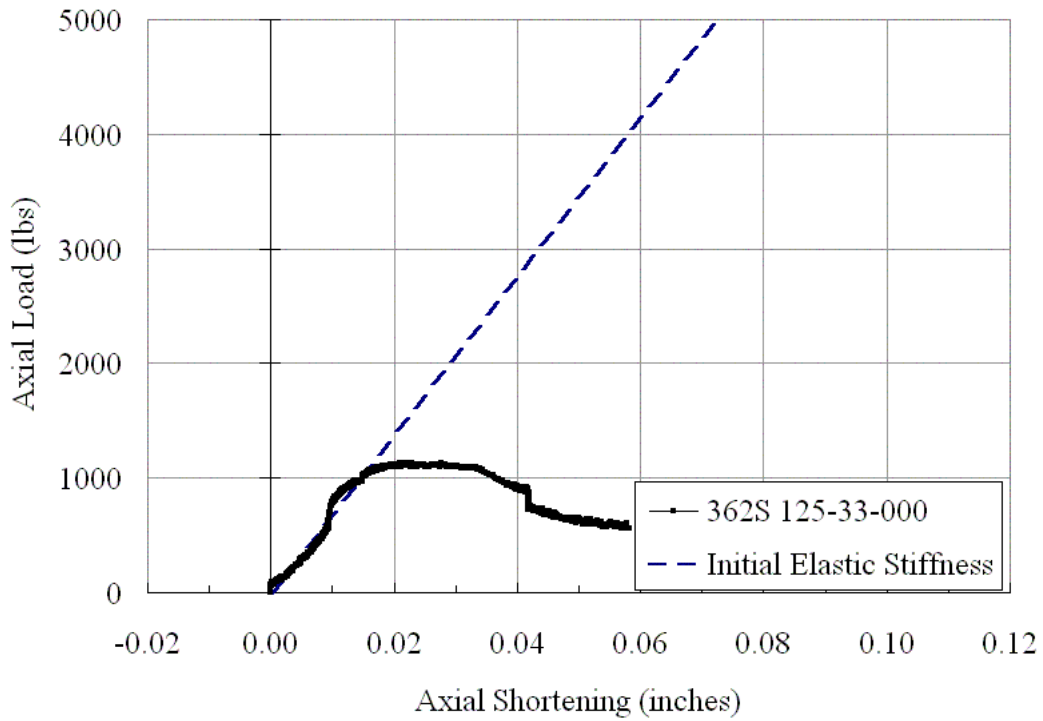


Figure A1.5 Plot of Axial Load vs. Axial Shortening

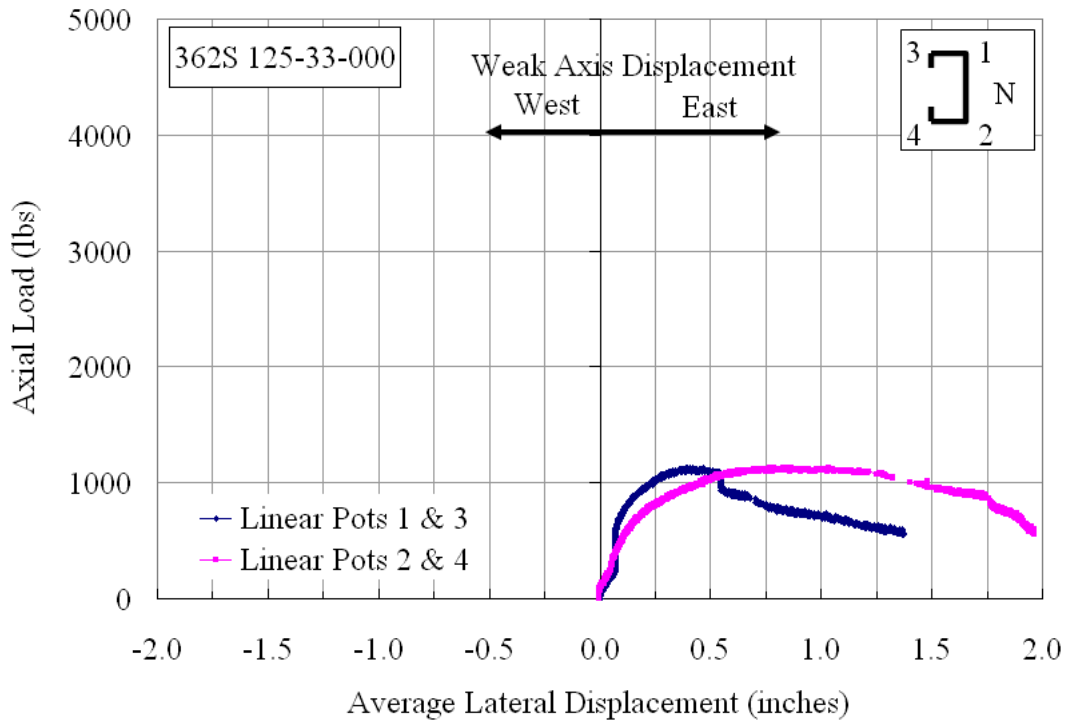


Figure A1.6 Plot of Axial Load vs. Weak Axis Displacement at Mid-Height

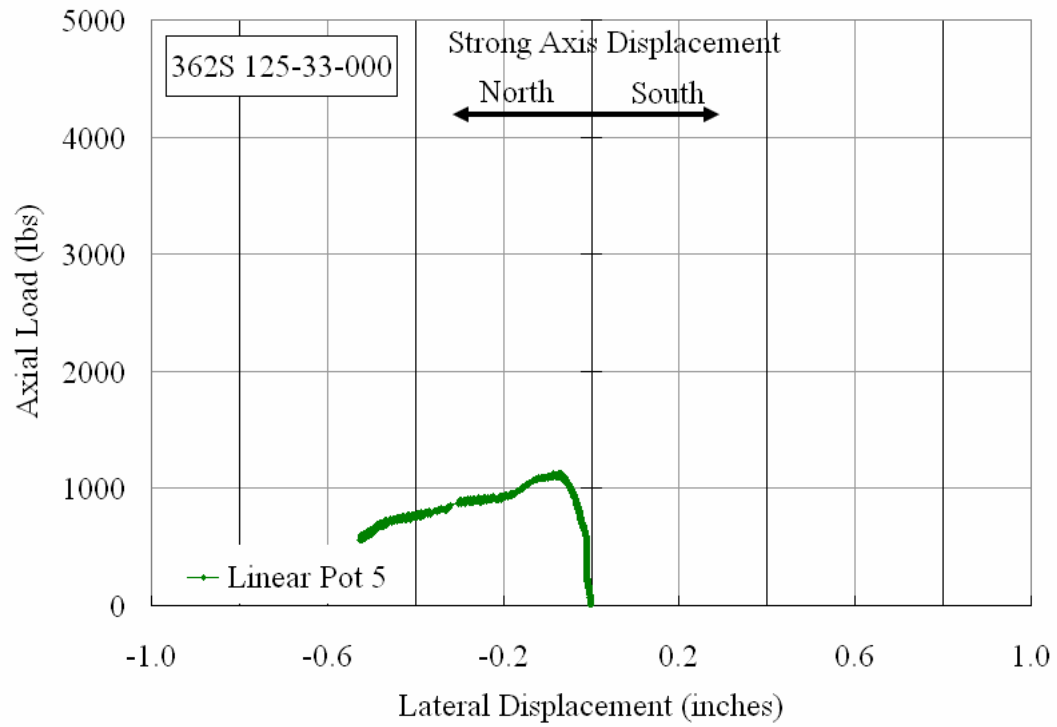


Figure A1.7 Plot of Axial Load vs. Strong Axis Displacement at Mid-Height

**362S125-33-100(1)**

The stud 362S125-33-100(1) was braced with total brace stiffness of 192 lbs/in. The brace stiffness was 2 times the required ideal bracing, as described in Chapter 3. Figure A2.1 shows the stud in the Riehle Universal Testing Machine before the test. The mid-height displacement of the two flanges was measured by linear potentiometers LP-1 & LP-3 attached to the north flange and LP-2 & LP-4 attached to the south flange. The mid-height strong axis lateral displacement was measured with LP-5 attached to the south flange. The stud was loaded at 5 lbs/sec to ensure static response to the applied loading.

From zero to about 650 lbs of axial load, the strong axis displaced south by 0.015 inches, as shown in Figure A2.8. From an axial load of 650 lbs to the maximum load, there was predominant strong axis displacement towards the north. It can be observed in Figure A2.2 that there is a differential movement in the two flanges at the top of the stud as compared to the movement at mid-height, indicating flexural-torsional buckling in the top-half of the stud. At an axial load of 2000 lbs, the north and south flanges had displaced relatively by the same amount of 0.065 inches and 0.070 inches, respectively. Both the flanges were moving at the same rate, without any torsion of the mid-height cross-section, as can be observed in Figure A2.7.

Figure A2.5 shows that, at 650 lbs of axial load, an axial shortening of 0.15 inches is measured on the north flange. From 650 lbs to 1350 lbs, the linear potentiometer did not record any axial shortening, which can be attributed to the beginning of the flexural buckling about the strong axis. During this period of loading, the axial shortening was the same as the elongation due to flexural buckling. With increase in the axial load up to 2000 lbs, the elongation in the north flange was greater than the axial shortening, and the strong axis had displaced north by 0.14 inches. Again, from 2000 lbs up to the maximum

load, the effect of axial shortening was neutralized by the elongation of the north flange due to strong axis movement. At the maximum load, the strong axis had moved north by 0.25 inches, whereas the weak axis had moved east by the same amount of 0.08 inches on both the flanges.

The brace forces, BF-3 and BF-4, were seen to increase linearly up an axial load of 1700 lbs, and at this load they measured 5 lbs and 6.6 lbs, respectively (see Figure A2.6). From 1700 lbs up to the maximum load of 2750 lbs, force in BF-4 dropped to 1.5 lbs, whereas force in BF-3 continued to increase and measured 7.7 lbs at the maximum load. There were no brace forces recorded in BF-1 and BF-2, indicating that the mid-height cross-section was under flexural buckling about the weak axis in second mode, along with torsional buckling in the top half of stud.



Figure A2.1 Overall View of Stud 362S125-33-100(1) in the Riehle Machine

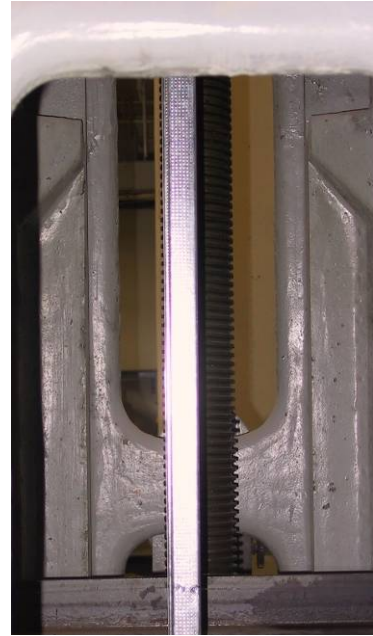


Figure A2.2 Flexural-torsion of the Top-half of the Stud 362S125-33-100(1)



Figure A2.3 Flexural-Torsional Buckling of the Stud 362S125-33-100(1) at an Axial Load of 2500 lbs



Figure A2.4 Overall View of Stud 362S125-33-100(1) at maximum load after Failure.

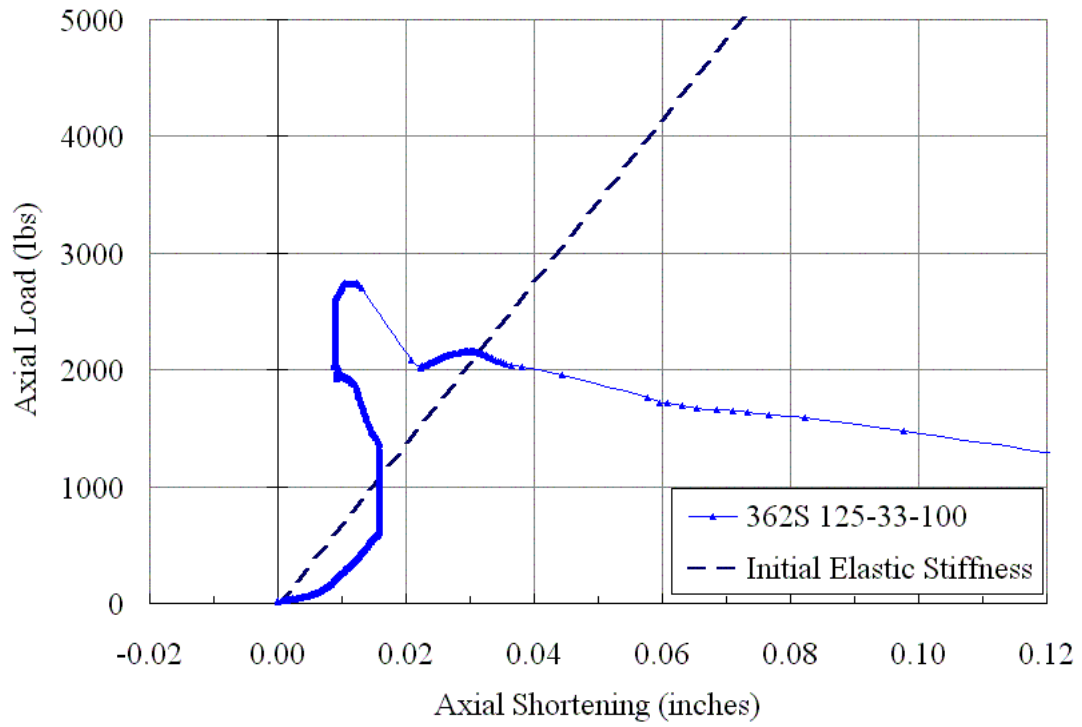


Figure A2.5 Plot of Axial Load vs. Axial Shortening

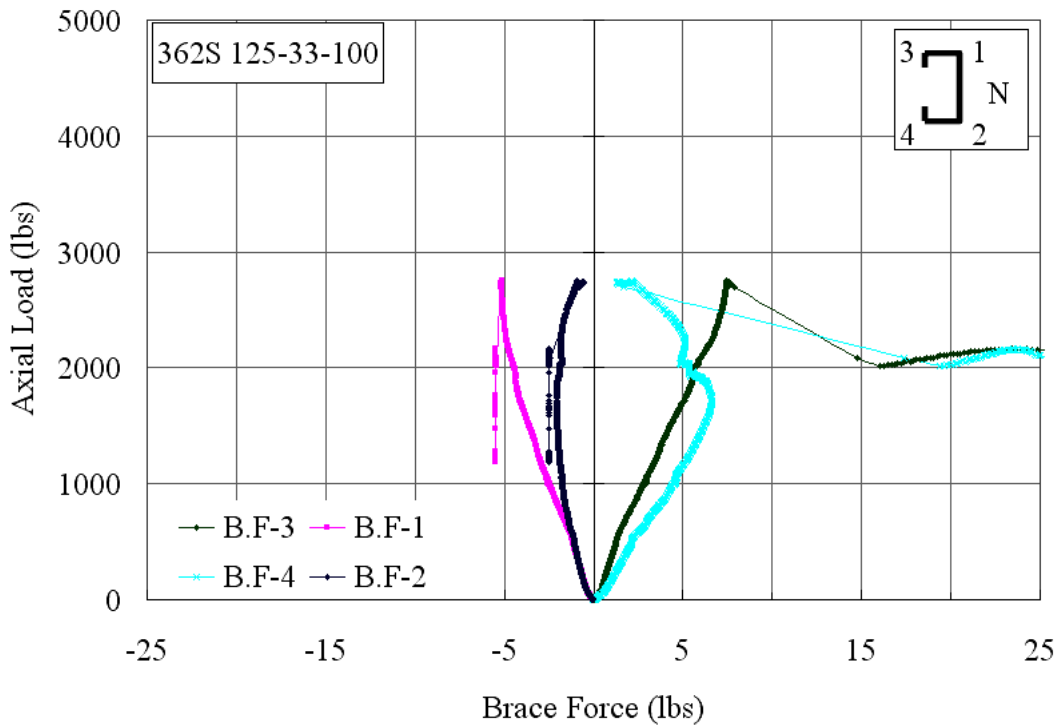


Figure A2.6 Plot of Axial Load vs. Brace Forces

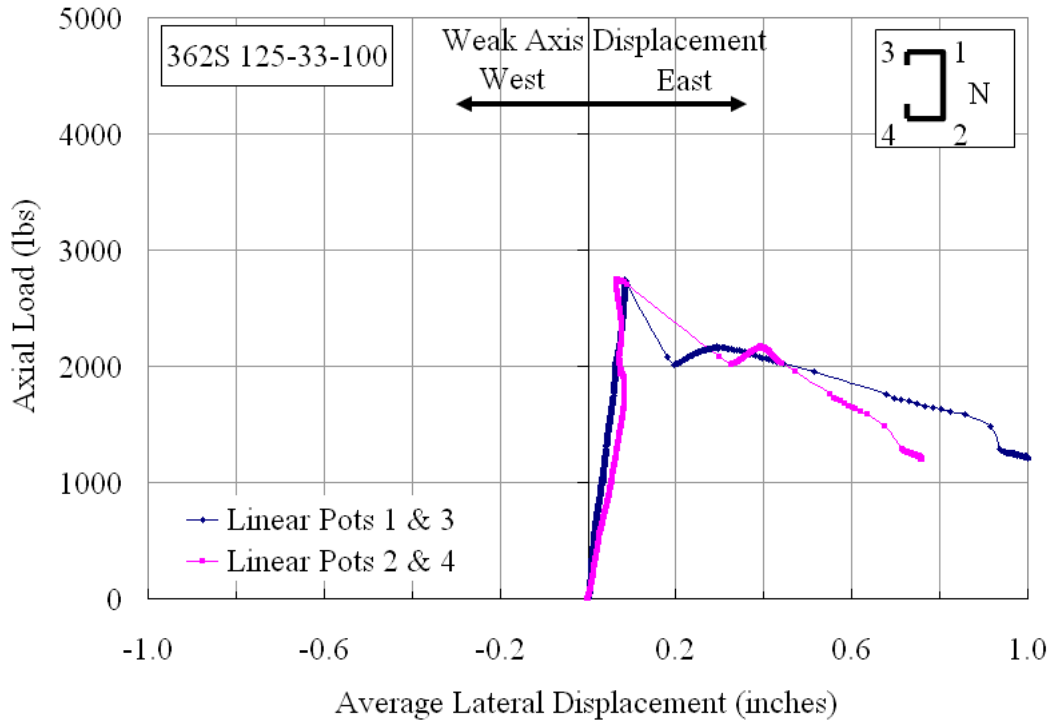


Figure A2.7 Plot of Axial Load vs. Weak Axis Displacement at Mid-Height

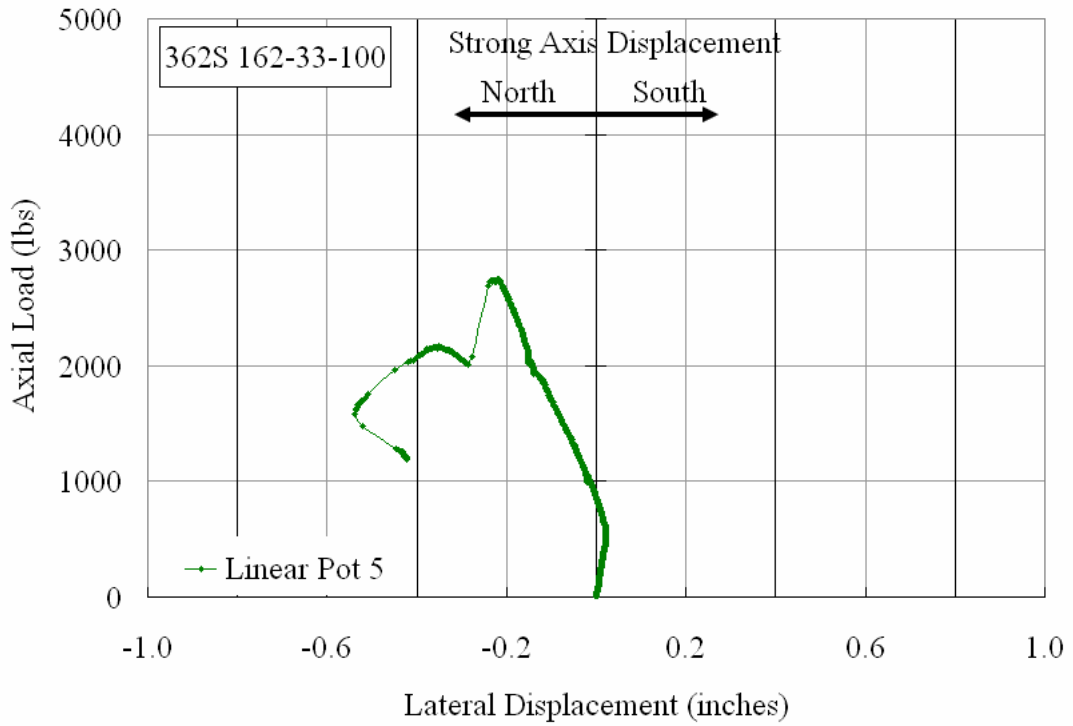


Figure A2.8 Plot of Axial Load vs. Strong Axis Displacement at Mid-Height

**362S125-33-100(2)**

The cee stud specimen, 362S125-33-100(2), had a total effective brace stiffness of 192 lbs/in., which was twice the ideal bracing stiffness requirement. Figure A4.1 shows the stud in the Riehle Universal Testing Machine before the test. The stud was loaded at 5 lbs/sec to 10 lbs/sec, to ensure static response of the stud. The weak axis lateral displacement at mid-height was measured with linear potentiometers LP-1 & LP-3 attached to the north flange, and LP-2 & LP-4 attached to the south flange. The mid-height lateral displacement of the strong axis was measured with LP-5. The axial shortening was measured with LP-6, which was connected to the north flange.

Initially, the slope of the load versus axial shortening was lesser than that of the initial elastic stiffness up to an axial load of about 400 lbs. At this point the stud started to undergo a multi mode buckling in strong axis flexural and torsional. This can be observed in Figure A3.8 with LP-5 measuring northward displacement. The brace forces up to this point measured zero and remained unchanged. From this load onwards to the ultimate load, there was strong axis flexural buckling which is evident in Figure A3.8. From an axial load of 400 lbs to 1400 lbs there was first mode torsional buckling of the stud as shown in Figure A3.2 in which there is clear differential movement of the north and south flanges. In Figure A3.6, the brace forces in BF-1 and BF-4 are increasing with increasing load, providing torsional restraint to buckling. At an axial load of 1000 lbs, the forces in BF-1 dropped off to zero, and force in BF-3 started to pick up, with force in BF-4 remaining mostly constant at 1.0 lbs. The strong axis had moved northward to 0.4 in. at this same load, whereas the displacement of the weak axis was insignificant and the axial shortening being 0.01 in.

When the axial load reached 1800 lbs, the brace force in BF-4 reached zero, and that in BF-2 started to increase from a previous value of zero, whereas BF-3 measured 8.18 lbs. This indicates the torsional buckling, which can be observed in Figure A3.7 but the torsional buckling began at 1500 lbs.

At the ultimate load of 2305 lbs, the stud had buckled in second mode flexural and second mode torsional buckling. Figure A3.4 shows the final buckled shape of the stud at the ultimate load.



Figure A3.1 Overall View of Stud 362S125-33-100(2) in the Riehle Machine (Looking East)



Figure A3.2 Beginning of Flexural-Torsional buckling of Stud 362S125-33-100(2) at an axial load of 400 lbs



Figure A3.3 Flexural Torsional buckling of Stud 362S125-33-100(3) at an Axial Load of 1800 lbs (Looking East)



Figure A3.4 Flexural Torsional buckling of Stud 362S125-33-100(3) at an Axial Load of 1800 lbs (Looking East)

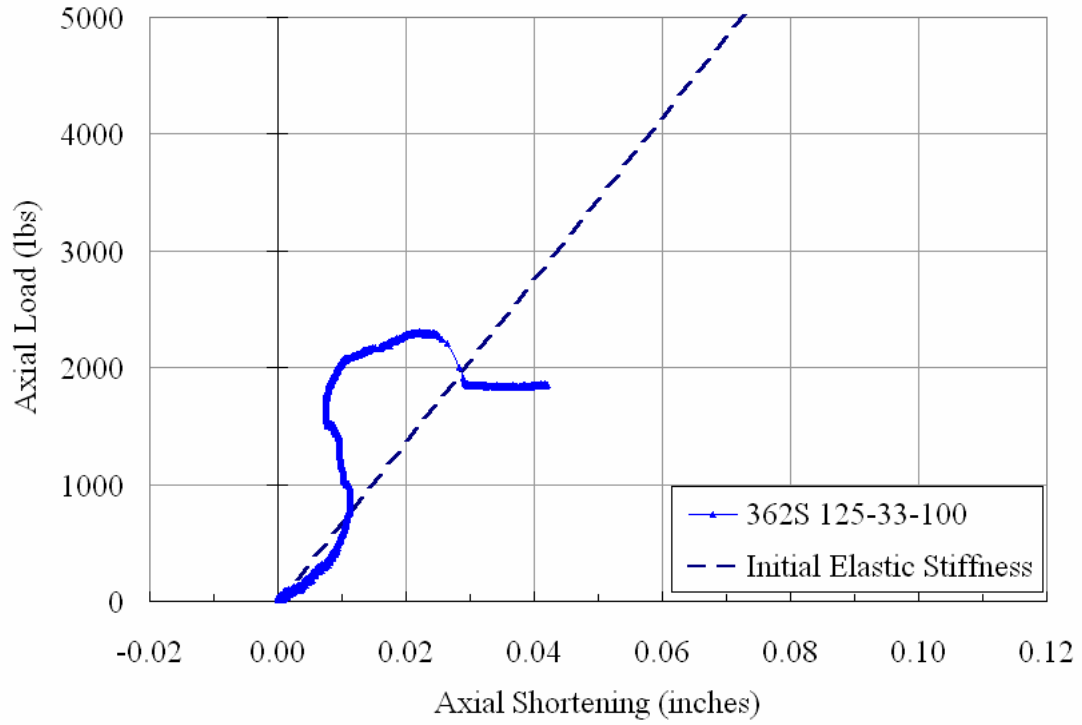


Figure A3.5 Plot of Axial Load vs. Axial Shortening

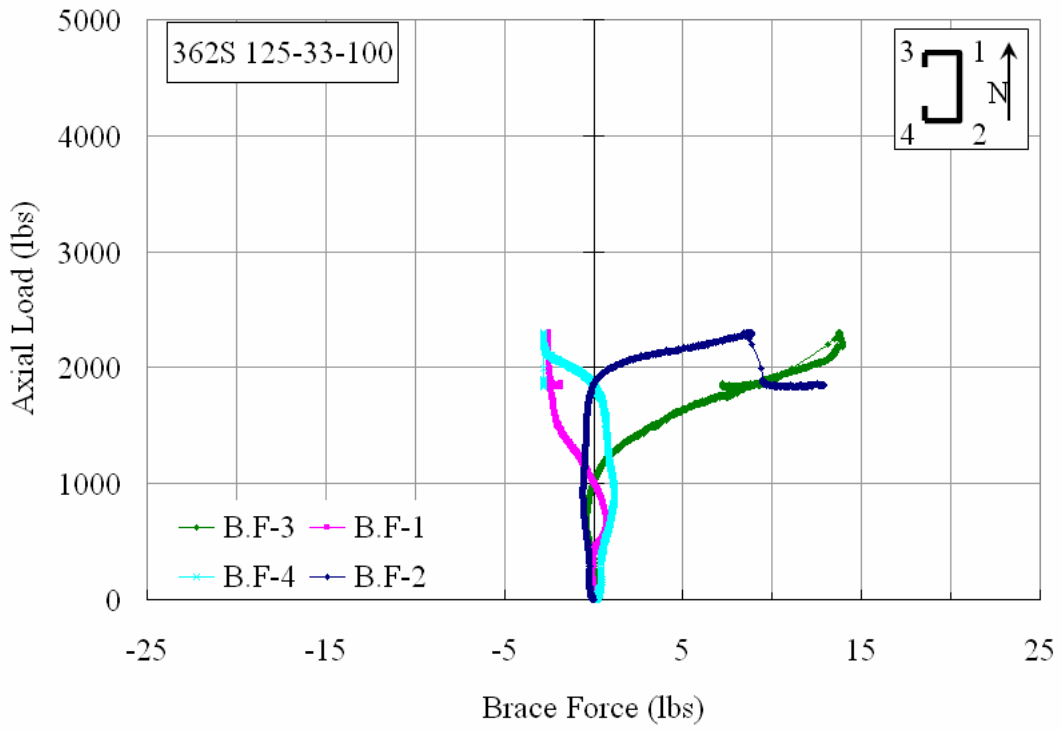


Figure A3.6 Plot of Axial Load vs. Brace Forces

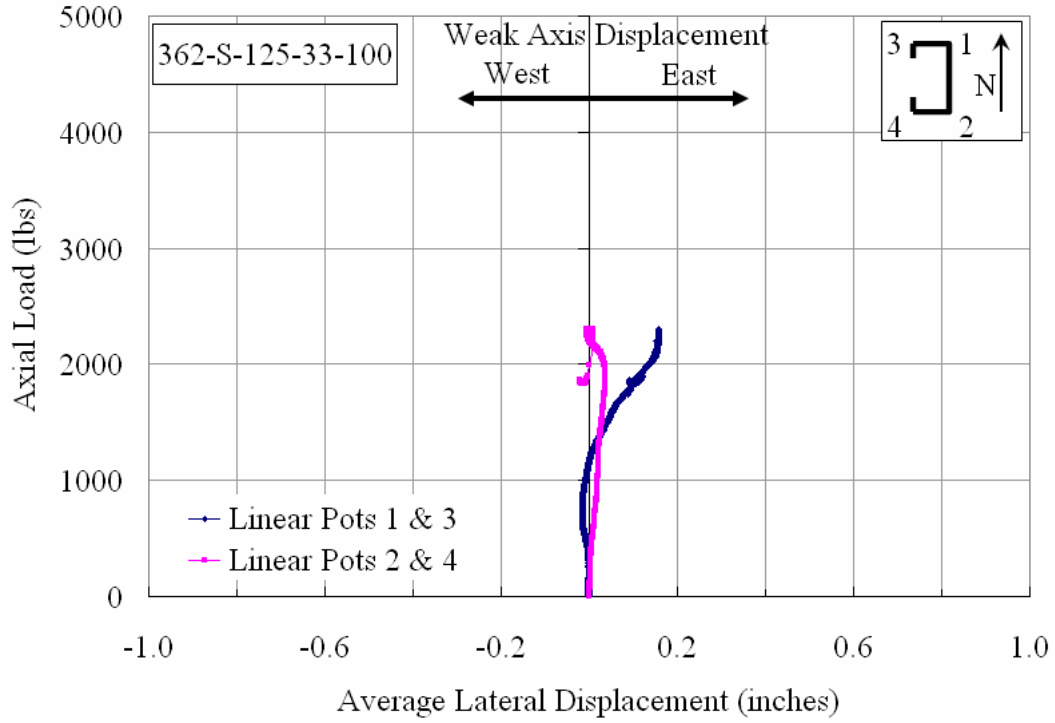


Figure A3.7 Plot of Axial Load vs. Weak Axis Displacement at Mid-Height

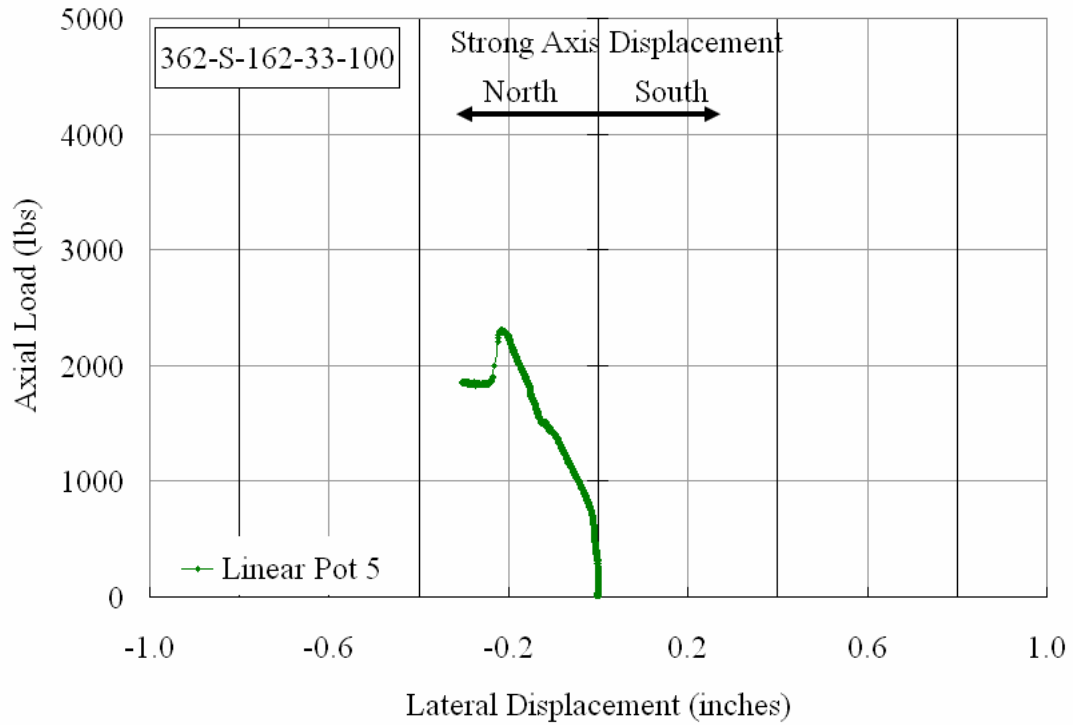


Figure A3.8 Plot of Axial Load vs. Strong Axis Displacement at Mid-Height

**362S125-33-100(3)**

The cee stud specimen, 362S125-33-100(3), had a total effective brace stiffness of 201 lbs/in, which was twice the ideal bracing stiffness requirement. Figure A3.1 shows the stud in the Riehle Universal Testing Machine before the test. The stud was loaded at 5 lbs/sec to 10lbs/sec, to ensure static response of the stud. The weak axis lateral displacement at mid-height was measured with linear potentiometers LP-1 & LP-3 attached to the north flange, and LP-2 & LP-4 attached to the south flange. The mid-height lateral displacement of the strong axis was measured with LP-5. The axial shortening was measured with LP-6, which was connected to the north flange.

The axial shortening was nearly parallel to the initial stiffness line and is shown in Figure A3.5. From an axial load of zero to 1000 lbs, the lateral displacement of both, the strong and the weak axes, was slight, and at 1000 lbs both axes had displaced laterally by approximately 0.02 inches north and east, respectively. At this load, the brace forces in both BF-3 and BF-4 were about 0.9 lb, as shown in Figure A3.6.

When the axial load reached 1200 lbs, the two flanges exhibited differential movement, indicating torsional buckling of the mid-height section. At an axial load of about 1500 lbs, the bottom end of the stud developed an end-zone failure due to section distortion. The flanges were prevented from softening by the vertical leg of the bottom track, as shown in Figure A3.2. From an axial load of 1450 lbs to 1650 lbs, the lateral displacement of the strong axis towards north changed from 0.052 inches to 0.090 inches (see Figure A3.8).

The test specimen reached an initial peak load of about 2250 lbs, and then gradually lost stiffness and reached a maximum axial load of 2400 lbs. Up to 2250 lbs, the axial shortening was parallel to the initial stiffness line, and at that load level, it was

0.03 inches and the brace forces in BF-3 & BF-4 were about 6 lbs and 2 lbs, respectively. At about 2300 lbs distortional buckling was observed at a punchout in the top-half of the cee stud, (see Figure A3.3). On reaching the maximum load, the axial shortening increased to 0.06 inches, the brace forces in BF-3 dropped to about 1.0 lb and that in BF-4 reached 15 lbs. At this load, the south flange had moved east by 0.16 inches and the north flange had moved to the initial position (see Figure A3.7). Failure of the test specimen was due to the bottom end-zone crumple (see Figure A3.4).



Figure A3.1 Overall View of Stud 362S125-33-100(3) in the Riehle Machine (Looking East)



Figure A3.2 Beginning of Distortion at Bottom of Stud 362S125-33-100(3) at an axial load of 1500 lbs

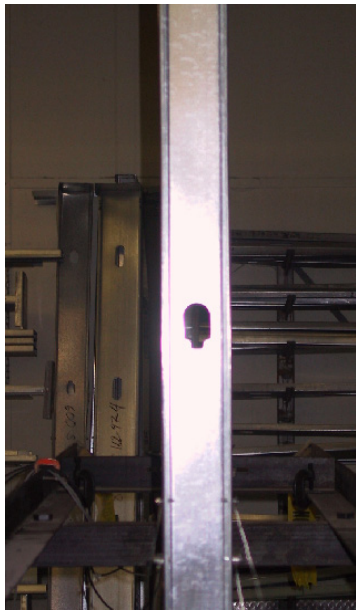


Figure A3.3 Distortion at a Web-perforation of Stud 362S125-33-100(3) at an Axial Load of 2300 lbs (Looking East)



Figure A3.4 Bottom Track-Stud End failure of Stud 362S125-33-100(3) at an axial load of 2400 lbs

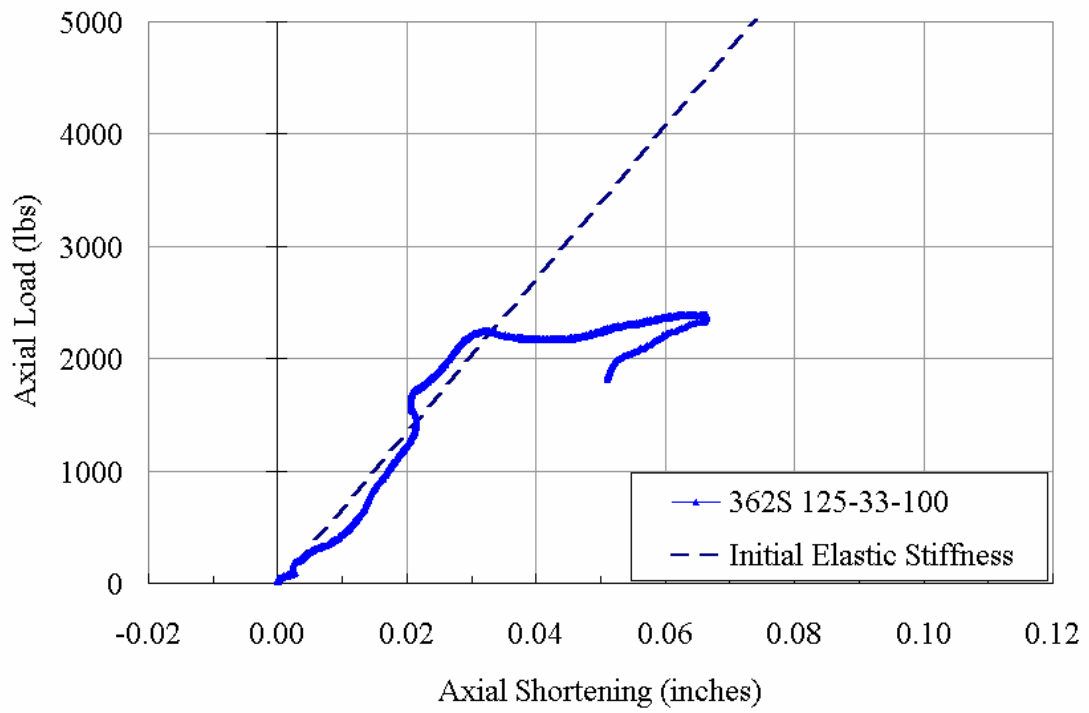


Figure A3.5 Plot of Axial Load vs. Axial Shortening

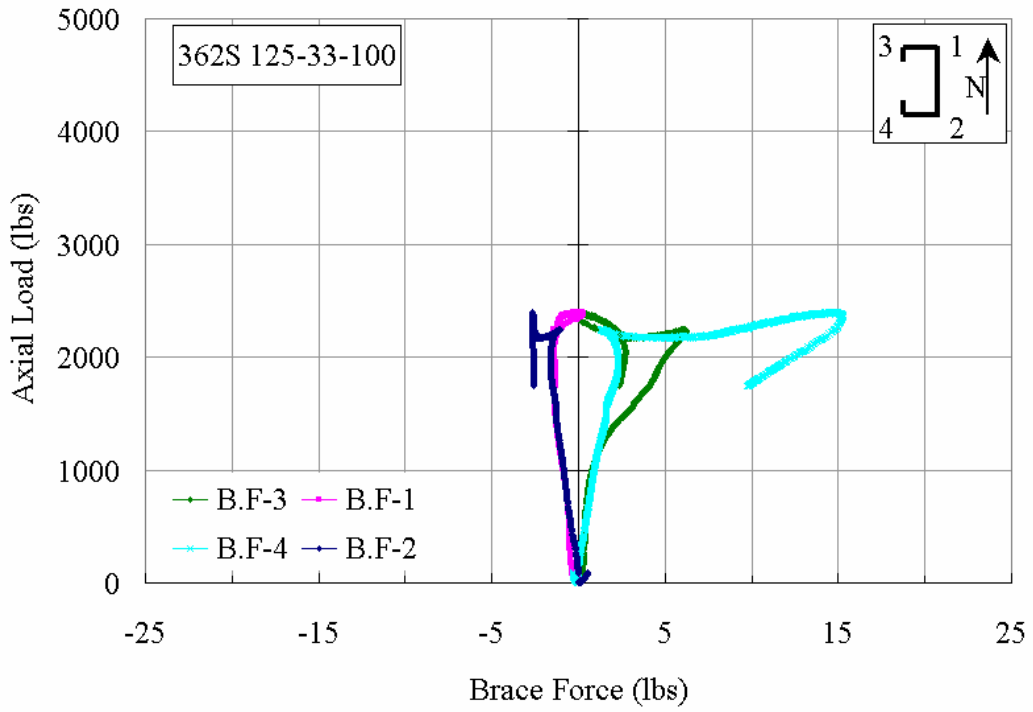


Figure A3.6 Plot of Axial Load vs. Brace Forces

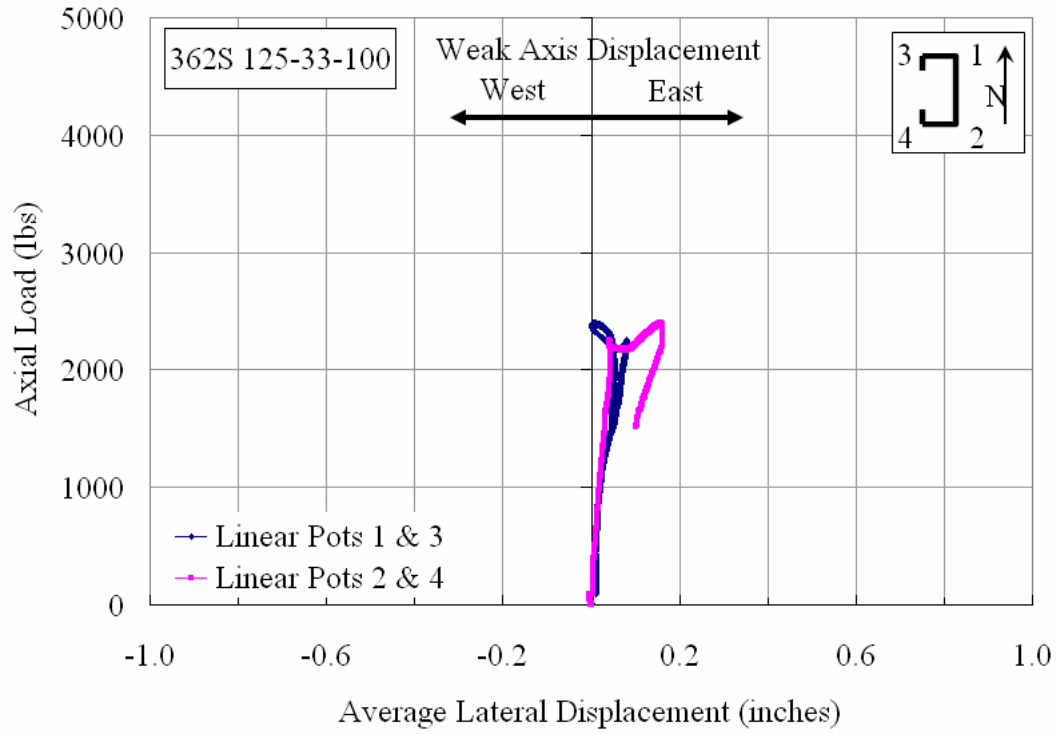


Figure A3.7 Plot of Axial Load vs. Weak Axis Displacement at Mid-Height

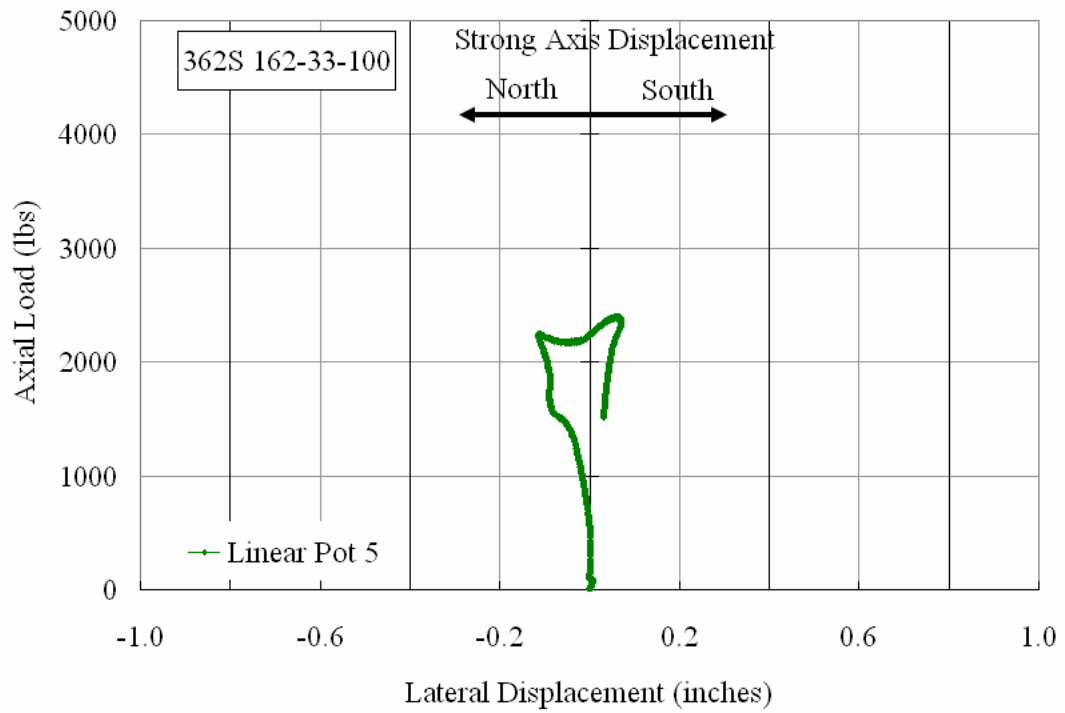


Figure A3.8 Plot of Axial Load vs. Strong Axis Displacement at Mid-Height

**362S125-33-200**

Figure A5.1 shows cee stud 362S125-33-200 in the Riehle Testing Machine. The stud was loaded at the rate of 5 to 15 lbs/sec and the axial load was measured with a 100 kip load cell mounted at the base. The weak axis lateral displacement was measured with linear potentiometers LP-1 & LP-3, attached to the north flange and LP-2 & LP-4 attached to the south flange. The strong axis displacement was measured using LP-5, attached to the south flange. Figure A5.5 shows the plot of axial load versus axial shortening of the stud. The brace forces were measured with four 150 lbs S-beam load cells and a plot of axial load versus brace forces is shown in Figure A5.6.

From zero to an axial load of 500 lbs, the forces in BF-1 & BF-2 reached 2.5 lbs each with a net change of 0.4 lbs, and can be associated with initial seating of the stud. On further loading these brace forces reduced to zero, at an axial load of about 1000 lbs. The forces in BF-3 and BF-4 showed a net increase of about 1.5 lb. At this load level, there was no axial shortening of the stud, the stud displaced about its strong axis and had moved north by 0.07 inches. When the axial load reached 1800 lbs, the stud had displaced about the strong axis and had moved north by 0.12 inches, as shown in Figure A5.8. There was minimal weak axis movement with the increase in axial load, because the stud seemed to be buckling in second mode flexure. At this load level, distortional buckling was observed above the bracing, as shown in Figure A5.2(a). With further increase in the load, the distortional buckling was observed to progress from the mid-height to both the top and bottom halves of the stud.

From an axial load of 1800 lbs to 2300 lbs, the brace forces in BF-3 increased linearly by a net of 4.5 kips, BF-2 changed from 0.2 to 0.9 lb, with the other two brace

wires recording zero. From this load level and up to the maximum load, the brace forces in BF-2 and BF-3 increased linearly and measured about 4.0 lbs and 7.0 lbs.

At an axial load of 2800 lbs, the distortional waves were seen all along the length of the stud, as shown in Figure A5.2(b). When the load reached 3000 lbs, a local buckle started to form in the two flanges and the two lips causing the stud to gradually fail, as shown in Figure A5.3. This local buckle was located at about 2'-0" from the top end of stud, and at this load level, the axial shortening of the stud increased from 0.02 inches to 0.03 inches. At failure, the stud's strong axis had moved north by 0.18 inches, and the weak axis had moved east by 0.018 inches. Figs. A5.4a and A5.4b show the top half and bottom half of the final buckled shape of the stud in second mode flexure.

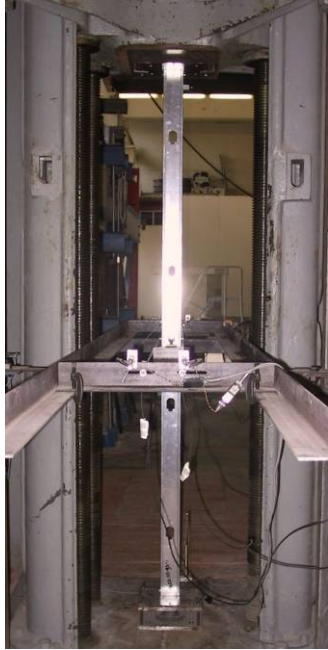
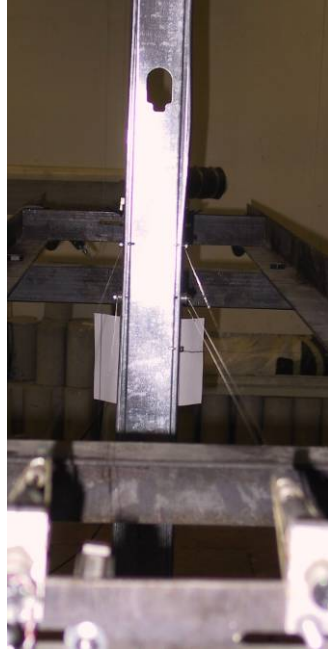
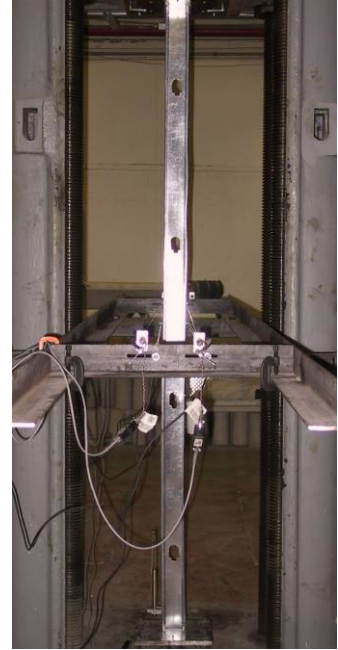


Figure A5.1 Overall View of Stud 362S125-33-200 in the Riehle Testing Machine (Looking East)



(a) at 1800 lbs



(b) at 2800 lbs

(Looking East)

Figure A5.2 Distortion Buckling of the Stud 362S125-33-200 at various Axial Load

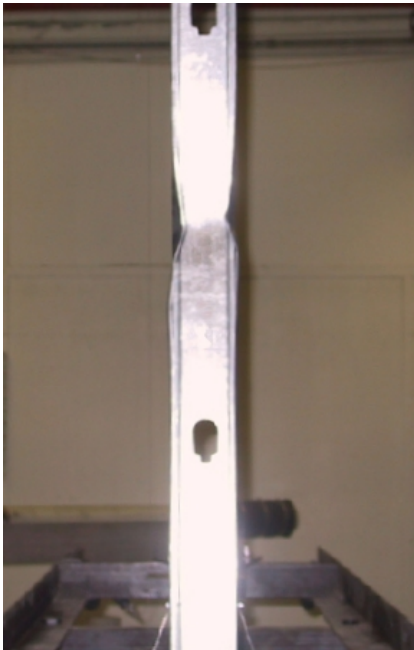


Figure A5.3 Local Buckling of Stud 362S125-33-200 at an axial load of 3000 lbs (Looking East)



(a) Top-half



(b) Bottom-half

(Looking North)

Figure A5.4 Final View of Stud 362S125-33-200

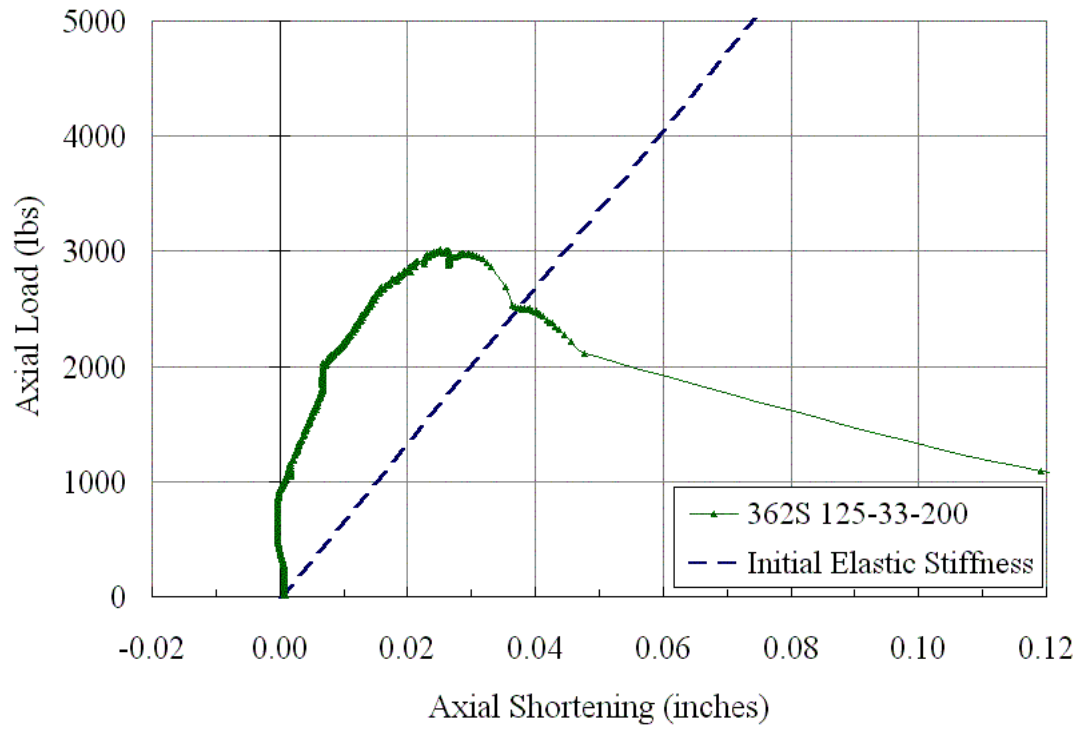


Figure A5.5 Plot of Axial Load vs. Axial Shortening

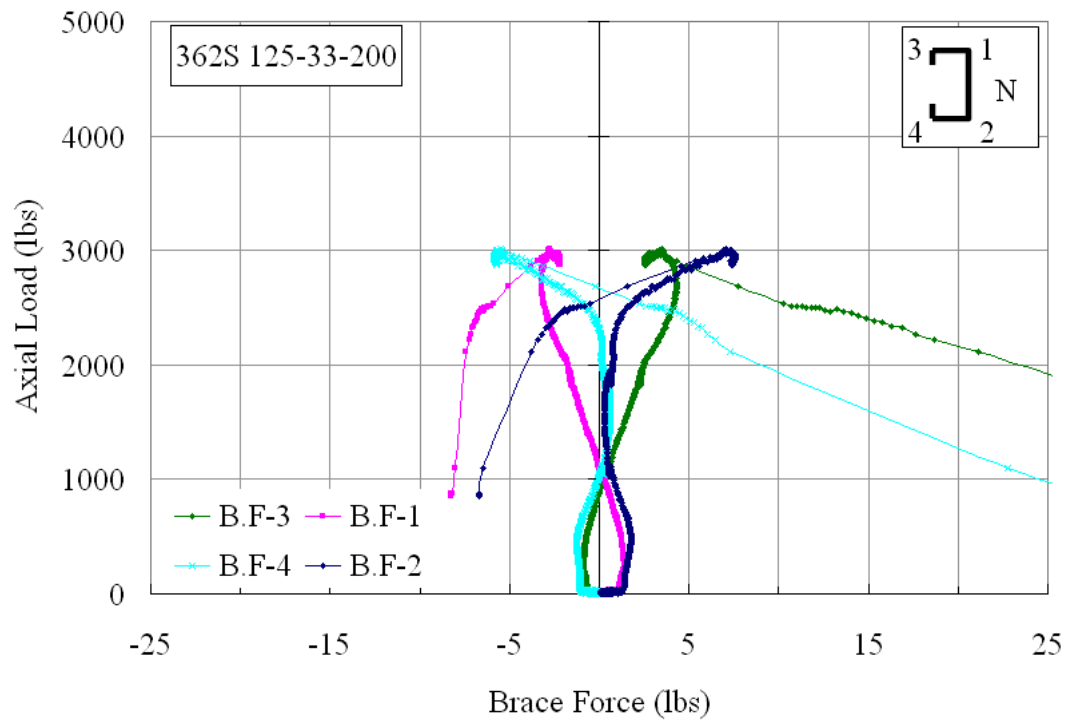


Figure A5.6 Plot of Axial Load vs. Brace Forces

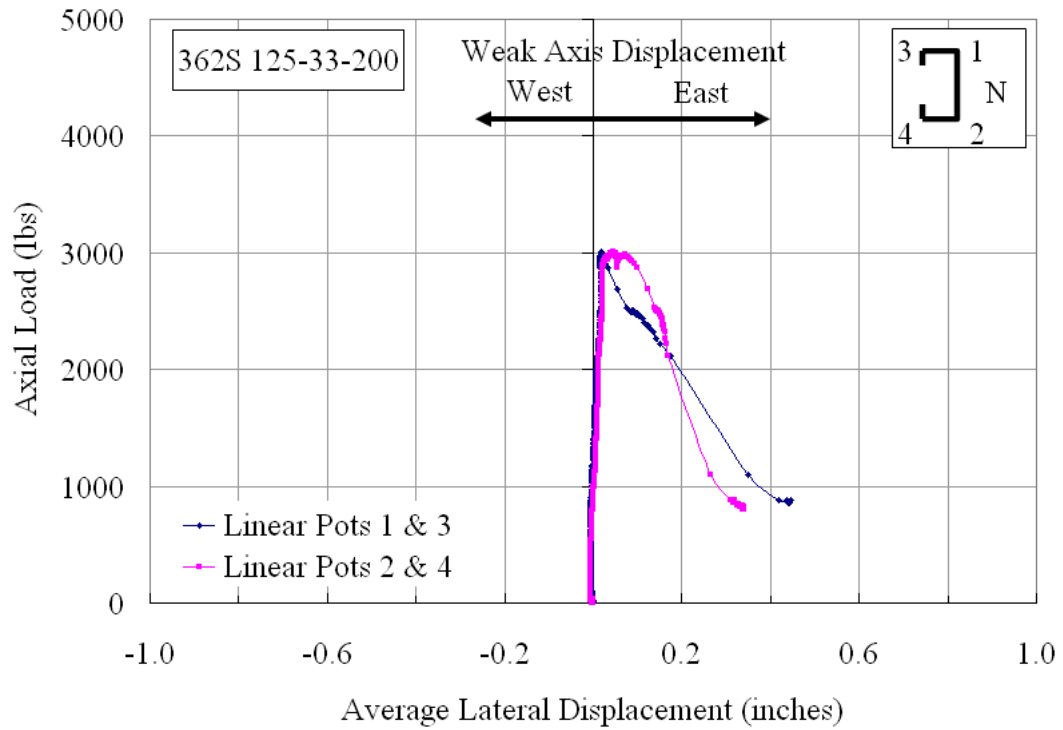


Figure A5.7 Plot of Axial Load vs. Weak Axis Displacement at Mid-Height

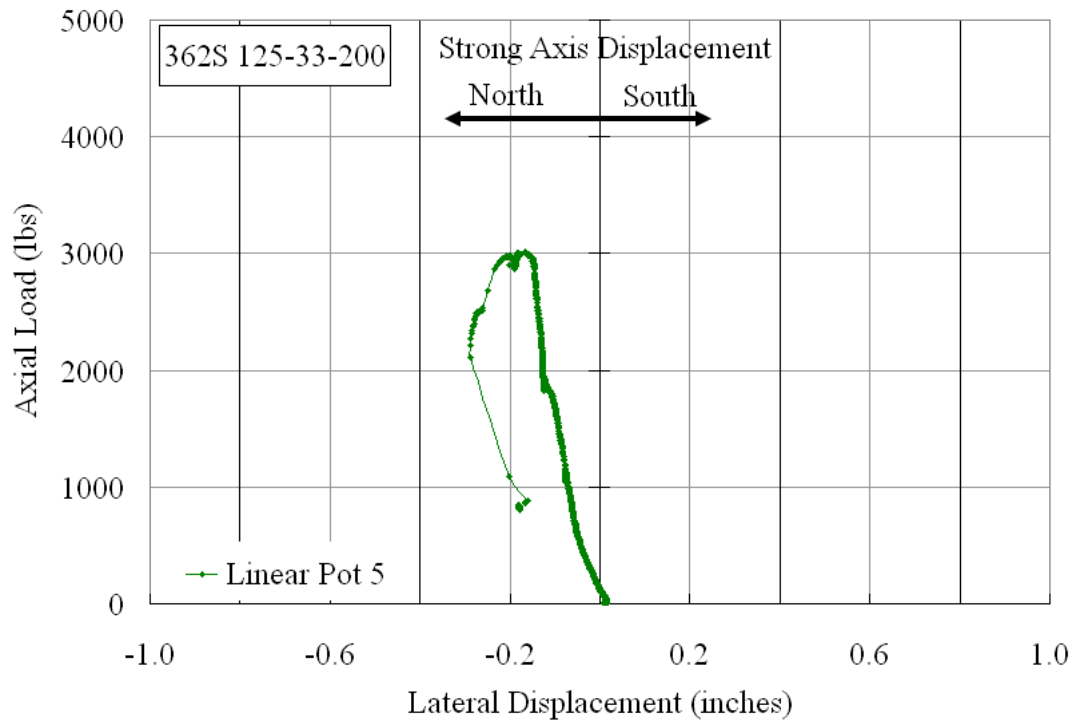


Figure A5.8 Plot of Axial Load vs. Strong Axis Displacement at Mid-Height

**362S125-33-400**

Figure A6.1 shows the overall view of the cee stud 362S125-33-400 in the Riehle Universal Testing Machine, prior to the test. The cee stud specimen was loaded at 5 to 15 lbs/sec to ensure static response of the stud to the applied load. The weak axis movement was measured by the linear potentiometers LP-1 & LP-3 attached to the north flange and LP-2 & LP-4 attached to the south flange. The strong axis movement was measured by LP-5 attached to the south flange. These instruments were located at mid-height of the stud.

The initial loading and unloading to 200 lbs ensured that the stud was properly seated within the end tracks. The plot of the axial load versus axial shortening is shown in Figure A6.5. From zero to about 1000 lbs, the axial shortening showed a linear increase. When the axial load reached 1000 lbs, the stud began to exhibit weak axis flexural-torsional buckling. The north and the south flanges had both moved east by 0.026 inches and by 0.045 inches, respectively (see Figure A6.7). At this load level, the strong axis movement was measured to be 0.45 inches towards the north by LP-5 (see Figure A6.8) and the brace forces BF-3 & BF-4 measured 3 lbs each (see Figure A6.6).

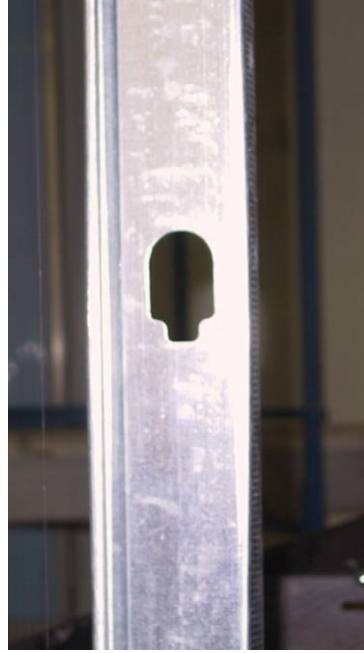
From 1000 lbs to 1800 lbs, the top-half of the stud twisted anti-clockwise and bottom-half of the stud twisted clockwise. Up to an axial load of 1800 lbs, the plot of axial shortening is relatively linear, but steeper than the initial stiffness line (see Figure A6.5). At an axial load of 1800 lbs, a distortional buckle in the flange was visible at about one foot above the location of the brace-wires (see Figure A6.2(a)). At this load, the north flange had moved east by 0.034 inches, the south flange had moved east by 0.075 inches, and the strong axis had moved north by 0.085 inches. The brace forces in both BF-3 & BF-4 measured 6.0 lbs.

From 1800 to 2000 lbs there was no incremental axial shortening. At an axial load of 2000 lbs elastic buckling waves were seen in the web, along with distortional buckling in the flanges. With increase in the axial load from 2000 lbs to 2800 lbs, the plot of axial shortening is seen to be parallel to the initial elastic stiffness line. When the axial load reached 2800 lbs, the distortional waves were seen along the full length of the stud on the flanges (see Figure A6.2(b)). At this load level, a local buckle on the south flange-lip was seen at about one foot above the braces (see Figure A6.3).

With further increase in axial load it was seen that the east displacement of the north flange was greater than that the south flange causing a greater force in BF-3 compared to BF-4. Beyond this load level up to the maximum load, the incremental load carrying capacity of the stud occurred with much larger axial deformation. The axial load increased gradually from 2800 lbs till it reached a maximum of 2960 lbs, with very large axial shortening owing to the flexural-torsional buckling of the stud. During this load plateau, the north flange displaced from 0.09 to 0.13 inches, and the south flange displaced from 0.13 to 0.26 inches while the strong axis displaced from 0.18 inches to 0.26 inches towards the north. The measured brace forces in BF-3 and BF-4 were 17 lbs and 13 lbs at the maximum load, respectively. The axial load then gradually dropped off to 2600 lbs as the brace forces increased to 30 lbs in both BF-3 and BF-4. There was a sudden drop in the axial load from this level to about 2200 lbs, and at this new load level, the stud underwent a constant axial deformation at a constant load. The test was concluded when the axial deformation was significant and measured 0.066 inches. The final buckled shape of the stud is shown in Figure A6.4 and can be measured as second max flexure-torsion.



Figure A6.1 Overall View of Stud 362S125-33-400 in UTM (Looking East)



(a) at 1800 lbs

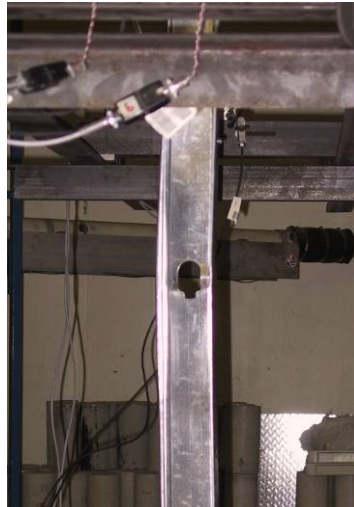


(b) at 2800 lbs

Figure A6.2 Distortional Buckling at various Axial Loads of Stud 362S125-33-400



(a) Top-Half



(b) Bottom-Half

Figure A6.3 Local Buckling at an Axial load of 2800 lbs in the Stud 362S125-33-400 in



Figure A6.4 Overall View of Stud 362S125-33-400 at maximum load (Looking North)

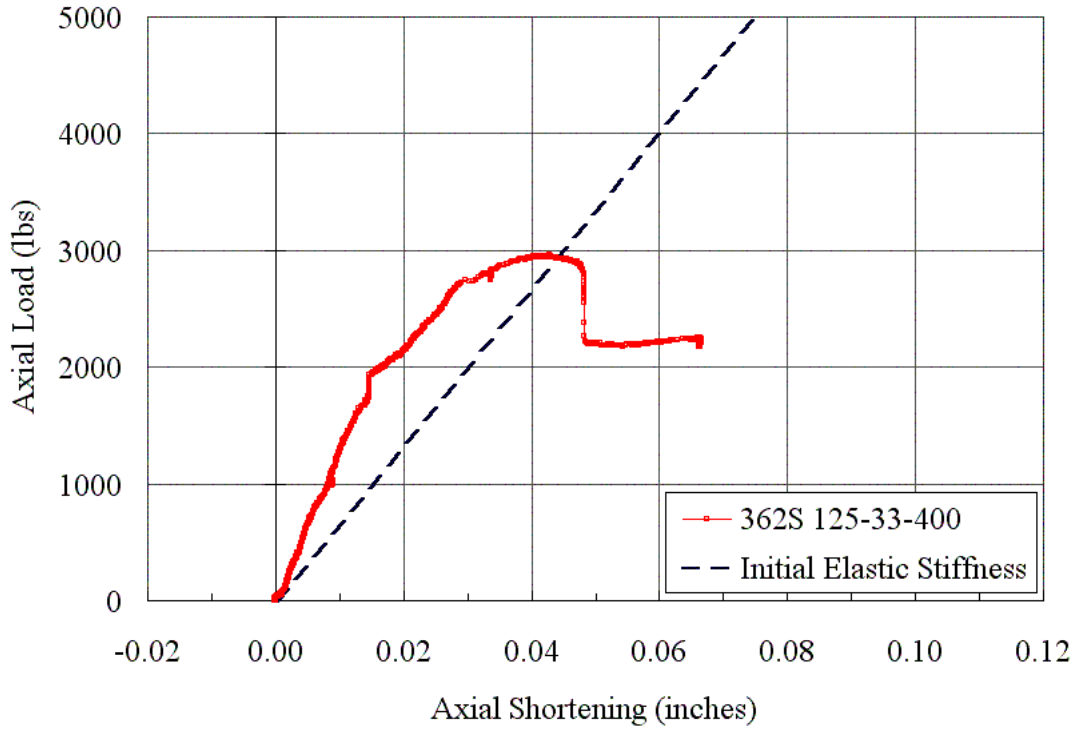


Figure A6.5 Plot of Axial Load vs. Axial Shortening

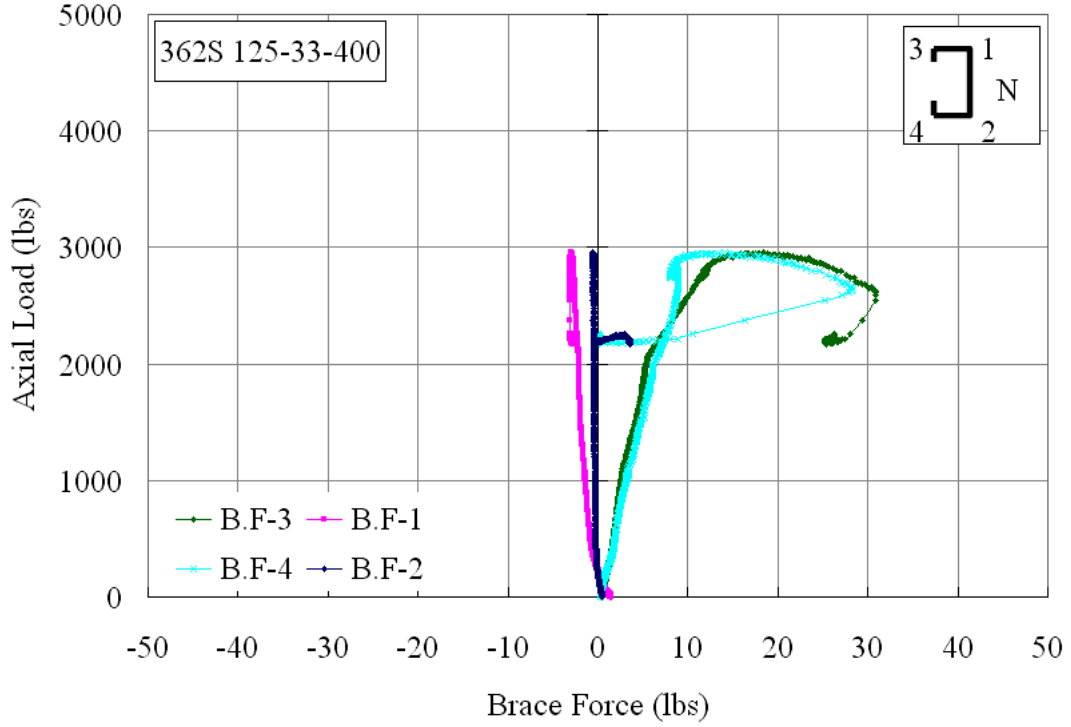


Figure A6.6 Plot of Axial Load vs. Brace Forces

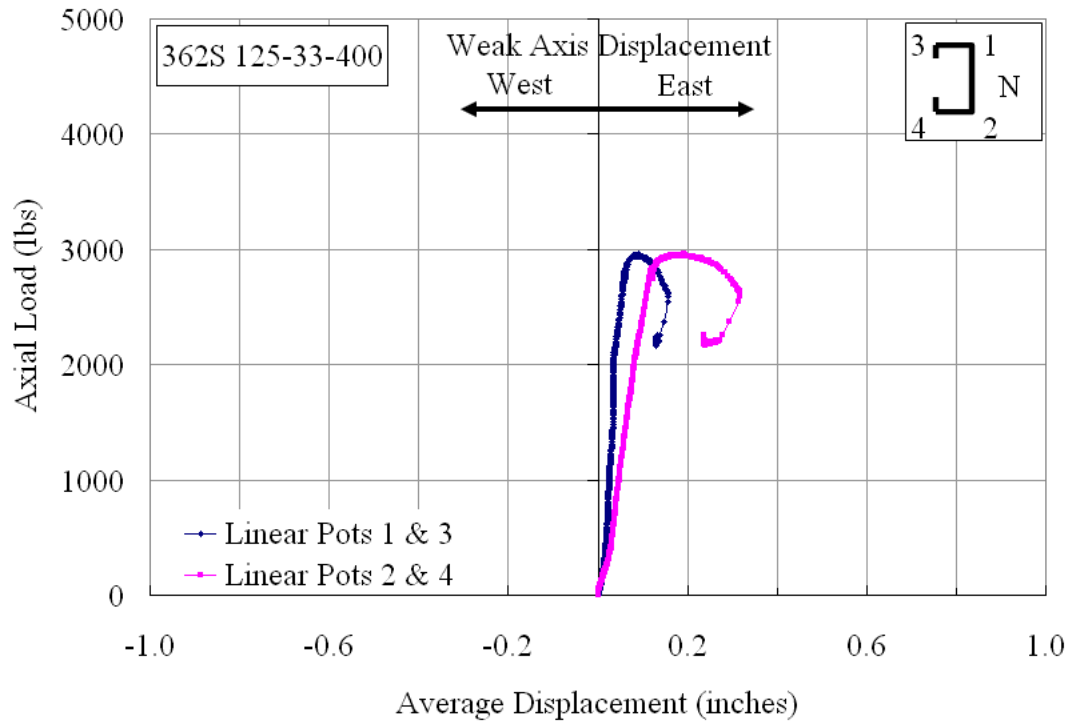


Figure A6.7 Plot of Axial Load vs. Weak Axis Displacement at Mid-height

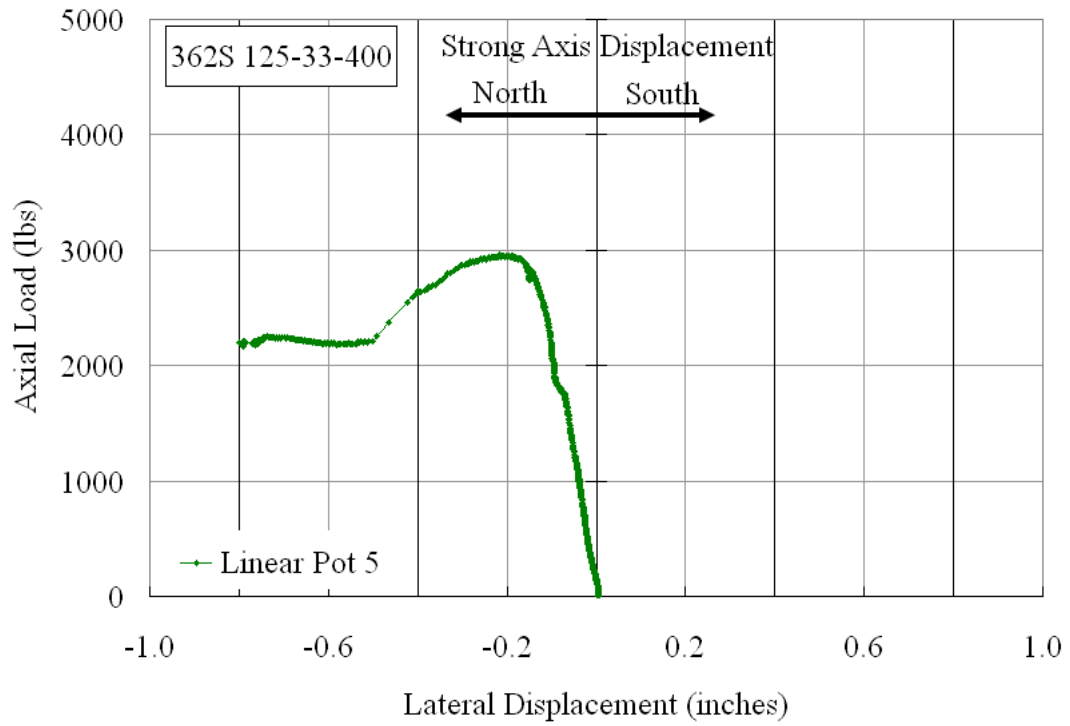


Figure A6.8 Plot of Axial Load vs. Strong Axis Displacement at Mid-Height

**362S162-43-000**

The cee stud specimen 362S162-43-000 was tested with no bracings. It was loaded at the rate of 8 to 10 lbs/sec, to ensure static response to the applied load. The overall view of the stud in the test frame is shown in Figure A7.1. The plot of the axial load versus the axial shortening, shown in Figure A7.5, is comparable and parallel to the initial elastic stiffness line for most of the test. Figure A7.6 shows the displacements of the mid-height cross-section with increasing axial load. Up to an axial load of 2500 lbs, first mode weak axis flexural buckling was observed. The linear potentiometers LP-1 & LP-3 and LP-2 & LP-4, attached to the north and south flanges, recorded a displacement of 0.25 inches each, respectively. At the same load, the strong axis had moved north by 0.08 inches (see Figure A7.7).

From 2500 lbs to the maximum axial load, the stud started to buckle in first mode flexural-torsion and the two flanges exhibited differential movement towards the east. The mid-height cross-section twisted clockwise. Figure A7.2 shows the stud at 4000 lbs and first mode flexural-torsional buckling is clearly observed. On reaching the maximum load of about 5250 lbs, the axial shortening was 0.05 inches, the north flange had moved east by 1.0 inch, and the south flange had moved back to 0.05 inches east. The strong axis had moved north by 0.5 inches. Figure A7.4 shows the stud at 5250 lbs with a local buckle in the south flange. Figure A7.4 shows the close-up view of the local buckle in the south flange-web junction.



Figure A7.1 Overall View of Stud 362S162-43-000 in the Riehle Machine (Looking East)



Figure A7.2 Flexural-torsion of the Stud 362S162-43-000 at an Axial Load of 4000 lbs (Looking East)



Figure A7.3 Flexural-torsion of the Stud 362S162-43-000 at an Axial Load of 5250 lbs (Looking North)



Figure A7.4 Final View of the Stud 362S162-43-000 at Failure (Looking North)

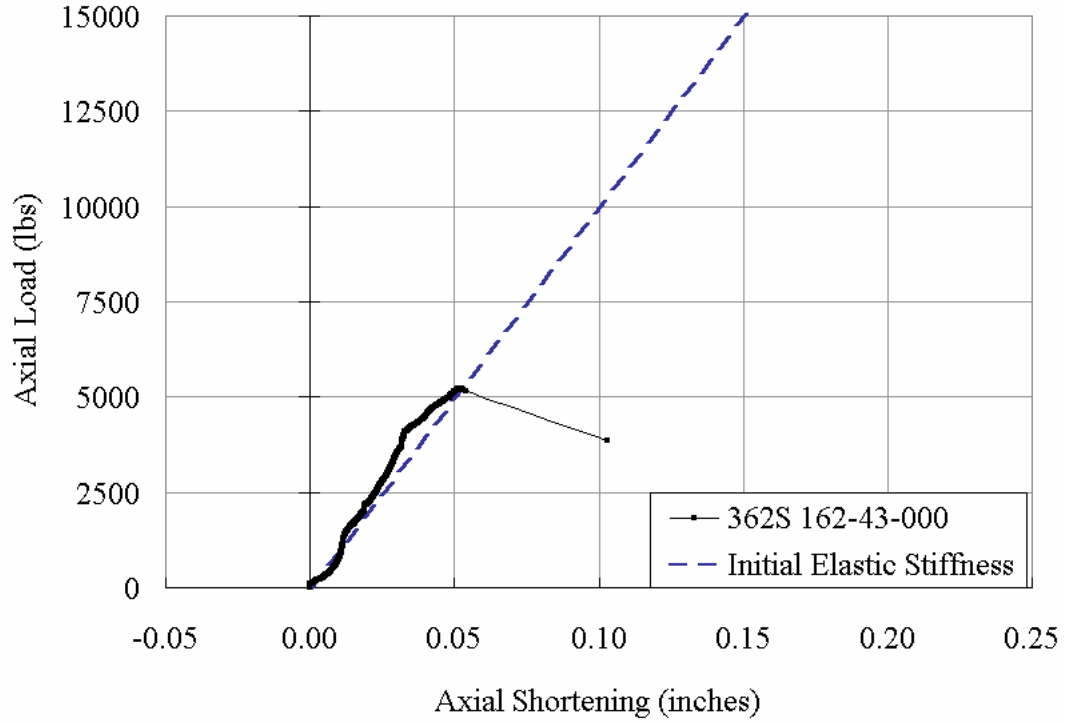


Figure A7.5 Plot of Axial Load vs. Axial Shortening

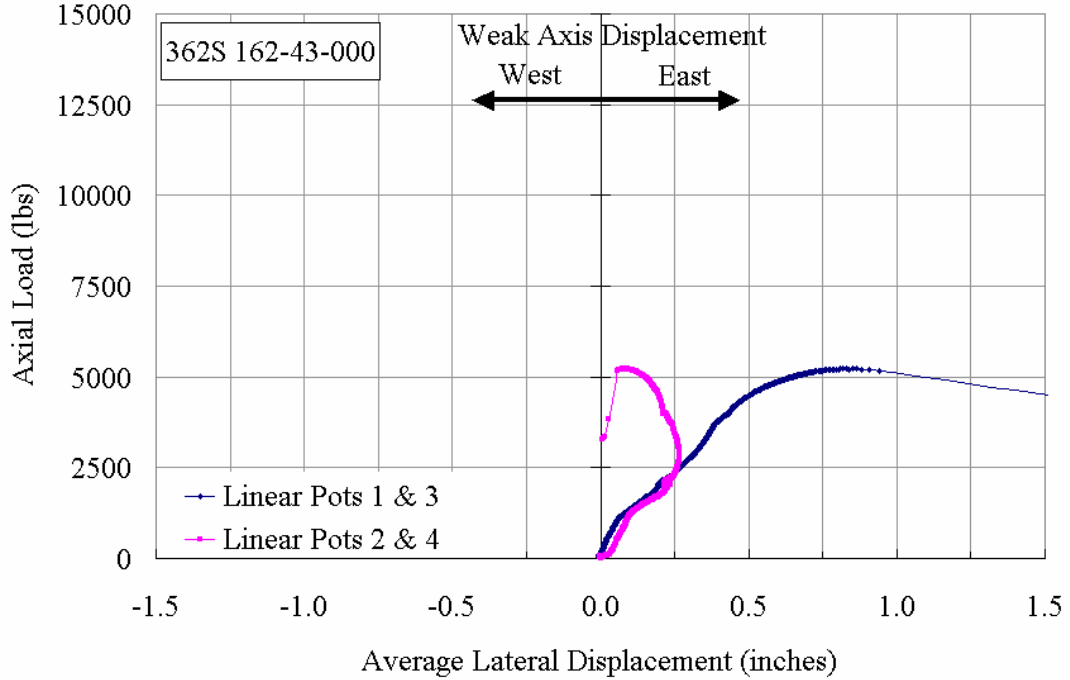


Figure A7.6 Plot of Axial Load vs. Weak Axis Displacement at Mid-Height

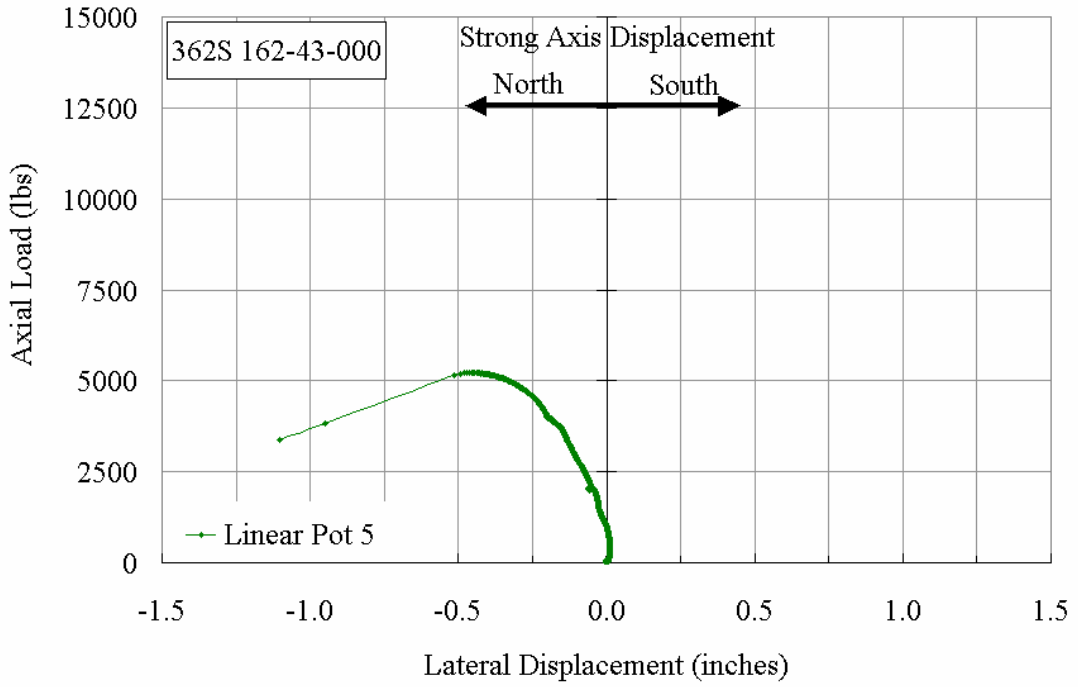


Figure A7.7 Plot of Axial Load vs. Strong Axis Displacement at Mid-Height

**362S162-43-200**

The cee stud specimen 362S162-43-200 was tested with effective total brace stiffness of 371 lbs/in. The bracing provided was close to twice the ideal bracing requirement. To ensure static response of the stud to the applied load, it was loaded at the rate of 8 to 12 lbs/sec. The overall view of the stud in the test frame is shown in Figure A8.1. The plot of the axial load versus the axial shortening, shown in Figure A8.5, is comparable and parallel to the initial elastic stiffness line.

From an axial load of zero to 2500 lbs, the mid-height displacement of the weak axis towards east indicates flexural buckling. At this load, the linear potentiometers LP-1 & LP-3 and LP-2 & LP-4, attached to the north and south flanges, respectively, recorded a lateral displacement of 0.05 inches on both flanges (see Figure A8.7). At this load level, the mid-height lateral displacement of the strong axis was 0.05 inches to the north (see Figure A8.8). The brace forces in BF-3 and BF-4 measured 8 lbs in both the braces, and is shown in Figure A8.6.

From 2500 lbs to the maximum axial load, the stud buckled in second mode flexural-torsion as differential lateral displacements were recorded between the two flanges (see Figure A8.7). The brace force in BF-3 continued to increase whereas the force in BF-4 remained constant at around 9 lbs. At an axial load of 4050 lbs, the cross-sectional distortion was visible close to a web punchout, as shown in Figure A8.2.

On reaching the maximum load of about 7250 lbs, the axial shortening was 0.09 inches, the north flange had moved by 0.1 inch to the east, and the south flange had moved back to 0.03 inches from its initial position. At the maximum load level, there was a local buckle formation in the web, and is shown in Figure A8.3.

The strong axis lateral displacement was 0.15 inches to the north. At failure the stud had buckled in first mode flexure with second mode torsion as shown in Figure

A8.4.



Figure A8.1 Overall View of Stud 362S162-43-200 in the Riehle Machine (Looking East)



Figure A8.2 Distortion at a Web-perforation of the Stud 362S162-43-200 at an Axial Load of 4050 lbs



Figure A8.3 Distortion of the Stud 362S162-43-200 at the Maximum Axial Load (Looking East)



Figure A8.4 Final View of the Stud 362S162-43-200 beyond the Maximum Axial Load (Looking East)

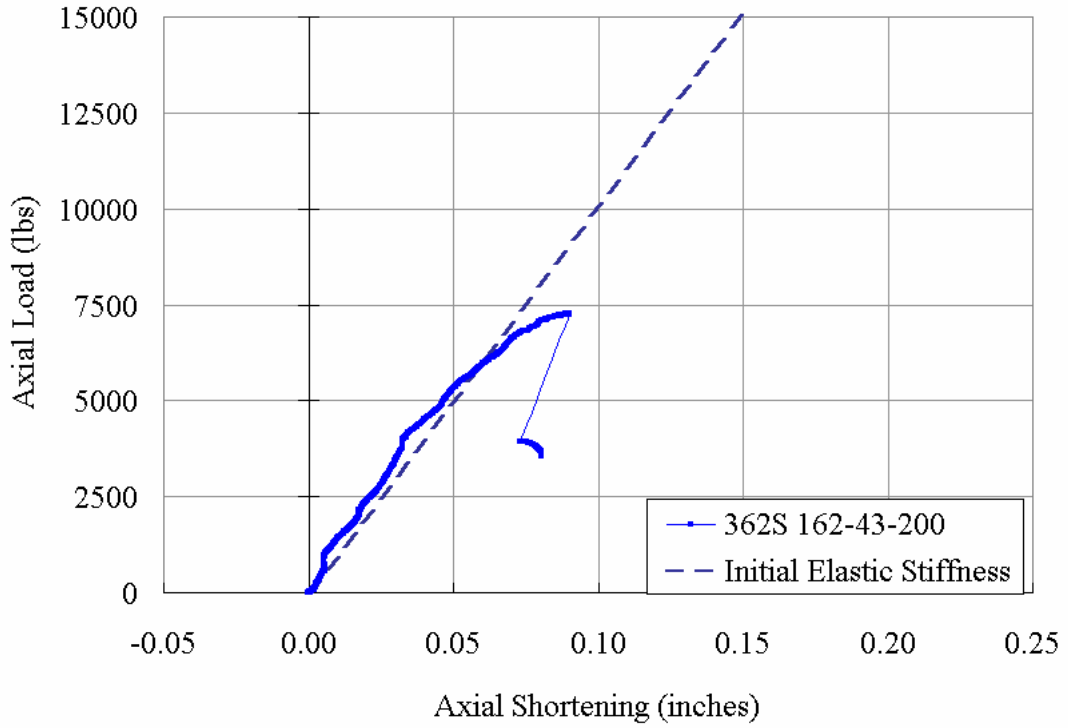


Figure A8.5 Plot of Axial Load vs. Axial Shortening

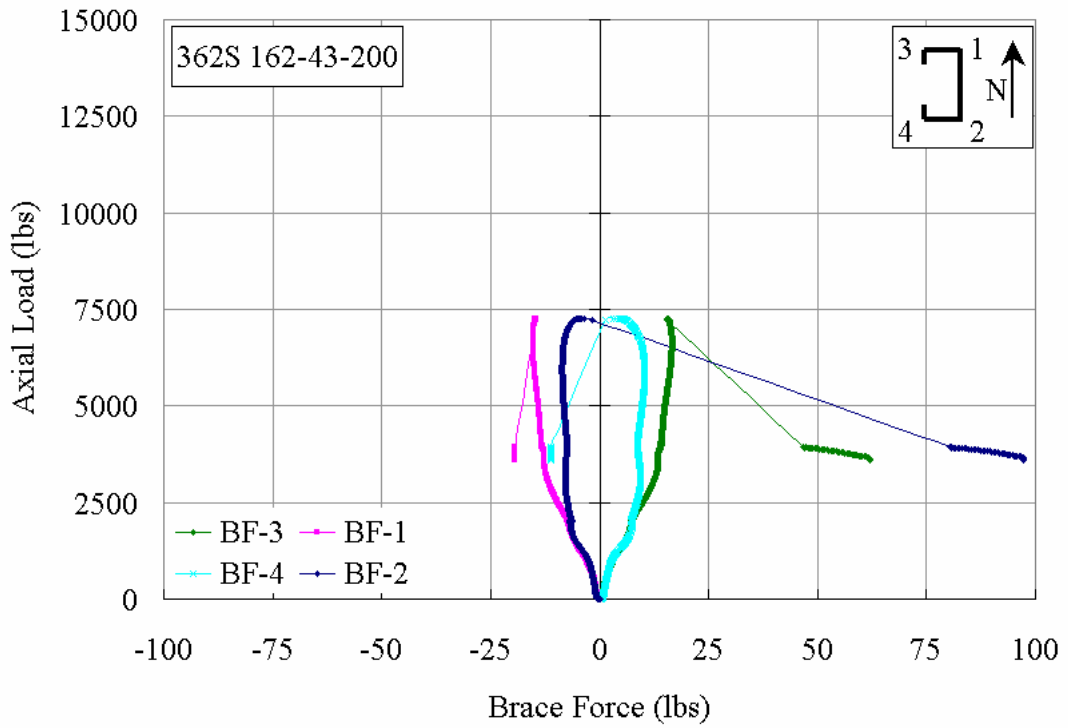


Figure A8.6 Plot of Axial Load vs. Brace Forces

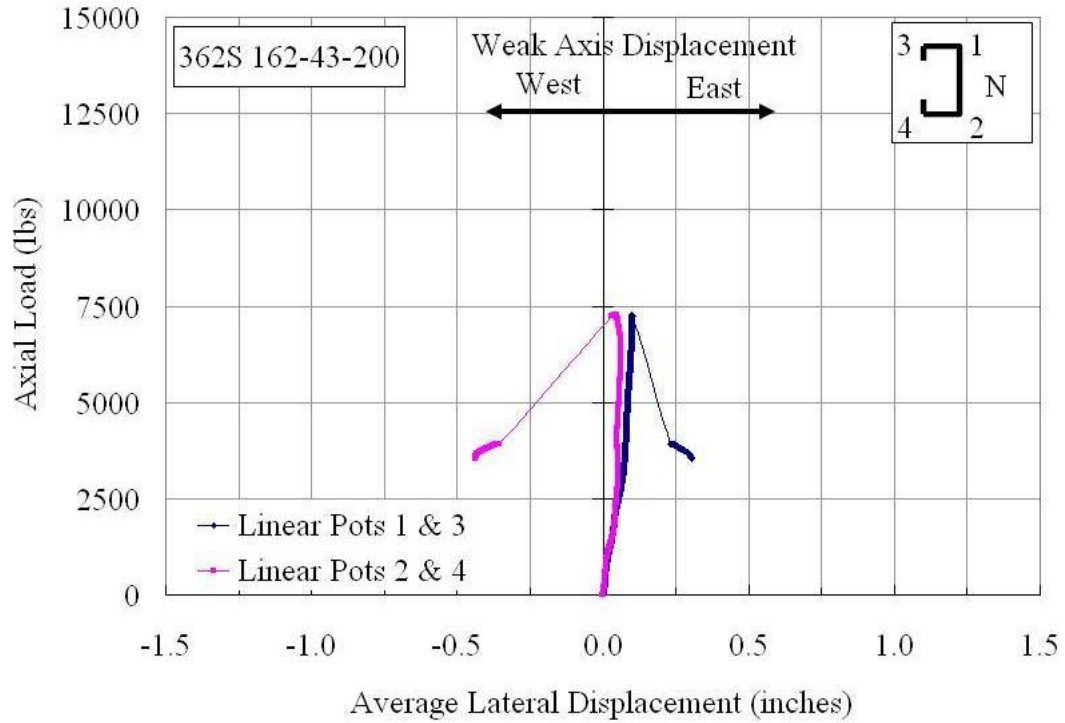


Figure A8.7 Plot of Axial Load vs. Weak Axis Displacement at Mid-Height

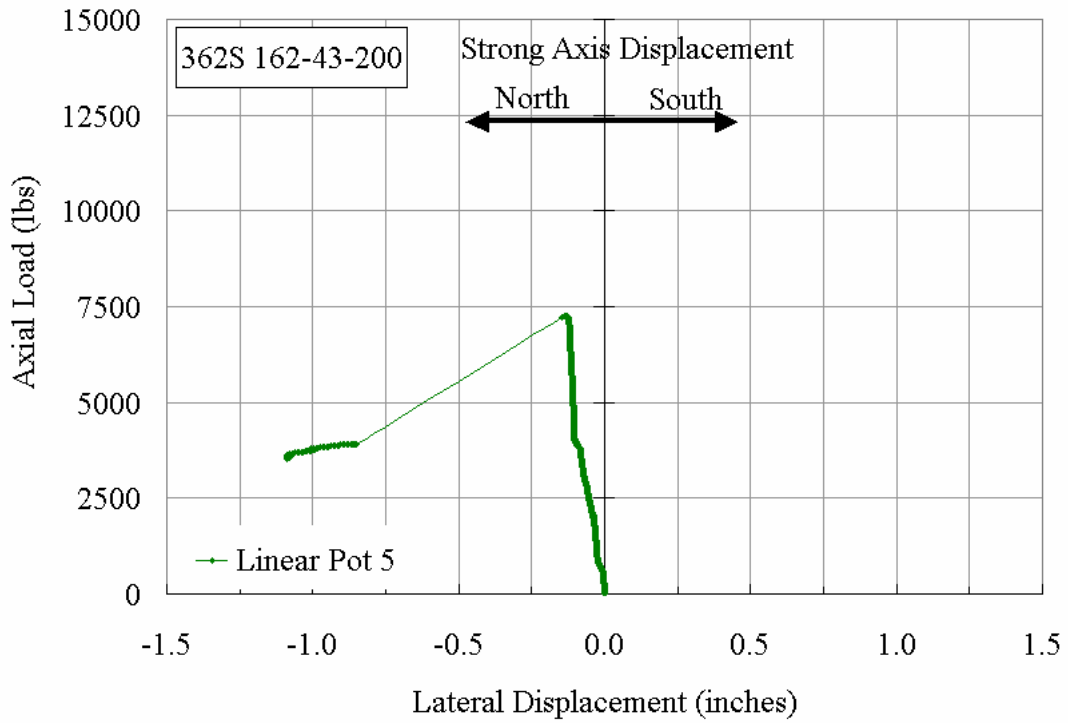


Figure A8.8 Plot of Axial Load vs. Strong Axis Displacement at Mid-Height

**362S162-43-400**

The cee stud specimen 362S162-43-400 was tested with a total bracing stiffness of 734 lbs/in. It was loaded at the rate of 10 to 15 lbs/sec, to ensure a static response. The overall view of the stud in the test frame is shown in Figure A9.1. The weak axis lateral displacement of the mid-height cross-section was measured by the linear potentiometers LP-1 & LP-3 and LP-2 & LP-4, attached to the north and south flanges, respectively, and the strong axis lateral displacement was measured by LP-5 attached to the south flange.

From zero to an axial load of 1400 lbs, the flexural buckling of the stud caused the weak axis to move east. At this load level, the north and south flanges had laterally displaced to the east by 0.019 inches, and the corresponding plot is shown in Figure A9.7. At this load level, the strong axis had moved north by 0.043 inches as shown in Figure A9.8. During this loading phase, the brace forces in BF-3 and BF-4 increased with increasing axial load and at 1400 lbs both measured about 7.0 lbs as shown in Figure A9.6. With further increase in axial load, the relative change in the brace forces in BF-3 and BF-4 was different and at 2500 lbs, they measured 20.5 lbs and 8.2 lbs, respectively.

From 1400 lbs to 4400 lbs of axial load, there was only a slight differential movement of the flanges that would be indicative of flexural buckling of the stud while brace forces in BF-3 and BF-4 continued to increase and at 4400 lbs they measured 29 lbs and 18 lbs, respectively. At an axial load of 4400 lbs, a local buckle was observed in the cross section in the vicinity of a web punchout, and is shown in Figure A9.2. When the axial load increased to 5400lbs, the force in BF-4 had reached a peak value of 20 lbs and then had started to decrease, whereas the force in BF-3 remained constant at 30 lbs. On reaching the maximum axial load of 7029 lbs, the axial shortening was 0.09 inches, the north flange had moved by 0.08 inch to the east, and the south flange had moved back to

0.03 inches from the initial position. The mid-height section had laterally displaced to the north by 0.21 inches. At the maximum load level, the brace forces in BF-3 and BF-4 measured 37 lbs and 0 lbs, respectively. The final buckled shape of the stud can be described as first mode flexure coupled with second mode torsion.



Figure A9.1 Overall View of Stud 362S162-43-400 in the Riehle Machine (Looking East)



Figure A9.2 Distortion at a Web-perforation of the Stud 362S162-43-400 at an Axial Load of 4400 lbs

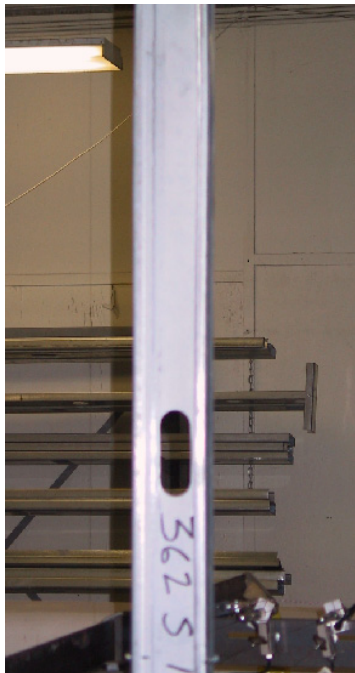


Figure A9.3 Distortional wave in the flanges of Stud 362S162-43-400 at 7000 lbs of Axial Load

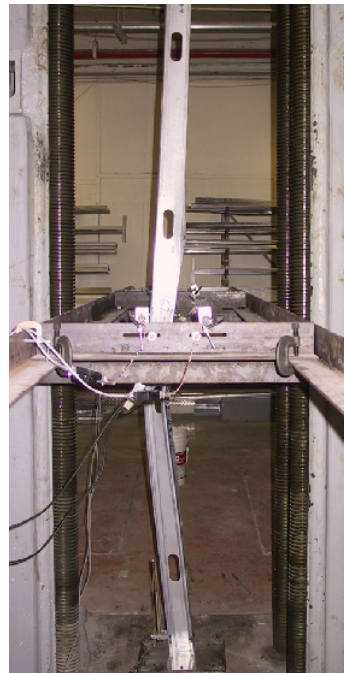


Figure A9.4 Final View of the Stud 362S162-43-400 beyond the Maximum Axial Load (Looking East)

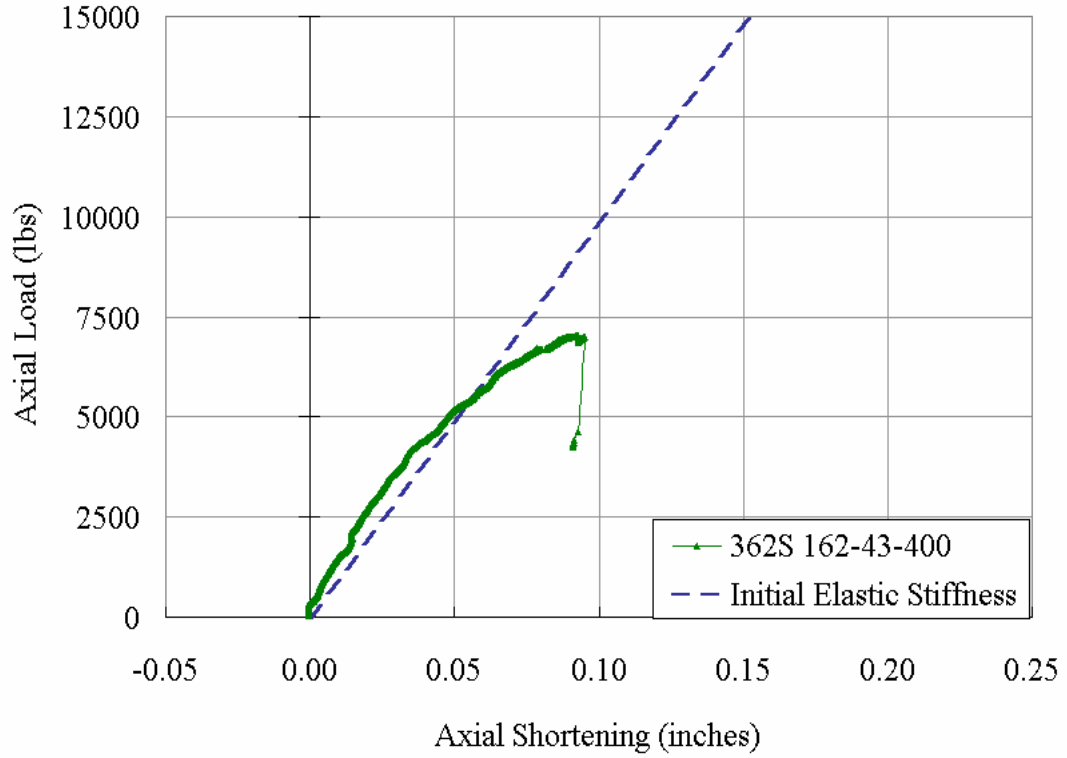


Figure A9.5 Plot of Axial Load vs. Axial Shortening

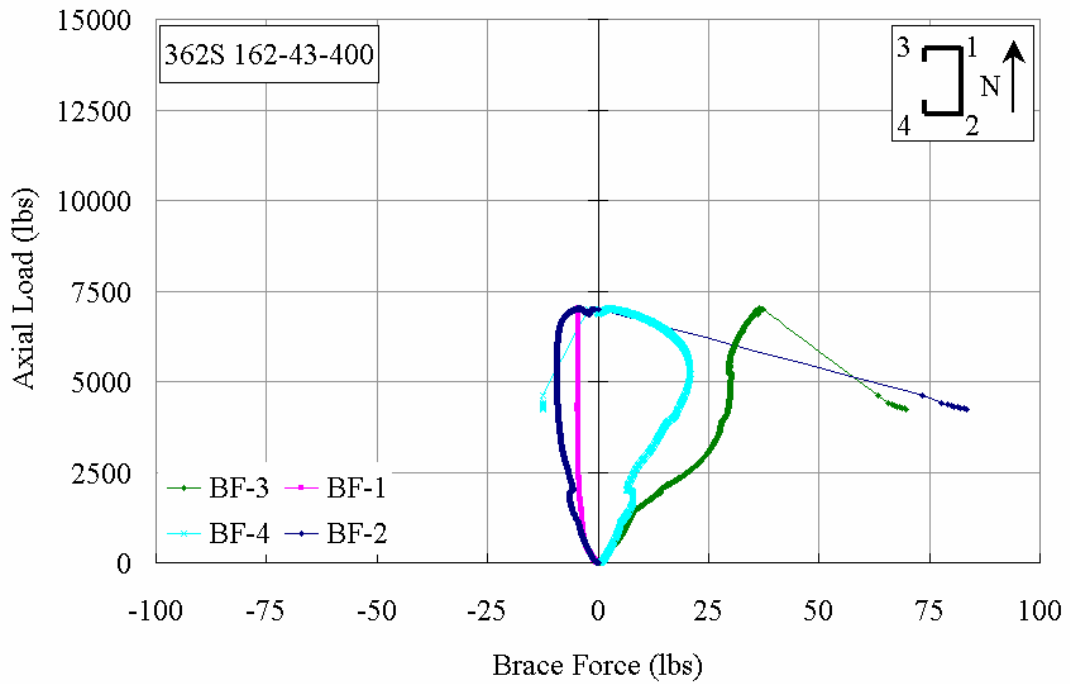


Figure A9.6 Plot of Axial Load vs. Brace Forces

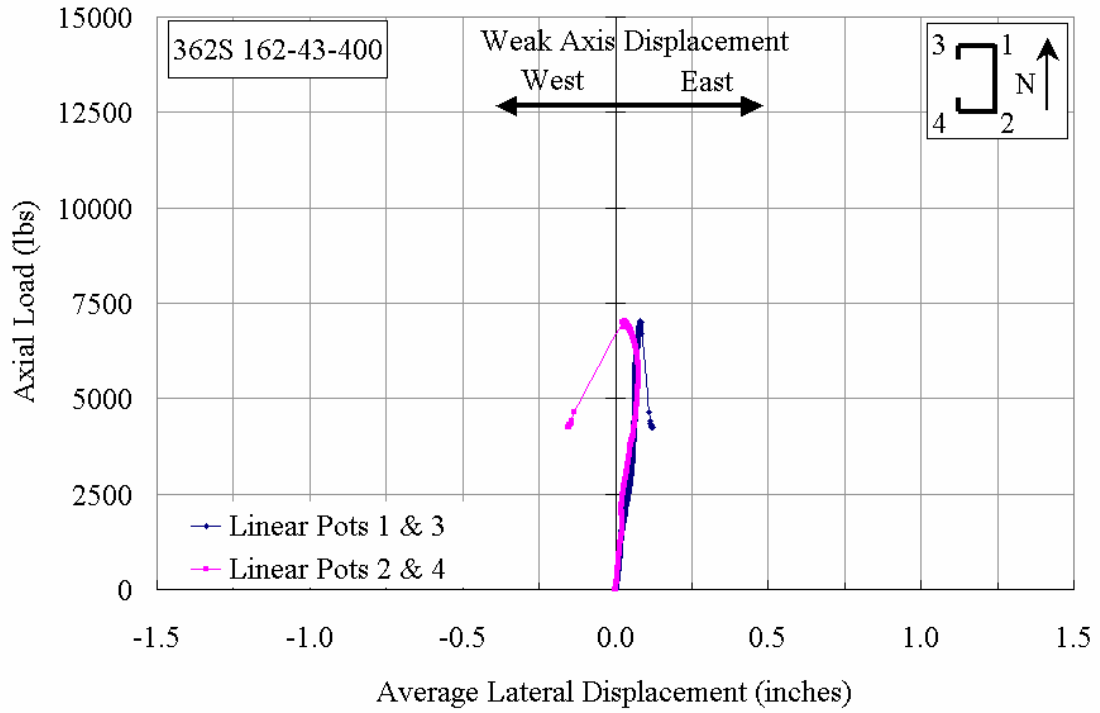


Figure A9.7 Plot of Axial Load vs. Weak Axis Displacement at Mid-Height

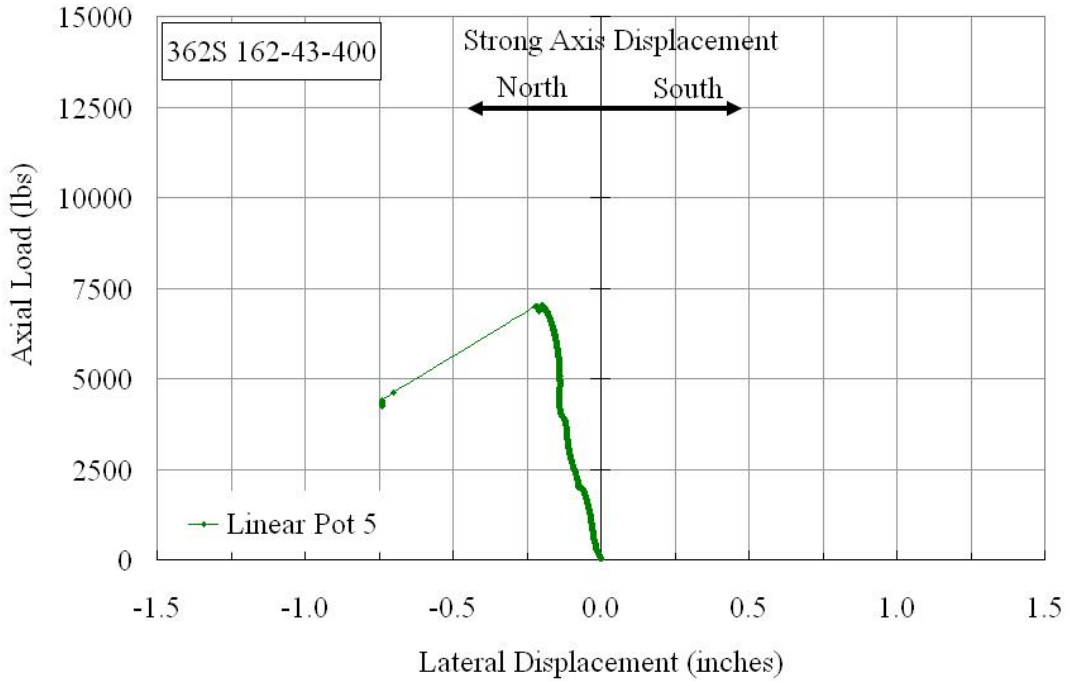


Figure A9.8 Plot of Axial Load vs. Strong Axis Displacement at Mid-Height

**362S162-43-800**

The overall view of the test specimen, prior to testing, in the Riehle Universal Testing Machine is shown in Figure A10.1. The stud 362S162-43-800 was braced with a total brace stiffness of 1478 lbs/in., which was about seven times the ideal bracing requirement. Axial load was applied at a rate of 10 lbs/sec, to ensure static response of the stud. The weak axis lateral displacement, at the mid-height of the stud, was measured with linear potentiometers LP-1 & LP-3 attached to the north flange, and LP-2 & LP-4 attached to the south flange. The strong axis lateral displacement was measured with LP-5 attached to the south flange of the stud.

From zero to an axial load of 1750 lbs, there was minimal strong and weak axis lateral displacement or any observable change in the geometry of the stud. During this loading phase, the stud was observed to be buckling in first mode flexure, though small, by the lateral displacement of the weak axis. From Figure A10.6, it is observed that from 1750 lbs onwards, there was a noticeable change in the measured brace forces in BF-3 and BF-4, indicating the inception of torsional buckling. At an axial load of 2000 lbs, the north and south flanges had moved east by 0.037 inches and 0.013 inches, respectively, with northward movement of the strong axis being 0.005 inches. At this same load, the brace forces in BF-3 and BF-4 measured 11.8 lbs and 7.92 lbs, respectively. The differential brace forces in BF-3 and BF-4 and the differential movement of the north and south flanges, as shown in Figs. A10.6 and A10.7, indicate that torsional buckling of the mid-height cross-section was occurring.

The plot of axial load versus axial shortening of the stud was parallel to the initial elastic stiffness line up to an axial load of about 5000 lbs as shown in Figure A10.5. With increase in the axial load the stud seemed to rotate about the southeast corner with

BF-3 preventing this rotation. At an axial load of 5000 lbs, a local buckle was observed to initiate near the vicinity of a web punchout, causing portion of a web to be ineffective in carrying the compressive load. Figure A10.2 shows the formation of the local buckle in the web at about 1.5 ft from the mid-height, in the upper half of the stud specimen.

When the axial load reached about 6400 lbs, the brace force in BF-4 measured zero and beyond this point, the force in BF-2 started to increase. At an axial load of about 6535 lbs, the stud failed by second-mode torsional buckling. At this load, the force in BF-3 measured 30 lbs, and that in BF-2 was 5 lbs. The strong axis had moved north by 0.09 inches, and the weak axis movement was defined by the displacement of the north flange towards the east by 0.09 inches and the south flange towards the west by 0.03 inches. Figure A10.3 shows the overall view of the stud at failure and Figure A10.4 shows a close view of the local buckle formed in both the south flange and the web of the stud, at about 1.5 ft from mid-height of the stud in the vicinity of a web punchout.



Figure A10.1 Overall view of Stud 362S162-43-800 in the Riehle Testing Machine (Looking East)



Figure A10.2 Local Buckling in the Web at an Axial Load of 5000 lbs, of the Stud 362S162-43-800 (Looking East)

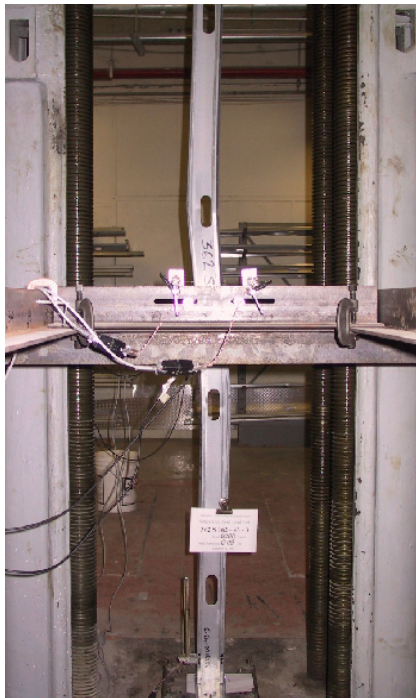


Figure A10.3 Final Buckled Shape of the Stud 362S162-43-800 (Looking East)

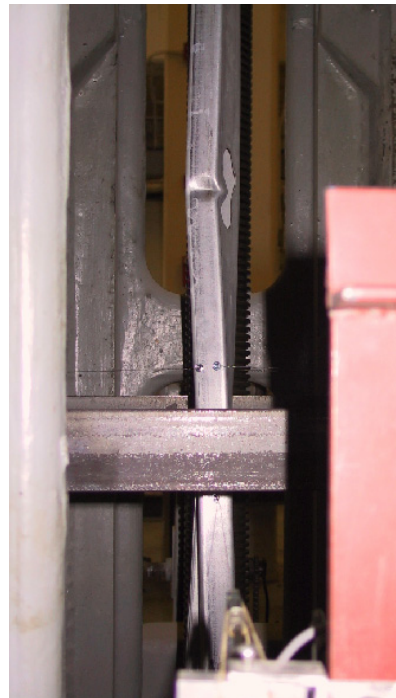


Figure A10.4 Final Buckled Shape of the Stud 362S162-43-800 (Looking North)

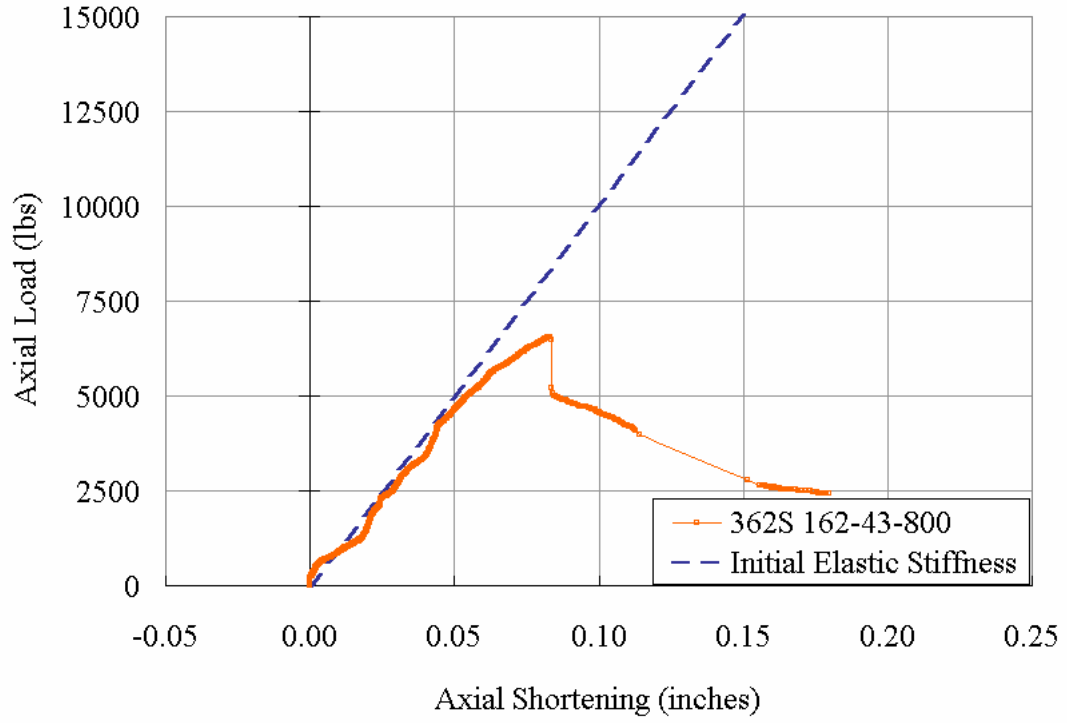


Figure A10.5 Plot of Axial Load vs. Axial Shortening

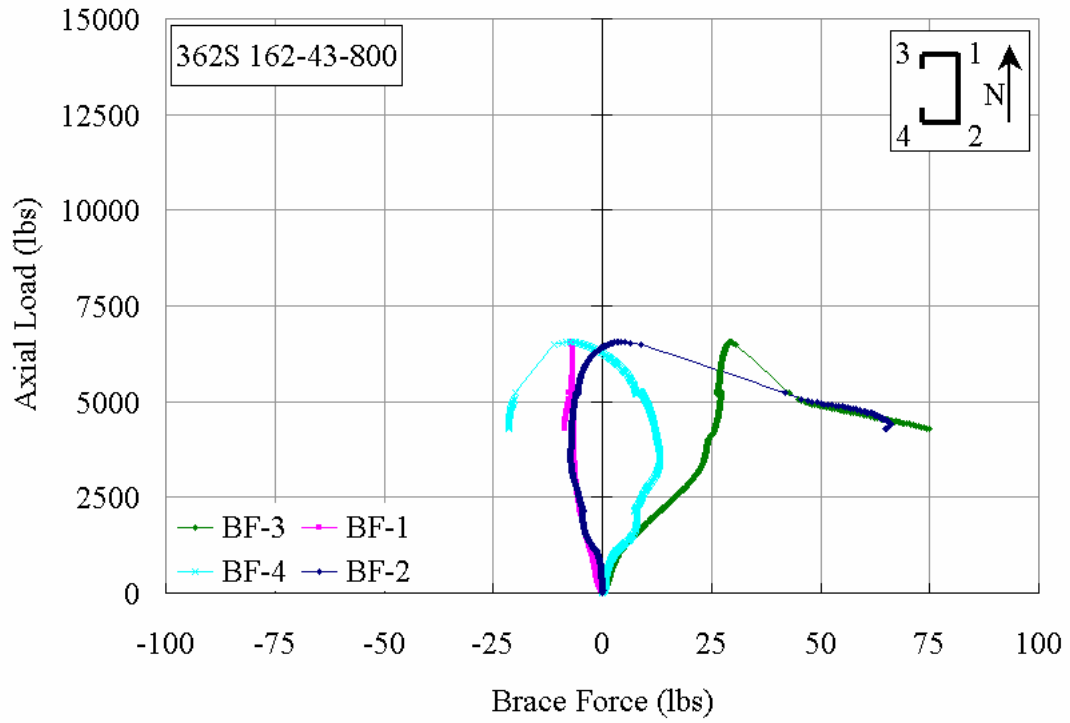


Figure A10.6 Plot of Axial Load vs. Brace Force

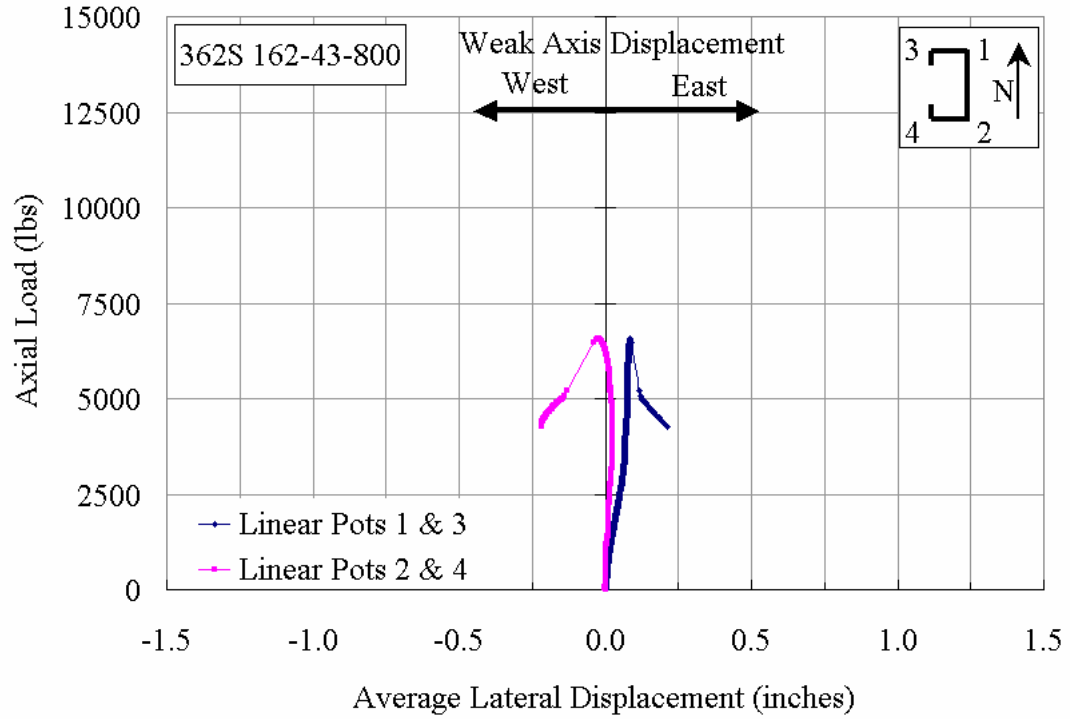


Figure A10.7 Plot of Axial Load vs. Weak Axis Displacement at Mid-Height

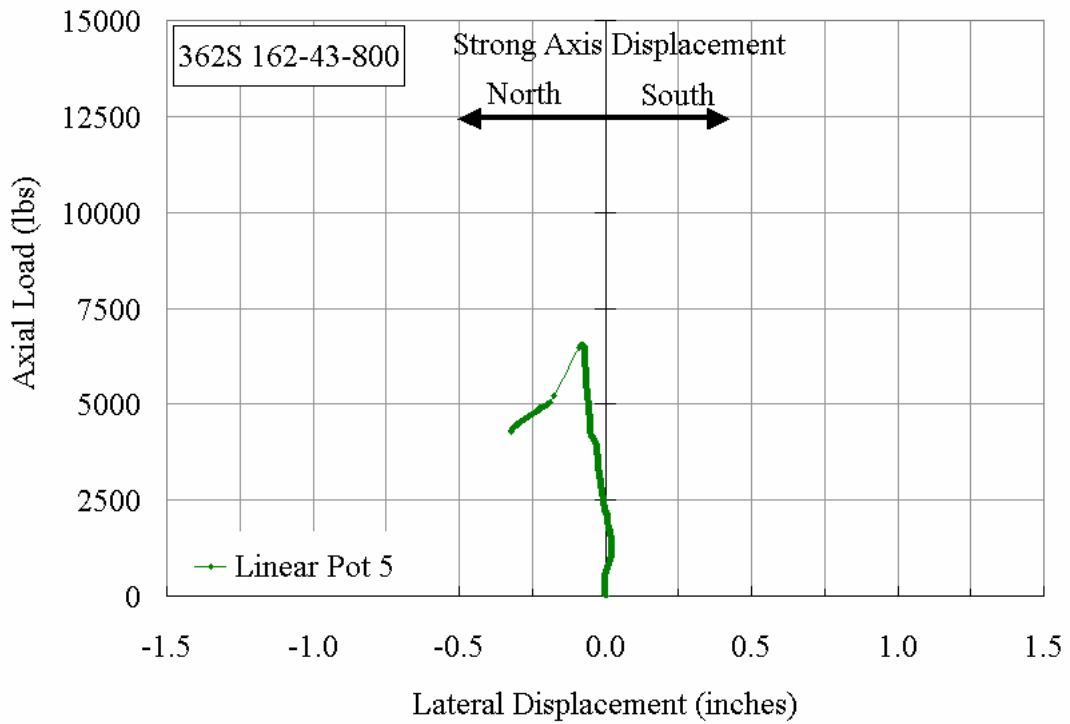


Figure A10.8 Plot of Axial Load vs. Strong Axis Displacement at Mid-Height

**362S162-68-000**

The stud 362S162-68-000 was tested without any bracing. The stud was loaded initially at 10 lbs/sec and then at 5 lbs/sec, to ensure static response of the stud to the applied load. The overall view of the stud in the Riehle Testing Machine, prior to testing, is shown in Figure A11.1. The weak axis lateral displacement at mid-height was measured with linear potentiometers LP-1 & LP-3 and LP-2 & LP-4, attached to the north and south flanges, respectively, and the strong axis was measured with LP-5 attached to the south flange.

From the very beginning of the testing, the stud exhibited first mode flexural-torsional buckling. The plot of the axial load versus average weak axis displacement shows that the north and south flanges were moving to the east due to combined first mode flexural buckling about weak axis and first mode torsional buckling. Torsional buckling of the stud caused the two flanges to move at different rates with respect to the applied load. From zero to 1000 lbs of axial load, no axial shortening was recorded, since it was nullified by the effect of elongation of the north flange. From 1000 lbs to 3300 lbs, the axial shortening was nearly parallel to the initial elastic stiffness line, and at 3300 lbs it was 0.02 inches (see Figure A11.5), equal to the computed value on the initial elastic stiffness line. At this load level, the north and the south flanges had moved east by 0.28 inches and 0.67 inches, respectively.

On further loading of the stud, slight increments in the applied load caused excessive buckling of the stud, which caused higher axial shortening than the computed value of the initial elastic stiffness, as shown in Figure A11.5. There was no appreciable strong axis buckling since the weak axis first mode flexure combined with first mode torsion was the controlling limit state. The plot of mid-height lateral displacement of the

strong axis is shown in Figure A11.7, and at 5400 lbs, a significant change in the strong axis displacement was observed. At an axial load of 5600 lbs, a distortional buckle was observed on the south flange causing the cross section become less effective in carrying the compressive load. At this load level, the lateral displacement of the north and south flanges to the east were 0.49 inches and 1.64 inches, respectively. Figure A11.3 shows a close-up view of the distortional buckle at 5800 lbs. The load then reached a maximum of approximately 6450 lbs, as part of the cross-section became ineffective in carrying the compressive load. At this load level, the axial deformation and the mid-height lateral displacement were sufficiently large to cause failure of the stud. The axial shortening was 0.165 inches, the lateral displacement of the north and south flanges to the east were 0.91 and 2.87 inches, respectively, and the displacement of the of strong axis was 0.47 inches to the north. The final buckled shape of the stud is shown in Figure A11.4, which is identified as first mode flexural-torsional buckling.



Figure A11.1 Overall View of Stud 362S162-68-000 in the Riehle Machine (Looking East)



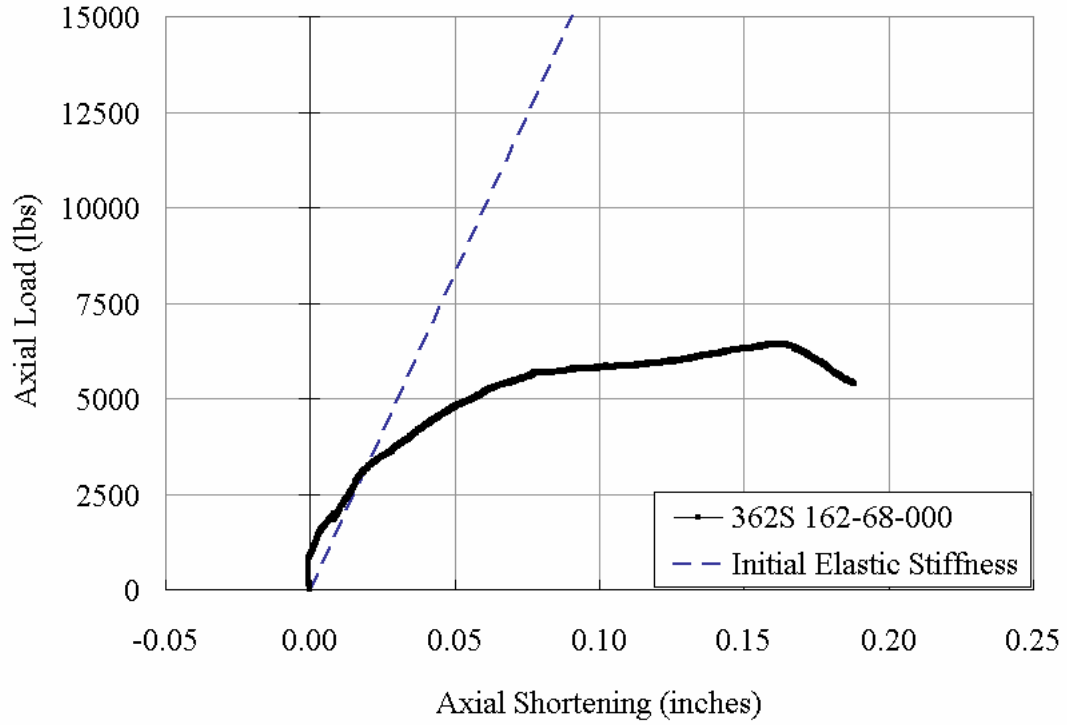
Figure A11.2 Flexural-Torsional Buckling of the Stud 362S162-68-000 at an axial load of 4000 lbs



Figure A11.3 Distortional buckling of the Stud 362S162-68-000 at 6100 lbs of axial load



(a) Looking East (b) Looking North  
Figure A11.4 Final View of the Buckled Shape of the Stud 362S162-68-000



FigureA11.5 Plot of Axial Load vs. Axial Shortening

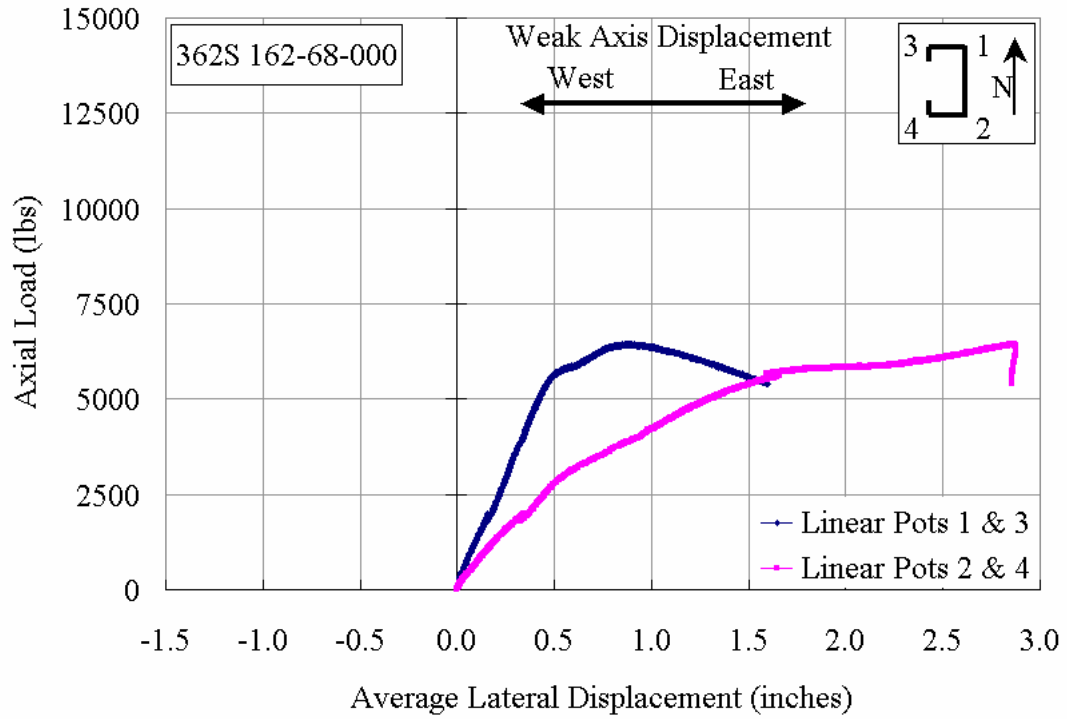


Figure A11.6 Plot of Axial Load vs. Weak Axis Displacement at Mid-Height

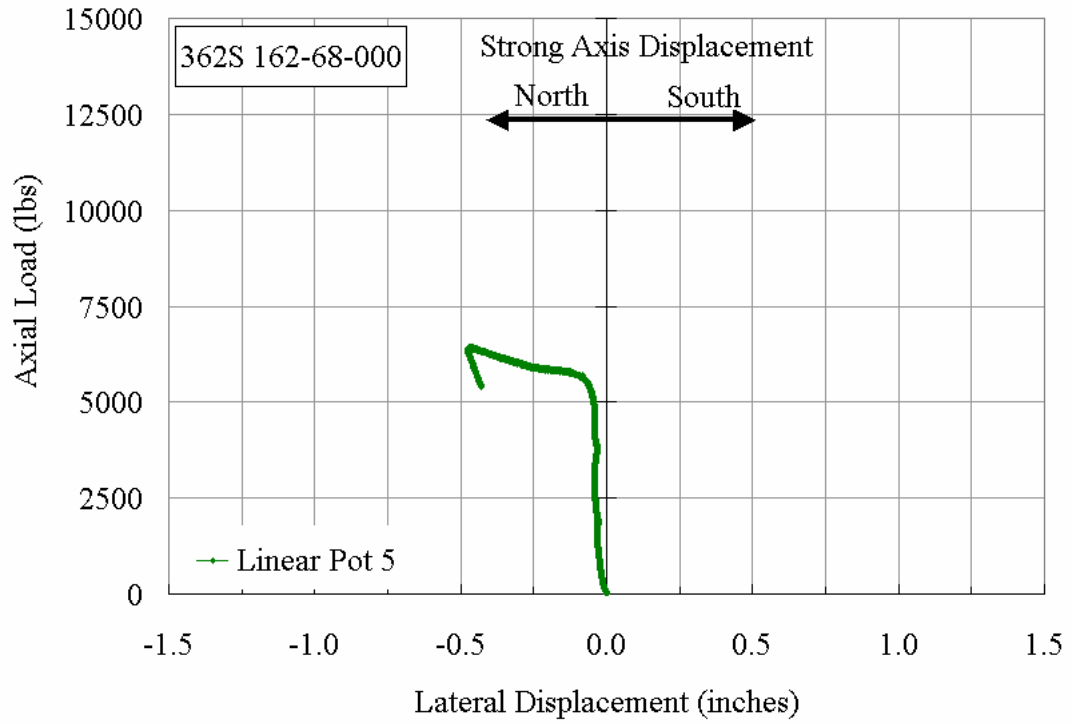


Figure A11.7 Plot of Axial Load vs. Strong Axis Displacement at Mid-Height

**362S162-68-500**

The test specimen 362S162-68-500 was braced with a total stiffness of 1023 lbs/in., which was about 2.4 times the ideal bracing requirement. To ensure static response of the stud to the applied load, it was loaded at the rate of 10 to 20 lbs/sec. Figure A12.1 shows the overall view of the stud in the Riehle Testing Machine, prior to testing. The mid-height lateral displacement of the weak axis was measured with linear potentiometers LP-1 & LP-3 and LP-2 & LP-4, attached to the north and south flanges, respectively, and that of the strong axis by LP-5 attached to the south flange. The weak axis movement was in the East-West direction and that of the strong axis was in North-South direction.

Figure A12.5 shows the plot of axial load versus axial shortening of the stud along with the initial elastic stiffness line. From an axial load of zero to 1500 lbs, the stud was buckling about the strong axis, causing an initial elongation of the north flange. At 1500 lbs, the lateral displacement of the strong axis was 0.08 inches to the north (see Figure A12.8). From the beginning of the test it was observed that there was differential movement of the two flanges, as shown in Figure A12.7. Up to an axial load of 3800 lbs, the brace forces in BF-3 & BF-4 increased at the same rate and at that load level both measured about 20 lbs (see Figure A12.6).

From 3800 lbs to 7500 lbs, the brace force in BF-3 increased at a higher rate than that of BF-4. The brace force in BF-4 increased at an almost constant rate up to 6900 lbs, and gradually attained a constant value of 37 lbs at an axial load of 7500 lbs. At this load level, the north and south flanges had moved east by 0.08 and 0.17 inches, respectively, and the strong axis had moved north by 0.11 inches. The brace forces in BF-3 and BF-4 measured 58 lbs and 37 lbs, respectively. During this loading phase, the stud was

flexural buckling in first mode about the weak axis, as well as torsional buckling in first mode. When the axial load reached 10000 lbs, there was distortion in the web of the cross section close to a web-punchout, as shown in Figure A12.2.

From an axial load of 7500 lbs to 13250 lbs, the brace force in BF-4 dropped to zero while the brace force in BF-3 continued to increase measuring 147 lbs at 13250 lbs of axial load. At this load level, BF-4 was no longer effective, but BF-2 was actively bracing the stud. This demonstrates that at any point in the testing two brace-wires are effective in bracing the stud.

On reaching the maximum load of 13384.0 lbs, the stud had axially shortened by 0.10 inches, the north flange had moved east by 0.414 inches and the south flange had moved west by 0.056 inches. The brace forces in BF-2 and BF-3 measured 5.2 lbs and 159.8 lbs, respectively. The strong axis had moved north by 0.13 inches. Figure A12.3 shows a close-up view of the local buckle that occurred in the bottom-half of the stud. Figure A12.4 shows the final buckled shape of the stud in first mode flexural buckling about the weak axis along with first-mode torsional buckling.



Figure A12.1 Overall View of Stud 362S162-68-500 in the Riehle Machine (Looking East)

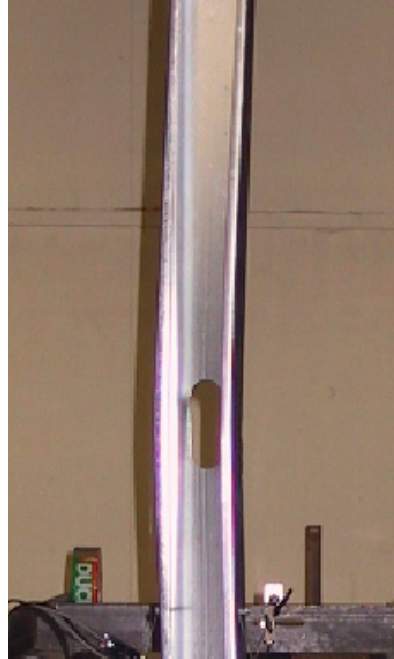


Figure A12.2 Distortional Buckling of the Stud 362S162-68-500 at an Axial Load of 10000 lbs (Looking East)

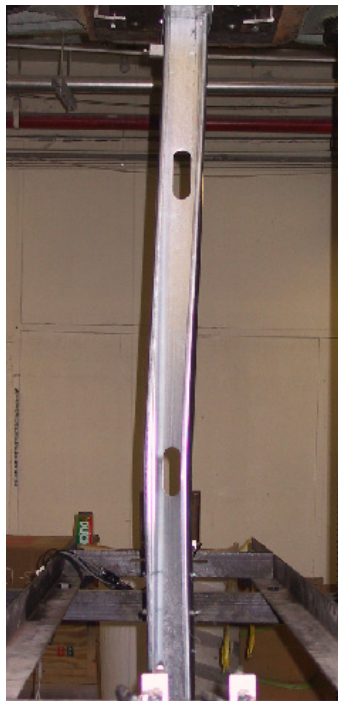


(a) Looking North



(b) Looking East

Figure A12.3 Close-up View of a Local Buckle of the Stud 362S162-68-500 at failure



(a) Top-Half



(b) Bottom-Half (Looking East)

Figure A12.4 Final View of the Buckled Shape in the Stud 362S162-68-500

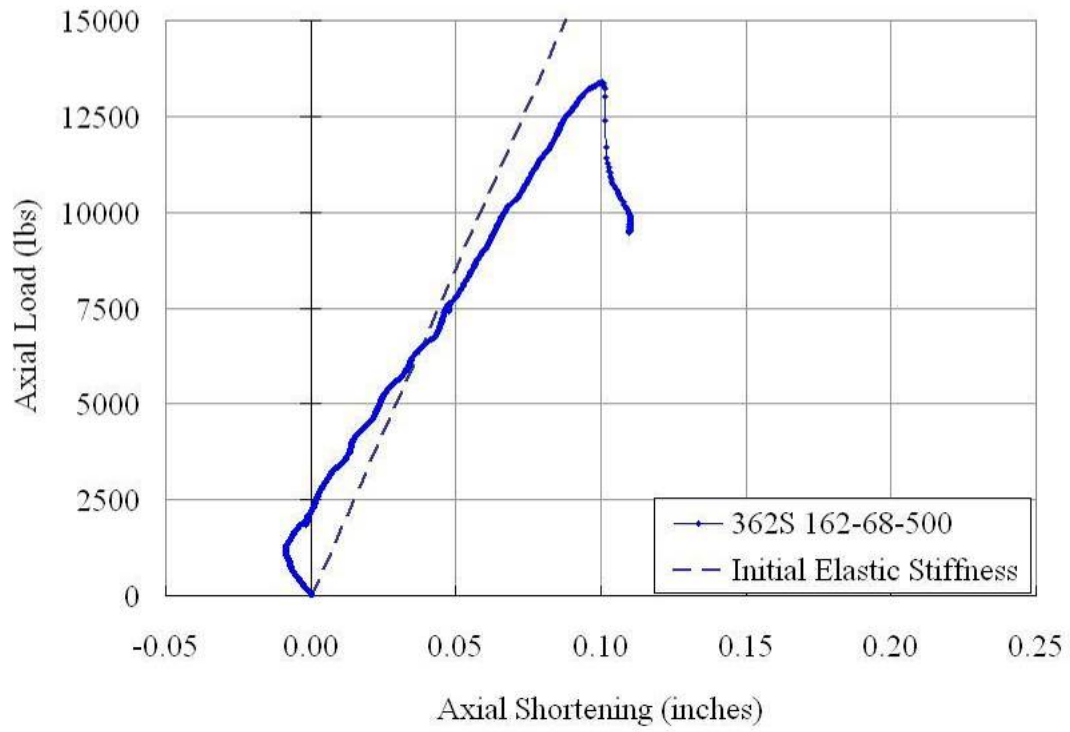


Figure A12.5 Plot of Axial Load vs. Axial Shortening

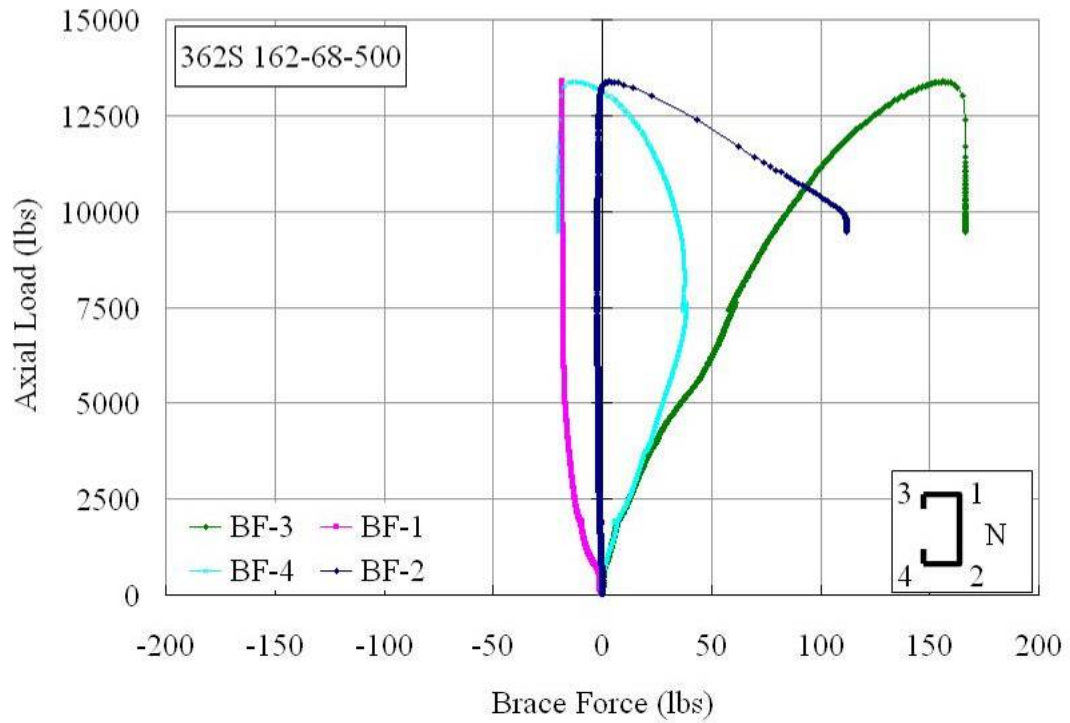


Figure A12.6 Plot of Axial Load vs. Brace Forces

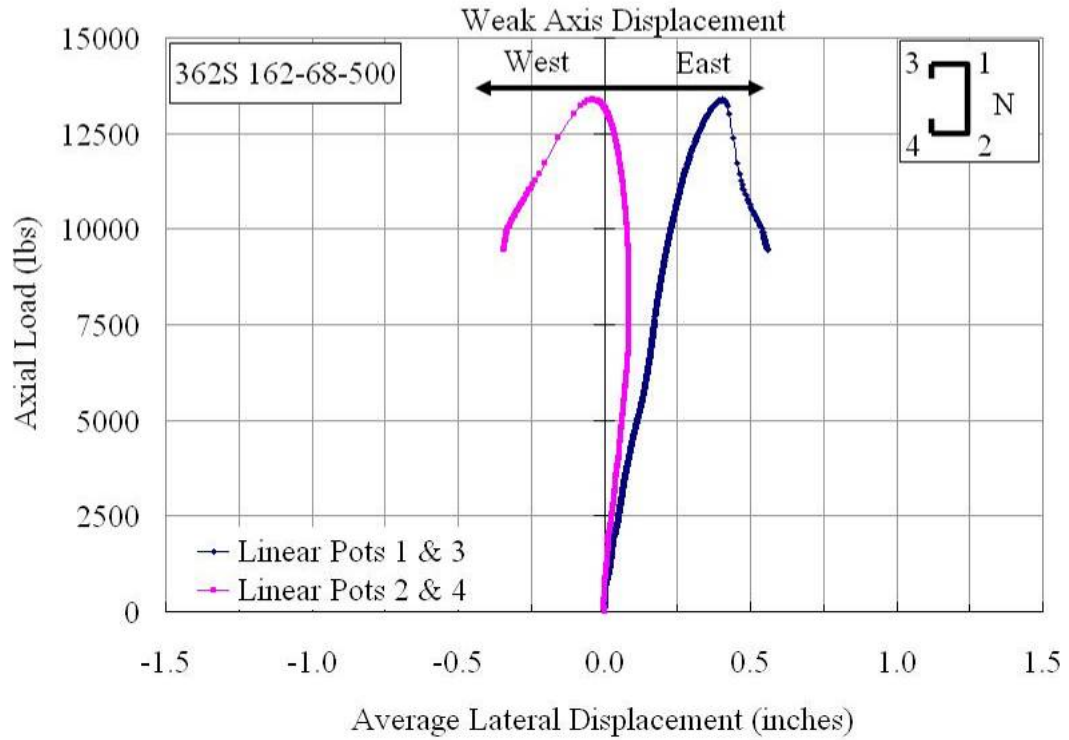


Figure A12.7 Plot of Axial Load vs. Weak Axis Displacement at Mid-Height

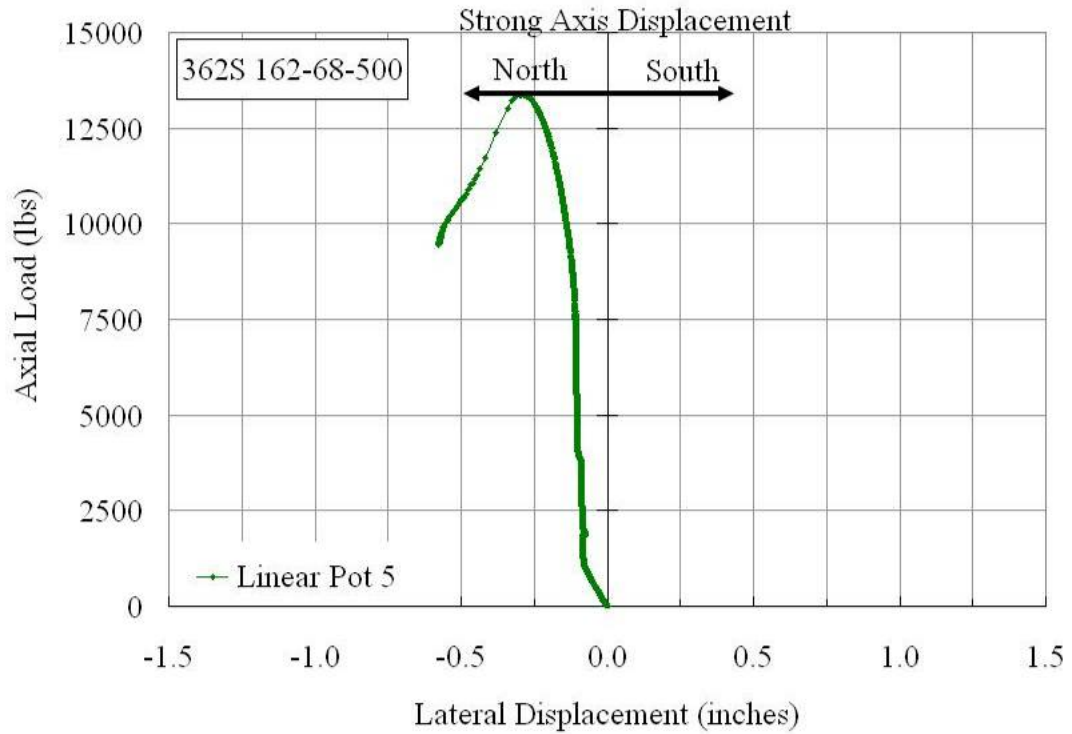


Figure A12.8 Plot of Axial Load vs. Strong Axis Displacement at Mid-Height

**362S162-68-750**

The cee stud specimen 362S162-68-750 was braced with a total brace stiffness of 1538 lbs/in., which was about 3.5 times the ideal bracing requirement. To ensure static response of the stud to the applied load, it was loaded at the rate of 10 to 25 lbs/sec. The overall view of the stud in the Riehle Testing Machine is shown in Figure A13.1. The weak axis lateral displacement was measured at mid-height by linear potentiometers LP-1 & LP-3 and LP-2 & LP-4, attached to the north and south flanges, respectively, and the strong axis displacement was measured with LP-5, attached to the south flange.

The plot of axial load versus axial shortening of the stud is mostly parallel to the initial elastic stiffness line and is shown in Figure A13.5. From zero to an axial load of 1700 lbs, the stud was buckling in first-mode flexure. At this load level, the strong axis had moved north by 0.012 inches, and the north and south flanges had moved east by 0.009 and 0.021 inches, respectively. During this loading phase, the brace forces in both BF-3 and BF-4 increased at the same rate and at 1700 lbs, both measured 11.0 lbs. With further increase in load, the brace forces in BF-3 and BF-4 increased at almost the same rate up to 5300 lbs, and at that load level the measured brace forces were 33.5 lbs each. At this load level, the strong axis had moved north by 0.09 inches and the weak axis had moved east, with the north and south flanges having moved by 0.03 inches and 0.07 inches, respectively.

From an axial load of 5300 lbs to 7500 lbs, the brace force in BF-4 increased at approximately the same rate, whereas BF-3 increased at a higher rate than earlier. At an axial load of 7500 lbs, BF-3 and BF-4 measured 64.0 lbs and 42.5 lbs, respectively. The weak axis had moved east with the north flange at 0.064 inches and the south flange at 0.094 inches, from its initial position. From 7500 lbs to about 8500 lbs the rate of

increase in brace force in BF-4 started to decrease and became constant measuring 43.6 lbs, whereas that in BF-3 measured 69.0 lbs and was increasing at an axial load of 8500 lbs.

When the load reached 11200 lbs, the axial shortening of the stud was 0.07 inches, and the brace forces in BF-3 and BF-4 measured 40.1 lbs and 85.5 lbs, respectively. At this load level, both the flanges had moved east by the same amount of 0.089 inches, and the strong axis had moved north by 0.14 inches. At this time second mode torsional buckling of the stud was observed. At about 12000 lbs there was a local buckle had formed in the top-half of the stud and it is as shown in Figure A13.2 at an axial load of 13000 lbs.

Up to 11500 lbs the stud was buckling predominantly in flexure, but from 11500 lbs to the maximum load of 14000 lbs, the mode changed to torsional buckling. This was observed by the top-half of the stud twisting clockwise and bottom-half twisting counterclockwise. At the maximum load, the north flange had moved east by 0.13 inches, whereas the south flange had moved back to its initial position, and the strong axis had moved north by 0.22 inches. Due to the local buckling of the web, the axial stiffness of the stud decreased causing it to fall below the initial elastic stiffness line. At the maximum load, the axial shortening measured 0.096 inches, whereas the initial elastic stiffness line would have given an axial shortening of 0.0844 inches. Fig A13.3 shows a close-up view of the local buckle in the top-half of the stud. Figure A13.4 shows the overall final buckled shape of the stud and the observed failure was identified as second-mode torsion.



Figure A13.1 Overall View of Stud 362S162-68-750 in the Riehle Machine (Looking East)



Figure A13.2 Buckled Shape of Stud 362S162-68-750 at an axial load of 13000 lbs (Looking East)

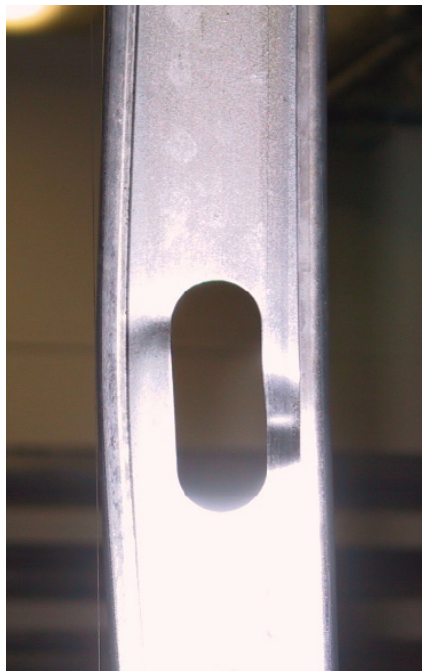


Figure A13.3 Close-up View of a Local Buckle of the Stud 362S162-68-750 at failure



(a) Looking North (b) Looking East  
Figure A13.4 Final View of the Buckled Shape of the Stud 362S162-68-750

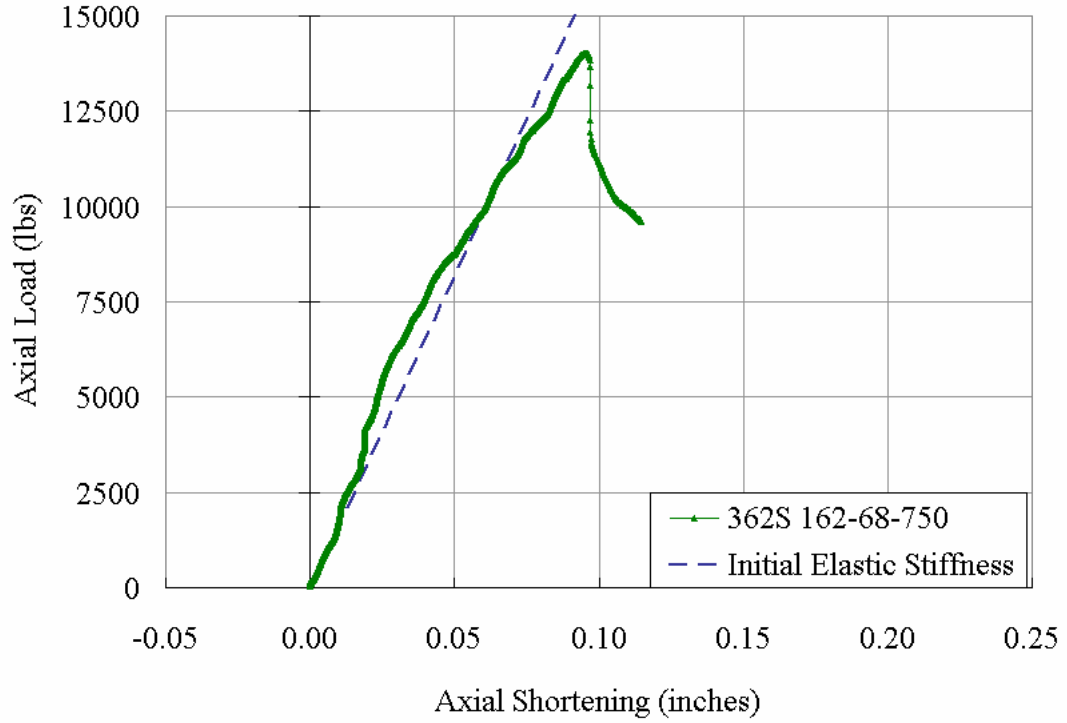


Figure A13.5 Plot of Axial Load vs. Axial Shortening

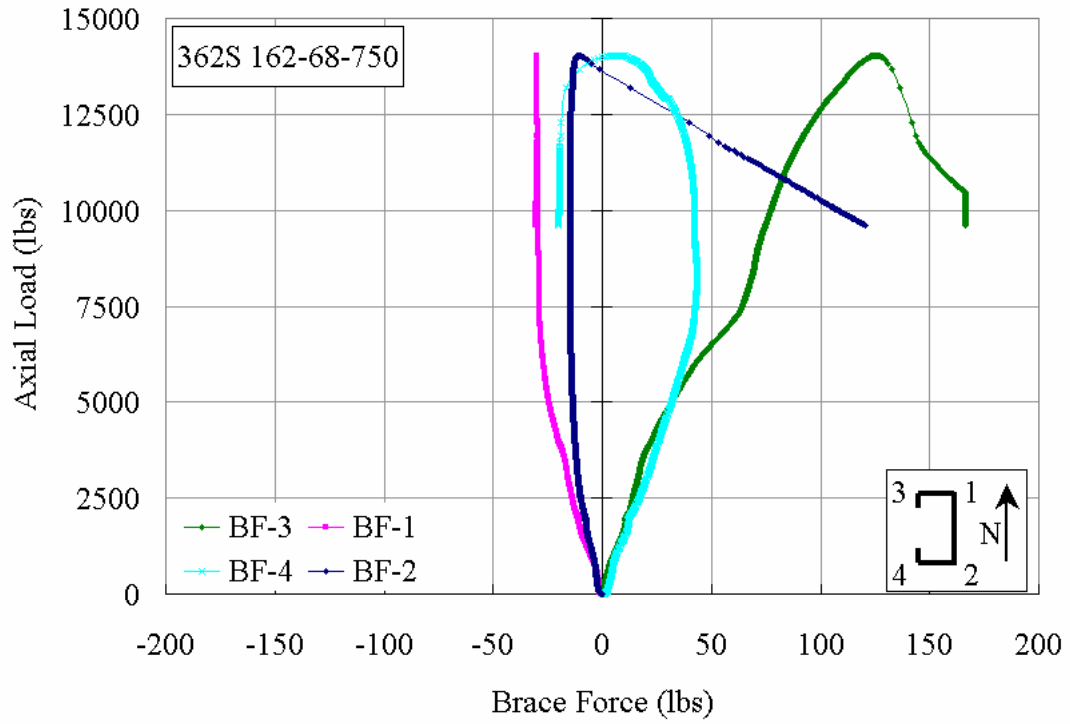


Figure A13.6 Plot of Axial Load vs. Brace Forces

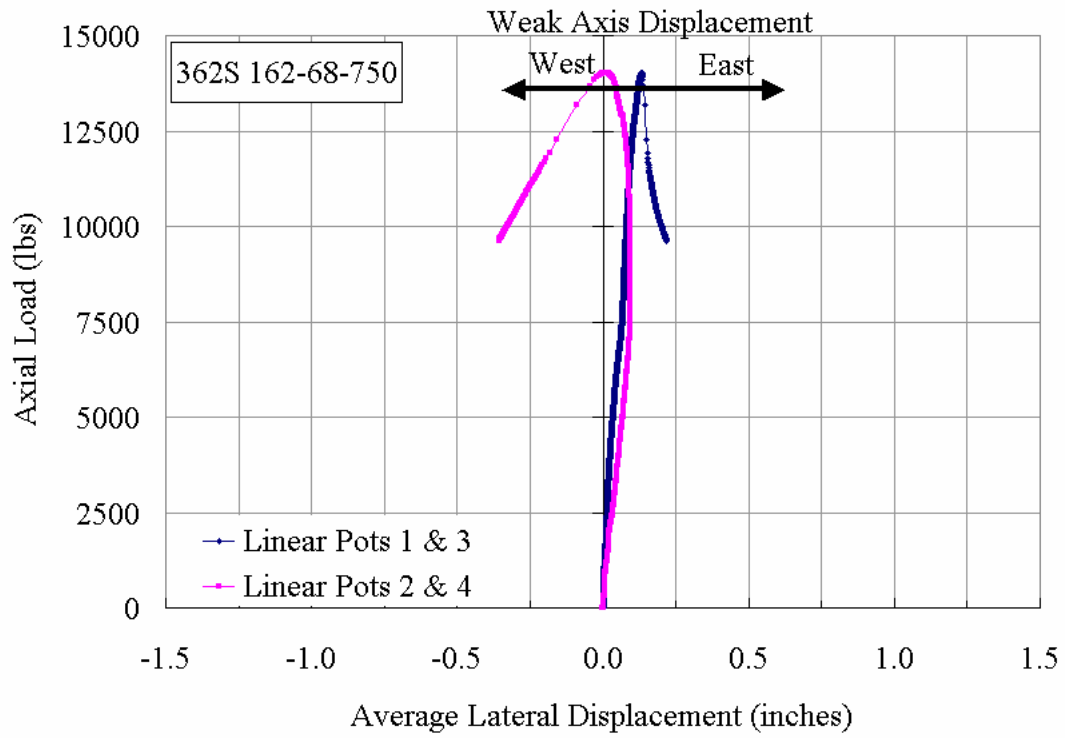


Figure A13.7 Plot of Axial Load vs. Weak Axis Displacement at Mid-Height

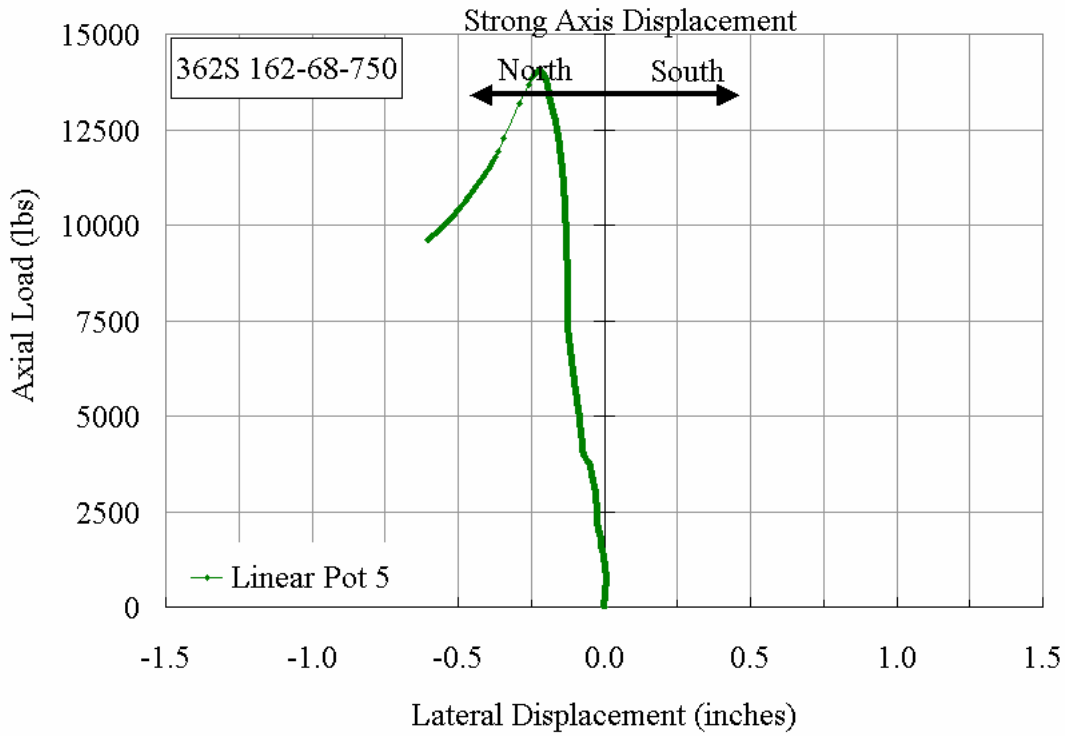


Figure A13.8 Plot of Axial Load vs. Strong Axis Displacement at Mid-Height

**362S162-68-1000**

The cee stud 362S162-68-1000 was tested with total brace stiffness of 2046 lbs/in., which was 4.7 times the ideal bracing requirement. The stud was loaded at the rate of 10 to 20 lbs/sec, to ensure a static response to the applied load. The overall view of the stud in the test frame is shown in Figure A14.1. The plot of the axial load versus the axial shortening and the initial stiffness line are shown in Figure A14.5. The mid-height weak axis lateral displacement was measured with linear potentiometers LP-1 & LP-3 and LP-2 & LP-4, attached to the north and south flanges, respectively, and the strong axis displacement was measured with LP-5.

From zero to an axial load of 950 lbs, the plot of axial shortening was steeper than the initial stiffness line and at 950 lbs it was 0.005 inches. Weak axis flexural buckling was observed, as shown in Figure A14.5. From 1000 lbs to 2500 lbs of axial load, the strong axis moved south by 0.036 inches at mid-height, and is shown in Figure A14.8. During this loading phase, the axial shortening was slightly greater than the initial elastic stiffness line and at 2500 lbs it was 0.023 inches. This was accompanied with flexural buckling about the weak axis, which had moved the stud to the east by 0.023 inches, as measured on each flange (see Figure A14.7). At this load level, the strong axis had moved south by 0.036 inches as can be observed in Figure A14.8. The brace forces in BF-3 and BF-4 had progressively increased and measured about 15 lbs each, as shown in Figure A14.6. With further increase in the axial load, the brace force in BF-4 continue to increase at the same rate, but the force in brace in BF-3 increased at a lower rate than previously observed. This is an indication that the beginning of torsional buckling of the stud has commenced.

When the axial load reached about 4000 lbs, the stud had buckled in second mode torsion with a slight first mode flexure, indicated by the weak axis movement of the two flanges in Figure A14.7. As the axial load increased, the brace forces in BF-3 and BF-4 continued to increase and at 7500 lbs they measured 45 lbs and 70 lbs, respectively. With further increase in the axial load, the force in BF-3 started to decrease, whereas the force in BF-4 continue to increase at the same rate up to the maximum load. The stud buckled gradually in second mode torsion. At an axial load of 10000 lbs, a local buckle in the web was observed near a punchout, in the bottom-half of the stud. At this load level, the second mode torsional buckling of lower-half of the stud can be seen in Figure A14.2.

On reaching the maximum load of about 14750 lbs, the axial shortening of the stud was 0.14 inches, the north and south flanges had moved east by 0.065 inches and 0.18 inches, respectively. The mid-height strong axis displacement was 0.11 inches to the south. At this maximum load, the brace forces in BF-3 & BF-4 measured 15 lbs and 128 lbs, respectively. Figure A14.3 shows a close-up view of the local buckle in the bottom-half of the stud and Figure A14.4 shows the overall final buckled shape of the stud as being predominantly second-mode torsion.



Figure A14.1 Overall View of Stud 362S162-68-1000 in the Riehle Machine (East View)



Figure A14.2 Local Buckling at a Web-perforation of the Stud 362S162-68-1000 at an Axial Load of 10000 lbs (East View)



Figure A14.3 Close-up View of the Local Buckle of the Stud 362S162-68-1000



Figure A14.4 Final View of the Buckled Shape of the Stud 362S162-68-1000 (East View)

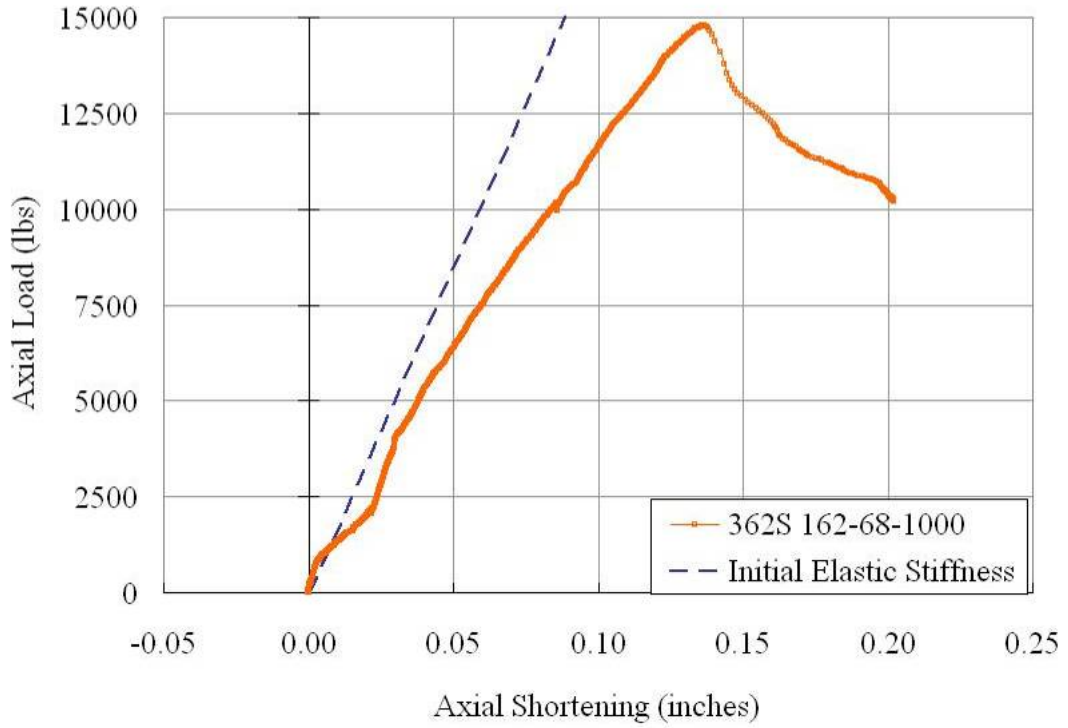


Figure A14.5 Plot of Axial Load vs. Axial Shortening

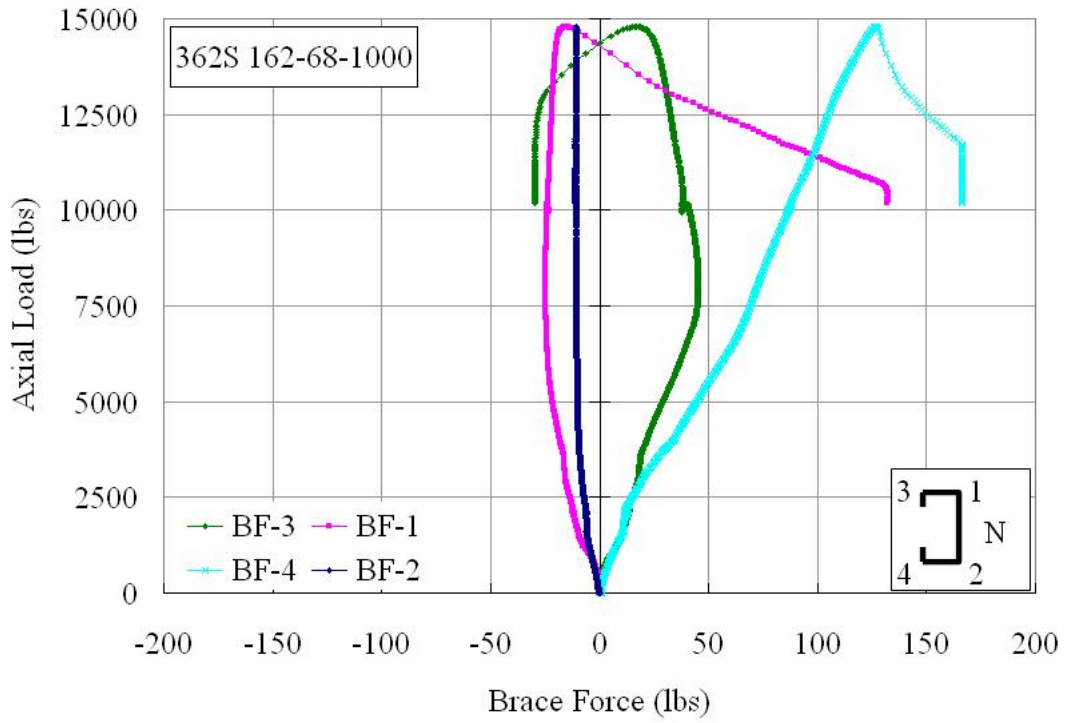


Figure A14.6 Plot of Axial Load vs. Brace Forces

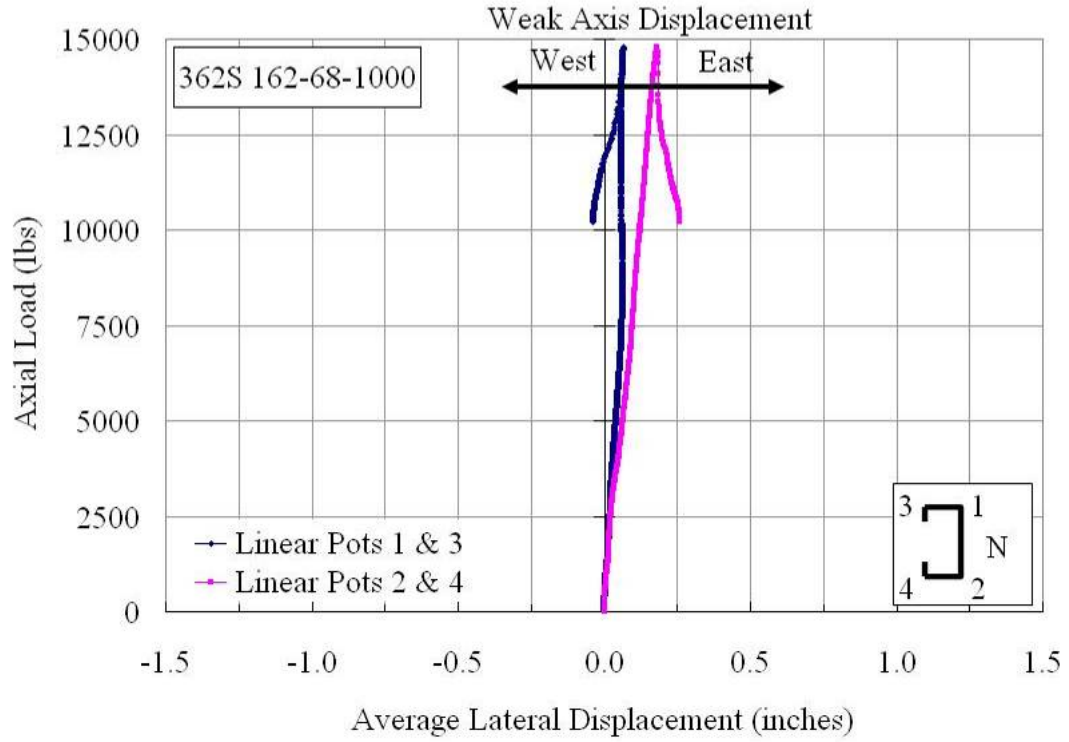


Figure 13.7 Plot of Axial Load vs. Weak Axis Displacement at Mid-Height

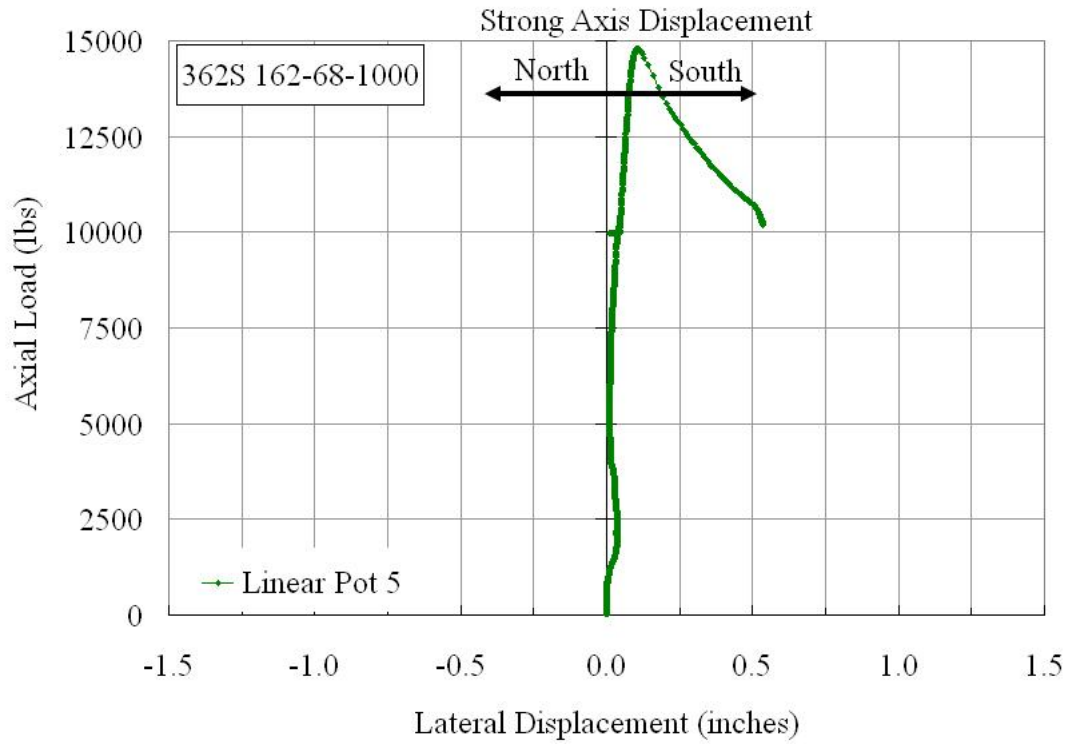


Figure A14.8 Plot of Axial Load vs. Strong Axis Displacement at Mid-Height

**600S125-33-000**

The stud 600S125-33-000 was tested without any lateral bracing. The overall view of the stud in the Riehle Testing Machine is shown in Figure A15.1. The load acting on the stud was measured as a response to an applied axial displacement. The specimen was loaded between 5 to 10 lbs/sec to ensure a static response to the applied load. The mid-height displacement was measured with linear potentiometers LP-1 & LP-3 and LP-2 & LP-4 attached to the north and south flanges, respectively. The strong axis displacement was measured with LP-5, attached to the south flange.

The plot of axial load versus axial shortening of the stud is shown in Figure A15.5. From zero to 800 lbs, the response of the stud was linear, and beyond this load it became non-linear. At 800 lbs, the weak axis displacement, as shown in Figure A15.6, indicates that the north and south flanges recorded differential movement towards the east, measuring 0.33 inches and 0.13 inches, respectively. The overall buckling of the stud seemed to be in first mode flexural-torsion. Though both distortional waves were visible in the flanges, elastic buckling waves in the web were observed as shown in Figure A15.2.

On further increasing the load, the stud continued buckling in first mode flexural-torsion as the north flange continued to move east at a rate more than that of the south flange. The non-linear axial shortening was due to a loss of cross-sectional stiffness because of the distortional buckling occurring in the flanges. At an axial load of approximately 984.4 lbs, the stud reached its maximum load carrying capacity. At this load level, the north and south flanges recorded lateral displacements of by 0.70 inches and 0.27 inches to the east, respectively and the axial shortening was 0.044 inches. With continued axial displacement there were no further increases in the displacement

response of the stud. The stud was considered to have reached failure when there was considerable distortion of the mid-height cross-section of the stud, as shown in Figure A15.3.

The stud was unloaded and except for some residual twist, the stud did not exhibit any other physical damage. The stud was reloaded at the same rate as shown in Figure A15.4, the stud reached a maximum load of 820 lbs, before the load started to decrease. The figure also shows the induced local buckles caused as a result of severity of distortional buckling waves in the flanges of the stud.



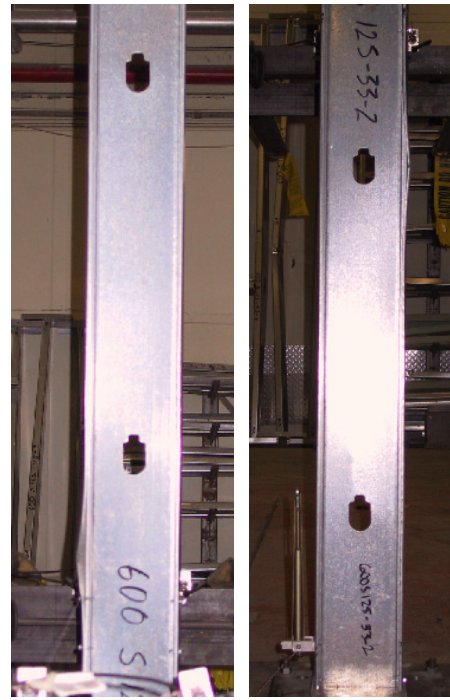
Figure A15.1 Overall View of Stud 600S125-33-000 in Riehle Machine Prior to Testing



Figure A15.2 Elastic buckling waves in the web of Stud 600S125-33-000 at an Axial



Figure A15.3 Cross-Section Distortion of the Stud 600S125-33-000 at an Axial Load of 980 lbs



(a) Top-half (b) Bottom-half  
Figure A15.4 Local Buckle & Distortion of the Stud 600S125-33-000 on Reloading to 800 lbs of Axial Load

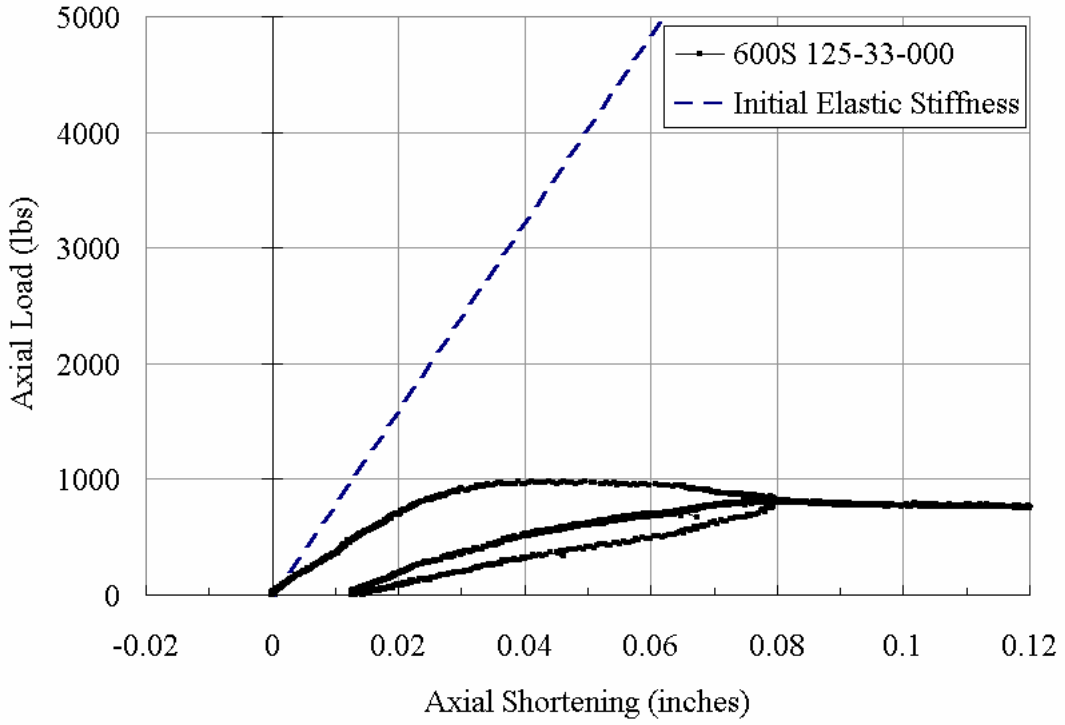


Figure A15.5 Plot of Axial Load vs. Axial Shortening

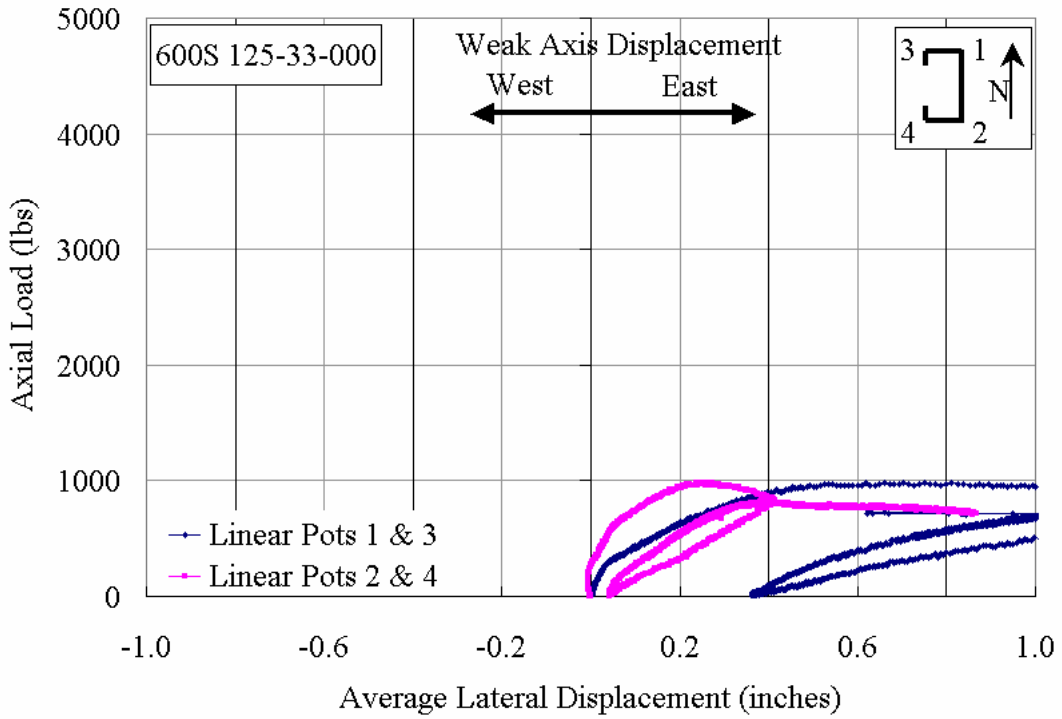


Figure A15.6 Plot of Axial Load vs. Weak Axis Displacement at Mid-Height

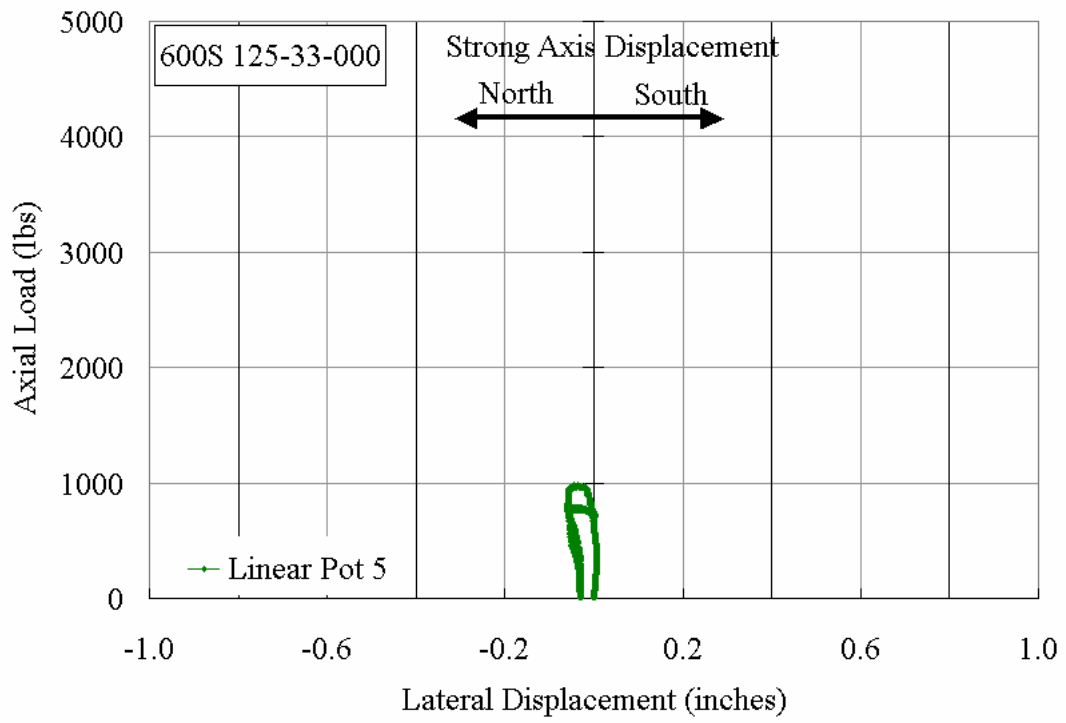


Figure A15.7 Plot of Axial Load vs. Strong Axis Displacement at Mid-Height

**600S125-33-030**

The stud 600S125-33-030 was braced at mid-height with a total brace stiffness of 61 lbs/inch, which was about 0.8 times the required ideal bracing. The overall view of the stud in the Riehle Machine is shown in Figure A16.1. It was loaded between 5 to 10 lbs/sec to ensure static response of the stud to the applied load. Figure A16.5 shows the plot of axial load versus axial shortening.

Initially, the stud exhibited predominantly first-mode flexural-torsional buckling, with some twisting being measured at the mid-height cross-section, as shown in Figure A16.7. The brace forces being measured in the four brace wires attached to the stud are given in Figure A16.6.

When the axial load on the stud reached 500 lbs, elastic buckling waves with a wavelength equal to the width of the stud, were seen running longitudinally in the web. On further loading, the amplitude of these elastic buckling waves increased. At an axial load of 1000 lbs, distortional buckling was observed in the flanges as the strong axis began to move north at this load level. Up to an axial load of about 1600 lbs, there were no significant changes in the stud, except the growth of the distortional buckling of the flanges, as shown in Figure A16.2. From 1600 lbs to 1900 lbs of axial load, the amplitude of the distortional wave above the braces was severe enough to cause a local buckle as shown in Figure A16.3. At approximately 1900 lbs, the strong axis had moved north by 0.15 inches, the north and south flanges had moved east by 0.64 inches and 0.24 inches, respectively, and the brace forces in BF-3 and BF-4 measured 19.4 lbs and 6.4 lbs, respectively.

The flanges of the stud were rendered ineffective in carrying the applied compressive load, after reaching a final maximum value of 2270 lbs the load on the stud

started to decrease. The final failure was considered to be first mode flexural buckling. With a brace stiffness less than the ideal requirement, this is the expected mode of buckling.



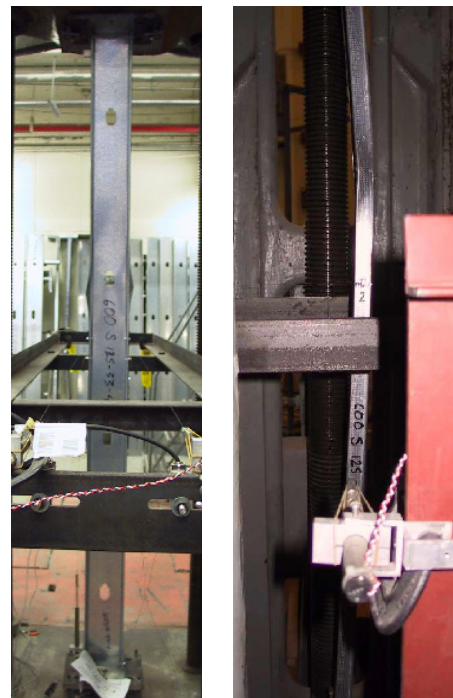
Figure A16.1 Overall View of Stud 600S125-33-030 in Riehle Machine Prior to Testing



Figure A16.2 Elastic Distortional waves in Stud 600S125-33-030 at an Axial Load of 1600 lbs



(a) at 1600 lbs (b) at 1900 lbs  
Figure A16.3 Distortional Wave in the Flanges of the Stud 600S125-33-030



(a) Looking East (b) Looking North  
Figure A16.4 Final View of the Top end of the Stud 600S125-33-060

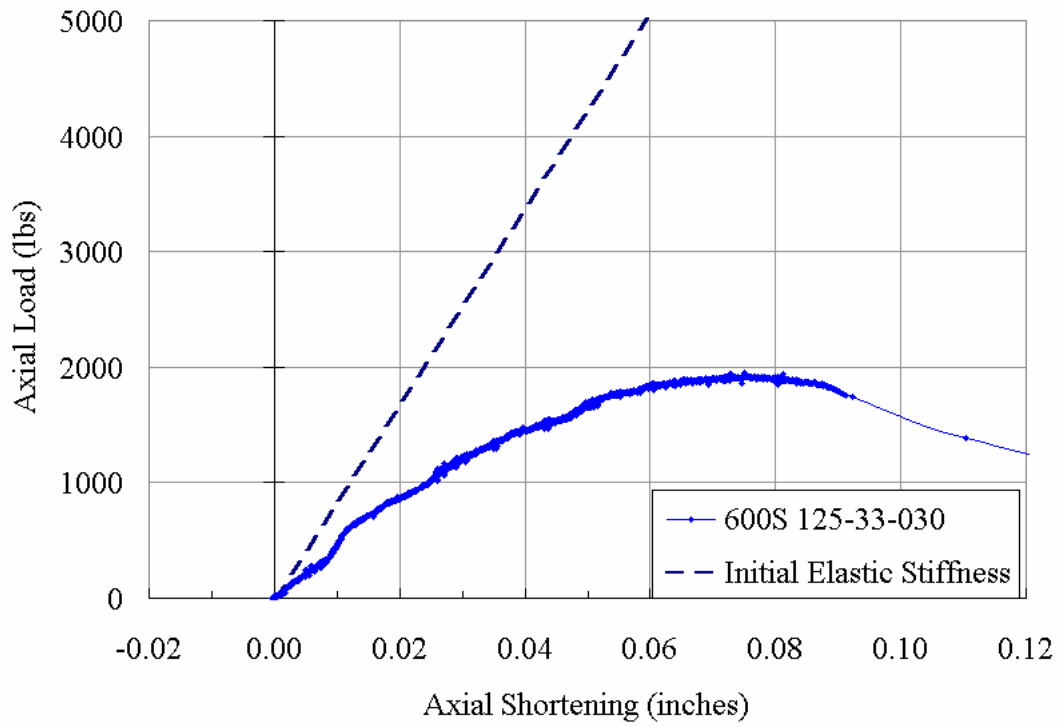


Figure A16.5 Plot of Axial Load vs. Axial Shortening

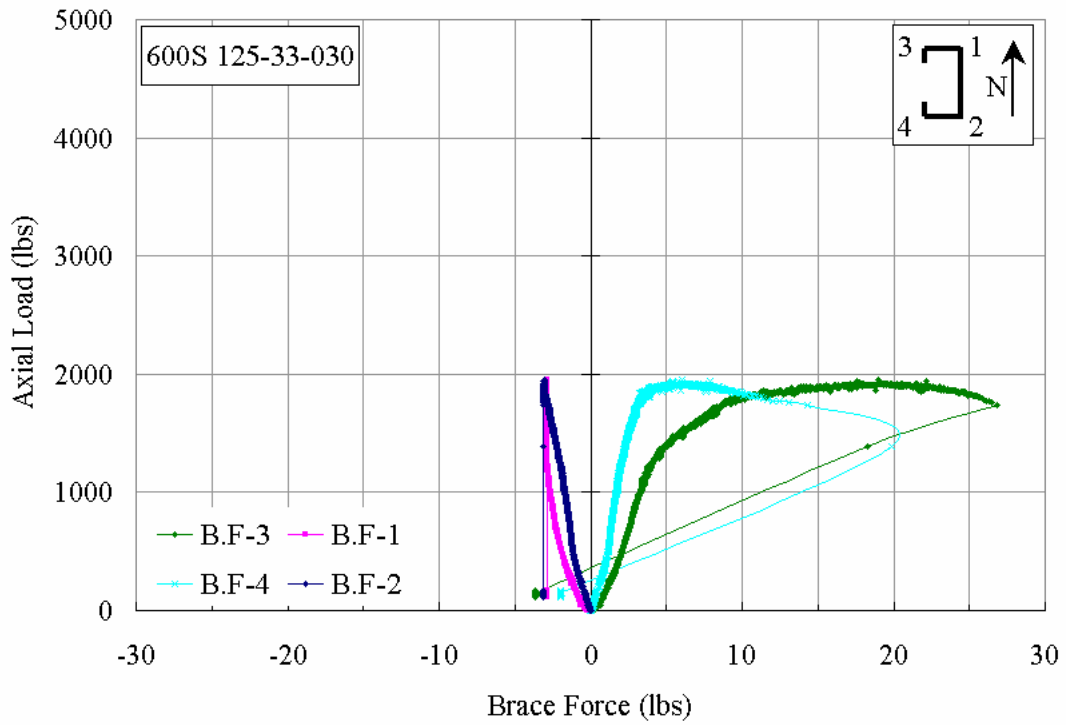


Figure A16.6 Plot of Axial Load vs. Brace Forces

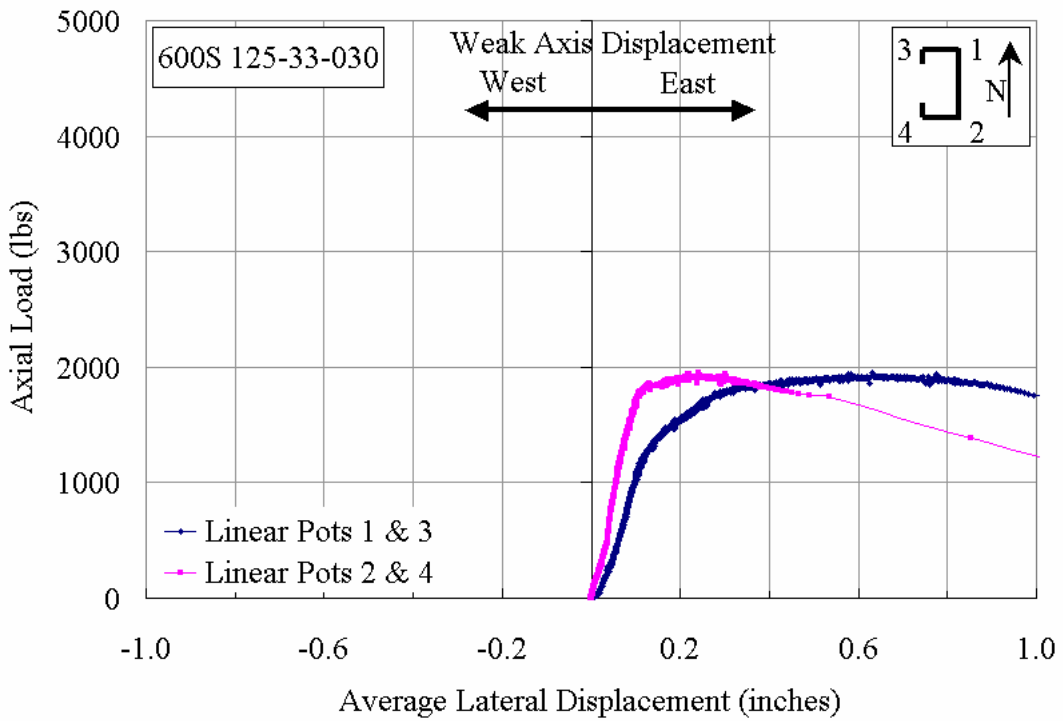


Figure A16.7 Plot of Axial Load vs. Weak Axis Movement at Mid-Height

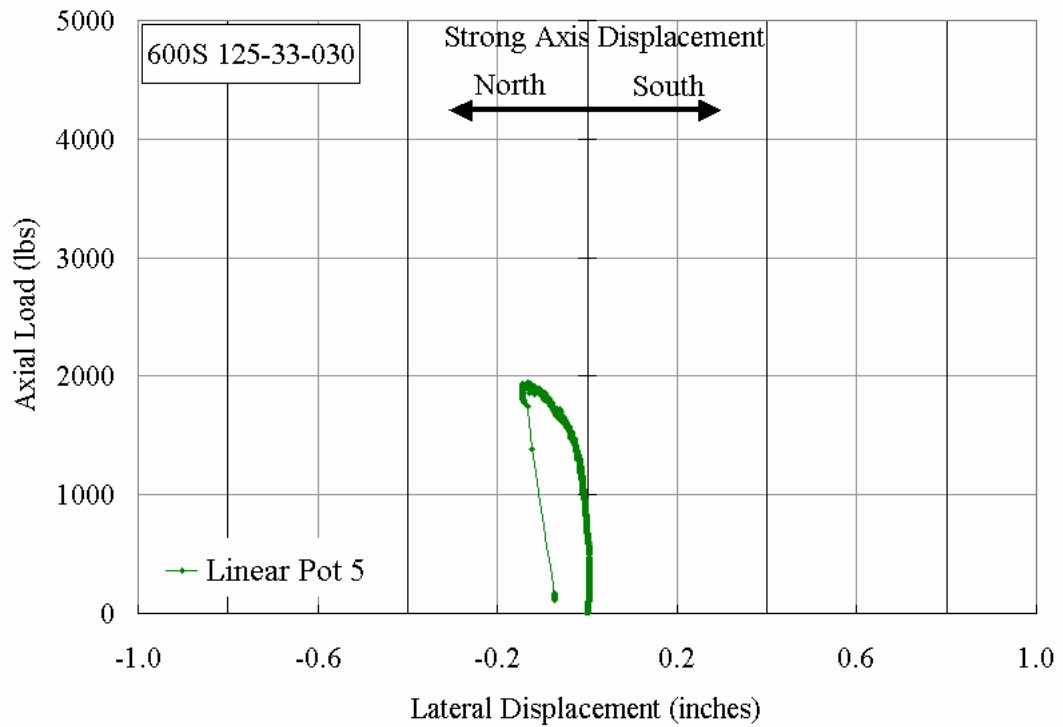


Figure A16.8 Plot of Axial Load vs. Strong Axis movement at Mid-Height

**600S125-33-060**

The cee stud specimen 600S125-33-060 was braced with a total brace stiffness of 123 lbs/inch, which was 1.6 times the required ideal bracing. The overall view of the stud in the Riehle Testing Machine is shown in Figure A17.1. It was loaded between 10 to 20 lbs/sec to ensure static response to the applied load. Figure A17.5 shows the plot of axial load versus axial shortening of the stud.

From an axial load of zero to 500 lbs, first mode weak axis flexural buckling governed the response of the stud. At an axial load of 500 lbs, the strong axis had moved south by 0.022 inches and the weak axis had moved west by 0.01 inches. Elastic buckling waves were observed in the web and distortional waves were observed in the flanges. The brace forces in BF-3 and BF-4 seemed to increase initially but only measured 0.24 lbs and 0.71 lbs, respectively at this load level.

When the load was approximately 1250 lbs, the upper-half of the stud near the top-end showed excessive distortion as shown in Figure A17.2. At this load, the north and south flanges had moved west by 0.05 inches and 0.005 inches, respectively, and the strong axis had moved south by 0.025 inches. The forces in BF-1 and BF-4 measured 2.4 lbs and 0.3 lbs, respectively. This indicates that the mid-height section was experiencing a slight torsional buckling along with some overall flexural buckling. With further increase in the applied load, the amplitude of the elastic buckling waves continued to increase and at an axial load of 1700 lbs, distortional buckling became predominantly visible.

When the load was about 1700 lbs, there was a snapping sound that caused sudden disturbance as can be seen in all the plots shown in Figures A17.5 through A17.8. On visual inspection it was concluded that the snapping sound was due to an elastic buckling

wave changing the direction and amplitude at a particular location close to the brace-wires. At this load, the strong axis displacement abruptly changed direction from southward and started to move north.

With further loading, the amplitude of the distortional waves in the flanges and the elastic buckling waves in the web still continued to increase and Figure A17.3 shows the overall appearance of the stud at an axial load of 2100 lbs. The brace force that had developed in BF-1 was preventing the movement of the north flange. The distortional wave, having its maximum amplitude at the top-end of the stud was causing the track to lose its stiffness and deform with increasing load.

At an axial load of about 2250 lbs, the distortional wave led to the formation of a local buckle, just below the top-track, which ultimately caused the failure of the stud. At this load the brace force in BF-1 measured about 11 lbs, and the north and south flanges had moved by 0.21 inches and 0.04 inches to the west, respectively. From these observations it was concluded that the stud failed by distortional buckling.



Figure A17.1 Overall View of Stud 600S125-33-060 in Riehle Machine Prior to Testing



Figure A17.2 Distortion of Top end of Stud 600S125-33-060 at an Axial Load of 1250 lbs



Figure A17.3 Elastic buckling waves in the Stud 600S 125-33-060 at an Axial Load of 2100 lbs



Figure A17.4 Final View of the Top-end of the Stud 600S125-33-060

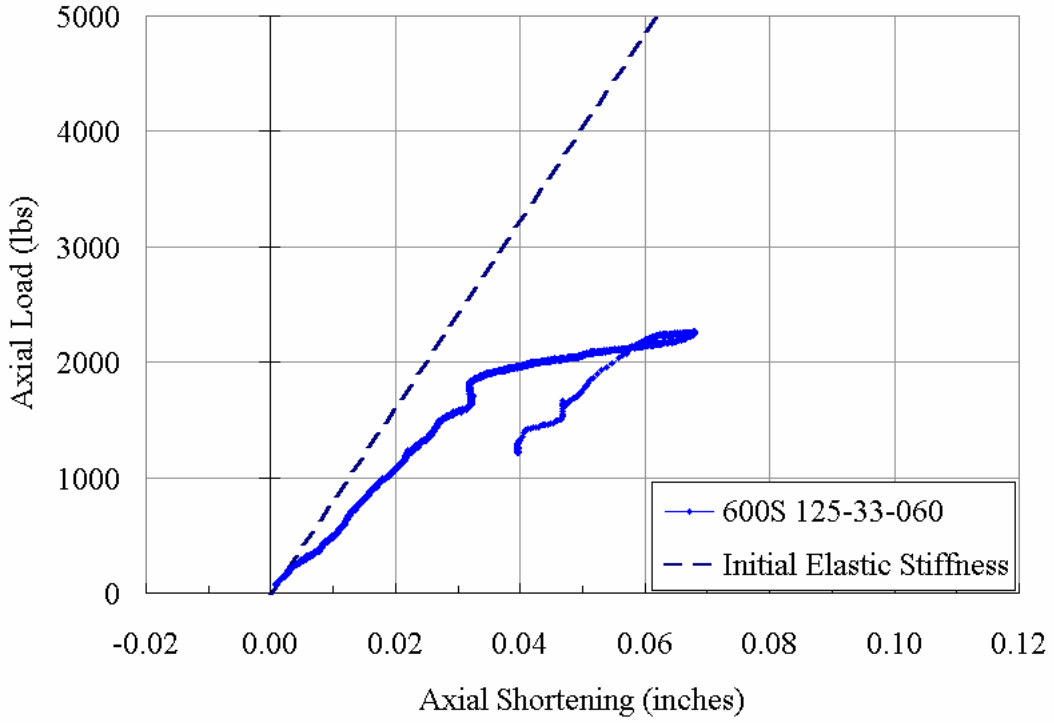


Figure A17.5 Plot of Axial Load vs. Axial Shortening

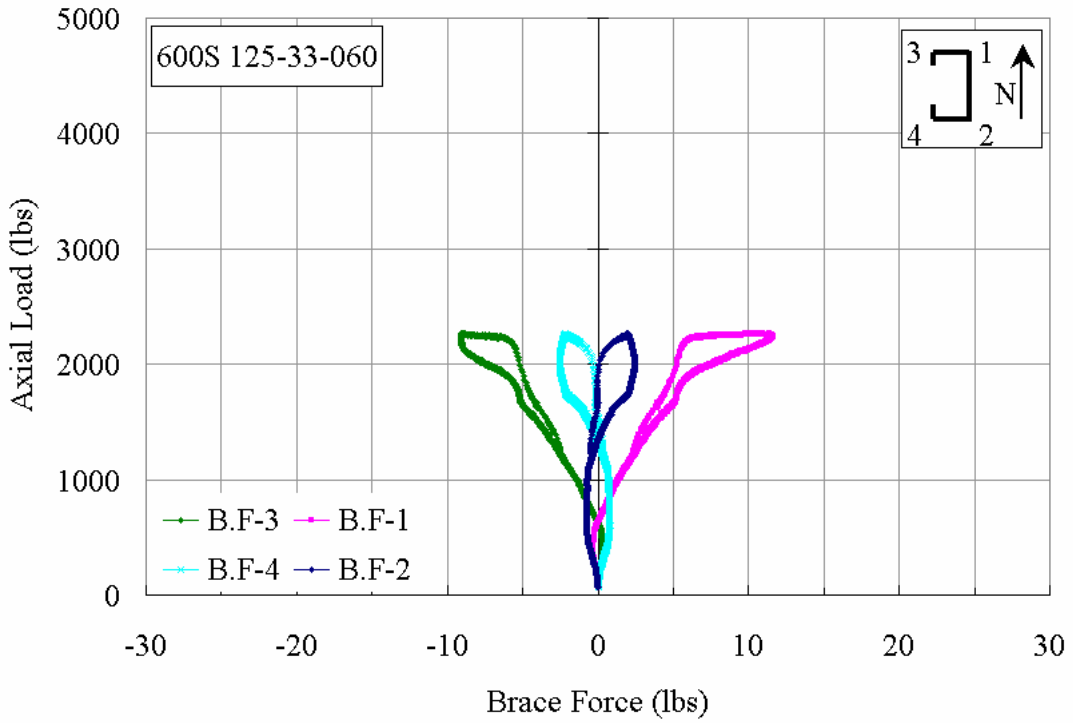


Figure A17.6 Plot of Axial Load vs. Brace Forces

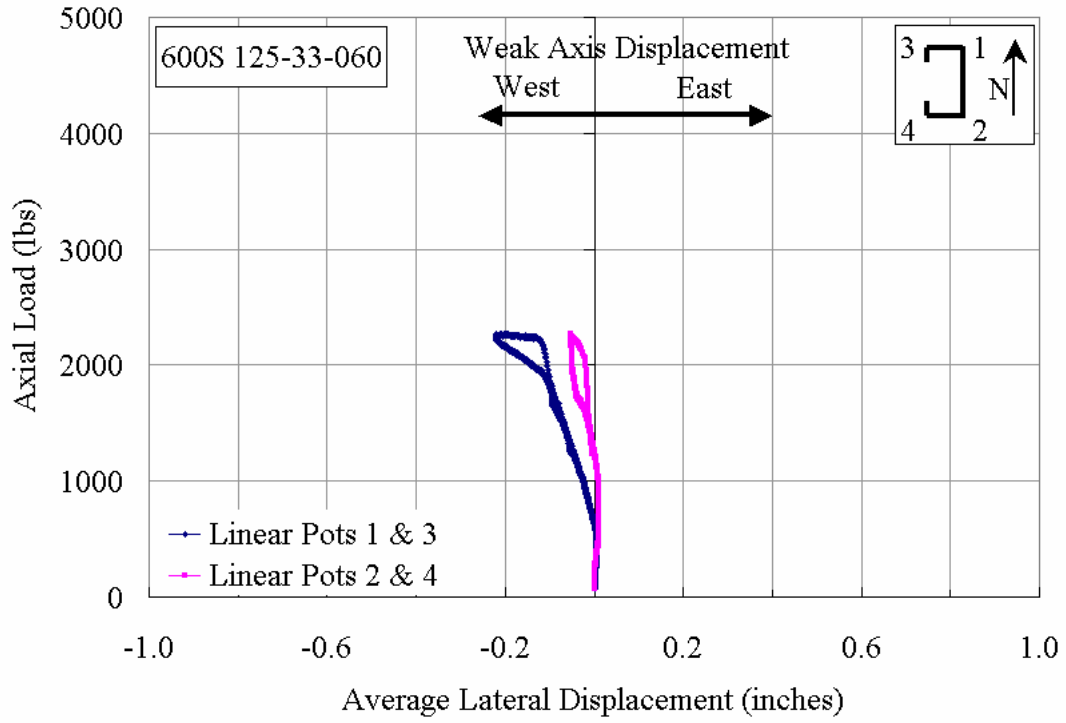


Figure A17.7 Plot of Axial Load vs. Weak Axis Movement at Mid-Height

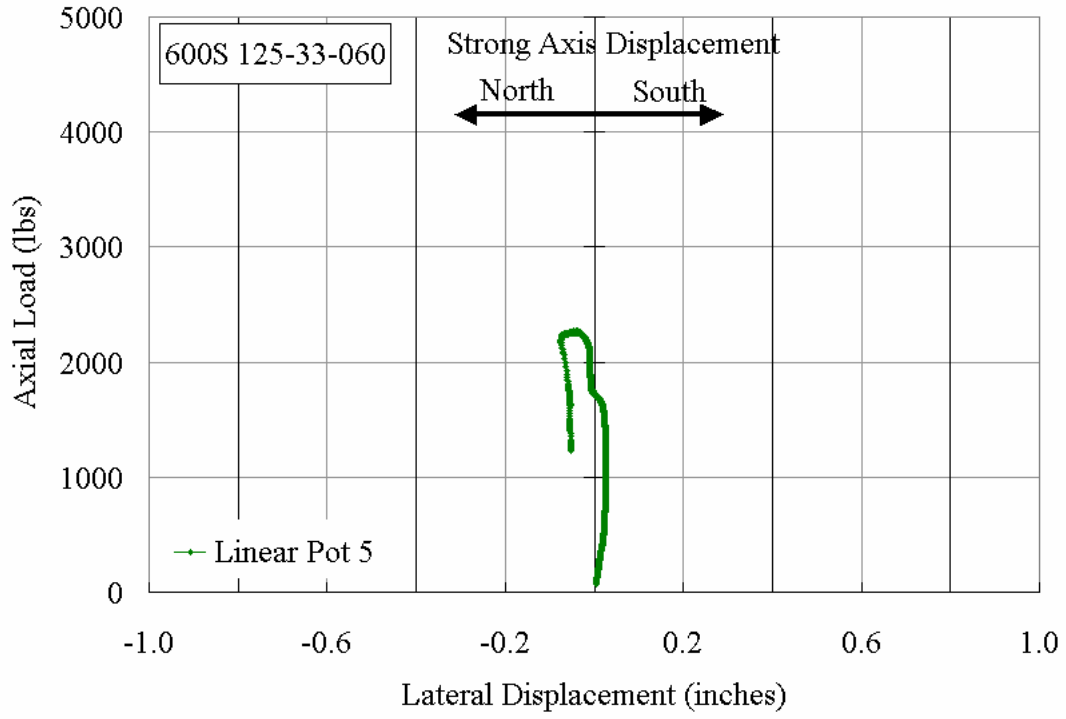


Figure A17.8 Plot of Axial Load vs. Strong Axis movement at Mid-Height

**600S125-33-200**

The test specimen 600S125-33-200 was braced with a total brace stiffness of 402 lbs/inch, which was 5.3 times the required ideal bracing. The overall view of the stud in the Riehle Testing Machine, prior to testing, is shown in Figure A18.1. It was loaded between 10 to 25 lbs/sec to ensure static response to the applied load. Figure A18.5 shows the plot of axial load versus axial shortening of the stud. The mid-height lateral displacement of the weak axis was measured with linear potentiometers LP-1 & LP-3 and LP-2 & LP-4 attached to the north and south flanges, respectively and the strong axis displacement was measured with LP-5, attached to the south flange.

From zero to an axial load of 1000 lbs, there was no lateral displacement at mid-height indicating that there was no flexural or torsional buckling of the stud occurring. At an axial load of approximately 1000 lbs, distortional buckling was observed at the top end of the stud, as shown in Figure A18.2. It can be seen in the figure that the north flange has deformed. Also at this load level, there was still no lateral displacement of the weak axis, whereas the strong axis had moved south by 0.025 inches (see Figures A18.7 and A18.8). The measured brace forces in BF-3 and BF-4 were 0.6 lbs and 2.2 lbs, respectively, as shown in Figure A18.6. With further increase in the axial load, distortional buckling waves were seen all along the length of the stud.

At an axial load of 1250 lbs, local elastic buckling waves were seen in the web and are clearly visible in Figure A18.3. As the axial load was increased, the elastic buckling waves became more predominant and the distortional waves became more severe. When the applied axial load reached 1700 lbs a snapping sound was heard, which can be seen as a disturbance in Figures A18.5 through A18.8. On visual inspection it was concluded

that the snapping sound was due to an elastic buckling wave changing direction and amplitude.

At a load of approximately 2125 lbs, the top of the stud failed as shown in Figure A18.4. The weak axis movement was about 0.02 inches towards west. The brace forces in all the brace-wires almost dropped to zero. The failure of the stud was neither due to flexural buckling nor torsional buckling, but because of the distortional buckling of the cross-sectional elements especially the flanges.



Figure A18.1 Overall View of Stud 600S125-33-200 in Riehle Machine Prior to Testing (Looking East)



Figure A18.2 Distortional Buckling of Stud 600S125-33-200 at an Axial Load of 1000 lbs (Looking East)



Figure A18.3 Elastic buckling waves in the Stud 600S125-33-200 at an Axial Load of 1250 lbs (Looking East)



Figure A18.4 Final View of the top-end of the Stud 600S125-33-200

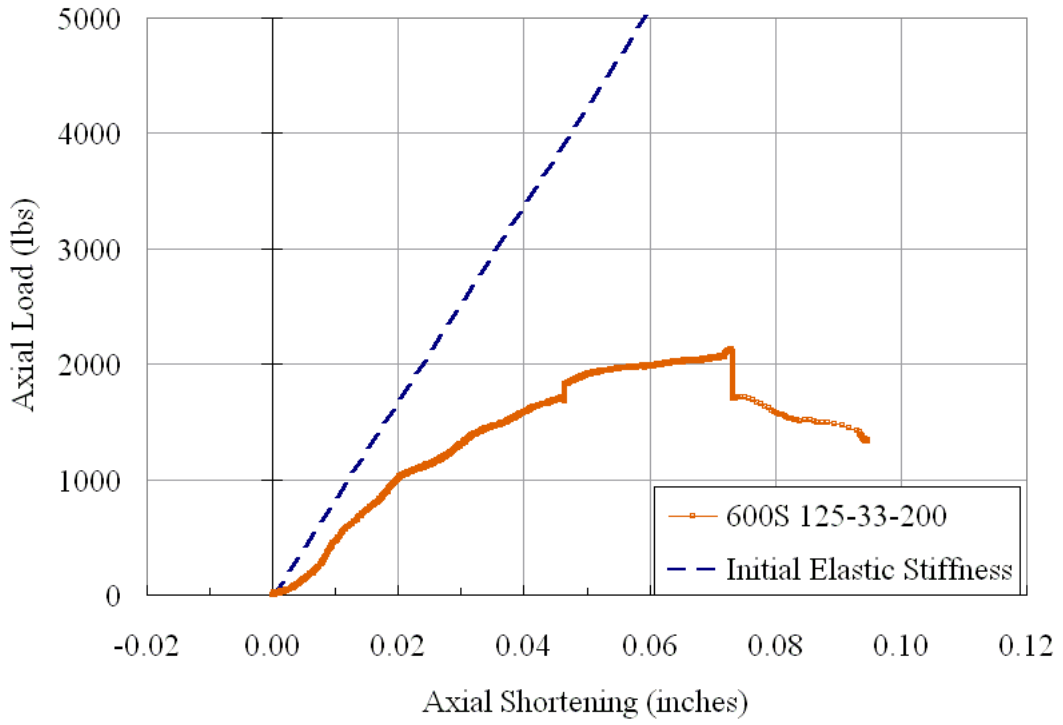


Figure A18.5 Plot of Axial Load vs. Axial Shortening

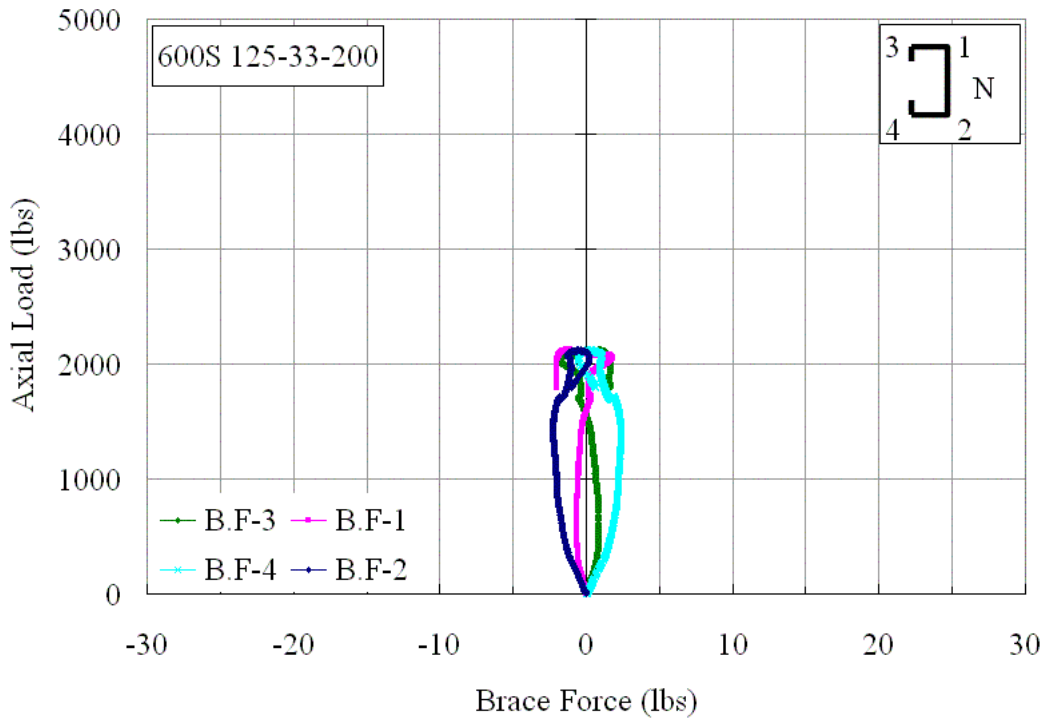


Figure A18.6 Plot of Axial Load vs. Brace Forces

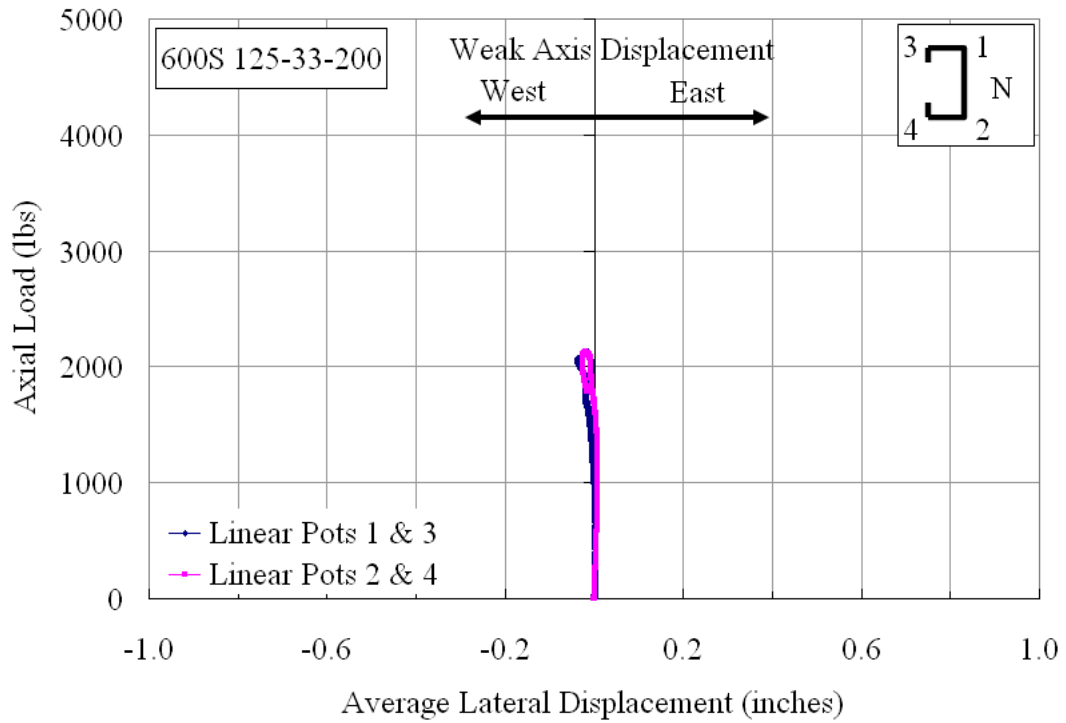


Figure A18.7 Plot of Axial Load vs. Weak Axis Displacement at Mid-Height

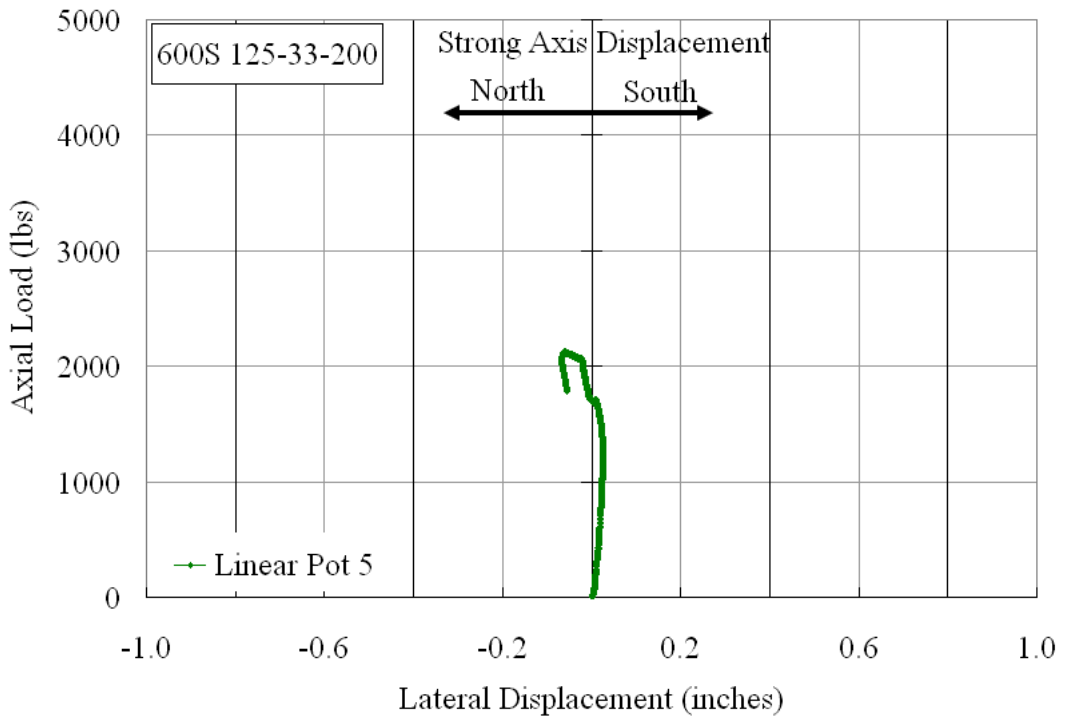


Figure A18.8 Plot of Axial Load vs. Strong Axis Displacement at Mid-Height

**600S162-43-000(1)**

The cee stud specimen 600S162-43-000(1) was tested without any lateral bracing. Figure A19.1 shows the stud in the Riehle Machine prior to the test. The stud was loaded at the rate between 8 to 10 lbs/sec, to ensure static response to the applied load. The weak axis lateral displacement at mid-height of the stud was measured with the linear potentiometers LP-1 & 3 and 2 & 4, attached to the north and south flanges, respectively, and the strong axis displacement was measured with LP-5, attached to the south flange. The axial shortening of the stud was measured by LP-6 attached on the north flange.

The plot of axial load versus axial shortening of the stud is shown in Figure A19.5. From zero up to an axial load of about 2500 lbs, the plot of the axial load versus axial shortening curve shows a negative value. In Figure A19.7 it can be observed that the stud is exhibiting strong axis buckling all through the duration of the test. Due to the strong axis flexural buckling, the north flange was continuously expanding causing LP-6 to record the negative axial shortening. In Figure A19.6 it can be observed that the north and south flanges are moving in opposite direction, indicating twisting of the mid-height cross-section due to torsional buckling of the stud. At an axial load of 2500 lbs, the measured displacement were 0.045 inches to the west on the south flange, 0.18 inches to the east on the north flange, while the strong axis displacement was 0.12 inches to the north. At approximately this load level, elastic buckling waves were observed in the web for the first time as shown in Figure A19.2.

Beyond this axial load, the stud exhibited first mode weak axis flexural buckling, which is evidently seen in Figure A19.6. The slope of the curve in Figure A19.1 is almost the same as the initial elastic stiffness line. With further increase in the axial load up to the maximum load, the stud exhibited flexural-torsional buckling. At loads just

prior to the maximum load, distortional buckling waves was observed in the flanges of the top-half of the cee-stud for the first time.

On attaining the maximum load, the distortional buckling led to formation of a local buckle in the flange-lip junction as shown in Figure A19.4(a). At this same load level, the axial shortening was 0.014 inches, the weak axis movement of the north and south flanges were 0.34 and 0.24 inches to the east, respectively, while the strong axis displacement was 0.19 inches to the north. Figure A19.4(b) shows the final view of the cee-stud at failure.



Figure A19.1 Overall View of the Stud 600S162-43-000(1) in the Riehle Testing Machine prior to testing



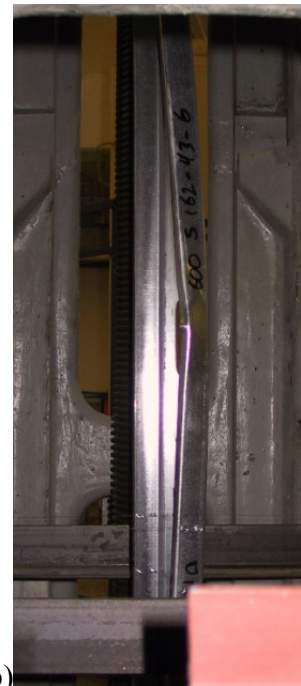
Figure A19.2 Elastic Buckling in the Stud 600S162-43-000(1) at an Axial Load 4500 lbs



Figure A19.3 First mode Flexural Buckling in the Stud 600S162-43-000 at an Axial Load of 5200 lbs



(a)



(b)

Figure A19.4 Distortional Buckling of the Stud 600S162-43-000 at (a) prior to Maximum (b) at Maximum load

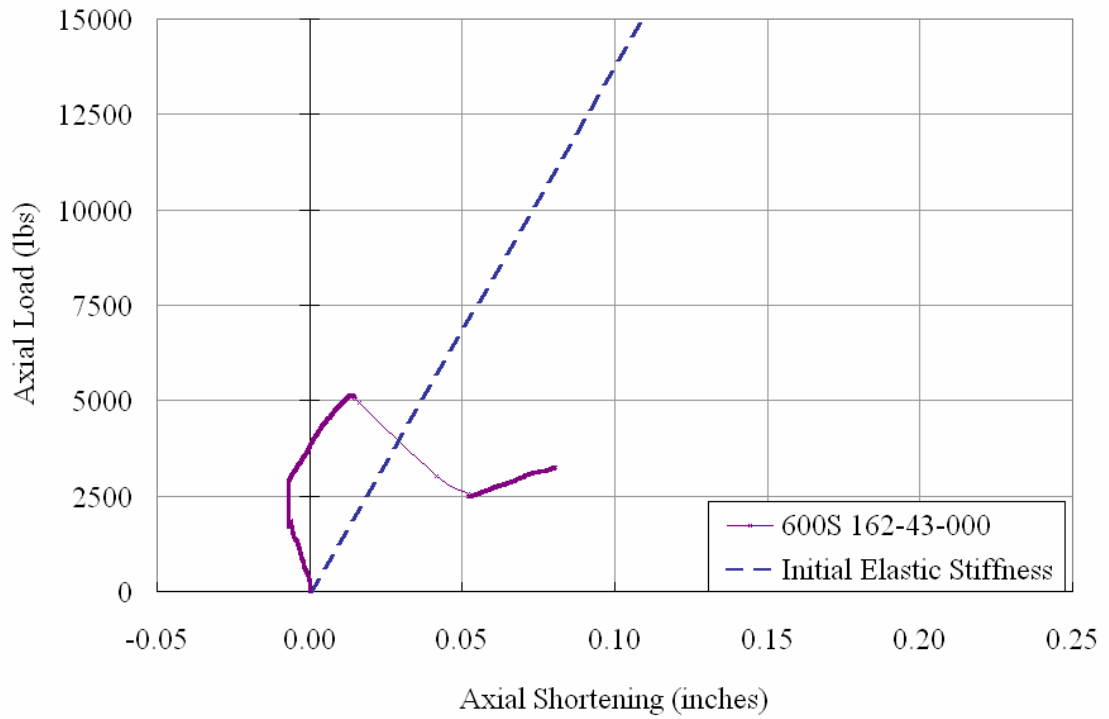


Figure A19.5 Plot of Axial Load vs. Axial Shortening

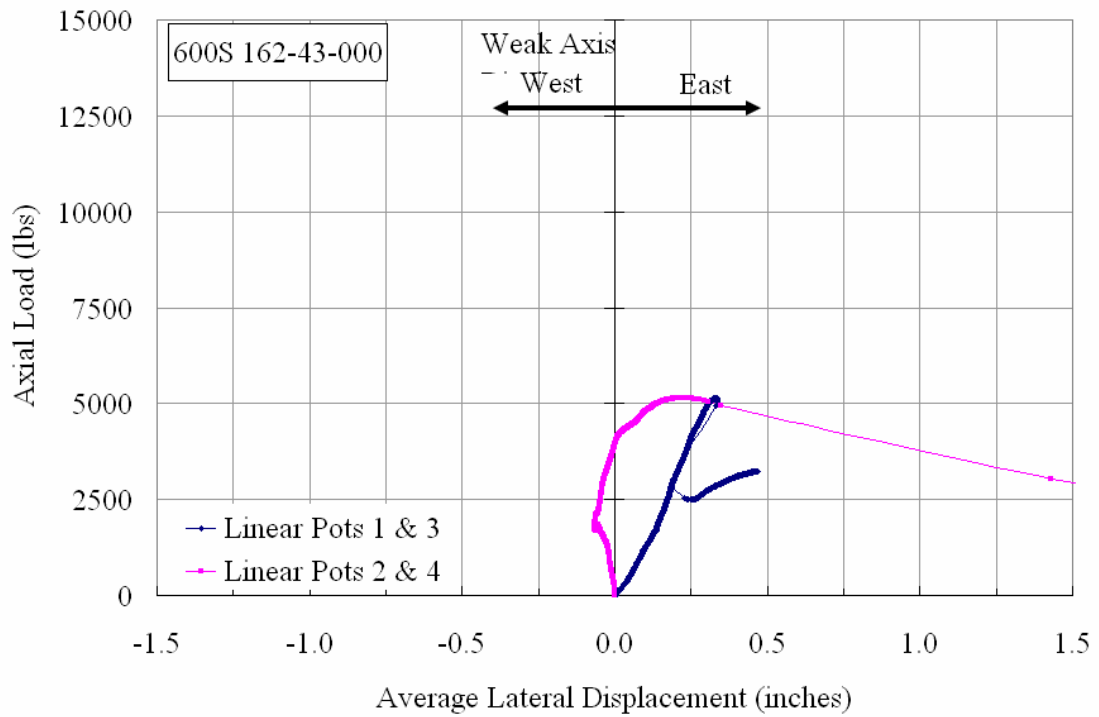


Figure A19.6 Plot of Axial Load vs. Weak Axis Displacement at Mid-Height

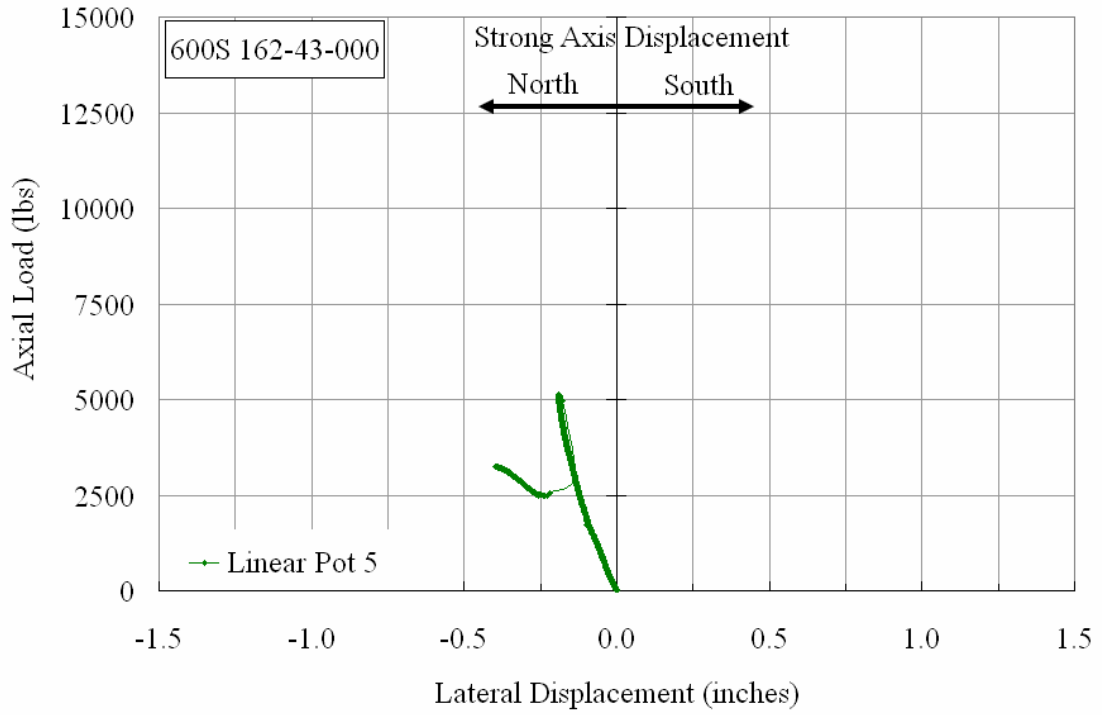


Figure A19.7 Plot of Axial Load vs. Strong Axis Displacement at Mid-Height

**600S162-43-000(2)**

The cee stud specimen 600S162-43-000 was tested without any lateral bracing. Figure A20.1 shows the stud in the Riehle Machine prior to the test. The stud was loaded at the rate between 8 to 12 lbs/sec, to ensure static response to the applied load. The weak axis lateral displacement at mid-height of the stud was measured with the linear potentiometers LP-1 & 3 and 2 & 4, attached to the north and south flanges, respectively, and the strong axis displacement was measured with LP-5, attached to the south flange.

The plot of axial load versus axial shortening of the stud is shown in Figure A20.5. From zero up to an axial load of about 2500 lbs, the plot coincides with the initial elastic stiffness, shown as a dashed line in Figure A20.5. At about 1000 lbs, the local elastic buckling waves were visible in the stud web, however their amplitude was very small. At an axial load of 2500 lbs, the axial shortening was 0.018 inches, the north and south flanges had moved west by 0.42 and 0.28 inches, respectively, as shown in Figure A20.6 and the strong axis had moved south by 0.032 inches (see Figure A20.7). From 2500 lbs up to the maximum load, the effective cross-sectional area reduced, and the stud started losing its stiffness. Figures A20.2 and 20.3 show the weak axis flexural buckling and distortional buckling in the flanges that was occurring at about 4000 lbs.

The stud reached its axial load carrying capacity at about 4250 lbs subsequently the load started to decrease as local buckling in the flanges had occurred. Figures 20.3 and 20.4 clearly shows first mode flexural buckling which agrees with the plot shown in Figure 20.6.



Figure A20.1 Overall View of the Stud 600S162-43-000 in the Riehle Testing Machine at an axial load of



Figure A20.2 Flexural Buckling of Top-half of the Stud 600S162-43-000 at an Axial Load of 4000 lbs



Figure A20.3 Distortional waves in the top-half of the Stud 600S162-43-000 at an Axial Load of 4000 lbs

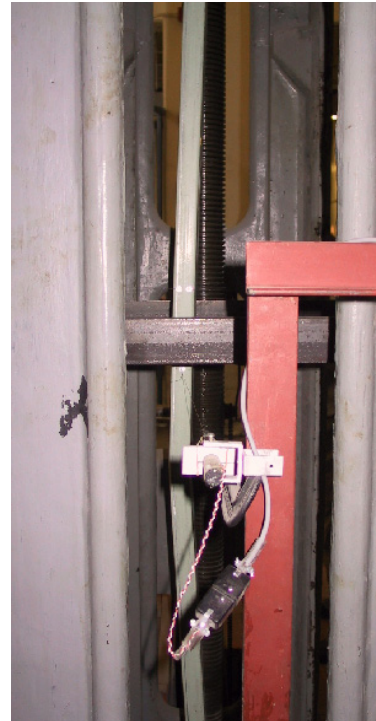


Figure A20.4 Final View of the Stud 600S162-43-000 at the maximum load

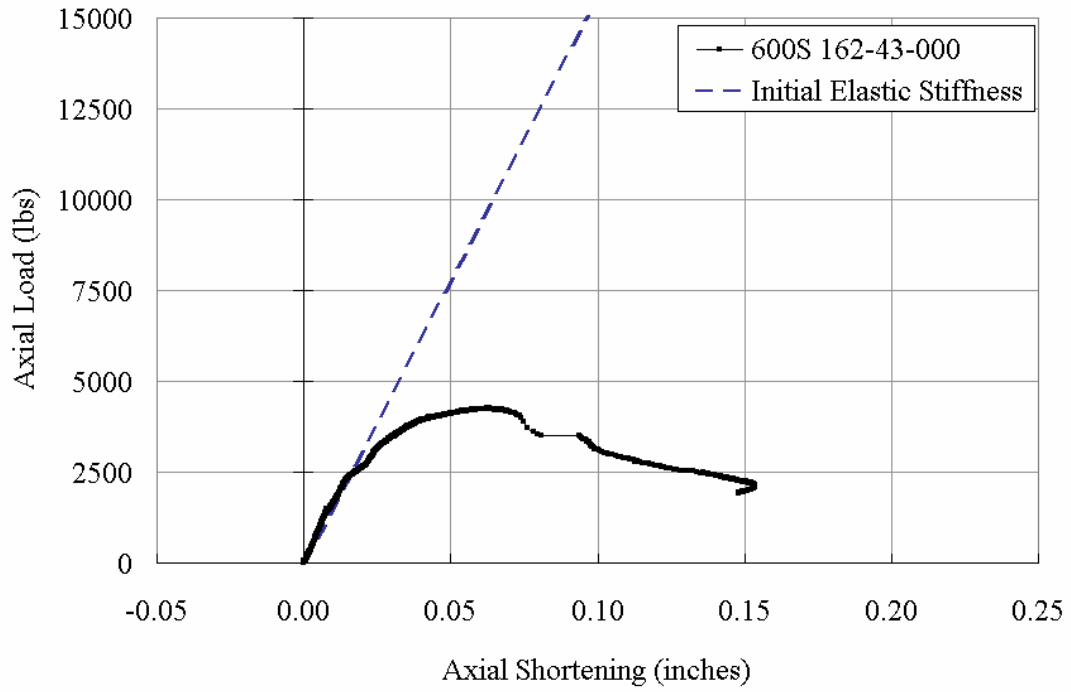


Figure A20.5 Plot of Axial Load vs. Axial Shortening

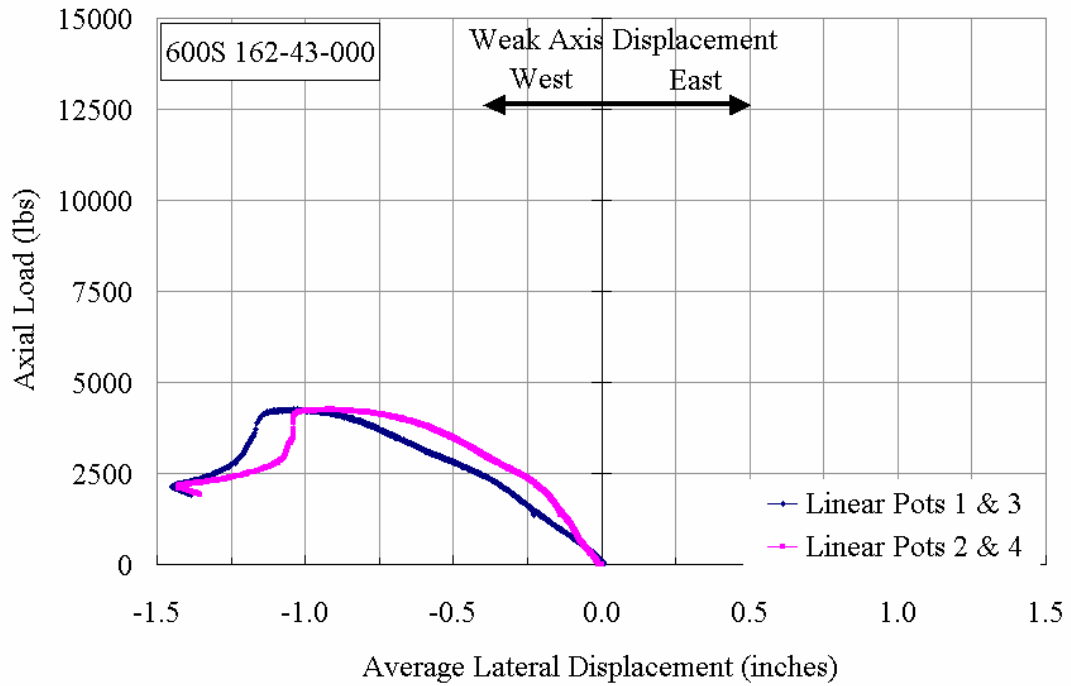


Figure A20.6 Plot of Axial Load vs. Weak Axis Displacement at Mid-Height

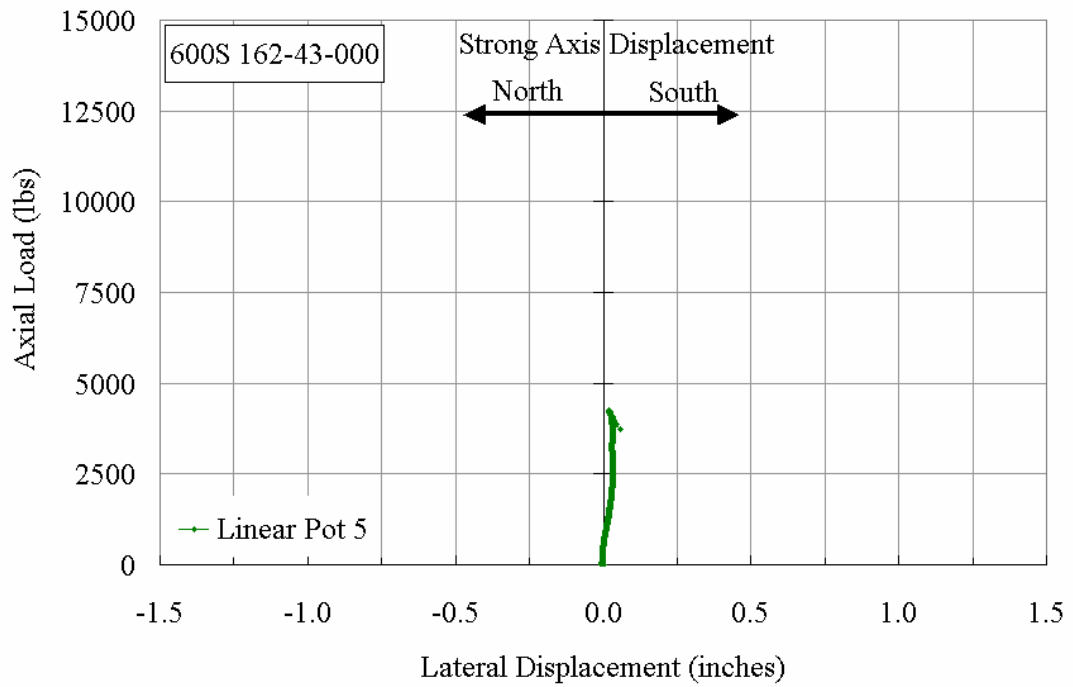


Figure A20.7 Plot of Axial Load vs. Strong Axis Displacement at Mid-Height

**600S162-43-030**

The cee stud specimen 600S162-43-030 was braced with a total brace stiffness of 61 lbs/inch which was equal to about 0.2 times the ideal bracing requirement. Figure A21.1 shows the stud in the Riehle Machine prior to the test. Figure A21.5 shows the plot of axial load versus axial shortening of the stud. The mid-height weak axis lateral displacement was measured by linear potentiometers LP-1 & LP-3 and LP-2 & LP-4, attached to the north and south flanges, respectively, and LP-5 recorded the strong axis lateral displacement.

Figure A21.7 shows that the stud exhibited first mode flexural buckling up to an axial load of about 1100 lbs, and the corresponding displacements of the north and south flanges, were 0.88 inches on both, respectively, with the strong axis starting to move southwards. The brace forces in BF-3 and BF-4 measured about 3.0 lbs each. The first elastic buckling waves in the web were observed at about 400 lbs of axial load, which were clearly visible at about 4000 lbs of axial load. With this increase in the axial load, there was only a slight change in the measured displacements, and the brace forces remained less than 5 lbs in both BF-3 and BF-4. When the load reached about 4500 lbs, the south flange started to move west and the strong axis started to move north with elastic distortional waves visible in the south flange along the top-half of the stud (see Figure A21.3). On reaching the maximum load of about 7150 lbs, the south flange had moved west by 0.40 inches, the north flange had remained at 0.02 inches to the east, and the strong axis had moved north by 0.13 inches. The corresponding brace force in BF-2 was about 15 lbs. The failure was considered to be distortional based on the severity of the elastic buckling waves and the distortional waves present, which led to a sudden simultaneous local buckling of the web and flanges, as shown in Figure A21.4.



Figure A21.1 Overall View of the Stud 600S162-43-030 in the Riehle Testing Machine, prior to the Test



Figure A21.2 Elastic buckling waves in the Web of Stud 600S162-43-030 at an Axial Load of 4000 lbs

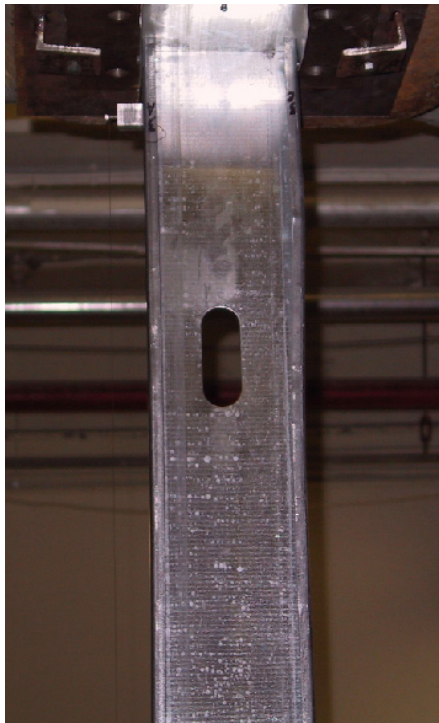
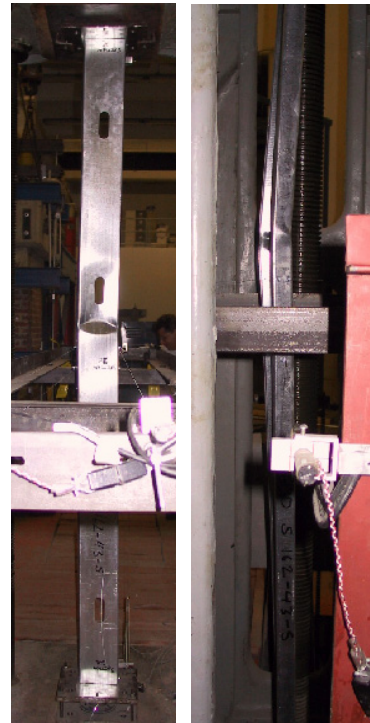


Figure A21.3 Distortional waves in the top-half of the Stud 600S162-43-030 at an Axial Load of 5000 lbs



(a) Looking West (b) Looking North  
Figure A21.4 Final View of the Stud 600S162-43-030 at the maximum load

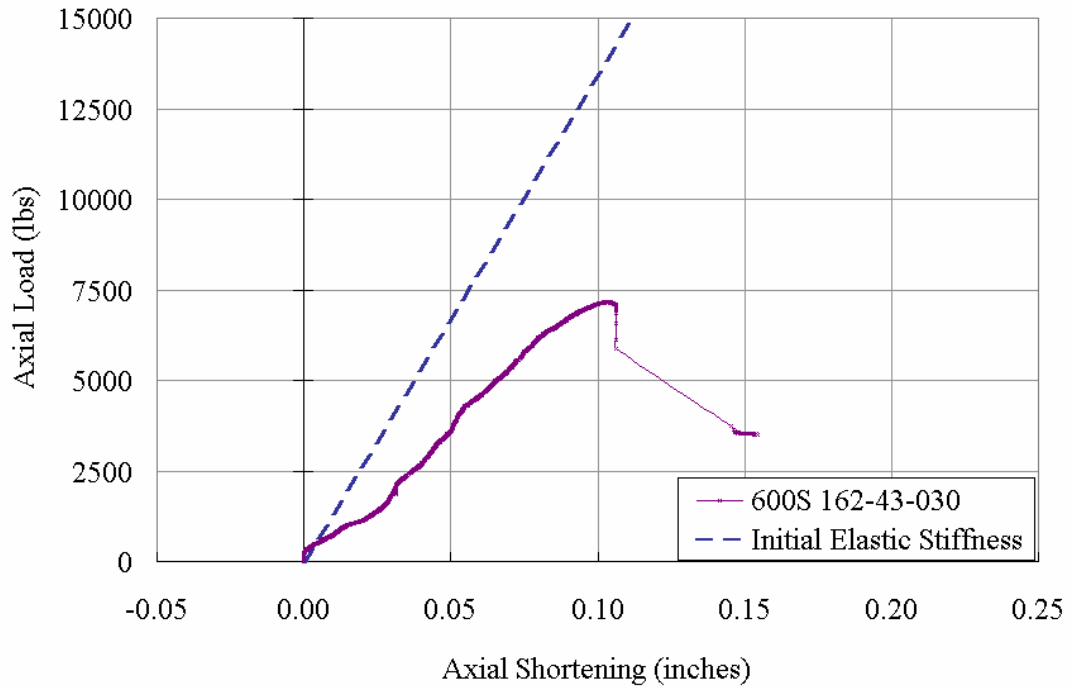


Figure A21.5 Plot of Axial Load vs. Axial Shortening

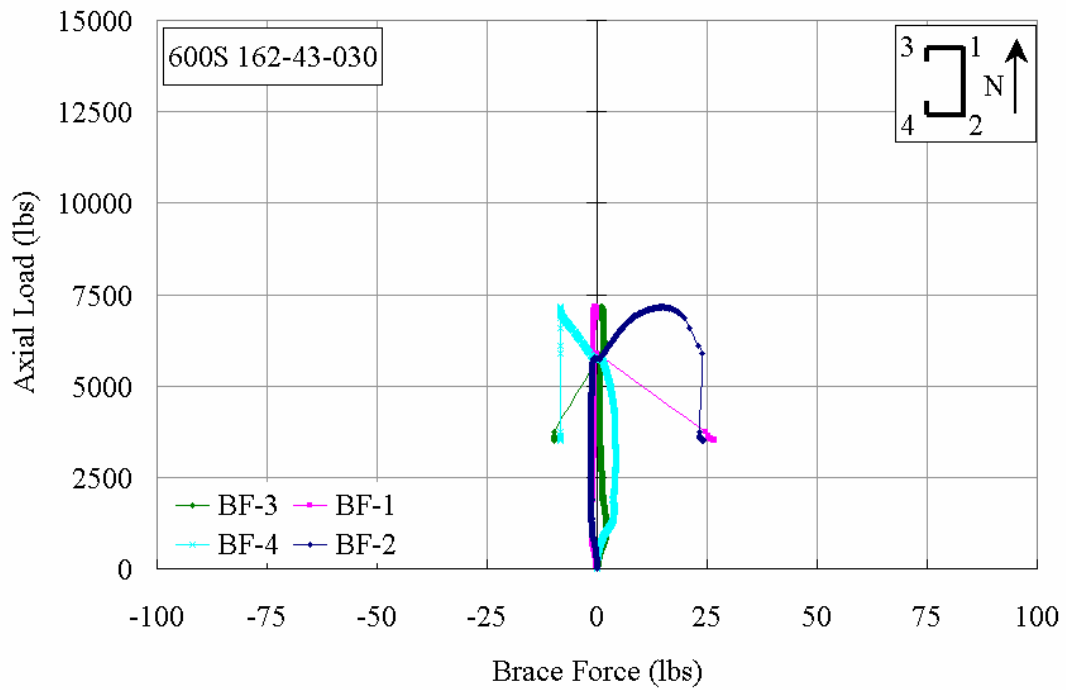


Figure A21.6 Plot of Axial Load vs. Brace Forces

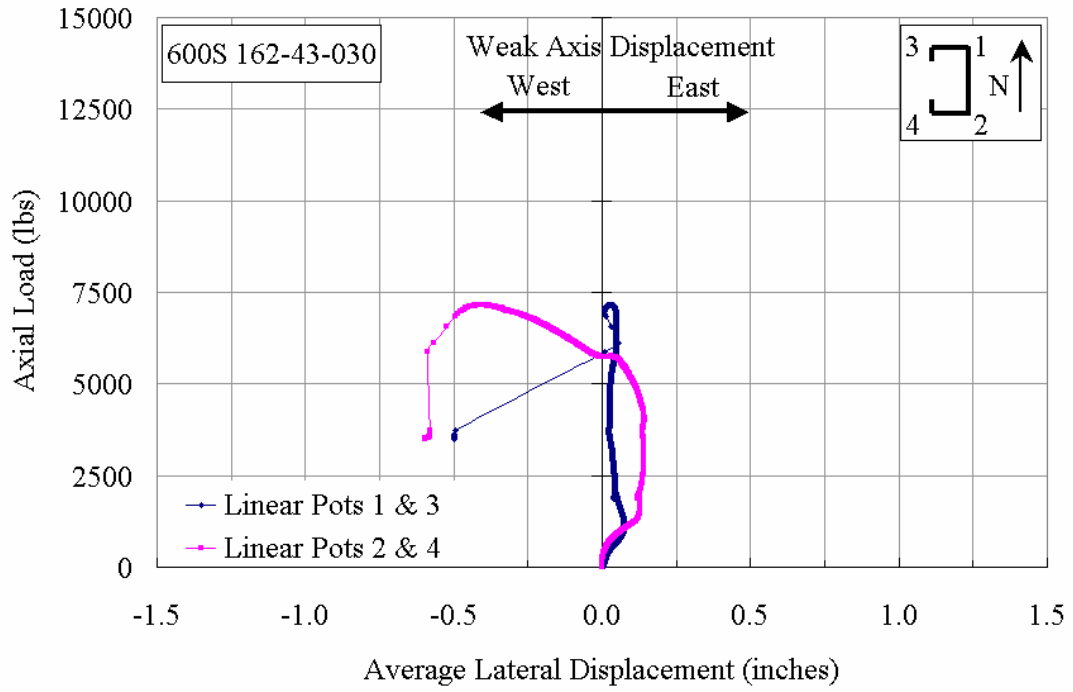


Figure A21.7 Plot of Axial Load vs. Weak Axis Displacement at Mid-Height

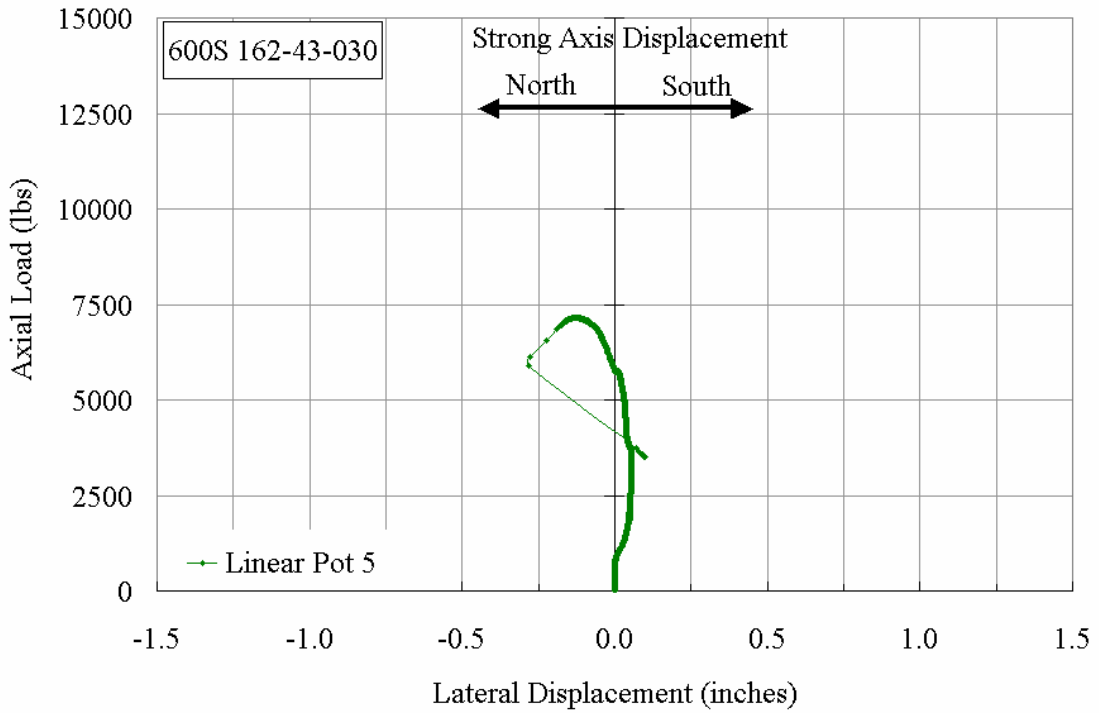


Figure A21.8 Plot of Axial Load vs. Strong Axis Displacement at Mid-Height

**600S162-43-075**

The cee stud specimen 600S162-43-075 was braced with a total brace stiffness of 148 lbs/inch which was equal to about 0.5 times the ideal bracing requirement. Figure A22.5 shows the plot of axial load versus axial shortening of the stud. It was observed that, from the start of the axial loading the axial deformation of the stud deviated from its initial elastic stiffness line. The stud reached two peak load capacities at two different axial deformations, as can be observed from Figure A22.5.

The weak axis displacement of the stud was measured by the linear potentiometers, LP-1 & LP-3 and LP-2 & LP-4, attached to the north and south flanges, respectively. Figure A22.8 shows that there was no strong axis displacement until the first peak load was reached as measured by linear potentiometer LP-5. The differential movement of the flanges though, indicates that the mid-height cross-section was twisting along with the weak axis movement prior to the peak being reached (see Figure A22.7).

The overall view of the stud before starting the test is shown in Figure A22.1. The stud was loaded at approximately 6 lbs/sec, to ensure static response of the stud. From zero up to the first peak load, the brace force in the BF-3 was increasing without much change in the other brace forces. Initially, up to 1500 lbs of axial load, the force in BF-3 reached 7 lbs, owing to the eastward movement of only the north flange, as shown in Figures A22.6 and A22.7. When the axial load reached approximately 2000 lbs, elastic buckling waves were observed in the web. These waves had a wavelength of about 6 inches across the web and 6 inches or more along the length of the stud, as shown in Figure A22.2. At about 4000 lbs, the elastic buckling waves were observed to decrease in wavelength. A close observation of Figure 22.3 shows the plate buckling of the stud's web. At this load, the brace force in BF-3 measured 9.75 lbs, the weak axis movement of

the north flange was 0.13 inch and that of the south flange was 0.04 inch, both towards the east. At approximately 5000 lbs, distortional waves were observed in the two flanges having a wavelength of about 24 inches.

At the first peak axial load of 6025 lbs, the top track started to loose stiffness owing to the distortional buckling of the flanges at the top of the stud, at an axial deformation of 0.1 inches. At about 24 inches from the top distortional wave, a local buckle formed on the north flange-lip junction, as shown in Figure 20.4. Soon after the formation of this local buckle, the axial load dropped to 5300 lbs. A brace force of 30 lbs was measured in BF-3 with an eastward movement of the north flange by 0.5 inch. The axial load started to increase again and reached a second maximum of about 6050 lbs, with the brace force in BF-3 now measuring 58 lbs at an axial shortening of 0.16 inches and a strong axis movement towards the north of 0.22 inches and a north flange movement of 1.0 inch towards the east. The failure of the stud is identified as distortional, as shown in Figure 20.4.



Figure A22.1 Overall View of Stud 600S162-43-075 in Riehle Machine Prior to Testing

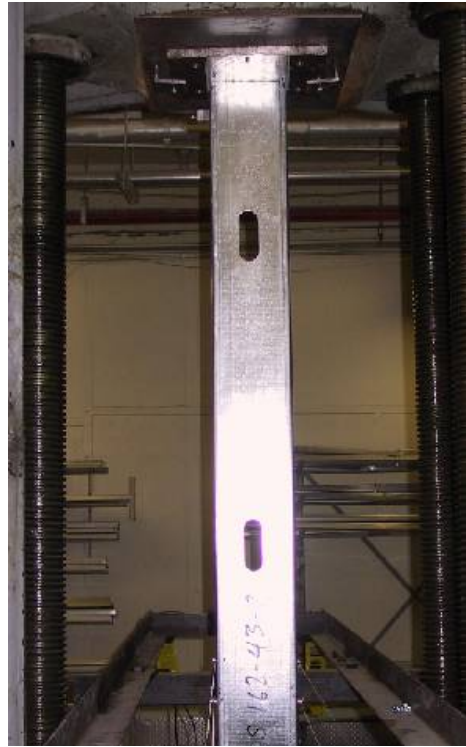


Figure A22.2 Elastic buckling waves in the Web of Stud 600S162-43-075 at an Axial Load

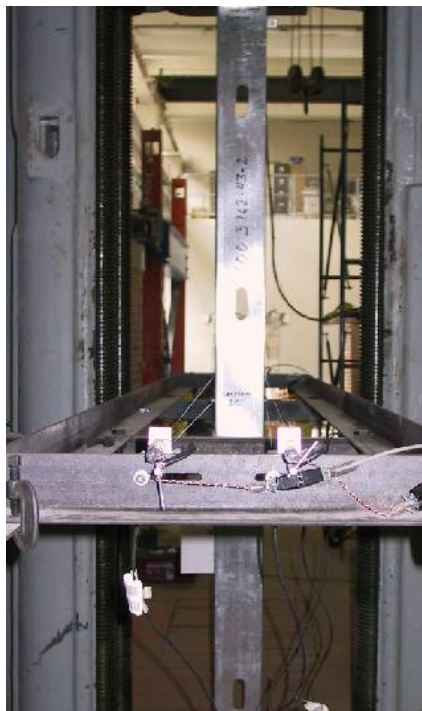


Figure A22.3 Elastic buckling waves in the Web of Stud 600S162-43-075 at an Axial Load

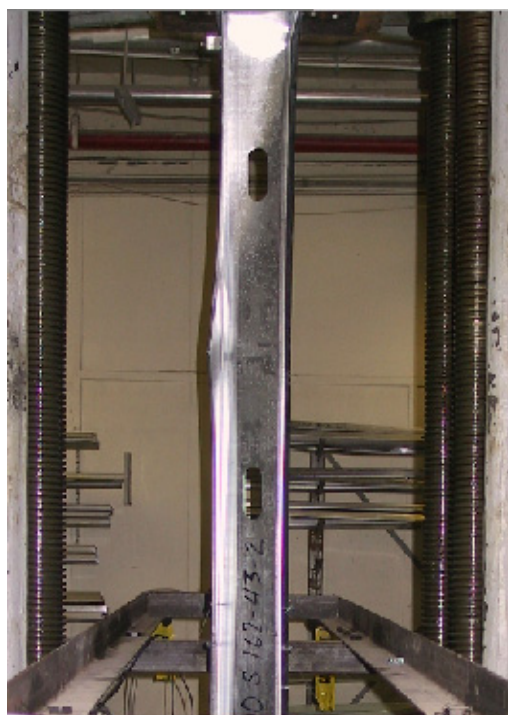


Figure A22.4 Distortional Wave & Formation of a Local Buckle in the Stud 600S162-43-075.

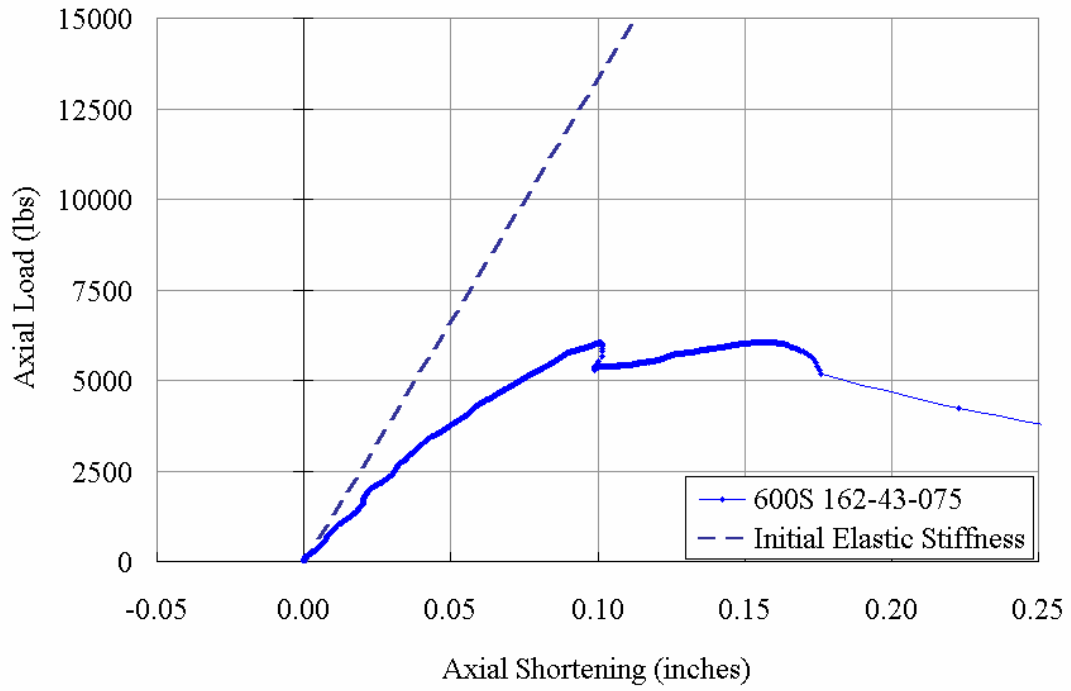


Figure A22.5 Plot of Axial Load vs. Axial Shortening

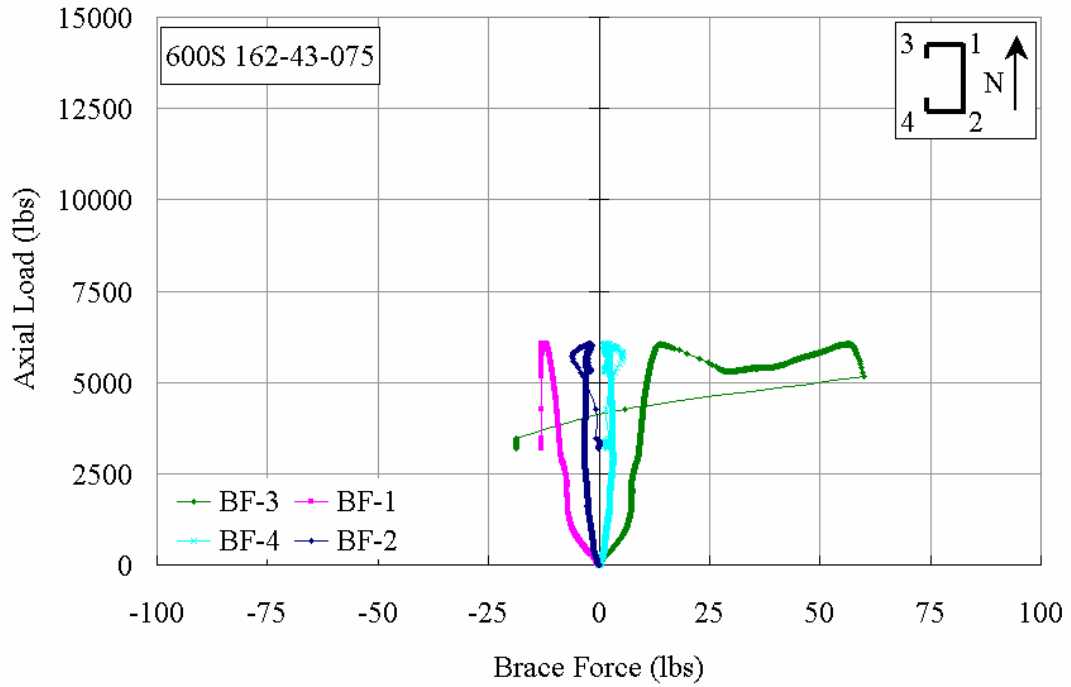


Figure 20.6 Plot of Axial Load vs. Brace Forces

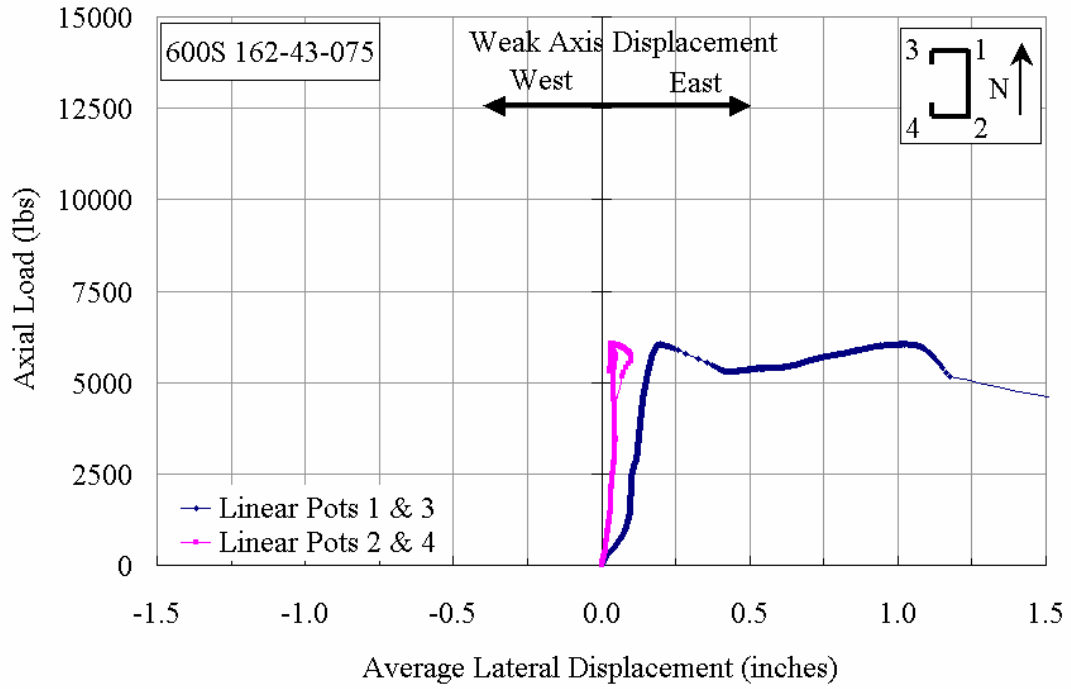


Figure 20.7 Plot of Axial Load vs. Weak Axis Displacement at Mid-Height

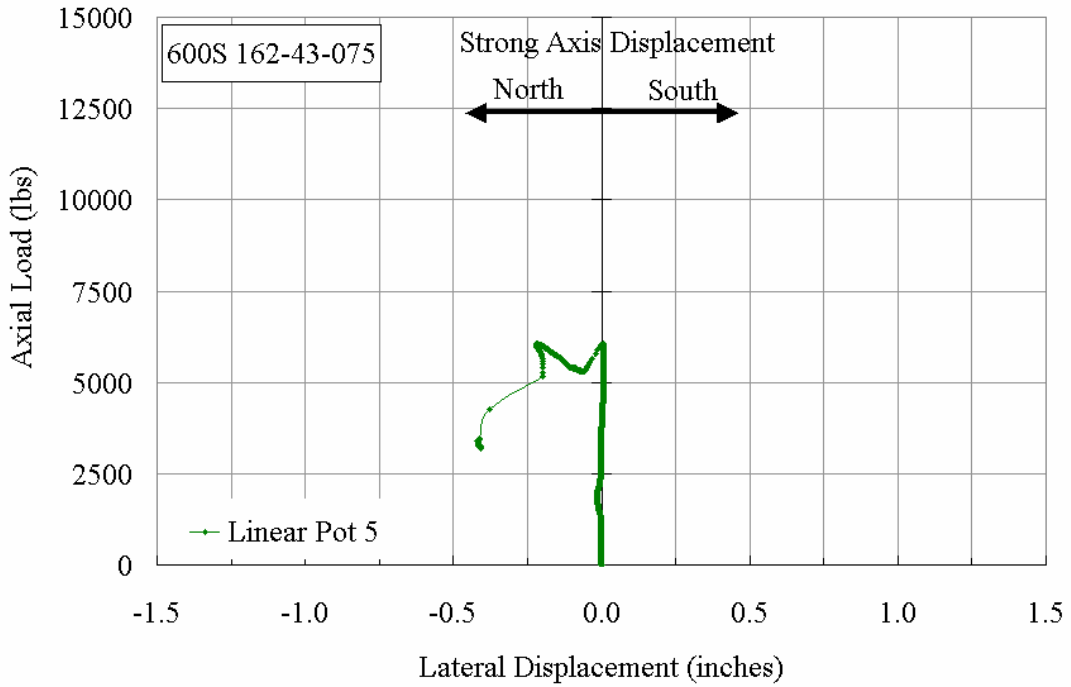


Figure A22.8 Plot of Axial Load vs. Strong Axis Displacement at Mid-Height

**600S162-43-250**

The cee stud specimen 600S162-43-250 was braced with a total bracing stiffness of 497 lbs/in., which was about 1.7 times the ideal bracing requirement. To ensure static response to the applied load, the stud was loaded initially at a rate of 10 lbs/sec, which was subsequently reduced to about 2 to 5 lbs/sec. The mid-height east-west displacement of the flanges was measured with two pairs of linear potentiometers LP-1 & LP-3 and LP-2 & LP-4 attached to the north and south flanges, respectively. The north-south displacement was measured with LP-5 attached to the south flange. Figure A23.1 shows the stud in the Riehle testing machine prior to testing.

Elastic buckling waves in the stud web were observed at an axial load between 500 and 1300 lbs as seen in Figure A23.2. At the 1300 lbs load level there was minimal weak axis lateral movement to the east of only 0.018 and 0.021 inches recorded on the north and south flanges, respectively. There was also a slight lateral movement to the south as measured by LP-5 of 0.022 inches (see Figure A23.8). The corresponding brace forces were also minimal, 4 lbs and 6 lbs at BF-3 and BF-4, respectively (see Figure A23.6). Above this nominal load level up to approximately the maximum axial capacity of the stud, there were only slight increases in the lateral movement of the stud at mid-height and the brace forces as measured by BF-3 and BF-4 remained less than 10 lbs.

The overall stud response from 1300 lbs up to 6500 lbs showed very little change with the axial stiffness staying fairly linear though the elastic buckling waves in the web had become more pronounced all along the length of the stud (see Figure A23.2). The recorded measurements at 6500 lbs of axial load were: weak axis movements of 0.037 inches (LP-1 & LP-3) to the west and 0.011 inches (LP-2 & LP-4) to the east, strong axis movement of 0.078 inches to the south, and brace forces in BF-1 and BF-4 of 7.0 lbs and

1.0 lbs, respectively. Above 6500 lbs, the axial stiffness of the stud began to gradually decrease, while the displacement measurements and brace force measurements continued to show only slight changes.

The stud reached its maximum load carrying capacity at a load of 7308 lbs. At this load, the force in BF-1 was only 6 lbs while the force in BF-2 was less than 2 lbs. The measured lateral movements of the stud at maximum load were 0.034 and 0.006 inches to the west measured on the north and south flanges, respectively, and 0.083 inches to the south. After the maximum load was attained, there was an immediate drop in axial load being carried by the stud. When the axial load had reduced to 6000 lbs, the force in the braces had again changed with BF-3 now measuring 42 lbs and the force in brace BF-4 at 9.0 lbs. The measured lateral movements of the stud also changed directions as the stud's ability to carry axial load decreased. The lateral displacements at mid-height now read 0.138 inches (LP-1 & LP-3) and 0.020 inches (LP-2 & LP-4) to the east and 0.012 inches to the north (LP-5). Shortly thereafter, the test was concluded and the stud unloaded.

The observed failure mode of the stud can be seen in Figure A23.4 that shows its final buckled shape. The overall failure mode can be described as distortional as the once elastic buckling waves in the web deepened and concentrated at the lowest punchout 12 inches above the bottom of the stud. Figure A23.3 shows a close up view of the distortional buckling failure that occurred in the web and progressed into the lipped flange of the stud adjacent to the punchout.



Figure A23.1 Overall View of Stud 600S162-43-250 in Riehle Machine Prior to Testing

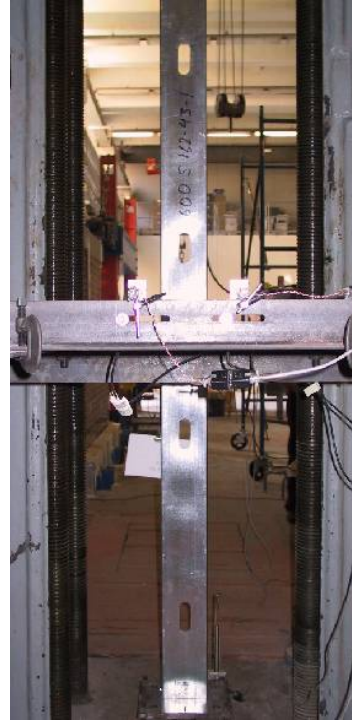


Figure A23.2 Elastic buckling waves in the Web of Stud 600S162-43-250 at an Axial Load

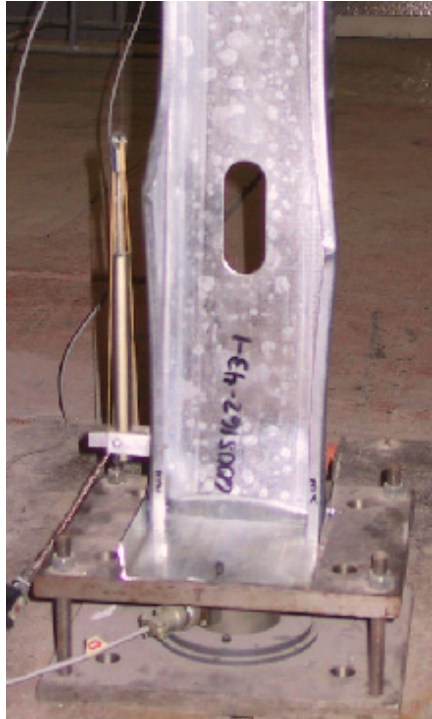


Figure A23.3 Distortional Wave & Formation of Local Buckle in flanges of the Stud 600S162-43-250



(a) Looking East (b) Looking North  
Figure A23.4 Final Buckled shape of bottom-half of the Stud 600S162-43-250

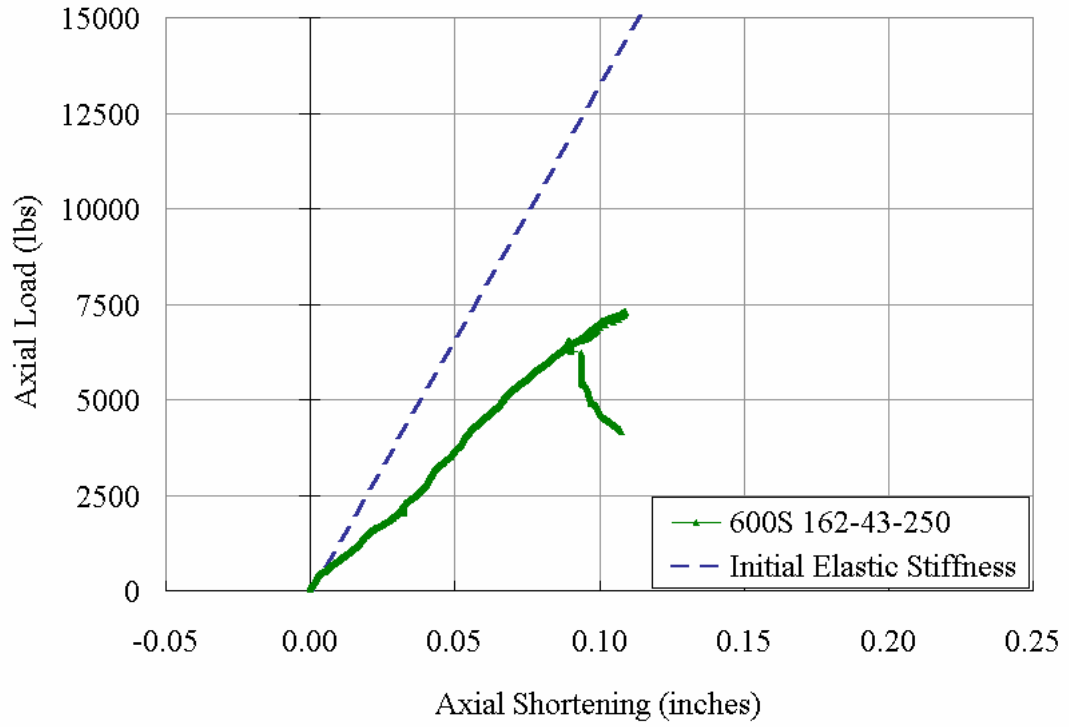


Figure A23.5 Plot of Axial Load vs. Axial Shortening

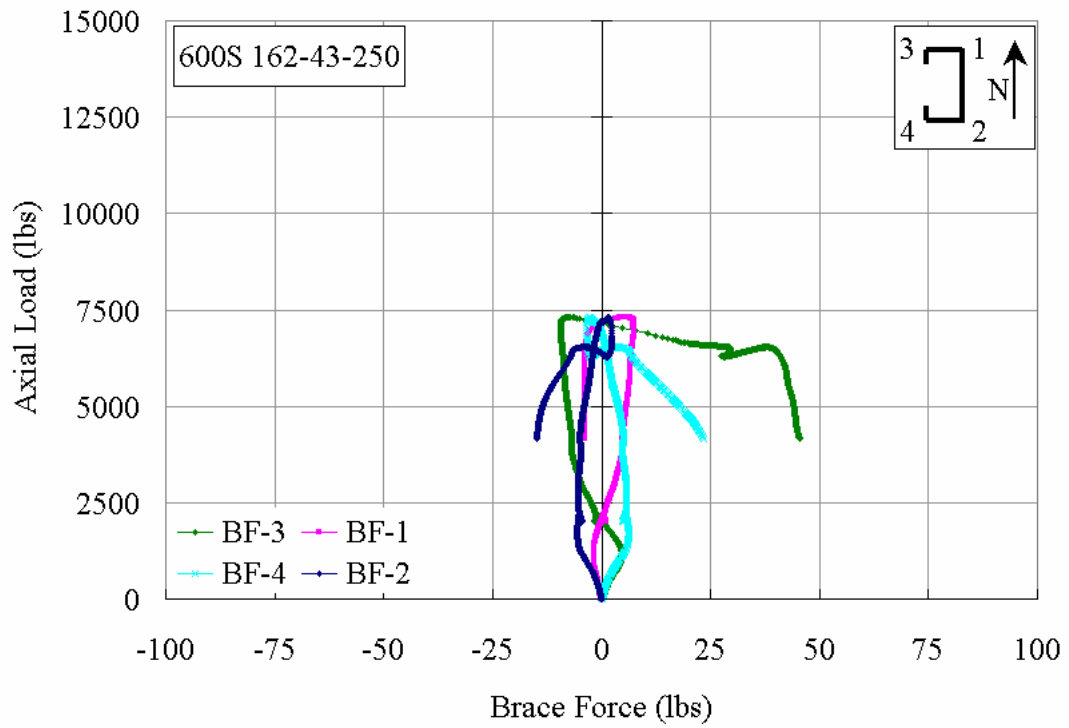


Figure A23.6 Plot of Axial Load vs. Brace Forces

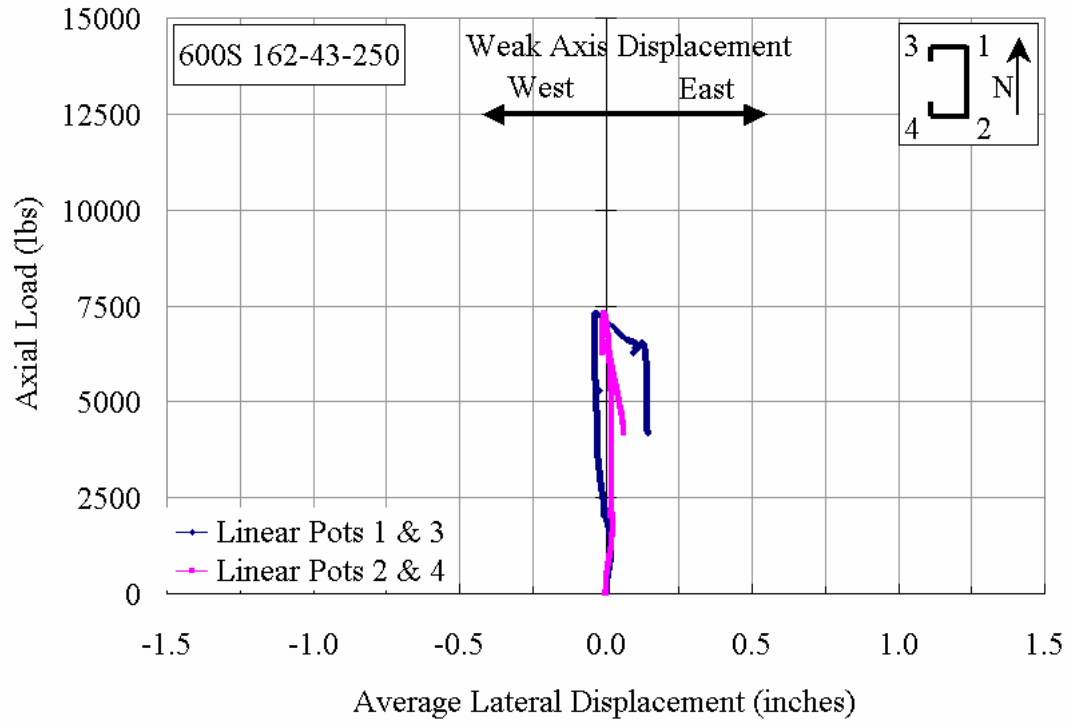


Figure A23.7 Plot of Axial Load vs. Weak Axis Displacement at Mid-Height

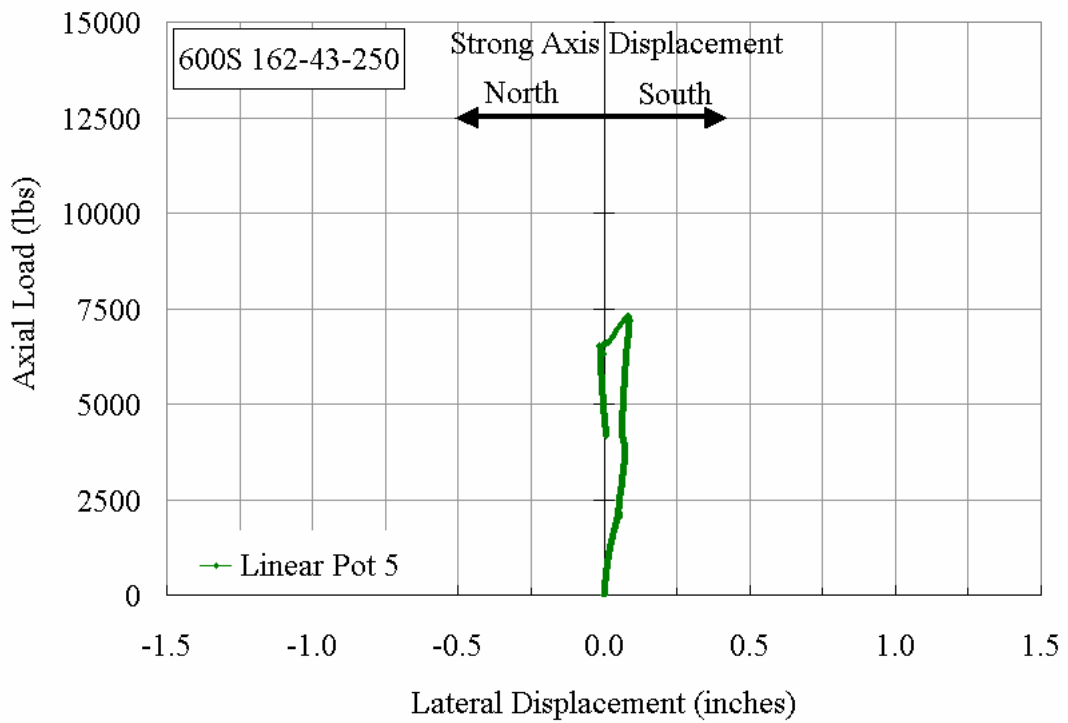


Figure A23.8 Plot of Axial Load vs. Strong Axis Displacement at Mid-Height

**600S162-43-500**

The stud 600S162-43-500 was braced with a total stiffness of 990 lbs/in. which was about 3.5 times the ideal bracing requirement. The load was applied at a rate of 5 to 10 lbs/sec to ensure that there would be a static response to the applied load. The weak axis displacement at mid-height of the stud was measured with linear potentiometers LP-1 & LP-3 and LP-2 & LP-4 attached to the north and south flanges, respectively. The strong axis movement, in the north-south direction, was measured with LP-5. Figure A24.1 shows the stud in the Riehle testing machine prior to testing. The axial deformation was measured with LP-6 attached along the north flange.

Elastic buckling waves in the web were first observed at an axial load of 1000 lbs as shown in Figure A24.2. At this load level the weak axis lateral displacement was 0.01 inches, on both flanges (see Figure A24.7). There was also a slight lateral movement to the South, as measured by LP-5, of 0.012 inches (see Figure A24.8). The brace forces in BF-3 and BF-4 were 4 lbs and 5 lbs, respectively (see Figure A24.6). As the load was increased from 1000 lbs to 2500 lbs, there was not much change in the weak axis displacement, whereas at approximately 2500 lbs of axial load, the strong axis had moved south by 0.46 inches. The force in BF-3 dropped to zero at 2000 lbs, and then increased to 3.0 lbs at 2500 lbs of axial load, whereas the force in BF-4 steadily increased to 10 lbs.

When the load reached about 4500 lbs, the force in BF-4 measured 14 lbs and then started to drop; the force in BF-3 measured 7 lbs. Up to an axial load of 7000 lbs, the axial shortening was relatively linear, as shown in Figure A24.5. As the axial load was increased from 7000 lbs to just prior to the maximum load being reached, the axial stiffness began to gradually decrease. At these same load levels the lateral displacement measurements showed very small changes.

At the maximum load of 7075 lbs, the brace force measurements in BF-3 and BF-4 were 12 lbs and 3 lbs, respectively. The measured lateral movements of the stud at maximum load were only 0.01 inches to the east, and 0.047 inches to the south. Distortional buckling had developed in the stud at this load as can be seen in Figure A24.3. After attaining the maximum load, there was gradual drop in axial load carried by the stud to about 6000 lbs. The force in braces BF-3 and BF-4 now measured 24.0 lbs and 0.0 lbs, respectively. Shortly thereafter, the test was concluded and the stud unloaded.

The observed failure mode of the stud and its final buckled shape is shown in Figure A24.4. The overall failure mode is identified as distortional buckling at about 12 inches from the bottom of the stud. Figure A24.4 also shows a close up view of the distortional buckling failure that occurred in the web and progressed into the lipped flange of the stud adjacent to the punchout.



Figure A24.1 Overall View of Stud 600S162-43-500 in Riehle Machine Prior to Testing



Figure A24.2 Elastic buckling waves in the Web of Stud 600S162-43-500 at an Axial Load



Figure A24.3 Distortional Wave in the South flange of the Stud 600S162-43-500



(a) Looking East (b) Looking North  
 Figure A24.4 Final Buckled shape of bottom-half of the Stud 600S162-43-500

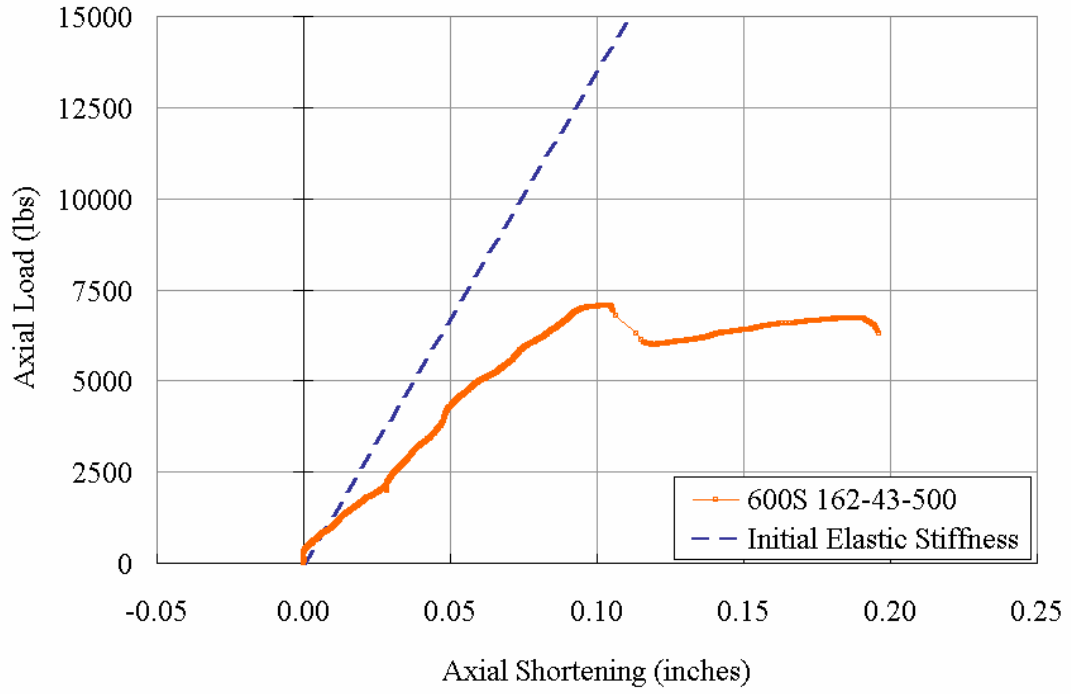


Figure A24.5 Plot of Axial Load vs. Axial Shortening

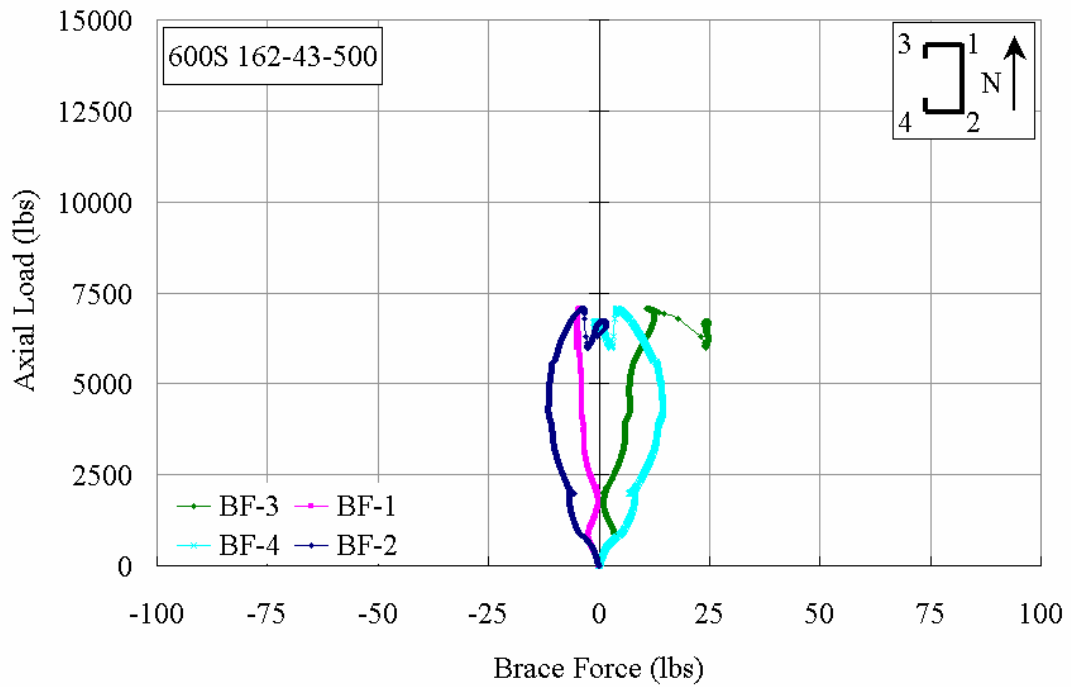


Figure A24.6 Plot of Axial Load vs. Brace Forces

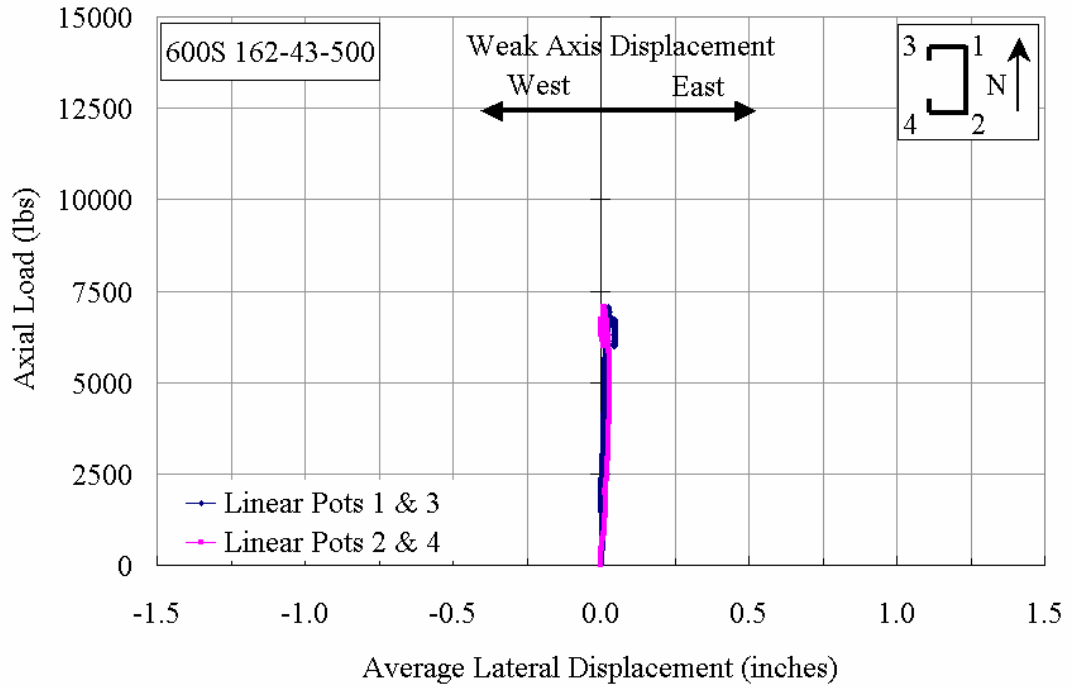


Figure A24.7 Plot of Axial Load vs. Weak Axis Displacement at Mid-Height

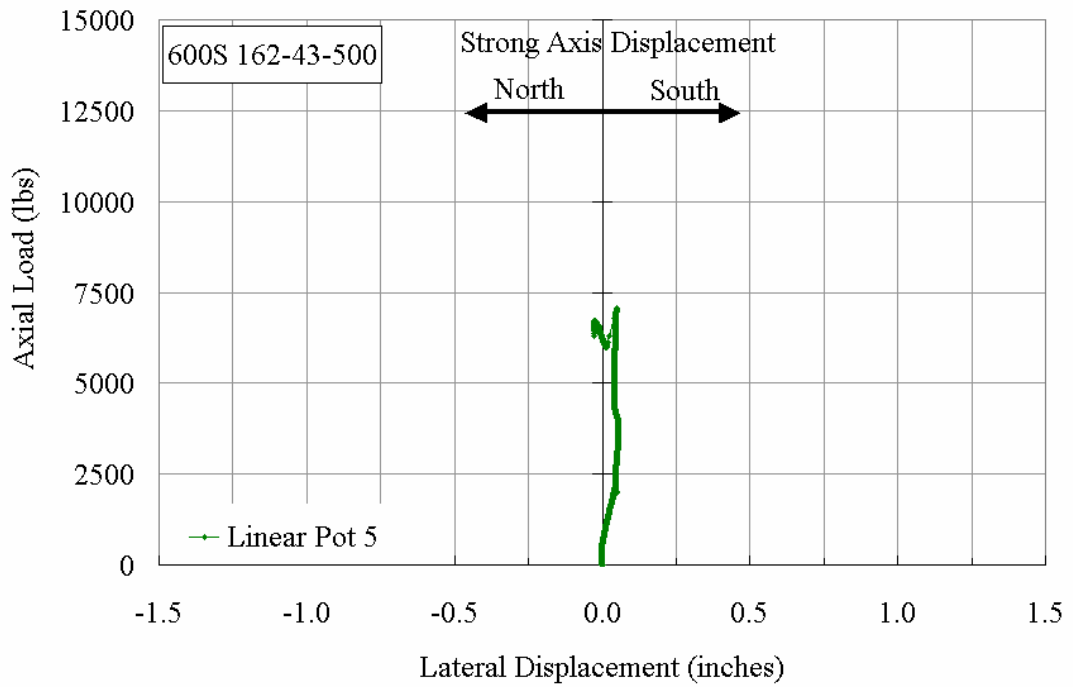


Figure A24.8 Plot of Axial Load vs. Strong Axis Displacement at Mid-Height

**600S162-97-000**

The stud 600S162-97-000 was tested without any lateral bracing. The stud was loaded initially at a rate of about 10 lbs/sec up to 5000 lbs and then at about 90 lbs/sec up to the maximum load. Figure A25.1 shows the overall view of the stud in the test frame. The plot of axial load versus axial shortening, as shown in Figure A25.5, closely follows the initial elastic stiffness once the load exceeds 5000 lbs. Lateral displacement of the two flanges in the east-west direction was measured with pairs of linear potentiometers LP-1 & LP-3 and LP-2 and LP-4, attached to the north and south flanges, respectively, at mid-height of the stud. The strong axis lateral displacement in the north-south direction was measured by LP-5, which was attached to the south flange.

Initially, up to 3000 lbs, the stud demonstrated flexural-torsional buckling about the weak axis, with the flanges moving in opposite directions, as shown in Figure A25.6, while the strong axis was moving towards north, as shown in Figure A25.7. At approximately 3000 lbs, the north flange had moved east by 0.028 inches, and by 5000 lbs, it had moved back to its initial position. Meanwhile, the south flange had moved by 0.198 inches west and the strong axis had moved north by 0.10 inches.

As the axial load reached 18000 lbs, the north flange had moved west by 0.04 inches while the south flange continued to move west by 0.45 inches, and the strong axis had moved north by 0.18 inches. At this load level, elastic buckling waves were seen in the web, as shown in Figure A25.2, close to the punchouts.

At the maximum axial load of about 21000 lbs, a local buckle developed close to a web punchout, as shown in Figure A25.3. At this load, the displacement of the north and south flanges increased to 0.18 inches and 1.0 inch to the west, respectively, and the strong axis had moved 0.35 inches towards the north.

The failure of the stud was by flexural-torsional buckling, but predominantly flexural, with local buckling occurring as a result of the global buckling modes. An overall view of the stud along with a close-up view is shown in Figure A25.4.



Figure A25.1 Overall View of Stud 600S162-97-000 in Riehle Machine Prior to Testing

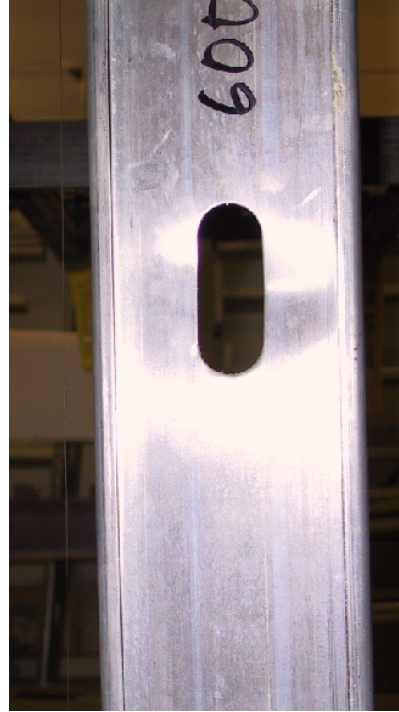
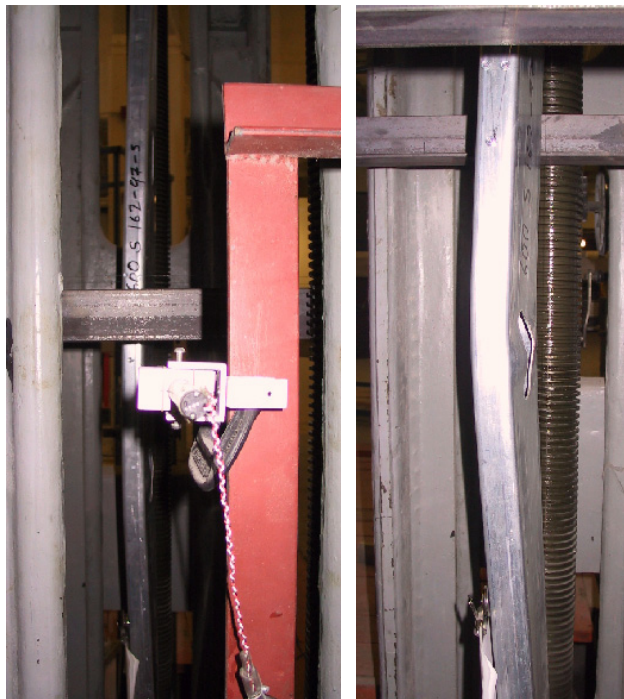


Figure A25.2 Elastic Wave in the web of the Stud 600S162-97-000 at an Axial Load of 19000 lbs



Figure A25.3 Local Buckling in the Web of the Stud 600S162-97-000 at an Axial Load of 19500 lbs



(a) Looking North (b) Close-up View  
Figure A25.4 Buckled Shape of the Stud 600S162-97-000 at the Maximum Axial Load

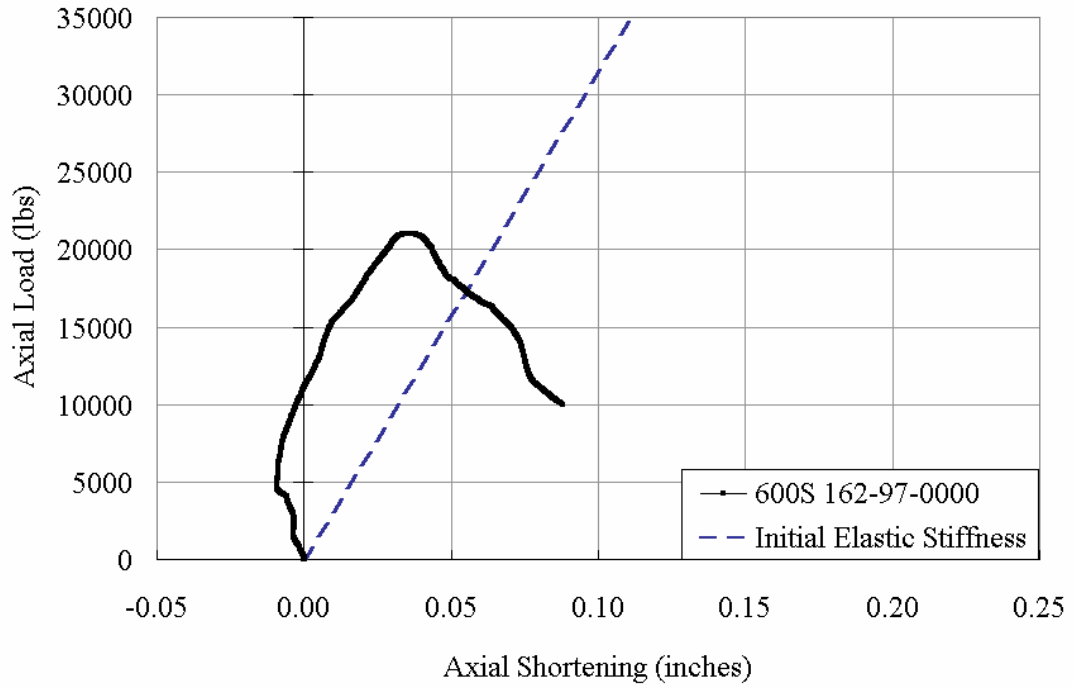


Figure A25.5 Plot of Axial Load vs. Axial Shortening

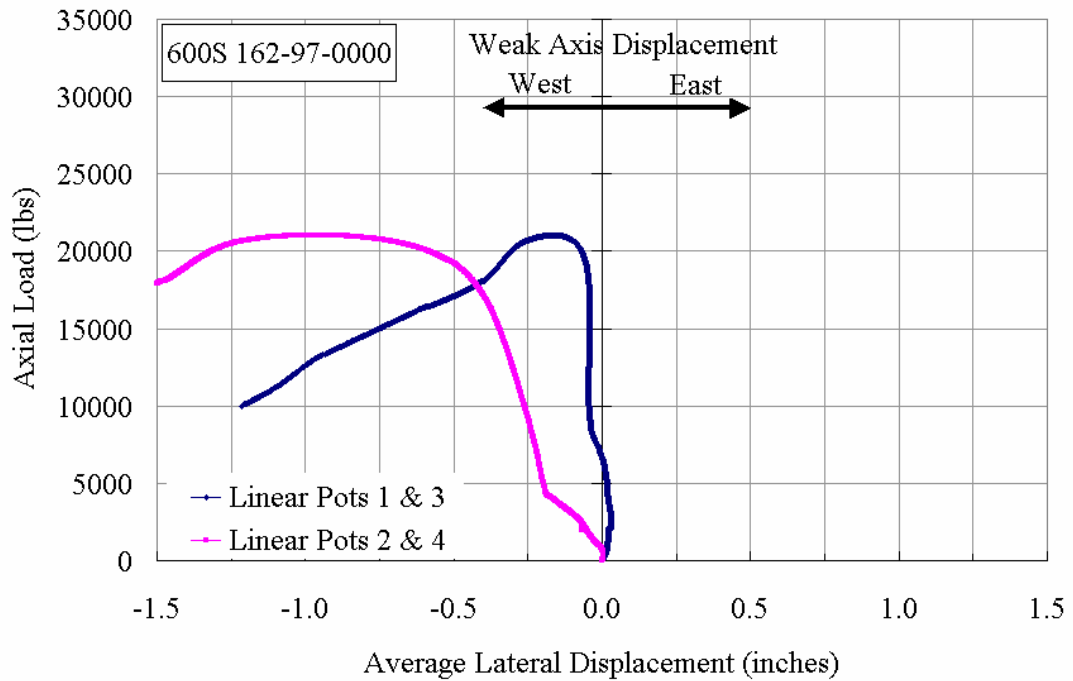


Figure A25.6 Plot of Axial Load vs. Weak Axis Displacement at Mid-Height

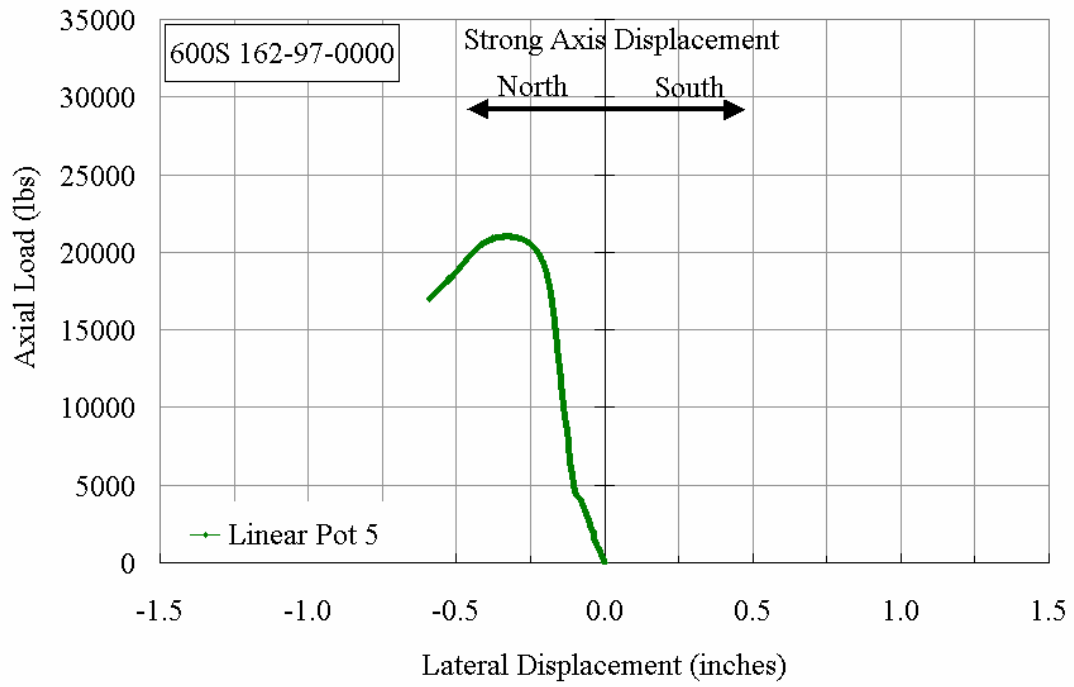


Figure A25.7 Plot of Axial Load vs. Strong Axis Displacement at Mid-Height

**600S162-97-160**

The stud 600S162-97-160 was braced with a total stiffness of 324 lbs/in. that was 0.3 times the ideal bracing requirement. The stud was loaded initially at the rate of about 10 lbs/sec up to 5000 lbs and then at about 45 lbs/sec till the maximum load was reached. Figure A26.1 shows the overall view of the stud in the test frame. The plot of axial load versus axial shortening as shown in Figure A26.5 closely follows the initial elastic stiffness once the load exceeded 10,000 lbs. Lateral displacement of the two flanges in the east-west direction was measured with pairs of linear potentiometers LP-1 & LP-3 and LP-2 and LP-4, attached to the north and south flanges, respectively, at mid-height of the stud. The strong axis lateral displacement in the north-south direction was measured by LP-5, which was attached to the south flange.

From the beginning of the test, the stud demonstrated flexural-torsional buckling about the weak axis as shown in Figure A26.7. The plot of the axial load versus brace forces, shown in Figure A26.6, also indicated that the diagonally opposite brace wires BF-2 & BF-3 were preventing the mid-height cross-section from twisting and allowing torsional buckling to occur. However, the bracing was not stiff enough to prevent the twist. As the axial load was increased, the strong axis was moving towards the north, as shown in Figure A26.8.

As the axial load reached 25000 lbs, the brace forces in BF-2 and BF-3 measured 20.0 lbs and 10.0 lbs, respectively. The north flange had moved east by 0.09 inches, the south flange had moved west by 0.10 inches, and the strong axis had moved north by 0.15 inches. At this load level, elastic buckling waves were observed in the web close to the punchouts as shown in Figure A26.2.

The stud reached its maximum load carrying capacity at an axial load of about 28000 lbs, when a local buckle developed close to a web punchout as shown in Figure A26.3. At this load, the forces in braces BF-2 and BF-3 measured about 35 lbs and 9 lbs, respectively. The displacement of the north and south flanges were 0.08 inches to the east and 0.02 inches to the west, respectively, with the strong axis moving 0.2 inches towards the north. An overall view of the stud at its maximum load is shown in Figure A26.4.

The failure of the stud was by first mode flexural-torsional buckling but predominantly torsional, with local buckling as a result of the severe twisting of the section.



Figure A26.1 Overall View of Stud 600S162-97-160 in Riehle Machine Prior to Testing

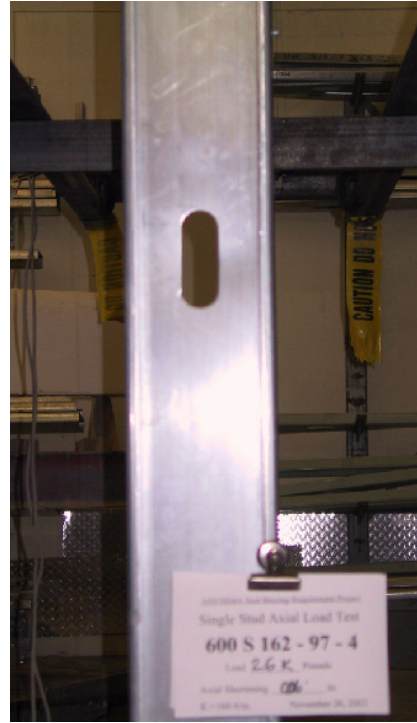


Figure A26.2 Elastic Wave in the web of the Stud 600S162-97-160 at an Axial Load of 25000 lbs

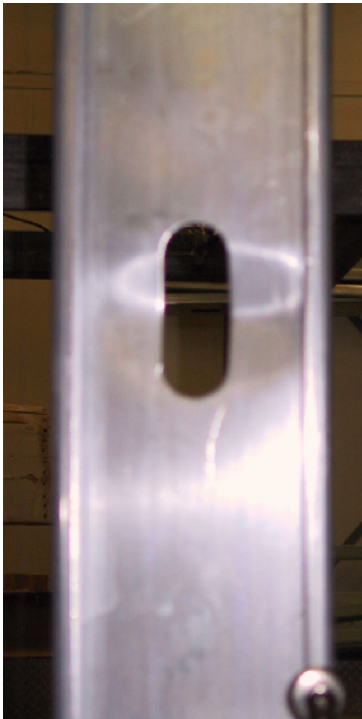


Figure A26.3 Local buckling in the web of the Stud 600S162-97-160 at an Axial Load of 28000 lbs



Figure A26.4 Final View of Stud 600S162-97-160 at Maximum Load

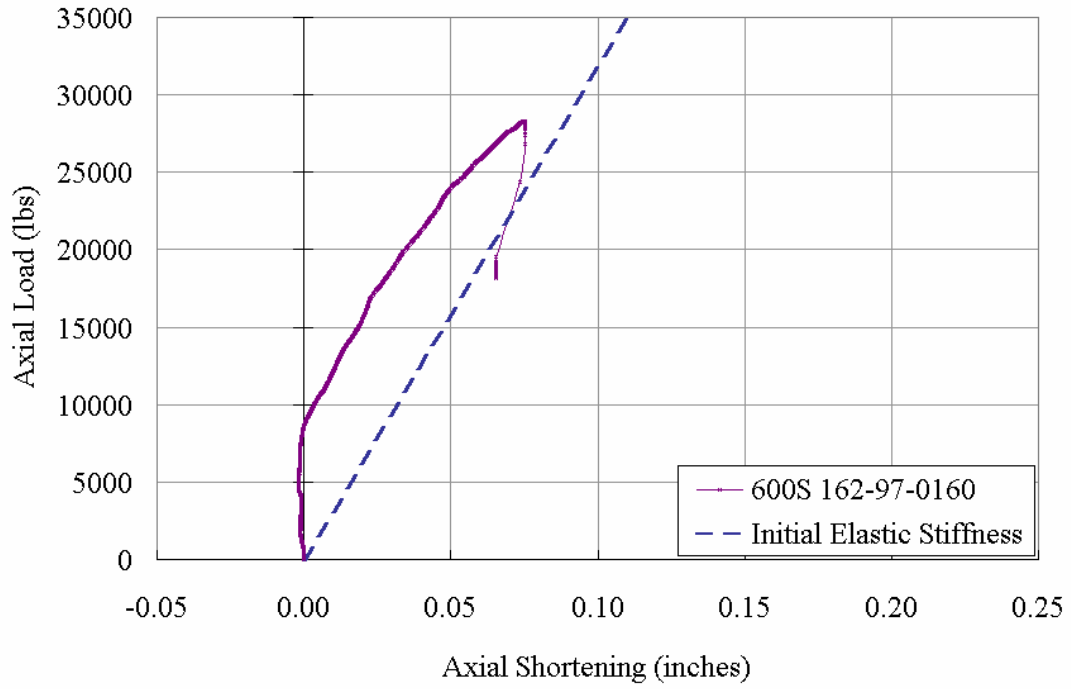


Figure A26.5 Plot of Axial Load vs. Axial Shortening

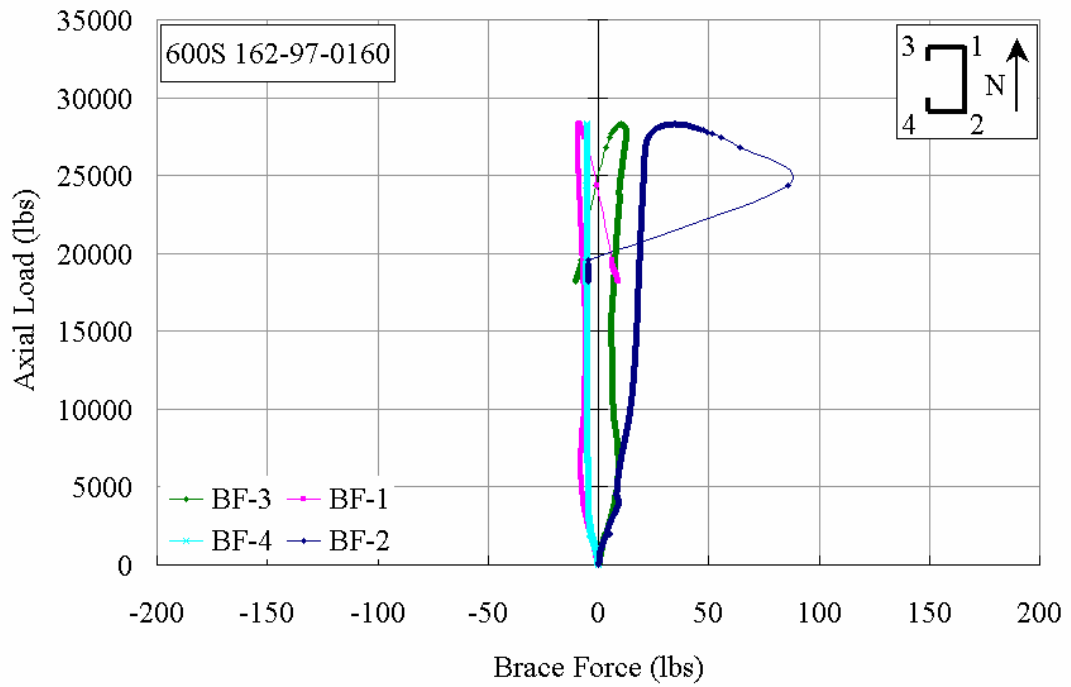


Figure A26.6 Plot of Axial Load vs. Brace Forces

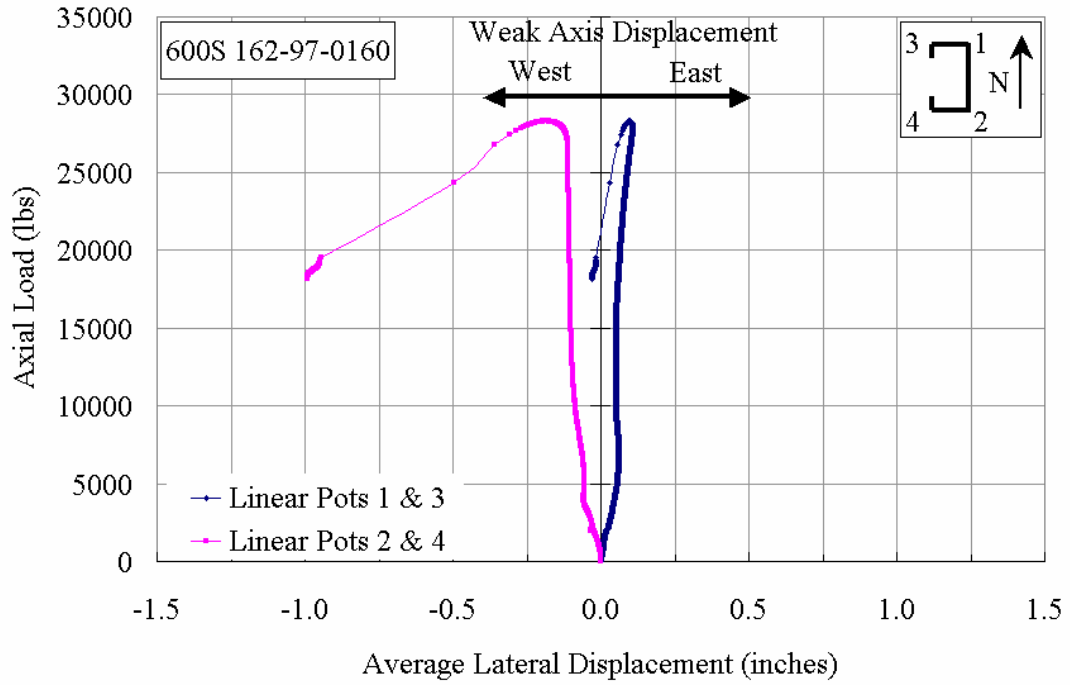


Figure A26.7 Plot of Axial Load vs. Weak Axis Displacement at Mid-Height

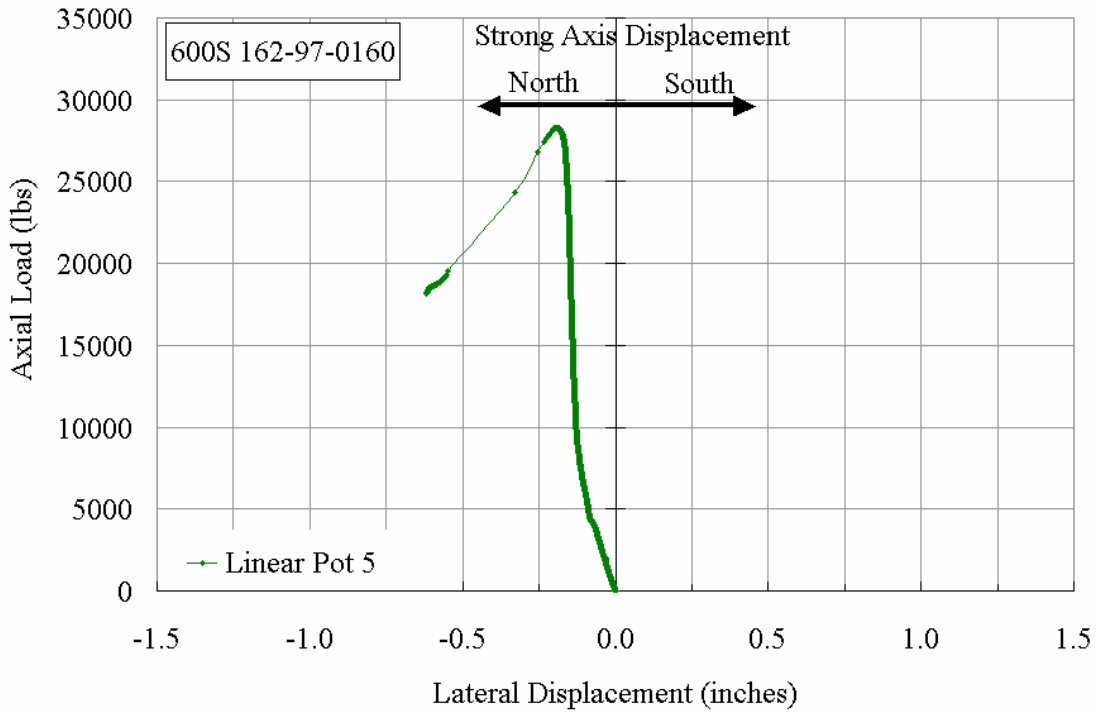


Figure A26.8 Plot of Axial Load vs. Strong Axis Displacement at Mid-Height

**600S162-97-500**

The stud 600S162-97-500 was braced with a total bracing stiffness of 1041 lbs/in. that was close to the ideal bracing requirement. The stud was loaded initially at the rate of about 20 lbs/sec up to 5000 lbs and then at about 125 lbs/sec till the maximum load was reached. Though this loading rate was higher than the rate at which the rest of the studs were tested, it still can be considered as being static loading as the behavior of the stud was not impacted by the loading rate. Figure A27.1 shows the overall view of the stud in the test frame. The plot of axial load versus axial shortening of the stud is shown in Figure A27.5 which closely follows the initial elastic stiffness line. Lateral displacement of the two flanges in the east-west direction was measured with pairs of linear potentiometers LP-1 & LP-3 and LP-2 and LP-4, attached to the north and south flanges, respectively, at mid-height of the stud. The strong axis lateral displacement in the north-south direction was measured by LP-5, which was attached to the south flange.

From the beginning of the test, the stud demonstrated flexural-torsional buckling about the weak axis as shown in Figure A27.7. The plot of the axial load versus brace forces, shown in Figure A27.6, also indicated that the diagonally opposite brace wires BF-1 and BF-4 were preventing the mid-height cross section from twisting and allowing torsional buckling to occur. However, the bracing was not stiff enough to ultimately prevent torsion of the section. The strong axis was also moving towards the south with increasing axial load, as shown in Figure A27.8.

As the axial load was increased up to 25000 lbs, the brace forces in BF-1 and BF-4 increased and measured 64.0 lbs and 20.0 lbs, respectively. The north flange had moved west by 0.15 inches and the south flange had moved east by 0.04 inches and the strong axis had moved south by 0.085 inches. At an axial load of about 28000 lbs a local buckle

developed close to a web punchout. Figure A27.2 shows the local buckle at an axial load of 29000 lbs. When the load reached about 30000 lbs, brace wire BF-1 broke and the stud almost instantaneously changed buckling modes from first mode flexural-torsional buckling to first mode flexural buckling. During this sudden process causing the brace-wire BF-2 also broke. Just before the wires snapped, the brace forces in BF-1 and BF-4 were 130 lbs and 6 lbs, respectively. The north and flange had moved west by 0.32 inches, whereas the south flange had moved back to initial position and the strong axis had moved south by 0.134 inches. The final buckled shape of the stud with the failed brace-wires is shown in Figure A27.3. However, the actual mode of failure would have been flexural-torsional buckling if the brace wires remained intact.



Figure A27.1 Overall View of Stud 600S162-97-500 in Riehle Machine Prior to Testing



Figure A27.2 Local buckling in the web of the Stud 600S162-97-500 at an Axial Load of 29000 lbs



Figure A27.3 Final Buckled Shape with the Broken Brace-wires of the Stud 600S162-97-500 at the Maximum Load

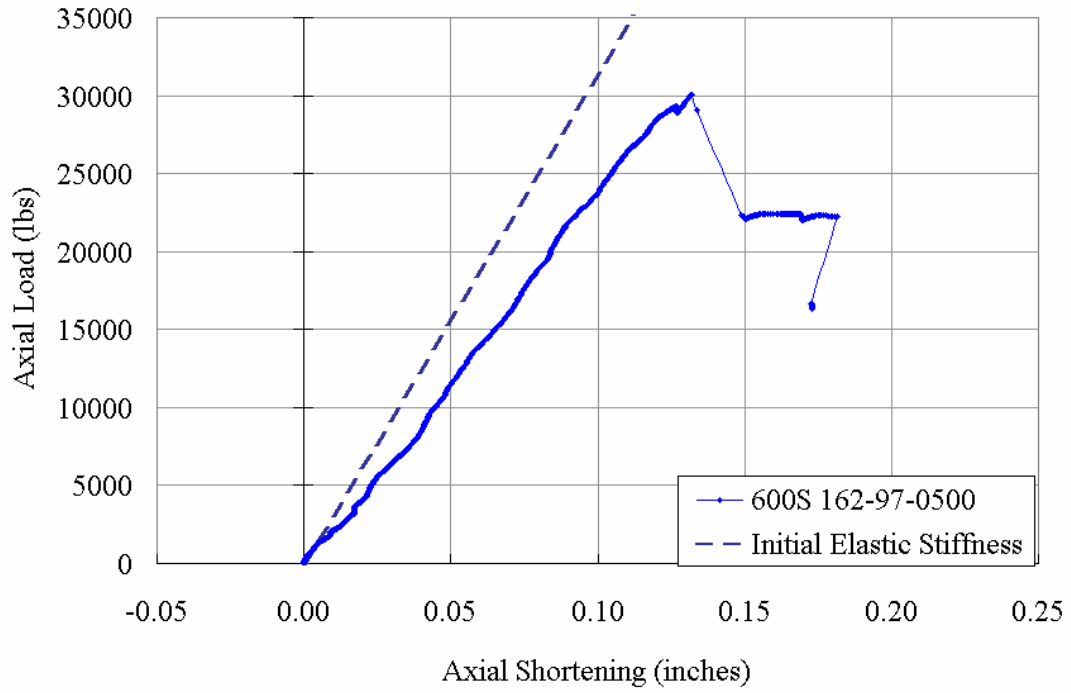


Figure A27.5 Plot of Axial Load vs. Axial Shortening

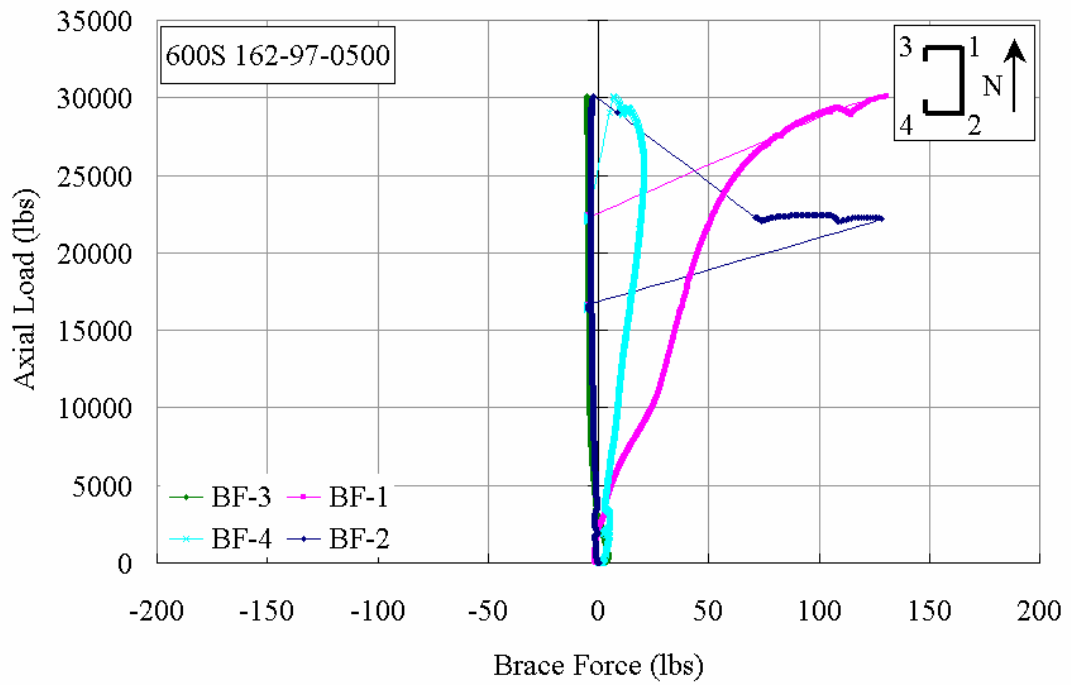


Figure A27.6 Plot of Axial Load vs. Brace Forces

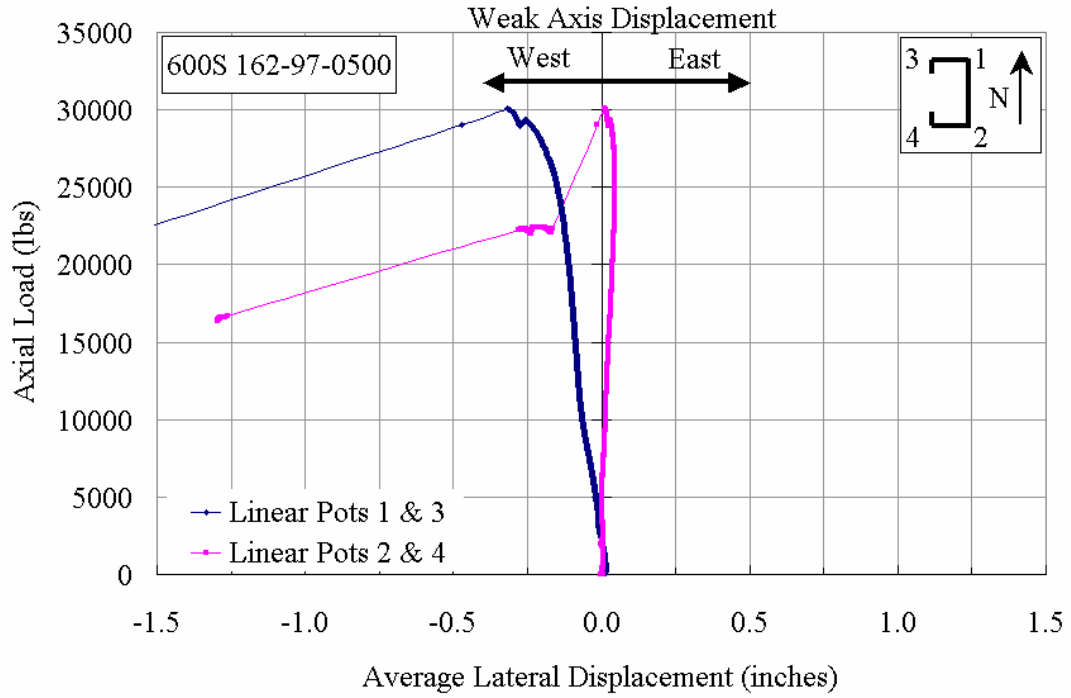


Figure A27.7 Plot of Axial Load vs. Weak Axis Displacement at Mid-Height

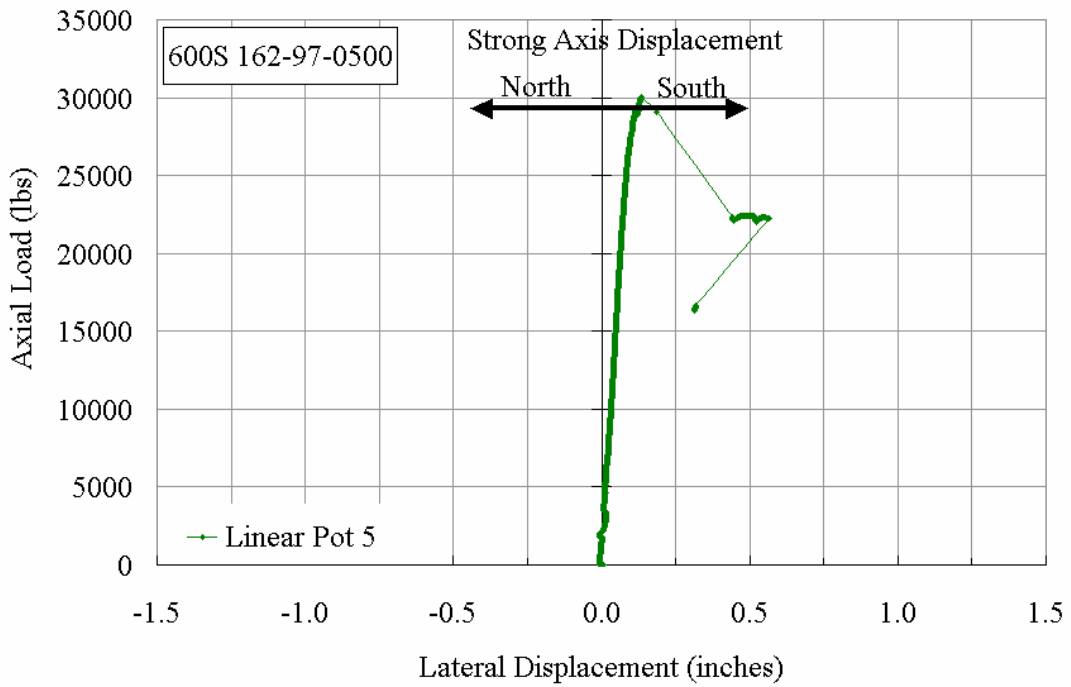


Figure A27.8 Plot of Axial Load vs. Strong Axis Displacement at Mid-Height

**600S162-97-1000**

The stud 600S162-97-1000 was braced with a total stiffness of 2069 lbs/in. and that was about 2.0 times the ideal bracing requirement. The stud was loaded initially at the rate of about 20 lbs/sec up to 5000 lbs and then at about 125 lbs/sec till it reached the maximum load. Though this loading rate was higher than the rate at which rest of the studs were tested, it still can be considered static loading as it did not affect the behavior of the stud. Figure A28.1 shows the overall view of the stud in the test frame. The plot of axial load versus axial shortening is shown in Figure A28.5, which closely the initial elastic stiffness line. Lateral displacement of the two flanges in the east-west direction was measured with pairs of linear potentiometers LP-1 & LP-3 and LP-2 and LP-4, attached to the north and south flanges, respectively, at mid-height of the stud. The strong axis lateral displacement in the north-south direction was measured by LP-5, which was attached to the south flange.

From zero to an axial load of 2250 lbs, the behavior of the stud showed first mode flexural buckling about the weak axis as can be observed by the increasing brace forces in BF-1 and BF-2 given in Figure A28.6, and the eastward displacement of the flanges in Figure A28.7. The strong axis movement, as shown in Figure A28.8, was negligible at this load level. With further increase in the applied load, the stud started to buckle in first mode flexural-torsion and the flanges began to exhibit differential displacement towards the west. Up to 7500 lbs, the brace forces in BF-1 and BF-2 measured 39.0 lbs and 11.0 lbs, respectively and at 25000 lbs they measured 88 lbs and 20 lbs, respectively. At the maximum load of about 28550 lbs, the brace forces in BF-1 and BF-2 measured 133 lbs and 41 lbs, and the north and south flanges had moved west by 0.39 inches and 0.05 inches, respectively, while the strong axis had moved south by 0.15 inches.

Figure A28.3 shows the local buckle developing in the web at the maximum load causing the load carrying capacity of the stud to decrease. The force in the brace BF-1 then began to decrease while the force in brace BF-2 continued to increase. The north flange displacement to the west increased rapidly as the stud started to shed load. The final observed failure was identified as first mode flexural-torsional buckling.



Figure A28.1 Overall View of Stud 600S162-97-1000 in the Riehle Machine Prior to Testing



Figure A28.2 Flexural-Torsional Buckling of the Stud 600S162-97-1000 at an Axial Load of 28500 lbs

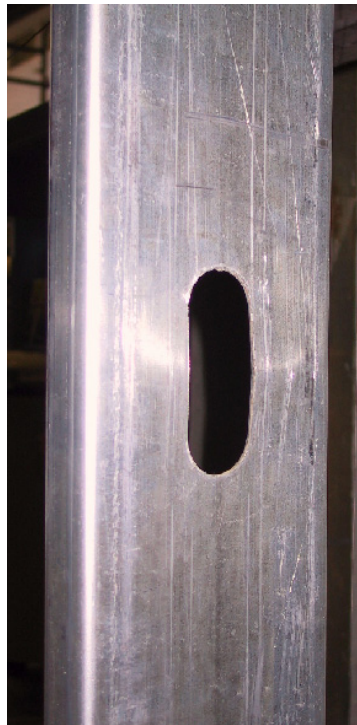


Figure A28.3 Local buckling of the Stud 600S162-97-1000 at the Maximum Load

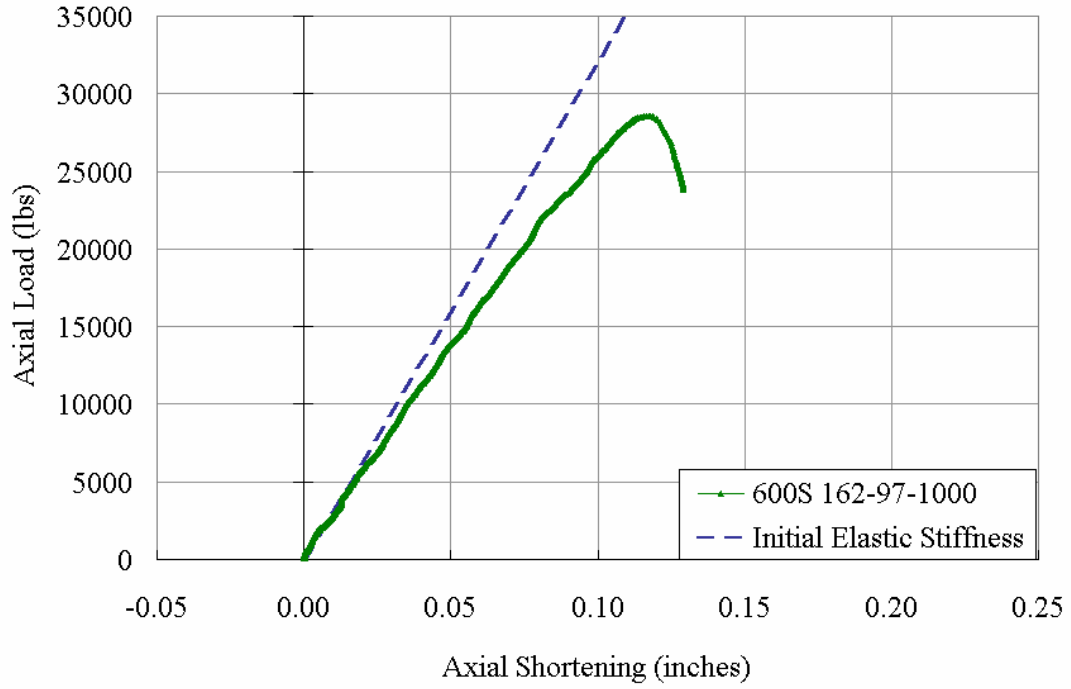


Figure A28.5 Plot of Axial Load vs. Axial Shortening

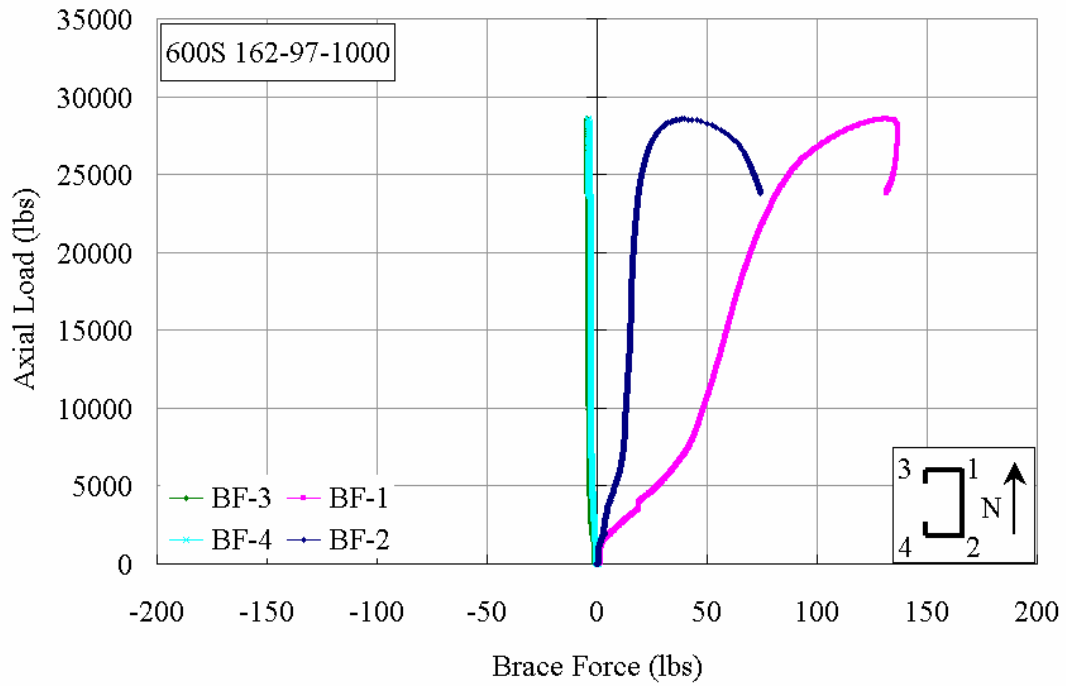


Figure A28.6 Plot of Axial Load vs. Brace Forces

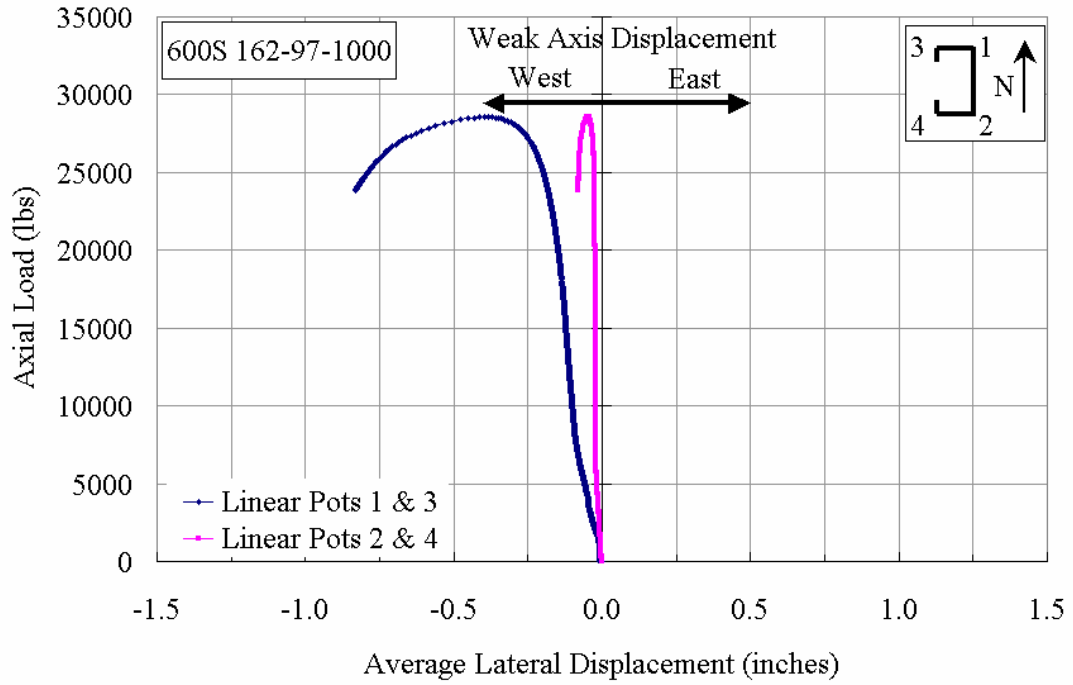


Figure A28.7 Plot of Axial Load vs. Weak Axis Displacement at Mid-Height

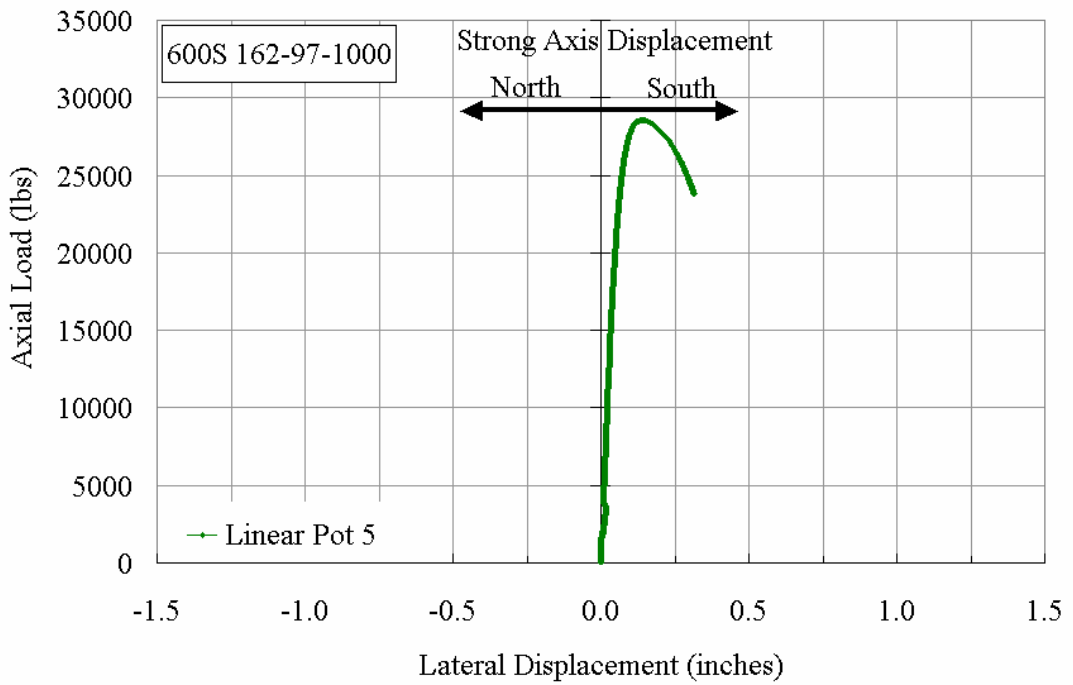


Figure A28.8 Plot of Axial Load vs. Strong Axis Displacement at Mid-Height

**600S162-97-1500**

The stud 600S162-97-1500 was braced with a total bracing stiffness of 3357 lbs/in. and that was about 3.4 times the ideal bracing requirement. The stud was loaded initially at the rate of about 20 lbs/sec up to 5000 lbs and then at about 125 lbs/sec till the maximum load. Though this loading rate was higher than the rate at which rest of the studs were tested, it still can be considered as static loading as it does not affect the behavior of the stud. Figure A29.1 shows the overall view of the stud in the test frame. The plot of axial load versus axial shortening is shown in Figure A29.5, which closely follows the initial elastic stiffness line, once the loading exceeded 10,000 lbs. Five linear potentiometers were used to record the mid-height lateral displacements, two on the north flange (LP-1 & LP-3) and two on the south flange (LP-2 & LP-4) for weak axis displacement, and one on the south flange (LP-5) for strong axis displacement. The axial shortening of the stud was measured by linear potentiometer LP-6 attached at top and bottom of the north flange.

From zero to an axial load of 7500 lbs, the behavior of the stud showed first mode flexural-torsional buckling. From Figures A29.7 and A29.8 it can be observed that there is lateral displacement of both the weak axis and the strong axis. At 7500 lbs, the brace forces in BF-1 and BF-2 measured 9.0 lbs and 72.0 lbs, respectively. With further increase in the applied load, the stud started to buckle in first mode torsional buckling, as the lateral displacement of the weak axis indicated a slight differential movement towards the west.

At 25000 lbs, the brace forces in BF-1 and BF-2 measured 18 lbs and 98 lbs, respectively. At the maximum load of about 29500 lbs, the brace forces in BF-1 and BF-2 measured 30 lbs and 125 lbs, respectively, while the north and south flanges had moved

west by 0.02 inches and 0.25 inches, respectively, and the strong axis had moved south by 0.17 inches.

As the maximum load was being achieved, a local buckle developed at a punchout in the bottom-half of the stud as can be seen in Figure A29.3. Afterwards, the stud began to unload as the brace force BF-1 continued to increase while the force in the brace BF-2 remained constant. Overall first mode torsional buckling was observed as the stud continued to twist as seen in the rapid westward displacement of the south flange while the north flange movement was minimal.



Figure A29.1 Overall View of Stud 600S162-97-1500 in Riehle Machine Prior to Testing



Figure A29.2 Torsional Buckling of the Stud 600S162-97-1500 at an Axial Load of 29000 lbs



Figure A29.3 Local buckling of the Stud 600S162-97-1500 at the Maximum Load of 29500 lbs

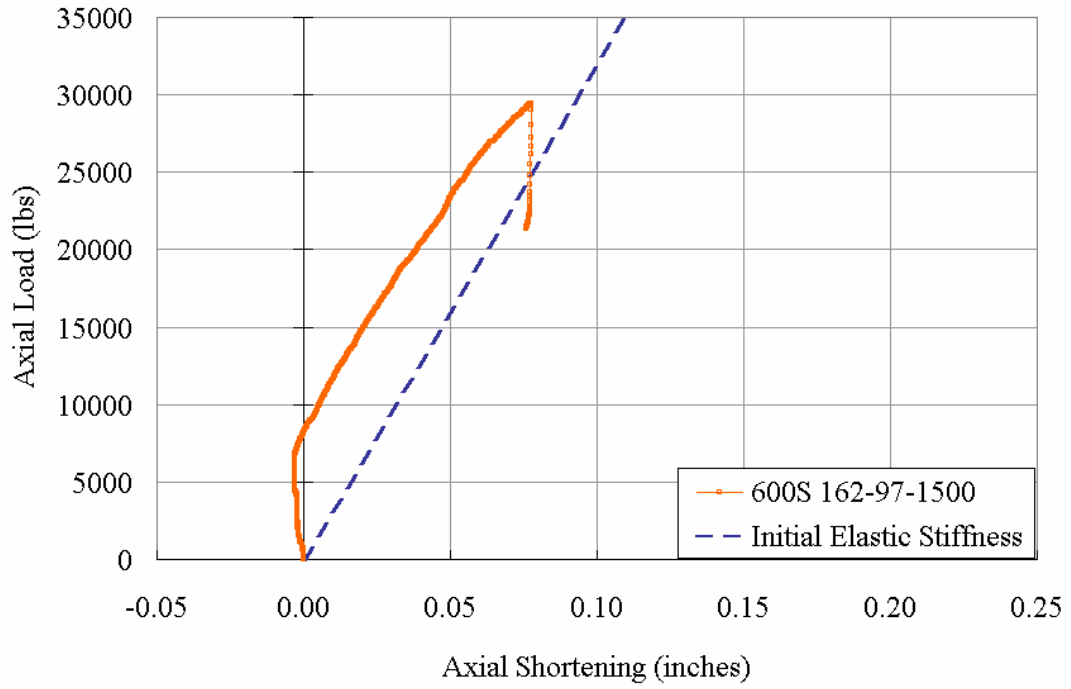


Figure A29.5 Plot of Axial Load vs. Axial Shortening

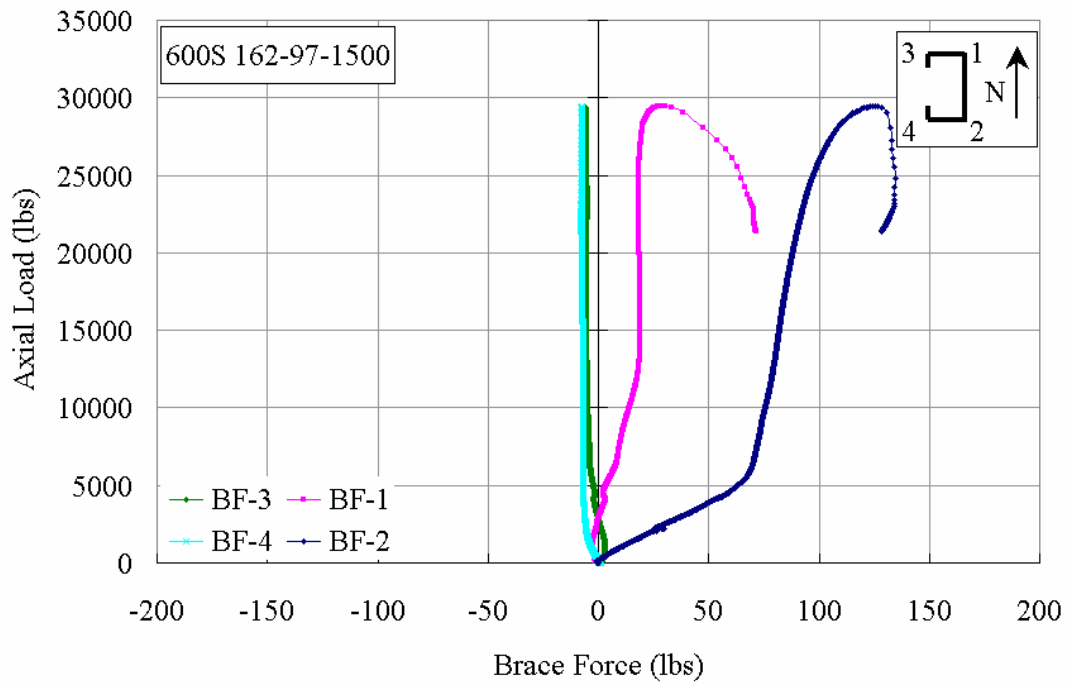


Figure A29.6 Plot of Axial Load vs. Brace Forces

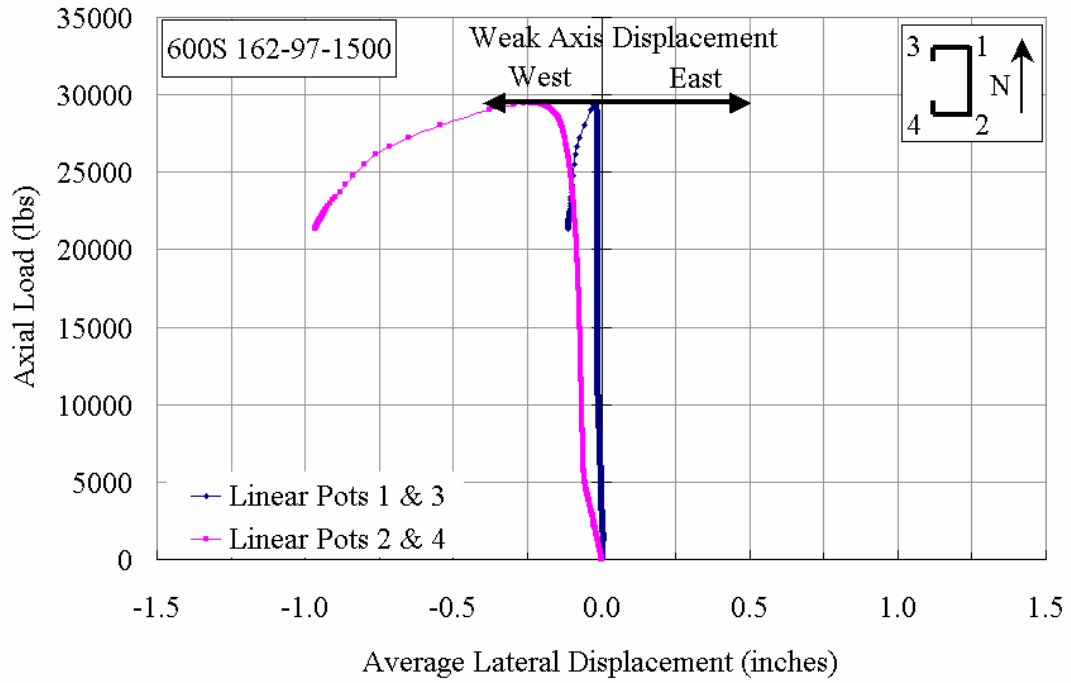


Figure A29.7 Plot of Axial Load vs. Weak Axis Displacement at Mid-Height

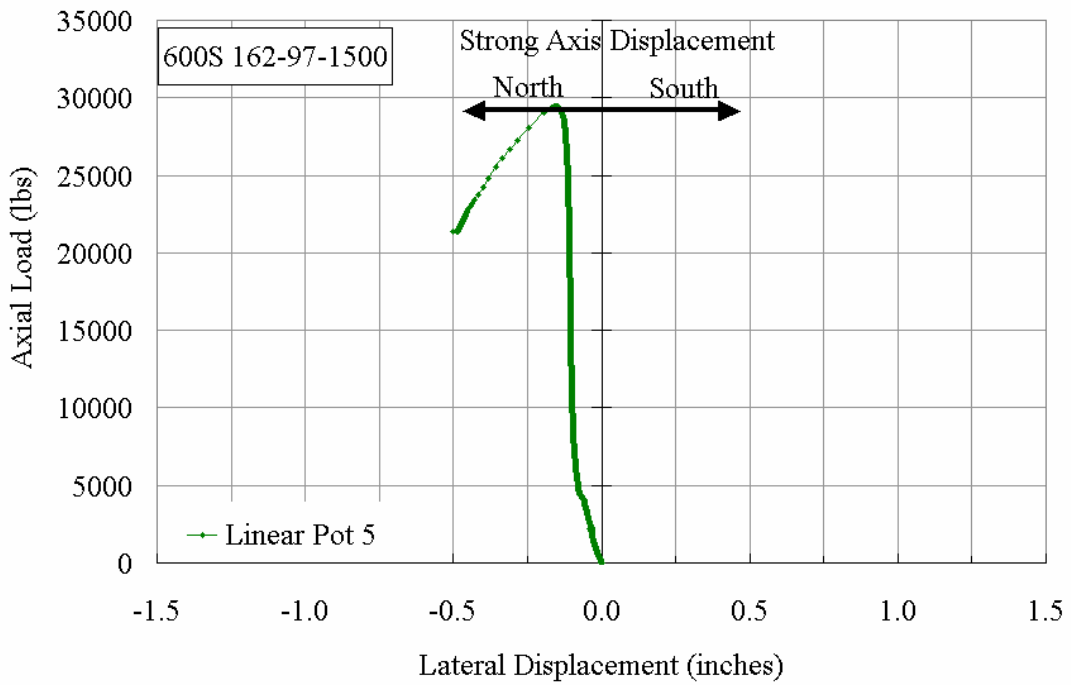


Figure A29.8 Plot of Axial Load vs. Strong Axis Displacement at Mid-Height

**800S162-43-000**

The cee stud specimen 800S162-43-000 was tested without any lateral bracing, so that it serves as a benchmark for comparison with other braced cee stud specimens. Figure A30.1 shows the stud in the Riehle Machine prior to the test. Figure A30.5 shows the plot of axial load versus axial shortening of the stud. The mid-height weak axis lateral displacement was measured by pairs of linear potentiometers LP-1 & LP-3 and LP-2 & LP-4, attached to the north and south flanges respectively, and the strong axis lateral displacement was measured by LP-5. The axial deformation was measured on the north flange by LP-6.

The slope of the axial load versus axial shortening curve of the stud traced the initial elastic stiffness line as shown in Figure A30.5 up to 3865 lbs, when the stud began to exhibit first mode flexural buckling. Initially up to an axial load of 1000 lbs, the weak axis flexural displacement of both the flanges was towards the east by 0.0129 inches, but with increasing axial load, the north flange started moving to the west as the south flange continued moving to the east. At an axial load of 1700 lbs the movement of the south flange to the east reached a maximum value of 0.0696 inches. Starting at about 1000 lbs, elastic buckling waves were seen in the web with amplitudes that continued to increase up to an axial load of 4000 lbs. When the axial load reached about 4000 lbs, distortional buckling waves were first observed in the flanges as shown in Figure A30.3.

The plot of axial load versus the mid-height lateral displacement of the strong axis is shown in Figure A30.7. The figure indicates that there was no strong axis movement up to an axial load of approximately 3850 lbs. Between this load level and 4500 lbs of axial load, the elastic buckling waves in the web and flanges caused the stud to lose a

portion of its axial stiffness. Appreciable strong axis flexural movement ensued at about this load level and continued up to the maximum load carrying capacity of the stud.

At about 4500 lbs, the distortional buckling of the stud at mid-height increased in intensity to cause the failure of the stud at 4591 lbs. The weak axis lateral displacement measured 0.42 and 0.88 inches to the west on the north and south flanges, respectively, while the strong axis had displaced to the north by about 0.15 inches. The final failure of the stud was predominantly first mode flexural buckling though distortional buckling was also present.



Figure A30.1 Overall View of the Stud 800S162-43-000 in the Riehle Testing Machine, prior to the Test



Figure A30.2 Elastic buckling waves in the Web of Stud 800S162-43-000 at an Axial Load 4000 lbs



Figure A30.3 Distortional Buckling in the Stud 800S162-43-000 at an Axial Load at 4000 lbs



(a) Overall view



(b) Close up

Figure A30.4 Final View of Stud 800S162-43-000 at the Ultimate load

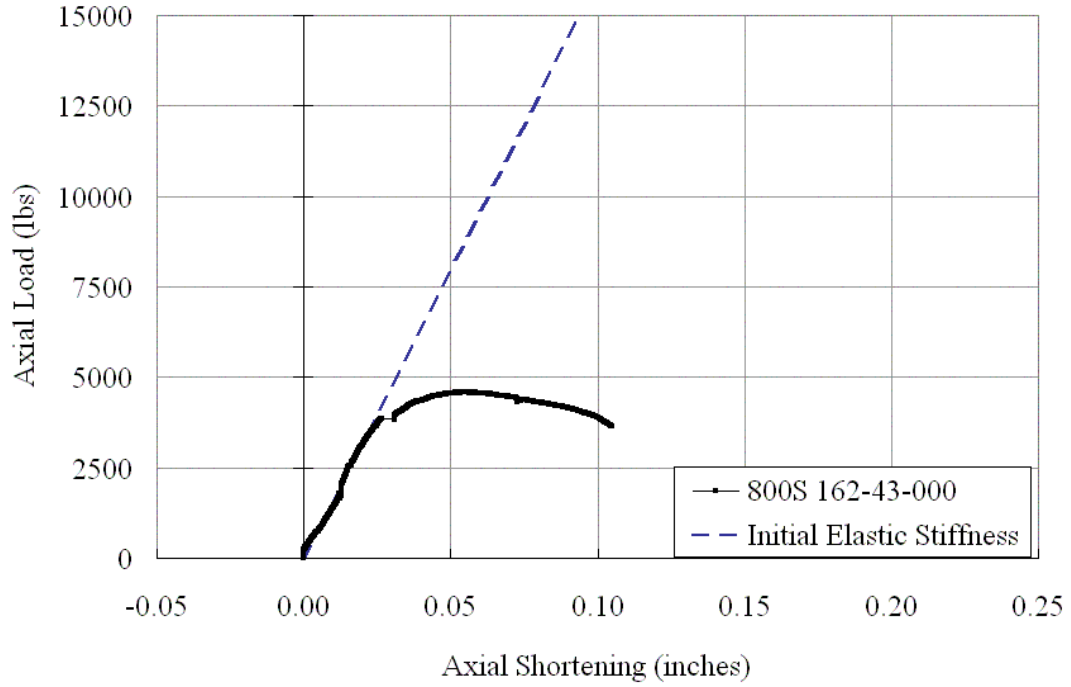


Figure A30.5 Plot of Axial Load vs. Axial Shortening

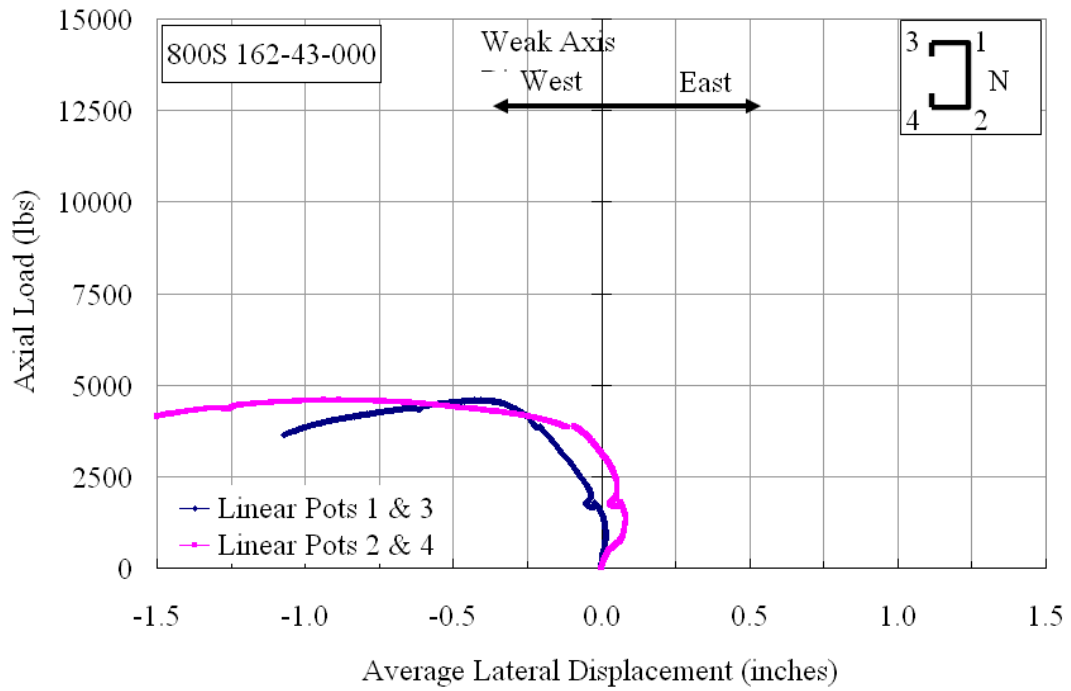


Figure A30.6 Plot of Axial Load vs. Weak Axis Displacement at Mid-Height

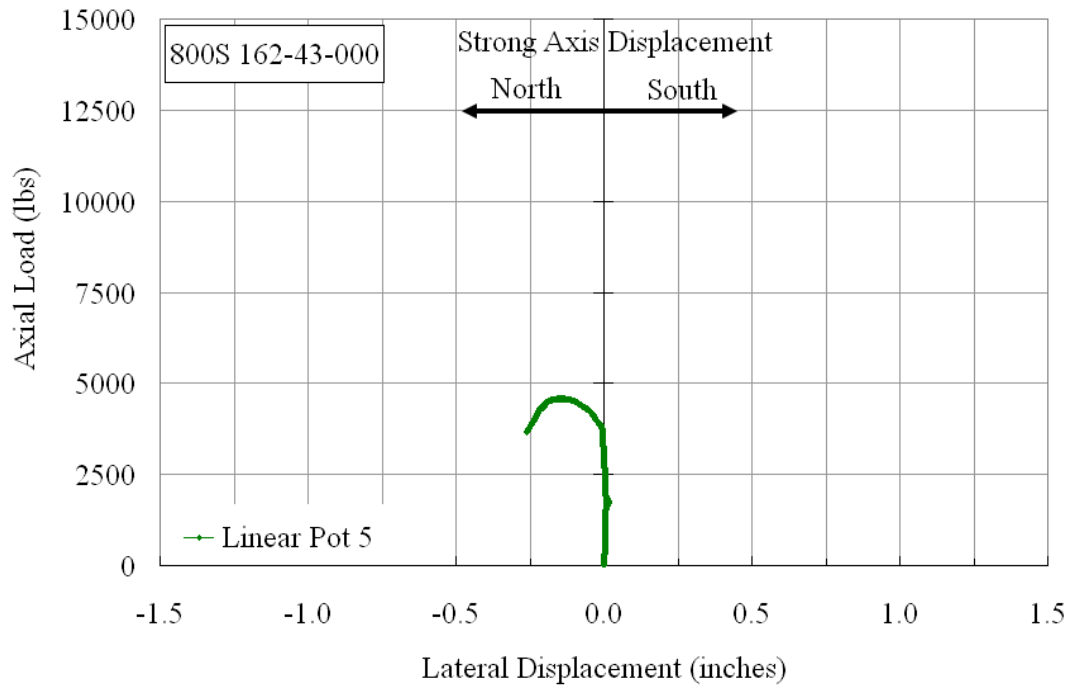


Figure A30.7 Plot of Axial Load vs. Strong Axis Displacement at Mid-Height

**800S162-43-075**

The cee stud specimen 800S162-43-075 was braced with a total bracing stiffness of 149 lbs/in. that was equal to 0.6 times the ideal bracing requirement. Figure A31.1 shows the stud in the Riehle Machine prior to the test. Figure A31.5 shows the plot of axial load versus axial shortening of the stud. The mid-height weak axis lateral displacement was measured by pairs of linear potentiometers LP-1 & LP-3 and LP-2 & LP-4, attached to the north and south flanges, respectively, and the strong axis lateral displacement was measured by LP-5. The axial shortening was measured by LP-6 attached to the north flange.

Initially, the stud seemed to be buckling in first mode flexure up to an axial load of approximately 1000 lbs. Though the corresponding lateral displacements of the north and south flanges were extremely small, 0.0017 and 0.0192 in. towards the east, respectively, and the strong axis displacement was 0.0174 in. towards the north. The brace forces in BF-3 and BF-4 measured approximately 1.2 lbs. At about this same load level, the weak axis movement of the stud started to change direction as the mid-height cross-section began to move in a westward direction. This change in direction caused the brace forces in BF-3 and BF-4 to drop and when they returned to zero at an axial load of approximately 1450 lbs, the other two braces, namely BF-1 and BF-2, started to pick up the brace forces.

Elastic buckling waves in the web were first observed at an axial load of approximately 400 lbs and were distinctly visible at an axial load of 4000 lbs as shown in Figure A31.2. At this same load, a local buckle began to develop at approximately 2'-0" from the top of the stud, on the south flange-lip junction as shown in Figure A31.3. The formation of this local buckle caused the cross-section that elevation to loose a

portion of its axial stiffness, causing the south flange to behave as an unstiffened element, which in turn allowed distortional buckling to occur in the flanges. At this load level, the measured brace forces in BF-1 and BF-2 were 11.2 and 6.3 lbs, respectively.

Above this load, the stud reached an initial peak capacity of 4211 lbs at a corresponding axial shortening of 0.038 inches with the two effective braces still preventing the stud from global buckling. Soon thereafter, the brace forces in both BF-1 and BF-2 started to drop. At this initial peak load, the measured brace forces were 0.87 and 1.87 lbs, respectively. From Figure A31.7 it can be observed that the mid-height cross-section started to move to the east after reaching this initial peak load. The stud then reached its ultimate axial load of 4306 lbs with a corresponding axial shortening of 0.080 inches. Between the 4211 lbs and 4306 lbs of axial load, the brace forces in BF-1 and BF-2 dropped to 0.0 lbs while the brace forces in BF-3 and BF-4 started to increase.

From the beginning of the test the stud was buckling about the strong axis until it reached the ultimate capacity, at which the measured lateral displacement was 0.036 in towards North. The observed first mode flexural buckling was considered to be the failure mode of the stud at the ultimate load of 4306 lbs. The final deformed shape of the stud is shown in Figure A31.4 (a) and (b), showing the close-up of the local and distortional buckling and the overall view of the stud, respectively.



Figure A31.1 Overall View of the Stud 800S162-43-075 in the Riehle Testing Machine, prior to the Test



Figure A31.2 Elastic buckling waves in the Web of Stud 800S162-43-075 at an Axial Load



Figure A31.3 Local and Distortional Buckling in the top-half of the Stud 800S162-43-075 at an Axial Load of 4000 lbs



(a) Close-up of Local Buckle (b) Looking North  
 Figure A31.4 Final View of the Stud 800S162-43-075 at the Maximum Load

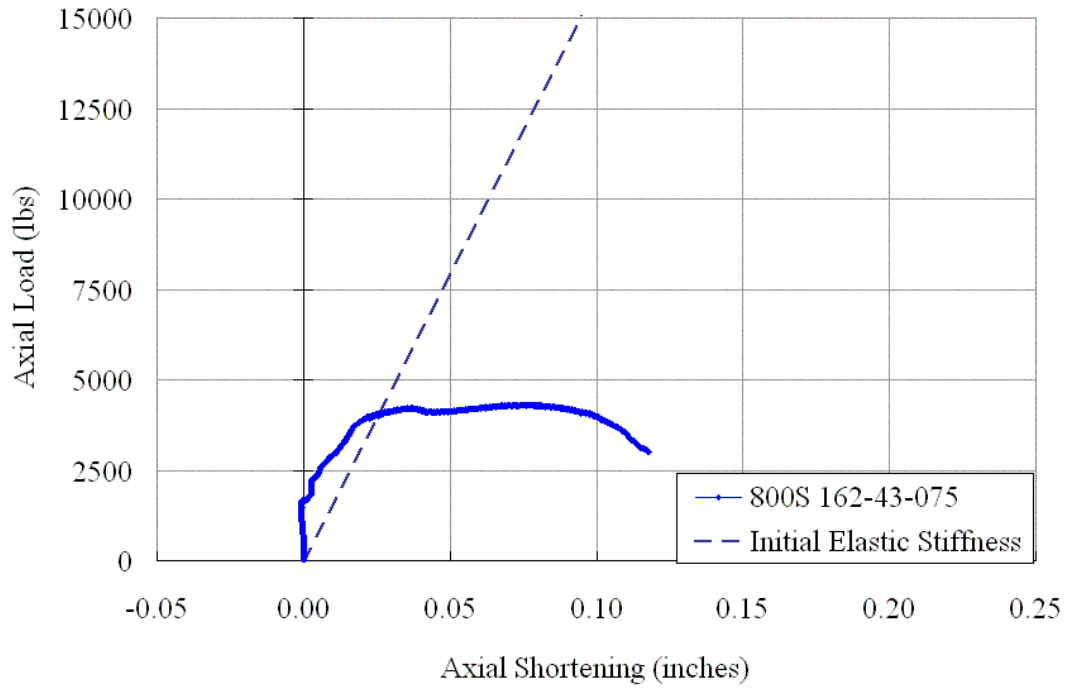


Figure A31.5 Plot of Axial Load vs. Axial Shortening

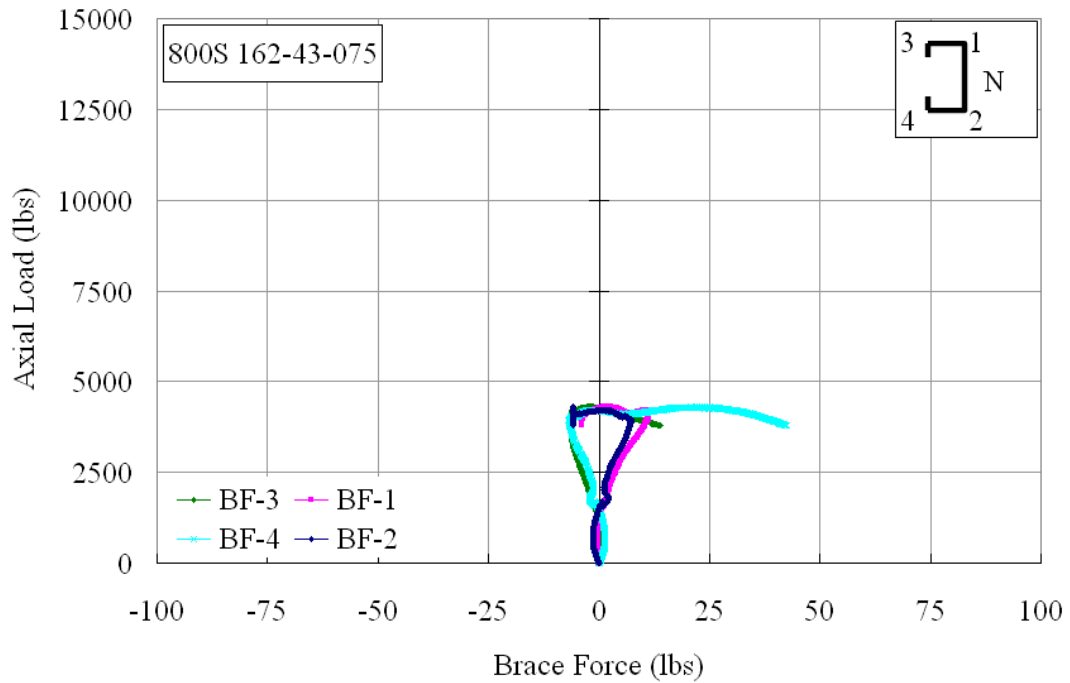


Figure A31.6 Plot of Axial Load vs. Brace Forces

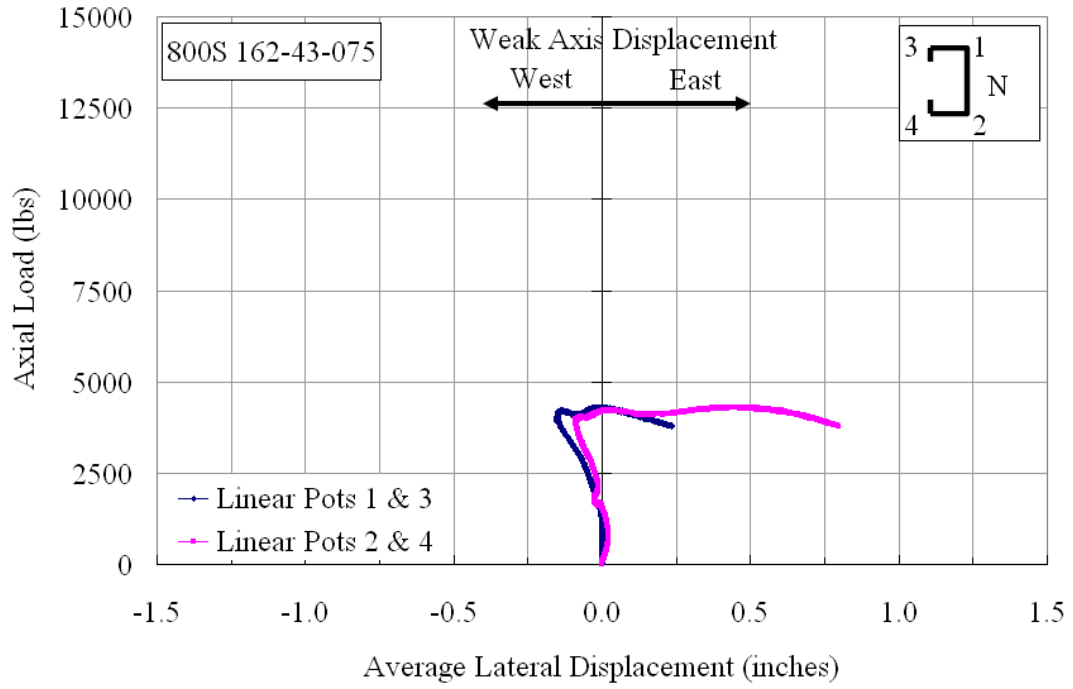


Figure A31.7 Plot of Axial Load vs. Weak Axis Displacement at Mid-Height

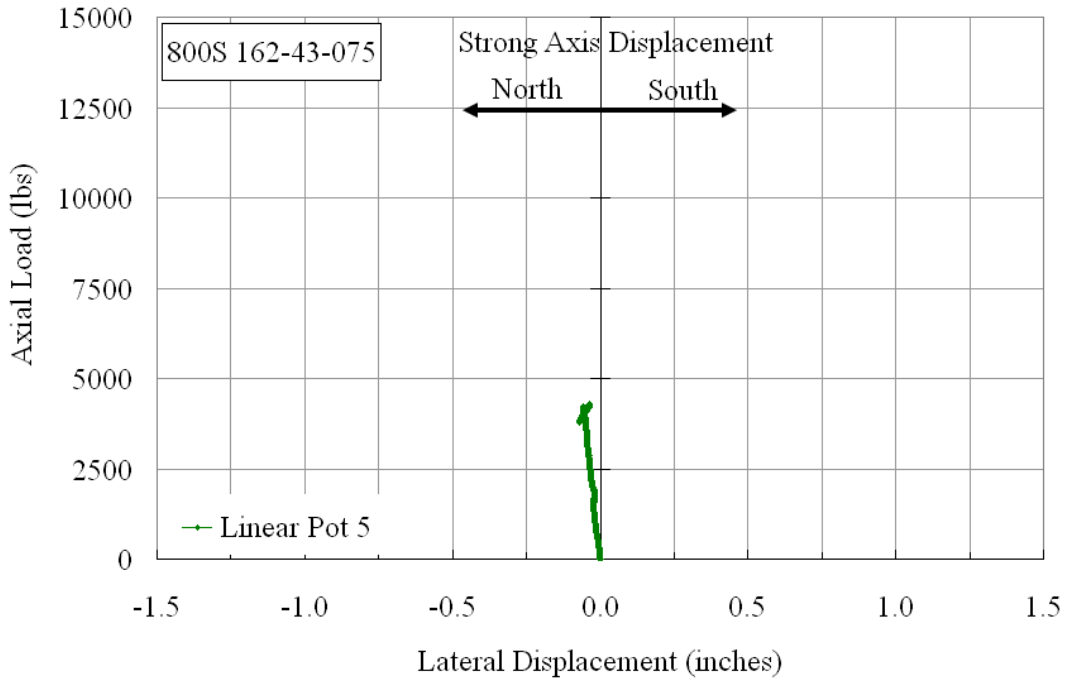


Figure A31.8 Plot of Axial Load vs. Strong Axis Displacement at Mid-Height

**800S162-43-150**

The cee stud specimen 800S162-43-150 was braced with a total bracing stiffness of 299 lbs/in. that was equal to about 1.2 times the ideal bracing requirement. Figure A32.1 shows the stud in the Riehle Machine prior to the test. Figure A32.5 shows the plot of axial load versus axial shortening of the stud. The mid-height weak axis lateral displacement was measured by pairs of linear potentiometers LP-1 & LP-3 and LP-2 & LP-4, attached to the north and south flanges respectively, and the strong axis lateral displacement was measured by LP-5. The axial shortening was measured on the north flange by LP-6.

Initially up to 2500 lbs, the slope of the axial load versus axial shortening curve of the stud followed the initial elastic stiffness line, as shown in Figure A32.5. The brace forces in BF-1 and BF-4 were gradually changing, and at 1000 lbs, they measured 0.4 and 3.0 lbs, respectively. At this same load level, elastic buckling waves were first observed in the web. Figure A32.2(a) shows these elastic buckling waves at an axial load of about 3500 lbs when the axial shortening was 0.029 inches and the weak axis and strong axis displacements were negligible as shown in Figures A32.7 and A32.8, respectively. The amplitude of the elastic buckling waves continued to increase with increase in the axial load as can be seen in Figure A32.2(b). The brace forces at this load level did not exhibit any appreciable change as BF-1 and BF-4 measured 0.0 lbs.

Distortional buckling in the flanges was first seen at 4300 lbs (see Figure A32.3(a)). When the axial load reached 5000 lbs, the distortional buckling was so severe that the effect of the stiffening of the lips and the flanges started to diminish and the axial load reached a maximum value of 5333 lbs. Figure A32.3(b) clearly shows the distortional buckling in the flanges at an axial load of 5000 lbs.

From 4700 lbs to an axial load of about 5000 lbs, the cee stud exhibited second mode flexural buckling with second mode torsional buckling. Beyond this load, the distortional buckling governed most of the deformation the stud. The failure of the stud was hence identified as due to distortional buckling. At this ultimate load, there were two local buckles in the flanges which rendered the flanges unstiffened as shown in Figure A32.4.



Figure A32.1 Overall View of the Stud 800S162-43-150 in the Riehle Testing Machine, prior to the Test



(a) at 3500 lbs



(b) at 4000 lbs

Figure A32.2 Elastic buckling waves in the Web of Stud 800S162-43-150 at various Loads



(a) at 4300 lbs



(b) at 5000 lbs

Figure A32.3 Distortional Buckling in the Stud 800S162-43-150 at various Axial Loads



Figure A32.4 Final View of bottom-half of the Stud 800S162-43-150 at the Maximum Load

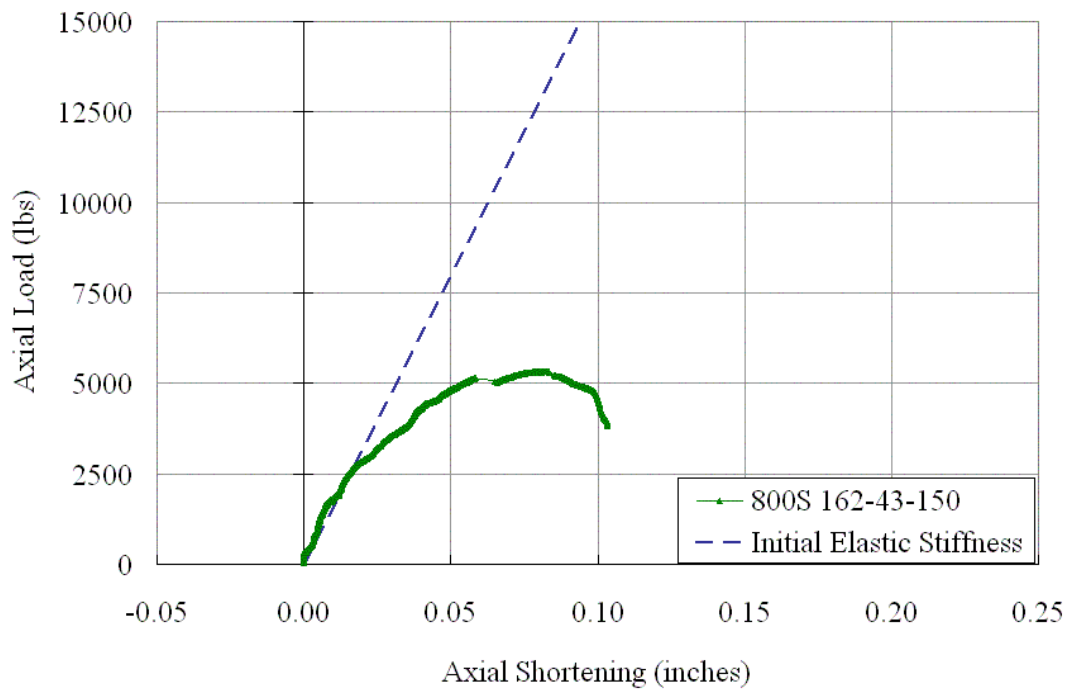


Figure A32.5 Plot of Axial Load vs. Axial Shortening

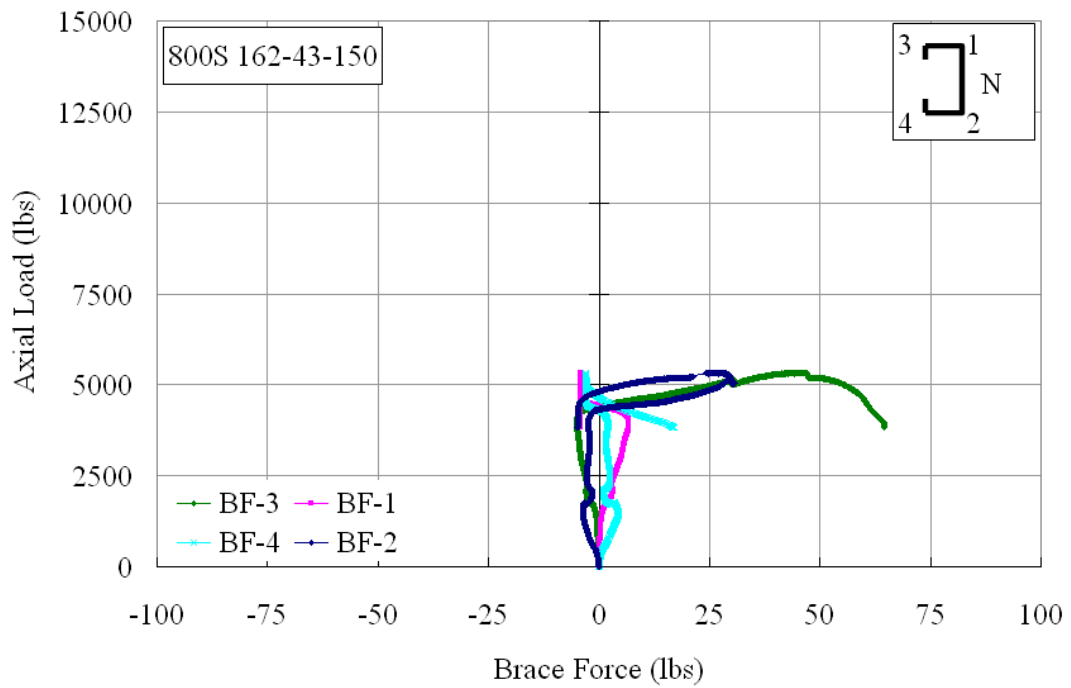


Figure A32.6 Plot of Axial Load vs. Brace Forces

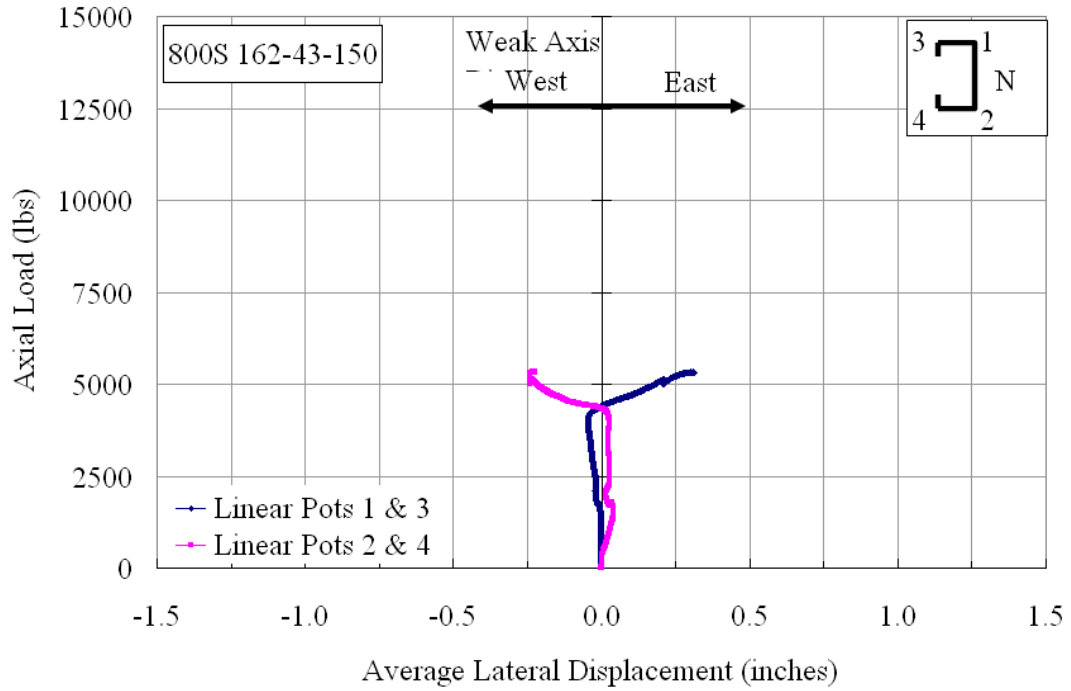


Figure A32.7 Plot of Axial Load vs. Weak Axis Displacement at Mid-Height

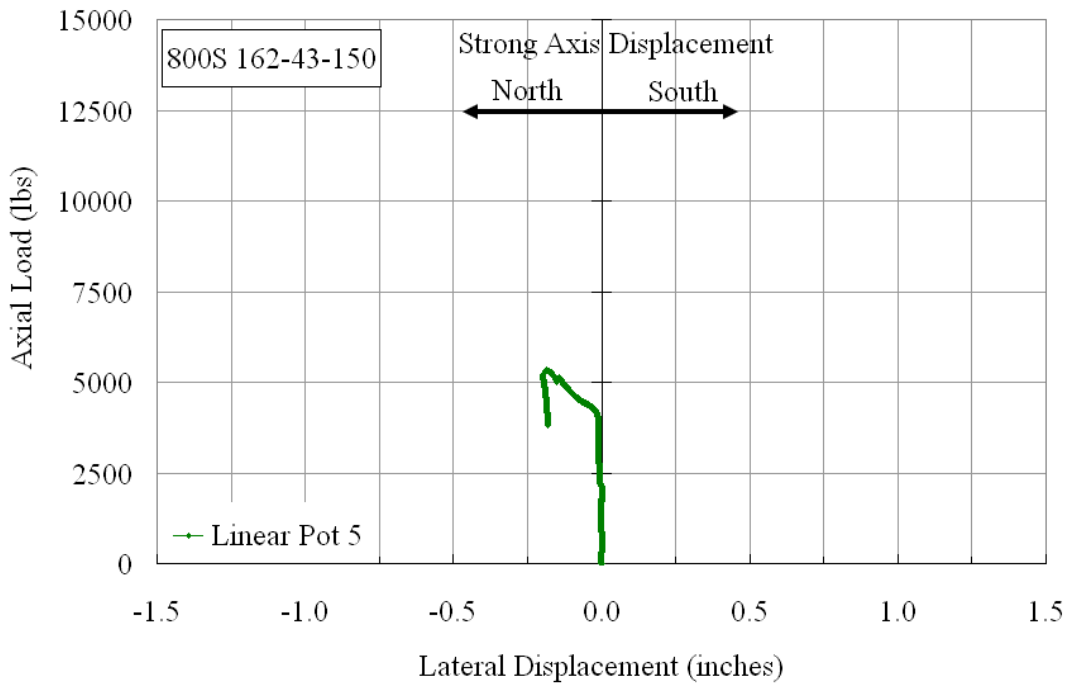


Figure A32.8 Plot of Axial Load vs. Strong Axis Displacement at Mid-Height

**800S162-43-300**

The cee stud specimen 800S162-43-300 was braced with a total bracing stiffness of 602 lbs/in. that was equal to about 2.4 times the ideal bracing requirement. Figure A33.1 shows the stud in the Riehle Machine prior to the test. Figure A33.5 shows the plot of axial load versus axial shortening of the stud. The mid-height weak axis lateral displacement was measured by linear potentiometers LP-1 & LP-3 and LP-2 & LP-4 (see Figure A33.7), attached to the north and south flanges respectively, and the strong axis lateral displacement was measured by LP-5. The axial shortening was measured by LP-6 attached on the north flange.

Initially up to an axial load of 2000 lbs, the slope of the axial load versus axial shortening curve of the stud deviated from the initial elastic stiffness line (see Figure A33.5). This was due to strong axis movement of the stud (see Figure A33.8). The brace forces in BF-3 and BF-4 were gradually increasing up to an axial load of about 1000 lbs, measuring 1.6 and 3.1 lbs, respectively. When the load reached 2000 lbs, elastic buckling waves were first observed in the web. Figure A33.2(a) shows these elastic buckling waves at an axial load of about 3500 lbs, when the axial shortening was 0.029 inches the strong axis had displaced to the north by 0.065 inches, and the weak axis displacement measured 0.033 and 0.135 inches on the north and south flanges, respectively. The amplitude of the elastic buckling waves continued to increase with increase in the axial load.

Weak axis movement of the stud, initially to the east, reversed direction at about 1000 lbs, when it was noted that the mid-height cross-section was displacing to the west. The corresponding brace forces in BF-3 and BF-4 also started to decrease. At an axial load of about 1500 lbs, all the brace forces measured approximately zero. As the

westward movement of mid-height cross-section of the stud continued with increasing load, the brace forces in BF-1 and BF-2 started to increase, and at about 4000 lbs, BF-1 and BF-2 measured 8.5 and 34 lbs, respectively. The weak axis displacement at this load level measured 0.16 and 0.034 inches to the west on the north and south flanges, respectively. Just beyond this load level, the weak axis stopped displacing laterally at mid-height, however the strong axis continued to displace north. The brace forces in BF-1 and BF-2 also started to decrease.

The brace force in BF-1 which had started to drop at about 4000 lbs of axial load, again began to gradually increase up to the ultimate load. Figure A33.2(b) shows an overall view of the stud at an axial load of 6000 lbs, and shows the elastic buckling waves that were present in the web.

With further increase in the axial load, second mode flexural buckling became clearly visible and Figure A33.3 shows the shape of the stud at an axial load of 6000 lbs. At this load level, the brace forces in BF-1 and BF-2 measured 10 and 15 lbs, respectively. The weak axis displacements on the north and south flanges were 0.05 and 0.10 inches to the west, respectively, and the strong axis displacement was 0.08 inches to the north.

The axial load reached a maximum value of 6213 lbs, when a local buckle developed in the web that led to the stud's failure. Even though this local buckle was present, the primary failure mode of the stud is considered to be second mode flexural buckling as shown in Figure A33.4.



Figure A33.1 Overall View of the Stud 800S162-43-300 in the Riehle Testing Machine, prior to the Test



(a) of 3500 lbs (b) of 6000 lbs  
Figure A33.2 Elastic buckling waves in the Web of Stud 800S162-43-300 at various Loads



Figure A33.3 Second Mode Flexural Buckling of the Stud 800S162-43-300 at an Axial Load 6000 lbs (Looking North)



(a) Looking North (b) Looking East  
Figure A33.4 Final View of Stud 800S162-43-150 at the Ultimate Load

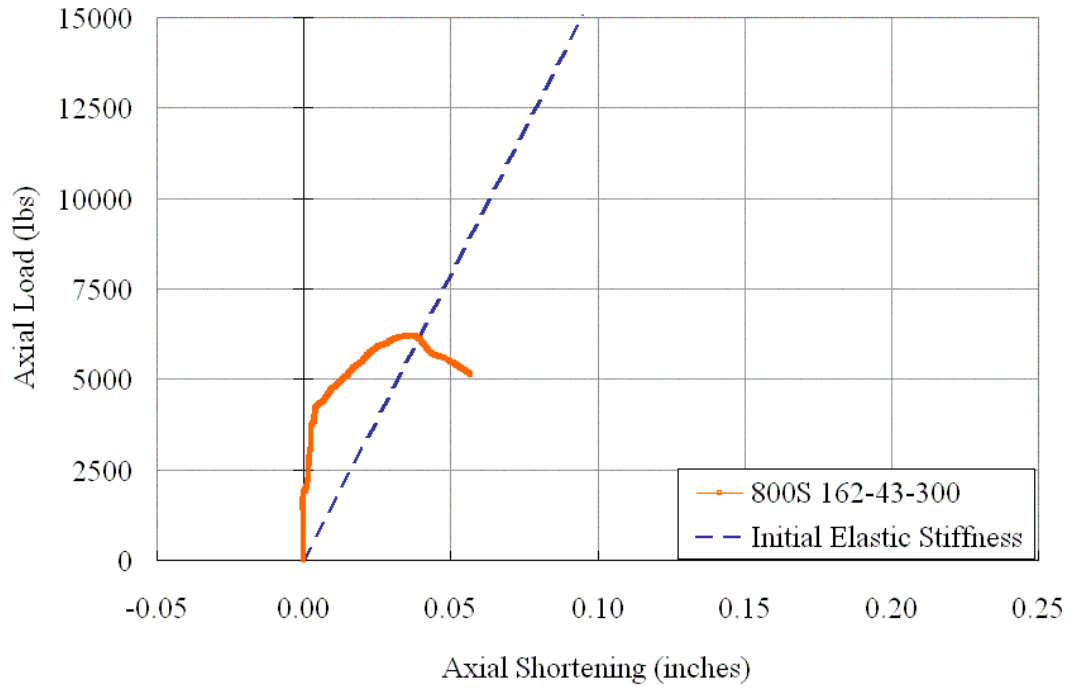


Figure A33.5 Plot of Axial Load vs. Axial Shortening

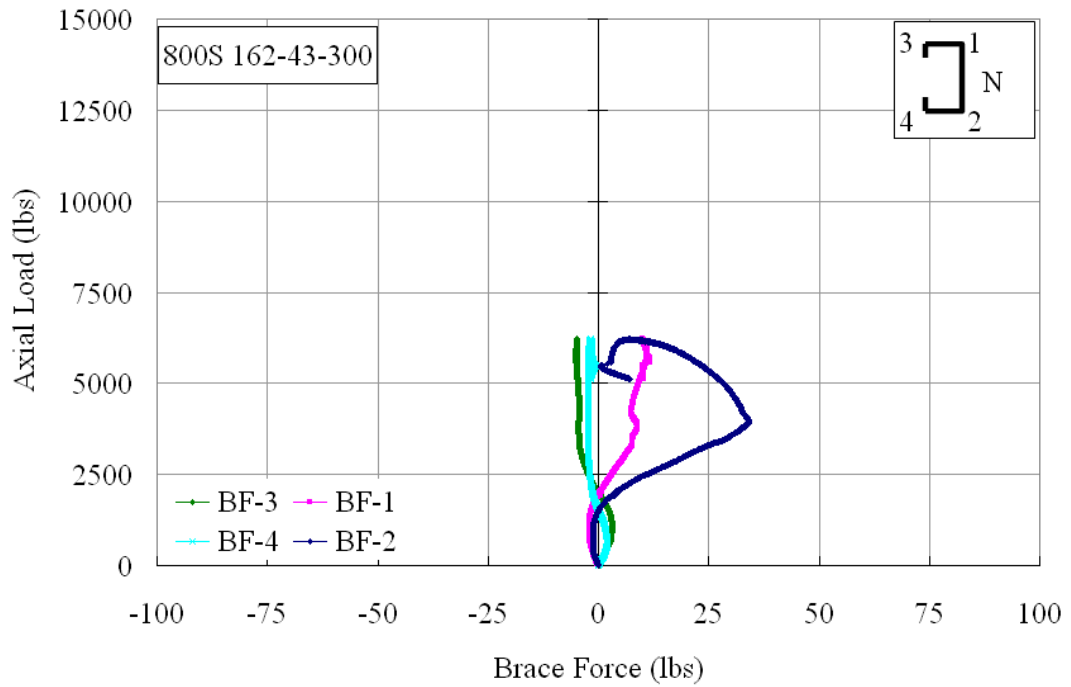


Figure A33.6 Plot of Axial Load vs. Brace Forces

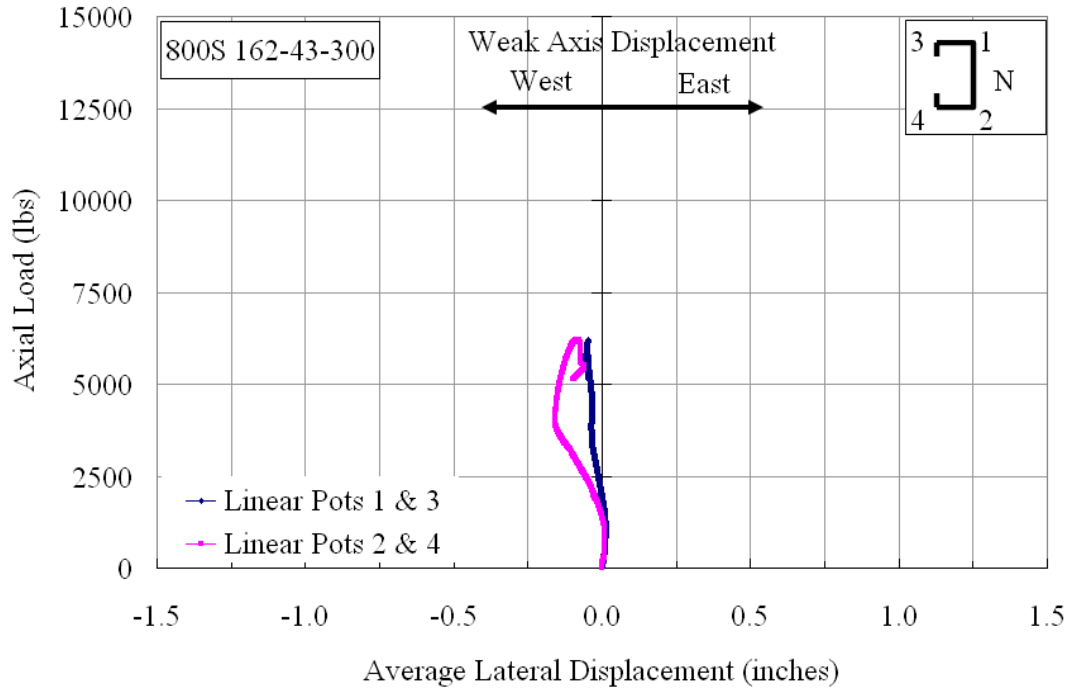


Figure A33.7 Plot of Axial Load vs. Weak Axis Displacement at Mid-Height

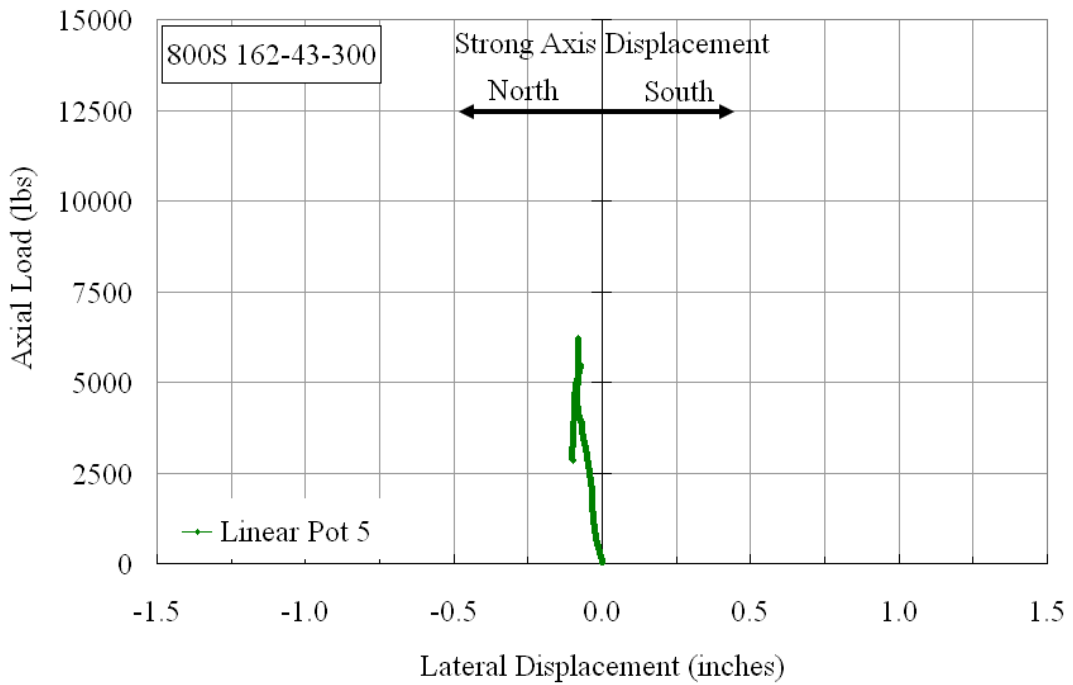


Figure A33.8 Plot of Axial Load vs. Strong Axis Displacement at Mid-Height

**800S162-97-000**

The cee stud specimen 800S162-97-000 was tested without any lateral bracing, so that it serves as a benchmark for comparison with other braced cee stud specimens. Figure A34.1 shows the stud in the Riehle Machine prior to the test. Figure A34.3 shows the plot of axial load versus axial shortening of the stud. The mid-height weak axis lateral displacement was measured with pairs of linear potentiometers LP-1 & LP-3 and LP-2 & LP-4, attached to the north and south flanges respectively, and the strong axis lateral displacement was measured with LP-5. The axial shortening of the stud was measured by LP-6, attached to the north flange.

The axial load was applied initially at the rate of 10 lbs/sec up to 5000 lbs of axial load and later increased to 40 lbs/sec till the maximum load was reached. With Initially the stud exhibited strong axis buckling, with LP-5 measuring 0.070 inches at 5000 lbs, beyond which there was no strong axis displacement measured. Up to this load level, there was no axial shortening since the strong axis buckling neutralized the effect of axial shortening. Along with strong axis buckling, the stud also exhibited weak axis buckling in first mode flexure as shown in Figure A34.4. Even though there was differential movement of the north and south flanges, the buckling was predominantly flexural rather than flexural-torsional. There was neither elastic buckling waves observed in the web nor any distortional buckling observed in the flanges, at any point of time during the complete test.

Figure A34.2 shows an overall final view of the stud at the maximum load. It can be observed in the figure that the stud is in first mode flexural buckling. At the ultimate load of 19703 lbs, the measured axial shortening was 0.051 inches, the weak axis lateral

displacement were 0.41 and 0.36 inches on the north and south flanges, respectively, and the strong axis lateral displacement measured 0.059 inches.



Figure A34.1 Overall View of the Stud 800S162-97-000 in the Riehle Testing Machine, prior to the Test



Figure A34.2 Final View of the of Stud 800S162-97-000 at the Ultimate load of 19703 lbs

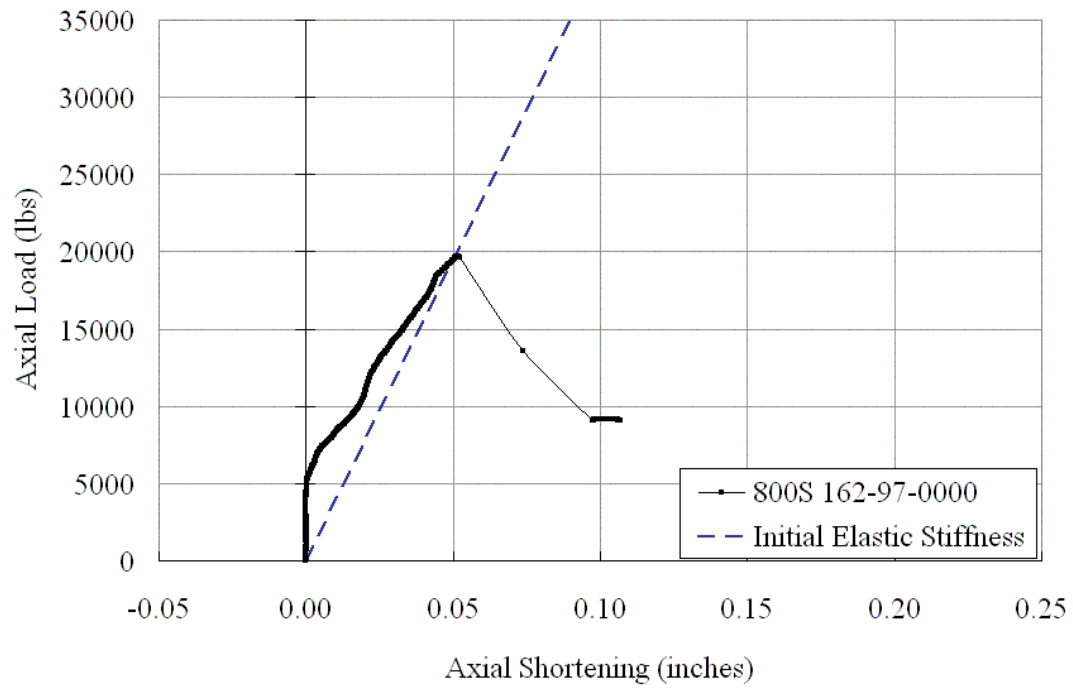


Figure A34.3 Plot of Axial Load vs. Axial Shortening

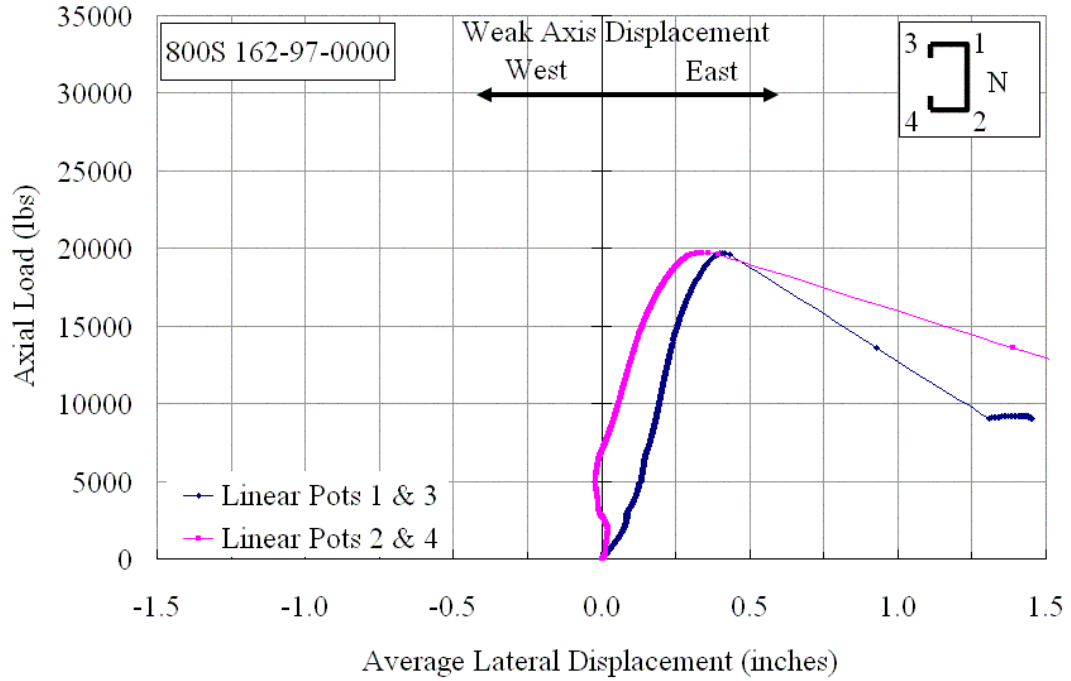


Figure A34.4 Plot of Axial Load vs. Weak Axis Displacement at Mid-Height

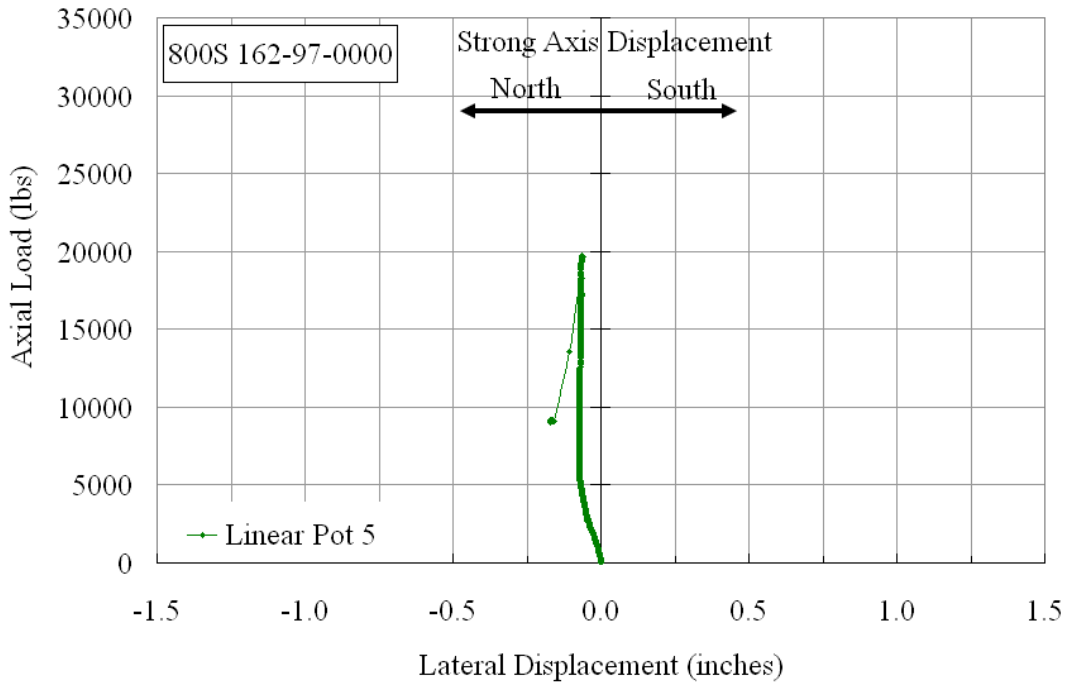


Figure A34.5 Plot of Axial Load vs. Strong Axis Displacement at Mid-Height

**800S162-97-500**

The cee stud specimen 800S162-97-500 was braced with a total bracing stiffness of 1041 lbs/in. that was equal to about 1.2 times the ideal bracing requirement. Figure A35.1 shows the stud in the Riehle Machine prior to the test. Figure A35.4 shows the plot of axial load versus axial shortening of the stud. The mid-height weak axis lateral displacement was measured by linear potentiometers LP-1 & LP-3 and LP-2 & LP-4, attached to the north and south flanges respectively, and LP-5 recorded the strong axis lateral displacement. The axial shortening was measured by LP-6, attached to the north flange.

The actual initial elastic stiffness of the stud was lesser than the calculated value, which can be observed in Figure A35.4. When the axial load reached 6500 lbs, there was a slight strong axis displacement of 0.0335 inches to the south, which moved back to the initial position with further increase in the axial load. At an axial load of 8000 lbs, the mid-height weak axis lateral displacement measured on the north and south flanges were 0.052 inches and 0.032 inches, respectively. When the axial load measured 15000 lbs, the weak axis displacement was zero on both the flanges (see Figure A35.6).

Initially the brace force in BF-3 was increased up to an axial load of approximately 7000 lbs and measured 17.87 lbs. The other brace wires did not develop any forces. When the axial load reached 11000 lbs the brace force in BF-2 started to increase, and at the ultimate load of 21626 lbs it measured about 54 lbs. A similar trend was seen in BF-1 with the brace force changed from 0.0 lbs at an axial load of 17000 lbs to 19.46 lbs at the ultimate load of 21626 lbs. At the ultimate load the north and south flanges had moved east by 0.125 inches and 0.25 inches, respectively, while the strong axis displacement was 0.038 inches to the south. At the ultimate load, the stud had buckled in first mode

flexural buckling as shown in Figure A35.3. There was a local buckle at t punchout that led to the final failure of the stud, however, the governing buckling mode is the global buckling mode, which was first mode flexural buckling.



Figure A35.1 Overall View of the Stud 800S162-97-500 in the Riehle Testing Machine, prior to the Test



Figure A35.2 Deformation of the Top and Bottom Tracks, at an Axial Load of 10000 lbs



Figure A35.3 Final View of Stud 800S97-500 at the Ultimate Load of 21626 lbs (Looking North)

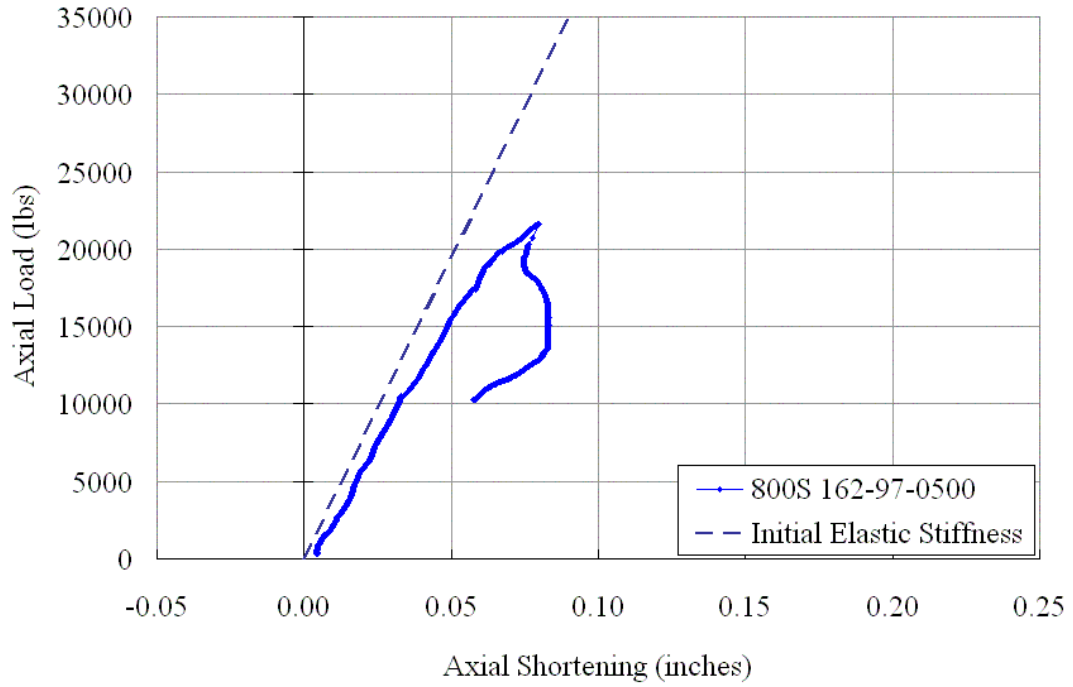


Figure A35.4 Plot of Axial Load vs. Axial Shortening

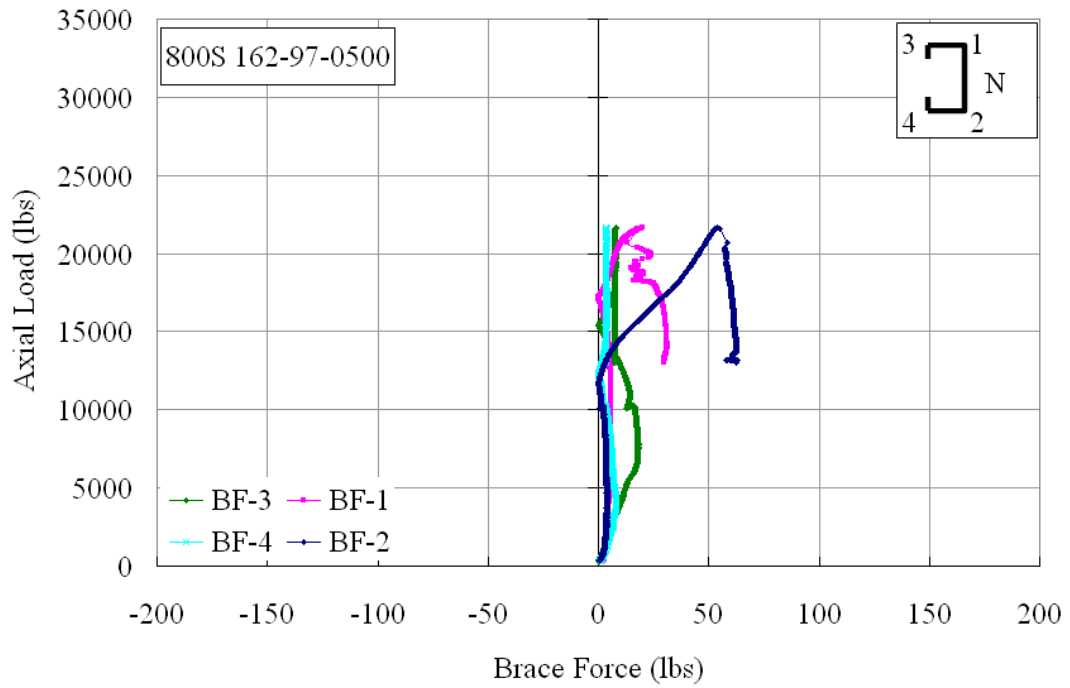


Figure A35.5 Plot of Axial Load vs. Brace Forces

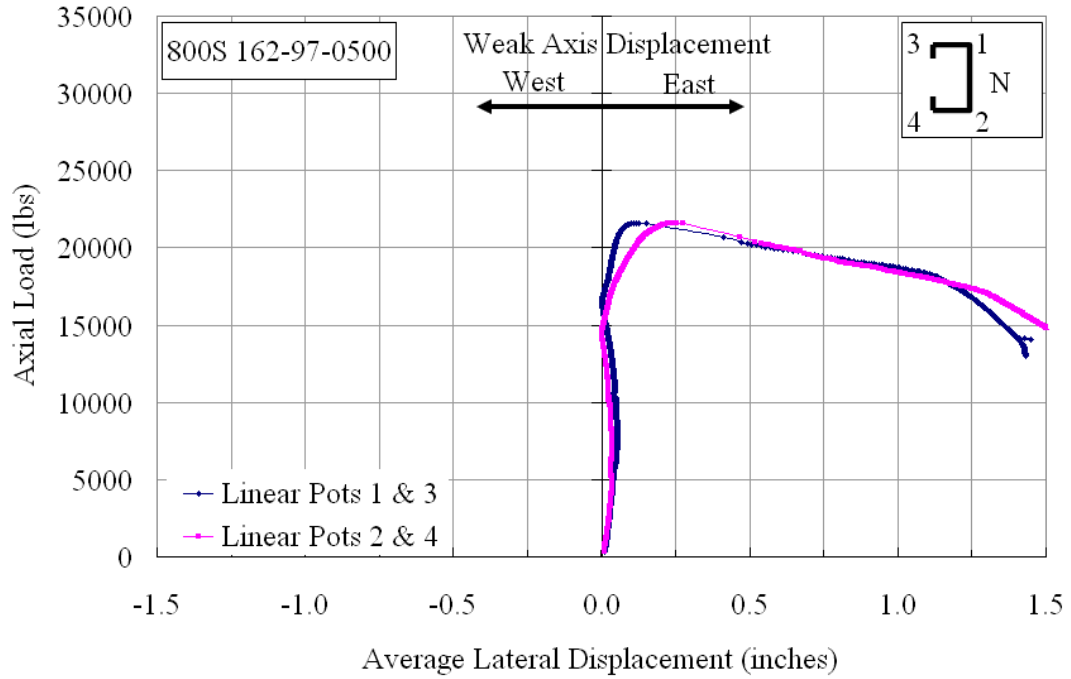


Figure A35.6 Plot of Axial Load vs. Weak Axis Displacement at Mid-Height

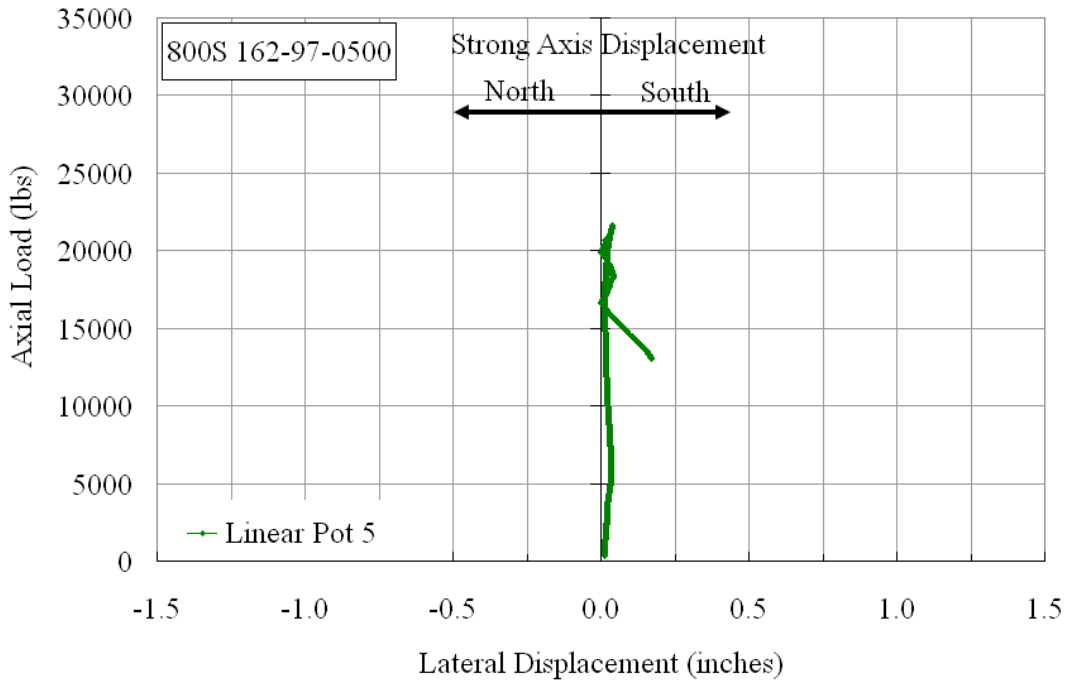


Figure A35.7 Plot of Axial Load vs. Strong Axis Displacement at Mid-Height

**800S162-97-1000**

The cee stud specimen 800S162-97-1000 was braced with a total bracing stiffness of 2093 lbs/in. that was equal to about 2.4 times the ideal bracing requirement. Figure A36.1 shows the stud in the Riehle Machine prior to the test. Figure A36.5 shows the plot of axial load versus axial shortening of the stud. The mid-height weak axis lateral displacement was measured by linear potentiometers LP-1 & LP-3 and LP-2 & LP-4, attached to the north and south flanges respectively, and LP-5 recorded the strong axis lateral displacement.

Initially the slope of the axial load versus axial shortening curve was lesser than the initial elastic stiffness line as shown in Figure A36.5, while the stud exhibited first mode flexural buckling with the mid-height cross-section laterally displacing to the east. Owing to the weak axis flexural buckling the brace forces in BF-3 and BF-4 increased almost linearly, up to an axial load of 5000 lbs, measuring 36.7 lbs and 29.5 lbs, respectively. Beyond this load, the brace force in BF-3 started to decrease gradually, and that in BF-4 increased gradually. The axial shortening measured at this load level was about 0.025 inches. There was no strong axis buckling up to an axial load of about 7500 lbs. From this load level to an axial load of 8500 lbs, there was no further lateral displacement of the mid-height cross-section and the measured weak axis movement at the new load level was 0.12 inches to the east.

Just prior to reaching an axial load of 14617 lbs, the brace forces in BF-3 and BF-4 measured 17.44 and 41.23 lbs. At this load level, there was almost an instantaneous drop in the forces in braces BF-3 and BF-4, measuring 0.67 lbs and 27.5 lbs, respectively. With further increase in the axial load, the brace forces again started to increase. The sudden drop may be due to slip in either of the two brace-wires.

Elastic buckling waves were first observed in the web at about 15000 lbs. Figure A36.2s shows the elastic buckling waves at an axial load of 22500 lbs. Between this load and a new load level of 23780 lbs, the brace forces in BF-3 and BF-4 measured 50 lbs, at which there could have been possible yielding of the brace-wires. At approximately 23811 lbs, the ultimate load was attained, beyond which both the brace-wires BF-3 and BF-4 snapped.

Just prior to the snapping of the brace wires, the stud exhibited second mode flexural buckling. After the snapping of the brace-wires, the buckling mode of the stud changed from second mode flexural buckling to first mode flexural buckling. Figure A36.3 shows the snapped brace-wires. The failure of the stud in first mode flexural buckling is shown in Figure A36.4, which is not the actual mode of failure.



Figure A36.1 Overall View of the Stud 800S162-97-1000 in the Riehle Testing Machine, prior to the Test



Figure A36.2 Elastic buckling waves in the Web of Stud 800S162-97-1000 at an Axial Load



Figure A36.3 View of the Snapped Brace-wires of Stud 800S162-97-1000, beyond the Ultimate load



Figure A36.4 Buckled Shape of Stud 800S162-97-1000, beyond the Ultimate load

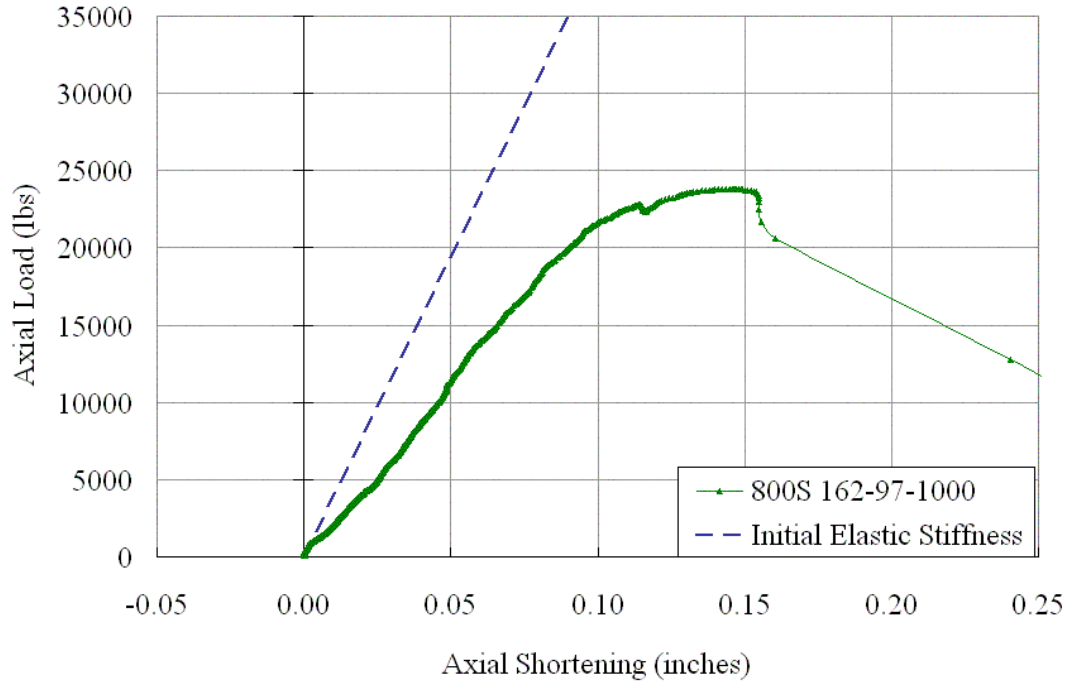


Figure A36.5 Plot of Axial Load vs. Axial Shortening

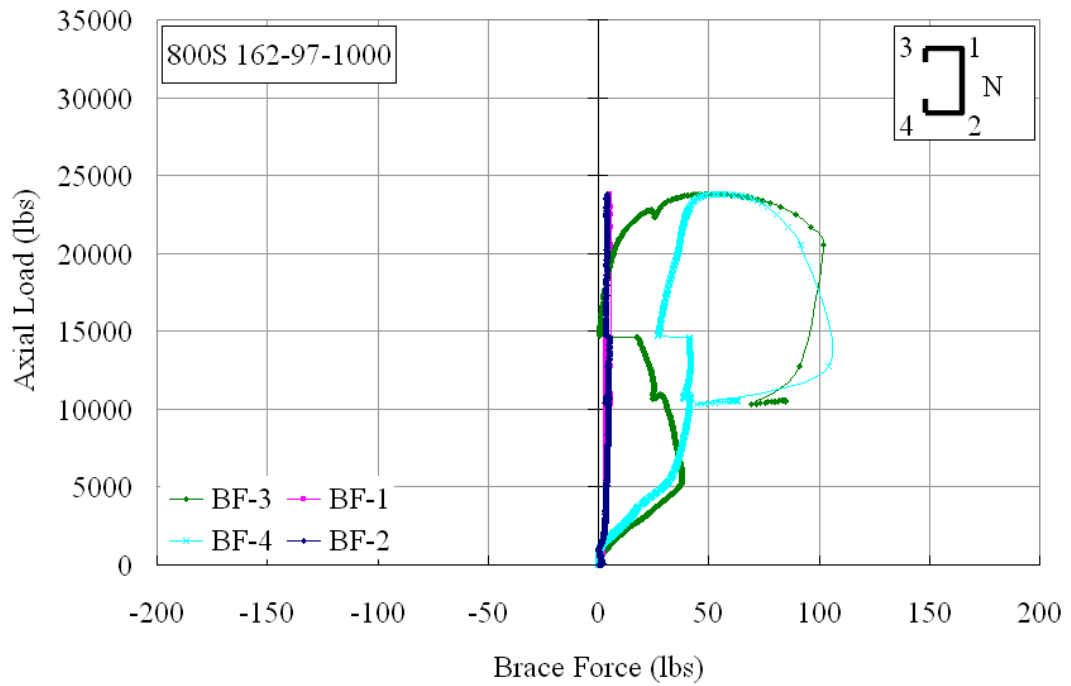


Figure A36.6 Plot of Axial Load vs. Brace Forces

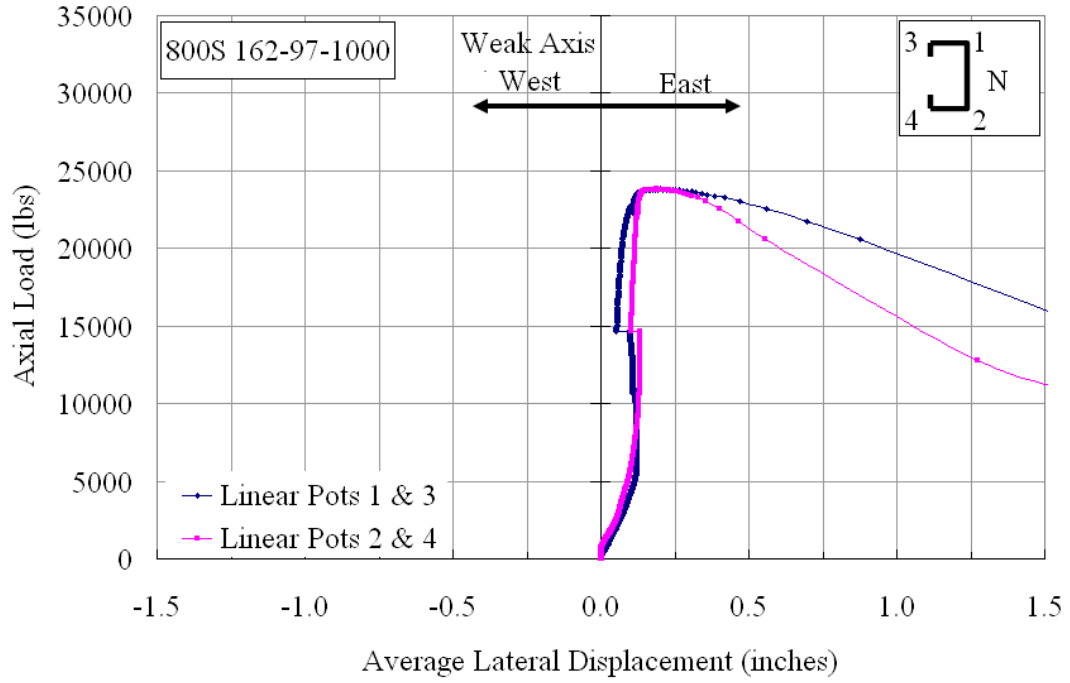


Figure A36.7 Plot of Axial Load vs. Weak Axis Displacement at Mid-Height

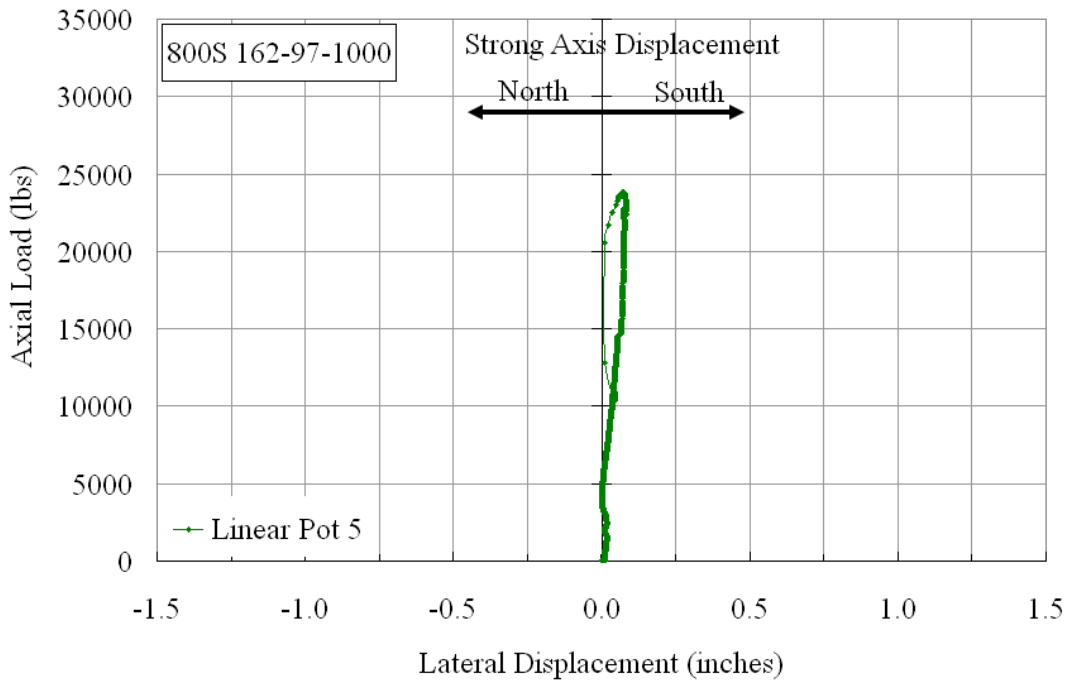


Figure A36.8 Plot of Axial Load vs. Strong Axis Displacement at Mid-Height

**800S162-97-2100**

The cee stud specimen 800S162-97-2100 was braced with a total bracing stiffness of 4195 lbs/in. that was equal to about 4.8 times the ideal bracing requirement. Figure A37.1 shows the stud in the Riehle Machine prior to the test. Figure A37.4 shows the plot of axial load versus axial shortening of the stud. The mid-height weak axis lateral displacement was measured by linear potentiometers LP-1 & LP-3 and LP-2 & LP-4, attached to the north and south flanges respectively, and LP-5 recorded the strong axis lateral displacement. The axial shortening was measured by LP-6, attached to the north flange.

The stud was loaded initially at a rate of approximately 7 lbs/sec up to an axial load of 5000 lbs, and then at 45 lbs/sec, to make sure that the stud had a static response to the applied load. The slope of the axial load versus axial shortening curve of the stud was less than that of the initial elastic stiffness line as shown in Figure A37.4. Initially up to an axial load of 7500 lbs, the brace force in BF-1 gradually increased to 16 lbs, and then began to decrease, while the forces in the other brace wires remained unchanged.

At approximately 14000 lbs, the brace force in BF-2 started to increase and measured 11 lbs at an axial load of 20000lbs. On reaching the ultimate load, the brace force in BF-2 dropped to 0.0 lbs.

There was no significant lateral movement of the weak axis up to an axial load of 23240 lbs. At the ultimate load of 23537 lbs, the north and south flanges had moved 0.233 and 0.073 inches to the east, respectively (see Figure A37.6). The strong axis displacement, which increased gradually, measured 0.050 inches at the ultimate load (see Figure A37.7).

At about 20000 lbs, elastic buckling waves were first observed in the web, which were predominantly seen around the web-punchouts. With the stud attaining its maximum axial load capacity, the stud exhibited first mode torsional buckling. Figure A37.3 shows the torsion in top-half of the stud, which was the cause of stud's failure.



Figure A37.1 Overall View of the Stud 800S162-97-2100 in the Riehle Testing Machine, prior to the Test



Figure A37.2 Elastic buckling waves in the Web of Stud 800S162-97-2100 at an Axial Load



Figure A37.3 Torsional Buckling in the top-half of the Stud 800S162-97-2100 at an Axial Load of 23000 lbs

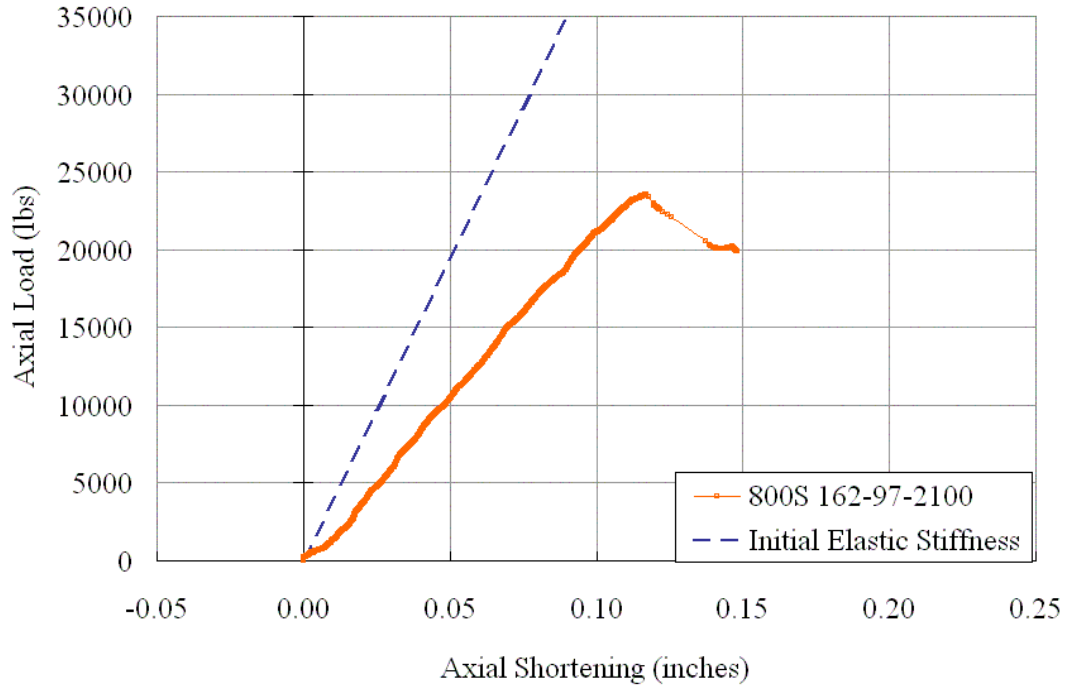


Figure A37.4 Plot of Axial Load vs. Axial Shortening

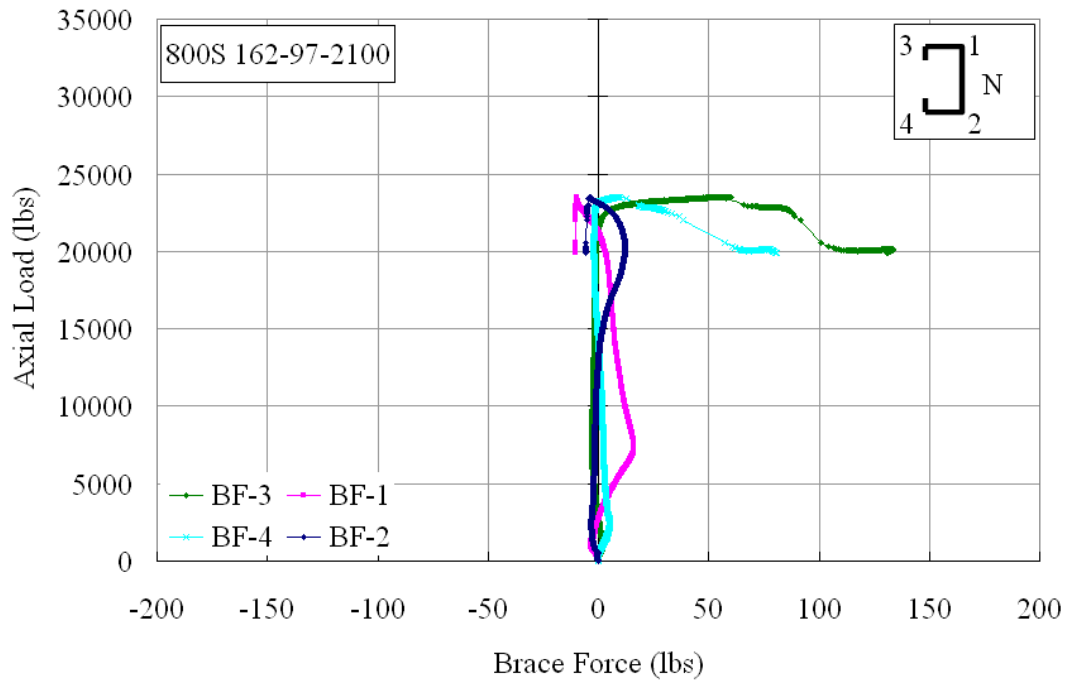


Figure A37.5 Plot of Axial Load vs. Brace Forces

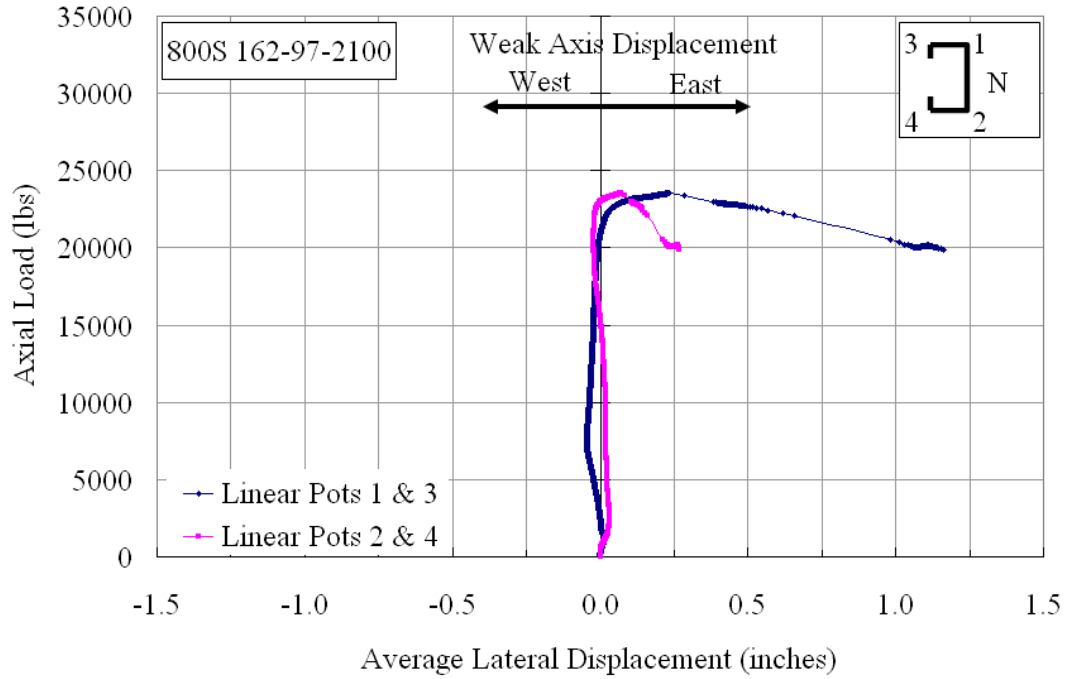


Figure A37.6 Plot of Axial Load vs. Weak Axis Displacement at Mid-Height

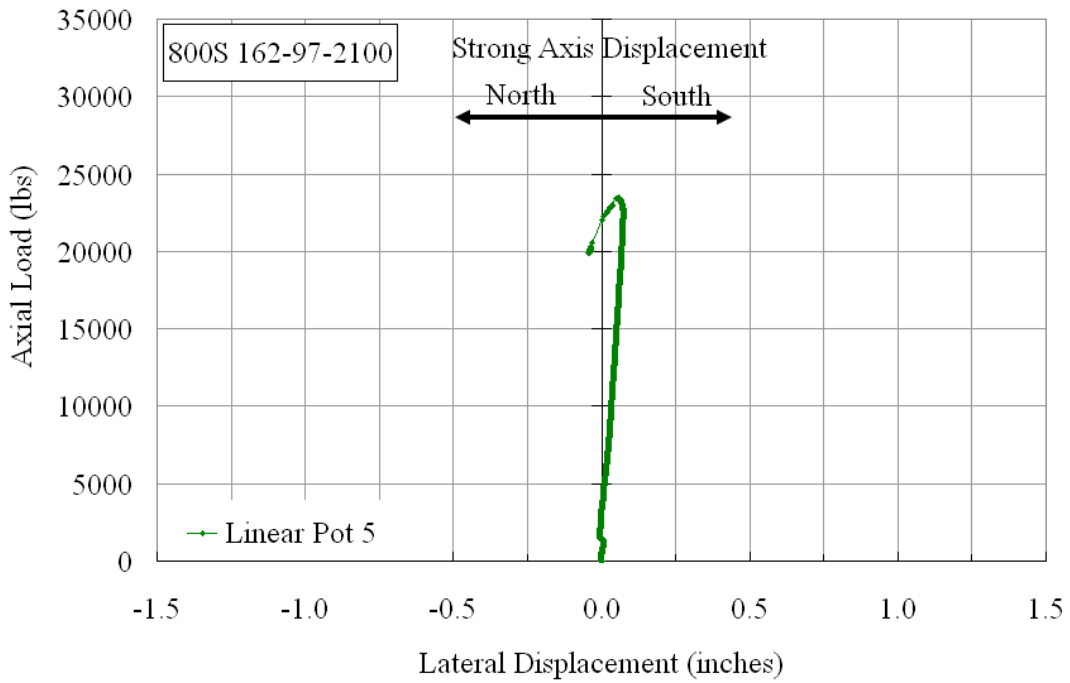


Figure A37.7 Plot of Axial Load vs. Strong Axis Displacement at Mid-Height

## APPENDIX B TEST RESULTS ON BRIDGING CONNECTIONS

The bridging connection tests were conducted on 54 cee-stud specimens, respectively, which were subdivided into two groups based on the loading condition. As described in Chapter 3, three types of bridging connections were tested for strength and stiffness. Load was applied perpendicular to the major axis or out-of-plane and along the major-axis or in-plane. Appendix B is subdivided into two sections based on the out-of-plane loading and in-plane loading conditions.

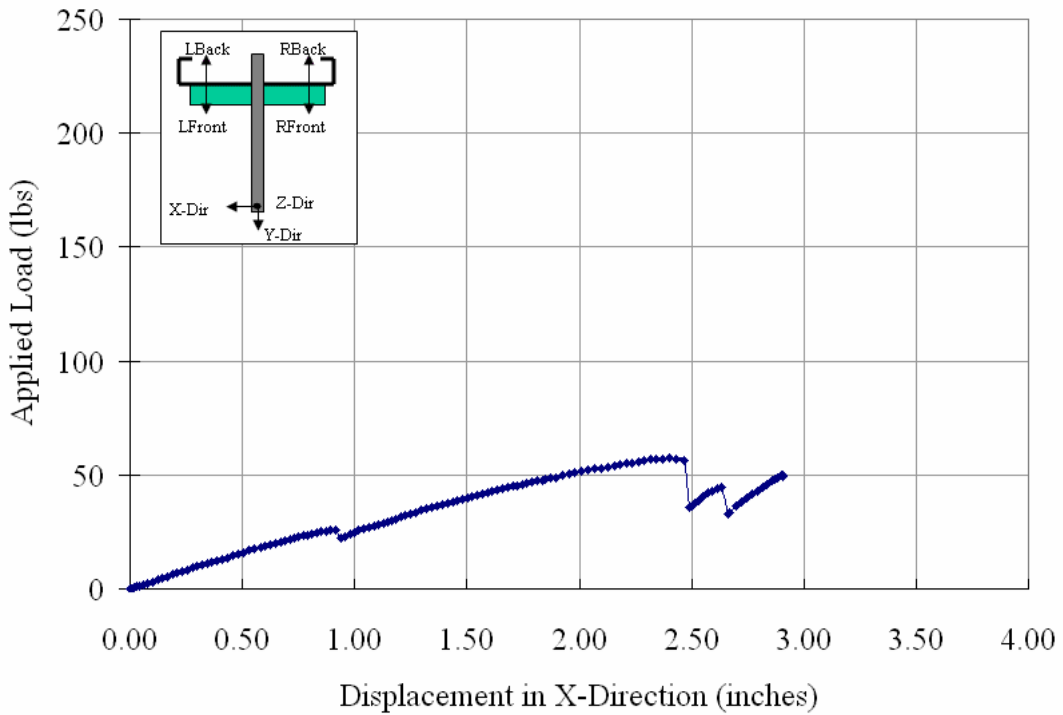
The photographs show either the initial or the final overall view of the test specimen and a close up view of the failure mechanism. The plot of applied load versus displacement, either out-of-plane or in-plane is shown for each of the bridging connections. Two test specimens were tested for each type of stud and connection.

In the out-of-plane load tests, the plot of applied load versus displacement in the X-Direction is shown, whereas for the in-plane load tests, the plot of applied load versus displacement in the Y-Direction is shown for each of the specimens. The observed failure mechanisms have been discussed in Chapter 4 for both the loadings.

**Out-Of-Plane Load Test on 362S125-33-1SS**

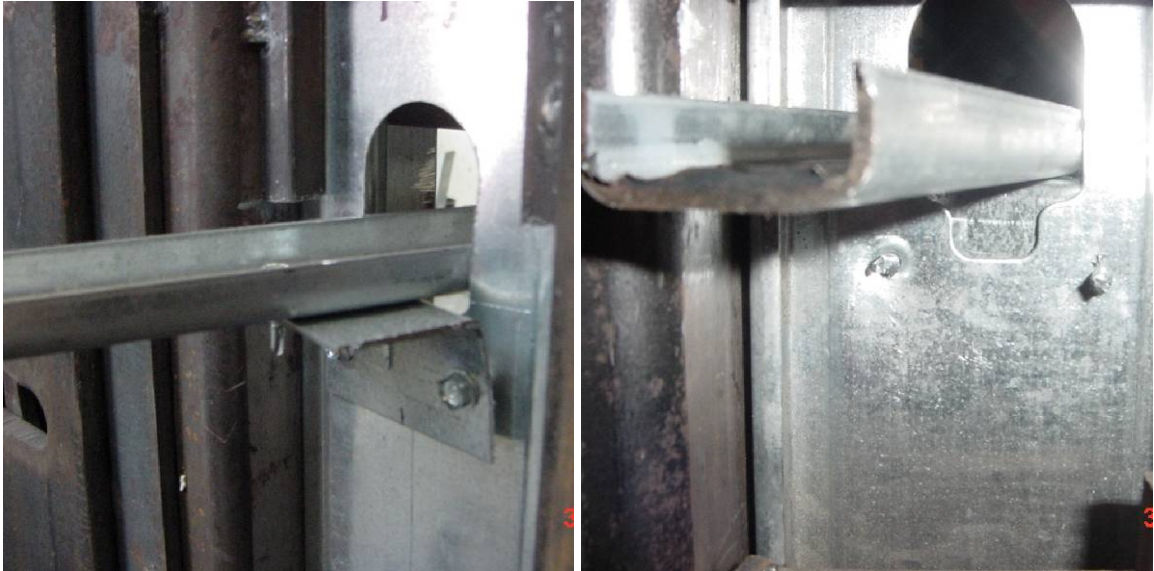


(a) Final Right Front View Showing Connection Deformation  
 (b) Close-up View Showing Web Plate Deformation and Screw Pull Out  
 362S 125-33-1 SS



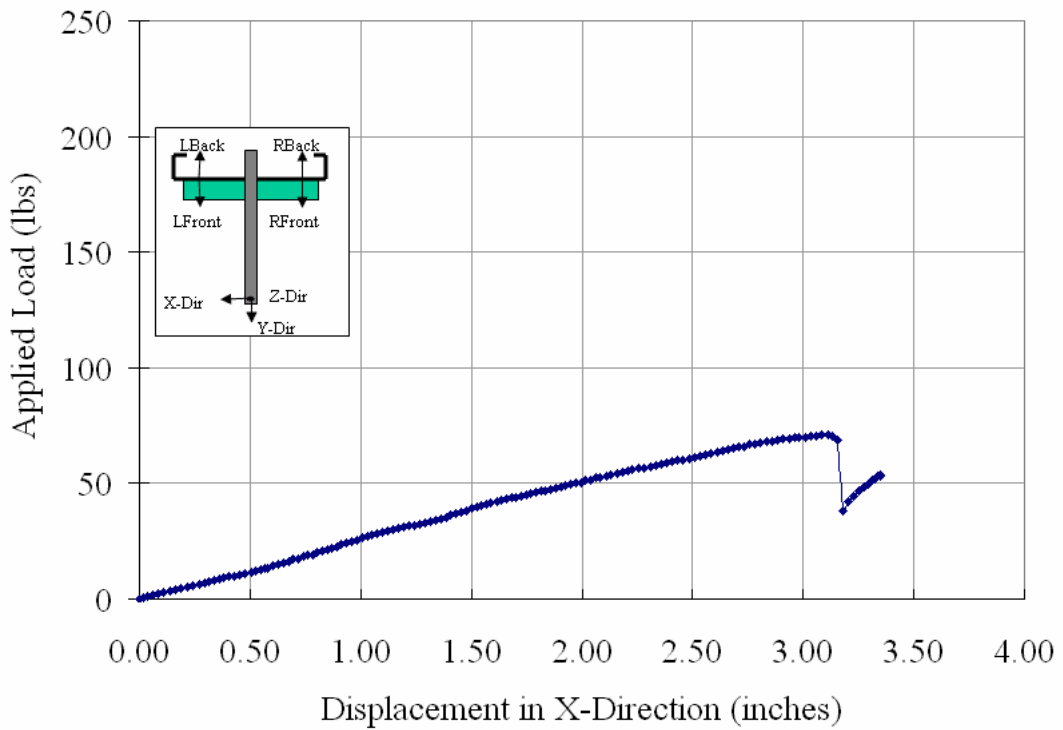
(c) Plot of Applied Load vs. Displacement in X-Direction  
 Figure B1.1

**Out-Of-Plane Load Test on 362S125-33-2SS**



(a) Final Right Front View Showing Screw Pull Out  
 (b) Close-up Backside View Showing Web Plate Deformation

362S 125-33-2 SS



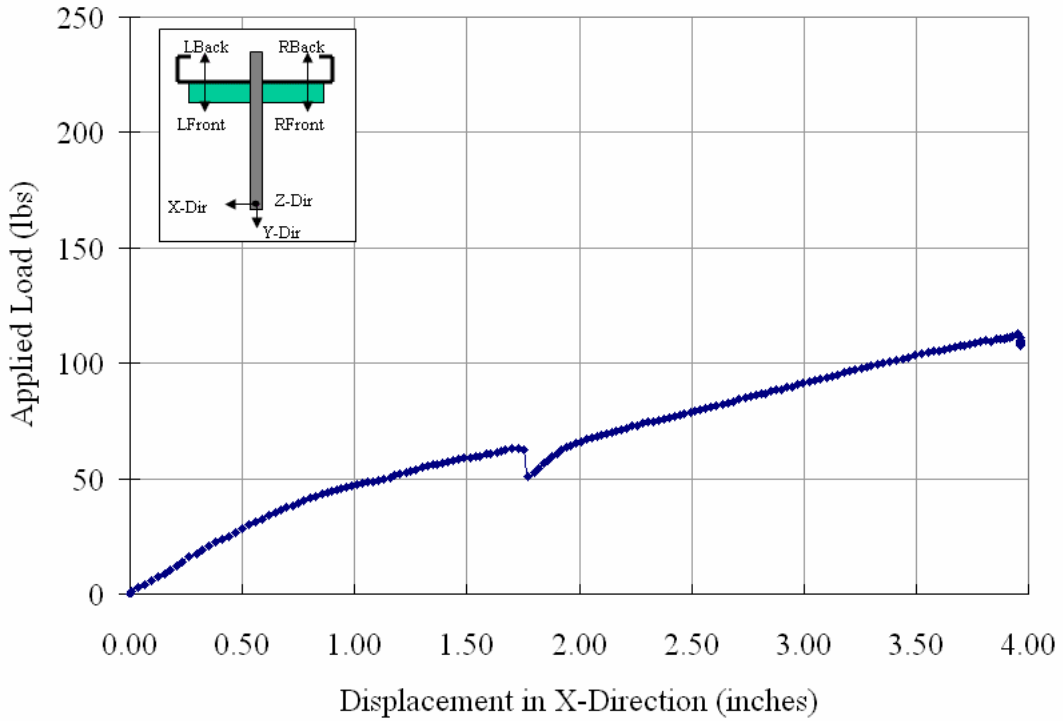
(c) Plot of Applied Load vs. Displacement in X-Direction  
 Figure B1.2

**Out-Of-Plane Load Test on 362S162-43-2SS**



(a) Final Right Front View Showing Connection Deformation  
 (b) Close-up View Showing Web Plate Deformation

362S 162-43-2



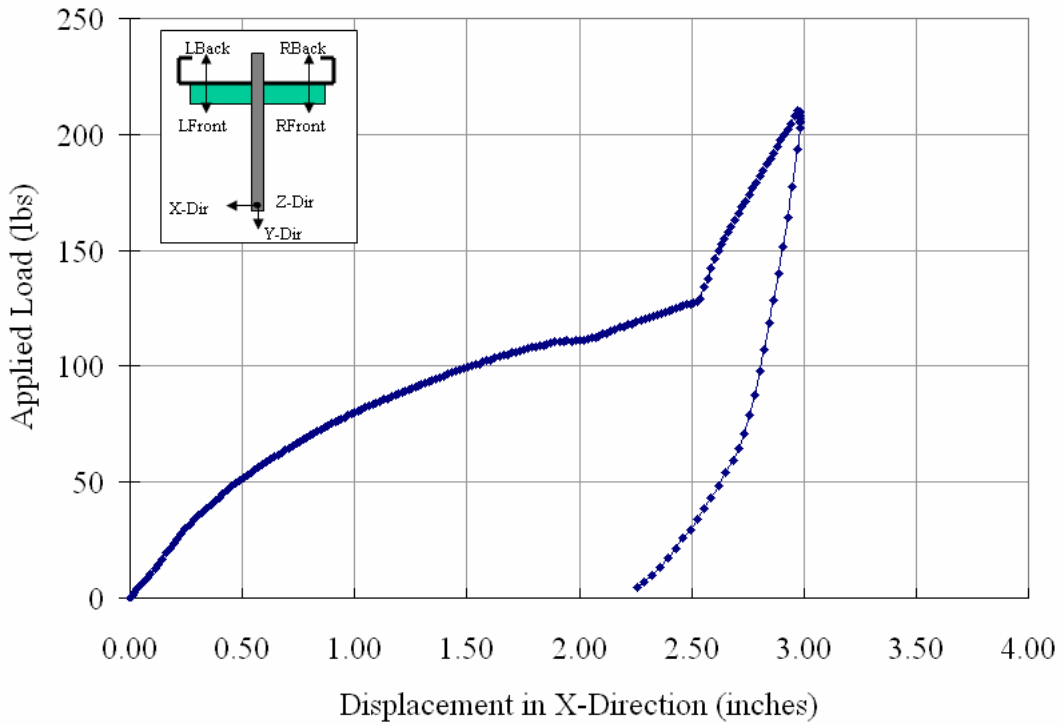
(c) Plot of Applied Load vs. Displacement in X-Direction  
 Figure B1.3

**Out-Of-Plane Load Test on 362S162-68-1SS**



(a) Right Front View Showing Clip Angle Deformation  
 (b) Top View Showing Clip Angle Deformation

362S 162-68-1 SS



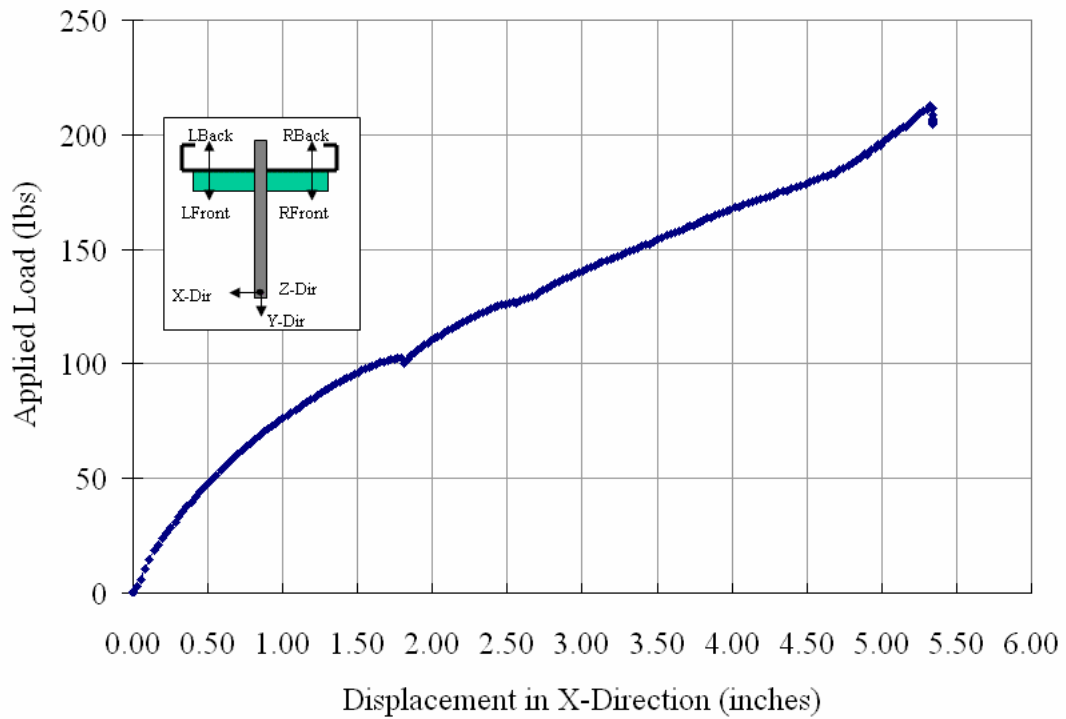
(c) Plot of Applied Load vs. Displacement in X-Direction  
 Figure B1.4

**Out-Of-Plane Load Test on 362S162-68-2SS**



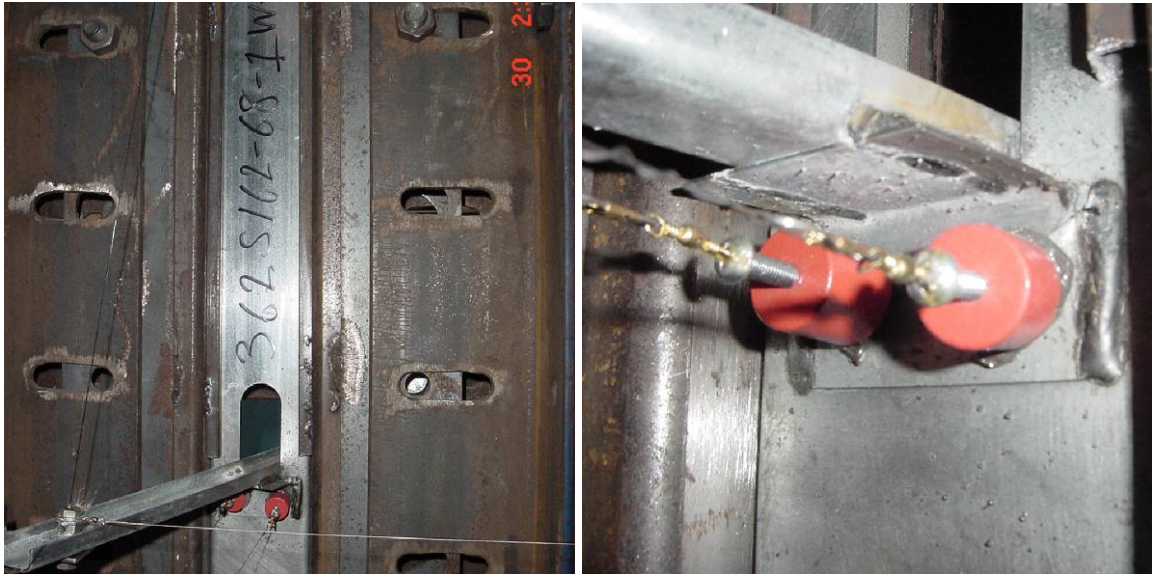
(a) Final Front View Showing Connection Deformation  
 (b) Close-up View Showing Web Plate Deformation

362S 162-68-2 SS



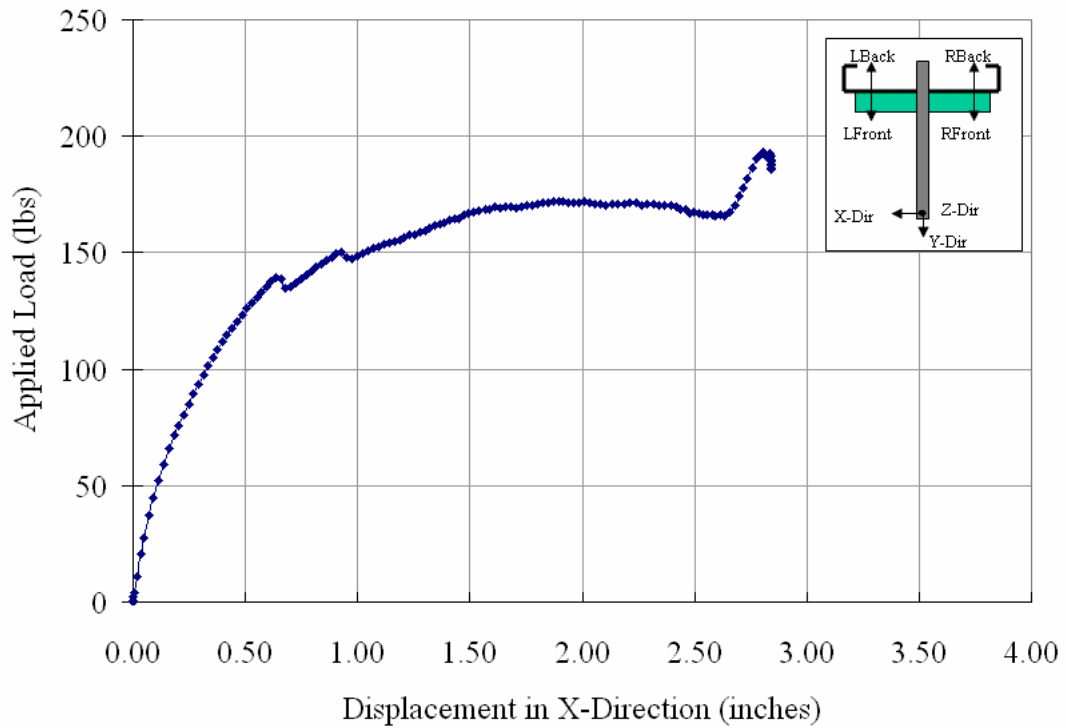
(c) Plot of Applied Load vs. Displacement in X-Direction  
 Figure B1.5

**Out-Of-Plane Load Test on 362S162-68-1WW**



(a) Final Front View Showing Connection Deformation  
 (b) Close-up View Showing Clip Angle Tear

362S 162-68-1 WW



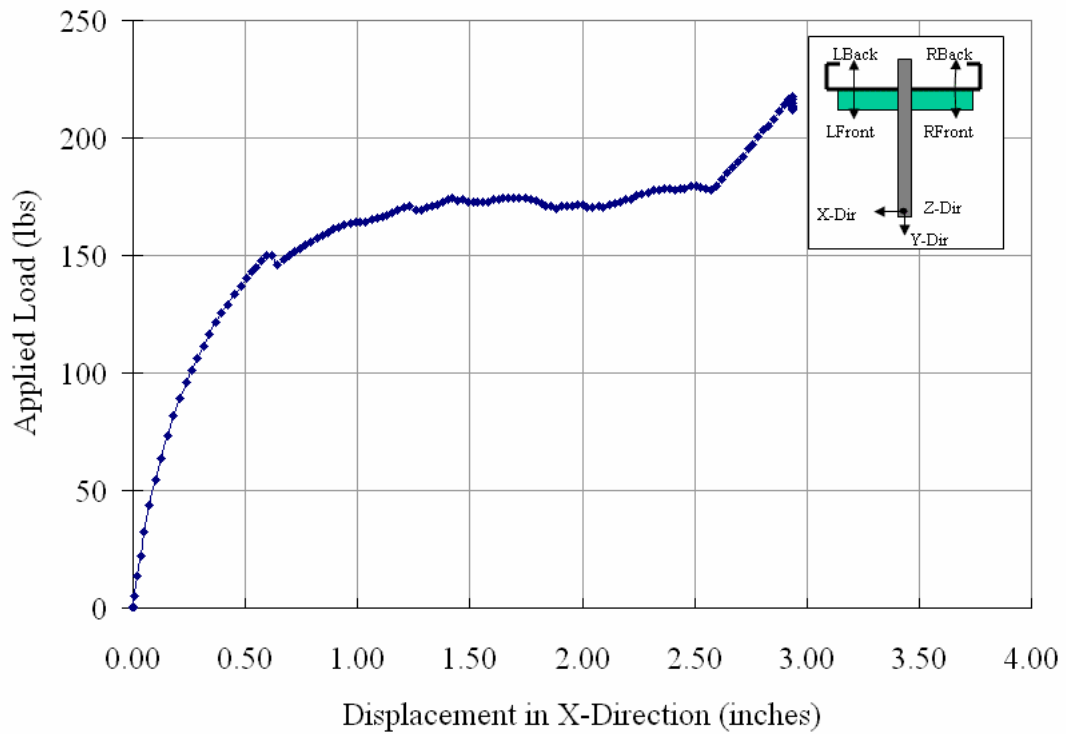
(c) Plot of Applied Load vs. Displacement in X-Direction  
 Figure B1.6

**Out-Of-Plane Load Test on 362S162-68-2WW**



(a) Final Front View Showing Connection Deformation  
 (b) Close-up View Showing Weld Tear

362S 162-68-2 WW



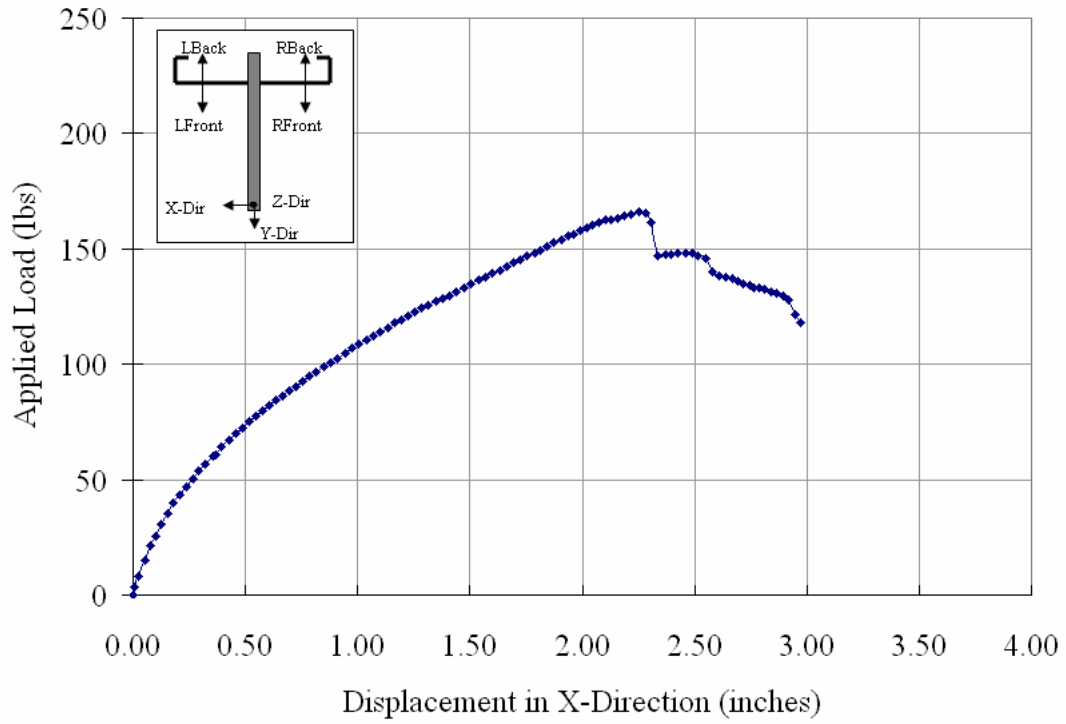
(c) Plot of Applied Load vs. Displacement in X-Direction  
 Figure B1.7

**Out-Of-Plane Load Test on 362S162-68-1DW**



(a) Final Front View Showing Connection Deformation  
 (b) Close-up View Showing Weld Tear

362S 162-68-1 DW



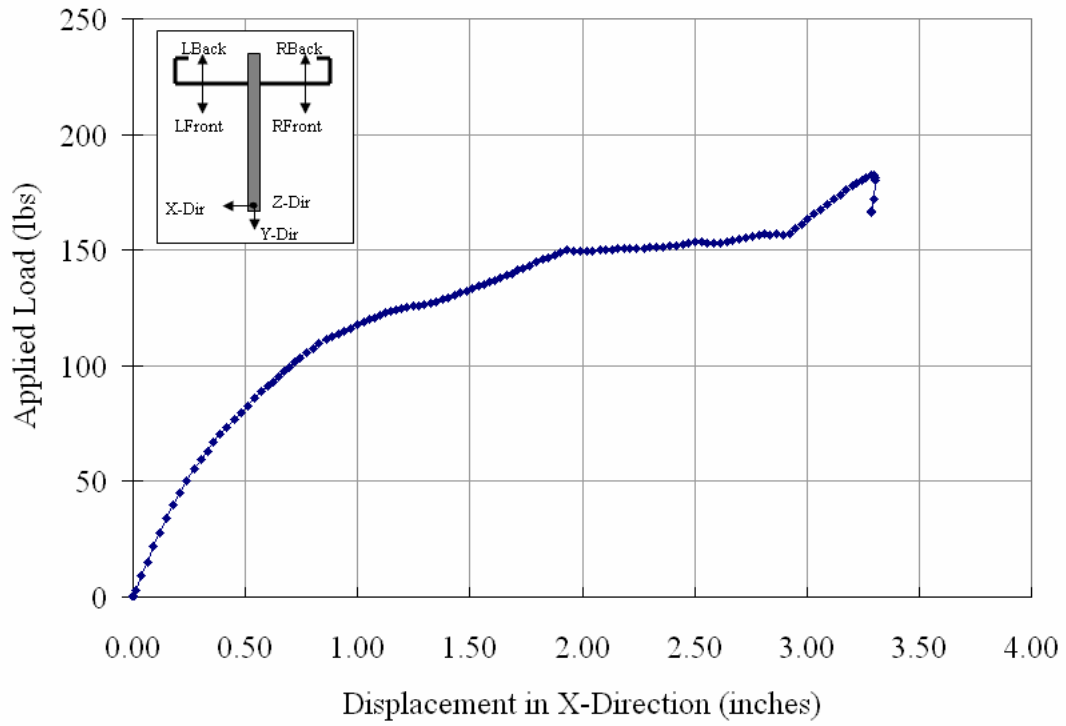
(c) Plot of Applied Load vs. Displacement in X-Direction  
 Figure B1.8

**Out-Of-Plane Load Test on 362S162-68-2DW**



(a) Final Front View Showing Connection Deformation  
 (b) Close-up View Showing Weld Tear

362S 162-68-2 DW



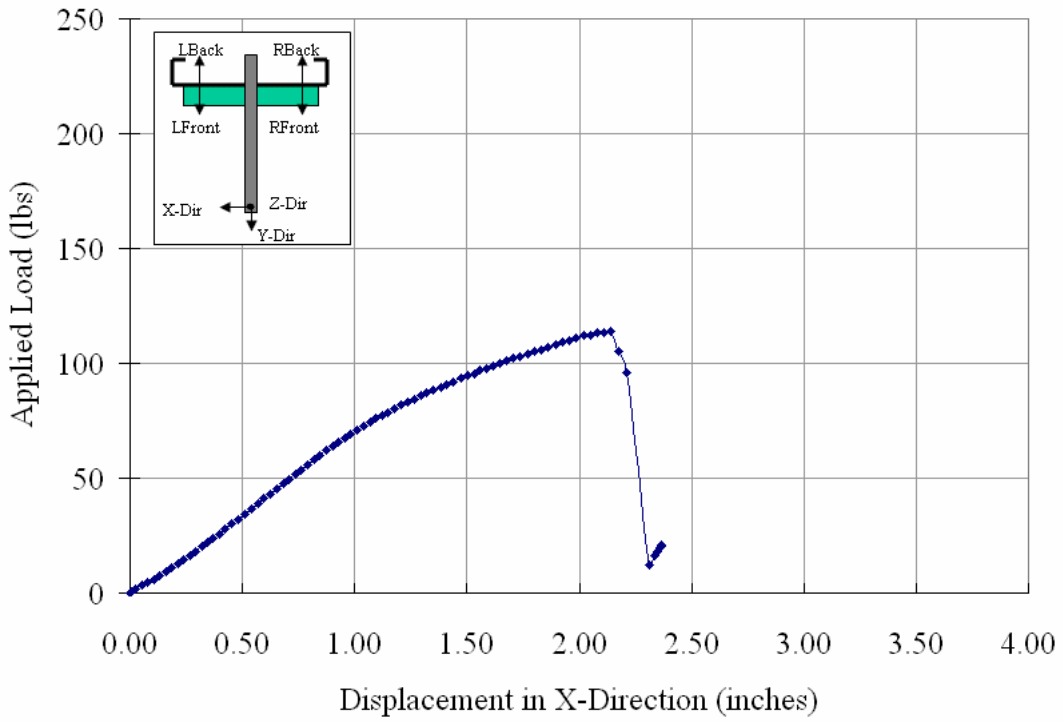
(c) Plot of Applied Load vs. Displacement in X-Direction  
 Figure B1.9

**Out-Of-Plane Load Test on 600S125-33-1SS**



(a) Final Front View Showing Connection Deformation  
 (b) Close-up View Showing Screw Pull Out

600S 125-33-1 SS



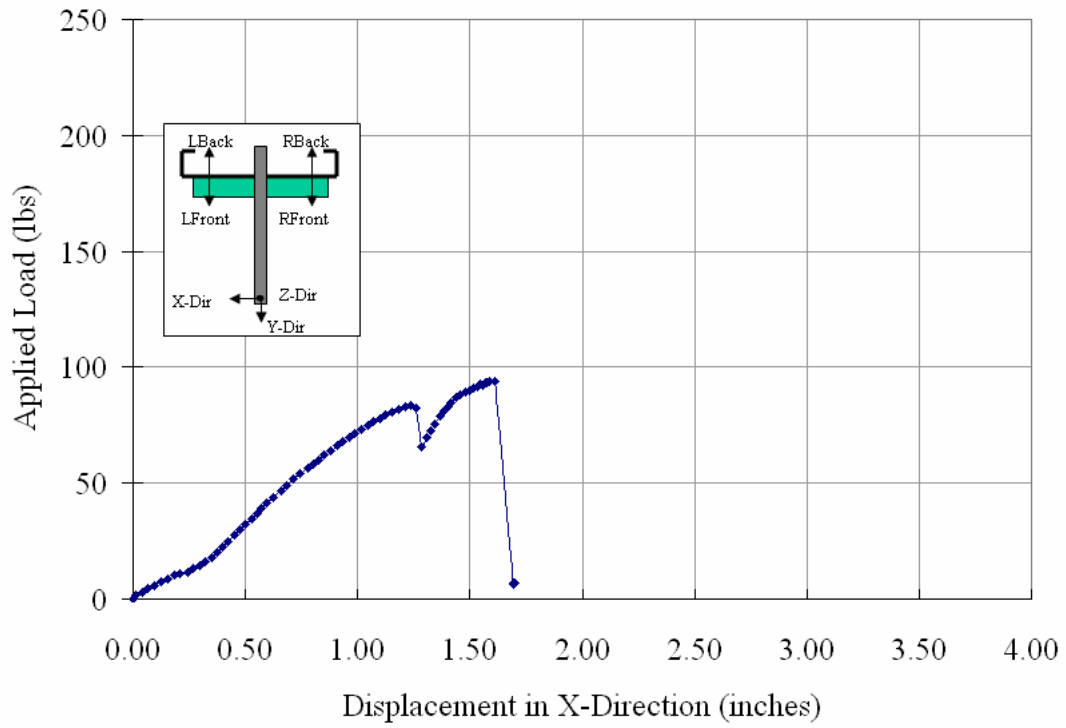
(c) Plot of Applied Load vs. Displacement in X-Direction  
 Figure B1.10

**Out-Of-Plane Load Test on 600S125-33-2SS**



(a) Front View Showing Connection Deformation  
 (b) Close-up View Showing Screw Pull Out

600S 125-33-2 SS



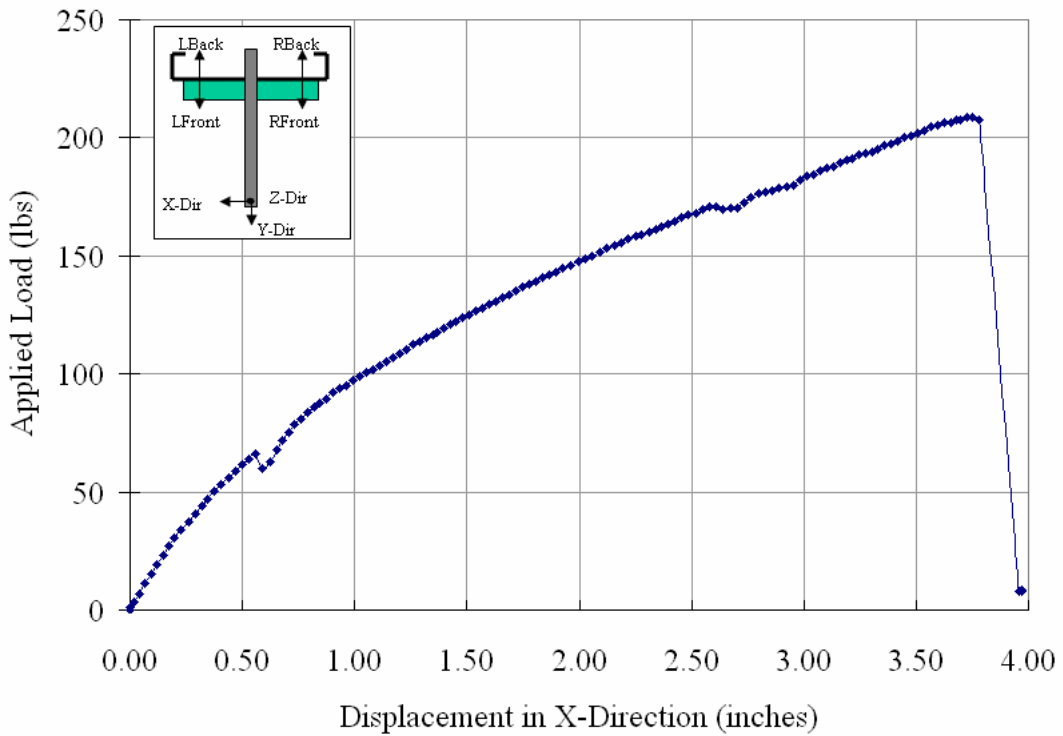
(c) Plot of Applied Load vs. Displacement in X-Direction  
 Figure B1.11

**Out-Of-Plane Load Test on 600S162-43-1SS**



(a) Front View Showing Connection Deformation  
 (b) Close-up View Showing Screw Pull Out

600S 162-43-1 S



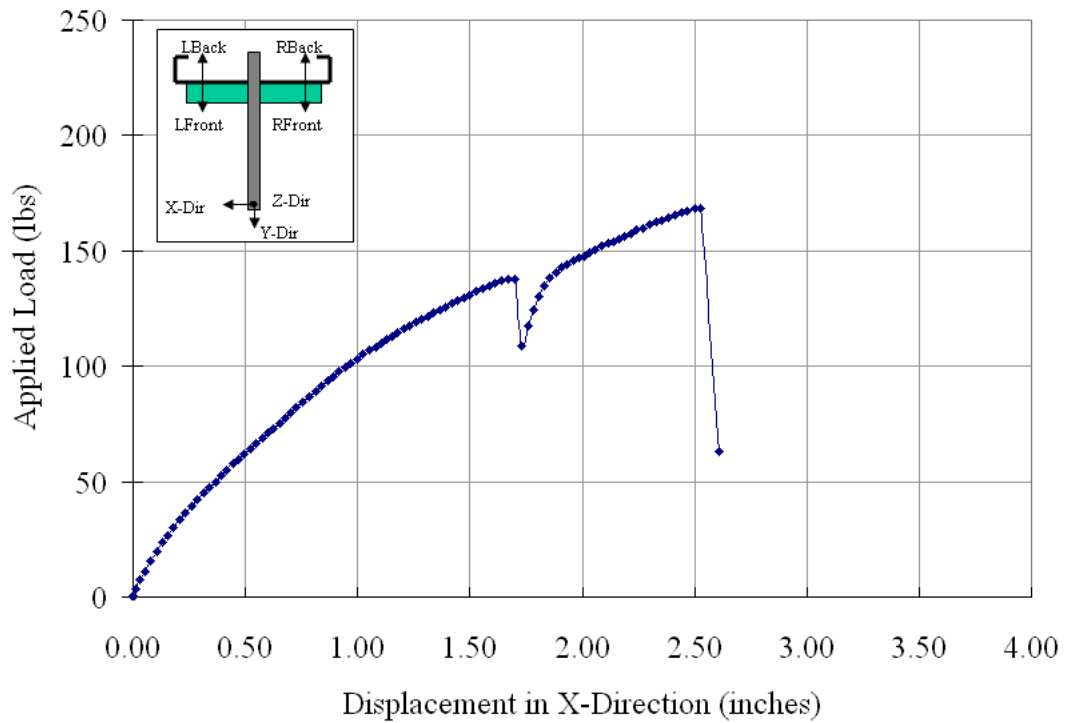
(c) Plot of Applied Load vs. Displacement in X-Direction  
 Figure B1.12

**Out-Of-Plane Load Test on 600S162-43-2SS**



(a) Front View Showing Connection Deformation in 600S162-43-2SS  
 (b) Close-up View Showing Screw Pull Out in 600S162-43-2SS

600S 162-43-2 SS



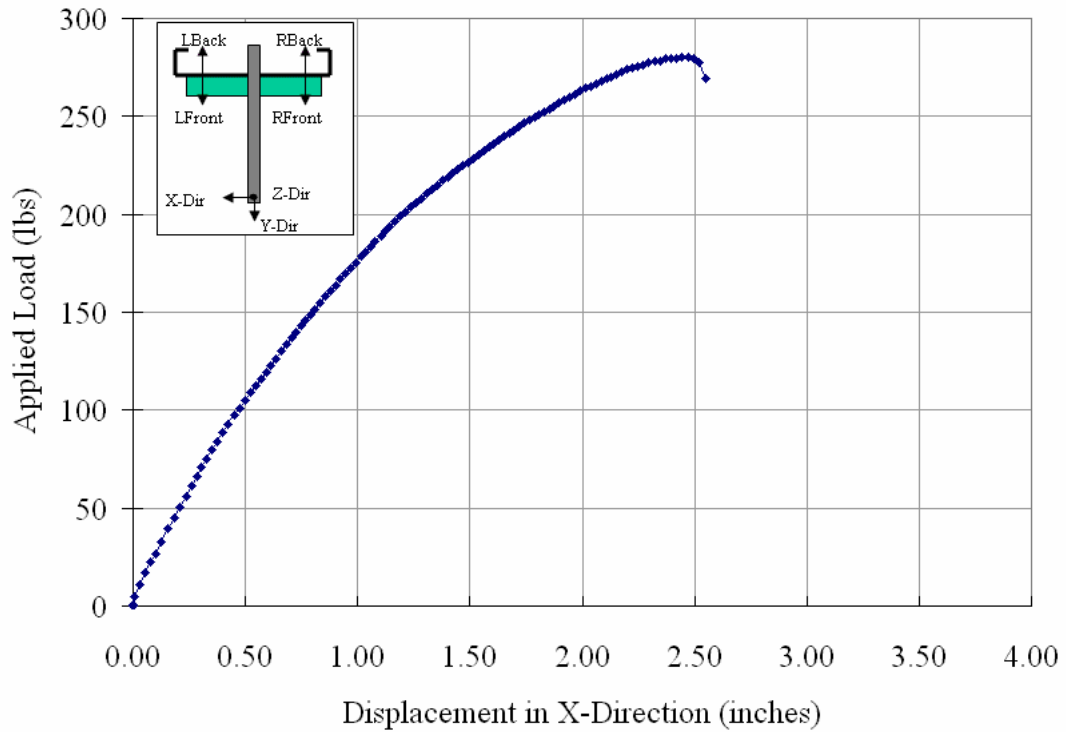
(c) Plot of Applied Load vs. Displacement in X-Direction  
 Figure B1.13

**Out-Of-Plane Load Test on 600S162-97-3SS**



(a) Front View Showing Connection Deformation in 600S162-97-3SS  
 (b) Top Close-up View Showing Screw Pull Out in 600S162-97-3SS

600S 162-97-3 SS



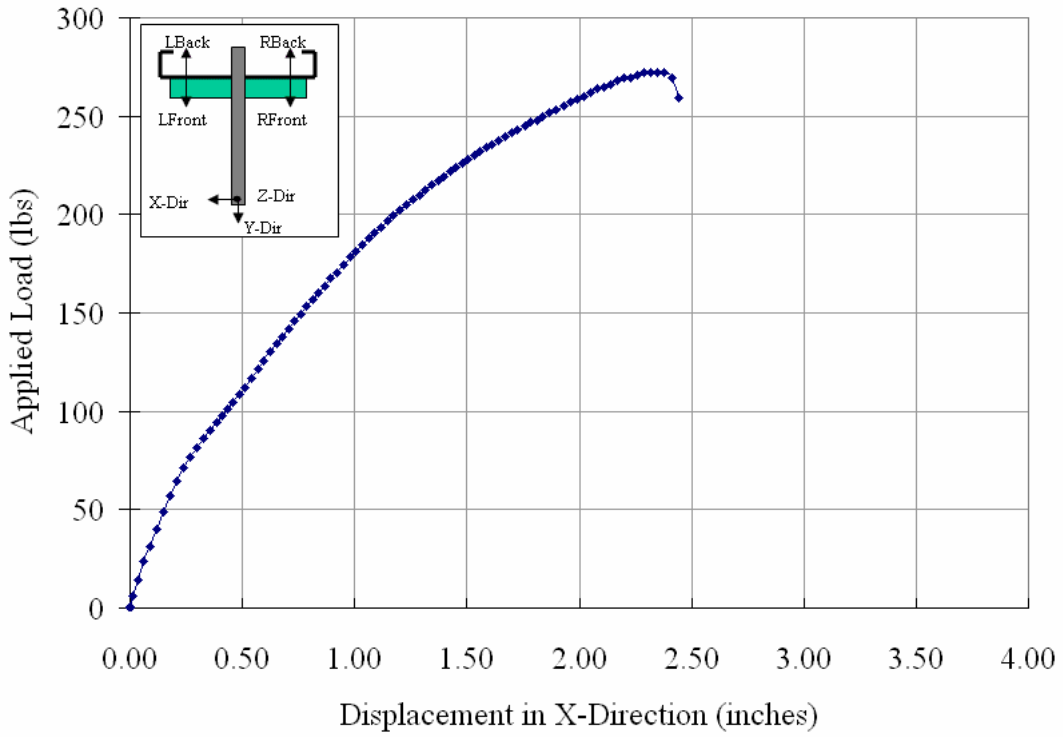
(c) Plot of Applied Load vs. Displacement in X-Direction  
 Figure B1.14

**Out-Of-Plane Load Test on 600S162-97-4SS**



(a) Front View Showing Connection Deformation in 600S162-97-4SS  
 (b) Top Close-up View Showing Screw Pull Out in 600S162-97-4SS

600S 162-97-4 SS



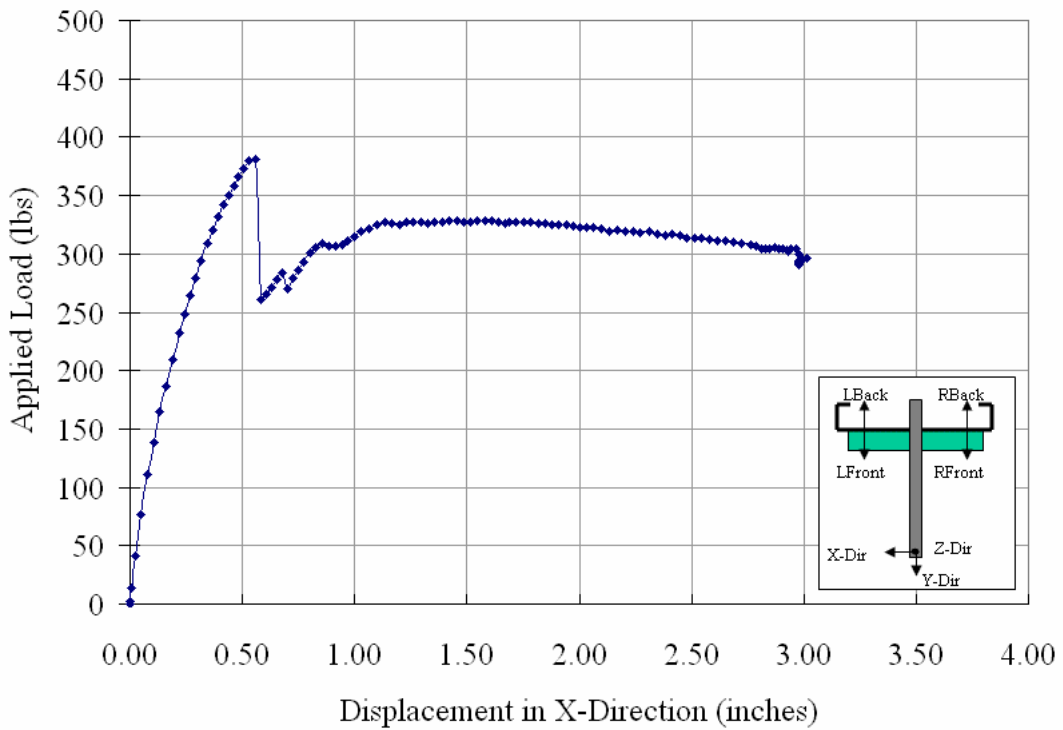
(c) Plot of Applied Load vs. Displacement in X-Direction  
 Figure B1.15

**Out-Of-Plane Load Test on 600S162-97-1WW**



(a) Front View Showing Connection Deformation in 600S162-97-1WW  
 (b) Close-up View Showing Clip Angle Tear in 600S162-97-1WW

600S 162-97-1 WW



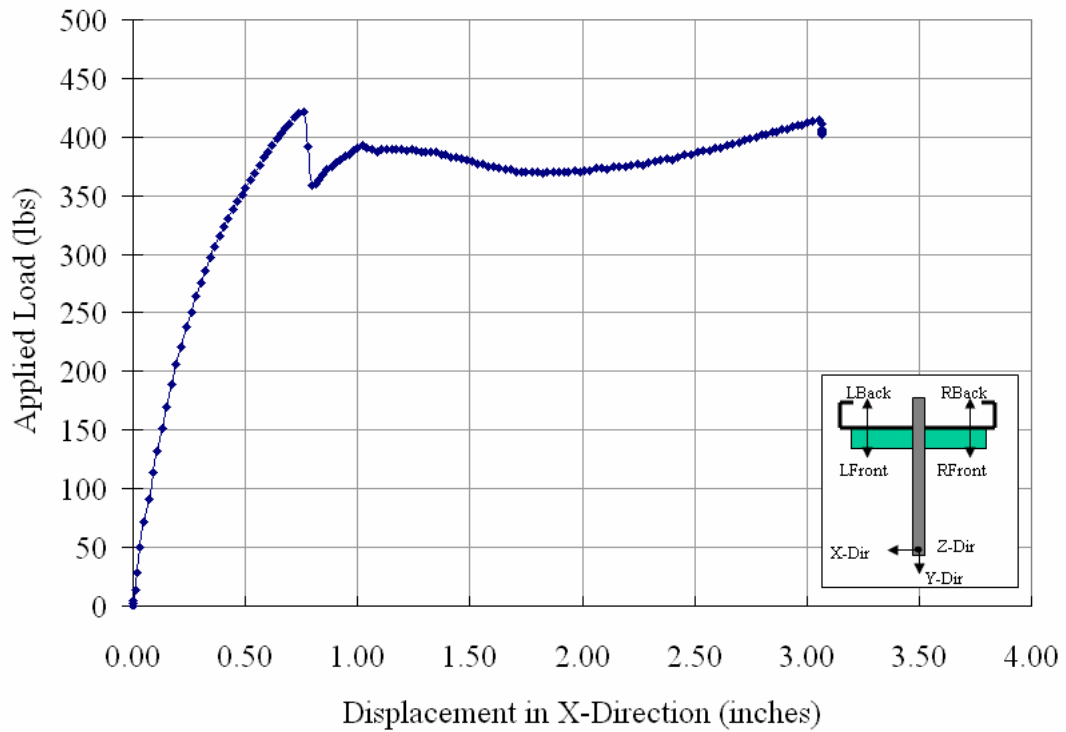
(c) Plot of Applied Load vs. Displacement in X-Direction  
 Figure B1.16

**Out-Of-Plane Load Test on 600S162-97-2WW**



(a) Front View Showing Connection Deformation in 600S162-97-2WW  
 (b) Close-up View Showing Clip Angle Tear and Deformation in 600S162-97-2WW

600S 162-97-2 WW



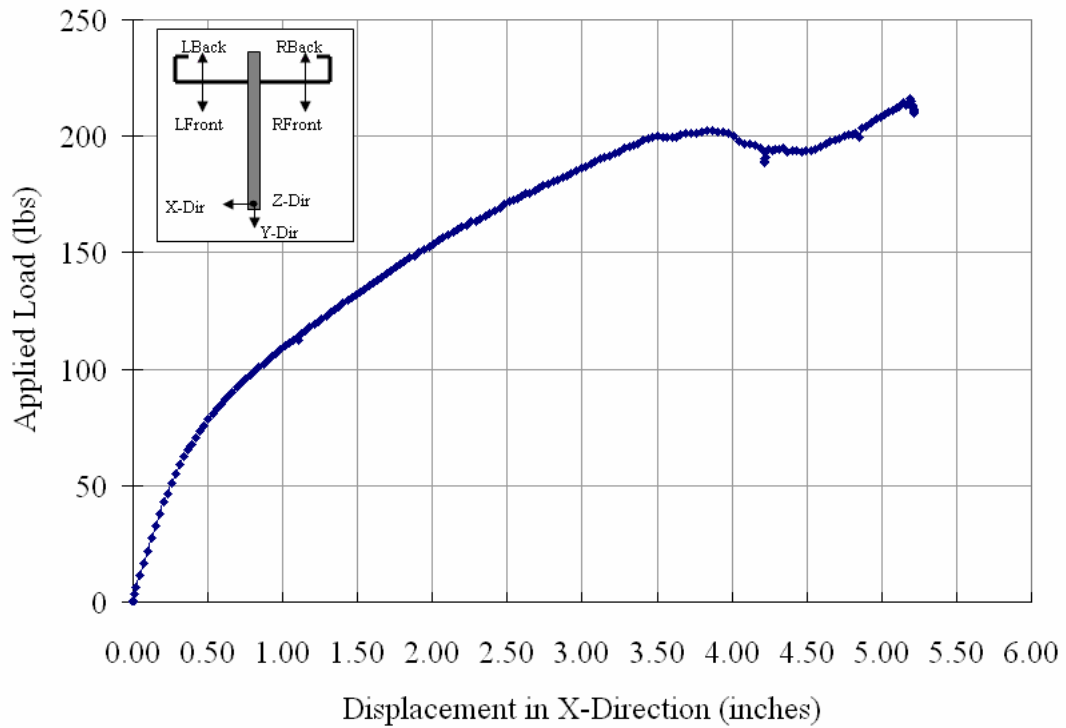
(c) Plot of Applied Load vs. Displacement in X-Direction  
 Figure B1.17

**Out-Of-Plane Load Test on 600S162-97-1DW**



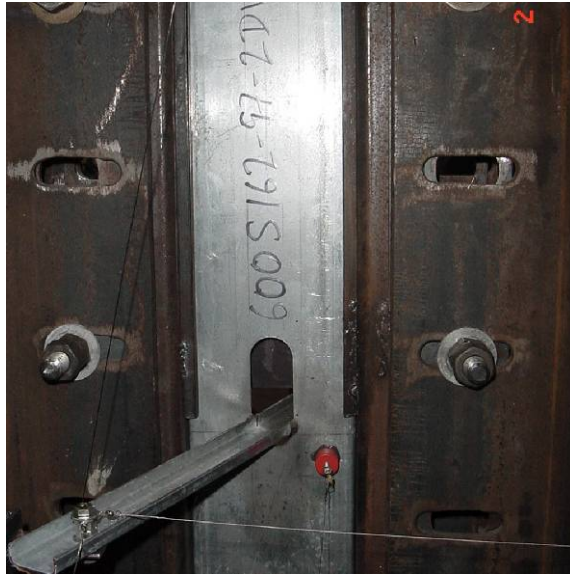
(a) Front View Showing Connection Deformation in 600S162-97-1DW  
 (b) Back View Showing Weld Tear and Plate Deformation in 600S162-97-1DW

600S 162-97-1 DW



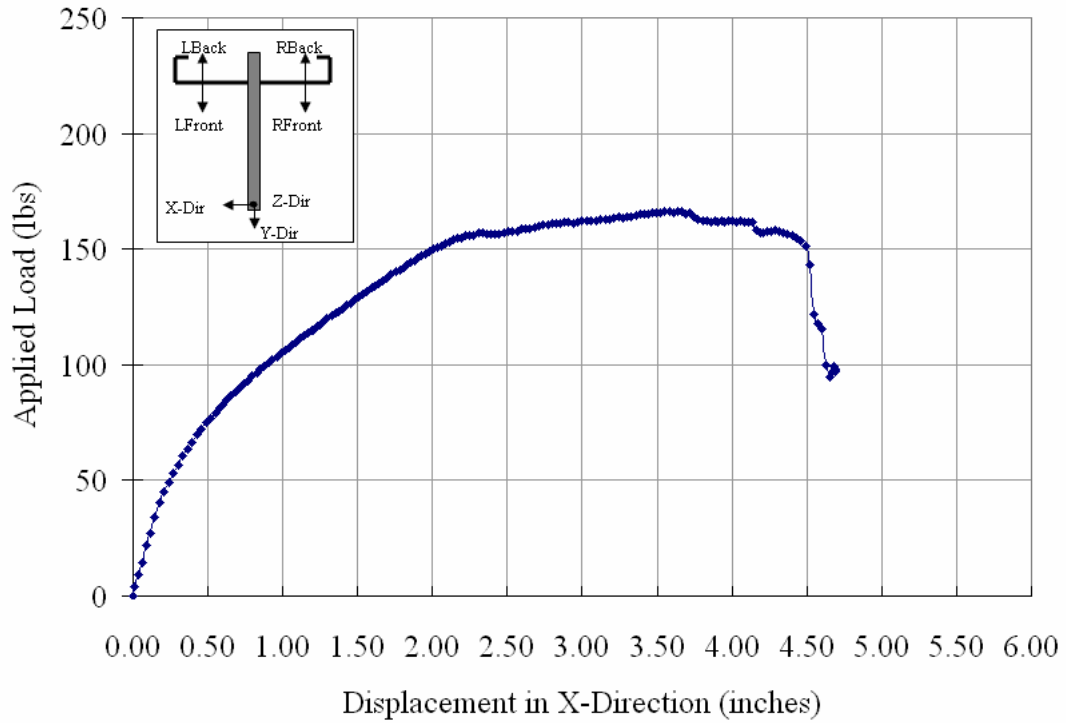
(c) Plot of Applied Load vs. Displacement in X-Direction  
 Figure B1.18

**Out-Of-Plane Load Test on 600S162-97-2DW**



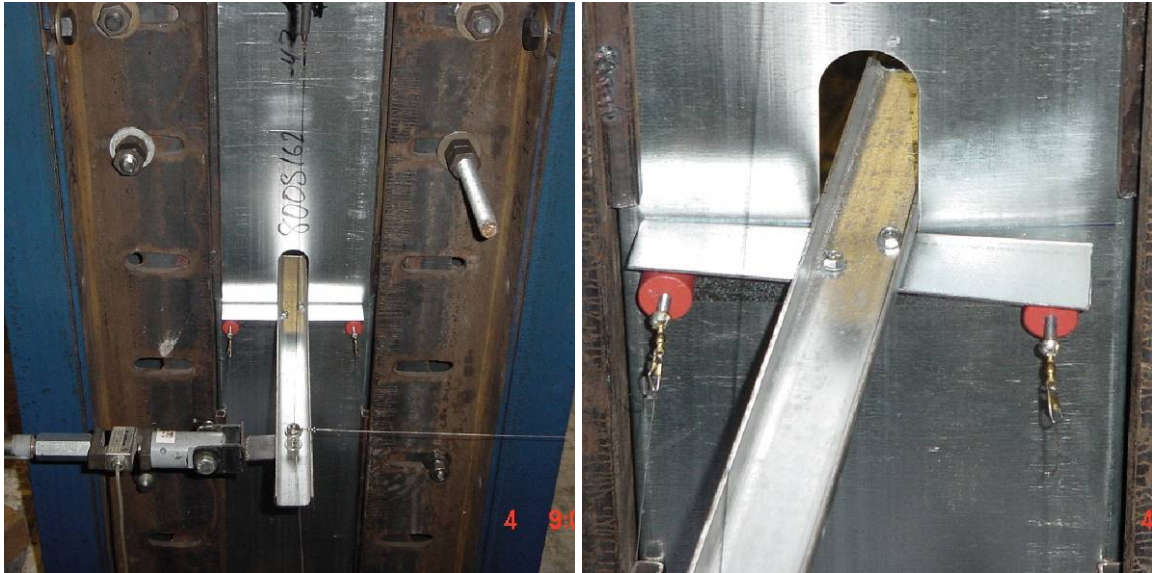
(a) Front View Showing Connection Deformation in 600S162-97-2DW

600S 162-97-2 DW



(b) Plot of Applied Load vs. Displacement in X-Direction  
Figure B1.19

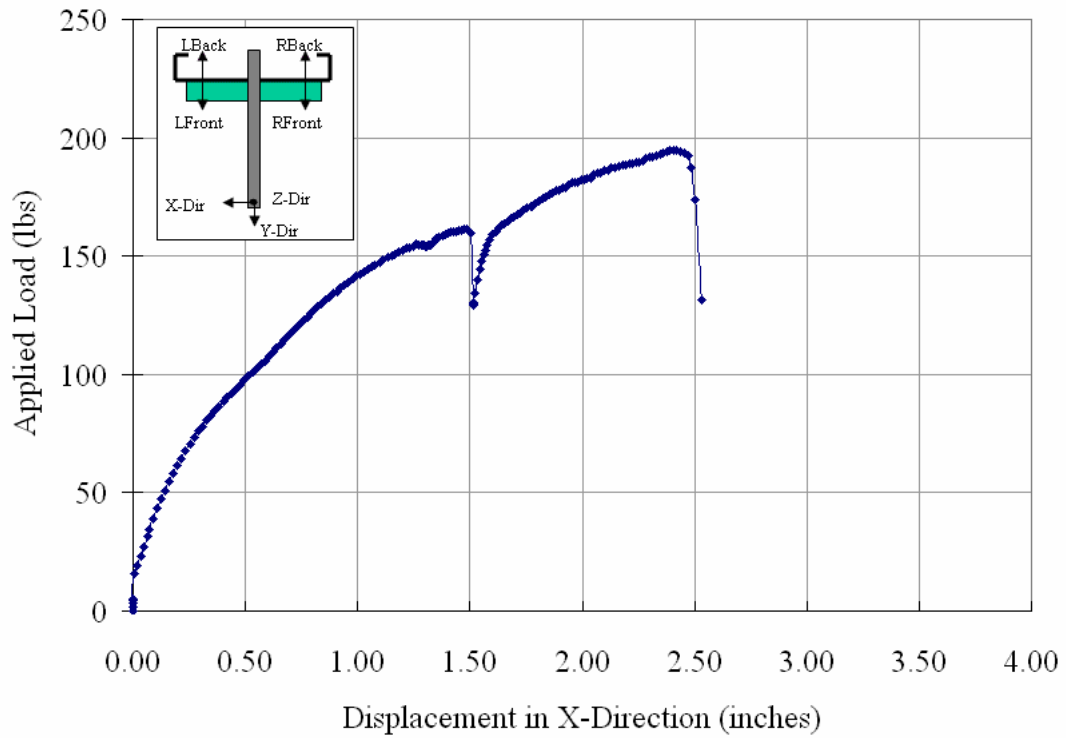
**Out-Of-Plane Load Test on 800162-43-1SS**



(a) Initial Front View of 800162-43-1SS

(b) Final Left Front View Showing Screw Pull Out and Clip Angle Deformation in 800S162-43-1SS

800S 162-43-1 SS



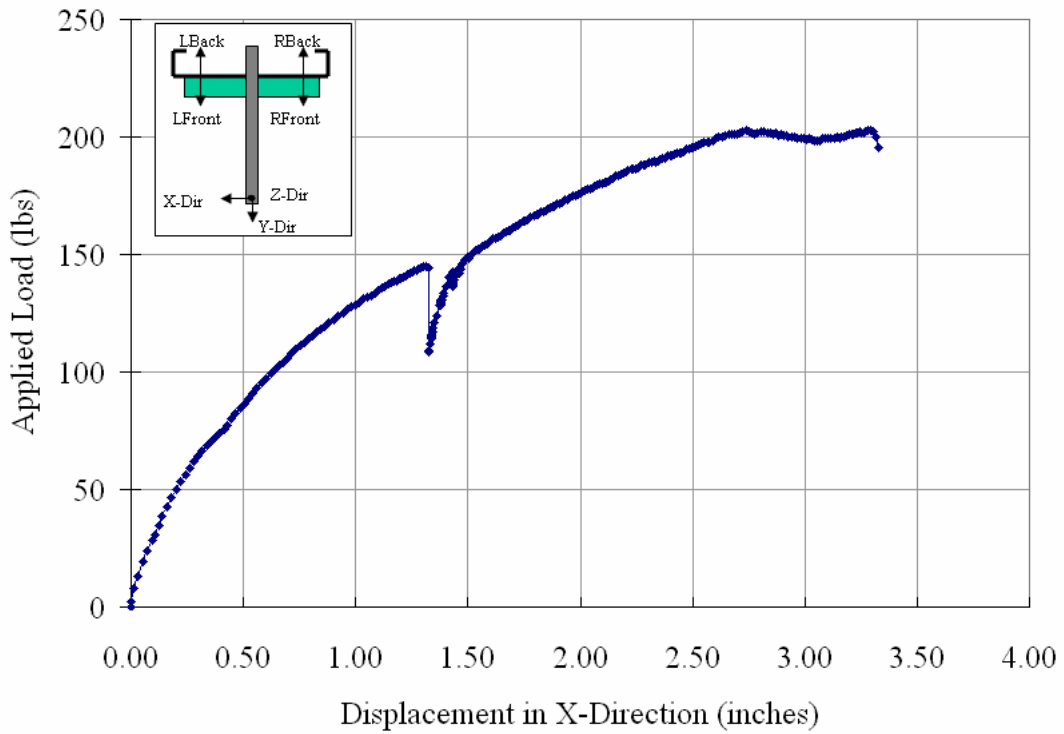
(c) Plot of Applied Load vs. Displacement in X-Direction  
Figure B1.20

**Out-Of-Plane Load Test on 800S162-43-2SS**



(a) Front View Showing Clip Angle Deformation in 800S162-43-2SS  
 (b) Top View Showing Screw Pull Out in 800S162-43-2SS

800S 162-43-2 SS



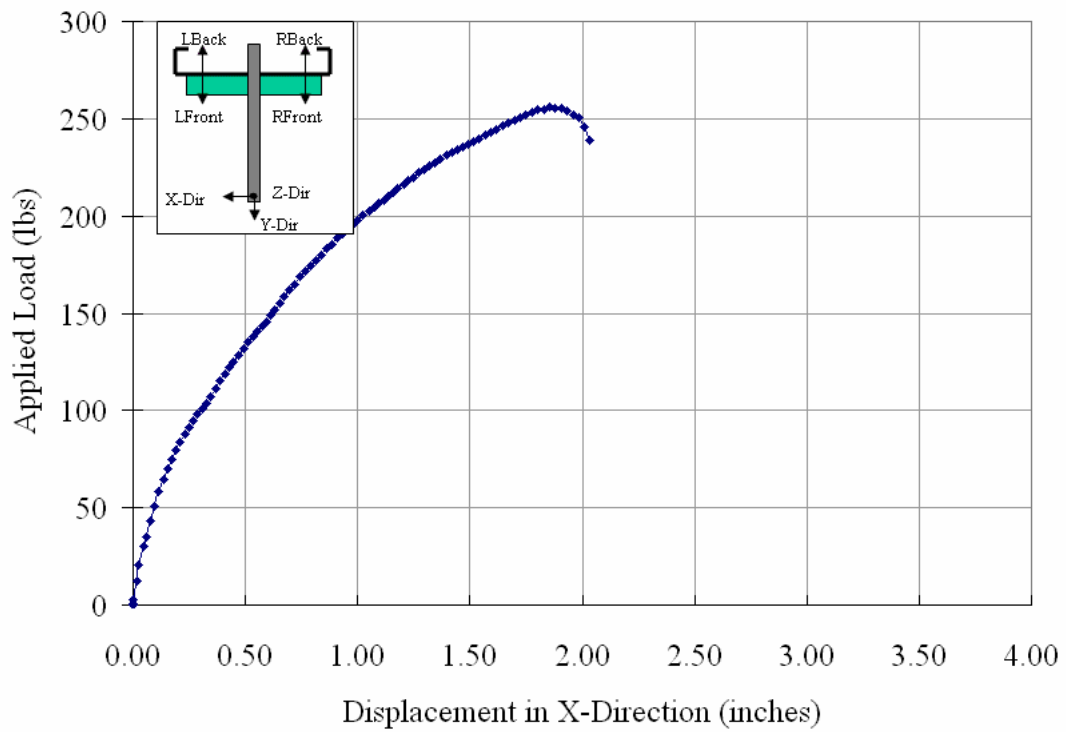
(c) Plot of Applied Load vs. Displacement in X-Direction  
 Figure B1.21

### Out-Of-Plane Load Test on 800S162-97-1SS



- (a) Front View Showing Connection Deformation in 800S162-97-1SS  
 (b) Top View Showing Connection Deformation in 800S162-97-1SS

800S 162-97-1 SS



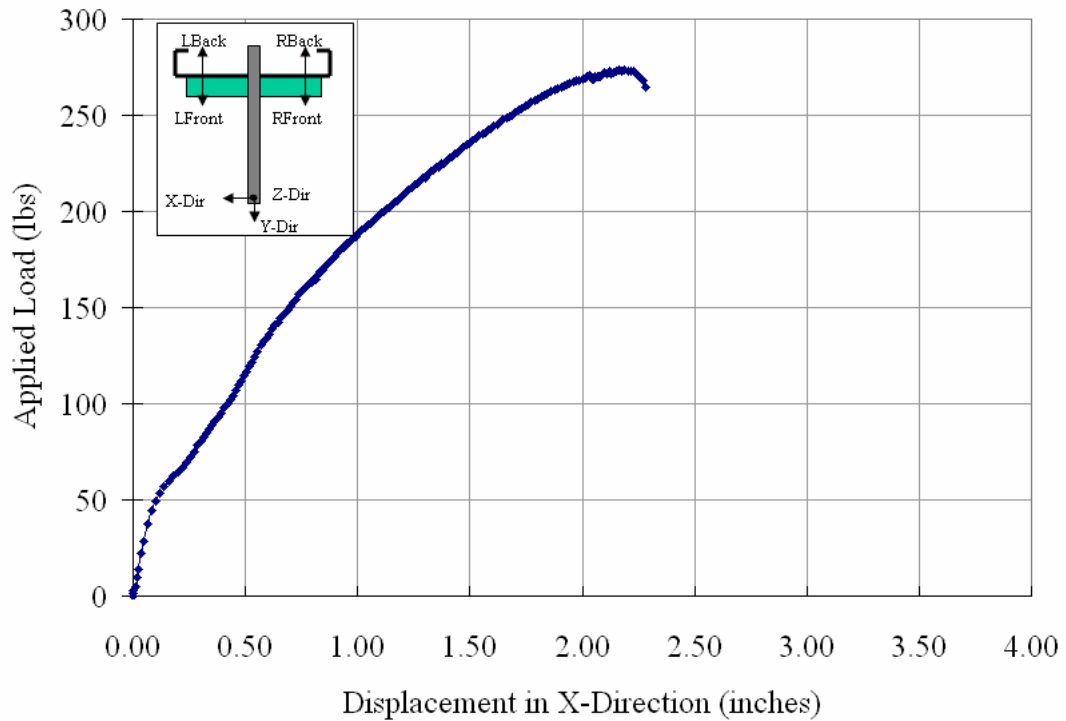
- (c) Plot of Applied Load vs. Displacement in X-Direction  
 Figure B1.22

### Out-Of-Plane Load Test on 800S162-97-2SS



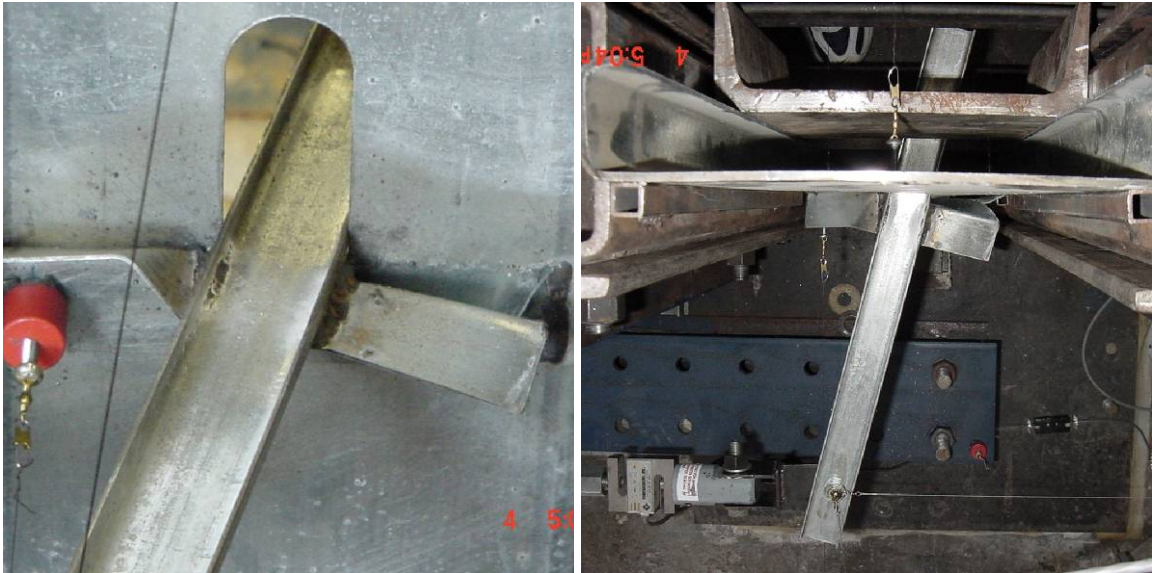
(a) Top View Showing Connection Deformation in 800S162-97-2SS  
 (b) Left Front View Showing Screw Shear in 800S162-97-2SS

800S 162-97-2 SS



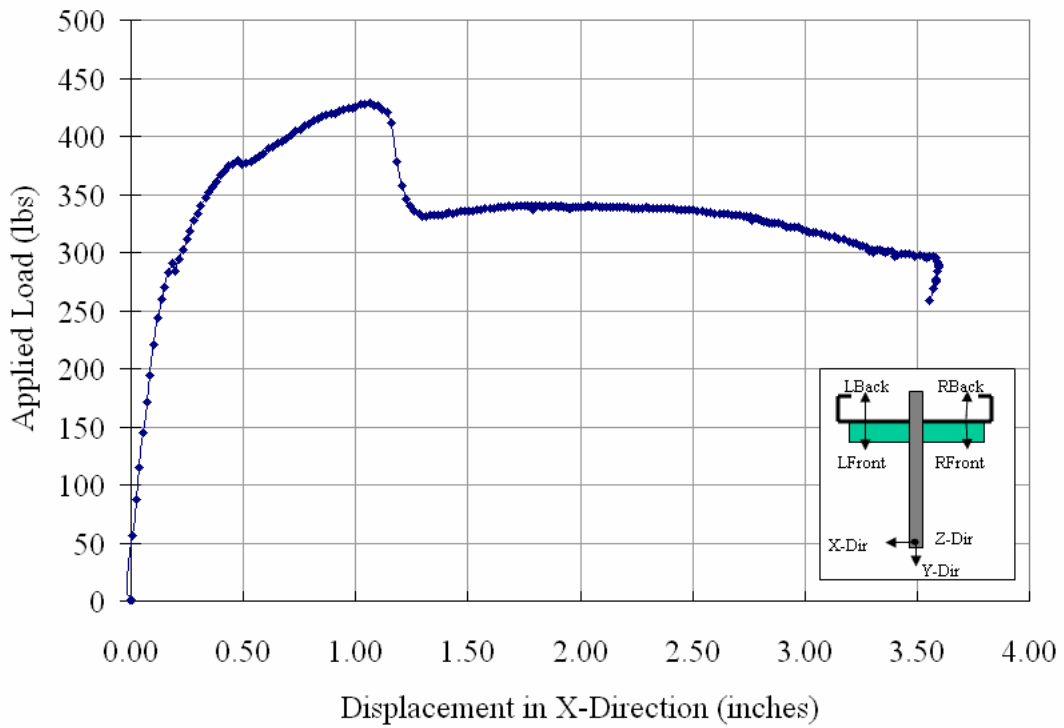
(c) Plot of Applied Load vs. Displacement in X-Direction  
 Figure B1.23

**Out-Of-Plane Load Test on 800S162-97-1WW**



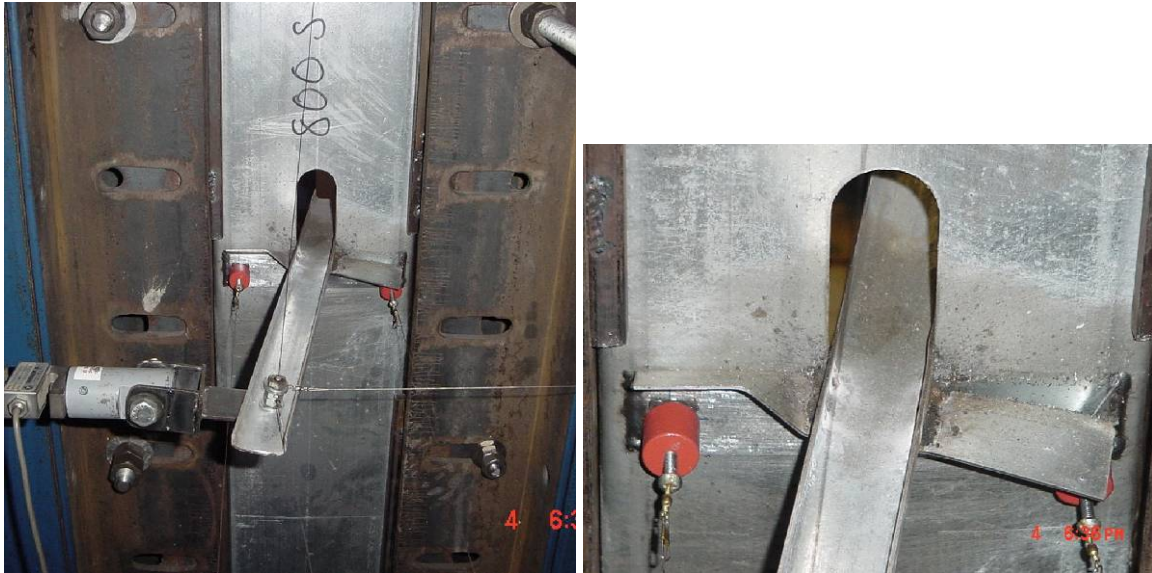
(a) Front View Showing Clip Angle Deformation in 800S162-97-1WW  
 (b) Top View Showing Connection Deformation in 800S162-97-1WW

800S 162-97-1 WW



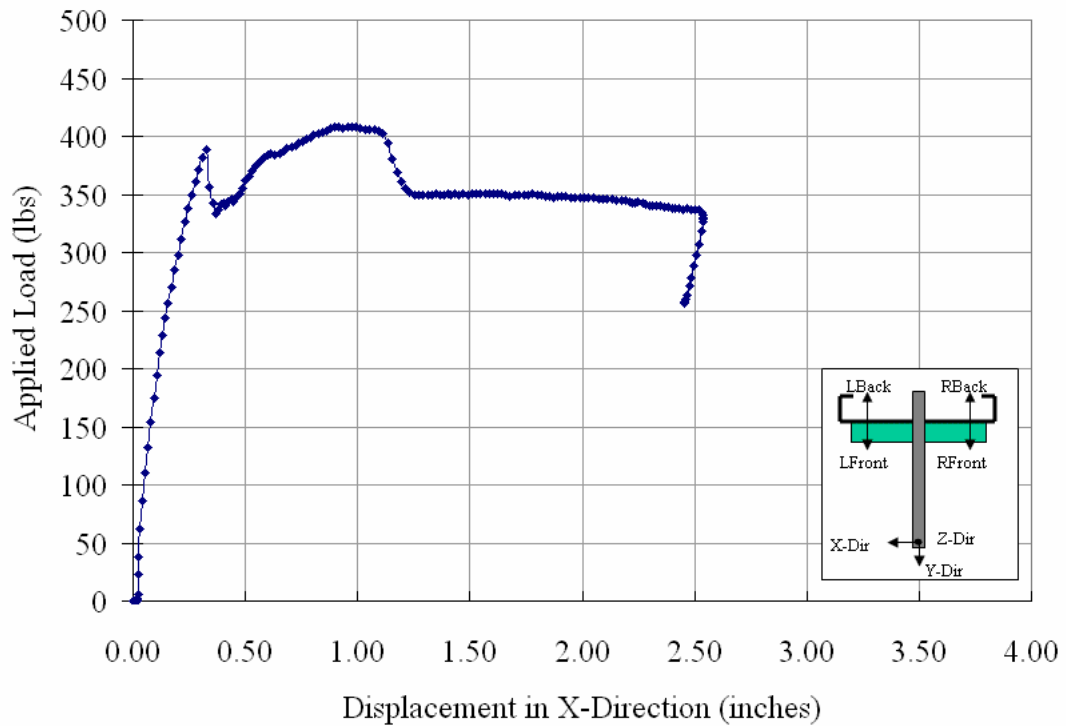
(c) Plot of Applied Load vs. Displacement in X-Direction  
 Figure B1.24

**Out-Of-Plane Load Test on 800S162-97-2WW**



(a) Front View Showing Clip Angle Deformation in 800S162-97-2WW  
 (b) Close-up View Showing Clip Angle Tear and Deformation in 800S162-97-2WW

800S 162-97-2 WW



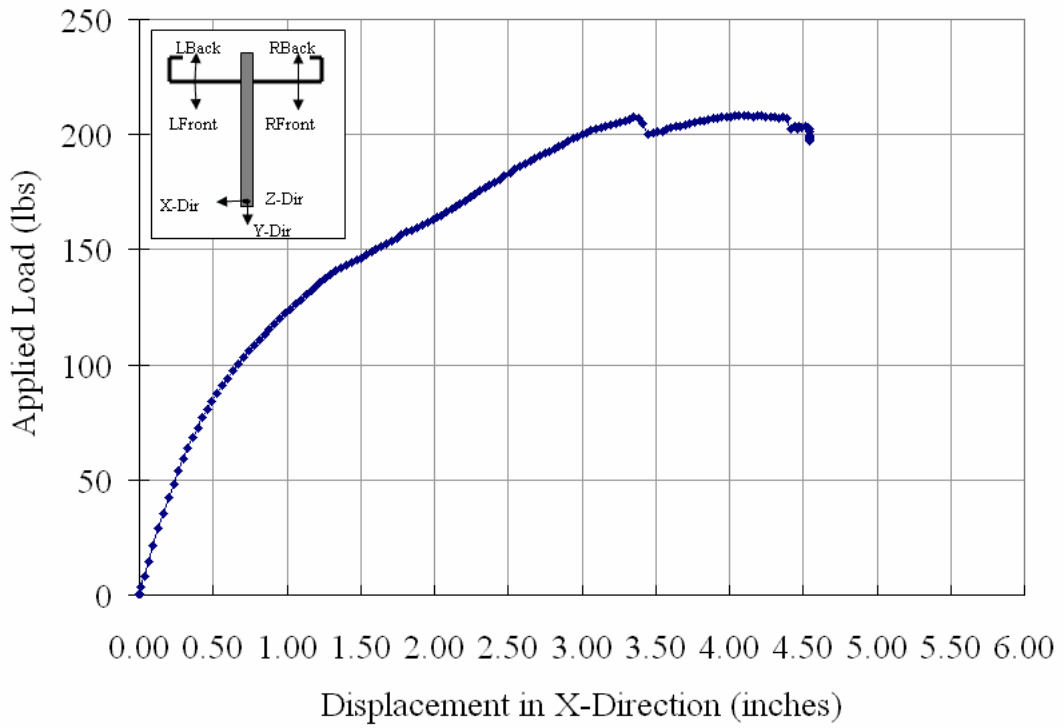
(c) Plot of Applied Load vs. Displacement in X-Direction  
 Figure B1.25

**Out-Of-Plane Load Test on 800S162-97-1DW**



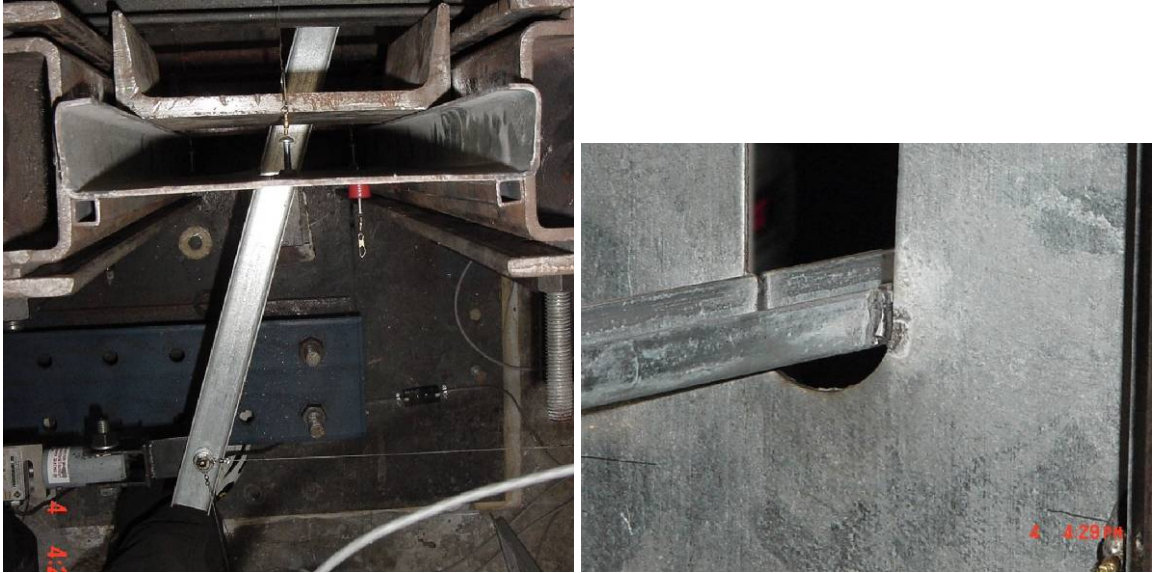
(a) Front View Showing Connection Deformation in 800S162-97-1DW  
 (b) Close-up View Showing Weld Tear in 800S162-97-1DW

800S 162-97-1 DW



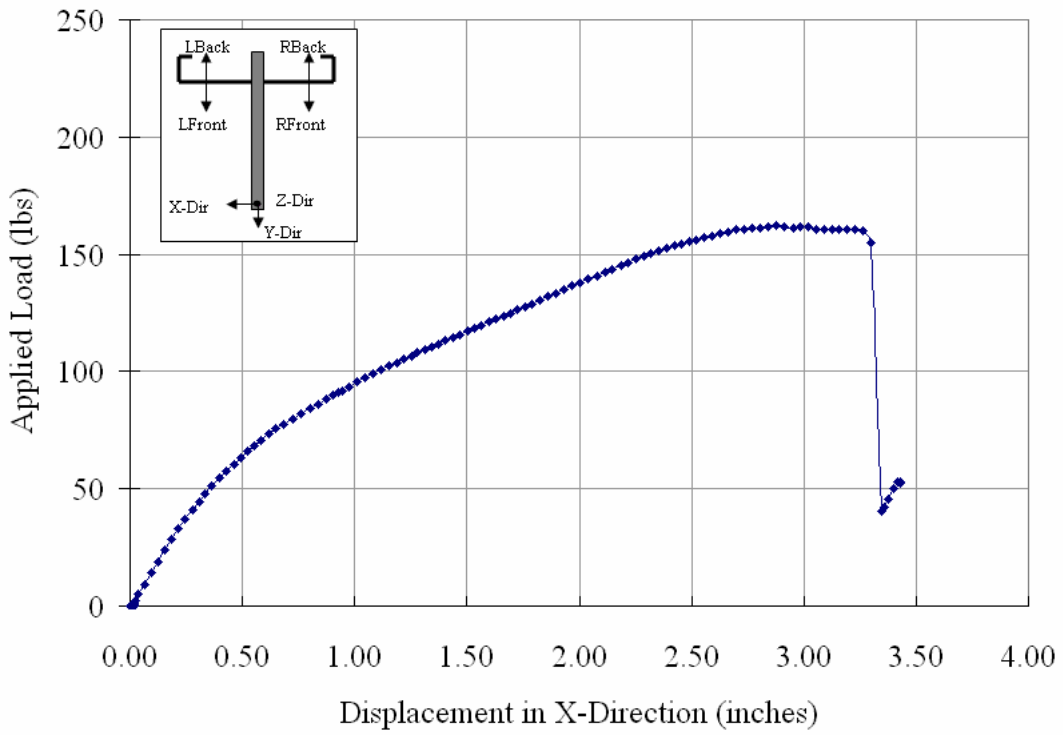
(c) Plot of Applied Load vs. Displacement in X-Direction  
 Figure B1.26

**Out-Of-Plane Load Test on 800S162-97-2DW**



(a) Top View Showing Connection Deformation in 800S162-97-2DW  
 (b) Close-up View Showing Weld Tear in 800S162-97-2DW

800S 162-97-2 DW



(c) Plot of Applied Load vs. Displacement in X-Direction  
 Figure B1.27

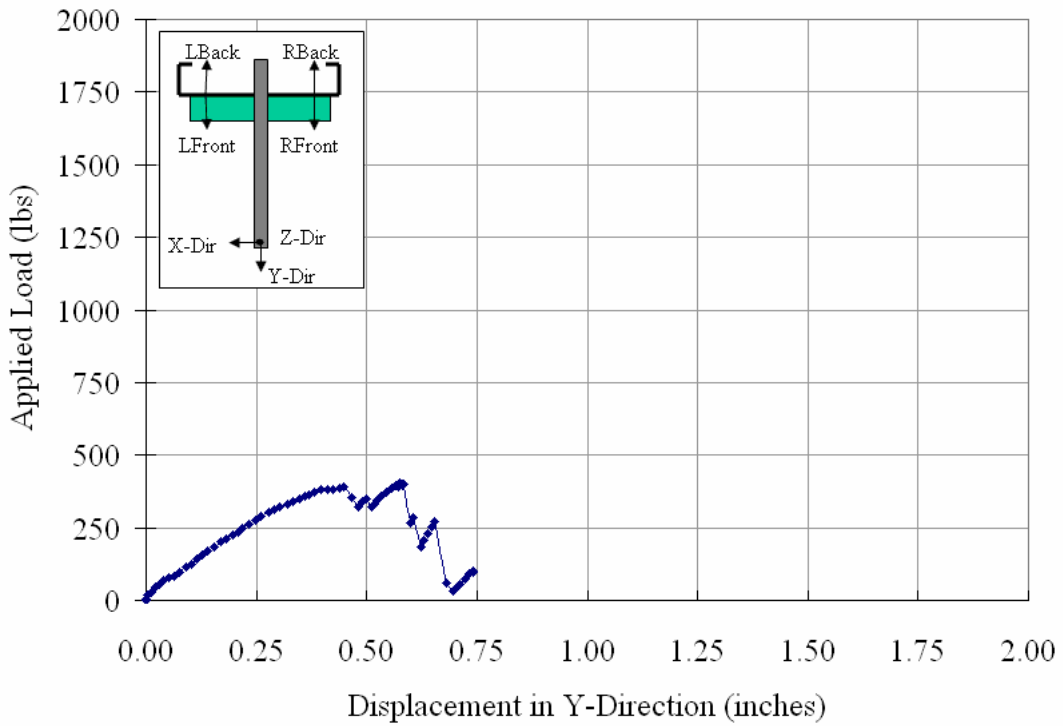
**In-Plane Load Test on 362S125-33-3SS**



(a) Initial View of 362S125-33-3SS

(b) Final View Showing Clip Angle Deformation, Screw Pull Out of 362S125-33-3SS

362S 125-33-3 SS



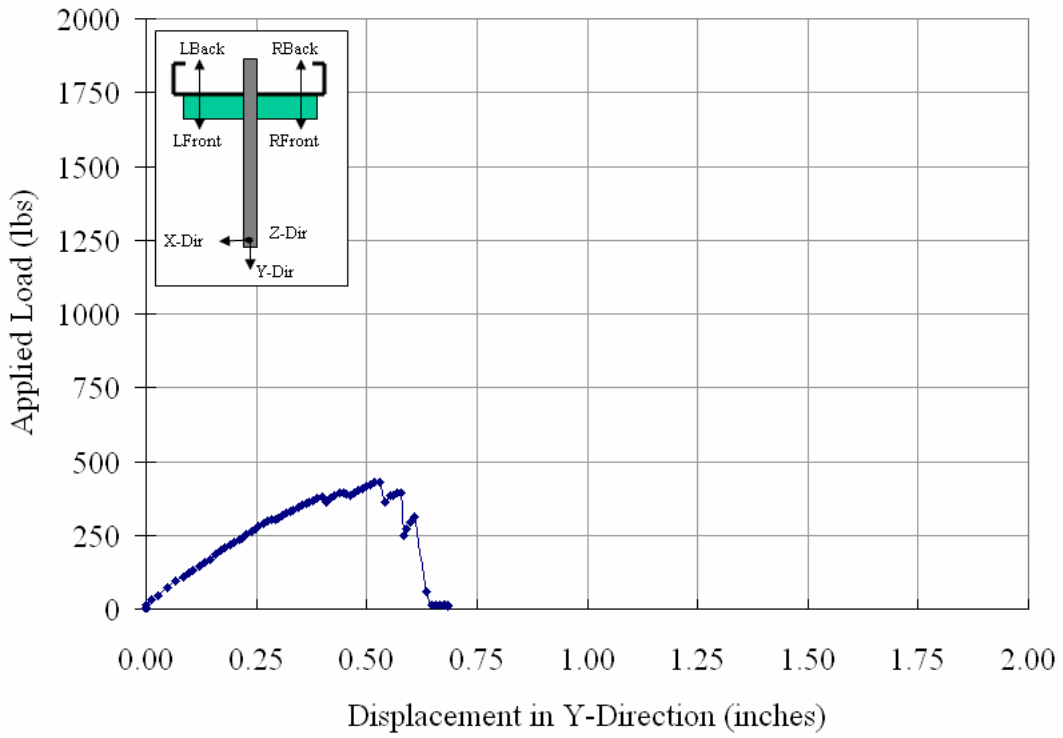
(c) Plot of Applied Load vs. Displacement in Y-Direction  
Figure B2.1

**In-Plane Load Test on 362S125-33-4SS**



(a) Initial View of 362S125-33-4SS  
 (b) Final View Showing Clip Angle Deformation, Screw Pull Out of 362S125-33-4SS

362S 125-33-4 SS



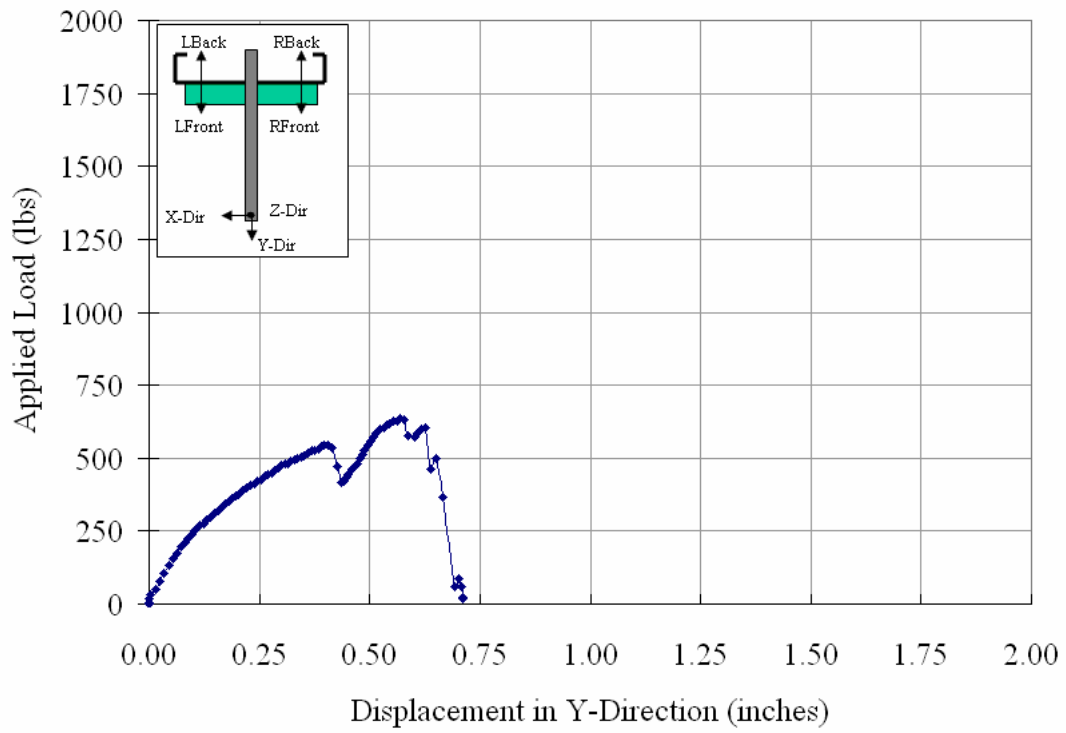
(c) Plot of Applied Load vs. Displacement in Y-Direction  
 Figure B2.2

**In-Plane Load Test on 362S162-43-3SS**



(a) Final Front View Showing Clip Angle Deformation of 362S162-43-3SS  
 (b) Top View Showing Clip Angle Deformation, Screw Pull Out of 362S162-43-3SS

362S 162-43-3 SS



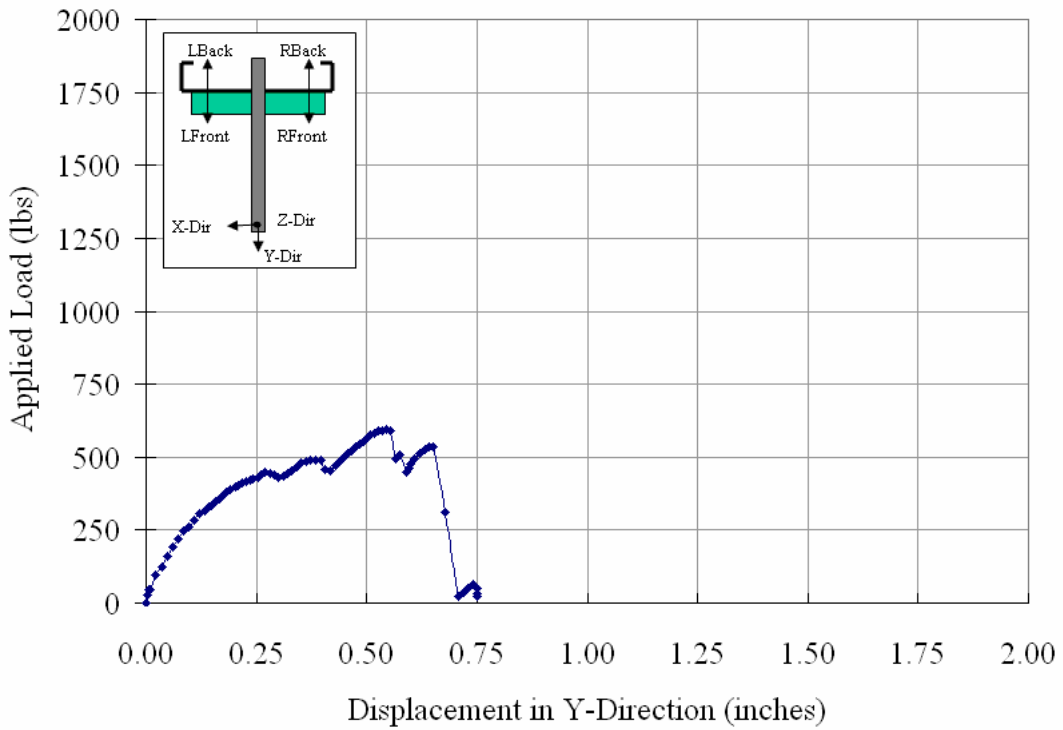
(c) Plot of Applied Load vs. Displacement in Y-Direction  
 Figure B2.3

**In-Plane Load Test on 362S162-43-4SS**



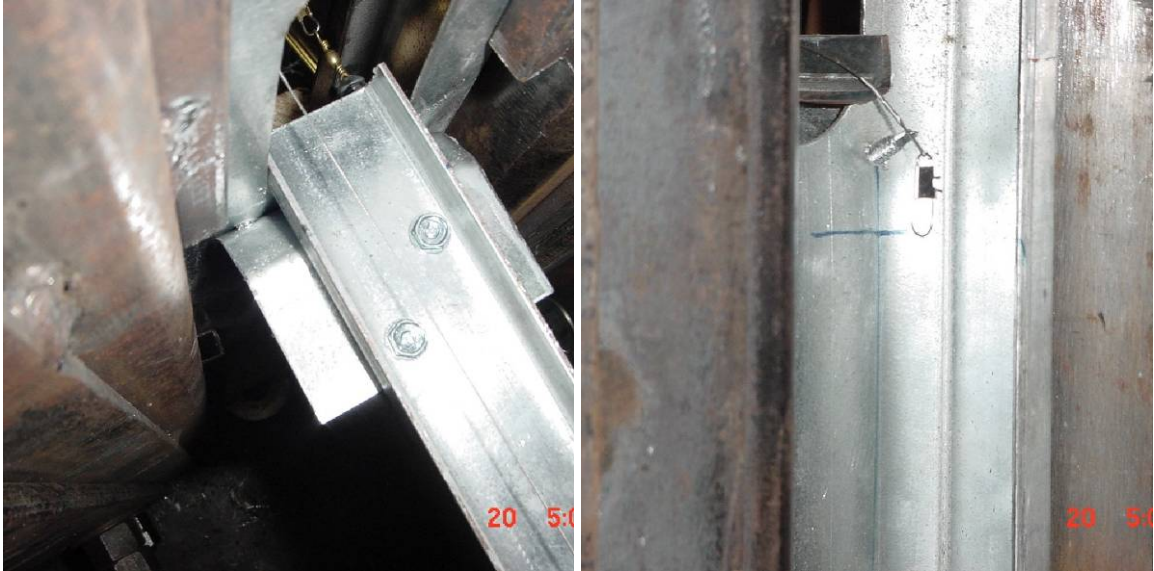
(a) Final Front View Showing Clip Angle Deformation of 362S162-43-4SS  
 (b) Top View Showing Clip Angle Deformation, Screw Pull Out of 362S162-43-4SS

362S 162-43-4 SS



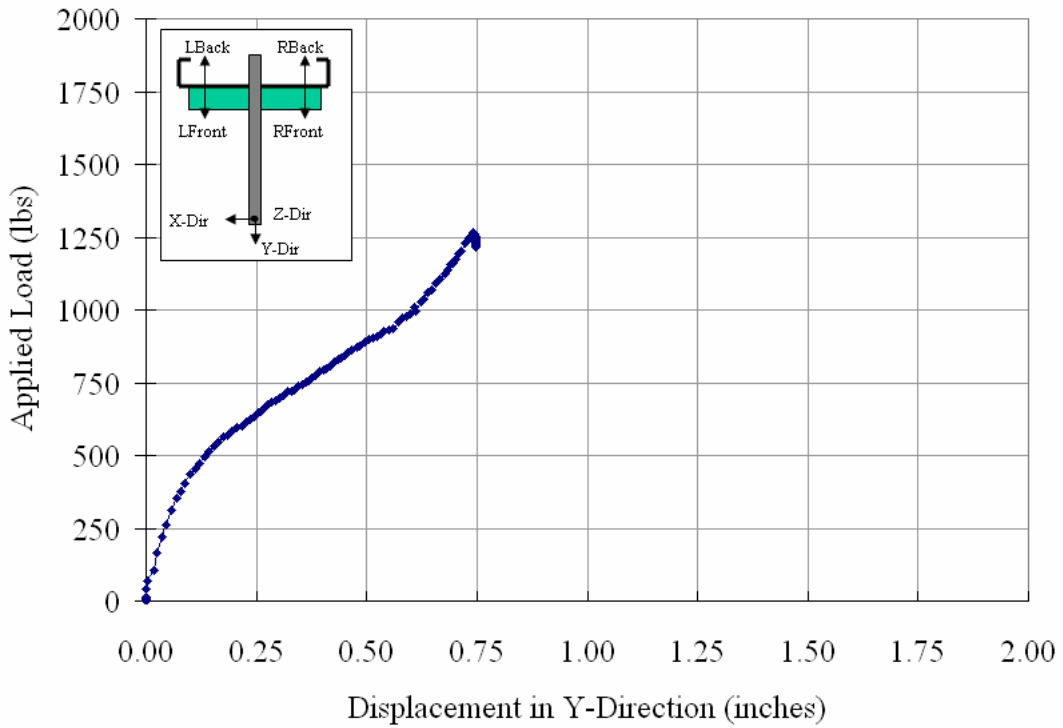
(c) Plot of Applied Load vs. Displacement in Y-Direction  
 Figure B2.4

**In-Plane Load Test on 362S162-68-3SS**



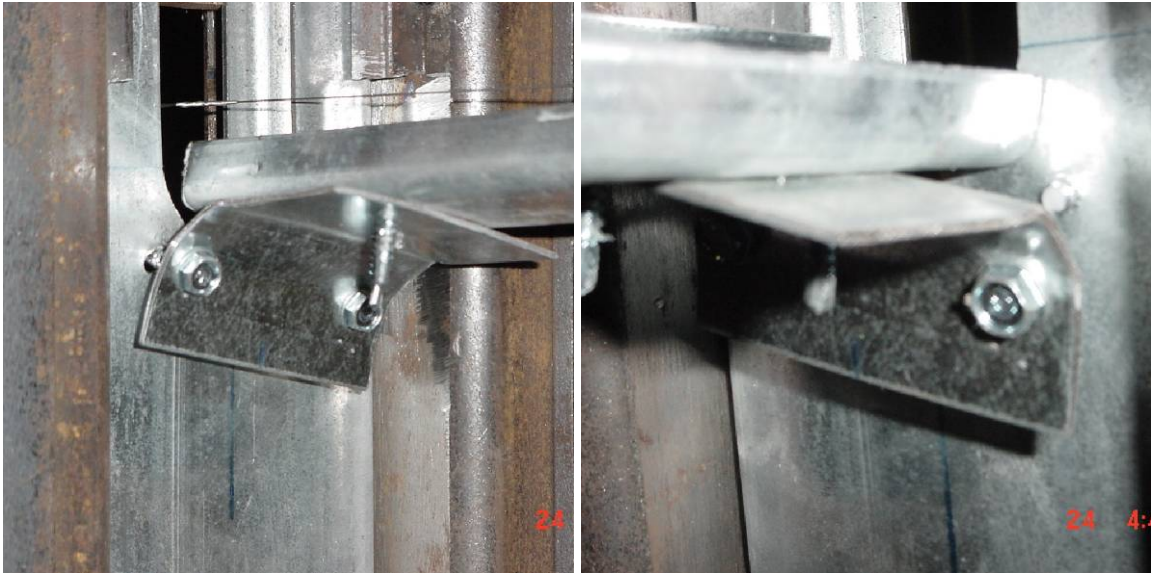
(a) Final Top View Showing Clip Angle Deformation of 362S162-68-3SS  
 (b) Left Back View showing Screw Rotation of 362S162-68-3SS

362S 162-68-3 SS



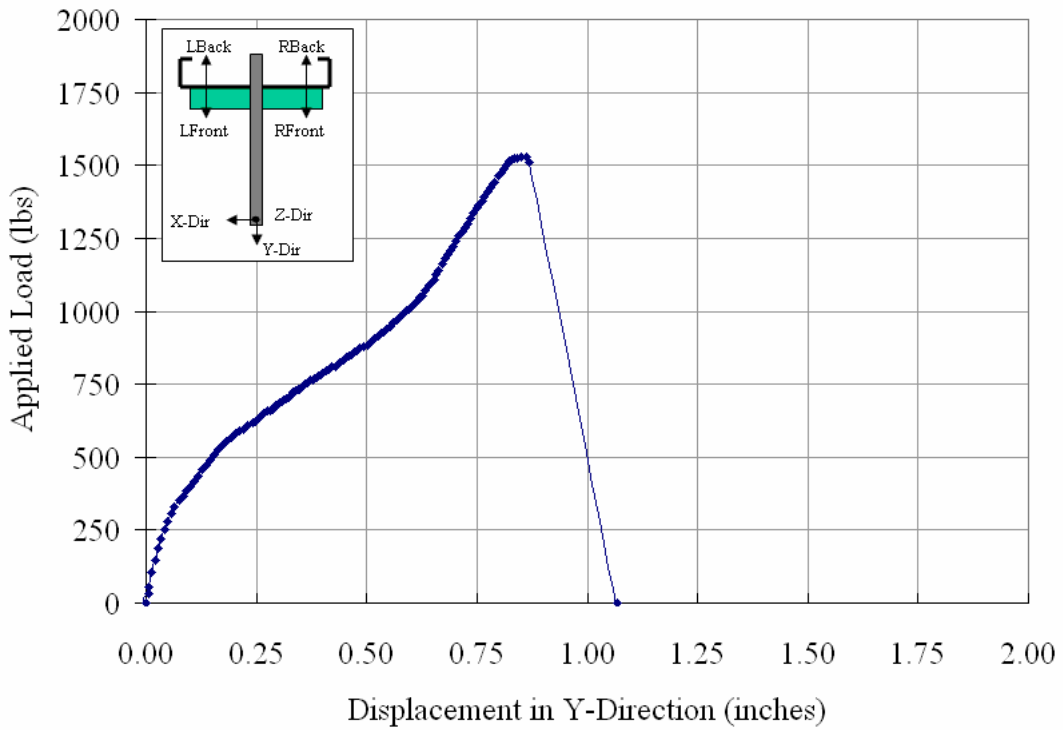
(c) Plot of Applied Load vs. Displacement in Y-Direction  
 Figure B2.5

**In-Plane Load Test on 362S162-68-4SS**



(a) Final Left View Showing Clip Angle Deformation of 362S162-68-4SS  
 (b) Final Right View showing Screw Failure of 362S162-68-4SS

362S 162-68-4 SS



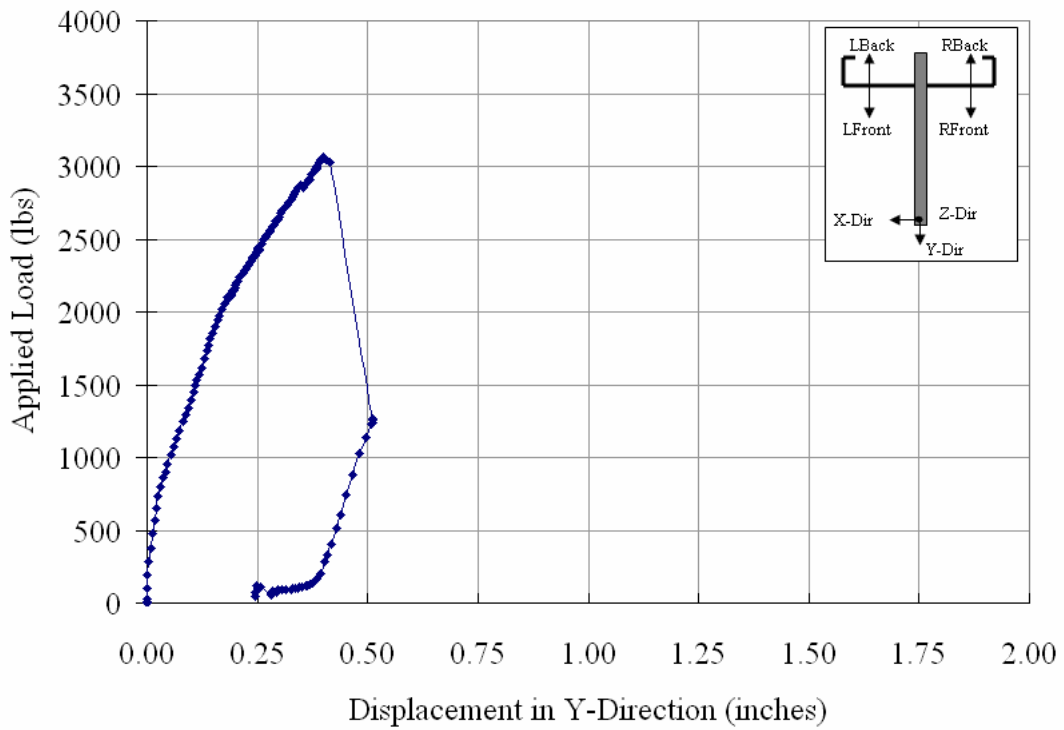
(c) Plot of Applied Load vs. Displacement in Y-Direction  
 Figure B2.6

**In-Plane Load Test on 362S162-68-3DW**



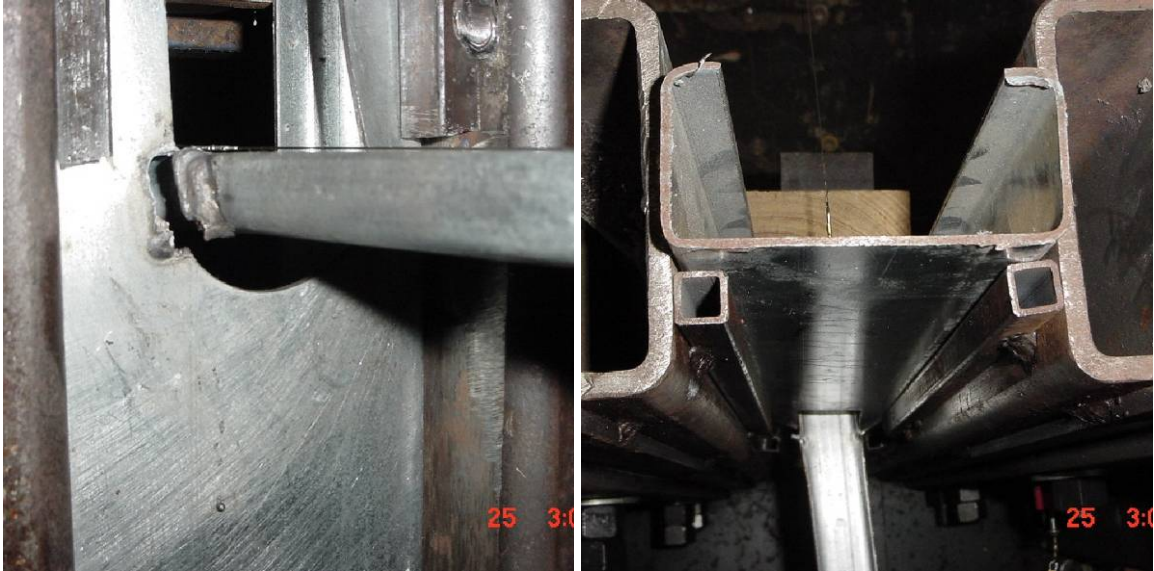
(a) Left-Front View Showing Weld Failure of 362S162-68-3DW  
 (b) Right-Front View Showing Block Shear Rupture of Web of 362S162-68-3DW

362S 162-68-3 DW



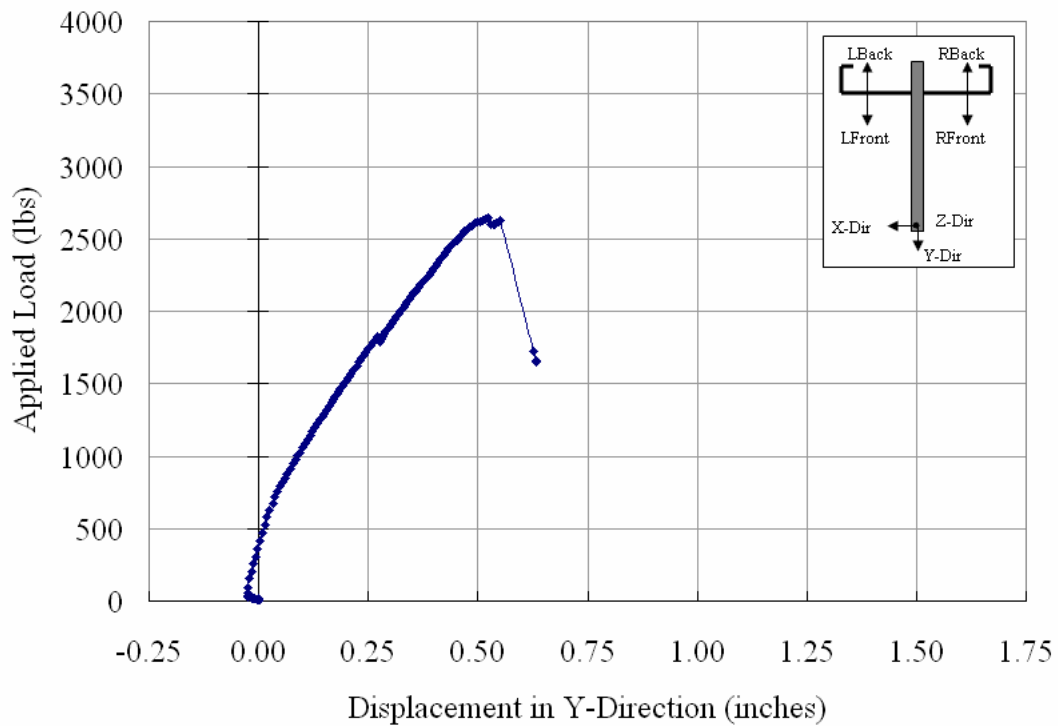
(c) Plot of Applied Load vs. Displacement in Y-Direction  
 Figure B2.7

### In-Plane Load Test on 362S162-68-4DW



- (a) Left-Front View Showing Block Shear Rupture of Web of 362S162-68-4DW  
 (b) Top View Showing the Connection Failure 362S162-68-4DW

362S 162-68-4 DW



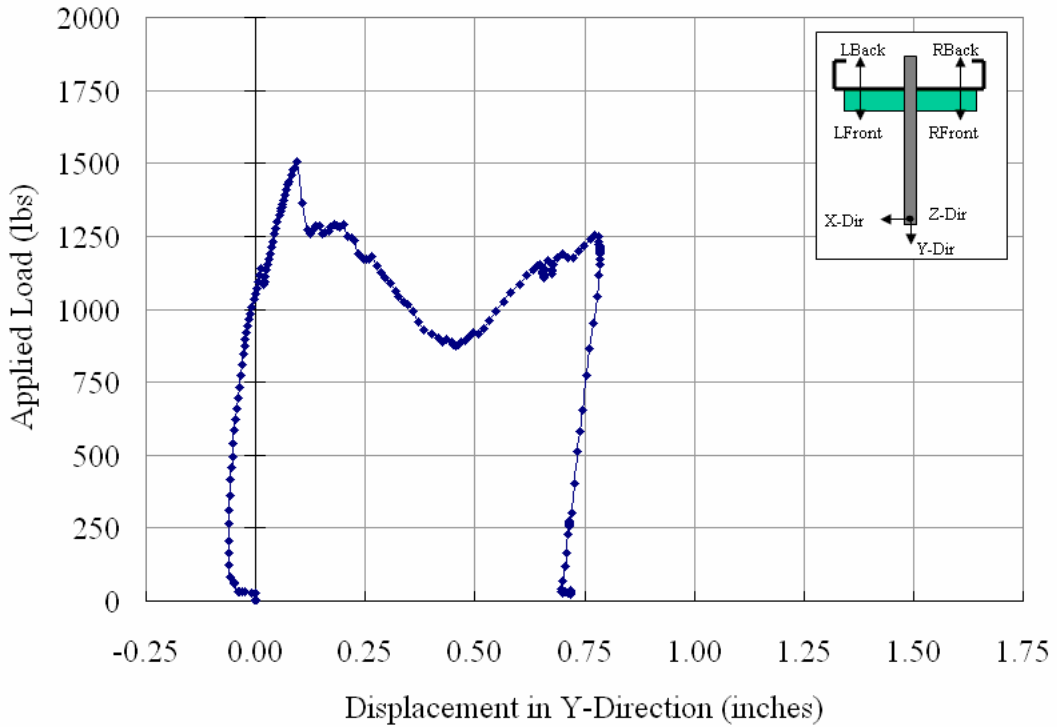
- (c) Plot of Applied Load vs. Displacement in Y-Direction  
 Figure B2.8

**In-Plane Load Test on 362S162-68-3WW**



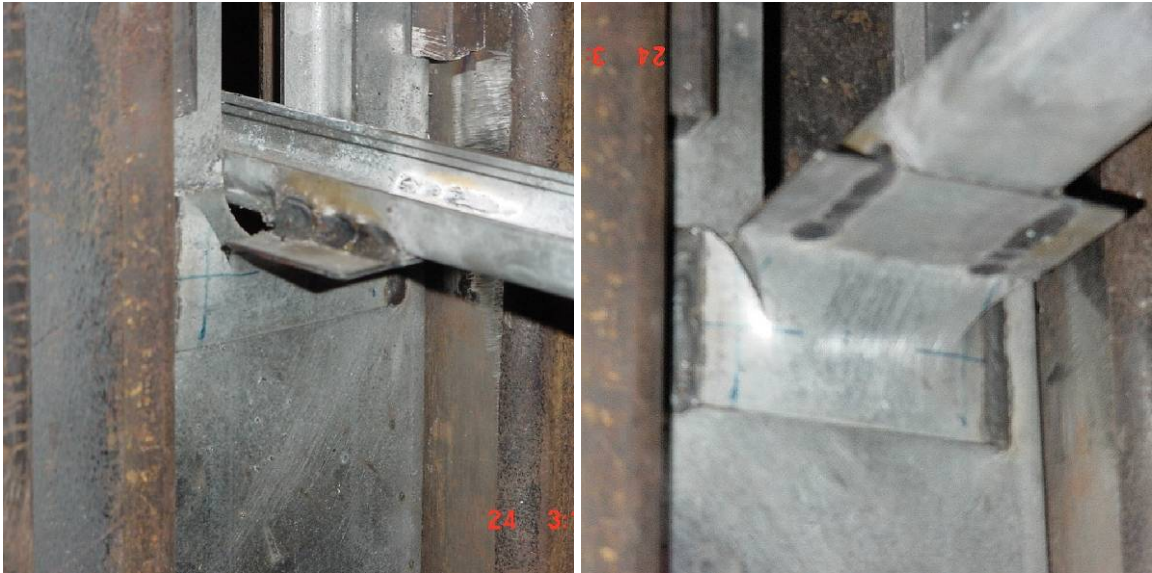
(a) Final View Showing Weld Tear in 362S162-68-3WW

362S 162-68-3 WW



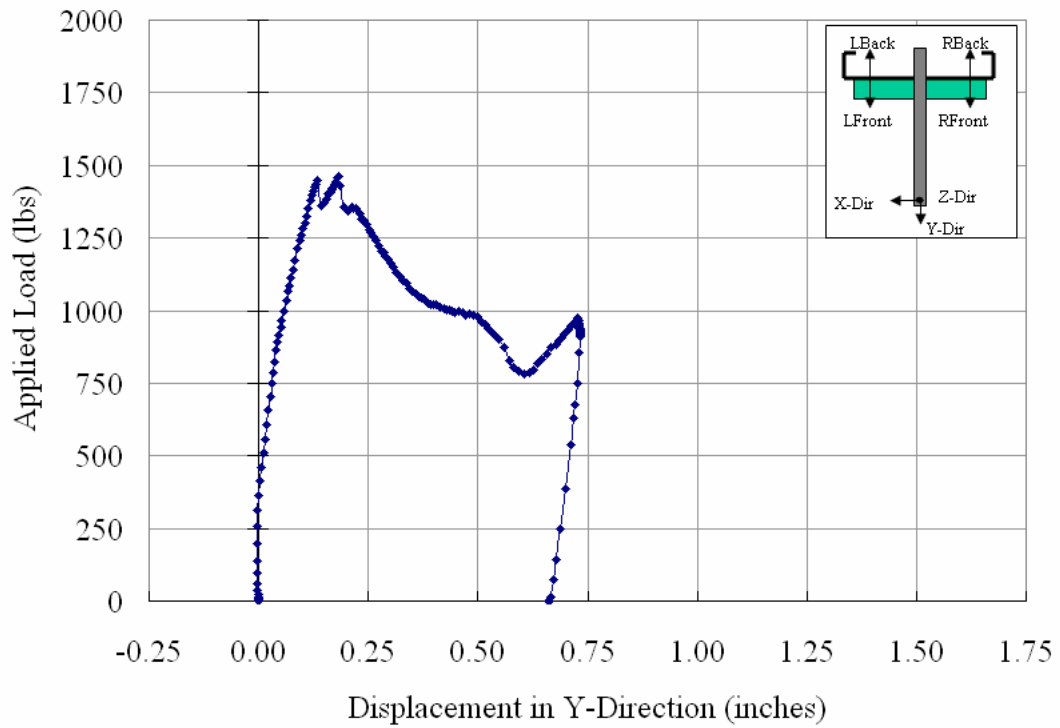
(b) Plot of Applied Load vs. Displacement in Y-Direction  
Figure B2.9

(a) In-Plane Load Test on 362S162-68-4WW



(b) Final Views Showing Clip Angle Tear in 362S162-68-4WW

362S 162-68-4 WW



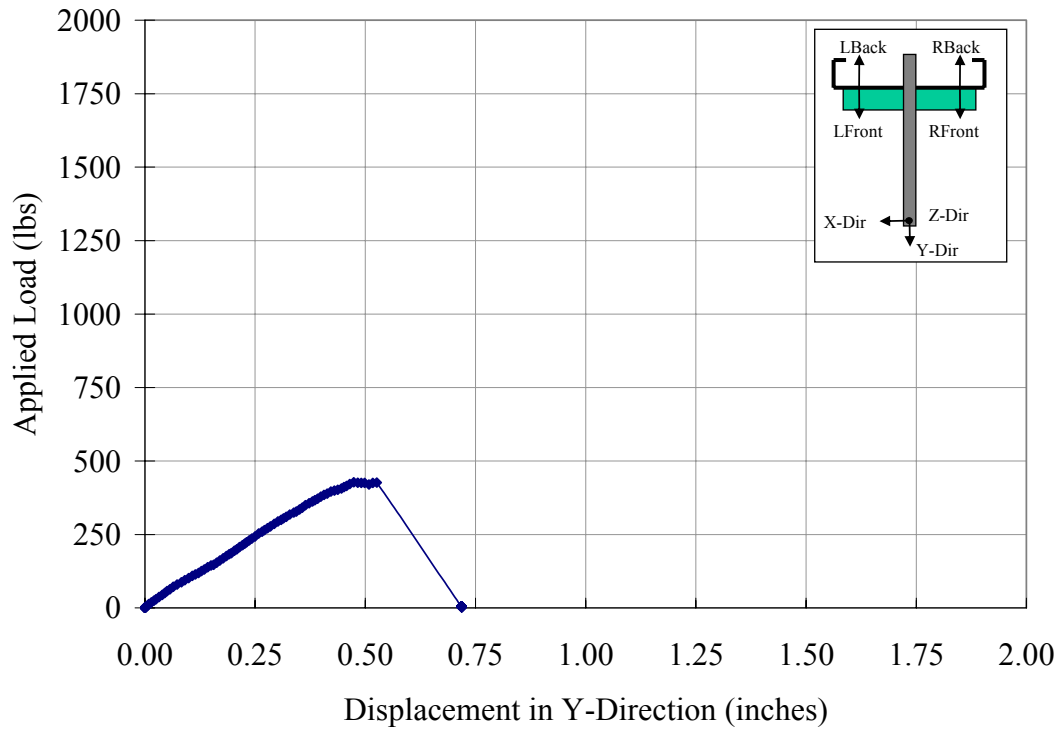
(c) Plot of Applied Load vs. Displacement in Y-Direction  
Figure B2.10

**In-Plane Load Test on 600S125-33-3SS**



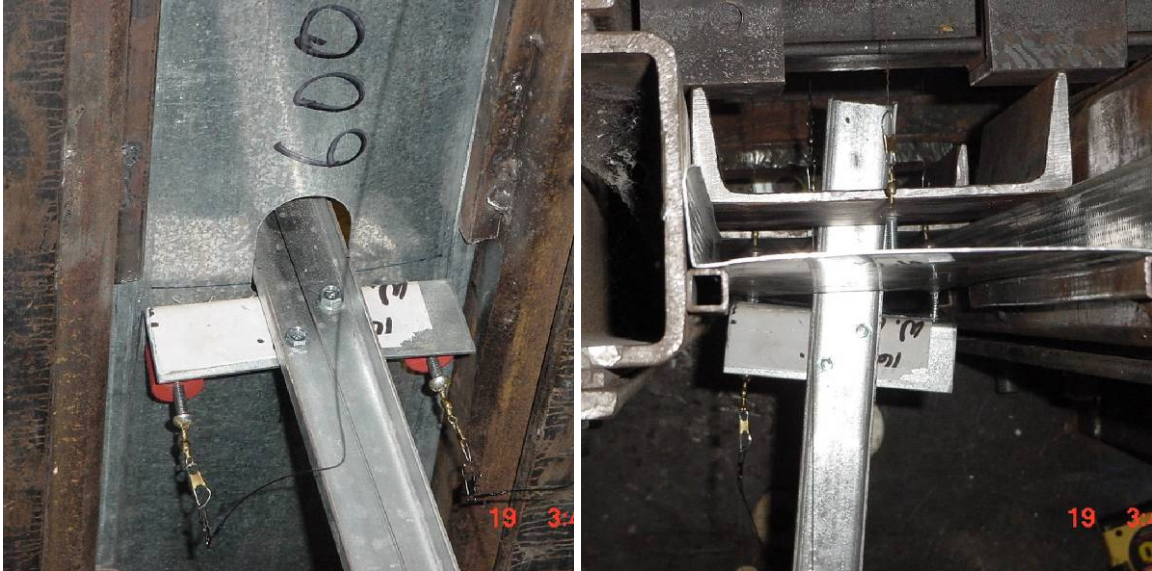
(a) Front View Screw Pull Out in 600S125-33-3SS  
 (b) Top View of Screw Pull Out in 600S125-33-3SS

600S 125-33-3 SS



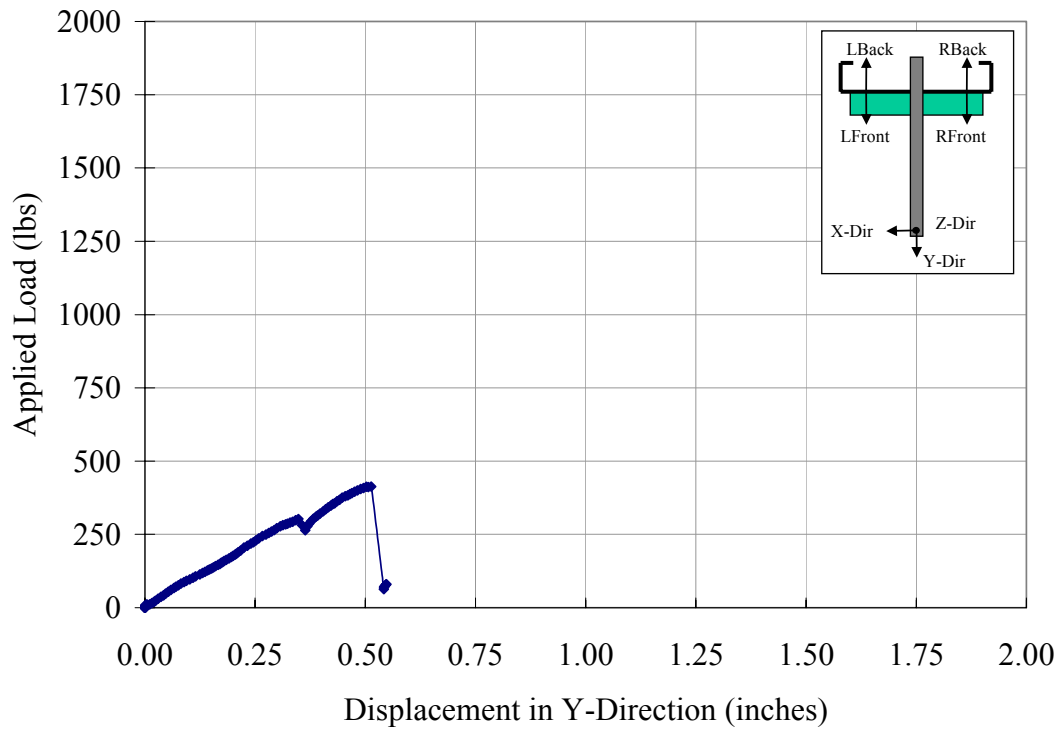
(c) Plot of Applied Load vs. Displacement in Y-Direction  
 Figure B2.11

**In-Plane Load Test on 600S125-33-4SS**



(a) Front View of Screw Pull Out in 600S125-33-4SS  
 (b) Top View of Screw Pull Out in 600S125-33-4SS

600S 125-33-4 SS



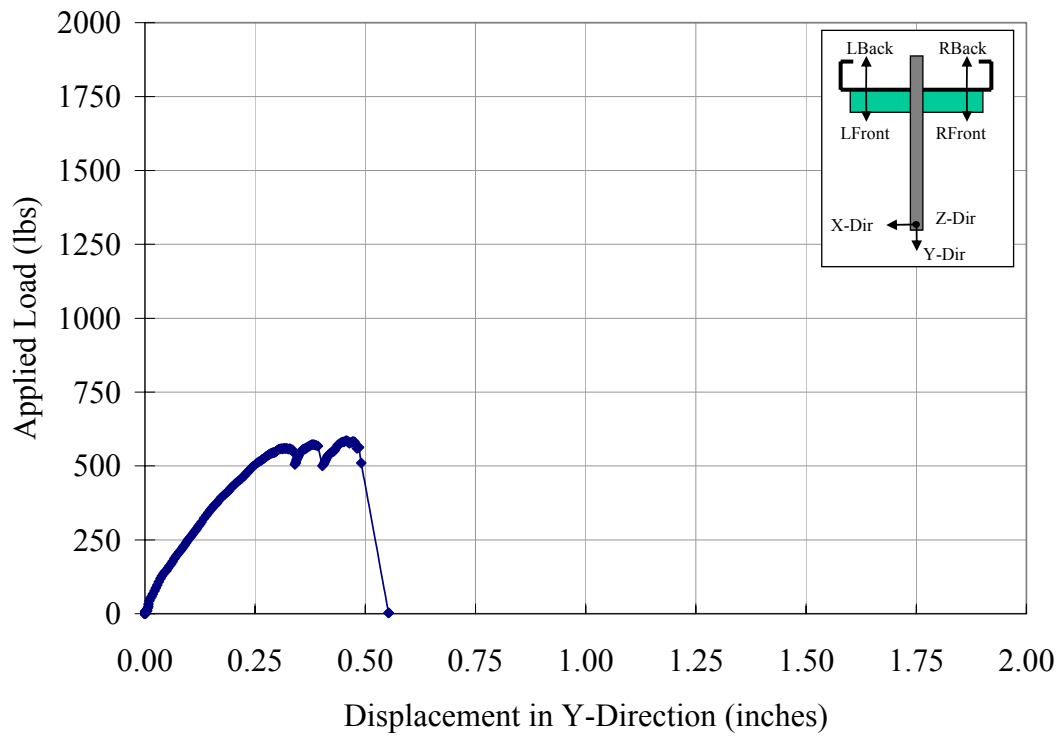
(c) Plot of Applied Load vs. Displacement in Y-Direction  
 Figure B2.12

**In-Plane Load Test on 600S162-43-3SS**



(a) Top View Showing Screw Pull Out of 600S162-43-3SS

600S 162-43-3 SS



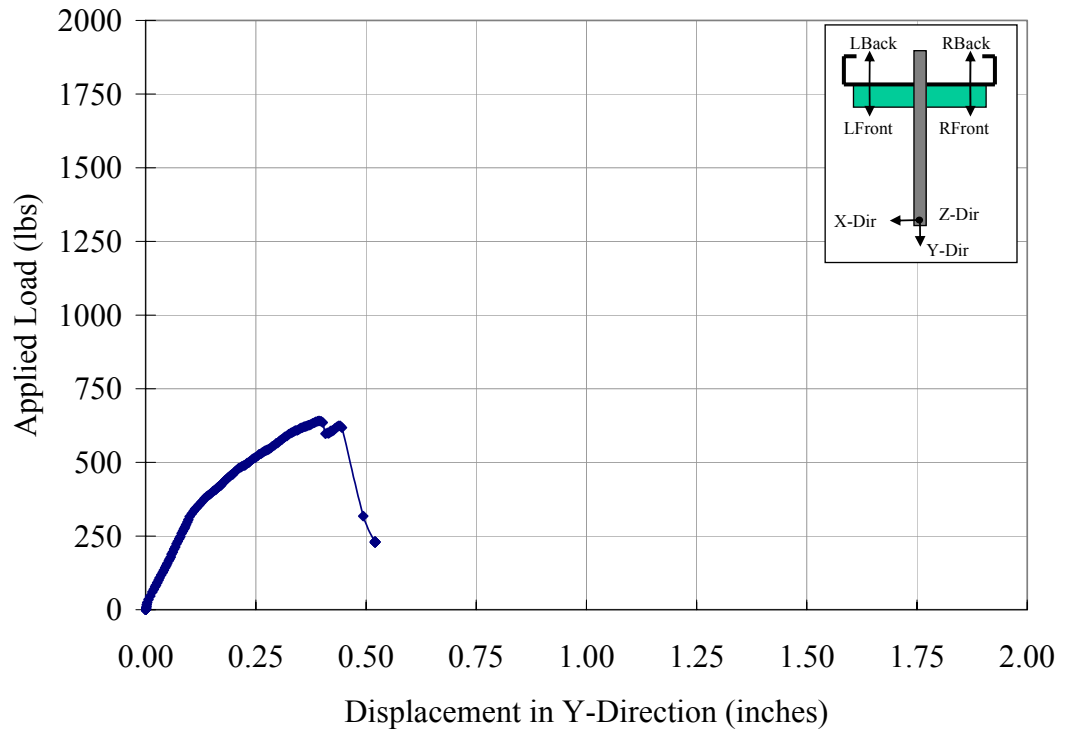
(b) Plot of Applied Load vs. Displacement in Y-Direction  
Figure B2.13

**In-Plane Load Test on 600S162-43-4SS**



(a) Front View of Screw Pull Out in 600S162-43-4SS  
 (b) Top View of Screw Pull Out in 600S162-43-4SS

600S 162-43-4 SS



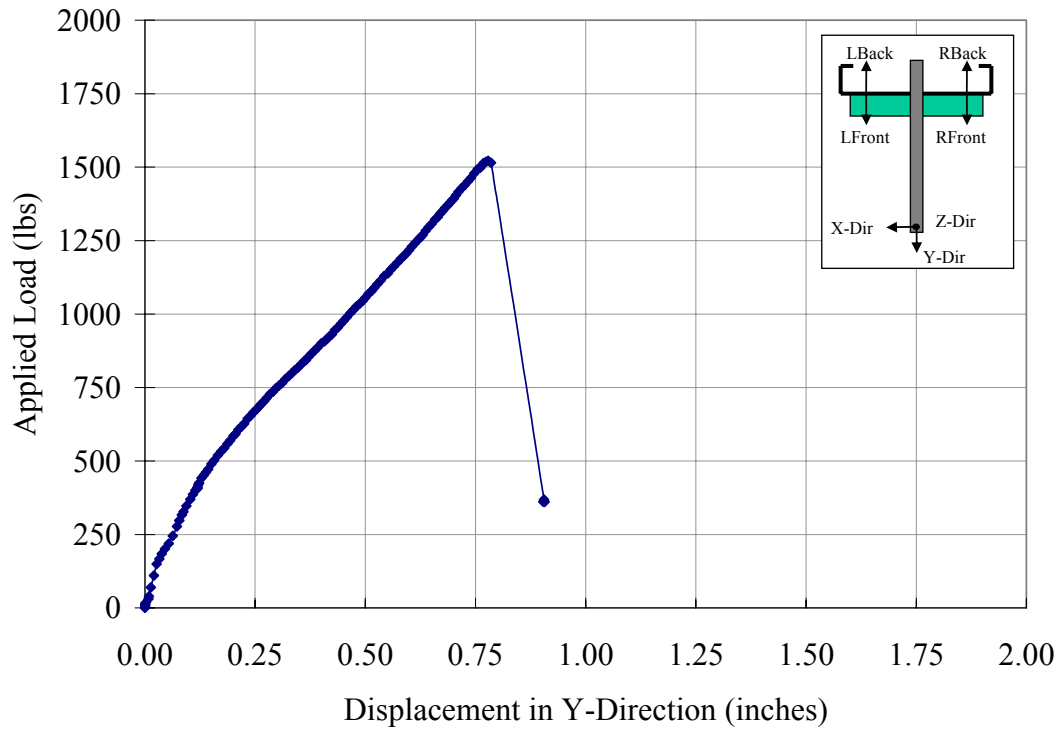
(c) Plot of Applied Load vs. Displacement in Y-Direction  
 Figure B2.14

**In-Plane Load Test on 600S162-97-1SS**



(a) Left Front View Showing Tension Failure of Screw of 600S162-97-1SS  
 (b) Front View Showing Clip Angle Deformation of 600S162-97-1SS

600S 162-97-1 SS



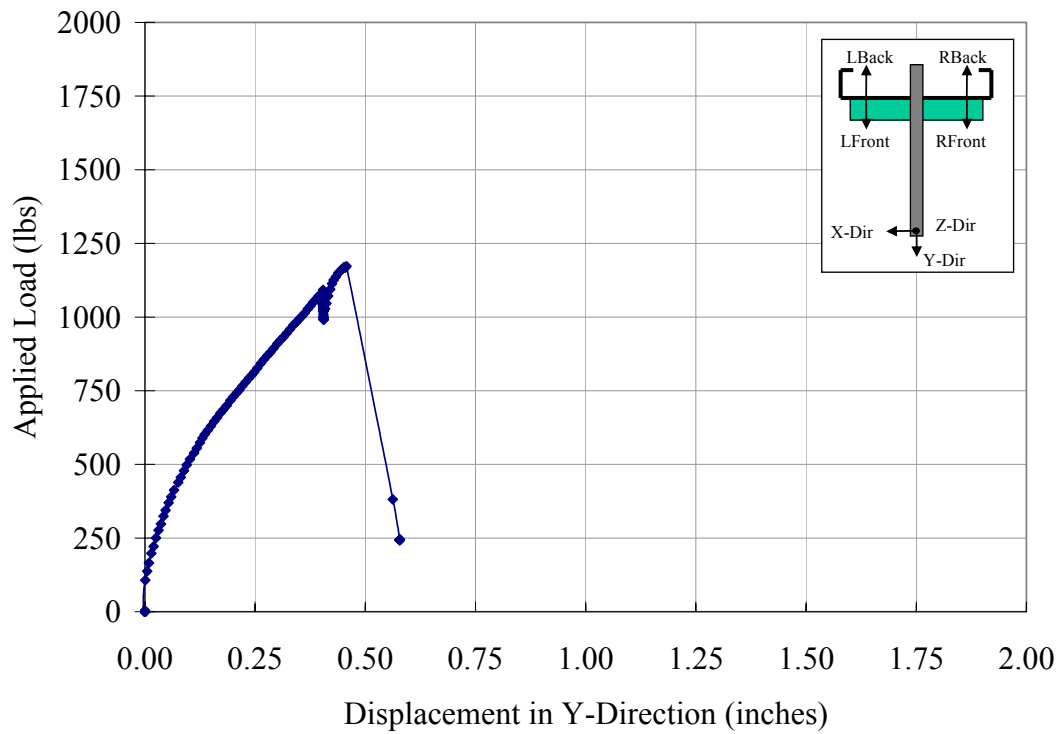
(c) Plot of Applied Load vs. Displacement in Y-Direction  
 Figure B2.15

**In-Plane Load Test on 600S162-97-2SS**



(a) Final View Tension Failure of Screw in 600S162-97-2SS  
 (b) Left Front View Showing in 600S162-97-2SS

600S 162-97-2 SS



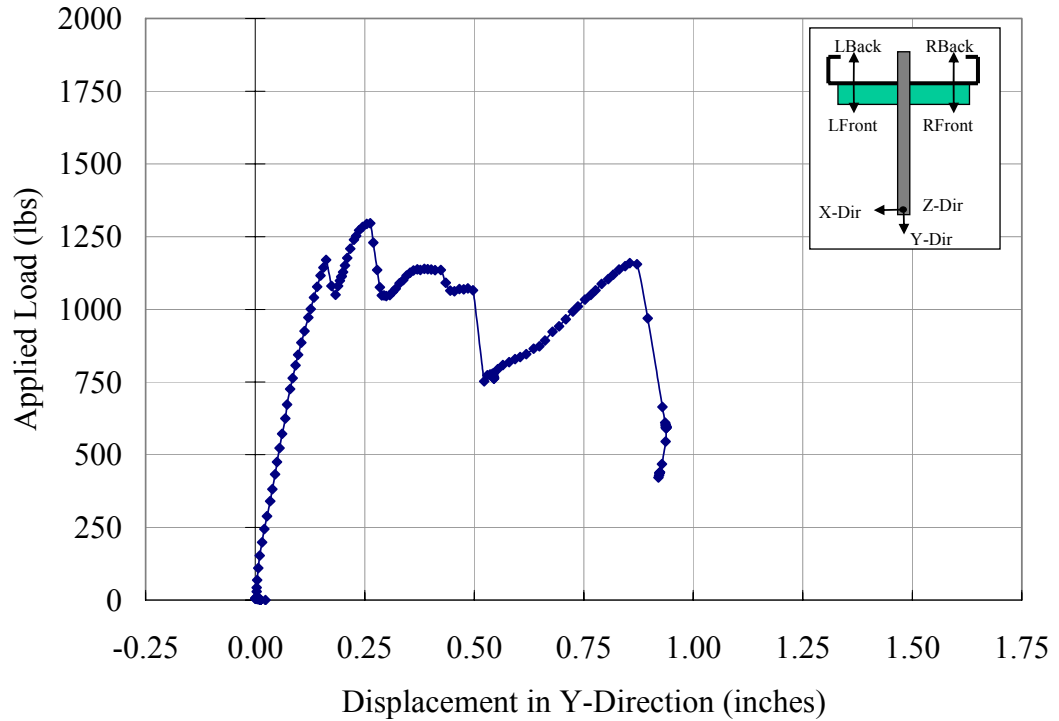
(c) Plot of Applied Load vs. Displacement in Y-Direction  
 Figure B2.16

**In-Plane Load Test on 600S162-97-3WW**



(a) Left Front View Showing Weld Failure in 600S162-97-3WW

600S 162-97-3 WW



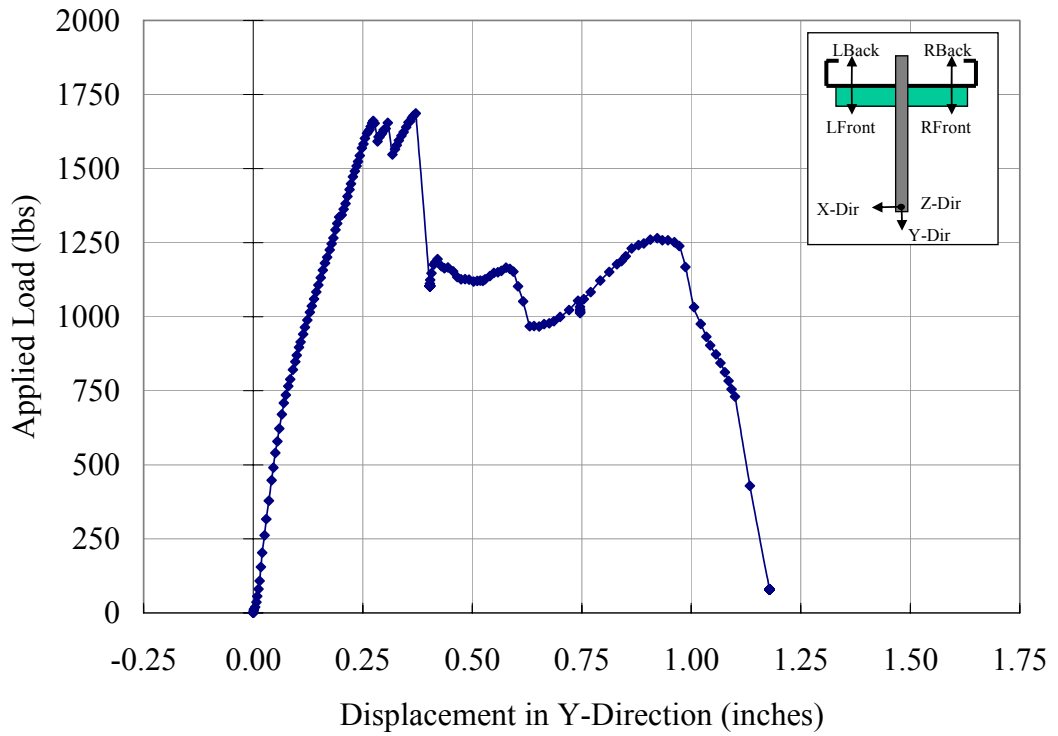
(b) Plot of Applied Load vs. Displacement in Y-Direction  
Figure B2.17

**In-Plane Load Test on 600S162-97-4WW**



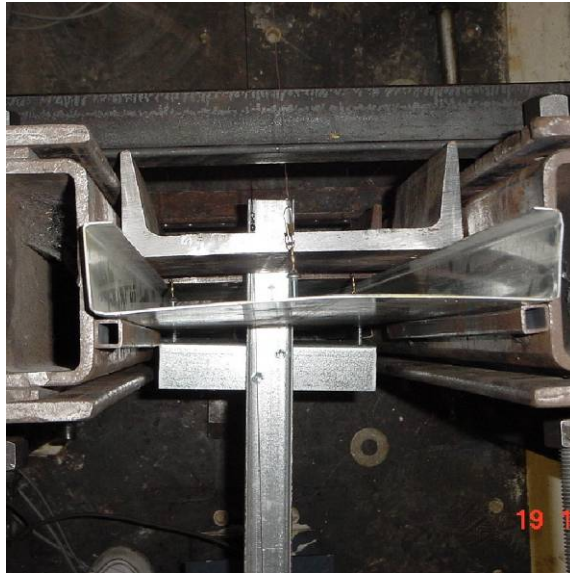
(a) Front View Showing Weld Failure in 600S162-97-4WW

600S 162-97-4 WW



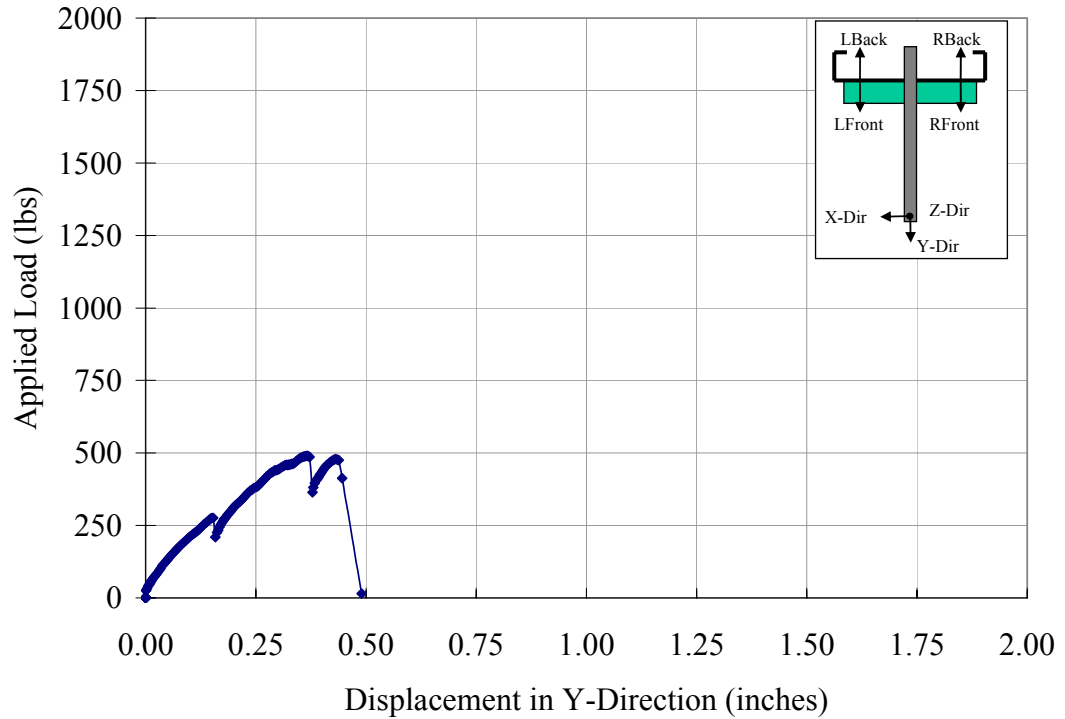
(b) Plot of Applied Load vs. Displacement in Y-Direction  
Figure B2.18

**In-Plane Load Test on 800S162-43-3SS**



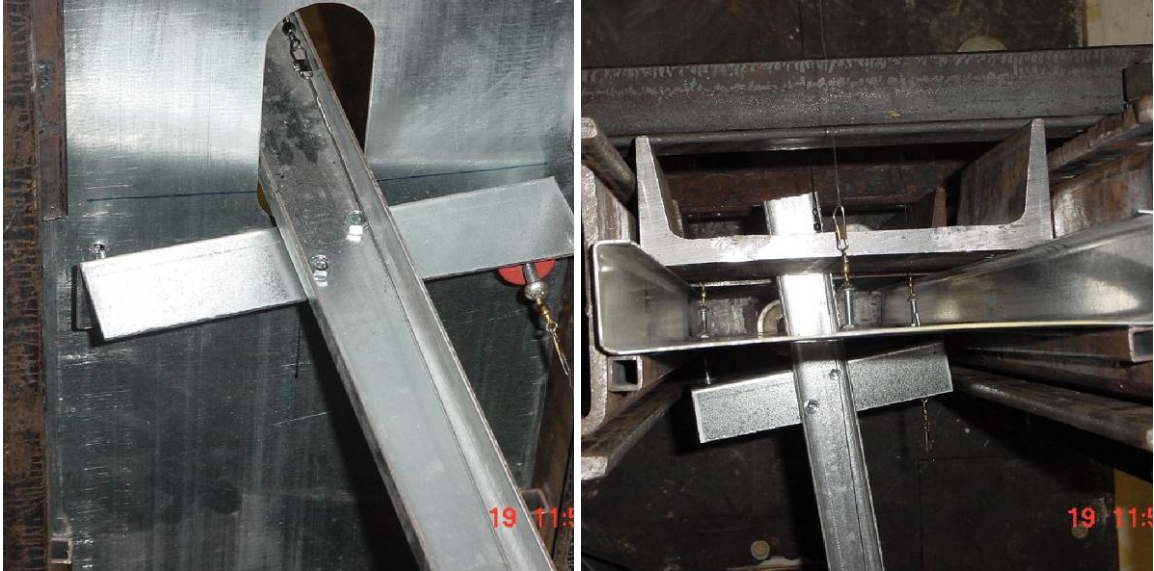
(a) Top View Showing Screw Pull Out in 800S162-43-3SS

800S 162-43-3 SS



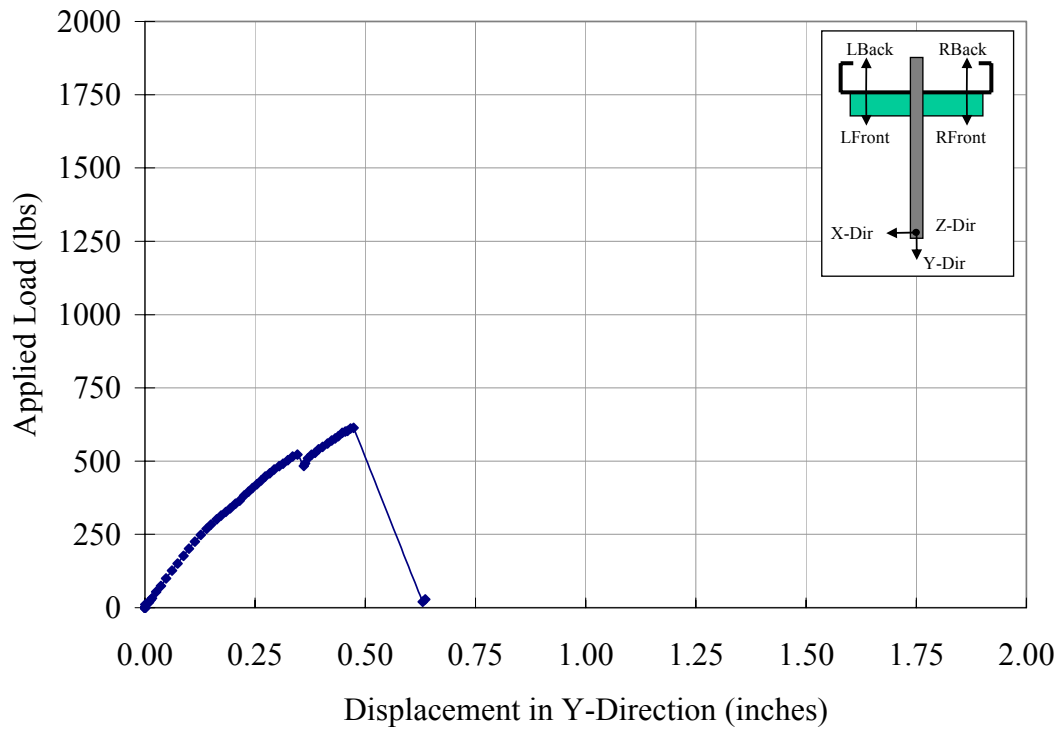
(b) Plot of Applied Load vs. Displacement in Y-Direction  
Figure B2.19

**In-Plane Load Test on 800S162-43-4SS**



(a) Front View Showing Tension Failure of Screw in 800S162-43-4SS  
 (b) Top View of 800S162-43-4SS

800S 162-43-4 SS



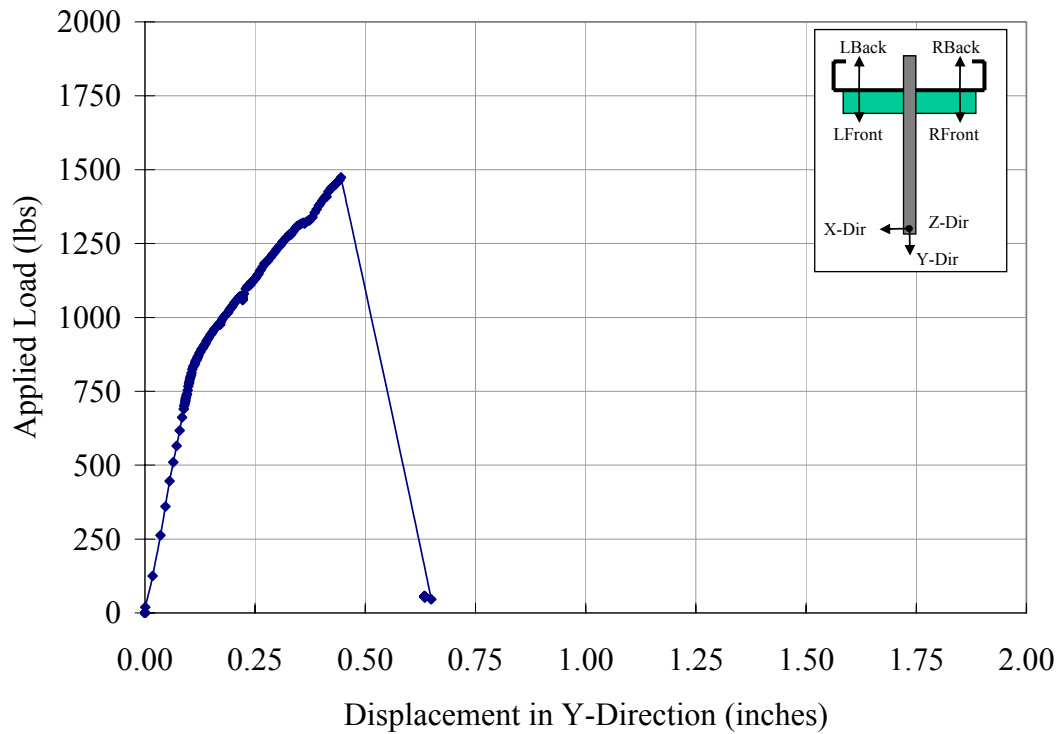
(c) Plot of Applied Load vs. Displacement in Y-Direction  
 Figure B2.20

**In-Plane Load Test on 800S162-97-3SS**



(a) Top View Showing Tension Failure of Screw in 800S162-97-3SS

800S 162-97-3 SS



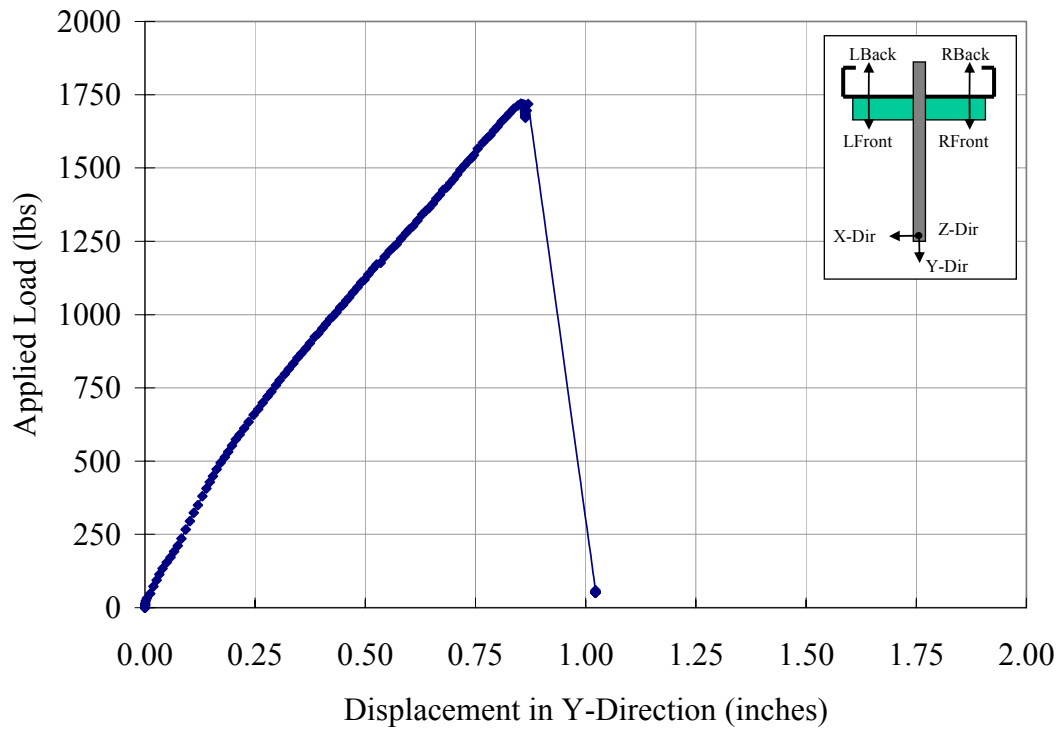
(b) Plot of Applied Load vs. Displacement in Y-Direction  
Figure B2.21

**In-Plane Load Test on 800S162-97-4SS**



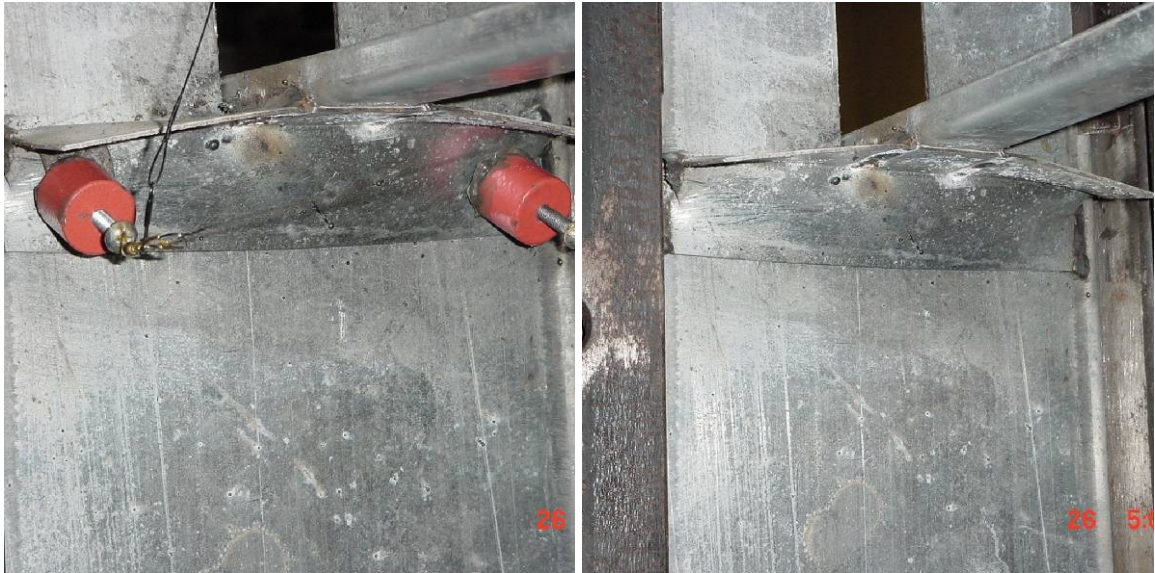
(a) Front View Showing Tension Failure of Screw in 800S162-97-4SS  
 (b) Top View Showing Clip Angle Deformation in 800S162-97-4SS

800S 162-97-4 SS



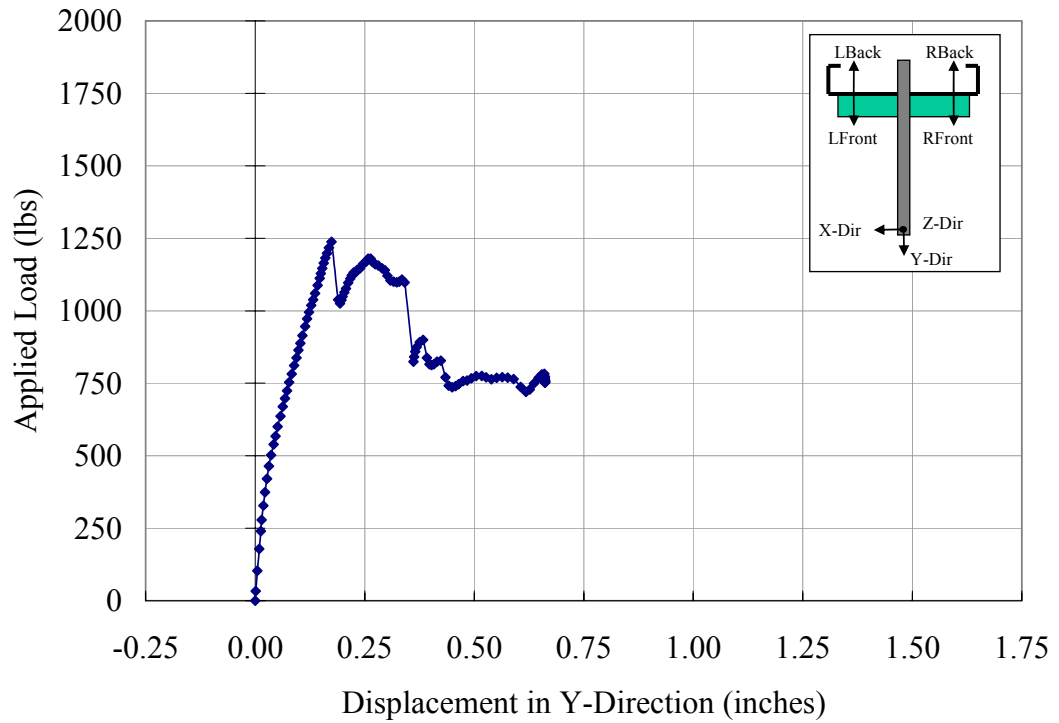
(c) Plot of Applied Load vs. Displacement in Y-Direction  
 Figure B2.22

**In-Plane Load Test on 800S162-97-3WW**



(a) Clip Angle Deformation in 800S162-97-3WW  
 (b) Angle Tear in 800S162-97-3WW

800S 162-97-3 WW



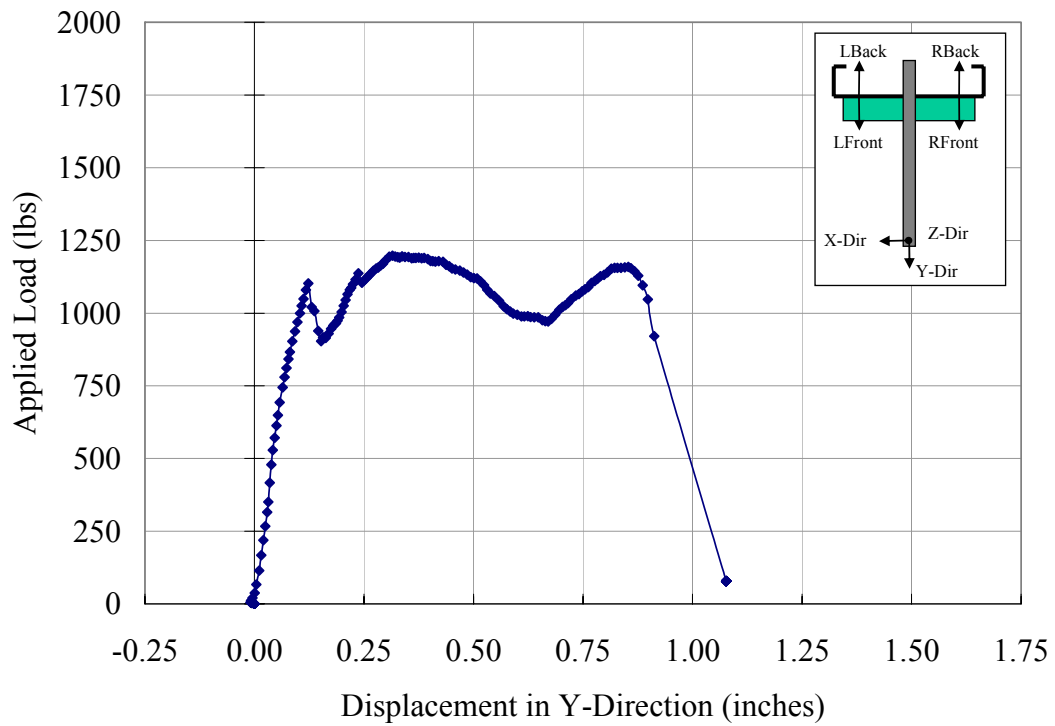
(c) Plot of Applied Load vs. Displacement in Y-Direction  
 Figure B2.23

**In-Plane Load Test on 800S162-97-4WW**



(a) Left Front View Showing Clip Angle Distortion in 800S162-97-4WW  
 (b) Front View Showing Clip Angle Tear in 800S162-97-4WW

800S 162-97-4 WW



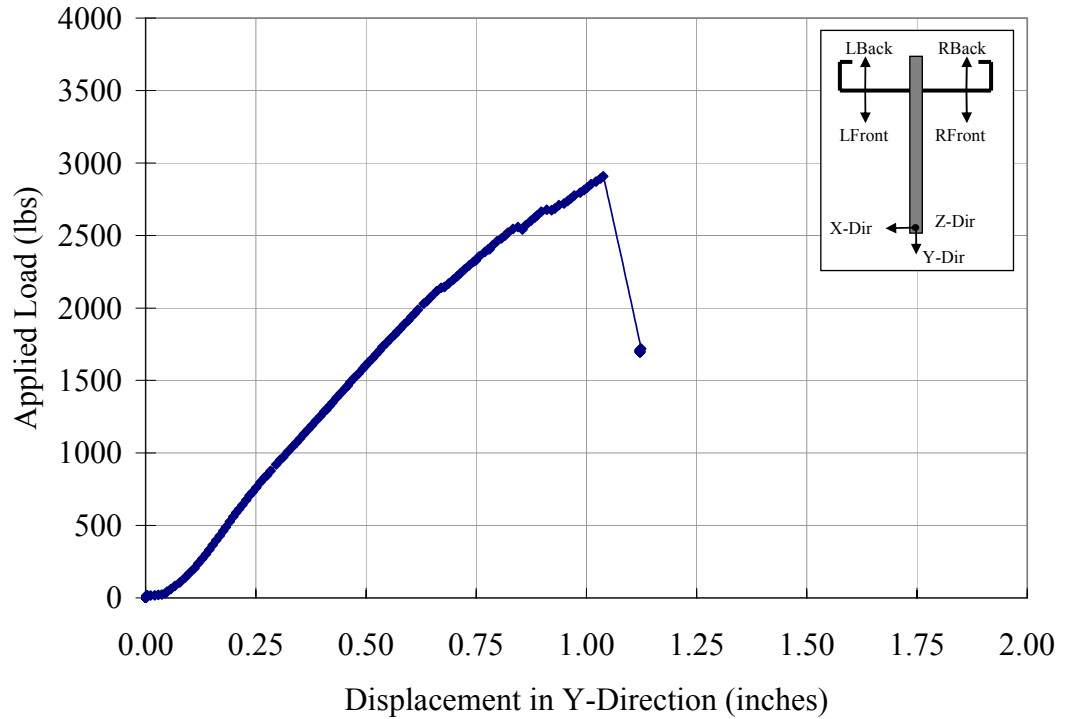
(c) Plot of Applied Load vs. Displacement in Y-Direction  
 Figure B2.24

**In-Plane Load Test on 800S162-97-3DW**



(a) Front Views Showing Weld Separation From the Web of 800S162-97-3DW

800S 162-97-3 DW



(b) Plot of Applied Load vs. Displacement in Y-Direction  
Figure B2.25

## APPENDIX C MATHCAD WORKSHEETS

The MathCAD worksheets are organized into following topics:

1. Axial load capacity of braced cee-stud: The MathCAD worksheet developed by Chen for AISI (1999) has been modified for the purposes of this research. One complete listing is provided for the 362S125-33 stud with no mid-height lateral brace. Input data and summary of results are provided for the 362S125-33 stud with full bracing (Winter 1960). It is assumed that the effective length factor for an infinitely stiff brace is 0.5 since the location of the brace acts as a pin support.
2. Initial Flexural Stiffness of the connection from the Out-Of-Plane tests: MathCAD worksheet has been developed from basic structural mechanics to determine the initial flexural stiffness of the bracing connection. A complete source code listing is given for all the eight groups of cee-studs for the three connection types.

## C.1 Axial Load Capacity of Unbraced Cee-Studs

### C.1.1 362S125-33 with Pinned Ends

Define Units:      ksi := 1000psi      kip := 1000lbf

#### Gross Section Properties of Channel and Hat Sections:

*This example calculates channel or hat section gross section properties: area (A), moments of inertia ( $I_x$ ,  $I_y$ ), section modulus ( $S_x$ ,  $S_y$ ), torsional constant (J), warping constant ( $C_w$ ), shear center location ( $x_0$ ), and parameter (j). Formulas used hereby are published in the AISI 1996 Cold-Formed Steel Design Manual. All the formulas consider the sections' round corners except torsional properties  $x_0$ , j and  $C_w$ .*

#### a. Input Data:

Section designation:      Designation := "362S125-33"

Enter capital "C" or "H" for channel or hat section, respectively:      SectTyp := "C"

Member Length:      L := 8ft

Dimension A:      A := 3.6131in

Dimension B:      B := 1.2876in

Dimension C:      C := 0.2287in

Corner Inner radius:      R := 0.0778in

Thickness:      t := 0.0319in

Effective Length Factors:       $K_x := 1.0$        $K_y := 1.0$        $K_t := 1.0$

Effective length of compression member for bending about x-axis       $KL_x := L \cdot K_x$        $KL_x = 8 \text{ ft}$

Effective length of compression member for bending about y-axis       $KL_y := L \cdot K_y$        $KL_y = 8 \text{ ft}$

Effective length of compression member for twisting       $KL_t := L \cdot K_t$        $KL_t = 8 \text{ ft}$

Yield stress:       $F_y := 33.0 \text{ ksi}$

Elastic modulus:      E := 29500ksi

Shear modulus      G := 11300ksi

Lip angle as shown in the figures above:       $\theta := 90 \text{ deg}$   
*Always 90 deg. for hat section.*

*Input perforation data. Enter zeros if no perforation exists.*

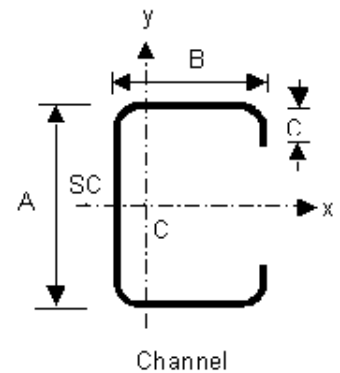
Hole shape:      shape := 2  
*Enter 1 for circle and 2 for others.*

Hole depth (or diameter for circular hole):       $d_h := 0 \text{ in}$

Hole width:       $b_h := 0 \text{ in}$

Hole spacing:       $s_h := 24 \text{ in}$

Distance between hole edge and end of member:       $s_{\text{end}} := 1.0625 \text{ in}$



**b. Gross Section Properties:**

Determine whether lips exist:  $\alpha := \begin{cases} 1 & \text{if } C \neq 0 \\ 0 & \text{otherwise} \end{cases}$

**Centerline dimensions without considering round corners:**

Centerline of dimension A:  $a_c := A - t$   $a_c = 3.5812\text{in}$

Centerline of dimension B:  $b_c := B - \left( \frac{t}{2} + \alpha \cdot \frac{t}{2} \right)$   $b_c = 1.2557\text{in}$

Centerline of dimension C:  $c_c := \alpha \cdot \left( C - \frac{t}{2} \right)$   $c_c = 0.2127\text{in}$

**The flat widths of flanges and web, and centerline arc length:**

Centerline radius:  $r := R + \frac{t}{2}$   $r = 0.0938\text{in}$

Flat width of Dim. A:  $a := A - (2 \cdot r + t)$   $a = 3.3937\text{in}$

Flat width of Dim. B:  $b := B - \left[ r + \frac{t}{2} + \alpha \cdot \left( r + \frac{t}{2} \right) \right]$   $b = 1.0682\text{in}$

Flat width of Dim. C:  $c := \alpha \cdot \left[ C - \left( r + \frac{t}{2} \right) \right]$   $c = 0.119\text{in}$

Arc length:  $u := \frac{\pi \cdot r}{2}$   $u = 0.1473\text{in}$

**Gross section properties:**

Gross area:  $A_g := t \cdot [a + 2 \cdot b + 2 \cdot u + \alpha \cdot (2 \cdot c + 2 \cdot u)]$   $A_g = 0.2028\text{in}^2$

Moment of inertia about x-axis of channel section:  $I_x := 2 \cdot t \cdot \left[ 0.0417a^3 + b \cdot \left( \frac{a}{2} + r \right)^2 + u \cdot \left( \frac{a}{2} + 0.637r \right)^2 + 0.149r^3 \dots \right. \\ \left. + \alpha \cdot \left[ 0.0833c^3 + \frac{c}{4} \cdot (a - c)^2 + u \cdot \left( \frac{a}{2} + 0.637r \right)^2 + 0.149r^3 \right] \right]$   $I_x = 0.4009\text{in}^4$

Section modulus about x-axis:  $S_x := \frac{I_x}{0.5 \cdot A}$   $S_x = 0.2219\text{in}^3$

Radius of gyration about x-axis:  $r_x := \sqrt{\frac{I_x}{A_g}}$   $r_x = 1.4059\text{in}$

Distance between centroid and web centerline:  $x_{\text{bar}} := \frac{2 \cdot t}{A_g} \cdot \left[ b \cdot \left( \frac{b}{2} + r \right) + u \cdot (0.363r) \dots \right. \\ \left. + \alpha \cdot [u \cdot (b + 1.637r) + c \cdot (b + 2r)] \right]$   $x_{\text{bar}} = 0.3162\text{in}$

Moment of inertia about y-axis:  $I_y := 2 \cdot t \cdot \left[ b \cdot \left( \frac{b}{2} + r \right)^2 + 0.0833b^3 + 0.356r^3 \dots \right. \\ \left. + \alpha \cdot [c \cdot (b + 2r)^2 + u \cdot (b + 1.637r)^2 + 0.149r^3] \right] - A_g \cdot x_{\text{bar}}^2$   $I_y = 0.0391\text{in}^4$

Distance between shear center  
and web centerline:

$$m := b_c \cdot \frac{[3 \cdot a_c^2 \cdot b_c + \alpha \cdot c_c \cdot (6 \cdot a_c^2 - 8 \cdot c_c^2)]}{a_c^3 + 6 \cdot a_c^2 \cdot b_c + \alpha \cdot c_c \cdot (8 \cdot c_c^2 - 12 \cdot a_c \cdot c_c + 6 \cdot a_c^2)} \quad m = 0.5165 \text{ in}$$

Distance between centroid  
and shear center:

$$x_0 := -(x_{\text{bar}} + m) \quad x_0 = -0.8327 \text{ in}$$

(Note: Negative sign indicates  $x_0$  is measured in negative x-direction)

Section modulus about y-axis:

$$S_{y\text{lip}} := \frac{I_y}{\left(B - x_{\text{bar}} - \frac{t}{2}\right)} \quad S_{y\text{web}} := \frac{I_y}{\left(x_{\text{bar}} + \frac{t}{2}\right)} \quad S_{y\text{lip}} = 0.0409 \text{ in}^3$$

$$S_{y\text{web}} = 0.1177 \text{ in}^3$$

Radius of gyration about y-axis:

$$r_y := \sqrt{\frac{I_y}{A_g}} \quad r_y = 0.439 \text{ in}$$

Polar radius of gyration:

$$r_0 := \sqrt{r_x^2 + r_y^2 + x_0^2} \quad r_0 = 1.692 \text{ in}$$

St. Venant torsional constant:

$$J := \frac{t^3}{3} \cdot [a + 2 \cdot b + 2 \cdot u + 2 \cdot \alpha \cdot (c + u)] \quad J = 0.0001 \text{ in}^4$$

Warping constant:

$$C_w := \frac{a_c^2 \cdot b_c^2 \cdot t}{12} \cdot \left[ \frac{2 \cdot a_c^3 \cdot b_c + 3 \cdot a_c^2 \cdot b_c^2 \dots + \alpha \cdot (48 \cdot c_c^4 + 112 \cdot b_c \cdot c_c^3 + 8 \cdot a_c \cdot c_c^3 + 48 \cdot a_c \cdot b_c \cdot c_c^2 \dots)}{6 \cdot a_c^2 \cdot b_c + (a_c + 2 \cdot \alpha \cdot c_c)^3 - 24 \cdot \alpha \cdot a_c \cdot c_c^2} \right] \quad C_w = 0.1007 \text{ in}^6$$

Parameter  $\beta_w$ ,  $\beta_f$ ,  $\beta_l$ :

$$\beta_w := -\left( \frac{t \cdot x_{\text{bar}} \cdot a_c^3}{12} + t \cdot x_{\text{bar}}^3 \cdot a_c \right) \quad \beta_w = -0.0422 \text{ in}^5$$

$$\beta_f := \frac{t}{2} \cdot [(b_c - x_{\text{bar}})^4 - x_{\text{bar}}^4] + \frac{t \cdot a_c^2}{4} \cdot [(b_c - x_{\text{bar}})^2 - x_{\text{bar}}^2] \quad \beta_f = 0.0923 \text{ in}^5$$

$$\beta_l := \alpha \cdot \left[ 2 \cdot c_c \cdot t \cdot (b_c - x_{\text{bar}})^3 + \frac{2}{3} \cdot t \cdot (b_c - x_{\text{bar}}) \cdot \left[ \left( \frac{a_c}{2} \right)^3 - \left( \frac{a_c}{2} - c_c \right)^3 \right] \right] \quad \beta_l = 0.0475 \text{ in}^5$$

Parameter  $j$ :

$$j := \frac{1}{2 \cdot I_y} \cdot (\beta_w + \beta_f + \beta_l) - x_0 \quad j = 2.081 \text{ in}$$

## Concentrically Loaded Compression Members

### b. Axial Compression Strength:

Elastic flexural buckling stress for bending about x-axis:

$$\sigma_{ex} := \frac{\pi^2 \cdot E}{\left(\frac{KL_x}{r_x}\right)^2} \quad \sigma_{ex} = 62.447\text{ksi} \quad (\text{Eq. C3.1.2-8})$$

Elastic flexural buckling stress for bending about y-axis:

$$\sigma_{ey} := \frac{\pi^2 \cdot E}{\left(\frac{KL_y}{r_y}\right)^2} \quad \sigma_{ey} = 6.0895\text{ksi} \quad (\text{Eq. C3.1.2-9})$$

Polar radius of gyration about shear center:

$$r_0 := \sqrt{r_x^2 + r_y^2 + x_0^2} \quad r_0 = 1.692\text{in} \quad (\text{Eq. C3.1.2-13})$$

Elastic torsional buckling stress:

$$\sigma_t := \frac{1}{A_g \cdot r_0^2} \left[ G \cdot J + \frac{\pi^2 \cdot E \cdot C_w}{(KL_t)^2} \right] \quad \sigma_t = 6.8189\text{ksi} \quad (\text{Eq. C3.1.2-10})$$

$$\beta := 1 - \left(\frac{x_0}{r_0}\right)^2 \quad \beta = 0.7578 \quad (\text{Eq. C4.2-3})$$

Elastic lateral torsional buckling stress:

$$F_{elt} := \frac{1}{2 \cdot \beta} \cdot \left[ (\sigma_{ex} + \sigma_t) - \sqrt{(\sigma_{ex} + \sigma_t)^2 - 4 \cdot \beta \cdot \sigma_{ex} \cdot \sigma_t} \right] \quad F_{elt} = 6.6282\text{ksi} \quad (\text{Eq. C4.2-1})$$

The critical elastic buckling stress will be the minimum stress of buckling about x or y axis, torsional buckling, and lateral-torsional buckling:

$$F_e := \min(\sigma_{ex} \quad \sigma_{ey} \quad \sigma_t \quad F_{elt}) \quad F_e = 6.0895\text{ksi}$$

$$\lambda_c := \sqrt{\frac{F_y}{F_e}} \quad \lambda_c = 2.3279 \quad (\text{Eq. C4-4})$$

$$F_n := \begin{cases} (0.658^{\lambda_c^2}) \cdot F_y & \text{if } \lambda_c \leq 1.5 \\ \left(\frac{0.877}{\lambda_c^2}\right) \cdot F_y & \text{otherwise} \end{cases} \quad F_n = 5.3405\text{ksi} \quad (\text{Eq. C4-2})$$

$$\left(\frac{0.877}{\lambda_c^2}\right) \cdot F_y \quad \text{otherwise} \quad (\text{Eq. C4-3})$$

## Effective Area for Channel with/without Perforations

This example calculates effective area of C-, Z- or hat section members with/without perforations as shown in the figures below when the member is subjected to an axial load. **AISI Specification Sections B2.2 and D4** are used to consider the perforation.

### b. Section Geometries:

$$\begin{aligned} \text{Stiffener moment of inertia:} \quad I_s &:= \frac{c^3 \cdot t \cdot \sin(\theta)^2}{12} & I_s = 0 \text{ in}^4 \\ \text{Nominal uniform compressive stress on section:} \quad f_n &:= F_n \end{aligned}$$

### c. Functions for Effective Width Calculation:

*The following function determines the effective width based on given stress level and buckling coefficient (Section B2.1).*

$$\text{Effective\_width}(w, f, k) := \left| \begin{array}{l} \lambda \leftarrow \frac{1.052}{\sqrt{k}} \cdot \left( \frac{w}{t} \right) \cdot \sqrt{\frac{f}{E}} \end{array} \right. \quad (\text{Eq. B2.1-4})$$

$$\left| \begin{array}{l} \rho \leftarrow \frac{\left( 1 - \frac{0.22}{\lambda} \right)}{\lambda} \end{array} \right. \quad (\text{Eq. B2.1-3})$$

$$\left| \begin{array}{l} b \leftarrow \text{if}(\lambda \leq 0.673, w, \rho \cdot w) \end{array} \right. \quad (\text{Eq. B2.1-1,2})$$

*The following function determines effective width of a stiffened element with a circular hole using Section B2.2.*

$$\text{beff\_B2\_2}(f, w) := \left| \begin{array}{l} k \leftarrow 4 \\ \lambda \leftarrow \frac{1.052}{\sqrt{k}} \cdot \left( \frac{w}{t} \right) \cdot \sqrt{\frac{f}{E}} \end{array} \right. \quad (\text{Eq. B2.1-4})$$

$$\left| \begin{array}{l} b \leftarrow w - d_h \text{ if } \lambda \leq 0.675 \end{array} \right. \quad (\text{Eq. B2.2-1})$$

$$\left| \begin{array}{l} \min \left[ \frac{w \cdot \left( 1 - \frac{0.22}{\lambda} - \frac{0.8 \cdot d_h}{w} \right)}{\lambda}, w - d_h \right] \text{ otherwise} \end{array} \right. \quad (\text{Eq. B2.2-2})$$

*The following function determines effective width assuming the element with perforation consists of two unstiffened sub-elements, one on each side of the perforation (assume hole is centered on the element). It follows Section D4.*

$$\text{beff\_D4}(f, w) := \left| \begin{array}{l} w_{\text{sub}} \leftarrow \frac{(w - d_h)}{2} \\ b_{\text{sub}} \leftarrow \text{Effective\_width}(w_{\text{sub}}, f, 0.43) \\ b \leftarrow b_{\text{sub}} \cdot 2 \end{array} \right.$$

The following function determines the effective width of uniformly compressed element with an edge stiffener (Section B4.2):

$$b_{\text{flange\_lip}}(w_{\text{lip}}, f_{\text{lip}}, w, f) := \begin{cases} S \leftarrow 1.28 \sqrt{\frac{E}{f}} & \text{(Eq. B4-1)} \\ \text{if } \frac{w}{t} \leq \frac{S}{3} & \\ \quad \left| \begin{aligned} d_s &\leftarrow \text{Effective\_width}(w_{\text{lip}}, f_{\text{lip}}, 0.43) \\ b &\leftarrow w \end{aligned} \right. & \text{(Eq. B4.2-1)} \\ \text{otherwise} & \\ \quad \left| \begin{aligned} n &\leftarrow \text{if} \left( \frac{S}{3} < \frac{w}{t} < S, \frac{1}{2}, \frac{1}{3} \right) \\ k_u &\leftarrow 0.43 \\ I_a &\leftarrow \begin{cases} 399t^4 \cdot \left( \frac{w}{t \cdot S} - \sqrt{\frac{k_u}{4}} \right)^3 & \text{if } \frac{S}{3} < \frac{w}{t} < S \\ t^4 \cdot \left[ 115 \cdot \left( \frac{w}{t \cdot S} \right) + 5 \right] & \text{otherwise} \end{cases} & \begin{aligned} &\text{(Eq. B4.2-4)} \\ &\text{(Eq. B4.2-11)} \end{aligned} \\ C_2 &\leftarrow \min \left( \left( \frac{I_s}{I_a} - 1 \right) \right) & \text{(Eq. B4.2-5)} \\ k_a &\leftarrow \min \left[ \left[ 5.25 - 5 \cdot \left( \frac{C}{w} \right) \right], 4.0 \right] & \text{(Eq. B4.2-8)} \\ k &\leftarrow C_2^n \cdot (k_a - k_u) + k_u & \text{(Eq. B4.2-7)} \\ b &\leftarrow \text{Effective\_width}(w, f, k) \\ d_s &\leftarrow C_2 \cdot \text{Effective\_width}(w_{\text{lip}}, f_{\text{lip}}, 0.43) & \text{(Eq. B4.2-9)} \\ b_e &\leftarrow (b \quad d_s)^T \end{aligned} \end{cases}$$

#### d. Check Perforation Limitations Set Forth in Section B2.2 or D4:

The following function checks whether limitations given in Section B2.2 are satisfied.

$$\text{Cond}_{B2\_2}(w) := \begin{cases} \text{Check1} \leftarrow \text{if} \left[ \left( 0.50 \geq \frac{d_h}{w} \geq 0 \right) \cdot \left( \frac{w}{t} \leq 70 \right) = 1, 1, 0 \right] \\ \text{Check2} \leftarrow \text{if} \left[ s_h \geq \max \left( (0.5 \cdot w - 3 \cdot d_h), 1, 0 \right) \right] \\ \text{cond} \leftarrow \text{if}(\text{Check1} \cdot \text{Check2} \cdot \text{shape} = 1, 1, 0) \end{cases}$$

*<- check if  $0.5 \geq \frac{d_h}{w} \geq 0$  and  $\frac{w}{t} \leq 70$ ; if*

*hole spacing larger than either  $0.5w$  or  $3d_h$ ; and if it is a circular hole.*

$$\text{Cond}_{B2\_2}(a) = 0$$

*Cond=1, indicates all the requirements given in Section B2.2 are satisfied. Otherwise, at least one of the conditions is not satisfied.*

The following function checks whether all the limitations given in Section D4 are satisfied.

$$\text{Cond}_{D4} := \begin{cases} \text{Check1} \leftarrow \text{if}(s_h \geq 24 \cdot \text{in}, 1, 0) \\ \text{Check2} \leftarrow \text{if}[d_h \leq \min((0.5 \cdot A - 2.5 \cdot \text{in}), 1), 0] \\ \text{Check3} \leftarrow \text{if}(b_h \leq 4.5 \cdot \text{in}, 1, 0) \\ \text{Check4} \leftarrow \text{if}\left(\frac{A}{t} \geq 20, 1, 0\right) \\ \text{Check5} \leftarrow \text{if}(s_{\text{end}} \geq 10 \cdot \text{in}, 1, 0) \\ \text{cond} \leftarrow \text{if}(\text{Check1} \cdot \text{Check2} \cdot \text{Check3} \cdot \text{Check4} \cdot \text{Check5} = 1, 1, 0) \end{cases}$$

$\text{Cond}_{D4} = 0$       *Cond=1, indicates all the requirements given in Section B2.2 are satisfied. Otherwise, at least one of the conditions is not satisfied.*

$$\text{Check} := \begin{cases} \text{"No hole exists. Chapter B is applicable."} & \text{if } d_h = 0 \\ \text{"Either Section B2.2 or D4 is applicable."} & \text{if } (\text{Cond}_{B2\_2}(a) + \text{Cond}_{D4}) \cdot (d_h \neq 0) \geq 1 \\ \text{"Specification is not applicable. Please revise the Section."} & \text{otherwise} \end{cases}$$

Check = "No hole exists. Chapter B is applicable."

*<-- Review this before going further*

### e. Effective Area under Given Compressive Stress:

$$A_{\text{eff}} := \begin{cases} b_{e\_B\_C} \leftarrow \begin{cases} b_{\text{flange\_lip}}(c, f_n, b, f_n) & \text{if } \alpha \neq 0 \\ \left( \text{Effective\_width}(b, f_n, 0.43) \ 0 \right)^T & \text{otherwise} \end{cases} & \text{--} b_e \text{ of Elems. B \& C with lips.} \\ b_{e\_A} \leftarrow \begin{cases} b_{\text{eff}_{B2\_2}}(f_n, a) & \text{if } (\text{Cond}_{B2\_2}(a) = 1) \cdot (d_h \neq 0) \\ b_{\text{eff}_{D4}}(f_n, a) & \text{if } (\text{Cond}_{D4} = 1) \cdot (d_h \neq 0) \cdot (\text{Cond}_{B2\_2}(a) = 0) \\ \text{Effective\_width}(a, f_n, 4) & \text{if } d_h = 0 \\ 0 \cdot \text{in} & \text{otherwise} \end{cases} & \begin{array}{l} \text{--} b_e \text{ of Elems. B \& C without} \\ \text{lips.} \\ \text{--} b_e \text{ of Elem. A satisfying B2.2} \\ \text{--} b_e \text{ of Elem. A satisfying D4} \\ \text{but not B2.2.} \\ \text{--} b_e \text{ of Elem. A without hole.} \end{array} \\ A_{\text{eff}} \leftarrow \left[ \left( b_{e\_B\_C_0} + \alpha \cdot b_{e\_B\_C_1} \right) \cdot 2 + b_{e\_A} + 2 \cdot (u + \alpha \cdot u) \right] \cdot t & \text{--} \text{Calculate effective area} \end{cases}$$

$$A_{\text{eff}} = 0.1963 \text{in}^2$$

$$P_n := F_n \cdot A_{\text{eff}}$$

$$P_n = 1048.3646 \text{bf}$$

(Eq. C4-1)

### Compression Strength for LRFD:

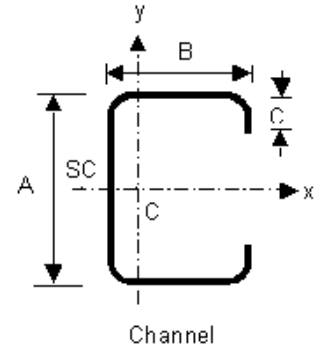
$$\phi_c := 0.85 \quad (\text{LRFD})$$

$$\phi_c \cdot P_n = 891.1099 \text{bf}$$

## Summary

### Gross Section Properties:

|   |  |              |              |
|---|--|--------------|--------------|
| Effective Length Factors:                   | $K_{xx} = 1$                           | $K_{yy} = 1$ | $K_{tw} = 1$ |
| Cross section area:                         | $A_g = 0.2028 \text{in}^2$             |              |              |
| Moment of inertia about x-axis:             | $I_x = 0.40085 \text{in}^4$            |              |              |
| Moment of inertia about y-axis:             | $I_y = 0.0391 \text{in}^4$             |              |              |
| Section modulus about x-axis:               | $S_x = 0.2219 \text{in}^3$             |              |              |
| Section modulus about y-axis:               | $S_{y\text{lip}} = 0.0409 \text{in}^3$ |              |              |
|   | $S_{y\text{web}} = 0.1177 \text{in}^3$ |              |              |
| Distance between shear center and centroid: | $x_0 = -0.8327 \text{in}$              |              |              |
| Radius of gyration about x-axis:            | $r_x = 1.4059 \text{in}$               |              |              |
| Radius of gyration about y-axis:            | $r_y = 0.439 \text{in}$                |              |              |
| Polar radius of gyration:                   | $r_0 = 1.692 \text{in}$                |              |              |
| St. Venant torsional constant:              | $J = 0.0001 \text{in}^4$               |              |              |
| Warping constant:                           | $C_w = 0.1007 \text{in}^6$             |              |              |
| Parameters $\beta_w, \beta_f, \beta_l$ :    | $\beta_w = -0.0422 \text{in}^5$        |              |              |
|   | $\beta_f = 0.0923 \text{in}^5$         |              |              |
|   | $\beta_l = 0.0475 \text{in}^5$         |              |              |
| Parameter j:                                | $j = 2.081 \text{in}$                  |              |              |



### Check Applicability:

|                              |  |
|------------------------------|--|
| $\text{Cond}_{B2\_2(a)} = 0$ | <i>Cond=1, indicates all the requirements given in Section B2.2 are satisfied. Otherwise, at least one of the conditions is not satisfied.</i> |
| $\text{Cond}_{D4} = 0$       | <i>Cond=1, indicates all the requirements given in Section B2.2 are satisfied. Otherwise, at least one of the conditions is not satisfied.</i> |

Check = "No hole exists. Chapter B is applicable."

### Result:

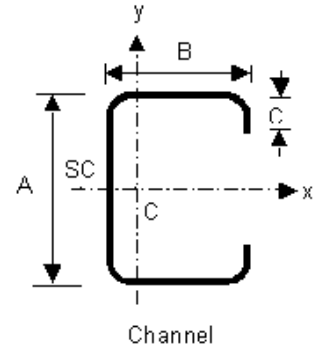
|  |  |
|--|--|
| Gross Area:  | $A_g = 0.2028 \text{in}^2$               |
| Effective area:  | $A_{\text{eff}} = 0.1963 \text{in}^2$    |
| Elastic flexural buckling stress for bending about x-axis:   | $\sigma_{\text{ex}} = 62.447 \text{ksi}$ |
| Elastic flexural buckling stress for bending about y-axis:   | $\sigma_{\text{ey}} = 6.0895 \text{ksi}$ |
| Elastic lateral torsional buckling stress:   | $F_{\text{elt}} = 6.6282 \text{ksi}$     |
| The critical elastic buckling stress will be the minimum stress of buckling about x or y axis, torsional buckling, and lateral-torsional buckling: | $F_e = 6.0895 \text{ksi}$                |
|  | $F_n = 5.3405 \text{ksi}$                |
|  | $P_n = 1048.36 \text{lb}$                |
| <b>Compression Strength for LRFD:</b>  | $\phi_c = 0.85$                          |
|  | $P_u := \phi_c P_n$                      |
|  | $P_u = 891.11 \text{lb}$                 |



## Summary

### Gross Section Properties:

|   |  |                |                 |
|---|--|----------------|-----------------|
| Effective Length Factors:                   | $K_{xx} = 0.5$                         | $K_{yy} = 0.5$ | $K_{tt} = 0.25$ |
| Cross section area:                         | $A_g = 0.2028 \text{in}^2$             |                |                 |
| Moment of inertia about x-axis:             | $I_x = 0.40085 \text{in}^4$            |                |                 |
| Moment of inertia about y-axis:             | $I_y = 0.0391 \text{in}^4$             |                |                 |
| Section modulus about x-axis:               | $S_x = 0.2219 \text{in}^3$             |                |                 |
| Section modulus about y-axis:               | $S_{y\text{lip}} = 0.0409 \text{in}^3$ |                |                 |
|   | $S_{y\text{web}} = 0.1177 \text{in}^3$ |                |                 |
| Distance between shear center and centroid: | $x_0 = -0.8327 \text{in}$              |                |                 |
| Radius of gyration about x-axis:            | $r_x = 1.4059 \text{in}$               |                |                 |
| Radius of gyration about y-axis:            | $r_y = 0.439 \text{in}$                |                |                 |
| Polar radius of gyration:                   | $r_0 = 1.692 \text{in}$                |                |                 |
| St. Venant torsional constant:              | $J = 0.0001 \text{in}^4$               |                |                 |
| Warping constant:                           | $C_w = 0.1007 \text{in}^6$             |                |                 |
| Parameters $\beta_w, \beta_f, \beta_l$ :    | $\beta_w = -0.0422 \text{in}^5$        |                |                 |
|   | $\beta_f = 0.0923 \text{in}^5$         |                |                 |
|   | $\beta_l = 0.0475 \text{in}^5$         |                |                 |
| Parameter j:                                | $j = 2.081 \text{in}$                  |                |                 |



### Check Applicability:

|                              |  |
|------------------------------|--|
| $\text{Cond}_{B2\_2(a)} = 0$ | <i>Cond=1, indicates all the requirements given in Section B2.2 are satisfied. Otherwise, at least one of the conditions is not satisfied.</i> |
| $\text{Cond}_{D4} = 0$       | <i>Cond=1, indicates all the requirements given in Section B2.2 are satisfied. Otherwise, at least one of the conditions is not satisfied.</i> |

Check = "No hole exists. Chapter B is applicable."

### Result:

|  |   |
|--|---|
| Gross Area:  | $A_g = 0.2028 \text{in}^2$                |
| Effective area:  | $A_{\text{eff}} = 0.15403 \text{in}^2$    |
| Elastic flexural buckling stress for bending about x-axis:   | $\sigma_{\text{ex}} = 249.788 \text{ksi}$ |
| Elastic flexural buckling stress for bending about y-axis:   | $\sigma_{\text{ey}} = 24.3578 \text{ksi}$ |
| Elastic lateral torsional buckling stress:   | $F_{\text{elt}} = 79.913 \text{ksi}$      |
| The critical elastic buckling stress will be the minimum stress of buckling about x or y axis, torsional buckling, and lateral-torsional buckling: | $F_e = 24.3578 \text{ksi}$                |
|  | $F_n = 18.7174 \text{ksi}$                |
|  | $P_n = 2882.98 \text{lb}$                 |
| <b>Compression Strength for LRFD:</b>  | $P_u = 2450.53 \text{lb}$                 |

### Compression Strength for LRFD:

$$\phi_c = 0.85$$

$$P_u := \phi_c P_n$$

## C.2 Initial Flexural Stiffness of the Connection from In-Plane Load tests

### C.2.1 SS Type Connection

The following mathcad worksheet is for Screwed-Screwed connection of Clip angle to the bridging and the stud-web and is used to determine the initial connection stiffness only, based on basic mechanics

ORIGIN:= 1

ksi := 1000psi

kip := 1000bf

#### STUD PROPERTIES:

Depth of studs  $D := (3.625 \ 3.625 \ 3.625 \ 6.000 \ 6.000 \ 6.000 \ 8.000 \ 8.000)^T$  in

Thickness of studs  $t := (0.033 \ 0.043 \ 0.068 \ 0.033 \ 0.043 \ 0.097 \ 0.043 \ 0.097)^T$  in  
 $i := \text{ORIGIN}.. \text{last}(D)$

Radius of bend  $r_{\text{bent}} := (0.094 \ 0.094 \ 0.141 \ 0.094 \ 0.094 \ 0.205 \ 0.094 \ 0.205)^T$  in

Effective flat width of web  $w_i := D_i - t_i - 2 \cdot r_{\text{bent}_i}$        $w_{\text{by}_t}_i := \frac{w_i}{t_i}$

Material properties  $w^T = (3.404 \ 3.394 \ 3.275 \ 5.779 \ 5.769 \ 5.493 \ 7.769 \ 7.493)$  in  
 $E_{\text{stud}_i} := 29500.\text{ksi}$        $\mu := 0.3$   
 $f_y := (48.53 \ 47.04 \ 52.01 \ 24.03 \ 46.24 \ 60.2 \ 40.23 \ 42.5)^T$  ksi

Punchout dimensions  $w_{h_i} := 4\text{in}$      $w_{h_1} := 1.5\text{in}$      $w_{h_4} := 1.5\text{in}$      $d_h := 1.5\text{in}$   
 Note: The 33 mil studs had smaller length punchouts

#### BRIDGING PROPERTIES:

Length of bridging  $L_{\text{bridging}} := 10.0\text{in}$

Thickness of bridging  $t_{\text{bridging}} := 0.054\text{in}$

Web depth of bridging  $D_{\text{bridging}} := 1.5\text{in}$

Area of bridging channel c/s  $A_{\text{bridging}} := D_{\text{bridging}} \cdot t_{\text{bridging}} + 0.55\text{in} \cdot t_{\text{bridging}} \cdot 2$

Material properties  $E_{\text{bridging}} := 29500\text{ksi}$        $A_{\text{bridging}} = 0.1404\text{in}^2$

#### CLIP ANGLE PROPERTIES:

Angle leg  $L_{\text{angle}} := 1.5\text{in}$

Thickness of angle  $t_{\text{angle}} := 0.054\text{in}$

Length of angle  $L_{\text{angle}} := D - 1.5\text{in}$   
 $L_{\text{angle}}^T = (2.125 \ 2.125 \ 2.125 \ 4.5 \ 4.5 \ 4.5 \ 6.5 \ 6.5)$  in

Material properties  $E_{\text{angle}} := 29500\text{ksi}$

Moment of inertia

$$I_x := \left( \frac{\text{Leg}_{\text{angle}} \cdot t_{\text{angle}}^3}{12} + \text{Leg}_{\text{angle}} \cdot \frac{t_{\text{angle}}^3}{4} \right) \dots$$

$$+ \left[ \frac{(\text{Leg}_{\text{angle}} - t_{\text{angle}})^3 \cdot t_{\text{angle}}}{12} + \frac{(\text{Leg}_{\text{angle}} - t_{\text{angle}}) \cdot \text{Leg}_{\text{angle}}^2}{4} \cdot t_{\text{angle}} \right]$$

$$I_x = 0.0576 \text{in}^4$$

### SELF DRILLING SCREW PROPERTIES

Diameter of screw

$$d_{\text{screw}} := 0.19 \text{in}$$

$$d_{\text{screw}} = 0.19 \text{in}$$

M.I of screw

$$I_{\text{screw}} := \frac{\pi}{64} d_{\text{screw}}^4$$

$$I_{\text{screw}} = 6.3971 \times 10^{-5} \text{in}^4$$

Area of c/s of screw

$$A_{\text{screw}} := \frac{\pi}{4} \cdot d_{\text{screw}}^2$$

$$A_{\text{screw}} = 0.0284 \text{in}^2$$

Material properties

$$E_{\text{screw}} := 29000.0 \text{ksi}$$

**Horizontal bridging channel:** Subjected to direct tension

$$\beta = \frac{P}{\Delta} = \frac{A \cdot E}{L}$$

$$\beta_{\text{bridging}} := \frac{(A_{\text{bridging}}) \cdot E_{\text{bridging}}}{L_{\text{bridging}}}$$

$$\beta_{1i} := \beta_{\text{bridging}}$$

$$\beta_{1T} = (414.18 \ 414.18 \ 414.18 \ 414.18 \ 414.18 \ 414.18 \ 414.18 \ 414.18) \frac{\text{kip}}{\text{in}}$$

**Clip angle:** Considered as a simply supported beam subjected to two symmetric point loads due the screws connecting the channel. Supported at the screws connecting the stud-web

$$a_i := \frac{L_{\text{angle}_i} - 1.0 \text{in}}{2}$$

$$I_{\text{angle}} := I_x$$

$$\text{inv} \beta_{\text{angle}_i} := \frac{1}{E_{\text{angle}} \cdot I_{\text{angle}}} \cdot \left[ \frac{1}{2} \cdot (a_i)^2 \cdot \left( \frac{2}{3} \cdot a_i \right) + a_i \cdot 0.5 \text{in} \cdot \left( a_i + \frac{0.5 \text{in}}{2} \right) \right]$$

$$\beta_{\text{angle}_i} := \frac{1}{\text{inv} \beta_{\text{angle}_i}}$$

$$\beta_{2i} := \beta_{\text{angle}_i}$$

$$\beta_{2T} = (5903.9163 \ 5903.9163 \ 5903.9163 \ 480.5355 \ 480.5355 \ 480.5355 \ 153.6899 \ 153.6899) \frac{\text{kip}}{\text{in}}$$

**Bending in screws** connecting bridging channel and the horizontal leg of clip angle, considering fixed-fixed condition...

$$L1_{\text{screw}} := t_{\text{angle}} + t_{\text{bridging}}$$

$$\beta = \frac{P}{\Delta} = \frac{12E \cdot I}{L^3} \quad \beta_{\text{screw1}} := 2 \frac{12 \cdot E_{\text{screw}} \cdot I_{\text{screw}}}{L1_{\text{screw}}^3} \quad \beta3_1 := \beta_{\text{screw1}}$$

$$\beta3^T = (35344.535 \ 35344.535 \ 35344.535 \ 35344.535 \ 35344.535 \ 35344.535 \ 35344.535 \ 35344.535) \frac{\text{kip}}{\text{in}}$$

**Screw in direct tension:** considering the length of screw being the sum of thickness of connecting plate members (clip angle and stud-web)...

$$L2_{\text{screw}_i} := (t_{\text{angle}} + t_i)$$

$$\beta = \frac{P}{\Delta} = \frac{A \cdot E}{L} \quad \beta_{\text{screw2}} := 2 \frac{(A_{\text{screw}}) \cdot E_{\text{screw}}}{(L2_{\text{screw}})} \quad \beta4 := \beta_{\text{screw2}}$$

$$\beta4^T = (18901.92 \ 16953.26 \ 13479.24 \ 18901.92 \ 16953.26 \ 10890.51 \ 16953.26 \ 10890.51) \frac{\text{kip}}{\text{in}}$$

**Web plate:** subjected to two point loads...

Plate aspect ratio  $a_r := 2$

The web plate was considered to be either simply supported or fixed on all four edges, and the plate stiffness equation from "Roark's formulas for stress and strain" was used which is as given below. In this equation, the width of the web was determined based on the Section B2.2 of the AISI-CFS Spec.

*For a simply supported plate:*

Plate buckling coefficient  $k1_b := 24$  Plate fixity coefficients:  $C_{ss} := 0.138$

Slenderness factor:  $\lambda1_i := \frac{1.052}{\sqrt{k1_b}} \frac{(w_i)}{t_i} \cdot \sqrt{\frac{f_{y_i}}{E_{\text{stud}_i}}}$

Effective width of web  $b_i := \begin{cases} \left[ \frac{w_i}{\lambda1_i} \left( 1 - \frac{0.22}{\lambda1_i} - \frac{0.8d_h}{w_i} \right) \right] & \text{if } \lambda1_i > 0.673 \\ w_i - d_h & \end{cases}$

$$\lambda1^T = (0.8984 \ 0.6768 \ 0.4343 \ 1.0733 \ 1.1406 \ 0.5493 \ 1.4328 \ 0.6296)$$

$$\frac{\Delta}{P} = C(1 - \mu^2) \cdot \frac{a \cdot b}{E \cdot t^3}$$

$$\beta_{SS_{web}_i} := \frac{E_{stud_i} \cdot (t_i)^3}{C_{SS} \cdot (1 - \mu^2) \cdot [b_i \cdot (w_i \cdot a_T)]}$$

For a fixed plate:

Plate buckling coefficient  $k_{2b} := 41$       Plate fixity coefficients:  $C_{ff} := 0.067$

Slenderness factor: 
$$\lambda_{2i} := \frac{1.052}{\sqrt{k_{2b}}} \frac{(w_i)}{t_i} \cdot \sqrt{\frac{f_{y_i}}{E_{stud_i}}}$$

Effective width of web 
$$b_i := \begin{cases} \left[ \frac{w_i}{\lambda_{2i}} \cdot \left( 1 - \frac{0.22}{\lambda_{2i}} - \frac{0.8d_h}{w_i} \right) \right] & \text{if } \lambda_{2i} > 0.673 \\ w_i - d_h & \end{cases}$$

$$\lambda^T = (0.6874 \ 0.5178 \ 0.3322 \ 0.8212 \ 0.8727 \ 0.4203 \ 1.0962 \ 0.4817)$$

$$\beta_{FF_{web}_i} := \frac{E_{stud_i} \cdot (t_i)^3}{C_{ff} \cdot (1 - \mu^2) \cdot [b_i \cdot (w_i \cdot a_T)]}$$

$$\frac{1}{\beta_{conn}} = \frac{1}{\beta_1} + \frac{1}{\beta_2} + \frac{1}{\beta_3} + \frac{1}{\beta_4} + \frac{1}{\beta_5}$$

$$\beta_{SS}^5 := \beta_{SS_{web}}$$

$$inv\beta_{SS_{conn}} := \frac{1}{\beta_1} + \frac{1}{\beta_2} + \frac{1}{\beta_3} + \frac{1}{\beta_4} + \frac{1}{\beta_{SS}^5}$$

$$\beta_{SS_{conn}_i} := \frac{1}{inv\beta_{SS_{conn}_i}}$$

$$\beta_{FF}^5 := \beta_{FF_{web}}$$

$$inv\beta_{FF_{conn}} := \frac{1}{\beta_1} + \frac{1}{\beta_2} + \frac{1}{\beta_3} + \frac{1}{\beta_4} + \frac{1}{\beta_{FF}^5}$$

$$\beta_{FF_{conn}_i} := \frac{1}{inv\beta_{FF_{conn}_i}}$$

$$\beta_{expLBV} := \begin{pmatrix} 1.683 \\ 3.574 \\ 6.102 \\ 1.000 \\ 3.785 \\ 5.571 \\ 2.066 \\ 2.947 \end{pmatrix} \cdot \frac{\text{kip}}{\text{in}} \quad \beta_{expUBV} := \begin{pmatrix} 2.068 \\ 4.200 \\ 7.942 \\ 1.143 \\ 3.822 \\ 6.860 \\ 2.463 \\ 7.082 \end{pmatrix} \cdot \frac{\text{kip}}{\text{in}} \quad \beta_{SS_{conn}} = \begin{pmatrix} 0.6501 \\ 1.4471 \\ 6.2465 \\ 0.1706 \\ 0.3785 \\ 4.7796 \\ 0.1914 \\ 2.3368 \end{pmatrix} \cdot \frac{\text{kip}}{\text{in}} \quad \beta_{FF_{conn}} = \begin{pmatrix} 1.3366 \\ 2.9685 \\ 12.6412 \\ 0.351 \\ 0.7782 \\ 9.6196 \\ 0.3935 \\ 4.7076 \end{pmatrix} \cdot \frac{\text{kip}}{\text{in}}$$

$$\beta_{SS} := (\beta_1 \ \beta_2 \ \beta_3 \ \beta_4 \ \beta_{SS}^5) \quad \beta_{FF} := (\beta_1 \ \beta_2 \ \beta_3 \ \beta_4 \ \beta_{FF}^5)$$

$$\beta_{SS} = \begin{pmatrix} (414.18) & (5903.9163) & (35344.5353) & (18901.9158) & (0.6513) \\ 414.18 & 5903.9163 & 35344.5353 & 16953.2647 & 1.4527 \\ 414.18 & 5903.9163 & 35344.5353 & 13479.235 & 6.3531 \\ 414.18 & 480.5355 & 35344.5353 & 18901.9158 & 0.1707 \\ 414.18 & 480.5355 & 35344.5353 & 16953.2647 & 0.3792 \\ 414.18 & 480.5355 & 35344.5353 & 10890.5078 & 4.8874 \\ 414.18 & 153.6899 & 35344.5353 & 16953.2647 & 0.1917 \\ (414.18) & (153.6899) & (35344.5353) & (10890.5078) & (2.3872) \end{pmatrix} \frac{\text{kip}}{\text{in}}$$

$$\beta_{FF} = \begin{pmatrix} (414.18) & (5903.9163) & (35344.5353) & (18901.9158) & (1.3414) \\ 414.18 & 5903.9163 & 35344.5353 & 16953.2647 & 2.9922 \\ 414.18 & 5903.9163 & 35344.5353 & 13479.235 & 13.0856 \\ 414.18 & 480.5355 & 35344.5353 & 18901.9158 & 0.3516 \\ 414.18 & 480.5355 & 35344.5353 & 16953.2647 & 0.781 \\ 414.18 & 480.5355 & 35344.5353 & 10890.5078 & 10.0666 \\ 414.18 & 153.6899 & 35344.5353 & 16953.2647 & 0.3949 \\ (414.18) & (153.6899) & (35344.5353) & (10890.5078) & (4.9169) \end{pmatrix} \frac{\text{kip}}{\text{in}}$$

Augmenting all the above values into one matrix...

$$A := \text{augment} \left( \frac{D}{\text{in}}, \frac{t}{\text{in}}, \frac{f_y}{\text{ksi}}, \lambda_1, \frac{\beta_{\text{expLBV}}}{\frac{\text{kip}}{\text{in}}}, \frac{\beta_{\text{expUBV}}}{\frac{\text{kip}}{\text{in}}}, \frac{\beta_{SS_{\text{conn}}}}{\frac{\text{kip}}{\text{in}}}, \frac{\beta_{FF_{\text{conn}}}}{\frac{\text{kip}}{\text{in}}}, w_{\text{by}_t} \right)$$

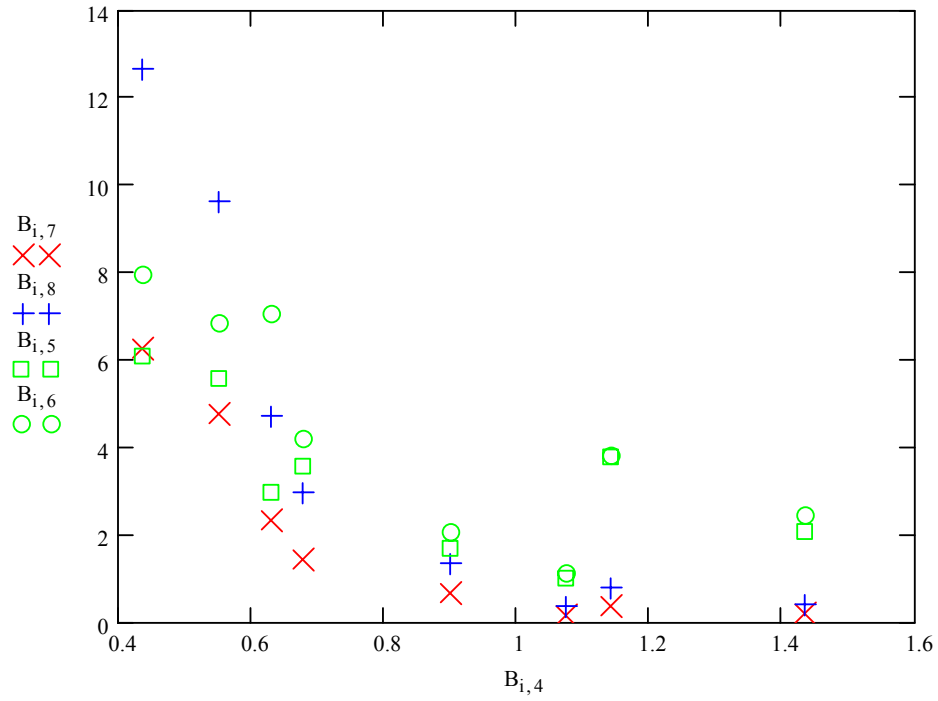
Sorting the augmented matrix in ascending order of slenderness...

$$B := \text{csort}(A, 4)$$

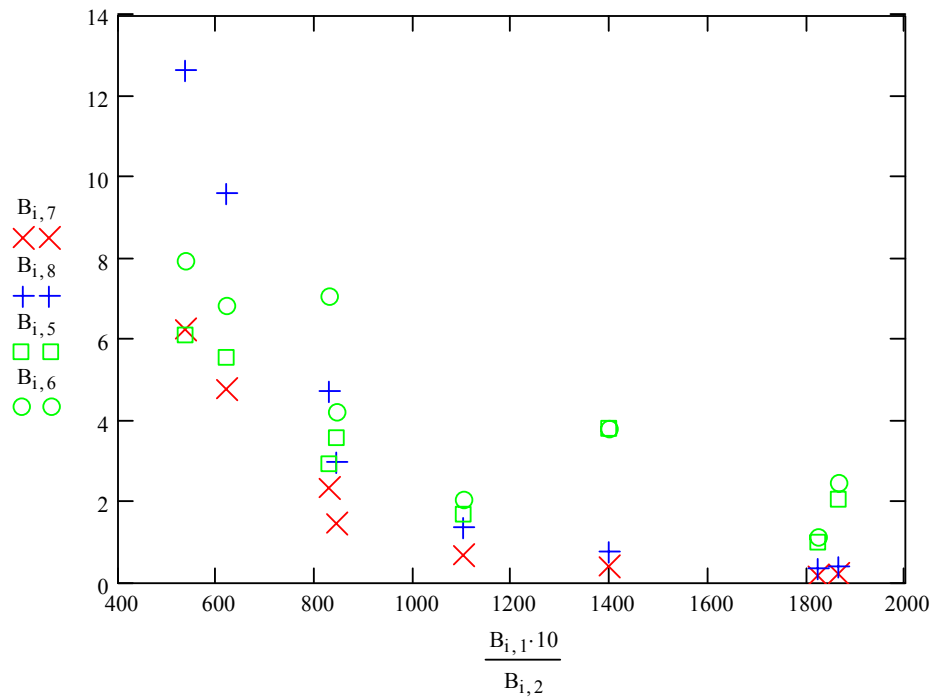
Each of the columns in the Matrix B (below) represents:

Stud Depth, Thickness, Yield Stress, Slenderness Factor, Lower Bound Expt. stiffness, Upper Bound Expt. stiffness, Calculated Stiffness for SS plate, Calculated Stiffness for FF plate, and w/t ratio, resp.

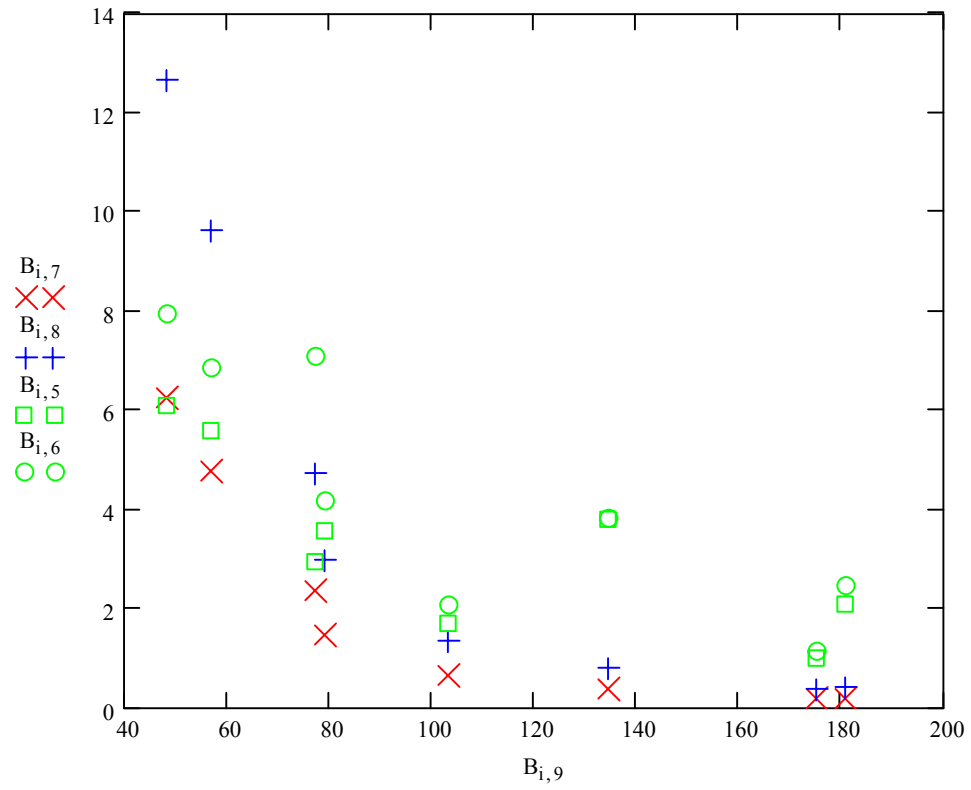
$$B = \begin{pmatrix} 3.625 & 0.068 & 52.01 & 0.4343 & 6.102 & 7.942 & 6.2465 & 12.6412 & 48.1618 \\ 6 & 0.097 & 60.2 & 0.5493 & 5.571 & 6.86 & 4.7796 & 9.6196 & 56.6289 \\ 8 & 0.097 & 42.5 & 0.6296 & 2.947 & 7.082 & 2.3368 & 4.7076 & 77.2474 \\ 3.625 & 0.043 & 47.04 & 0.6768 & 3.574 & 4.2 & 1.4471 & 2.9685 & 78.9302 \\ 3.625 & 0.033 & 48.53 & 0.8984 & 1.683 & 2.068 & 0.6501 & 1.3366 & 103.1515 \\ 6 & 0.033 & 24.03 & 1.0733 & 1 & 1.143 & 0.1706 & 0.351 & 175.1212 \\ 6 & 0.043 & 46.24 & 1.1406 & 3.785 & 3.822 & 0.3785 & 0.7782 & 134.1628 \\ 8 & 0.043 & 40.23 & 1.4328 & 2.066 & 2.463 & 0.1914 & 0.3935 & 180.6744 \end{pmatrix}$$



Plot of Experimental LBV, UBV [squares & circles], Analytical [x and +] VS. slenderness factor...



Plot of Experimental LBV, UBV [squares & Circles], Analytical [x and +], VS. D/t ratio



Plot of Experimental LBV, UBV [squares & Circles], Analytical [x and +], versus flat w/t ratio...

## C.2.2 WW Type Connection

The following mathcad worksheet is for Welded-Welded connection of Clip angle to the bridging channel and the stud-web, and is used to determine the initial connection stiffness only, based on basic mechanics

ORIGIN:= 1

ksi := 1000psi

kip := 1000bf

### STUD PROPERTIES:

Depth of studs  $D := (3.625 \ 6.000 \ 8.000)^T$  in

Thickness of studs  $t := (0.068 \ 0.097 \ 0.097)^T$  in

$i := \text{ORIGIN} \cdot \text{last}(D)$

Radius of bend  $r_{\text{bent}} := (0.141 \ 0.205 \ 0.205)^T$  in

Effective flat width of web  $w := D - t - 2 \cdot r_{\text{bent}}$

$w^T = (3.275 \ 5.493 \ 7.493)$  in  $w_{\text{by}_t} := \frac{w_i}{t_i}$

Material properties  $E_{\text{stud}_i} := 29500$ ksi  $\mu := 0.3$

$f_y := (52.01 \ 60.20 \ 42.50)^T$  ksi

punchout dimensions  $w_{h_i} := 4$ in  $d_h := 1.5$ in

### BRIDGING PROPERTIES:

Length of bridging  $L_{\text{bridging}} := 10.0$ in

Thickness of bridging  $t_{\text{bridging}} := 0.054$ in

Web depth of bridging  $D_{\text{bridging}} := 1.5$ in

Area of bridging channel c/s  $A_{\text{bridging}} := D_{\text{bridging}} \cdot t_{\text{bridging}} + 0.55 \text{in} \cdot t_{\text{bridging}} \cdot 2$

Material properties  $E_{\text{bridging}} := 29500$ ksi

$A_{\text{bridging}} = 0.1404 \text{in}^2$

### CLIP ANGLE PROPERTIES:

Angle leg  $\text{Leg}_{\text{angle}} := 1.5$ in

Thickness of angle  $t_{\text{angle}} := 0.054$ in

Length of angle  $L_{\text{angle}} := D - 1.5$ in

$L_{\text{angle}}^T = (2.125 \ 4.5 \ 6.5)$  in

Material properties  $E_{\text{angle}} := 29500$ ksi

Moment of inertia

$$I_x := \left( \frac{\text{Leg}_{\text{angle}} \cdot t_{\text{angle}}^3}{12} + \text{Leg}_{\text{angle}} \cdot \frac{t_{\text{angle}}^3}{4} \right) \dots$$

$$+ \left[ \frac{(\text{Leg}_{\text{angle}} - t_{\text{angle}})^3 \cdot t_{\text{angle}}}{12} + \frac{(\text{Leg}_{\text{angle}} - t_{\text{angle}}) \cdot \text{Leg}_{\text{angle}}^2}{4} \cdot t_{\text{angle}} \right]$$

$$I_x = 0.0576 \text{ in}^4$$

Horizontal bridging channel; considering under direct tension

$$\beta = \frac{P}{\Delta} = \frac{A \cdot E}{L} \beta_{\text{bridging}} := \frac{(A_{\text{bridging}}) \cdot E_{\text{bridging}}}{L_{\text{bridging}}} \quad \beta 1_i := \beta_{\text{bridging}} \quad \beta 1^T = (414.18 \ 414.18 \ 414.18) \frac{\text{kip}}{\text{in}}$$

Neglecting the effect of weld, since it does not contribute to the stiffness significantly.

Clip angle; considering as a fixed-fixed beam subjected to two symmetric point loads due to the welds...

$$a_i := \frac{L_{\text{angle}_i} - 1.5 \text{ in}}{2} \quad b_i := L_{\text{angle}_i} - a_i - 1.5 \text{ in} \quad I_{\text{angle}} := I_x \quad M_{\text{fem}_i} := \frac{a_i \cdot b_i}{L_{\text{angle}_i}}$$

$$\text{inv} \beta_{\text{angle}_i} := \frac{1}{E_{\text{angle}} \cdot I_{\text{angle}}} \cdot \left[ \frac{1}{2} \cdot (a_i)^2 \cdot \left( \frac{2}{3} \cdot a_i \right) + a_i \cdot 0.75 \text{ in} \cdot \left( a_i + \frac{0.75 \text{ in}}{2} \right) - \frac{M_{\text{fem}_i} \cdot L_{\text{angle}_i}}{2} \cdot \frac{L_{\text{angle}_i}}{4} \right]$$

$$\beta_{\text{angle}_i} := \frac{1}{\text{inv} \beta_{\text{angle}_i}} \quad \beta 2_i := \beta_{\text{angle}_i} \quad \beta 2^T = (1.169 \times 10^4 \ 863.1842 \ 307.8147) \frac{\text{kip}}{\text{in}}$$

Web plate subjected to two point loads...

Plate aspect ratio  $a_r := 2$

Plate buckling coefficient  $k 1_b := 24$  Plate fixity coefficients:  $C_{SS} := 0.138$

Slenderness factor:  $\lambda 1_i := \frac{1.052}{\sqrt{k 1_b}} \cdot \frac{(w_i)}{t_i} \cdot \sqrt{\frac{f_{y_i}}{E_{\text{stud}_i}}}$  correction1<sub>i</sub> := 1

$$\lambda 1^T = (0.4343 \ 0.5493 \ 0.6296)$$

$$\frac{\Delta}{P} = C \left( 1 - \mu^2 \right) \cdot \frac{a \cdot b}{E \cdot t^3}$$

$$\beta_{SS_{\text{web}_i}} := \frac{(\text{correction}1_i) \cdot E_{\text{stud}_i} \cdot (t_i + t_{\text{angle}})^3}{C_{SS} \cdot (1 - \mu^2) \cdot [(w_i) \cdot (a_r \cdot w_i) - d_h \cdot w_{h_i}]}$$

$$\beta_{SS3} := \beta_{SS_{\text{web}}}$$

Plate buckling coefficient  $k 2_b := 41$  Plate fixity coefficients:  $C_{ff} := 0.067$

Slenderness factor:  $\lambda_{2i} := \frac{1.052}{\sqrt{k_2 b}} \frac{(w_i)}{t_i} \sqrt{\frac{f_{y_i}}{E_{\text{stud}_i}}}$       correction2<sub>i</sub> := 1

$$\lambda_2^T = (0.3322 \ 0.4203 \ 0.4817)$$

$$\beta_{\text{FF}_{\text{web}_i}} := \frac{(\text{correction2}_i) \cdot E_{\text{stud}_i} \cdot (t_i + t_{\text{angle}})^3}{C_{\text{FF}} (1 - \mu^2) \cdot [(w_i) \cdot (a_i \cdot w_i) - d_h \cdot w_{h_i}]}$$

$$\beta_{\text{FF3}} := \beta_{\text{FF}_{\text{web}}}$$

$$\beta_{\text{SS}_{\text{web}}}^T = (27.6069 \ 14.8821 \ 7.6092) \frac{\text{kip}}{\text{in}}$$

$$\beta_{\text{FF}_{\text{web}}}^T = (56.8619 \ 30.6527 \ 15.6727) \frac{\text{kip}}{\text{in}}$$

$$\frac{1}{\beta_{\text{conn}}} = \frac{1}{\beta_1} + \frac{1}{\beta_2} + \frac{1}{\beta_3}$$

$$\text{inv}\beta_{\text{SS}_{\text{conn}}} := \frac{1}{\beta_1} + \frac{1}{\beta_2} + \frac{1}{\beta_{\text{SS3}}}$$

$$\beta_{\text{SS}_{\text{conn}_i}} := \frac{1}{\text{inv}\beta_{\text{SS}_{\text{conn}_i}}}$$

$$\text{inv}\beta_{\text{FF}_{\text{conn}}} := \frac{1}{\beta_1} + \frac{1}{\beta_2} + \frac{1}{\beta_{\text{FF3}}}$$

$$\beta_{\text{FF}_{\text{conn}_i}} := \frac{1}{\text{inv}\beta_{\text{FF}_{\text{conn}_i}}}$$

$$\beta_{\text{expLBV}} := \begin{pmatrix} 30.423 \\ 15.241 \\ 10.512 \end{pmatrix} \cdot \frac{\text{kip}}{\text{in}} \quad \beta_{\text{expUBV}} := \begin{pmatrix} 40.788 \\ 16.524 \\ 19.668 \end{pmatrix} \cdot \frac{\text{kip}}{\text{in}} \quad \beta_{\text{SS}_{\text{conn}}} = \begin{pmatrix} 25.8246 \\ 14.1307 \\ 7.2949 \end{pmatrix} \frac{\text{kip}}{\text{in}} \quad \beta_{\text{FF}_{\text{conn}}} = \begin{pmatrix} 49.7849 \\ 27.627 \\ 14.395 \end{pmatrix} \frac{\text{kip}}{\text{in}}$$

$$\beta_{\text{SS}} := (\beta_1 \ \beta_2 \ \beta_{\text{SS3}})$$

$$\beta_{\text{FF}} := (\beta_1 \ \beta_2 \ \beta_{\text{FF3}})$$

$$\beta_{\text{SS}} = \begin{bmatrix} (414.18) & (11690.498) & (27.6069) \\ 414.18 & 863.1842 & 14.8821 \\ (414.18) & (307.8147) & (7.6092) \end{bmatrix} \frac{\text{kip}}{\text{in}} \quad \beta_{\text{FF}} = \begin{bmatrix} (414.18) & (11690.498) & (56.8619) \\ 414.18 & 863.1842 & 30.6527 \\ (414.18) & (307.8147) & (15.6727) \end{bmatrix} \frac{\text{kip}}{\text{in}}$$

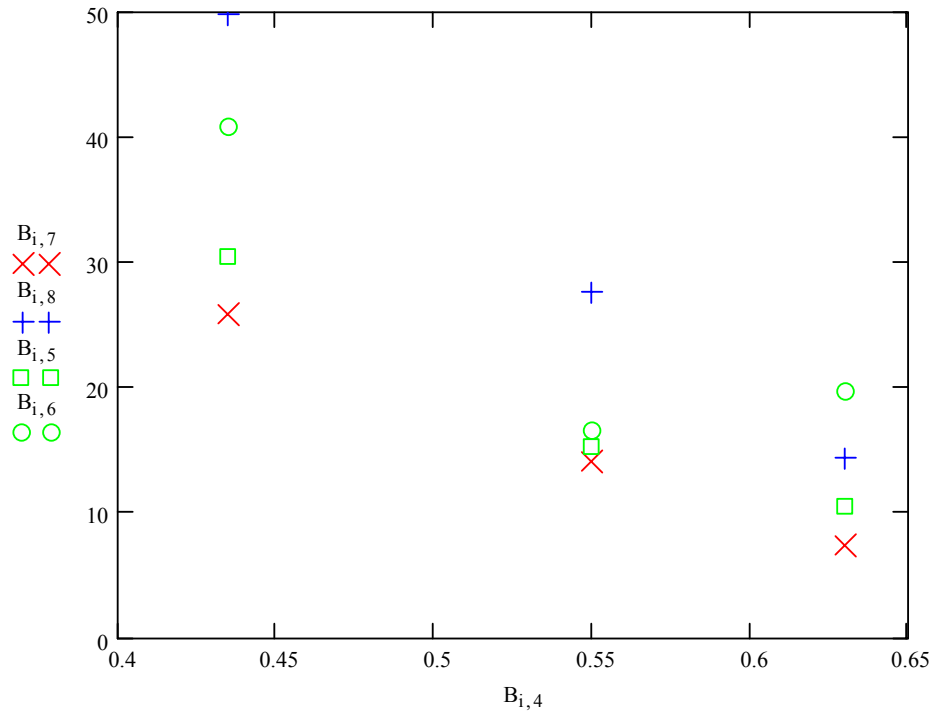
Augmenting all the above values into one matrix...

$$A := \text{augment} \left( \frac{D}{\text{in}}, \frac{t}{\text{in}}, \frac{f_y}{\text{ksi}}, \lambda_1, \frac{\beta_{\text{expLBV}}}{\frac{\text{kip}}{\text{in}}}, \frac{\beta_{\text{expUBV}}}{\frac{\text{kip}}{\text{in}}}, \frac{\beta_{\text{SS}_{\text{conn}}}}{\frac{\text{kip}}{\text{in}}}, \frac{\beta_{\text{FF}_{\text{conn}}}}{\frac{\text{kip}}{\text{in}}}, w_{\text{by}_t} \right)$$

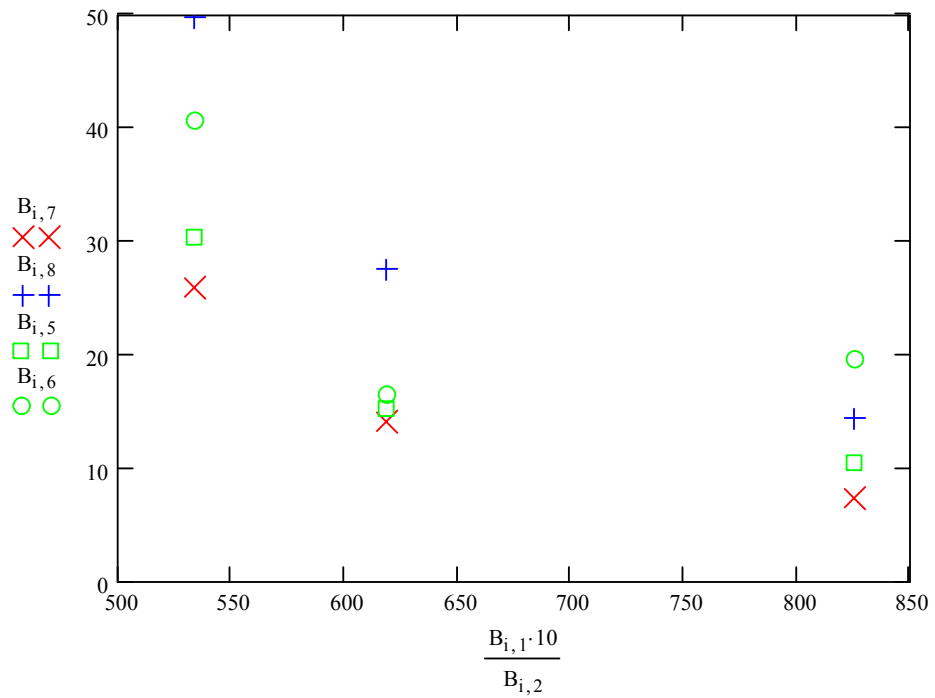
Sorting the augmented matrix in ascending order of slenderness...

$$B := \text{csort}(A, 4)$$

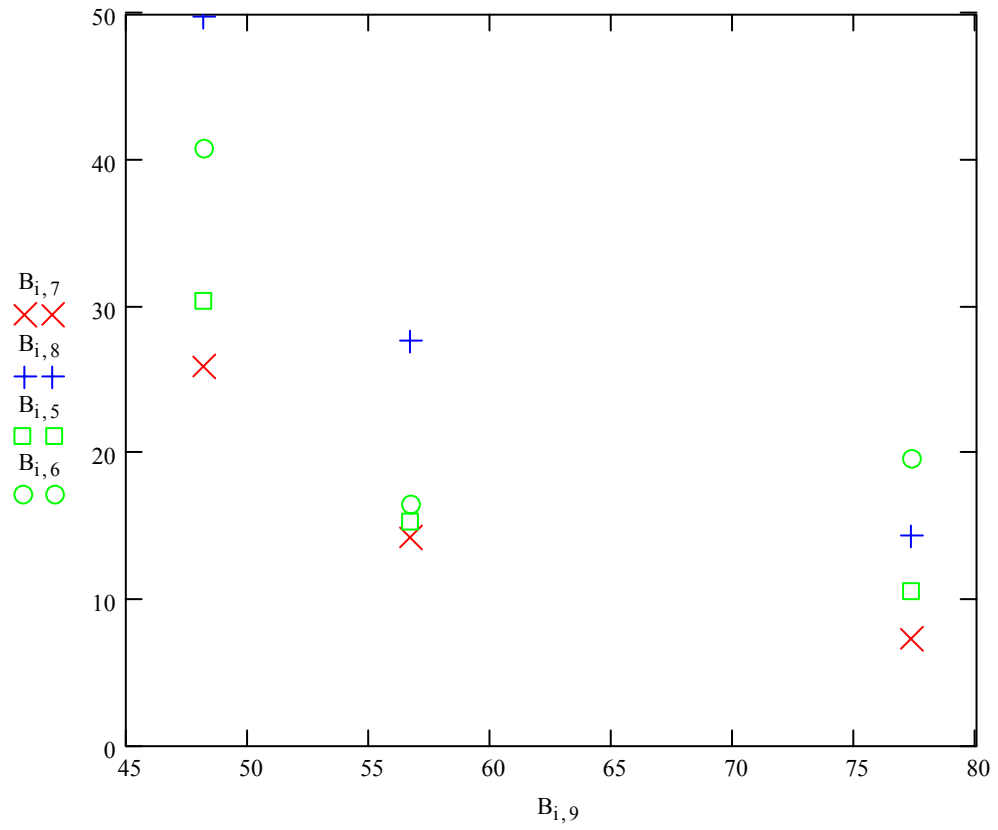
$$B = \begin{pmatrix} 3.625 & 0.068 & 52.01 & 0.4343 & 30.423 & 40.788 & 25.8246 & 49.7849 & 48.1618 \\ 6 & 0.097 & 60.2 & 0.5493 & 15.241 & 16.524 & 14.1307 & 27.627 & 56.6289 \\ 8 & 0.097 & 42.5 & 0.6296 & 10.512 & 19.668 & 7.2949 & 14.395 & 77.2474 \end{pmatrix}$$



Plot of Experimental [squares(LBV) and circles], Analytical [x and +], versus slenderness factor...



Plot of Experimental [squares(LBV) and circles], Analytical [x and +], versus D/t ratio



Plot of Experimental [squares(LBV) and circles], Analytical [x and +], versus flat w/t ratio...

## LIST OF REFERENCES

- American Institute of Steel Construction (AISC), 1999, *Load and Resistance Factor Design Specification for Structural Steel Buildings*, Third Edition, American Institute of Steel Construction, Chicago, IL.
- American Iron and Steel Institute (AISI), 1996, Specification for the Design of Cold-Formed Steel Structural Members, American Iron and Steel Institute, Washington, D.C.
- American Iron and Steel Institute (AISI), 1999, Specification for the Design of Cold-Formed Steel Structural Members Supplement No.-1, American Iron and Steel Institute, Washington, D.C.
- American Iron and Steel Institute (AISI), 2001a, North American Specification for the Design of Cold-Formed Steel Structural Members – Code and Commentary, AISI, Washington, D.C.
- American Iron and Steel Institute (AISI), 2001b, Commentary on North American Specification for the Design of Cold-Formed Steel Structural Members – Code and Commentary, AISI, Washington, D.C.
- AISIWIN V5.0, 2002, Devco Software, Inc. 245, NE Conifer, P.O. Box 1211, Corvallis, OR.
- American Society for Testing Materials (ASTM), 2000, Standard Specification for Nonstructural Steel Framing Members, ASTM C645-00, American Society for Testing and Materials, Philadelphia, PA.
- American Society for Testing Materials (ASTM), 2001, *Standard Test Methods for Tension Testing of Metallic Materials*, ASTM E8-01e2, American Society for Testing and Materials, Philadelphia, PA.
- American Society for Testing Materials (ASTM), 2001, Standard Specification for Load-Bearing (Transverse and Axial) Steel Studs, Runners (Tracks), and Bracing or Bridging for Screw Application of Gypsum Panel Products and Metal Plaster Bases, ASTM C955-01, American Society for Testing and Materials, Philadelphia, PA.
- Beshara, B., LaBoube, R.A., 2001, “Pilot Study: Lateral Braced C-Sections Under Bending,” *Thin Walled Structures*, Vol. 39, p 827-839.

- Bleich, F., 1952, *Buckling Strength of Metal Structures*, McGraw-Hill, New York, NY.
- Chajes, A., 1974, *Principles of Structural Stability*, Prentice-Hall, Englewood Cliffs, NJ.
- Galambos, T.V., 1998, *Guide to Stability Design Criteria for Metal Structures*, Fifth Edition, John Wiley & Sons, New York.
- Helwig, T.A., Yura, J.A., 1999, "Torsional Bracing of Columns," *Journal of Structural Engineering*, Vol. 125, No. 5, p 547-555.
- Kwon, Y.B., Hancock, G.J., 1991, "Strength Tests of Cold-Formed Channel Sections Undergoing Local and Distortional Buckling," Research Report No. R640, School of Civil and Mining Engineering, University of Sydney, Australia.
- Kavanagh, K.T., Ellifritt, D.S., 1993, "Bracing of Cold-Formed Channels Not Attached to Deck or Sheeting," *Bracing for Stability*, Structural Stability Research Council, Bethlehem, PA.
- Miller, T.H., 1990, "Behavior of Cold-Formed Steel Wall Stud Assemblies Subject to Eccentric Axial Loads," Ph.D. Thesis, Cornell University, Ithaca, N.Y.
- Miller, T.H., Pekoz, T., 1994, "Behavior of Gypsum-Sheathed Cold-Formed Steel Wall Studs," *Journal of Structural Engineering*, Vol. 120, No. 5, p 1644-1650.
- Plaut, R.H., 1993, "Requirements for Lateral Bracing of Columns with Two Spans," *Journal of Structural Engineering*, Vol. 119, No. 10, p 2913-2931.
- Shanley, F.R., 1947, "Inelastic Column Theory," *Journal of the Aeronautical Sciences*, Vol. 14, No. 5, p 261-268.
- Shanley, F.R., 1957, *Strength of Materials*, McGraw-Hill, New York, NY.
- Schafer, B.W., 2000, "Distortional Buckling of Cold-Formed Steel Columns," *Final Report to the American Iron and Steel Institute*, Washington, D.C.
- Steel Studs Manufacturers Association (SSMA), 2001, *Product Technical Information*, Steel Studs Manufacturers Association, ICBO ER-4943P, Chicago, IL.
- Winter, G., 1959, "Cold-Formed, Light-Gage Steel Construction," *Journal of Structural Engineering*, Vol. 85, No. ST 9, p 151-171.
- Winter, G., 1960, "Lateral Bracing of Columns and Beams," *Transactions of the American Society of Civil Engineers*, Vol. 125, p 807-845.
- Young, B., Rasmussen, K.J.R., 1999, "Behavior of Cold-Formed Singly Symmetric Columns," *Thin Walled Structures*, Vol. 33, p 83-102.
- Young, B., Rasmussen, K.J.R., 2000, "Inelastic Bifurcation of Cold-Formed Singly Symmetric Columns," *Thin Walled Structures*, Vol. 36, p 213-230.

- Yu, W-W., 1991, *Cold-Formed Steel Design*, Third Edition, John Wiley and Sons, New York, NY.
- Yura, J.A., 1996, "Winter's Bracing Model Revisited," *Engineering Structures Journal*, Elsevier, Vol. 18, No. 10, pp 821-825.
- Yura, J.A., 1995, "Bracing for Stability – State of the Art," *Bracing for Stability*, Structural Stability Research Council, Bethlehem, PA.
- Zuk, W., (1956), "Lateral Bracing Forces on Beams and Columns," *Journal of Engineering Mechanics*, Vol. 82, EM3, p 1032-1 – 1032-16.

## BIOGRAPHICAL SKETCH

Mr. Viswanath Urala was born on April 10, 1976, in Bangalore City, Karnataka State, India, to Mrs. Padma Balaramu and Mr. H.N. Balaramu. He went to Central School Malleswaram, Bangalore, for his primary, secondary and high school education. The author completed a Bachelor of Civil Engineering degree (1993 to 1997) at Bangalore Institute of Technology, Bangalore University, and a Master of Civil Engineering (1998 to 2000) at University of Visweswaraya - College of Engineering, Bangalore University. With this educational background, he worked for a couple of years as a Structural Detailer, Structural Designer and as a Civil Engineering Consultant.

Mr. Viswanath enrolled for a Master of Engineering degree with a major in structures at the Department of Civil and Coastal Engineering, University of Florida, Gainesville, FL, USA. He received a Graduate Research Assistantship for conducting research and a Graduate Teaching Assistantship for an undergraduate course on project development and visualization techniques. He worked on a research topic entitled Bracing Requirements of Cold-Formed Steel Cee-Studs Subjected to Axial Compressive Loading, co-sponsored by AISI and SSMA. He has co-authored three conference papers for the Structural Stability Research Council. As a teaching assistant, he taught computer aided drafting in AutoCAD for two consecutive semesters. He plans to receive his Master of Engineering degree in August 2004 after which he will pursue a career in the field of structural engineering.